

DYNAMIC FRICTIONAL CONTACT PROBLEMS INVOLVING
FUNCTIONALLY GRADED MATERIALS

A THESIS SUBMITTED TO
THE GRADUATE SCHOOL OF NATURAL AND APPLIED SCIENCES
OF
MIDDLE EAST TECHNICAL UNIVERSITY

BY

MEHMET NURULLAH BALCI

IN PARTIAL FULFILLMENT OF THE REQUIREMENTS
FOR
THE DEGREE OF DOCTOR OF PHILOSOPHY
IN
MECHANICAL ENGINEERING

OCTOBER 2018

Approval of the thesis:

**DYNAMIC FRICTIONAL CONTACT PROBLEMS INVOLVING
FUNCTIONALLY GRADED MATERIALS**

submitted by **MEHMET NURULLAH BALCI** in partial fulfillment of the requirements for the degree of **Doctor of Philosophy in Mechanical Engineering Department, Middle East Technical University** by,

Prof. Dr. Halil Kalıpçılar
Dean, Graduate School of **Natural and Applied Sciences**

Prof. Dr. M. A. Sahir Arıkan
Head of Department, **Mechanical Engineering**

Prof. Dr. Serkan Dağ
Supervisor, **Mechanical Engineering Dept., METU**

Examining Committee Members:

Assoc. Prof. Dr. Hüsnü Dal
Mechanical Engineering Dept., METU

Prof. Dr. Serkan Dağ
Mechanical Engineering Dept., METU

Prof. Dr. Recep Güneş
Mechanical Engineering Dept., Erciyes University

Assoc. Prof. Demirkan Çöker
Aerospace Engineering Dept., METU

Assoc. Prof. Dr. Barış Sabuncuoğlu
Mechanical Engineering Dept., Hacettepe University

Date: *19/10/2018*

I hereby declare that all information in this document has been obtained and presented in accordance with academic rules and ethical conduct. I also declare that, as required by these rules and conduct, I have fully cited and referenced all material and results that are not original to this work.

Name, Last Name: Mehmet Nurullah Balci

Signature:

ABSTRACT

DYNAMIC FRICTIONAL CONTACT PROBLEMS INVOLVING FUNCTIONALLY GRADED MATERIALS

Balci, Mehmet Nurullah
Ph.D., Department of Mechanical Engineering
Supervisor: Prof. Dr. Serkan Dağ
October 2018, 317 pages

The main aim of this study is to analyze the dynamic frictional contact problem of layered and functionally graded materials. Investigating contact problems including dynamic effects has a significant importance in mechanical engineering applications since many contact problems arise between moving structures. In moving contact problems, speed of the punch may not be so small to ignore dynamic effects. Hence, contact problem should be examined using elastodynamics theory. In this study, both frictional moving contact problems of homogenous elastic coatings and functionally graded coatings pressed by a moving rigid punch with various punch profiles are considered. The rigid punch is pressed against the coating and it moves at a constant subsonic speed. Governing partial differential equations are solved analytically using Galilean and Fourier transformation techniques. Displacement fields in both coating and the substrate are found by applying boundary and interface continuity conditions. Equations for the mixed boundary value problem is reduced to a singular integral equation of the second kind including unknown normal contact stress. The singular integral equation is solved numerically using a suitable expansion-collocation technique and normal contact stress is found. A verification study for elastostatic contact analysis is carried out using computational results generated by the use of finite element method. A verification study for elastodynamic contact analysis is conducted by utilizing available results in the literature. Consequently, the influences

of punch profile, punch sliding speed, material inhomogeneity, coefficient of friction and coating thickness on contact stresses and punch stress intensity factors are investigated.

Keywords: Dynamic Contact Mechanics, Moving Rigid Punch, Friction, Functionally Graded Coatings, Contact Stresses, Stress Intensity Factors, Singular Integral Equation.

ÖZ

FONKSİYONEL DERECELENDİRİLMİŞ MALZEMELER İÇEREN DİNAMİK SÜRTÜNMELİ TEMAS PROBLEMLERİ

Balci, Mehmet Nurullah
Doktora, Makina Mühendisliği Bölümü
Tez Yöneticisi: Prof. Dr. Serkan Dağ
Ekim 2018, 317 sayfa

Bu çalışmanın temel amacı katmanlı ve fonksiyonel derecelendirilmiş malzemeler içeren dinamik sürtünmeli temas problemini analiz etmektir. Makine mühendisliği uygulamalarında temas probleminin dinamik etkiler katılarak incelenmesi büyük önem taşımaktadır çünkü birçok temas hareketli yapılarda meydana gelmektedir. Hareketli temas problemlerinde, zımba hızı dinamik etkileri ihmal edecek kadar küçük olmayabilir. Bu yüzden, temas problemi elastodinamik teori kullanılarak incelenmelidir. Bu çalışmada, farklı profillere sahip hareketli rijit bir zımba tarafından bastırılan hem homojen elastik kaplama hem de fonksiyonel derecelendirilmiş kaplamaların sürtünmeli ve hareketli temas problemi ele alınmıştır. Rijit zımba kaplamaya bastırılmakta ve sabit ses altı bir hızda hareket etmektedir. Yürütücü kısmi diferansiyel denklemler Galilean ve Fourier dönüşümü tekniği kullanılarak analitik olarak çözülmüştür. Kaplama ve alt katman için yer-değiştirme alanları sınır ve ara-yüzey devamlılık koşulları uygulanarak bulunmuştur. Karma sınır değer problemi için denklemler içerisinde bilinmeyen normal temas gerilmesi içeren ikinci tip tekil integral denkleme indirgenmiştir. Tekil integral denklemini uygun bir açılım-düzenleme tekniği ile sayısal olarak çözülmüş ve normal temas gerilmesi bulunmuştur. Elastostatik temas analizi için doğrulama çalışması sonlu elemanlar metodu kullanılarak üretilen hesaplamalı sonuçlar ile yapılmıştır. Elastodinamik temas analizi için doğrulama çalışması literatürde mevcut olan

sonular kullanılarak yapılmıřtır. Sonu olarak, zımba profili, zımba kayma hızı, malzeme homojensizlięi, srtnme katsayısı ve kaplama kalınlıęının temas gerilmeleri ve zımba gerilme řiddeti arpanına olan etkileri arařtırılmıřtır.

Anahtar Kelimeler: Dinamik Temas Mekaniięi, Hareketli Rijit Zımba, Srtnme, Fonksiyonel Derecelendirilmiř Kaplamalar, Temas Gerilmeleri, Gerilme řiddeti arpanları, Tekil İntegral Denklemi.

ACKNOWLEDGEMENTS

Firstly, the author would like to express his sincere thanks and gratitudes to the advisor Prof. Dr. Serkan Dađ for his continuous support, patience and valuable suggestions throughout the Ph.D. study and related research. Besides his advisor, the author would like to thank to the members of the thesis monitoring committee Assoc. Prof. Dr. Demirkan öker and Assoc. Prof. Dr. Hüsnu Dal for their valuable comments, discussions, encouragement and collobration which incented the author to widen his research from various perspectives. The author would also like to thank to Prof. Dr. Bora Yıldırım at Hacettepe University, for his useful ideas and guidance.

The author would like to thank to TÜBİTAK – BİDEB (Bilim İnsanı Destekleme Dairesi Başkanlığı) for giving financial support during Ph.D. study.

The author wishes to express his grateful appreciation to his parents Mrs. Kezban Balcı and Mr. Prof. Dr. Sabahattin Balcı for their support, patience and understanding throughout the Ph. D. study.

Lastly, the author would like to thank to his wife Fatma Betül for her patience and understanding during the Ph. D. thesis study.

TABLE OF CONTENTS

ABSTRACT.....	v
ÖZ.....	vii
ACKNOWLEDGEMENTS.....	ix
TABLE OF CONTENTS.....	xi
LIST OF TABLES.....	xiv
LIST OF FIGURES.....	xxiv
CHAPTERS	
1. INTRODUCTION.....	1
1.1. Functionally Graded Materials.....	1
1.2. Tribological Applications.....	4
1.3. Literature Survey.....	7
1.4. Scope of the Study.....	13
2. PROBLEM STATEMENT AND FORMULATION.....	17
2.1. Interface Continuity and Boundary Conditions.....	32
2.1.1. Continuity Conditions along the Interface.....	35
2.1.2. Boundary Conditions.....	47
2.2. Singular integral equation of the problem.....	54
2.3. The derivation of the lateral contact stress on the contact surface.....	69
3. NUMERICAL SOLUTION OF THE SINGULAR INTEGRAL EQUATION ..	73
3.1. Flat punch problem.....	73

3.2. Triangular punch problem	83
3.3. Semi-circular punch problem	92
3.4. Cylindrical punch problem	103
4. NUMERICAL RESULTS FOR THE HOMOGENOUS ELASTIC COATING AND THE SUBSTRATE SYSTEM.....	115
4.1. Finite Element Analysis Study	118
4.2. Numerical Results for the Rigid Flat Punch.....	120
4.3. Numerical Results for the Rigid Triangular Punch	139
4.4. Numerical Results for the Rigid Semi-circular Punch	156
4.5. Numerical Results for the Rigid Cylindrical Punch	173
5. NUMERICAL RESULTS FOR THE FUNCTIONALLY GRADED COATING AND THE SUBSTRATE SYSTEM.....	189
5.1. Numerical Results for the Rigid Flat Punch.....	191
5.2. Numerical Results for the Rigid Triangular Punch	211
5.3. Numerical Results for the Rigid Semi-circular Punch	231
5.4. Numerical Results for the Rigid Cylindrical Punch	252
6. CONCLUSIONS AND FUTURE WORK	271
6.1. Concluding Remarks	271
6.2. Future work	282
REFERENCES.....	285
APPENDICES	
APPENDIX-A FIRST TERMS OF ASYMPTOTIC EXPRESSIONS	295
APPENDIX-B METHOD TO CALCULATE INDEFINITE INTEGRALS	296
APPENDIX-C USEFUL PROPERTIES OF JACOBI POLYNOMIALS	298

APPENDIX-D THE METHOD OF EVALUATION OF THE FREDHOLM KERNELS.....	301
APPENDIX-E THE EFFECT OF MASS DENSITY RATIO ON DYNAMIC CONTACT MECHANICS OF HOMOGENOUS ELASTIC COATINGS	308
APPENDIX-F SOLUTION OF DYNAMIC CONTACT PROBLEM BETWEEN A RIGID PUNCH AND A HALF PLANE BY COMPLEX FUNCTIONS	315
CURRICULUM VITAE	317

LIST OF TABLES

TABLES

Table 3.1: The powers of stress singularity for a flat punch $\nu_1 = 0.25$	82
Table 3.2: The powers of stress singularity for a triangular punch $\nu_1 = 0.25$. .91	91
Table 3.3: The powers of stress singularity for a semi-circular punch $\nu_1 = 0.25$	102
Table 3.4: The powers of stress singularity for a cylindrical punch $\nu_1 = 0.25$	114
Table 4.1: Dimensionless punch speed ratios	122
Table 4.2: Normalized stress intensity factors for the moving flat punch $c_1 = 0.0$, $\eta = 0.0$, $\nu_1 / \nu_2 = 0.8$	135
Table 4.3: Normalized stress intensity factors for the moving flat punch $a/h_1 = 0.1$, $\eta = 0.3$, $\rho_1 / \rho_2 = 1/8$, $\nu_1 / \nu_2 = 0.8$	135
Table 4.4: Normalized stress intensity factors for the moving flat punch $a/h_1 = 0.4$, $\eta = 0.3$, $\rho_1 / \rho_2 = 1/8$, $\nu_1 / \nu_2 = 0.8$	135
Table 4.5: Normalized stress intensity factors for the moving flat punch $a/h_1 = 0.4$, $\mu_1 / \mu_2 = 1/5$, $\rho_1 / \rho_2 = 1/8$, $\nu_1 / \nu_2 = 0.8$	136
Table 4.6: Normalized stress intensity factors for the moving flat punch $a/h_1 = 0.4$, $\mu_1 / \mu_2 = 5$, $\rho_1 / \rho_2 = 1/8$, $\nu_1 / \nu_2 = 0.8$	136
Table 4.7: Percent difference between elastostatic and elastodynamic normal contact stresses $\mu_1 / \mu_2 = 1/10$, $a/h_1 = 0.1$, $\eta = 0.3$, $\rho_1 / \rho_2 = 1/8$, $\nu_1 / \nu_2 = 0.8$	137

Table 4.8: Percent difference between elastostatic and elastodynamic lateral contact stresses $\mu_1 / \mu_2 = 1/10, a/h_1 = 0.1, \eta = 0.3, \rho_1 / \rho_2 = 1/8, \nu_1 / \nu_2 = 0.8$.
.....137

Table 4.9: Percent difference between elastostatic and elastodynamic normal contact stresses $\mu_1 / \mu_2 = 10, a/h_1 = 0.1, \eta = 0.3, \rho_1 / \rho_2 = 1/8, \nu_1 / \nu_2 = 0.8$.138

Table 4.10: Percent difference between elastostatic and elastodynamic lateral contact stresses $\mu_1 / \mu_2 = 10, a/h_1 = 0.1, \eta = 0.3, \rho_1 / \rho_2 = 1/8, \nu_1 / \nu_2 = 0.8$.138

Table 4.11: The normalized load for homogenous coating indented by a moving triangular punch $c_1 = 0, \eta = 0.0, \nu_1 / \nu_2 = 0.8$150

Table 4.12: The normalized load for homogenous coating indented by a moving triangular punch $b/h_1 = 0.2, \eta = 0.3, \rho_1 / \rho_2 = 1/8, \nu_1 / \nu_2 = 0.8$150

Table 4.13: The normalized load for homogenous coating indented by a moving triangular punch $b/h_1 = 0.4, \eta = 0.3, \rho_1 / \rho_2 = 1/8, \nu_1 / \nu_2 = 0.8$150

Table 4.14: The normalized load for homogenous coating indented by a moving triangular punch $b/h_1 = 0.4, \mu_1 / \mu_2 = 1/5, \rho_1 / \rho_2 = 1/8, \nu_1 / \nu_2 = 0.8$151

Table 4.15: The normalized load for homogenous coating indented by a moving triangular punch $b/h_1 = 0.4, \mu_1 / \mu_2 = 5, \rho_1 / \rho_2 = 1/8, \nu_1 / \nu_2 = 0.8$151

Table 4.16: Normalized stress intensity factors for a moving triangular punch $c_1 = 0, \eta = 0.0, \nu_1 / \nu_2 = 0.8$151

Table 4.17: Normalized stress intensity factors for a moving triangular punch $b/h_1 = 0.2, \eta = 0.3, \rho_1 / \rho_2 = 1/8, \nu_1 / \nu_2 = 0.8$152

Table 4.18: Normalized stress intensity factors for a moving triangular punch $b/h_1 = 0.4, \eta = 0.3, \rho_1 / \rho_2 = 1/8, \nu_1 / \nu_2 = 0.8$152

Table 4.19: Normalized stress intensity factors for a moving triangular punch $b/h_1 = 0.4, \mu_1 / \mu_2 = 1/5, \rho_1 / \rho_2 = 1/8, \nu_1 / \nu_2 = 0.8$152

Table 4.20: Normalized stress intensity factors for a moving triangular punch $b/h_1 = 0.4$, $\mu_1/\mu_2 = 5$, $\rho_1/\rho_2 = 1/8$, $\nu_1/\nu_2 = 0.8$153

Table 4.21: Percent difference between elastostatic and elastodynamic normal contact stresses $\mu_1/\mu_2 = 1/10$, $b/h_1 = 0.2$, $\eta = 0.3$, $\rho_1/\rho_2 = 1/8$, $\nu_1/\nu_2 = 0.8$153

Table 4.22: Percent difference between elastostatic and elastodynamic lateral contact stresses $\mu_1/\mu_2 = 1/10$, $b/h_1 = 0.2$, $\eta = 0.3$, $\rho_1/\rho_2 = 1/8$, $\nu_1/\nu_2 = 0.8$154

Table 4.23: Percent difference between elastostatic and elastodynamic normal contact stresses $\mu_1/\mu_2 = 10$, $b/h_1 = 0.2$, $\eta = 0.3$, $\rho_1/\rho_2 = 1/8$, $\nu_1/\nu_2 = 0.8$. 154

Table 4.24: Percent difference between elastostatic and elastodynamic lateral contact stresses $\mu_1/\mu_2 = 10$, $b/h_1 = 0.2$, $\eta = 0.3$, $\rho_1/\rho_2 = 1/8$, $\nu_1/\nu_2 = 0.8$. 155

Table 4.25: The normalized load for homogenous coating indented by a moving semi-circular punch $c_1 = 0$, $R_1/h_1 = 20$, $\eta = 0.0$, $\nu_1/\nu_2 = 0.8$167

Table 4.26: The normalized load for homogenous coating indented by a moving semi-circular punch $b/R_1 = 0.01$, $R_1/h_1 = 20$, $\eta = 0.3$, $\rho_1/\rho_2 = 1/8$, $\nu_1/\nu_2 = 0.8$167

Table 4.27: The normalized load for homogenous coating indented by a moving semi-circular punch $b/R_1 = 0.04$, $R_1/h_1 = 20$, $\eta = 0.3$, $\rho_1/\rho_2 = 1/8$, $\nu_1/\nu_2 = 0.8$167

Table 4.28: The normalized load for homogenous coating indented by a moving semi-circular punch $b/R_1 = 0.01$, $R_1/h_1 = 20$, $\mu_1/\mu_2 = 1/5$, $\rho_1/\rho_2 = 1/8$, $\nu_1/\nu_2 = 0.8$168

Table 4.29: The normalized load for homogenous coating indented by a moving semi-circular punch $b/R_1 = 0.01$, $R_1/h_1 = 20$, $\mu_1/\mu_2 = 5$, $\rho_1/\rho_2 = 1/8$, $\nu_1/\nu_2 = 0.8$	168
Table 4.30: Normalized stress intensity factors for a moving semi-circular punch $c_1 = 0$, $R_1/h_1 = 20$, $\eta = 0.0$, $\nu_1/\nu_2 = 0.8$	168
Table 4.31: Normalized stress intensity factors for a moving semi-circular punch $b/R_1 = 0.01$, $R_1/h_1 = 20$, $\eta = 0.3$, $\rho_1/\rho_2 = 1/8$, $\nu_1/\nu_2 = 0.8$	169
Table 4.32: Normalized stress intensity factors for a moving semi-circular punch $b/R_1 = 0.04$, $R_1/h_1 = 20$, $\eta = 0.3$, $\rho_1/\rho_2 = 1/8$, $\nu_1/\nu_2 = 0.8$	169
Table 4.33: Normalized stress intensity factors for a moving semi-circular punch $b/R_1 = 0.01$, $R_1/h_1 = 20$, $\mu_1/\mu_2 = 1/5$, $\rho_1/\rho_2 = 1/8$, $\nu_1/\nu_2 = 0.8$	169
Table 4.34: Normalized stress intensity factors for a moving semi-circular punch $b/R_1 = 0.01$, $R_1/h_1 = 20$, $\mu_1/\mu_2 = 5$, $\rho_1/\rho_2 = 1/8$, $\nu_1/\nu_2 = 0.8$	170
Table 4.35: Percent difference between elastostatic and elastodynamic normal contact stresses $\mu_1/\mu_2 = 1/10$, $b/R_1 = 0.01$, $R_1/h_1 = 20$, $\eta = 0.3$, $\rho_1/\rho_2 = 1/8$, $\nu_1/\nu_2 = 0.8$	170
Table 4.36: Percent difference between elastostatic and elastodynamic lateral contact stresses $\mu_1/\mu_2 = 1/10$, $b/R_1 = 0.01$, $R_1/h_1 = 20$, $\eta = 0.3$, $\rho_1/\rho_2 = 1/8$, $\nu_1/\nu_2 = 0.8$	171
Table 4.37: Percent difference between elastostatic and elastodynamic normal contact stresses $\mu_1/\mu_2 = 10$, $b/R_1 = 0.01$, $R_1/h_1 = 20$, $\eta = 0.3$, $\rho_1/\rho_2 = 1/8$, $\nu_1/\nu_2 = 0.8$	171
Table 4.38: Percent difference between elastostatic and elastodynamic lateral contact stresses $\mu_1/\mu_2 = 10$, $b/R_1 = 0.01$, $R_1/h_1 = 20$, $\eta = 0.3$, $\rho_1/\rho_2 = 1/8$, $\nu_1/\nu_2 = 0.8$	172

Table 4.39: The normalized load for homogenous coating indented by a moving cylindrical punch $c_1 = 0$, $R_1 / h_1 = 100$, $\eta = 0.0$, $\nu_1 / \nu_2 = 1.0$185

Table 4.40: The normalized load for homogenous coating indented by a moving cylindrical punch $(b + a) / R_1 = 0.01$, $R_1 / h_1 = 100$, $\eta = 0.3$, $\rho_1 / \rho_2 = 1/8$, $\nu_1 / \nu_2 = 0.8$185

Table 4.41: The normalized load for homogenous coating indented by a moving cylindrical punch $(b + a) / R_1 = 0.05$, $R_1 / h_1 = 100$, $\eta = 0.3$, $\rho_1 / \rho_2 = 1/8$, $\nu_1 / \nu_2 = 0.8$185

Table 4.42: The normalized load for homogenous coating indented by a moving cylindrical punch $(b + a) / R_1 = 0.01$, $R_1 / h_1 = 100$, $\mu_1 / \mu_2 = 1/5$, $\rho_1 / \rho_2 = 1/8$, $\nu_1 / \nu_2 = 0.8$186

Table 4.43: The normalized load for homogenous coating indented by a moving cylindrical punch $(b + a) / R_1 = 0.01$, $R_1 / h_1 = 100$, $\mu_1 / \mu_2 = 5$, $\rho_1 / \rho_2 = 1/8$, $\nu_1 / \nu_2 = 0.8$186

Table 4.44: Percent difference between elastostatic and elastodynamic normal contact stresses $\mu_1 / \mu_2 = 1/10$, $(b + a) / R_1 = 0.01$, $R_1 / h_1 = 100$, $\eta = 0.3$, $\rho_1 / \rho_2 = 1/8$, $\nu_1 / \nu_2 = 0.8$187

Table 4.45: Percent difference between elastostatic and elastodynamic lateral contact stresses $\mu_1 / \mu_2 = 1/10$, $(b + a) / R_1 = 0.01$, $R_1 / h_1 = 100$, $\eta = 0.3$, $\rho_1 / \rho_2 = 1/8$, $\nu_1 / \nu_2 = 0.8$187

Table 4.46: Percent difference between elastostatic and elastodynamic normal contact stresses $\mu_1 / \mu_2 = 10$, $(b + a) / R_1 = 0.01$, $R_1 / h_1 = 100$, $\eta = 0.3$, $\rho_1 / \rho_2 = 1/8$, $\nu_1 / \nu_2 = 0.8$188

Table 4.47: Percent difference between elastostatic and elastodynamic lateral contact stresses $\mu_1 / \mu_2 = 10, (b + a) / R_1 = 0.01, R_1 / h_1 = 100, \eta = 0.3, \rho_1 / \rho_2 = 1/8, \nu_1 / \nu_2 = 0.8.$	188
Table 5.1: Normalized stress intensity factors for the contact between a rigid flat punch and an FGM coating $a / h_1 = 0.1, c_1 = 0.0.$	206
Table 5.2: Normalized stress intensity factors for the moving rigid flat punch $c_1 = 0.0, \eta = 0.0, \nu_1 / \nu_2 = 1.$	206
Table 5.3: Normalized stress intensity factors for the moving rigid flat punch $a / h_1 = 0.1, \eta = 0.3, \nu_1 / \nu_2 = 1.$	206
Table 5.4: Normalized stress intensity factors for the moving rigid flat punch $a / h_1 = 0.25, \eta = 0.3, \nu_1 / \nu_2 = 1.$	207
Table 5.5: Normalized stress intensity factors for the moving rigid flat punch $a / h_1 = 0.4, \eta = 0.3, \nu_1 / \nu_2 = 1.$	207
Table 5.6: Normalized stress intensity factors for the rigid flat punch $a / h_1 = 0.1, \Gamma_1 = 1/6, \nu_1 / \nu_2 = 1.$	207
Table 5.7: Normalized stress intensity factors for the moving rigid flat punch $a / h_1 = 0.1, \Gamma_1 = 6, \nu_1 / \nu_2 = 1.$	208
Table 5.8: Percent difference between elastostatic and elastodynamic normal contact stresses $\Gamma_1 = 1/6, a / h_1 = 0.1, \eta = 0.3, \nu_1 / \nu_2 = 1.$	208
Table 5.9: Percent difference between elastostatic and elastodynamic lateral contact stresses $\Gamma_1 = 1/6, a / h_1 = 0.1, \eta = 0.3, \nu_1 / \nu_2 = 1.$	209
Table 5.10: Percent difference between elastostatic and elastodynamic normal contact stresses $\Gamma_1 = 6, a / h_1 = 0.1, \eta = 0.3, \nu_1 / \nu_2 = 1.$	209
Table 5.11: Percent difference between elastostatic and elastodynamic lateral contact stresses $\Gamma_1 = 6, a / h_1 = 0.1, \eta = 0.3, \nu_1 / \nu_2 = 1.$	210

Table 5.12: The normalized load for FGM coating indented by a moving triangular punch $c_1 = 0, \eta = 0.0, \nu_1 / \nu_2 = 1.0$	225
Table 5.13: The normalized load for FGM coating indented by a moving triangular punch $b / h_1 = 0.2, \eta = 0.3, \nu_1 / \nu_2 = 1$	225
Table 5.14: The normalized load for FGM coating indented by a moving triangular punch $b / h_1 = 0.4, \eta = 0.3, \nu_1 / \nu_2 = 1$	225
Table 5.15: The normalized load for FGM coating indented by a moving triangular punch $b / h_1 = 0.4, \eta = 0.3, \nu_1 / \nu_2 = 1.0$	226
Table 5.16: The normalized load for FGM coating indented by a moving triangular punch $b / h_1 = 0.2, \Gamma_1 = 1/6, \nu_1 / \nu_2 = 1.0$	226
Table 5.17: The normalized load for FGM coating indented by a moving triangular punch $b / h_1 = 0.2, \Gamma_1 = 6, \nu_1 / \nu_2 = 1.0$	226
Table 5.18: Normalized stress intensity factors for the moving rigid triangular punch $b / h_1 = 0.2, c_1 = 0.0$	227
Table 5.19: Normalized stress intensity factors for the moving triangular punch $c_1 = 0, \eta = 0.0, \nu_1 / \nu_2 = 1.0$	227
Table 5.20: Normalized stress intensity factors for the moving triangular punch $b / h_1 = 0.2, \eta = 0.3, \nu_1 / \nu_2 = 1.0$	227
Table 5.21: Normalized stress intensity factors for the moving triangular punch $b / h_1 = 0.4, \eta = 0.3, \nu_1 / \nu_2 = 1.0$	228
Table 5.22: Normalized stress intensity factors for the moving triangular punch $b / h_1 = 0.2, \Gamma_1 = 1/6, \nu_1 / \nu_2 = 1.0$	228
Table 5.23: Normalized stress intensity factors for the moving triangular punch $b / h_1 = 0.2, \Gamma_1 = 6, \nu_1 / \nu_2 = 1.0$	228

Table 5.24: Percent difference between elastostatic and elastodynamic normal contact stresses $\Gamma_1 = 1/6$, $b/h_1 = 0.2$, $\eta = 0.3$, $\nu_1/\nu_2 = 1.0$	229
Table 5.25: Percent difference between elastostatic and elastodynamic lateral contact stresses $\Gamma_1 = 1/6$, $b/h_1 = 0.2$, $\eta = 0.3$, $\nu_1/\nu_2 = 1.0$	229
Table 5.26: Percent difference between elastostatic and elastodynamic normal contact stresses $\Gamma_1 = 6$, $b/h_1 = 0.2$, $\eta = 0.3$, $\nu_1/\nu_2 = 1.0$	230
Table 5.27: Percent difference between elastostatic and elastodynamic lateral contact stresses $\Gamma_1 = 6$, $b/h_1 = 0.2$, $\eta = 0.3$, $\nu_1/\nu_2 = 1.0$	230
Table 5.28: The normalized load for FGM coating indented by a moving semi-circular punch $c_1 = 0$, $\eta = 0.0$, $R_1/h_1 = 20$, $\nu_1/\nu_2 = 1.0$	245
Table 5.29: The normalized load for FGM coating indented by a moving semi-circular punch $b/R_1 = 0.01$, $R_1/h_1 = 20$, $\eta = 0.3$, $\nu_1/\nu_2 = 1.0$	245
Table 5.30: The normalized load for FGM coating indented by a moving semi-circular punch $b/R_1 = 0.02$, $R_1/h_1 = 20$, $\eta = 0.3$, $\nu_1/\nu_2 = 1.0$	245
Table 5.31: The normalized load for FGM coating indented by a moving semi-circular punch $b/R_1 = 0.04$, $R_1/h_1 = 20$, $\eta = 0.3$, $\nu_1/\nu_2 = 1.0$	246
Table 5.32: The normalized load for FGM coating indented by a moving semi-circular punch $b/R_1 = 0.02$, $R_1/h_1 = 20$, $\Gamma_1 = 1/6$, $\nu_1/\nu_2 = 1.0$	246
Table 5.33: The normalized load for FGM coating indented by a moving semi-circular punch $b/R_1 = 0.02$, $R_1/h_1 = 20$, $\Gamma_1 = 6$, $\nu_1/\nu_2 = 1.0$	246
Table 5.34: Normalized stress intensity factors for the moving rigid semi-circular punch $b/R_1 = 0.025$, $R_1/h_1 = 20$, $c_1 = 0.0$	247
Table 5.35: Normalized stress intensity factor for the moving semi-circular punch $c_1 = 0.0$, $\eta = 0.0$, $R_1/h_1 = 20$, $\nu_1/\nu_2 = 1.0$	247

Table 5.36: Normalized stress intensity factor for the moving semi-circular punch $b/R_1 = 0.01$, $R_1/h_1 = 20$, $\eta = 0.3$, $\nu_1/\nu_2 = 1.0$	247
Table 5.37: Normalized stress intensity factor for the moving semi-circular punch $b/R_1 = 0.02$, $R_1/h_1 = 20$, $\eta = 0.3$, $\nu_1/\nu_2 = 1.0$	248
Table 5.38: Normalized stress intensity factor for the moving semi-circular punch $b/R_1 = 0.04$, $R_1/h_1 = 20$, $\eta = 0.3$, $\nu_1/\nu_2 = 1.0$	248
Table 5.39: Normalized stress intensity factor for the moving semi-circular punch $b/R_1 = 0.02$, $R_1/h_1 = 20$, $\Gamma_1 = 1/6$, $\nu_1/\nu_2 = 1.0$	248
Table 5.40: Normalized stress intensity factor for the moving semi-circular punch $b/R_1 = 0.02$, $R_1/h_1 = 20$, $\Gamma_1 = 6$, $\nu_1/\nu_2 = 1.0$	249
Table 5.41: Percent difference between elastostatic and elastodynamic normal contact stresses $\Gamma_1 = 1/6$, $b/R_1 = 0.01$, $R_1/h_1 = 20$, $\eta = 0.3$, $\nu_1/\nu_2 = 1.0$	249
Table 5.42: Percent difference between elastostatic and elastodynamic lateral contact stresses $\Gamma_1 = 1/6$, $b/R_1 = 0.01$, $R_1/h_1 = 20$, $\eta = 0.3$, $\nu_1/\nu_2 = 1.0$	250
Table 5.43: Percent difference between elastostatic and elastodynamic normal contact stresses $\Gamma_1 = 6$, $b/R_1 = 0.01$, $R_1/h_1 = 20$, $\eta = 0.3$, $\nu_1/\nu_2 = 1.0$	250
Table 5.44: Percent difference between elastostatic and elastodynamic lateral contact stresses $\Gamma_1 = 6$, $b/R_1 = 0.01$, $R_1/h_1 = 20$, $\eta = 0.3$, $\nu_1/\nu_2 = 1.0$	251
Table 5.45: The normalized load for FGM coating indented by a moving cylindrical punch $c_1 = 0$, $\eta = 0.0$, $R_1/h_1 = 100$, $\nu_1/\nu_2 = 1.0$	267
Table 5.46: The normalized load for FGM coating indented by a moving cylindrical punch $(b+a)/R_1 = 0.01$, $R_1/h_1 = 100$, $\eta = 0.3$, $\nu_1/\nu_2 = 1.0$	267
Table 5.47: The normalized load for FGM coating indented by a moving cylindrical punch $(b+a)/R_1 = 0.02$, $R_1/h_1 = 100$, $\eta = 0.3$, $\nu_1/\nu_2 = 1.0$	267

Table 5.48: The normalized load for FGM coating indented by a moving cylindrical punch $(b+a)/R_1 = 0.04$, $R_1/h_1 = 100$, $\eta = 0.3$, $\nu_1/\nu_2 = 1.0$268

Table 5.49: The normalized load for FGM coating indented by a moving cylindrical punch $(b+a)/R_1 = 0.04$, $R_1/h_1 = 100$, $\Gamma_1 = 1/6$, $\nu_1/\nu_2 = 1.0$268

Table 5.50: The normalized load for FGM coating indented by a moving cylindrical punch $(b+a)/R_1 = 0.04$, $R_1/h_1 = 100$, $\Gamma_1 = 6$, $\nu_1/\nu_2 = 1.0$268

Table 5.51: Percent difference between elastostatic and elastodynamic normal contact stresses $\Gamma_1 = 1/6$, $(b+a)/R_1 = 0.01$, $R_1/h_1 = 100$, $\eta = 0.3$, $\nu_1/\nu_2 = 1.0$.
.....269

Table 5.52: Percent difference between elastostatic and elastodynamic lateral contact stresses $\Gamma_1 = 1/6$, $(b+a)/R_1 = 0.01$, $R_1/h_1 = 100$, $\eta = 0.3$, $\nu_1/\nu_2 = 1.0$.
.....269

Table 5.53: Percent difference between elastostatic and elastodynamic normal contact stresses $\Gamma_1 = 6$, $(b+a)/R_1 = 0.01$, $R_1/h_1 = 100$, $\eta = 0.3$, $\nu_1/\nu_2 = 1.0$. 270

Table 5.54: Percent difference between elastostatic and elastodynamic lateral contact stresses $\Gamma_1 = 6$, $(b+a)/R_1 = 0.01$, $R_1/h_1 = 100$, $\eta = 0.3$, $\nu_1/\nu_2 = 1.0$. 270

LIST OF FIGURES

FIGURES

Figure 1.1: A particulate FGM with the volume fractions of constituent phases	4
Figure 2.1: A dynamic contact problem between a coating and a rigid punch of an arbitrary profile (a) homogenous coating (b) FGM coating	19
Figure 2.2: Rigid punch in stationary and moving coordinates	21
Figure 3.1: The moving rigid flat punch on (a) homogenous elastic coating (b) functionally graded coating	74
Figure 3.2: The moving rigid triangular punch on (a) homogenous elastic coating (b) functionally graded coating	83
Figure 3.3: The moving rigid semi-circular punch on (a) homogenous elastic coating (b) functionally graded coating	92
Figure 3.4: The moving rigid cylindrical punch on (a) homogenous elastic coating (b) functionally graded coating	103
Figure 4.1: Constructed finite element model: (a) Quadrilateral finite element and its 8-noded triangular option; (b) Dimensions in the finite element mesh; (c) close-up view of the contact zone	119
Figure 4.2: General schematic for the contact between a homogenous elastic coating and a rigid flat punch	120
Figure 4.3: Normal and lateral contact stress distribution on the homogenous coating indented by a flat punch for different stiffness ratio of the coating and the substrate (a) Normal contact stress distribution; (b) Lateral contact stress distribution, $a/h_1 = 0.1$, $\eta = 0.3$, $c_1 = 0.0$	127

Figure 4.4: Normal and lateral contact stress distribution on the homogenous coating indented by a flat punch for different stiffness ratio of the coating and the substrate (a) Normal contact stress distribution; (b) Lateral contact stress distribution, $a/h_1 = 0.25$, $\eta = 0.3$, $c_1 = 0.0$127

Figure 4.5: Normal and lateral contact stress distribution on the homogenous coating indented by a flat punch for different stiffness ratio of the coating and the substrate (a) Normal contact stress distribution; (b) Lateral contact stress distribution, $a/h_1 = 0.5$, $\eta = 0.3$, $c_1 = 0.0$128

Figure 4.6: Normal and lateral contact stress distribution on the half-plane indented by frictionless moving punch for various punch speed $\eta = 0.0$. (a) Normal contact stress distribution; (b) Lateral contact stress distribution.128

Figure 4.7: Normal and lateral elastodynamic contact stresses on homogenous coating indented by a moving flat punch for various mass density ratio (a) Normal contact stress distribution; (b) Lateral contact stress distribution, $\mu_1/\mu_2 = 1/10$, $a/h_1 = 0.2$, $c_1 = 0.6$, $\eta = 0.3$, $\nu_1/\nu_2 = 0.8$129

Figure 4.8: Normal and lateral elastodynamic contact stresses on homogenous coating indented by a moving flat punch for various mass density ratio (a) Normal contact stress distribution; (b) Lateral contact stress distribution, $\mu_1/\mu_2 = 10$, $a/h_1 = 0.2$, $c_1 = 0.6$, $\eta = 0.3$, $\nu_1/\nu_2 = 0.8$129

Figure 4.9: Normal and lateral elastodynamic contact stresses on homogenous coating indented by a moving flat punch for various values of punch speed (a) Normal contact stress distribution; (b) Lateral contact stress distribution, $\mu_1/\mu_2 = 1/10$, $a/h_1 = 0.1$, $\eta = 0.3$, $\rho_1/\rho_2 = 1/8$, $\nu_1/\nu_2 = 0.8$130

Figure 4.10: Normal and lateral elastodynamic contact stresses on homogenous coating indented by a moving flat punch for various values of punch speed (a)

Normal contact stress distribution; (b) Lateral contact stress distribution,
 $\mu_1 / \mu_2 = 10, a / h_1 = 0.1, \eta = 0.3, \rho_1 / \rho_2 = 1/8, \nu_1 / \nu_2 = 0.8$130

Figure 4.11: Normal and lateral elastodynamic contact stresses on homogenous coating indented by a moving flat punch for various values of punch speed (a) Normal contact stress distribution; (b) Lateral contact stress distribution,
 $\mu_1 / \mu_2 = 1/10, a / h_1 = 0.4, \eta = 0.3, \rho_1 / \rho_2 = 1/8, \nu_1 / \nu_2 = 0.8$131

Figure 4.12: Normal and lateral elastodynamic contact stresses on homogenous coating indented by a moving flat punch for various values of punch speed (a) Normal contact stress distribution; (b) Lateral contact stress distribution,
 $\mu_1 / \mu_2 = 10, a / h_1 = 0.4, \eta = 0.3, \rho_1 / \rho_2 = 1/8, \nu_1 / \nu_2 = 0.8$131

Figure 4.13: Normal and lateral elastodynamic contact stresses on homogenous coating indented by a moving flat punch for various values of coefficient of friction (a) Normal contact stress distribution; (b) Lateral contact stress distribution,
 $\mu_1 / \mu_2 = 1/10, a / h_1 = 0.4, c_1 = 0.4, \rho_1 / \rho_2 = 1/8, \nu_1 / \nu_2 = 0.8$. ..132

Figure 4.14: Normal and lateral elastodynamic contact stresses on homogenous coating indented by a moving flat punch for various values of coefficient of friction (a) Normal contact stress distribution; (b) Lateral contact stress distribution,
 $\mu_1 / \mu_2 = 10, a / h_1 = 0.4, c_1 = 0.4, \rho_1 / \rho_2 = 1/8, \nu_1 / \nu_2 = 0.8$132

Figure 4.15: Normal and lateral elastodynamic contact stresses on homogenous coating indented by a moving flat punch for various values of relative coating thickness (a) Normal contact stress distribution; (b) Lateral contact stress distribution,
 $\mu_1 / \mu_2 = 1/10, c_1 = 0.4, \eta = 0.3, \rho_1 / \rho_2 = 1/8, \nu_1 / \nu_2 = 0.8$133

Figure 4.16: Normal and lateral elastodynamic contact stresses on homogenous coating indented by a moving flat punch for various values of relative coating thickness (a) Normal contact stress distribution; (b) Lateral contact stress distribution,
 $\mu_1 / \mu_2 = 10, c_1 = 0.4, \eta = 0.3, \rho_1 / \rho_2 = 1/8, \nu_1 / \nu_2 = 0.8$133

Figure 4.17: Normal and lateral elastodynamic contact stresses on homogenous coating indented by a moving flat punch for various values of Poisson's ratio (a) Normal contact stress distribution; (b) Lateral contact stress distribution, $\mu_1 / \mu_2 = 1/10, a/h_1 = 0.5, c_1 = 0.6, \eta = 0.3, \rho_1 / \rho_2 = 1/8, \nu_1 / \nu_2 = 0.8$134

Figure 4.18: Normal and lateral elastodynamic contact stresses on homogenous coating indented by a moving flat punch for various values of Poisson's ratio (a) Normal contact stress distribution; (b) Lateral contact stress distribution, $\mu_1 / \mu_2 = 10, a/h_1 = 0.5, c_1 = 0.6, \eta = 0.3, \rho_1 / \rho_2 = 1/8, \nu_1 / \nu_2 = 0.8$134

Figure 4.19: General schematic for the contact between a homogenous elastic coating and a rigid triangular punch139

Figure 4.20: Normal and lateral elastodynamic contact stresses on homogenous coating indented by a moving triangular punch for various mass density ratios (a) Normal contact stress distribution; (b) Lateral contact stress distribution, $\mu_1 / \mu_2 = 1/10, b/h_1 = 0.4, c_1 = 0.6, \eta = 0.3, \nu_1 / \nu_2 = 0.8$144

Figure 4.21: Normal and lateral elastodynamic contact stresses on homogenous coating indented by a moving triangular punch for various mass density ratios (a) Normal contact stress distribution; (b) Lateral contact stress distribution, $\mu_1 / \mu_2 = 10, b/h_1 = 0.4, c_1 = 0.6, \eta = 0.3, \nu_1 / \nu_2 = 0.8$144

Figure 4.22: Normal and lateral elastodynamic contact stresses on homogenous coating indented by a moving triangular punch for various values of punch speed (a) Normal contact stress distribution; (b) Lateral contact stress distribution, $\mu_1 / \mu_2 = 1/10, b/h_1 = 0.2, \eta = 0.3, \rho_1 / \rho_2 = 1/8, \nu_1 / \nu_2 = 0.8$145

Figure 4.23: Normal and lateral elastodynamic contact stresses on homogenous coating indented by a moving triangular punch for various values of punch speed (a) Normal contact stress distribution; (b) Lateral contact stress distribution, $\mu_1 / \mu_2 = 10, b/h_1 = 0.2, \eta = 0.3, \rho_1 / \rho_2 = 1/8, \nu_1 / \nu_2 = 0.8$145

Figure 4.24: Normal and lateral elastodynamic contact stresses on homogenous coating indented by a moving triangular punch for various values of punch speed (a) Normal contact stress distribution; (b) Lateral contact stress distribution, $\mu_1 / \mu_2 = 1/10, b/h_1 = 0.5, \eta = 0.3, \rho_1 / \rho_2 = 1/8, v_1 / v_2 = 0.8$146

Figure 4.25: Normal and lateral elastodynamic contact stresses on homogenous coating indented by a moving triangular punch for various values of punch speed (a) Normal contact stress distribution; (b) Lateral contact stress distribution, $\mu_1 / \mu_2 = 10, b/h_1 = 0.5, \eta = 0.3, \rho_1 / \rho_2 = 1/8, v_1 / v_2 = 0.8$146

Figure 4.26: Normal and lateral elastodynamic contact stresses on homogenous coating indented by a moving triangular punch for various values of coefficient of friction (a) Normal contact stress distribution; (b) Lateral contact stress distribution, $\mu_1 / \mu_2 = 1/10, b/h_1 = 0.2, c_1 = 0.4, \rho_1 / \rho_2 = 1/8, v_1 / v_2 = 0.8$. .147

Figure 4.27: Normal and lateral elastodynamic contact stresses on homogenous coating indented by a moving triangular punch for various values of coefficient of friction (a) Normal contact stress distribution; (b) Lateral contact stress distribution, $\mu_1 / \mu_2 = 10, b/h_1 = 0.2, c_1 = 0.4, \rho_1 / \rho_2 = 1/8, v_1 / v_2 = 0.8$147

Figure 4.28: Normal and lateral elastodynamic contact stresses on homogenous coating indented by a moving triangular punch for various values of relative coating thickness (a) Normal contact stress distribution; (b) Lateral contact stress distribution, $\mu_1 / \mu_2 = 1/10, c_1 = 0.4, \eta = 0.3, \rho_1 / \rho_2 = 1/8, v_1 / v_2 = 0.8$148

Figure 4.29: Normal and lateral elastodynamic contact stresses on homogenous coating indented by a moving triangular punch for various values of relative coating thickness (a) Normal contact stress distribution; (b) Lateral contact stress distribution, $\mu_1 / \mu_2 = 10, c_1 = 0.4, \eta = 0.3, \rho_1 / \rho_2 = 1/8, v_1 / v_2 = 0.8$. 148

Figure 4.30: Normal and lateral elastodynamic contact stresses on homogenous coating indented by a moving triangular punch for various values of Poisson's

ratio (a) Normal contact stress distribution; (b) Lateral contact stress distribution, $\mu_1 / \mu_2 = 1/10, b/h_1 = 0.2, c_1 = 0.6, \eta = 0.3, \rho_1 / \rho_2 = 1/8$	149
Figure 4.31: Normal and lateral elastodynamic contact stresses on homogenous coating indented by a moving triangular punch for various values of Poisson's ratio (a) Normal contact stress distribution; (b) Lateral contact stress distribution, $\mu_1 / \mu_2 = 10, b/h_1 = 0.2, c_1 = 0.6, \eta = 0.3, \rho_1 / \rho_2 = 1/8$	149
Figure 4.32: General schematic for the contact between a homogenous elastic coating and a rigid triangular punch	156
Figure 4.33: Normal and lateral elastodynamic contact stresses on homogenous coating indented by a moving semi-circular punch for various mass density ratios (a) Normal contact stress distribution; (b) Lateral contact stress distribution, $\mu_1 / \mu_2 = 1/10, b/R_1 = 0.025, R_1/h_1 = 20, c_1 = 0.6, \eta = 0.3, \nu_1 / \nu_2 = 0.8$	161
Figure 4.34: Normal and lateral elastodynamic contact stresses on homogenous coating indented by a moving semi-circular punch for various mass density ratios (a) Normal contact stress distribution; (b) Lateral contact stress distribution, $\mu_1 / \mu_2 = 10, b/R_1 = 0.025, R_1/h_1 = 20, c_1 = 0.6, \eta = 0.3, \nu_1 / \nu_2 = 0.8$	161
Figure 4.35: Normal and lateral elastodynamic contact stresses on homogenous coating indented by a moving semi-circular punch for various values of punch speed (a) Normal contact stress distribution; (b) Lateral contact stress distribution, $\mu_1 / \mu_2 = 1/10, b/R_1 = 0.01, R_1/h_1 = 20, \eta = 0.3, \rho_1 / \rho_2 = 1/8, \nu_1 / \nu_2 = 0.8$	162
Figure 4.36: Normal and lateral elastodynamic contact stresses on homogenous coating indented by a moving semi-circular punch for various values of punch speed (a) Normal contact stress distribution; (b) Lateral contact stress	

distribution, $\mu_1 / \mu_2 = 10, b / R_1 = 0.01, R_1 / h_1 = 20, \eta = 0.3, \rho_1 / \rho_2 = 1/8,$
 $\nu_1 / \nu_2 = 0.8.$ 162

Figure 4.37: Normal and lateral elastodynamic contact stresses on homogenous coating indented by a moving semi-circular punch for various values of punch speed (a) Normal contact stress distribution; (b) Lateral contact stress

distribution, $\mu_1 / \mu_2 = 1/10, b / R_1 = 0.05, R_1 / h_1 = 20, \eta = 0.3, \rho_1 / \rho_2 = 1/8,$
 $\nu_1 / \nu_2 = 0.8.$ 163

Figure 4.38: Normal and lateral elastodynamic contact stresses on homogenous coating indented by a moving semi-circular punch for various values of punch speed (a) Normal contact stress distribution; (b) Lateral contact stress

distribution, $\mu_1 / \mu_2 = 10, b / R_1 = 0.05, R_1 / h_1 = 20, \eta = 0.3, \rho_1 / \rho_2 = 1/8,$
 $\nu_1 / \nu_2 = 0.8.$ 163

Figure 4.39: Normal and lateral elastodynamic contact stresses on homogenous coating indented by a moving semi-circular punch for various values of coefficient of friction (a) Normal contact stress distribution; (b) Lateral contact stress

distribution, $\mu_1 / \mu_2 = 1/10, b / R_1 = 0.01, R_1 / h_1 = 20, c_1 = 0.4,$
 $\rho_1 / \rho_2 = 1/8, \nu_1 / \nu_2 = 0.8.$ 164

Figure 4.40: Normal and lateral elastodynamic contact stresses on homogenous coating indented by a moving semi-circular punch for various values of coefficient of friction (a) Normal contact stress distribution; (b) Lateral contact

stress distribution, $\mu_1 / \mu_2 = 10, b / R_1 = 0.01, R_1 / h_1 = 20, c_1 = 0.4, \rho_1 / \rho_2 = 1/8,$
 $\nu_1 / \nu_2 = 0.8.$ 164

Figure 4.41: Normal and lateral elastodynamic contact stresses on homogenous coating indented by a moving semi-circular punch for various values of relative coating thickness (a) Normal contact stress distribution; (b) Lateral contact

stress distribution, $\mu_1 / \mu_2 = 1/10$, $b / R_1 = 0.025$, $c_1 = 0.4$, $\eta = 0.3$, $\rho_1 / \rho_2 = 1/8$, $\nu_1 / \nu_2 = 0.8$165

Figure 4.42: Normal and lateral elastodynamic contact stresses on homogenous coating indented by a moving semi-circular punch for various values of relative coating thickness (a) Normal contact stress distribution; (b) Lateral contact stress distribution, $\mu_1 / \mu_2 = 10$, $b / R_1 = 0.025$, $c_1 = 0.4$, $\eta = 0.3$, $\rho_1 / \rho_2 = 1/8$, $\nu_1 / \nu_2 = 0.8$165

Figure 4.43: Normal and lateral elastodynamic contact stresses on homogenous coating indented by a moving semi-circular punch for various values of Poisson's ratio (a) Normal contact stress distribution; (b) Lateral contact stress distribution, $\mu_1 / \mu_2 = 1/10$, $b / R_1 = 0.05$, $c_1 = 0.6$, $\eta = 0.3$, $\rho_1 / \rho_2 = 1/8$166

Figure 4.44: Normal and lateral elastodynamic contact stresses on homogenous coating indented by a moving semi-circular punch for various values of Poisson's ratio (a) Normal contact stress distribution; (b) Lateral contact stress distribution, $\mu_1 / \mu_2 = 10$, $b / R_1 = 0.05$, $c_1 = 0.6$, $\eta = 0.3$, $\rho_1 / \rho_2 = 1/8$166

Figure 4.45: General schematic for the contact between a homogenous elastic coating and a rigid cylindrical punch.....173

Figure 4.46: Normal and lateral elastodynamic contact stresses on homogenous coating indented by a moving cylindrical punch for various mass density ratios (a) Normal contact stress distribution; (b) Lateral contact stress distribution, $\mu_1 / \mu_2 = 1/10$, $(b + a) / R_1 = 0.02$, $R_1 / h_1 = 100$, $c_1 = 0.6$, $\eta = 0.3$, $\nu_1 / \nu_2 = 0.8$178

Figure 4.47: Normal and lateral elastodynamic contact stresses on homogenous coating indented by a moving cylindrical punch for various mass density ratios (a) Normal contact stress distribution; (b) Lateral contact stress distribution,

$\mu_1 / \mu_2 = 1/10$, $(b + a) / R_1 = 0.02$, $R_1 / h_1 = 100$, $c_1 = 0.6$, $\eta = 0.3$, $v_1 / v_2 = 0.8$.
178

Figure 4.48: Normal and lateral elastodynamic contact stresses on homogenous coating indented by a moving cylindrical punch for various values of punch speed (a) Normal contact stress distribution; (b) Lateral contact stress distribution, $\mu_1 / \mu_2 = 1/10$, $(b + a) / R_1 = 0.01$, $R_1 / h_1 = 100$, $\eta = 0.0$,

$\rho_1 / \rho_2 = 1/8$, $v_1 / v_2 = 0.8$179

Figure 4.49: Normal and lateral elastodynamic contact stresses on homogenous coating indented by a moving cylindrical punch for various values of punch speed (a) Normal contact stress distribution; (b) Lateral contact stress distribution, $\mu_1 / \mu_2 = 1$, $(b + a) / R_1 = 0.01$, $R_1 / h_1 = 100$, $\eta = 0.0$, $\rho_1 / \rho_2 = 1/8$,

$v_1 / v_2 = 1.0$179

Figure 4.50: Normal and lateral elastodynamic contact stresses on homogenous coating indented by a moving cylindrical punch for various values of punch speed (a) Normal contact stress distribution; (b) Lateral contact stress distribution, $\mu_1 / \mu_2 = 10$, $(b + a) / R_1 = 0.01$, $R_1 / h_1 = 100$, $\eta = 0.0$, $\rho_1 / \rho_2 = 1/8$,

$v_1 / v_2 = 0.8$180

Figure 4.51: Normal and lateral elastodynamic contact stresses on homogenous coating indented by a moving cylindrical punch for various values of punch speed (a) Normal contact stress distribution; (b) Lateral contact stress distribution, $\mu_1 / \mu_2 = 1/10$, $(b + a) / R_1 = 0.01$, $R_1 / h_1 = 100$, $\eta = 0.3$,

$\rho_1 / \rho_2 = 1/8$, $v_1 / v_2 = 0.8$180

Figure 4.52: Normal and lateral elastodynamic contact stresses on homogenous coating indented by a moving cylindrical punch for various values of punch speed (a) Normal contact stress distribution; (b) Lateral contact stress

distribution, $\mu_1 / \mu_2 = 1$, $(b + a) / R_1 = 0.01$, $R_1 / h_1 = 100$, $\eta = 0.3$, $\rho_1 / \rho_2 = 1/8$, $\nu_1 / \nu_2 = 1.0$181

Figure 4.53: Normal and lateral elastodynamic contact stresses on homogenous coating indented by a moving cylindrical punch for various values of punch speed (a) Normal contact stress distribution; (b) Lateral contact stress distribution, $\mu_1 / \mu_2 = 10$, $(b + a) / R_1 = 0.01$, $R_1 / h_1 = 100$, $\eta = 0.3$, $\rho_1 / \rho_2 = 1/8$, $\nu_1 / \nu_2 = 0.8$181

Figure 4.54: Normal and lateral elastodynamic contact stresses on homogenous coating indented by a moving cylindrical punch for various values of coefficient of friction (a) Normal contact stress distribution; (b) Lateral contact stress distribution, $\mu_1 / \mu_2 = 1/5$, $(b + a) / R_1 = 0.02$, $R_1 / h_1 = 100$, $c_1 = 0.4$, $\rho_1 / \rho_2 = 1/8$, $\nu_1 / \nu_2 = 0.8$182

Figure 4.55: Normal and lateral elastodynamic contact stresses on homogenous coating indented by a moving cylindrical punch for various values of coefficient of friction (a) Normal contact stress distribution; (b) Lateral contact stress distribution, $\mu_1 / \mu_2 = 5$, $(b + a) / R_1 = 0.02$, $R_1 / h_1 = 100$, $c_1 = 0.4$, $\rho_1 / \rho_2 = 1/8$, $\nu_1 / \nu_2 = 0.8$182

Figure 4.56: Normal and lateral elastodynamic contact stresses on homogenous coating indented by a moving cylindrical punch for various values of relative coating thickness (a) Normal contact stress distribution; (b) Lateral contact stress distribution, $\mu_1 / \mu_2 = 1/5$, $(b + a) / R_1 = 0.02$, $c_1 = 0.4$, $\eta = 0.3$, $\rho_1 / \rho_2 = 1/8$, $\nu_1 / \nu_2 = 0.8$183

Figure 4.57: Normal and lateral elastodynamic contact stresses on homogenous coating indented by a moving cylindrical punch for various values of relative coating thickness (a) Normal contact stress distribution; (b) Lateral contact

stress distribution, $\mu_1 / \mu_2 = 5$, $(b + a) / R_1 = 0.02$, $c_1 = 0.4$, $\eta = 0.3$, $\rho_1 / \rho_2 = 1/8$, $\nu_1 / \nu_2 = 0.8$	183
Figure 4.58: Normal and lateral elastodynamic contact stresses on homogenous coating indented by a moving cylindrical punch for various values of Poisson's ratio (a) Normal contact stress distribution; (b) Lateral contact stress distribution, $\mu_1 / \mu_2 = 1/10$, $(b + a) / R_1 = 0.02$, $R_1 / h_1 = 100$, $c_1 = 0.6$, $\eta = 0.3$, $\rho_1 / \rho_2 = 1/8$	184
Figure 4.59: Normal and lateral elastodynamic contact stresses on homogenous coating indented by a moving cylindrical punch for various values of Poisson's ratio (a) Normal contact stress distribution; (b) Lateral contact stress distribution, $\mu_1 / \mu_2 = 10$, $(b + a) / R_1 = 0.02$, $R_1 / h_1 = 100$, $c_1 = 0.6$, $\eta = 0.3$, $\rho_1 / \rho_2 = 1/8$	184
Figure 5.1: The schematic of the flat punch on the surface of the FGM coating bonded to a homogenous substrate	191
Figure 5.2: Normal and lateral contact stress distribution on FGM coating indented by a flat punch for different stiffness ratio of the coating (a) Normal contact stress distribution; (b) Lateral contact stress distribution, $a / h_1 = 0.1$, $\Gamma_1 = \mu_2 / \mu_{10}$, $\eta = 0.0$, $c_1 = 0.0$	197
Figure 5.3: Normal and lateral contact stress distribution on FGM coating indented by a flat punch for different stiffness ratio of the coating (a) Normal contact stress distribution; (b) Lateral contact stress distribution, $a / h_1 = 0.5$, $\Gamma_1 = \mu_2 / \mu_{10}$, $\eta = 0.0$, $c_1 = 0.0$	197
Figure 5.4: Normal and lateral contact stress distribution on FGM coating indented by a flat punch for different stiffness ratio of the coating (a) Normal contact stress distribution; (b) Lateral contact stress distribution, $a / h_1 = 0.05$, $\Gamma_1 = \mu_2 / \mu_{10}$, $\eta = 0.3$, $c_1 = 0.0$	198

Figure 5.5: Normal and lateral contact stress distribution on FGM coating indented by a flat punch for different stiffness ratio of the coating (a) Normal contact stress distribution; (b) Lateral contact stress distribution, $a/h_1 = 0.1$, $\Gamma_1 = \mu_2 / \mu_{10}$, $\eta = 0.5$, $c_1 = 0.0$198

Figure 5.6: Normal and lateral elastodynamic contact stresses on FGM coating indented by a moving flat punch for various values of punch speed (a) Normal contact stress distribution; (b) Lateral contact stress distribution, $a/h_1 = 0.1$, $\Gamma_1 = 1$, $\eta = 0.0$, $\nu_1/\nu_2 = 1$199

Figure 5.7: Normal and lateral elastodynamic contact stresses on FGM coating indented by a moving flat punch for various values of punch speed (a) Normal contact stress distribution; (b) Lateral contact stress distribution, $a/h_1 = 0.1$, $\Gamma_1 = 1$, $\eta = 0.3$, $\nu_1/\nu_2 = 1$199

Figure 5.8: Normal and lateral elastodynamic contact stresses on FGM coating indented by a moving flat punch for various values of punch speed (a) Normal contact stress distribution; (b) Lateral contact stress distribution, $a/h_1 = 0.05$, $\Gamma_1 = 1/6$, $\eta = 0.3$, $\nu_1/\nu_2 = 1$200

Figure 5.9: Normal and lateral elastodynamic contact stresses on FGM coating indented by a moving flat punch for various values of punch speed (a) Normal contact stress distribution; (b) Lateral contact stress distribution, $a/h_1 = 0.05$, $\Gamma_1 = 6$, $\eta = 0.3$, $\nu_1/\nu_2 = 1$200

Figure 5.10: Normal and lateral elastodynamic contact stresses on FGM coating indented by a moving flat punch for various values of punch speed (a) Normal contact stress distribution; (b) Lateral contact stress distribution, $a/h_1 = 0.1$, $\Gamma_1 = 1/6$, $\eta = 0.3$, $\nu_1/\nu_2 = 1$201

Figure 5.11: Normal and lateral elastodynamic contact stresses on FGM coating indented by a moving flat punch for various values of punch speed (a) Normal contact stress distribution; (b) Lateral contact stress distribution, $a/h_1 = 0.1$, $\Gamma_1 = 6$, $\eta = 0.3$, $\nu_1/\nu_2 = 1$201

Figure 5.12: Normal and lateral elastodynamic contact stresses on FGM coating indented by a moving flat punch for various values of punch speed (a) Normal contact stress distribution; (b) Lateral contact stress distribution, $a/h_1 = 0.2$, $\Gamma_1 = 1/6$, $\eta = 0.3$, $\nu_1/\nu_2 = 1$202

Figure 5.13: Normal and lateral elastodynamic contact stresses on FGM coating indented by a moving flat punch for various values of punch speed (a) Normal contact stress distribution; (b) Lateral contact stress distribution, $a/h_1 = 0.2$, $\Gamma_1 = 6$, $\eta = 0.3$, $\nu_1/\nu_2 = 1$202

Figure 5.14: Normal and lateral elastodynamic contact stresses on FGM coating indented by a moving flat punch for various values of coefficient of friction (a) Normal contact stress distribution; (b) Lateral contact stress distribution, $a/h_1 = 0.1$, $\Gamma_1 = 1/6$, $c_1 = 0.4$, $\nu_1/\nu_2 = 1$203

Figure 5.15: Normal and lateral elastodynamic contact stresses on FGM coating indented by a moving flat punch for various values of coefficient of friction (a) Normal contact stress distribution; (b) Lateral contact stress distribution, $a/h_1 = 0.1$, $\Gamma_1 = 6$, $c_1 = 0.4$, $\nu_1/\nu_2 = 1$203

Figure 5.16: Normal and lateral elastodynamic contact stresses on FGM coating indented by a moving flat punch for various values of stiffness ratio (a) Normal contact stress distribution; (b) Lateral contact stress distribution, $a/h_1 = 0.1$, $c_1 = 0.4$, $\eta = 0.3$, $\nu_1/\nu_2 = 1$204

Figure 5.17: Normal and lateral elastodynamic contact stresses on FGM coating indented by a moving flat punch for various values of stiffness ratio (a) Normal

contact stress distribution; (b) Lateral contact stress distribution, $a/h_1 = 0.4$, $c_1 = 0.4$, $\eta = 0.3$, $\nu_1/\nu_2 = 1$	204
Figure 5.18: Normal and lateral elastodynamic contact stresses on FGM coating indented by a moving flat punch for various values of relative coating thickness (a) Normal contact stress distribution; (b) Lateral contact stress distribution, $\Gamma_1 = 1/6$, $c_1 = 0.6$, $\eta = 0.3$, $\nu_1/\nu_2 = 1$	205
Figure 5.19: Normal and lateral elastodynamic contact stresses on FGM coating indented by a moving flat punch for various values of relative coating thickness (a) Normal contact stress distribution; (b) Lateral contact stress distribution, $\Gamma_1 = 6$, $c_1 = 0.6$, $\eta = 0.3$, $\nu_1/\nu_2 = 1$	205
Figure 5.20: The schematic of the triangular punch on the surface of the FGM coating bonded to a homogenous substrate	211
Figure 5.21: Normal and lateral contact stress distribution on FGM coating indented by a triangular punch for different stiffness ratio of the coating (a) Normal contact stress distribution; (b) Lateral contact stress distribution, $b/h_1 = 0.2$, $\eta = 0.0$, $c_1 = 0.0$	216
Figure 5.22: Normal and lateral contact stress distribution on FGM coating indented by a triangular punch for different stiffness ratio of the coating (a) Normal contact stress distribution; (b) Lateral contact stress distribution, $b/h_1 = 0.5$, $\eta = 0.0$, $c_1 = 0.0$	216
Figure 5.23: Normal and lateral contact stress distribution on FGM coating indented by a frictional triangular punch for different stiffness ratio of the coating (a) Normal contact stress distribution; (b) Lateral contact stress distribution, $b/h_1 = 0.2$, $\eta = 0.3$, $c_1 = 0.0$	217
Figure 5.24: Normal and lateral contact stress distribution on FGM coating indented by a frictional triangular punch for different stiffness ratio of the	

coating (a) Normal contact stress distribution; (b) Lateral contact stress distribution, $b/h_1 = 0.2$, $\eta = 0.5$, $c_1 = 0.0$	217
Figure 5.25: Normal and lateral elastodynamic contact stresses on FGM coating indented by a moving triangular punch for various values of punch speed (a) Normal contact stress distribution; (b) Lateral contact stress distribution, $b/h_1 = 0.1$, $\Gamma_1 = 1$, $\eta = 0.0$, $\nu_1/\nu_2 = 1$	218
Figure 5.26: Normal and lateral elastodynamic contact stresses on FGM coating indented by a moving triangular punch for various values of punch speed (a) Normal contact stress distribution; (b) Lateral contact stress distribution, $b/h_1 = 0.1$, $\Gamma_1 = 1$, $\eta = 0.3$, $\nu_1/\nu_2 = 1$	218
Figure 5.27: Normal and lateral elastodynamic contact stresses on FGM coating indented by a moving triangular punch for various values of punch speed (a) Normal contact stress distribution; (b) Lateral contact stress distribution, $b/h_1 = 0.1$, $\Gamma_1 = 1/6$, $\eta = 0.3$, $\nu_1/\nu_2 = 1$	219
Figure 5.28: Normal and lateral elastodynamic contact stresses on FGM coating indented by a moving triangular punch for various values of punch speed (a) Normal contact stress distribution; (b) Lateral contact stress distribution, $b/h_1 = 0.1$, $\Gamma_1 = 6$, $\eta = 0.3$, $\nu_1/\nu_2 = 1$	219
Figure 5.29: Normal and lateral elastodynamic contact stresses on FGM coating indented by a moving triangular punch for various values of punch speed (a) Normal contact stress distribution; (b) Lateral contact stress distribution, $b/h_1 = 0.2$, $\Gamma_1 = 1/6$, $\eta = 0.3$, $\nu_1/\nu_2 = 1$	220
Figure 5.30: Normal and lateral elastodynamic contact stresses on FGM coating indented by a moving triangular punch for various values of punch speed (a) Normal contact stress distribution; (b) Lateral contact stress distribution, $b/h_1 = 0.2$, $\Gamma_1 = 6$, $\eta = 0.3$, $\nu_1/\nu_2 = 1$	220

Figure 5.31: Normal and lateral elastodynamic contact stresses on FGM coating indented by a moving triangular punch for various values of punch speed (a) Normal contact stress distribution; (b) Lateral contact stress distribution, $b/h_1 = 0.4, \Gamma_1 = 1/6, \eta = 0.3, \nu_1/\nu_2 = 1$221

Figure 5.32: Normal and lateral elastodynamic contact stresses on FGM coating indented by a moving triangular punch for various values of punch speed (a) Normal contact stress distribution; (b) Lateral contact stress distribution, $b/h_1 = 0.4, \Gamma_1 = 6, \eta = 0.3, \nu_1/\nu_2 = 1$221

Figure 5.33: Normal and lateral elastodynamic contact stresses on FGM coating indented by a moving triangular punch for various values of coefficient of friction (a) Normal contact stress distribution; (b) Lateral contact stress distribution, $b/h_1 = 0.2, \Gamma_1 = 1/6, c_1 = 0.4, \nu_1/\nu_2 = 1$222

Figure 5.34: Normal and lateral elastodynamic contact stresses on FGM coating indented by a moving triangular punch for various values of coefficient of friction (a) Normal contact stress distribution; (b) Lateral contact stress distribution, $b/h_1 = 0.2, \Gamma_1 = 6, c_1 = 0.4, \nu_1/\nu_2 = 1$222

Figure 5.35: Normal and lateral elastodynamic contact stresses on FGM coating indented by a moving triangular punch for various values of stiffness ratio (a) Normal contact stress distribution; (b) Lateral contact stress distribution, $b/h_1 = 0.2, \eta = 0.3, c_1 = 0.4, \nu_1/\nu_2 = 1$223

Figure 5.36: Normal and lateral elastodynamic contact stresses on FGM coating indented by a moving triangular punch for various values of stiffness ratio (a) Normal contact stress distribution; (b) Lateral contact stress distribution, $b/h_1 = 0.4, \eta = 0.3, c_1 = 0.4, \nu_1/\nu_2 = 1$223

Figure 5.37: Normal and lateral elastodynamic contact stresses on FGM coating indented by a moving triangular punch for various values of relative coating

thickness (a) Normal contact stress distribution; (b) Lateral contact stress distribution, $\Gamma_1 = 1/6$, $\eta = 0.3$, $c_1 = 0.4$, $\nu_1/\nu_2 = 1$224

Figure 5.38: Normal and lateral elastodynamic contact stresses on FGM coating indented by a moving triangular punch for various values of relative coating thickness (a) Normal contact stress distribution; (b) Lateral contact stress distribution, $\Gamma_1 = 6$, $\eta = 0.3$, $c_1 = 0.4$, $\nu_1/\nu_2 = 1$224

Figure 5.39: The schematic of the semi-circular punch on the surface of the FGM coating bonded to a homogenous substrate231

Figure 5.40: Normal and lateral contact stress distribution on FGM coating indented by a frictional semi-circular punch for different stiffness ratio of the coating (a) Normal contact stress distribution; (b) Lateral contact stress distribution, $\Gamma_1 = \mu_2 / \mu_{10}$, $\eta = 0.0$, $b/R_1 = 0.01$, $R_1/h_1 = 20$236

Figure 5.41: Normal and lateral contact stress distribution on FGM coating indented by a frictional semi-circular punch for different stiffness ratio of the coating (a) Normal contact stress distribution; (b) Lateral contact stress distribution, $\Gamma_1 = \mu_2 / \mu_{10}$, $\eta = 0.0$, $b/R_1 = 0.05$, $R_1/h_1 = 20$236

Figure 5.42: Normal and lateral elastodynamic contact stresses on FGM coating indented by a moving semi-circular punch for various values of punch speed (a) Normal contact stress distribution; (b) Lateral contact stress distribution, $b/R_1 = 0.01$, $R_1/h_1 = 20$, $\Gamma_1 = 1$, $\eta = 0.0$, $\nu_1/\nu_2 = 1$237

Figure 5.43: Normal and lateral elastodynamic contact stresses on FGM coating indented by a moving semi-circular punch for various values of punch speed (a) Normal contact stress distribution; (b) Lateral contact stress distribution, $b/R_1 = 0.01$, $R_1/h_1 = 20$, $\Gamma_1 = 1$, $\eta = 0.3$, $\nu_1/\nu_2 = 1$237

Figure 5.44: Normal and lateral elastodynamic contact stresses on FGM coating indented by a moving semi-circular punch for various values of punch speed (a)

Normal contact stress distribution; (b) Lateral contact stress distribution, $b/R_1 = 0.01, R_1/h_1 = 20, \Gamma_1 = 1/6, \eta = 0.3, \nu_1/\nu_2 = 1$	238
Figure 5.45: Normal and lateral elastodynamic contact stresses on FGM coating indented by a moving semi-circular punch for various values of relative coating thickness (a) Normal contact stress distribution; (b) Lateral contact stress distribution, $b/R_1 = 0.01, R_1/h_1 = 20, \Gamma_1 = 6, \eta = 0.3, \nu_1/\nu_2 = 1$	238
Figure 5.46: Normal and lateral elastodynamic contact stresses on FGM coating indented by a moving semi-circular punch for various values of punch speed (a) Normal contact stress distribution; (b) Lateral contact stress distribution, $b/R_1 = 0.02, R_1/h_1 = 20, \Gamma_1 = 1/6, \eta = 0.3, \nu_1/\nu_2 = 1$	239
Figure 5.47: Normal and lateral elastodynamic contact stresses on FGM coating indented by a moving semi-circular punch for various values of punch speed (a) Normal contact stress distribution; (b) Lateral contact stress distribution, $b/R_1 = 0.02, R_1/h_1 = 20, \Gamma_1 = 6, \eta = 0.3, \nu_1/\nu_2 = 1$	239
Figure 5.48: Normal and lateral elastodynamic contact stresses on FGM coating indented by a moving semi-circular punch for various values of punch speed (a) Normal contact stress distribution; (b) Lateral contact stress distribution, $b/R_1 = 0.04, R_1/h_1 = 20, \Gamma_1 = 1/6, \eta = 0.3, \nu_1/\nu_2 = 1$	240
Figure 5.49: Normal and lateral elastodynamic contact stresses on FGM coating indented by a moving semi-circular punch for various values of punch speed (a) Normal contact stress distribution; (b) Lateral contact stress distribution, $b/R_1 = 0.04, R_1/h_1 = 20, \Gamma_1 = 6, \eta = 0.3, \nu_1/\nu_2 = 1$	240
Figure 5.50: Normal and lateral elastodynamic contact stresses on FGM coating indented by a moving semi-circular punch for various values of coefficient of friction (a) Normal contact stress distribution; (b) Lateral contact stress distribution, $b/R_1 = 0.02, R_1/h_1 = 20, \Gamma_1 = 1/6, c_1 = 0.4, \nu_1/\nu_2 = 1$	241

Figure 5.51: Normal and lateral elastodynamic contact stresses on FGM coating indented by a moving semi-circular punch for various values of coefficient of friction (a) Normal contact stress distribution; (b) Lateral contact stress distribution, $b/R_1 = 0.02$, $R_1/h_1 = 20$, $\Gamma_1 = 6$, $c_1 = 0.4$, $\nu_1/\nu_2 = 1$241

Figure 5.52: Normal and lateral elastodynamic contact stresses on FGM coating indented by a moving semi-circular punch for various values of stiffness ratio (a) Normal contact stress distribution; (b) Lateral contact stress distribution, $b/R_1 = 0.01$, $R_1/h_1 = 20$, $c_1 = 0.4$, $\eta = 0.3$, $\nu_1/\nu_2 = 1$242

Figure 5.53: Normal and lateral elastodynamic contact stresses on FGM coating indented by a moving semi-circular punch for various values of stiffness ratio (a) Normal contact stress distribution; (b) Lateral contact stress distribution, $b/R_1 = 0.02$, $R_1/h_1 = 20$, $c_1 = 0.4$, $\eta = 0.3$, $\nu_1/\nu_2 = 1$242

Figure 5.54: Normal and lateral elastodynamic contact stresses on FGM coating indented by a moving semi-circular punch for various values of relative coating thickness (a) Normal contact stress distribution; (b) Lateral contact stress distribution, $b/R_1 = 0.02$, $\Gamma_1 = 1/6$, $c_1 = 0.4$, $\eta = 0.3$, $\nu_1/\nu_2 = 1$243

Figure 5.55: Normal and lateral elastodynamic contact stresses on FGM coating indented by a moving semi-circular punch for various values of relative coating thickness (a) Normal contact stress distribution; (b) Lateral contact stress distribution, $b/R_1 = 0.02$, $\Gamma_1 = 6$, $c_1 = 0.4$, $\eta = 0.3$, $\nu_1/\nu_2 = 1$243

Figure 5.56: Normal and lateral elastodynamic contact stresses on FGM coating indented by a moving semi-circular punch for various values of punch radius (a) Normal contact stress distribution; (b) Lateral contact stress distribution, $\Gamma_1 = 1/6$, $R_1/h_1 = 20$, $c_1 = 0.4$, $\eta = 0.3$, $\nu_1/\nu_2 = 1$244

Figure 5.57: Normal and lateral elastodynamic contact stresses on FGM coating indented by a moving semi-circular punch for various values of punch radius (a)

Normal contact stress distribution; (b) Lateral contact stress distribution, $\Gamma_1 = 6$, $R_1/h_1 = 20$, $c_1 = 0.4$, $\eta = 0.3$, $\nu_1/\nu_2 = 1$	244
Figure 5.58: The schematic of the cylindrical punch on the surface of the FGM coating bonded to a homogenous substrate	252
Figure 5.59: Normal and lateral contact stress distribution on FGM coating indented by a cylindrical punch for different stiffness ratio of the coating (a) Normal contact stress distribution; (b) Lateral contact stress distribution, $\Gamma_1 = \mu_2/\mu_{10}$, $(b+a)/R_1 = 0.01$, $R_1/h_1 = 100$, $\eta = 0.0$, $c_1 = 0.0$	257
Figure 5.60: Normal and lateral contact stress distribution on FGM coating indented by a cylindrical punch for different stiffness ratio of the coating (a) Normal contact stress distribution; (b) Lateral contact stress distribution, $\Gamma_1 = \mu_2/\mu_{10}$, $(b+a)/R_1 = 0.03$, $R_1/h_1 = 100$, $\eta = 0.0$, $c_1 = 0.0$	257
Figure 5.61: Normal and lateral contact stress distribution on FGM coating indented by a cylindrical punch for different stiffness ratio of the coating (a) Normal contact stress distribution; (b) Lateral contact stress distribution, $\Gamma_1 = \mu_2/\mu_{10}$, $(b+a)/R_1 = 0.02$, $R_1/h_1 = 50$, $\eta = 0.3$, $c_1 = 0.0$	258
Figure 5.62: Normal and lateral contact stress distribution on FGM coating indented by a cylindrical punch for different stiffness ratio of the coating (a) Normal contact stress distribution; (b) Lateral contact stress distribution, $\Gamma_1 = \mu_2/\mu_{10}$, $(b+a)/R_1 = 0.01$, $R_1/h_1 = 100$, $\eta = 0.3$, $c_1 = 0.0$	258
Figure 5.63: Normal and lateral elastodynamic contact stresses on FGM coating indented by a moving cylindrical punch for various values of punch speed (a) Normal contact stress distribution; (b) Lateral contact stress distribution, $(b+a)/R_1 = 0.01$, $R_1/h_1 = 100$, $\Gamma_1 = 1$, $\eta = 0.0$, $\nu_1/\nu_2 = 1$	259
Figure 5.64: Normal and lateral elastodynamic contact stresses on FGM coating indented by a moving cylindrical punch for various values of punch speed (a)	

Normal contact stress distribution; (b) Lateral contact stress distribution, ($b+a$)/ $R_1 = 0.01$, $R_1/h_1 = 100$, $\Gamma_1 = 1$, $\eta = 0.3$, $\nu_1/\nu_2 = 1$	259
Figure 5.65: Normal and lateral elastodynamic contact stresses on FGM coating indented by a moving cylindrical punch for various values of punch speed (a) Normal contact stress distribution; (b) Lateral contact stress distribution, ($b+a$)/ $R_1 = 0.01$, $R_1/h_1 = 100$, $\Gamma_1 = 1/6$, $\eta = 0.3$, $\nu_1/\nu_2 = 1$	260
Figure 5.66: Normal and lateral elastodynamic contact stresses on FGM coating indented by a moving cylindrical punch for various values of punch speed (a) Normal contact stress distribution; (b) Lateral contact stress distribution, ($b+a$)/ $R_1 = 0.01$, $R_1/h_1 = 100$, $\Gamma_1 = 6$, $\eta = 0.3$, $\nu_1/\nu_2 = 1$	260
Figure 5.67: Normal and lateral elastodynamic contact stresses on FGM coating indented by a moving cylindrical punch for various values of punch speed (a) Normal contact stress distribution; (b) Lateral contact stress distribution, ($b+a$)/ $R_1 = 0.02$, $R_1/h_1 = 100$, $\Gamma_1 = 1/6$, $\eta = 0.3$, $\nu_1/\nu_2 = 1$	261
Figure 5.68: Normal and lateral elastodynamic contact stresses on FGM coating indented by a moving cylindrical punch for various values of punch speed (a) Normal contact stress distribution; (b) Lateral contact stress distribution, ($b+a$)/ $R_1 = 0.02$, $R_1/h_1 = 100$, $\Gamma_1 = 6$, $\eta = 0.3$, $\nu_1/\nu_2 = 1$	261
Figure 5.69: Normal and lateral elastodynamic contact stresses on FGM coating indented by a moving cylindrical punch for various values of punch speed (a) Normal contact stress distribution; (b) Lateral contact stress distribution, ($b+a$)/ $R_1 = 0.04$, $R_1/h_1 = 100$, $\Gamma_1 = 1/6$, $\eta = 0.3$, $\nu_1/\nu_2 = 1$	262
Figure 5.70: Normal and lateral elastodynamic contact stresses on FGM coating indented by a moving cylindrical punch for various values of punch speed (a) Normal contact stress distribution; (b) Lateral contact stress distribution, ($b+a$)/ $R_1 = 0.04$, $R_1/h_1 = 100$, $\Gamma_1 = 6$, $\eta = 0.3$, $\nu_1/\nu_2 = 1$	262

Figure 5.71: Normal and lateral elastodynamic contact stresses on FGM coating indented by a moving cylindrical punch for various values of coefficient of friction (a) Normal contact stress distribution; (b) Lateral contact stress distribution, $(b+a)/R_1 = 0.01$, $R_1/h_1 = 100$, $\Gamma_1 = 1/6$, $c_1 = 0.4$, $\nu_1/\nu_2 = 1$263

Figure 5.72: Normal and lateral elastodynamic contact stresses on FGM coating indented by a moving cylindrical punch for various values of coefficient of friction (a) Normal contact stress distribution; (b) Lateral contact stress distribution, $(b+a)/R_1 = 0.01$, $R_1/h_1 = 100$, $\Gamma_1 = 6$, $c_1 = 0.4$, $\nu_1/\nu_2 = 1$263

Figure 5.73: Normal and lateral elastodynamic contact stresses on FGM coating indented by a moving cylindrical punch for various values of stiffness ratio (a) Normal contact stress distribution; (b) Lateral contact stress distribution, $(b+a)/R_1 = 0.02$, $R_1/h_1 = 100$, $c_1 = 0.4$, $\eta = 0.3$, $\nu_1/\nu_2 = 1$264

Figure 5.74: Normal and lateral elastodynamic contact stresses on FGM coating indented by a moving cylindrical punch for various values of stiffness ratio (a) Normal contact stress distribution; (b) Lateral contact stress distribution, $(b+a)/R_1 = 0.04$, $R_1/h_1 = 100$, $c_1 = 0.4$, $\eta = 0.3$, $\nu_1/\nu_2 = 1$264

Figure 5.75: Normal and lateral elastodynamic contact stresses on FGM coating indented by a moving cylindrical punch for various values of relative coating thickness (a) Normal contact stress distribution; (b) Lateral contact stress distribution, $(b+a)/R_1 = 0.02$, $\Gamma_1 = 1/6$, $c_1 = 0.4$, $\eta = 0.3$, $\nu_1/\nu_2 = 1$265

Figure 5.76: Normal and lateral elastodynamic contact stresses on FGM coating indented by a moving cylindrical punch for various values of relative coating thickness (a) Normal contact stress distribution; (b) Lateral contact stress distribution, $(b+a)/R_1 = 0.02$, $\Gamma_1 = 6$, $c_1 = 0.4$, $\eta = 0.3$, $\nu_1/\nu_2 = 1$265

Figure 5.77: Normal and lateral elastodynamic contact stresses on FGM coating indented by a moving cylindrical punch for various values of $(b+a)/R_1$ (a)

Normal contact stress distribution; (b) Lateral contact stress distribution,
 $R_1/h_1 = 100, \Gamma_1 = 1/6, c_1 = 0.4, \eta = 0.3, \nu_1/\nu_2 = 1$266

Figure 5.78: Normal and lateral elastodynamic contact stresses on FGM coating
indented by a moving cylindrical punch for various values of $(b+a)/R_1$ (a)

Normal contact stress distribution; (b) Lateral contact stress distribution,
 $R_1/h_1 = 100, \Gamma_1 = 6, c_1 = 0.4, \eta = 0.3, \nu_1/\nu_2 = 1$266

CHAPTER 1

INTRODUCTION

The main aim of this study is to develop an analytical method to investigate dynamic frictional contact problems involving layered structures and functionally graded coatings. A moving rigid punch slides at a constant subsonic speed over the functionally graded coating which is bonded perfectly to the homogenous substrate. The speed of the sliding rigid punch is not assumed to be so small hence, dynamic effects are taken into account in this study. Main interest is to examine dynamic effects and influences of geometrical and material properties on contact stresses and contact related results. This study covers both elastodynamic contact mechanics of homogenous elastic coatings and functionally graded coatings. Current chapter consists of four parts. First part describes the concept of functionally graded material and its development, second part gives some information about tribology and tribological applications, third part is the literature survey and fourth part is scope of this study.

1.1 Functionally Graded Materials

Development of technology enables the invention of new and innovative materials which are able to withstand the conditions of advanced environments. Generally, in engineering applications, two types of advanced composite materials are used. First is the advanced composites with very high strength and stiffness that are used in a

broad range of industry such as automobiles, aircraft, space vehicles, offshore structures, containers, piping, electronics, etc., Agarwal [1]. Second is the bonded or coating type composite materials. In many engineering applications, protective coatings are designed to withstand wear, thermal loadings and the corrosion, and substrates are designed for toughness and strength. New coating and treatment methods are being developed. For instance, devices and bearing systems which operate under near-vacuum conditions as in space mechanisms or satellites or engine components operating under hot corrosive and erosive conditions as in aero gas turbines could not function without advanced tribological coatings. Hard coatings such as titanium nitride, titanium carbide and aluminium oxide are commonly used on cutting tools in the manufacturing industry. Chromium nitride and molybdenum disulphide coatings are used on metal forming tools. Very hard but also low friction diamond like carbon coatings are deposited for wear protection on magnetic storage devices produced for computers. Various carbon based coatings are used in automotive industry to reduce energy consumption (Holmberg and Matthews [2]). Thermal barrier coatings (TBCs) are used on combustors and blades of aircraft engines (Parks et al. [3]). Y_2O_3 stabilized ZrO_2 is the most commonly used ceramic layer with a low thermal conductivity and it has a capability to keep metallic substrate from high thermal gradients. Various types of coatings in many applications such as sandwich coatings, graded coatings, duplex coatings, multilayer, superlattice, etc. are described in the work conducted by Hogmark [4]. Manufacturing of coatings on substrates are generally accomplished by deposition techniques which are mainly categorized as gaseous state process, solution state process, molten state process and solid state process. Solid state process is used to produce thicker coatings (Rickerby and Matthews [5]). Thickness of the coating and the deposition temperature are two important parameters to produce coatings. Typical coating thickness may vary from $0.1 \mu m$ to $10 mm$. Some recent research is examining the possibility of using much thinner coatings such as $1-3 nm$ for tribological purposes (Wang et al. [6]). Gaseous

state process includes chemical vapor deposition (CVD), ion implantation (II), and physical vapor deposition techniques (PVD). Solution state consists of chemical solution deposition, electrochemical deposition, and sol-gel techniques. Molten state process involves plasma variants techniques such as laser, thermal spraying and welding.

Although homogenous coatings are used to keep the metallic substrate from harsh surface environments (combinations of excessive wear, high thermal gradients and temperatures), these ceramic based layers have some shortcomings. Ceramic based coatings are vulnerable due to poor bonding strength, high residual stress, and the brittle nature of the ceramic layer. Use of metal/ceramic functionally graded coatings instead of conventional ceramic based coatings can be reasonable to eliminate these shortcomings.

Functionally graded material (FGM) concept was initially proposed in 1987 by material scientists in Sendai area in Japan during space plane research and development [7]. The objective was to develop a thermal barrier material which can withstand 2000 K temperature difference during operation. Test samples which were manufactured by chemical vapor deposition (CVD) and physical vapor deposition (PVD) and low pressure plasma spray methods were respectively Si-C, Ti-C and ZrO₂-NiCr functionally graded layers. It was concluded that FGMs had a great potential to reduce the thermal stress due to the mismatch of thermal expansion coefficients (Niino and Maeda [8]).

Functionally graded materials (FGMs) are a kind of advanced composites involving two or more constituent phases with a gradual and functionally variable composition of microstructure and material properties. In Figure 1.1, a particulate FGM which is graded in the thickness direction is shown [9]. Generally, metal and ceramic are the constituent phases of FGMs, and there is a smooth variation in volume fractions of constituent phases across the thickness direction. While one surface consists of 100%

ceramic, the other surface consists of 100% metal. The primary objective of using FGMs as protective coatings and interfacial zones is to reduce residual stress resulting from thermomechanical mismatch, overcome delamination or spallation problems due to poor bonding strength and provide toughness.

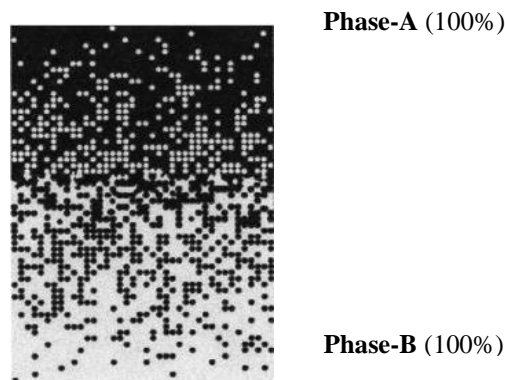


Figure 1.1: A particulate FGM with the volume fractions of constituent phases

1.2 Tribological Applications

Tribology is a field of science and technology which concerns contacting surfaces in relative motion. The major purpose is to reduce and control friction and wear in order to extend the lifetime of machine components and correspondingly increase efficiency. There are various type tribological components in engineering applications. Some tribological components are sliding and rolling contact bearings, gears, cams, sealings, piston rings and cutting tools. These components are utilized in industrial applications such as internal combustion engines in automotive, gas turbines in turbomachinery, railroad in transportation, magnetic storage devices in informatics industries. In tribological applications, many factors have to be considered for design process of contacting components. Selection of bulk materials is the most important design factor among them. Materials such as cast irons, stainless steels, high temperature alloys, ceramics, solid lubricants and polymers are utilized in many tribological applications. Main aim is to reduce friction and

correspondingly wear by selecting appropriate materials. Thus, mechanical components have enhanced durability and prolonged machine life. Descriptions depending on different perspectives of tribology are provided in the books by Bhushan [10] and Suh [11].

In recent years, the utilization of surface coatings is increasing trend in tribological applications. Coatings are mainly categorized as hard coatings and soft coatings. Hard coatings are considered for high wear resistance and moderate friction while soft coatings or solid lubricant coatings are considered with low friction. Ceramics, Steel, Ni or Co based intermetallic alloys and some metals like Ni, Cr, Mo are used as hard coatings. Soft metals such as Au, Ag, Pb, polymers and some materials such as MoS₂ and graphite are used as soft coatings. It is reported that the most successful tribological application of thin surface coatings is seen in cutting tool industry, [10]. Generally, ceramics based hard coating material is deposited on the tool surface as a hard coating and cutting tools have lower friction and wear and correspondingly they have extended tool life. Thin hard coatings made of nitrides and carbides such as TiN, TiC, ZrC, ZrN and TiAlN are used successfully in industry. In cutting tools, coatings made of oxide ceramics such as single crystal alumina (sapphire), polycrystalline Al₂O₃ and ZrO₂ are also utilized.

Roller bearings are utilized in various engineering components such as wheels, pistons, camshafts in automotive, aerospace and wind turbine industry [12]. The contact pressures may vary from 0.5 up to 3 GPa, depending on the application [2, 13]. The deposition of a protective low friction coating on the surface of rollers extends the lifetime of the component [13-15].

Abradable seals are used in aircraft gas turbine engines. They are used in blade-stator interface in the compressor and blade-shroud interface in the turbine to minimize the clearance without catastrophic failure [16].

Contact fatigue damage is a common mode of gear failure. Alanou et al. [17] experimentally showed that thin hard coatings may enhance the scuffing and micro-pitting performance of gears since they exhibit very high levels of surface hardness combined with a low traction against dry steel. However, they found poor adherence under some cases.

The failure mechanism resulting from surface cracking in brittle surfaces subject to severe contact stresses is investigated by many researchers. In practice, fracture behavior of the hard and brittle coatings is examined using indentation or scratch tests [18-19]. Indentation tests were conducted by Page and Knight [18] on a CVD coated TiN-steel composite structure. Radial cracks emerge across the surface of the coating from the corners of the Vicker's indenter at relatively high normal loads. These radial cracks are vertical half-penny shaped cracks which are one of the crack systems observed in brittle materials during indentation tests by a Vicker's indenter [20]. When blunt indenter is loaded normally on a thick elastic specimen, Hertzian cone crack system forms [21]. In Hertzian cone crack system, crack initiates at the surface and propagates in the form of a truncated cone into the material. If the blunt indenter (for example sphere) is translated laterally across the surface, tensile lateral stress increases at the trailing end of the contact zone due to friction. This is known as scratch test. Spallation of the coating from the substrate, Hertzian cracking and tensile cracking are reported as the three major failure modes under contact loading (Bull [19]).

Functionally graded materials (FGMs) have been used as either bulk materials or protective coatings to improve the structural resistance of machine components. Functionally graded materials (FGMs) have great potential in tribological applications. Suresh et al. [22] carried out experimental and computational studies and results of these studies showed that controlled gradients in elastic modulus alone can result in a pronounced enhancement in the resistance of a surface to frictional

sliding contact. Cho and Park [23] investigated the thermoelastic characteristics of functionally graded lathe cutting tools composed of Cr-Mo steel shank and ceramic tip in order to explore thermomechanical superiority. According to the results, the peak effective stress is reduced to almost by two and half times by inserting FGM cutting bite. Therefore, thermomechanical stress concentration was relaxed significantly. ZrO₂ based functionally ceramic coatings are developed as abradable seals in turbine parts of aircraft engines that seals with controlled ceramic microstructure exhibited reduced thermal cracking and better spallation resistance [24].

1.3 Literature Survey

Contact problems have been very known topic of interest within the theory of elasticity for over hundred years. The semi-infinite elastic solid under the compressive load of a rigid body was first analyzed by Boussinesq and the main aim was to find the stress distribution in a semi-infinite solid. Hence, this problem was called as *Boussinesq problem*. General description of the *Boussinesq problem* can be found in the study conducted by Hertz [25].

The foundation of the contact mechanics analysis is based on Hertz assumption. If the contact area is small compared to the geometry of the contacting bodies and if the contact area is far removed from other surfaces, then the contacting bodies may be approximated as semi-infinite planes. The Hertz assumption pioneered to analyze contact problems for half-planes.

Either the integral transformation approach or the finite element method may be used to examine the contact mechanics of solids. Analytical solutions to contact problems have significant applications in aerospace, automotive, manufacturing and marine industries. Since the knowledge of the contact stress distribution gives an idea of regions where potential damage may occur, determination of contact stresses on any machine element under contact loads is crucial.

Solutions to many plane and axisymmetric problems may be found in the work of Galin. [26]. The general method of solving frictionless plane contact problems was given by Muskhelishvili [27]. Analytical solutions where elastic half-planes were loaded by different type of tractions were presented by Johnson [28]. The numerical methods such as finite element method and boundary element method were used to obtain solutions for contact problems with complicated geometry and material properties [29]. Studies conducted by Kikuchi and Oden [30] and Khludnev and Sokolowski [31] proposed various finite element treatments for contact problems. Ratwani and Erdoğan [32] considered the frictionless plane contact problem for an elastic layer lying on an elastic half-space. Contact problems of a rigid punch on a non-homogenous medium were solved for small values of the inhomogeneity parameter by Bakirtas [33].

Contact mechanics analysis of a layered elastic solid pressed by an elastic cylinder was examined by Gupta and Walowit [34] in the state of plane strain. The formulation of the contact problem was reduced to an integral equation using Green functions. Results were obtained for both rigid and elastic punch models in order to see the practical applications of the study. Gupta et al. [35] examined the mechanical behavior of coated materials for bearings. Stress distribution in layered structure was provided by Fourier transforms of Airy stress function. Hence, the possibility of surface fracture caused by high stresses were investigated. Three dimensional contact analysis of layered solids was conducted by Chiu and Hartnett [36]. Numerical solutions were obtained to simulate the contact of a steel rolling component with a steel bearing supported by aluminum housing. Komvopoulos [37] performed finite element analysis to solve the contact problem between a layered elastic semi-infinite solid and a rigid surface. Stiff coating lying on a substrate was considered and solutions for the subsurface stress and deformation fields were presented for relatively thin, intermediate and thick layers. Contact stresses on stiff coatings

subjected to sliding contact were found by Kulchytsky-Zhyhailo and Rogowski [38]. The contact problem of elastic substrate coated by an elastic layer in contact with a rigid cylindrical indenter was considered. Solutions were obtained for various values of the stiffness ratio and the coefficient of friction and obtained results were compared to those obtained from Hertz solution.

Giannakopoulos and Pallot [39] proposed closed form analytical solutions for two dimensional isothermal contact of rigid cylinders on functionally graded substrates whose elastic property was expressed by power law. Giannakopoulos and Suresh [40] carried out analytical work for point force indentation of the gradient materials and the elastic modulus varied according to both exponential and power law functions. In their study, flat ended and cylindrical punches were considered. Giannakopoulos and Suresh [41] used both analytical and computational approaches to obtain stress and deformation fields in a graded half plane in contact with a rigid axisymmetric indenter. Suresh et al. [42] compared the computational results to those obtained from experimental studies for a spherical indenter. Barber [43] studied contact problems of thin layers on a rigid foundation indented by a frictionless punch. Guler [44] solved the quasi-static frictional contact problem for the stiffening medium. Frictional contact problem between a rigid punch and a functionally graded coating was investigated and the influences of punch profile, coefficient of friction, material inhomogeneity and length parameters on contact stresses were determined by Guler [45] and results were presented in manuscripts by Guler and Erdogan [46-47]. Analytical solutions to the coupled surface crack and contact problem in functionally graded half-plane were developed and contact stresses and the stress intensity factors at the tip of a surface crack were presented by Dag and Erdogan [48].

Ke and Wang [49] investigated two dimensional frictionless contact mechanics of functionally graded coatings with arbitrary spatial variations of elastic properties. In the plane stress deformation, functionally graded coating was made up a series of

layers with elastic modulus varying linearly in each. However, friction on the contact surface was not considered. Moreover, Ke and Wang [50] considered the same contact problem in frictional case and contact stress results were presented with respect to various parameters. Liu and Wang [51] examined the contact problem of functionally graded coatings without friction in axisymmetric condition. In their study, elastic modulus of the functionally graded layer was defined by exponential function.

Frictional contact problem between a rigid flat punch and a functionally graded coating which involves an interface crack was analyzed by Choi and Paulino [52]. In their study, the effect of the interface crack on contact stress and stress intensity factors were examined for different loading conditions. Choi and Paulino [53] carried out a research on the frictional contact problem with heat generation for coating, graded interlayer and the substrate system and thermal effects were added to the frictional contact problem. In their study, contact stresses with respect to various mechanical and thermal loading were presented. Balci et al. [54] conducted a study on the investigation of subsurface stresses in graded coatings subjected to frictional contact with heat generation. Subsurface stresses were presented for various thermoelastic and geometric parameters. Dag et al. [55] carried out a research on the frictional contact problem between a rigid punch and a laterally graded elastic medium. In their study, both flat and triangular punch profiles were considered and results obtained by analytical method were compared to those generated by finite element analysis. The influence of lateral gradation on contact stress distributions was shown. Dag [56] considered the spatial variation of coefficient of friction for laterally graded materials subjected to sliding contact by a rigid flat punch. Contact stresses were presented to reveal the effect of the spatial variation of the coefficient of friction in laterally graded materials. Dag et al. [57] examined the contact problem in the presence of a surface crack in a functionally graded coating subjected to a

sliding frictional contact. Stress intensity factors at the crack tip with respect to various elastic and geometric parameters were presented. Chen and Chen [58] analyzed contact behavior between a rigid punch and a homogenous half-space coated with linear graded layer. It was shown that the gradation law of material property and thickness of the surface layer have significant influences on the stress intensity factors and contact stress distributions.

Guler et al. [59] carried out a research on the tractive rolling contact mechanics of functionally graded coatings. The influence of the gradation of the material property on the contact stress field was examined by Alinia et al. [60] and contour plots of contact stresses in the contacting medium were provided.

Contact problems mentioned in the foregoing paragraphs are quasi-static or static type contact problems. In practical applications of many engineering problems, the speed of the one of the contacting bodies may be relatively quite high with respect to the other body. Hence, dynamic contributions may be significant in such contact problems.

The steady motion of a line load on the surface of the isotropic half plane was examined by Sneddon [61] and later by Cole and Huth [62]. The problem of a moving heavy cylinder rolling over the surface of an isotropic elastic half-space for sub-Rayleigh and supersonic moving speeds was conducted by Craggs and Roberts [63]. They extended the Sneddon's method to examine the mixed boundary value problem. The main aim was to discuss the limitations of the previous studies and to explore the anomalies that happen at high speeds close to Rayleigh wave speed. Georgidas and Barber [64] examined the elastodynamic super-Rayleigh/subseismic indentation paradox. They provided conclusions on separation of the contact associated with the punch speed. Barber and Comninou [65] studied the problem of an elastic cylinder rolling with friction on an elastic half-space with constant velocity which is supersonic with respect to the speed of wave propagation in materials of the

contacting bodies. Zhou et al. [66] analyzed the influences of the punch speed and material property variations on frictionless contact problem between an orthotropic material and a rigid moving punch, and they provided contact stress results for various elastic properties. Furthermore, Zhou et al. [67] investigated the same dynamic contact problem in frictional case and effects of punch speed, coefficient of friction and orthotropic constants on contact stresses were presented. Zhou and Lee [68] carried out a study on dynamic contact mechanics of anisotropic half-plane loaded by both moving rigid flat and cylindrical punches. In their study, it was concluded that the coefficient of friction and the speed of the punch have significant effects on contact stresses. Contact stresses on the surface of piezomagnetic materials subjected to frictional contact by a moving rigid flat punch were determined by Zhou and Kim [69] and influences found for various values of punch speed, coefficient of friction and magnetic induction were shown. Comez [70] solved the frictionless contact problem between a moving rigid cylindrical indenter and a functionally graded layer by an analytical method.

Examination of the literature survey indicates that, there is no previous work related to the dynamic contact mechanics problems involving homogenous elastic coatings and functionally graded coatings. In the current study, we put forward an analytical method based on singular integral equation technique to solve the dynamic frictional contact problem between a moving punch and a coating made of either homogenous elastic material or functionally graded material. The coating is perfectly bonded to a substrate material. Governing partial differential equations are derived by means of putting stress displacement relations into the equations of motion. Obtained partial differential equations of elastodynamics are solved analytically utilizing Galilean and Fourier transformation techniques. Equations of elastodynamics for the contact problem is then reduced to a singular integral equation of the second kind which involves Cauchy singularity and Fredholm kernels. The singular integral equation of

the contact problem is solved numerically by a suitable expansion-collocation technique. Developed analytical procedure is verified through comparisons made to the results available in the literature and those generated by means of the finite element method. Presented numerical results clearly show the influences of punch speed, coefficient of friction, material and geometric properties upon the normal and lateral contact stresses and punch stress intensity factors. It is shown that there is significant difference between contact stresses computed considering elastodynamic and elastostatic theories. Hence, especially for contact problems involving punches sliding with relatively higher speeds, elastodynamic contact model is necessary for accurate and realistic computation of contact stresses and other contact related quantities such as punch stress intensity factors.

1.4 Scope of the Study

This study puts forward an analytical method to investigate dynamic frictional contact mechanics of functionally graded coatings indented by various type of rigid punches. There are many studies in the literature concerning static or quasi-static contact mechanics of functionally graded coatings. Although there are few studies associated with the dynamic contact mechanics of homogenous half-planes or anisotropic substrates, there has not been any work related to the dynamic contact mechanics of functionally graded coatings. Section 1.1 gives brief information about functionally graded material concept and its history. Section 1.2 describes tribology, tribological applications and potential usage of functionally graded coatings. Section 1.3 is the literature survey, which includes previous studies related to the contact mechanics of functionally graded materials and dynamic problems. As also described in literature survey, there is not any previous study investigating dynamic contact mechanics of functionally graded coatings.

In Chapter 2, problem statement is described and analytical formulation is performed to develop solutions for dynamic contact mechanics of functionally graded coatings.

Dynamic contact mechanics of homogenous elastic coatings is also examined by changing the inhomogeneity constant in general formulation. Therefore, we are aimed to solve two different problems which are:

- Dynamic frictional contact problem between a rigid moving punch and a homogenous elastic coating,
- Dynamic frictional contact problem between a rigid moving punch and a functionally graded coating.

Formulation of the problem is made considering general theory of elastodynamics. Governing partial differential equations are solved analytically using Galilean and Fourier transformation techniques. Punch sliding speed is normalized using the shear wave propagation speed in solids. Displacement fields are written in terms of unknown functions and these unknown functions are determined through imposing interface continuity and boundary conditions. Then, displacement gradients on the contact surface are written and contact problem is reduced to a singular integral equation of the second kind which has Cauchy singularity and Fredholm kernels. Asymptotic analysis is performed to extract the singularities from the kernels of the integral equation. Thus, influential parameters which determine the powers of stress singularities are found.

For both homogenous elastic coating and functionally graded coating contact problems, four different punch profiles are considered. Flat, triangular, semi-circular and cylindrical punch profiles are utilized for solutions. Solution techniques of singular integral equation are mentioned in Chapter 3. Basically, singular integral equations can be solved by a function theoretic method or numerical methods. In this study, we use numerical methods (expansion - collocation technique) to solve the singular integral equation. Normalization procedures and solution techniques for each punch profile are provided.

Singular integral equation is solved for unknown normal contact stress. Using formulation shown in Section 2.4, lateral contact stress distribution on the contact surface is found. Moreover, contact related parameters such as normalized punch load and normalized stress intensity factors are also presented. Numerical results for dynamic frictional contact problems between a rigid moving punch and homogenous elastic coatings are presented in Chapter 4. Obtained results based on present analytical method are compared to those generated using finite element analysis in elastostatic case. Comparison of the results show that obtained results are in excellent agreement with those found by finite element analysis. One more comparison study is carried out for elastodynamic contact stresses. Elastodynamic contact stresses generated by frictionless moving punch on homogenous half-plane are compared to those available in the literature and it is seen that an excellent agreement is also achieved. Hence, verification of the present analytical method is accomplished. Elastodynamic contact stress results for the moving rigid flat, triangular, semi-circular and cylindrical punches are provided in sections 4.2, 4.3, 4.4 and 4.5, respectively. The influences of various elastodynamic and geometrical parameters (punch speed, mass density ratio, coefficient of friction, relative contact length and Poisson's ratio) on contact stress results are shown.

Numerical results for dynamic frictional contact problem between a rigid moving punch and functionally graded coatings are presented in Chapter 5. Contact stresses and other contact related results in elastostatic case are compared with those available in the literature. Comparisons show that results of the present analytical study are in very good agreement with available results in the literature. Numerical results are presented for rigid flat, triangular, semi-circular and cylindrical punches and they are provided in sections 5.1, 5.2, 5.3 and 5.4, respectively. Contact stresses and other contact related results are presented for various values of punch speed, coefficient of

friction, stiffness ratio (or material inhomogeneity), coating thickness and relative contact length parameters.

In Chapter 6, we summarize the concluding remarks obtained in this study and give some recommendations and new ideas for future work.

CHAPTER 2

PROBLEM STATEMENT AND FORMULATION

There are several causes of failure in mechanical structures. Fracture and fatigue are the most common causes of these failure mechanisms. Crack initiation and propagation may happen in the regions of high stress. Investigation of contact problems has a great importance since contact regions are responsible for development of high stress and wear. In many mechanical elements such as gears, cams, cutting tools, turbine blades etc. contacts are moving rather than stationary. Generally, contact problems may be mainly categorized as deformable-deformable, rigid-deformable, frictionless, frictional, static and dynamic. In deformable-deformable contacts, two contacting bodies have similar stiffness values so they can be modeled as elastic bodies whereas in rigid-deformable contacts, one of the contacting bodies has much greater stiffness value than the other body. Hence, a contacting body which has a much greater stiffness may be modeled as a rigid punch. Contact mechanics solutions where friction is neglected may be a good approximation of well lubricated machine component contacts. Frictionless contact modeling of these type of problems is applicable and considerably simplifies the solution. However, many of the contact problems involve frictional surfaces where friction effect cannot be neglected. In this study, the frictional rigid punch slides over the coating at a constant subsonic speed and dynamic effects are considered. The speed of the sliding punch has a significant effect on contact stresses and stress intensity factors. Generally, in contact mechanics, if $\sigma_{xy} < \eta \sigma_{yy}$ a rigid stick occurs,

if $\sigma_{xy} > \eta \sigma_{yy}$ a relative slip would take place between contacting bodies, if $\sigma_{xy} = \eta \sigma_{yy}$ normal and tangential (frictional) forces are developed according to Coulomb's law.

where η denotes the coefficient of friction. For example, gas turbine blade and the sealing section may be represented by a rigid punch and a ceramic rich graded metal/low density ceramic layer. In the present work, the stiffness of the punch is assumed to be much greater than those of the coating and the substrate. Hence, contact problem is considered as a rigid deformable contact. In the analytical solution, the homogenous isotropic substrate is considered as an elastic half-plane. It is assumed that the rigid punch and the coated medium are in relative motion and dynamic effects exist. Since coefficient of friction is assumed constant along the contact surface, the tangential force $Q = \eta P$, is generated according to Coulomb's law. General schematic of the dynamic contact problems involving homogenous elastic coatings and FGM coatings are shown in Fig. 2.1.

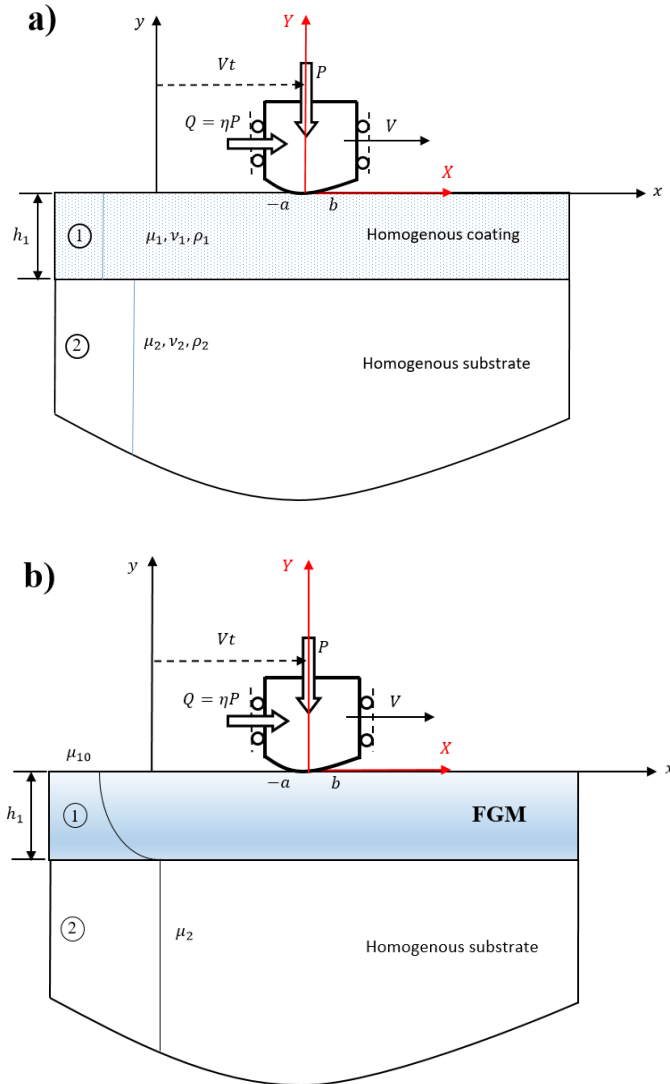


Figure 2.1: A dynamic contact problem between a coating and a rigid punch of an arbitrary profile (a) homogenous coating (b) FGM coating

A coating layer of thickness h_1 is perfectly bonded to the homogenous isotropic substrate. The shear modulus of the functionally graded coating is defined by an exponential function defined by $\mu_1(y) = \mu_{10} e^{\gamma_1 y}$, where μ_{10} is the shear modulus of FGM coating on the contact surface. Gradation of the coating is in the thickness

direction. The Poisson's ratio of the coating and the substrate are ν_1 and ν_2 , respectively. The Poisson's ratio is assumed to be constant for both FGM coating and the substrate. FGM coating and homogenous substrate are labeled as Medium 1 and Medium 2, respectively. Two elastic constants of the homogenous isotropic substrate are defined by μ_2 and κ_2 where μ_2 is the shear modulus and κ_2 is the Kolosov's constant. The inhomogeneity constant of FGM coating is denoted by γ_1 . Hence, $\mu_1(y)$ expresses the smooth behavior of the shear modulus along the thickness of the graded coating.

$$\mu_1(y) = \mu_{10} e^{\gamma_1 y}, \quad -h_1 < y < 0, \quad (2.1)$$

At the interface surface $y = -h_1$, the shear modulus of the graded coating equals to μ_{20} which denotes the shear modulus of the FGM coating at the interface between the coating and the substrate. In this study, μ_2 may not be equal to μ_{20} . Hence general formulations are derived to cover the mismatch on material properties at the interface.

$$\mu_{20} = \mu_{10} e^{-\gamma_1 h_1}, \quad (2.2)$$

$$\gamma_1 h_1 = -\ln \Gamma_1, \quad (2.3)$$

The shear modulus ratio between the interface and the contact surface of the graded coating is defined by Γ_1 . Hence, Γ_1 relatively controls the gradient of the coating depend on the shear moduli of the constituent materials.

$$\Gamma_1 = \frac{\mu_{20}}{\mu_{10}}, \quad (2.4)$$

Another parameter χ_1 is introduced to express the mismatch on material properties at the interface. It is the ratio between the shear modulus of FGM coating at the interface and that of the homogenous substrate as written below.

$$\chi_1 = \frac{\mu_{20}}{\mu_2}, \quad (2.5)$$

- When $\chi_1 = 1.0$, continuity on material properties at the interface between the coating and the substrate is satisfied. Dynamic contact mechanics analysis of functionally graded coatings are carried out by equating χ_1 to 1.0.
- When $\chi_1 \neq 1.0$, continuity on material properties at the interface between the coating and the substrate is not satisfied. Dynamic contact mechanics analysis of homogenous elastic coatings are carried out by equating χ_1 not to 1.0.

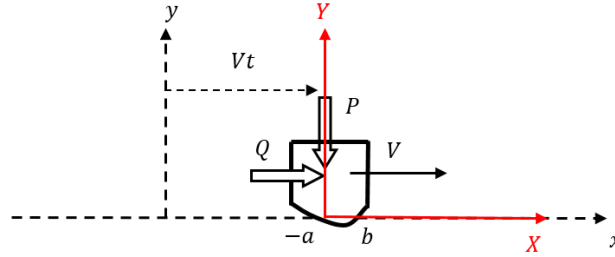


Figure 2.2: Rigid punch in stationary and moving coordinates

For the plane elastic contact problem, Hooke's law can be written for the FGM coating in the stationary coordinate system as follows:

$$\sigma_{1xx}(x, y) = \frac{\mu_{10}e^{\gamma_1 y}}{\kappa_1 - 1} \left[(\kappa_1 + 1) \frac{\partial u_1}{\partial x} + (3 - \kappa_1) \frac{\partial v_1}{\partial y} \right], \quad -h_1 < y < 0, \quad (2.6)$$

$$\sigma_{1yy}(x, y) = \frac{\mu_{10}e^{\gamma_1 y}}{\kappa_1 - 1} \left[(3 - \kappa_1) \frac{\partial u_1}{\partial x} + (\kappa_1 + 1) \frac{\partial v_1}{\partial y} \right], \quad -h_1 < y < 0, \quad (2.7)$$

$$\sigma_{1,xy}(x, y) = \mu_{10} e^{\gamma_1 y} \left[\frac{\partial u_1}{\partial y} + \frac{\partial v_1}{\partial x} \right], \quad -h_1 < y < 0, \quad (2.8)$$

For the homogenous substrate we have,

$$\sigma_{2,xx}(x, y) = \frac{\mu_2}{\kappa_2 - 1} \left[(\kappa_2 + 1) \frac{\partial u_2}{\partial x} + (3 - \kappa_2) \frac{\partial v_2}{\partial y} \right], \quad -\infty < y < -h_1, \quad (2.9)$$

$$\sigma_{2,yy}(x, y) = \frac{\mu_2}{\kappa_2 - 1} \left[(3 - \kappa_2) \frac{\partial u_2}{\partial x} + (\kappa_2 + 1) \frac{\partial v_2}{\partial y} \right], \quad -\infty < y < -h_1, \quad (2.10)$$

$$\sigma_{2,xy}(x, y) = \mu_2 \left[\frac{\partial u_2}{\partial y} + \frac{\partial v_2}{\partial x} \right], \quad -\infty < y < -h_1. \quad (2.11)$$

where

$$\kappa_1 = \begin{cases} 3 - 4\nu_1 & \text{plane strain} \\ \frac{3 - \nu_1}{1 + \nu_1} & \text{plane stress} \end{cases} \quad (2.12)$$

$$\kappa_2 = \begin{cases} 3 - 4\nu_2 & \text{plane strain} \\ \frac{3 - \nu_2}{1 + \nu_2} & \text{plane stress} \end{cases} \quad (2.13)$$

In planar elastodynamics, governing equations for the dynamic frictional contact problem in the absence of body force can be written as follows:

$$\sigma_{j,i,j} + F_i = \rho \ddot{u}_i, \quad i, j = 1, 2. \quad (2.14)$$

When equation (2.14) is expanded, for FGM coating, we may write the following equations:

$$\frac{\partial \sigma_{1,xx}}{\partial x} + \frac{\partial \sigma_{1,xy}}{\partial y} = \rho_1 \frac{\partial^2 u_1}{\partial t^2}, \quad (2.15)$$

$$\frac{\partial \sigma_{1xy}}{\partial x} + \frac{\partial \sigma_{1yy}}{\partial y} = \rho_1 \frac{\partial^2 v_1}{\partial t^2}, \quad (2.16)$$

For the homogenous substrate, the governing equations are,

$$\frac{\partial \sigma_{2xx}}{\partial x} + \frac{\partial \sigma_{2xy}}{\partial y} = \rho_2 \frac{\partial^2 u_2}{\partial t^2}, \quad (2.17)$$

$$\frac{\partial \sigma_{2xy}}{\partial x} + \frac{\partial \sigma_{2yy}}{\partial y} = \rho_2 \frac{\partial^2 v_2}{\partial t^2}. \quad (2.18)$$

where t is time and ρ represents the mass density. Along the graded coating, since the gradation is only in thickness direction, the mass density of the graded coating along the thickness direction is expressed by,

$$\rho_1(y) = \rho_{10} e^{\gamma_1 y}. \quad (2.19)$$

When stresses expressed by equations (2.6) - (2.11) are substituted into governing equilibrium equations, we obtain governing PDEs. Equations of motion for the FGM coating are,

$$\frac{(\kappa_1 + 1)}{(\kappa_1 - 1)} \frac{\partial^2 u_1}{\partial x^2} + \frac{2}{(\kappa_1 - 1)} \frac{\partial^2 v_1}{\partial x \partial y} + \gamma_1 \left(\frac{\partial u_1}{\partial y} + \frac{\partial v_1}{\partial x} \right) + \frac{\partial^2 u_1}{\partial y^2} = \frac{\rho_{10}}{\mu_{10}} \frac{\partial^2 u_1}{\partial t^2}, \quad (2.20)$$

$$\begin{aligned} \frac{\partial^2 v_1}{\partial x^2} + \gamma_1 \left[\frac{(3 - \kappa_1)}{(\kappa_1 - 1)} \frac{\partial u_1}{\partial x} + \frac{(\kappa_1 + 1)}{(\kappa_1 - 1)} \frac{\partial v_1}{\partial y} \right] + \frac{2}{(\kappa_1 - 1)} \frac{\partial^2 u_1}{\partial x \partial y} + \frac{(\kappa_1 + 1)}{(\kappa_1 - 1)} \frac{\partial^2 v_1}{\partial y^2} = \\ = \frac{\rho_{10}}{\mu_{10}} \frac{\partial^2 v_1}{\partial t^2}, \end{aligned} \quad (2.21)$$

Equations of motion for the homogenous substrate are,

$$\frac{(\kappa_1 + 1)}{(\kappa_2 - 1)} \frac{\partial^2 u_2}{\partial x^2} + \frac{2}{(\kappa_2 - 1)} \frac{\partial^2 v_2}{\partial x \partial y} + \frac{\partial^2 u_2}{\partial y^2} = \frac{\rho_2}{\mu_2} \frac{\partial^2 u_2}{\partial t^2}, \quad (2.22)$$

$$\frac{\partial^2 v_2}{\partial x^2} + \frac{2}{(\kappa_2 - 1)} \frac{\partial^2 u_1}{\partial x \partial y} + \frac{(\kappa_1 + 1)}{(\kappa_1 - 1)} \frac{\partial^2 v_2}{\partial y^2} = \frac{\rho_2}{\mu_2} \frac{\partial^2 v_2}{\partial t^2}. \quad (2.23)$$

In order to make the time dependent contact problem tractable, the ‘‘Galilean Transformation’’ is introduced. As it can be seen from Figure 2.2 that motion is only in the x -direction. Stationary coordinate system is denoted by (x, y) whereas moving coordinate system is defined by (X, Y) and moving coordinate system is attached to the rigid punch. Between the stationary and moving coordinates, one can write the following identities:

$$x = X + Vt, \quad (2.24)$$

$$y = Y. \quad (2.25)$$

where $+$ sign indicates that the direction of movement towards the right. In the analytical formulation steps, we use the translating coordinate system (X, Y) . Displacement components are $u(x, y)$ and $v(x, y)$ which can be rewritten as:

$$u(x + Vt, Y), \quad (2.26)$$

$$v(x + Vt, Y). \quad (2.27)$$

In moving coordinate system, V is the punch sliding speed. In analytical formulation and due to the requirement of the parametric studies, dimensionless punch speed is introduced. Dimensionless punch speed in FGM coating and homogenous substrate are expressed as:

$$c_1 = \frac{V}{c_{s1}}, \quad (2.28)$$

$$c_2 = \frac{V}{c_{s2}}, \quad (2.29)$$

where c_s is the shear wave propagation speed in solids. Shear wave propagation speed in FGM coating and homogenous substrate are expressed by,

$$c_{s1} = \sqrt{\frac{\mu_1(y)}{\rho_1(y)}} = \sqrt{\frac{\mu_{10} e^{\gamma_1 y}}{\rho_{10} e^{\gamma_1 y}}} = \sqrt{\frac{\mu_{10}}{\rho_{10}}}. \quad (2.30)$$

Note that in this study, the material non-homogeneity constant for the mass density should be equal to that for the shear modulus of the functionally graded material. Therefore, dimensionless speed is defined by using the properties of FGM coating on the contact surface. This assumption may be regarded as a limitation of this study. The shear wave propagation speed for the homogenous substrate is expressed as follows:

$$c_{s2} = \sqrt{\frac{\mu_2}{\rho_2}}. \quad (2.31)$$

where μ_2 is the shear modulus of the homogenous substrate and it is constant. When we substitute equations (2.28) - (2.29) into equations (2.20) - (2.23) and making further arrangements, we obtain the final form of the PDEs for the dynamic contact problem of FGM coating and the substrate. In order to solve governing partial differential equations analytically, Fourier transformation technique is used. The Fourier transformations of the displacement components for the FGM coating and the homogenous substrate can be written as follows:

$$F_1(\lambda, Y) = \int_{-\infty}^{\infty} u_1(X, Y) e^{-i\lambda X} dX, \quad (2.32)$$

$$F_2(\lambda, Y) = \int_{-\infty}^{\infty} u_2(X, Y) e^{-i\lambda X} dX, \quad (2.33)$$

$$G_1(\lambda, Y) = \int_{-\infty}^{\infty} v_1(X, Y) e^{-i\lambda X} dX, \quad (2.34)$$

$$G_2(\lambda, Y) = \int_{-\infty}^{\infty} v_2(X, Y) e^{-i\lambda X} dX. \quad (2.35)$$

where λ is the Fourier transform variable. Displacement components for the FGM coating are shown by $u_1(X, Y)$, $v_1(X, Y)$ and displacement components for the homogenous substrate are shown by $u_2(X, Y)$, $v_2(X, Y)$ and they are given by the following inverse Fourier transforms.

$$u_1(X, Y) = \frac{1}{2\pi} \int_{-\infty}^{\infty} F_1(\lambda, Y) e^{i\lambda X} d\lambda, \quad (2.36)$$

$$u_2(X, Y) = \frac{1}{2\pi} \int_{-\infty}^{\infty} F_2(\lambda, Y) e^{i\lambda X} d\lambda, \quad (2.37)$$

$$v_1(X, Y) = \frac{1}{2\pi} \int_{-\infty}^{\infty} G_1(\lambda, y) e^{i\lambda X} d\lambda, \quad (2.38)$$

$$v_2(X, Y) = \frac{1}{2\pi} \int_{-\infty}^{\infty} G_2(\lambda, y) e^{i\lambda X} d\lambda, \quad (2.39)$$

Displacement components shown by (2.36) - (2.39) are substituted into the governing partial differential equations given by (2.20) - (2.23). We obtain a system of partial differential equations for the graded coating and the homogenous substrate as follows:

$$\left(\frac{\kappa_1 + 1}{\kappa_1 - 1} - c_1^2 \right) \frac{\partial^2 u_1}{\partial X^2} + \gamma_1 \left(\frac{\partial u_1}{\partial Y} + \frac{\partial v_1}{\partial X} \right) + \frac{2}{(\kappa_1 - 1)} \frac{\partial^2 v_1}{\partial X \partial Y} + \frac{\partial^2 u_1}{\partial Y^2} = 0, \quad (2.40)$$

$$\begin{aligned} (1-c_1^2) \frac{\partial^2 v_1}{\partial X^2} + \gamma_1 \left[\frac{(3-\kappa_1) \partial u_1}{(\kappa_1-1) \partial X} + \frac{(\kappa_1+1) \partial v_1}{(\kappa_1-1) \partial Y} \right] + \frac{2}{(\kappa_1-1)} \frac{\partial^2 u_1}{\partial X \partial Y} + \\ + \frac{(\kappa_1+1) \partial^2 v_1}{(\kappa_1-1) \partial Y^2} = 0, \end{aligned} \quad (2.41)$$

$$\left(\frac{\kappa_2+1}{\kappa_2-1} - c_2^2 \right) \frac{\partial^2 u_2}{\partial X^2} + \frac{2}{(\kappa_2-1)} \frac{\partial^2 v_2}{\partial X \partial Y} + \frac{\partial^2 u_2}{\partial Y^2} = 0, \quad (2.42)$$

$$(1-c_2^2) \frac{\partial^2 v_2}{\partial X^2} + \frac{2}{(\kappa_2-1)} \frac{\partial^2 u_2}{\partial X \partial Y} + \frac{(\kappa_2+1) \partial^2 v_2}{(\kappa_2-1) \partial Y^2} = 0. \quad (2.43)$$

Assume solutions for $F_1(\lambda, Y)$ and $G_1(\lambda, Y)$ as follows:

$$F_1(\lambda, Y) = \sum_{j=1}^4 M_j(\lambda) N_j(\lambda) e^{s_j Y}, \quad (2.44)$$

$$G_1(\lambda, Y) = \sum_{j=1}^4 M_j(\lambda) e^{s_j Y}, \quad (2.45)$$

Displacement components in the FGM coating can be written using inverse Fourier transformation as shown below.

$$u_1(X, Y) = \frac{1}{2\pi} \int_{-\infty}^{\infty} \sum_{j=1}^4 M_j(\lambda) N_j(\lambda) e^{(s_j Y + i\lambda X)} d\lambda, \quad -h_1 < Y < 0, \quad -\infty < X < \infty, \quad (2.46)$$

$$v_1(X, Y) = \frac{1}{2\pi} \int_{-\infty}^{\infty} \sum_{j=1}^4 M_j(\lambda) e^{(s_j Y + i\lambda X)} d\lambda, \quad -h_1 < Y < 0, \quad -\infty < X < \infty. \quad (2.47)$$

When we substitute equations (2.46) and (2.47) and their required derivatives into the governing partial differential equations (2.40) and (2.41), the following equations are obtained:

$$\left\{ -\lambda^2 \left(\frac{\kappa_1 + 1}{\kappa_1 - 1} - c_1^2 \right) + \gamma_1 s_j + s_j^2 \right\} M_j N_j + \left\{ \frac{3 - \kappa_1}{\kappa_1 - 1} (i\lambda)(s_j) + \gamma_1 (i\lambda) + s_j (i\lambda) \right\} M_j = 0, \quad (2.48)$$

$$\left\{ -i\lambda s_j + \gamma_1 \frac{3 - \kappa_1}{\kappa_1 - 1} (i\lambda) + \frac{3 - \kappa_1}{\kappa_1 - 1} (i\lambda) s_j \right\} M_j N_j + \left\{ -(1 - c_1^2) \lambda^2 + \gamma_1 \frac{\kappa_1 + 1}{\kappa_1 - 1} (s_j) + \frac{\kappa_1 + 1}{\kappa_1 - 1} (s_j)^2 \right\} M_j = 0 \quad (2.49)$$

This equation system can be clearly expressed by the following matrix form.

$$\begin{vmatrix} -\lambda^2 \left(\frac{\kappa_1 + 1}{\kappa_1 - 1} - c_1^2 \right) + \gamma_1 s_j + s_j^2 & \left(\frac{2i\lambda}{\kappa_1 - 1} \right) s_j + \gamma_1 (i\lambda) \\ \left(\frac{2i\lambda}{\kappa_1 - 1} \right) s_j + \gamma_1 \frac{3 - \kappa_1}{\kappa_1 - 1} (i\lambda) & \frac{\kappa_1 + 1}{\kappa_1 - 1} (s_j)^2 + \gamma_1 \frac{\kappa_1 + 1}{\kappa_1 - 1} (s_j) - (1 - c_1^2) \lambda^2 \end{vmatrix} = 0. \quad (2.50)$$

Characteristic equation of the dynamic contact problem of graded coatings is obtained as follows:

$$s_j^4 + 2\gamma_1 s_j^3 + \left\{ \frac{2\lambda^2 (\kappa_1 c_1^2 - (\kappa_1 + 1))}{\kappa_1 + 1} + \gamma_1^2 \right\} s_j^2 + \left\{ 2\lambda^2 \gamma_1 \left(\frac{\kappa_1 c_1^2 - (\kappa_1 + 1)}{\kappa_1 + 1} \right) \right\} s_j + \lambda^4 \left\{ \frac{\kappa_1 (1 - c_1^2)^2 + (1 - c_1^4)}{\kappa_1 + 1} \right\} + \lambda^2 \gamma_1^2 \frac{3 - \kappa_1}{\kappa_1 + 1} = 0. \quad (2.51)$$

The roots of the characteristic equation of the dynamic contact problem can be expressed as follows:

$$s_1 = \frac{1}{2} \left\{ -\gamma_1 + \sqrt{\gamma_1^2 + 4 \left(1 - \frac{\kappa_1 c_1^2}{\kappa_1 + 1} \right) \lambda^2 + 4i\lambda \frac{\sqrt{\gamma_1^2 (3 - \kappa_1)(\kappa_1 + 1) - \lambda^2 c_1^4}}{\kappa_1 + 1}} \right\};$$

$\Re(s_1) > 0, \quad (2.52)$

$$s_2 = \frac{1}{2} \left\{ -\gamma_1 - \sqrt{\gamma_1^2 + 4 \left(1 - \frac{\kappa_1 c_1^2}{\kappa_1 + 1} \right) \lambda^2 + 4i\lambda \frac{\sqrt{\gamma_1^2 (3 - \kappa_1)(\kappa_1 + 1) - \lambda^2 c_1^4}}{\kappa_1 + 1}} \right\};$$

$\Re(s_2) < 0, \quad (2.53)$

$$s_3 = \frac{1}{2} \left\{ -\gamma_1 + \sqrt{\gamma_1^2 + 4 \left(1 - \frac{\kappa_1 c_1^2}{\kappa_1 + 1} \right) \lambda^2 - 4i\lambda \frac{\sqrt{\gamma_1^2 (3 - \kappa_1)(\kappa_1 + 1) - \lambda^2 c_1^4}}{\kappa_1 + 1}} \right\};$$

$\Re(s_3) > 0, \quad (2.54)$

$$s_4 = \frac{1}{2} \left\{ -\gamma_1 - \sqrt{\gamma_1^2 + 4 \left(1 - \frac{\kappa_1 c_1^2}{\kappa_1 + 1} \right) \lambda^2 - 4i\lambda \frac{\sqrt{\gamma_1^2 (3 - \kappa_1)(\kappa_1 + 1) - \lambda^2 c_1^4}}{\kappa_1 + 1}} \right\};$$

$\Re(s_4) < 0. \quad (2.55)$

Assume solutions for $G_2(\lambda, Y)$ and $F_2(\lambda, Y)$ of the form,

$$G_2(\lambda, Y) = (R_1 + YR_2) e^{-|\lambda|Y} + (R_3 + YR_4) e^{|\lambda|Y}, \quad (2.56)$$

$$F_2(\lambda, Y) = (R_5 + YR_6) e^{-|\lambda|Y} + (R_7 + YR_8) e^{|\lambda|Y}. \quad (2.57)$$

Constants R_1, R_2, R_3, R_6 should be equal to zero due to the regularity/radiation boundary condition. Regularity boundary condition states that displacement fields in the homogenous substrate $u_2(X, Y)$ and $v_2(X, Y)$ vanish as $Y \rightarrow \infty$. Therefore,

$$G_2(\lambda, Y) = (R_3 + YR_4) e^{|\lambda|Y}, \quad (2.58)$$

$$F_2(\lambda, Y) = (R_7 + YR_8) e^{|\lambda|Y}. \quad (2.59)$$

where R_3, R_4, R_7, R_8 are unknown functions of λ . In the final form, displacement components for the homogenous substrate can be written as follows:

$$u_2(X, Y) = \frac{1}{2\pi} \int_{-\infty}^{\infty} (R_7 + YR_8) e^{(|\lambda|Y + i\lambda X)} d\lambda, \quad -\infty < Y < -h_1, \quad -\infty < X < \infty, \quad (2.60)$$

$$v_2(X, Y) = \frac{1}{2\pi} \int_{-\infty}^{\infty} (R_3 + YR_4) e^{(|\lambda|Y + i\lambda X)} d\lambda, \quad -\infty < Y < -h_1, \quad -\infty < X < \infty, \quad (2.61)$$

Displacement components in the homogenous coating are found. We can write their required derivatives as:

$$\frac{\partial v_2(X, Y)}{\partial X} = \frac{i\lambda}{2\pi} \int_{-\infty}^{\infty} (R_3 + YR_4) e^{(|\lambda|Y + i\lambda X)} d\lambda, \quad (2.62)$$

$$\frac{\partial^2 v_2(X, Y)}{\partial X^2} = -\frac{\lambda^2}{2\pi} \int_{-\infty}^{\infty} (R_3 + YR_4) e^{(|\lambda|Y + i\lambda X)} d\lambda, \quad (2.63)$$

$$\frac{\partial u_2(X, Y)}{\partial X} = \frac{i\lambda}{2\pi} \int_{-\infty}^{\infty} (R_7 + YR_8) e^{(|\lambda|Y + i\lambda X)} d\lambda, \quad (2.64)$$

$$\frac{\partial^2 u_2(X, Y)}{\partial X \partial Y} = \frac{i\lambda}{2\pi} \int_{-\infty}^{\infty} (R_8 + |\lambda|R_7 + |\lambda|YR_8) e^{(|\lambda|Y + i\lambda X)} d\lambda, \quad (2.65)$$

$$\frac{\partial v_2(X, Y)}{\partial Y} = \frac{1}{2\pi} \int_{-\infty}^{\infty} (R_4 + |\lambda|R_3 + |\lambda|YR_4) e^{(|\lambda|Y + i\lambda X)} d\lambda, \quad (2.66)$$

$$\frac{\partial^2 v_2(X, Y)}{\partial Y^2} = \frac{1}{2\pi} \int_{-\infty}^{\infty} (|\lambda|^2 R_3 + 2|\lambda|R_4 + |\lambda|^2 YR_4) e^{(|\lambda|Y + i\lambda X)} d\lambda. \quad (2.67)$$

When equations (2.62) - (2.67) are substituted into the governing partial differential equations (2.42) - (2.43), the relations between unknown functions appear in the displacement components R_3 , R_4 , R_7 and R_8 are found. These relations can be written explicitly as follows:

$$R_8 = \frac{i \Lambda_1 |\lambda|}{2\lambda} R_4, \quad (2.68)$$

$$R_7 = \frac{i \Lambda_1 |\lambda|}{2\lambda} R_3 + \frac{i \Lambda_2 |\lambda|}{2\lambda} R_4, \quad (2.69)$$

$$\Lambda_1 = (\kappa_2 + 1) - (\kappa_2 - 1)(1 - c_2^2), \quad (2.70)$$

$$\Lambda_2 = (\kappa_2 + 1) + (\kappa_2 - 1)(1 - c_2^2). \quad (2.71)$$

After rearranging displacement fields for the functionally graded coating and the homogenous substrate, displacement field for FGM coating and the homogenous substrate become:

$$u_1(X, Y) = \frac{1}{2\pi} \int_{-\infty}^{\infty} M_j(\lambda) N_j(\lambda) e^{(s_j Y + i\lambda X)} d\lambda, \quad -h_1 < Y < 0, \quad -\infty < X < \infty, \quad (2.72)$$

$$v_1(X, Y) = \frac{1}{2\pi} \int_{-\infty}^{\infty} M_j(\lambda) e^{(s_j Y + i\lambda X)} d\lambda, \quad -h_1 < Y < 0, \quad -\infty < X < \infty. \quad (2.73)$$

where

$$N_j(\lambda) = \frac{1}{\lambda} \frac{(2 - c_1^2) i \lambda^2 - |\lambda| |\gamma_1| \sqrt{(3 - \kappa_1)(\kappa_1 + 1) - \frac{\lambda^2}{\gamma_1^2} c_1^4}}{2s_j + \gamma_1(3 - \kappa_1)}, \quad j = 1, \dots, 4, \quad (2.74)$$

$$u_2(X, Y) = \frac{1}{2\pi} \int_{-\infty}^{\infty} (R_7 + YR_8) e^{(|\lambda|Y + i\lambda X)} d\lambda, \quad -\infty < Y < -h_1, \quad -\infty < X < \infty, \quad (2.75)$$

$$v_2(X, Y) = \frac{1}{2\pi} \int_{-\infty}^{\infty} (R_3 + YR_4) e^{(|\lambda|Y + i\lambda X)} d\lambda, \quad -\infty < Y < -h_1, \quad -\infty < X < \infty. \quad (2.76)$$

Hence displacement expressions for the homogenous substrate are,

$$\begin{aligned} u_2(X, Y) = & \frac{1}{2\pi} \int_{-\infty}^{\infty} \left(\frac{i\Lambda_1 |\lambda|}{2\lambda} R_3 \right) \exp(|\lambda|Y + i\lambda X) d\lambda + \\ & + \frac{1}{2\pi} \int_{-\infty}^{\infty} \left(\frac{i\Lambda_2 |\lambda|}{2\lambda} R_4 \right) \exp(|\lambda|Y + i\lambda X) d\lambda + \\ & + \frac{1}{2\pi} \int_{-\infty}^{\infty} \left(Y \frac{i\Lambda_1 |\lambda|}{2\lambda} R_4 \right) \exp(|\lambda|Y + i\lambda X) d\lambda, \end{aligned} \quad (2.77)$$

$$v_2(X, Y) = \frac{1}{2\pi} \int_{-\infty}^{\infty} (R_3 + Y R_4) \exp(|\lambda|Y + i\lambda X) d\lambda. \quad (2.78)$$

2.1 Interface Continuity and Boundary Conditions

The unknown functions appear in the displacement components of dynamic contact problem are determined from interface matching conditions and boundary conditions along the contact surface. The unknown functions appear in the displacement equations are M_j ($j=1, \dots, 4$) and R_k ($k=3, 4$). Therefore, six unknown functions must be determined. Contact problem has four interface continuity conditions and two boundary conditions. These conditions are clearly described in this section. In the following subsections, we determine these unknown functions through utilizing continuity and boundary conditions. Since dynamic contact problem is analyzed in moving coordinate system, we need to determine the derivatives of the displacement fields in moving coordinates. Between the stationary and moving coordinate systems, partial derivatives of displacement fields with respect to the space variables can be written as follows:

Remember that $y = Y$ and $x = X + Yt$.

$$\frac{\partial^n u_1}{\partial x^n} = \frac{\partial^n u_1}{\partial X^n}, \quad \frac{\partial^n u_1}{\partial y^n} = \frac{\partial^n u_1}{\partial Y^n}, \quad n = 1, 2. \quad (2.79)$$

$$\frac{\partial^n v_1}{\partial x^n} = \frac{\partial^n v_1}{\partial X^n}, \quad \frac{\partial^n v_1}{\partial y^n} = \frac{\partial^n v_1}{\partial Y^n}, \quad n = 1, 2. \quad (2.80)$$

$$\frac{\partial^n u_2}{\partial x^n} = \frac{\partial^n u_2}{\partial X^n}, \quad \frac{\partial^n u_2}{\partial y^n} = \frac{\partial^n u_2}{\partial Y^n}, \quad n = 1, 2. \quad (2.81)$$

$$\frac{\partial^n v_2}{\partial x^n} = \frac{\partial^n v_2}{\partial X^n}, \quad \frac{\partial^n v_2}{\partial y^n} = \frac{\partial^n v_2}{\partial Y^n}, \quad n = 1, 2. \quad (2.82)$$

Stress and displacement relations are written in the moving coordinate system as follows:

$$\sigma_{1xx}(X, Y) = \frac{\mu_{10} e^{\gamma Y}}{\kappa_1 - 1} \left[(\kappa_1 + 1) \frac{\partial u_1}{\partial X} + (3 - \kappa_1) \frac{\partial v_1}{\partial Y} \right], \quad -h_1 < Y < 0, \quad (2.83)$$

$$\sigma_{1yy}(X, Y) = \frac{\mu_{10} e^{\gamma Y}}{\kappa_1 - 1} \left[(3 - \kappa_1) \frac{\partial u_1}{\partial X} + (\kappa_1 + 1) \frac{\partial v_1}{\partial Y} \right], \quad -h_1 < Y < 0, \quad (2.84)$$

$$\sigma_{1xy}(X, Y) = \mu_{10} e^{\gamma Y} \left[\frac{\partial u_1}{\partial Y} + \frac{\partial v_1}{\partial X} \right], \quad -h_1 < Y < 0, \quad (2.85)$$

$$\sigma_{2xx}(X, Y) = \frac{\mu_2}{\kappa_2 - 1} \left[(\kappa_2 + 1) \frac{\partial u_2}{\partial X} + (3 - \kappa_2) \frac{\partial v_2}{\partial Y} \right], \quad -\infty < Y < -h_1, \quad (2.86)$$

$$\sigma_{2yy}(X, Y) = \frac{\mu_2}{\kappa_2 - 1} \left[(3 - \kappa_2) \frac{\partial u_2}{\partial X} + (\kappa_2 + 1) \frac{\partial v_2}{\partial Y} \right], \quad -\infty < Y < -h_1, \quad (2.87)$$

$$\sigma_{2xy}(X, Y) = \mu_4 \left[\frac{\partial u_2}{\partial Y} + \frac{\partial v_2}{\partial X} \right], \quad -\infty < Y < -h_1. \quad (2.88)$$

Formulation of the contact problem is made considering the generality. The generalized problem is the FGM coating/homogenous substrate problem. Following statements indicate the generality of the problem.

- Formulations are derived for functionally graded coating and the homogenous substrate structure. However, setting the material inhomogeneity constant γ_1 to zero, addressed contact problem becomes homogenous elastic coating and homogenous substrate or homogenous half-plane problems.

Homogenous coating problem is obtained by the following change of parameters:

$$\gamma_1 = 0.0, \quad \Gamma_1 = \frac{\mu_{20}}{\mu_{10}} = 1.0, \quad \chi_1 = \frac{\mu_{20}}{\mu_2} \neq 1.0.$$

Homogenous half-plane is obtained by the following change of variables:

$$\gamma_1 = 0.0, \quad \Gamma_1 = \frac{\mu_{20}}{\mu_{10}} = 1.0, \quad \chi_1 = \frac{\mu_{20}}{\mu_2} = 1.0.$$

Functionally graded coating problem is obtained by the following change of variables:

$$\gamma_1 \neq 0.0, \quad \Gamma_1 = \frac{\mu_{20}}{\mu_{10}} \neq 1.0, \quad \chi_1 = \frac{\mu_{20}}{\mu_2} = 1.0.$$

- The shear modulus at the interface of the functionally graded coating is calculated by $\mu_{20} = \mu_{10} e^{-\gamma_1 h_1}$, and this shear modulus may not be equal to the shear modulus of homogenous substrate defined by μ_2 .
- Poisson's ratio of the functionally graded coating is denoted by ν_1 and variation of the Poisson's ratio along the thickness of the coating is ignored since it has very small effect on contact stresses [46]. On the other hand, the Poisson's ratio

of the functionally graded coating ν_1 may not be equal to the Poisson's ratio of the homogenous substrate which is defined by ν_2 .

2.1.1 Continuity Conditions along the Interface

Lateral and normal displacement components in the functionally graded coating were defined by $u_1(X, Y)$ and $v_1(X, Y)$. Lateral and normal displacement components in the homogenous substrate were defined by $u_2(X, Y)$ and $v_2(X, Y)$.

First interface matching condition states that the lateral displacement component in the FGM coating must be equal to the lateral displacement component in the homogenous substrate and this condition can be explicitly written as follows:

$$u_1(X, -h_1) = u_2(X, -h_1), \quad (2.89)$$

$$\left(\frac{i\Lambda_1 |\lambda| R_3}{2\lambda} + \frac{i\Lambda_2 R_4}{2\lambda} - \frac{i\Lambda_1 |\lambda| h R_4}{2\lambda} \right) e^{(-|\lambda|h)} - \sum_{j=1}^4 M_j(\lambda) N_j(\lambda) e^{(-s_j h)} = 0. \quad (2.90)$$

Second interface matching condition states that the normal displacement component in the FGM coating must be equal to the normal displacement component in the homogenous substrate. This condition can be clearly written as follows:

$$v_1(X, -h_1) = v_2(X, -h_1), \quad (2.91)$$

$$(R_3 - h R_4) e^{(-|\lambda|h)} - \sum_{j=1}^4 M_j(\lambda) e^{(-s_j h)} = 0. \quad (2.92)$$

In addition to these conditions, normal and shear stress components must be equal at the interface.

The following equation indicates that the normal stress component in the FGM coating must be equal to the normal stress component in the homogenous coating at the interface,

$$\sigma_{1YY}(X, -h_1) = \sigma_{2YY}(X, -h_1). \quad (2.93)$$

By substituting displacement components into the normal stress expressions shown by equation (2.84) - (2.87), normal stress for the FGM coating and the homogenous substrate can be given by,

$$\begin{aligned} \sigma_{1YY}(X, Y) = & \frac{\mu_{10} e^{\gamma_1 Y}}{\kappa_1 - 1} \left[(3 - \kappa_1) \frac{\partial}{\partial X} \left\{ \frac{1}{2\pi} \int_{-\infty}^{\infty} \sum_{j=1}^4 M_j N_j \exp(s_j Y + i\lambda X) d\lambda \right\} \right. \\ & \left. + (\kappa_1 + 1) \frac{\partial}{\partial Y} \left\{ \frac{1}{2\pi} \int_{-\infty}^{\infty} \sum_{j=1}^4 M_j \exp(s_j Y + i\lambda X) d\lambda \right\} \right], \end{aligned} \quad (2.94)$$

$$\begin{aligned} \sigma_{2YY}(X, Y) = & \frac{\mu_2}{\kappa_2 - 1} \left[(3 - \kappa_2) \frac{\partial}{\partial X} \left(\frac{1}{2\pi} \left(\frac{i\Lambda_1 |\lambda|}{2\lambda} R_3 + \frac{i\Lambda_2 |\lambda|}{2\lambda} R_4 + Y \frac{i\Lambda_1 |\lambda|}{2\lambda} R_4 \right) \right) \right] \times \\ & \times \exp(|\lambda| Y + i\lambda X) d\lambda + \\ & + (\kappa_2 + 1) \frac{\partial}{\partial Y} \left\{ \frac{1}{2\pi} \int_{-\infty}^{\infty} (R_4 + |\lambda| (R_3 + Y R_4)) \exp(|\lambda| Y + i\lambda X) d\lambda \right\} \right]. \end{aligned} \quad (2.95)$$

The shear stress in the FGM coating must be equal to the shear stress in the homogenous substrate at the interface. This equality can be shown by the following equation:

$$\sigma_{1XY}(X, -h_1) = \sigma_{2XY}(X, -h_1), \quad (2.96)$$

By substituting displacement components into the shear stress expression shown by equation (2.85) - (2.88), shear stress for the FGM coating and the homogenous substrate can be given by,

$$\begin{aligned} \sigma_{1XY}(X, Y) = \mu_{10} e^{\gamma Y} & \left[\frac{\partial}{\partial Y} \left\{ \frac{1}{2\pi} \int_{-\infty}^{\infty} \sum_{j=1}^4 M_j N_j \exp(s_j Y + i\lambda X) d\lambda \right\} \right. \\ & \left. + \frac{\partial}{\partial X} \left\{ \frac{1}{2\pi} \int_{-\infty}^{\infty} \sum_{j=1}^4 M_j \exp(s_j Y + i\lambda X) d\lambda \right\} \right], \end{aligned} \quad (2.97)$$

$$\begin{aligned} \sigma_{2XY}(X, Y) = \mu_2 & \left[\frac{\partial}{\partial Y} \left(\frac{1}{2\pi} \left(\frac{i\Lambda_1 |\lambda|}{2\lambda} R_3 + \frac{i\Lambda_2}{2\lambda} R_4 + Y \frac{i\Lambda_1 |\lambda|}{2\lambda} R_4 \right) \right) \times \right. \\ & \times \exp(|\lambda| Y + i\lambda X) d\lambda \\ & \left. + \frac{\partial}{\partial X} \left\{ \frac{1}{2\pi} \int_{-\infty}^{\infty} (R_3 + Y R_4) \exp(|\lambda| Y + i\lambda X) d\lambda \right\} \right]. \end{aligned} \quad (2.98)$$

Remind that unknown functions appear in displacement fields are M_1, M_2, M_3, M_4, R_3 and R_4 . Thus, six unknown functions must be determined in total. Four of them are determined from the prescribed continuity conditions along the coating interface. The remaining two unknown functions are determined from the boundary conditions.

Let's define new parameters such as:

$$R_3 \exp(-|\lambda| h_1) = R_3^*, \quad (2.99)$$

$$R_4 \exp(-|\lambda| h_1) = R_4^*, \quad (2.100)$$

$$M_j N_j \exp(-s_j h_1) = M_j^* N_j, \quad (2.101)$$

$$M_j \exp(-s_j h_1) = M_j^*. \quad (2.102)$$

When lateral displacement continuity condition shown by equation (2.89) is imposed, the following equation is obtained:

$$\frac{i\Lambda_1 |\lambda|}{2\lambda} R_3^* + \frac{i\Lambda_2 - i\Lambda_1 |\lambda| h_1}{2\lambda} R_4^* = N_1 M_1^* + N_2 M_2^* + N_3 M_3^* + N_4 M_4^*. \quad (2.103)$$

When normal displacement continuity condition shown by (2.91) is imposed, the following equation is obtained:

$$R_3^* - h_1 R_4^* = M_1^* + M_2^* + M_3^* + M_4^*. \quad (2.104)$$

Equations found from displacement continuity conditions can be written in matrix form as follows:

$$\begin{bmatrix} \frac{i\Lambda_1|\lambda|}{2\lambda} & \frac{i\Lambda_2 - i\Lambda_1|\lambda|h_1}{2\lambda} \\ 1 & -h_1 \end{bmatrix} \begin{Bmatrix} R_3^* \\ R_4^* \end{Bmatrix} = \begin{bmatrix} N_1 & N_2 & N_3 & N_4 \\ 1 & 1 & 1 & 1 \end{bmatrix} \begin{Bmatrix} M_1^* \\ M_2^* \\ M_3^* \\ M_4^* \end{Bmatrix}. \quad (2.105)$$

It is required to find R_3^* and R_4^* . Let's define the coefficient matrix of the linear system as follows:

$$[A] = \begin{bmatrix} \frac{i\Lambda_1|\lambda|}{2\lambda} & \frac{i\Lambda_2 - i\Lambda_1|\lambda|h_1}{2\lambda} \\ 1 & -h_1 \end{bmatrix}, \quad (2.106)$$

$$\begin{Bmatrix} R_3^* \\ R_4^* \end{Bmatrix} = [A]^{-1} \begin{bmatrix} N_1 & N_2 & N_3 & N_4 \\ 1 & 1 & 1 & 1 \end{bmatrix} \begin{Bmatrix} M_1^* \\ M_2^* \\ M_3^* \\ M_4^* \end{Bmatrix}, \quad (2.107)$$

$$\begin{Bmatrix} R_3^* \\ R_4^* \end{Bmatrix} = \begin{bmatrix} 1+h_1b_1 & 1+h_1b_2 & 1+h_1b_3 & 1+h_1b_4 \\ b_1 & b_2 & b_3 & b_4 \end{bmatrix} \begin{Bmatrix} M_1^* \\ M_2^* \\ M_3^* \\ M_4^* \end{Bmatrix}. \quad (2.108)$$

Then, b_1 , b_2 , b_3 and b_4 can be found from the matrix inversion.

$$b_1 = -\frac{\Lambda_1 |\lambda|}{\Lambda_2} - \frac{2i\lambda}{\Lambda_2} N_1, \quad (2.109)$$

$$b_2 = -\frac{\Lambda_1 |\lambda|}{\Lambda_2} - \frac{2i\lambda}{\Lambda_2} N_2, \quad (2.110)$$

$$b_3 = -\frac{\Lambda_1 |\lambda|}{\Lambda_2} - \frac{2i\lambda}{\Lambda_2} N_3, \quad (2.111)$$

$$b_4 = -\frac{\Lambda_1 |\lambda|}{\Lambda_2} - \frac{2i\lambda}{\Lambda_2} N_4. \quad (2.112)$$

In compact form equations (2.109)-(2.112) can be written as follows:

$$b_j = -\frac{\Lambda_1 |\lambda|}{\Lambda_2} - \frac{2i\lambda}{\Lambda_2} N_j(\lambda), \quad j=1, \dots, 4. \quad (2.113)$$

Two of unknown functions denoted by R_3^* and R_4^* can be written explicitly by the following equations:

$$R_3^* = (1 + h_1 b_1) M_1^* + (1 + h_1 b_2) M_2^* + (1 + h_1 b_3) M_3^* + (1 + h_1 b_4) M_4^*, \quad (2.114)$$

$$R_4^* = b_1 M_1^* + b_2 M_2^* + b_3 M_3^* + b_4 M_4^*. \quad (2.115)$$

The normal stress component in the FGM coating at the interface can be expressed by,

$$\begin{aligned} \sigma_{IYY}(X, -h_1) = & \frac{\mu_{10} e^{-\gamma_1 h_1}}{\kappa_1 - 1} \left[(3 - \kappa_1) \left\{ \frac{i\lambda}{2\pi} \int_{-\infty}^{\infty} \sum_{j=1}^4 M_j N_j \exp(-s_j h_1 + i\lambda X) d\lambda \right\} \right. \\ & \left. + (\kappa_1 + 1) \left\{ \frac{1}{2\pi} \int_{-\infty}^{\infty} \sum_{j=1}^4 s_j M_j \exp(-s_j h_1 + i\lambda X) d\lambda \right\} \right]. \end{aligned} \quad (2.116)$$

The normal stress component in the homogenous coating at the interface can be expressed by,

$$\begin{aligned}
\sigma_{2YY}(X, -h_1) = & \frac{\mu_2}{\kappa_2 - 1} \left[(3 - \kappa_2) \left(\frac{i\lambda}{2\pi} \left(\frac{i\Lambda_1 |\lambda|}{2\lambda} R_3 + \frac{i\Lambda_2 |\lambda|}{2\lambda} R_4 - h_1 \frac{i\Lambda_1 |\lambda|}{2\lambda} R_4 \right) \right) \right] \times \\
& \times \exp(-|\lambda| h_1 + i\lambda X) d\lambda \\
& + (\kappa_2 + 1) \left\{ \frac{1}{2\pi} \int_{-\infty}^{\infty} (R_4 + |\lambda| R_3 - |\lambda| h_1 R_4) \exp(-|\lambda| h_1 + i\lambda X) d\lambda \right\} \Bigg].
\end{aligned} \tag{2.117}$$

The shear modulus of FGM coating at the interface surface can be calculated by the following equation:

$$\mu_{10} e^{-\gamma_1 h_1} = \mu_{20}, \tag{2.118}$$

Note that μ_{20} shows the shear modulus of the FGM coating at the interface surface. The shear modulus of the FGM coating at the interface may not be equal to that of homogenous substrate. The ratio between the shear modulus of FGM coating and the homogenous substrate at the interface is defined by,

$$\chi_1 = \frac{\mu_{20}}{\mu_2}. \tag{2.119}$$

In this study, χ_1 is taken as 1.0 for functionally graded coating contact problem and χ_1 is assumed to be different from 1.0 for homogenous coating contact problem.

When normal stress continuity condition imposed, the following equation is obtained:

$$\begin{aligned}
\chi_1 \frac{\kappa_2 - 1}{\kappa_1 - 1} & \left(\left[(3 - \kappa_1) i\lambda \sum_{j=1}^4 M_j^* N_j + (\kappa_1 + 1) s_j \sum_{j=1}^4 M_j^* \right] \right) \\
= (3 - \kappa_2) & \left\{ \left(\frac{\Lambda_1 |\lambda|}{2} R_3^* - \frac{\Lambda_2}{2} R_4^* + \frac{\Lambda_1 |\lambda| h_1}{2} R_4^* \right) + (\kappa_2 + 1) (|\lambda| R_3^* + R_4^* - |\lambda| h_1 R_4^*) \right\}.
\end{aligned} \tag{2.120}$$

Substituting equations (2.116) and (2.117) into the normal stress continuity condition expressed by equation (2.93) and after performing lengthy mathematical manipulations, we have found the coefficients of unknown functions M_1^* , M_2^* , M_3^* and M_4^* .

The coefficient of M_1^* ,

$$\begin{aligned} & \left((\kappa_2 + 1)|\lambda| + \frac{-2(\kappa_2 + 1)i\lambda N_1 + K_1|\lambda|}{\Lambda_2} + (3 - \kappa_2)i\lambda N_1 - \right. \\ & \left. - \chi_1 \frac{\kappa_2 - 1}{\kappa_1 - 1} [(3 - \kappa_1)i\lambda N_1 + (\kappa_1 + 1)s_1] \right), \end{aligned} \quad (2.121)$$

The coefficient of M_2^* ,

$$\begin{aligned} & \left(-(\kappa_2 + 1)|\lambda| + \frac{2(\kappa_2 + 1)i\lambda N_2 - K_1|\lambda|}{\Lambda_2} - (3 - \kappa_2)i\lambda N_2 + \right. \\ & \left. + \chi_1 \frac{\kappa_2 - 1}{\kappa_1 - 1} [(3 - \kappa_1)i\lambda N_2 + (\kappa_1 + 1)s_2] \right), \end{aligned} \quad (2.122)$$

The coefficient of M_3^* ,

$$\begin{aligned} & \left((\kappa_2 + 1)|\lambda| + \frac{-2(\kappa_2 + 1)i\lambda N_3 + K_1|\lambda|}{\Lambda_2} + (3 - \kappa_2)i\lambda N_3 - \right. \\ & \left. - \chi_1 \frac{\kappa_2 - 1}{\kappa_1 - 1} [(3 - \kappa_1)i\lambda N_3 + (\kappa_1 + 1)s_3] \right), \end{aligned} \quad (2.123)$$

The coefficient of M_4^* ,

$$\begin{aligned} & \left(-(\kappa_2 + 1)|\lambda| + \frac{2(\kappa_2 + 1)i\lambda N_4 - K_1|\lambda|}{\Lambda_2} + (3 - \kappa_2)i\lambda N_4 + \right. \\ & \left. + \chi_1 \frac{\kappa_2 - 1}{\kappa_1 - 1} [(3 - \kappa_1)i\lambda N_4 + (\kappa_1 + 1)s_4] \right), \end{aligned} \quad (2.124)$$

where

$$K_1 = (\kappa_2^2 - 1)(1 - c_2^2) - (\kappa_2 + 1)^2. \quad (2.125)$$

The mathematical procedure which was done for the normal stress continuity condition is also performed for the shear stress continuity at the interface.

$$\begin{aligned} \sigma_{1XY}(X, -h_1) = \mu_{10} e^{-\gamma_1 h_1} & \left[\left\{ \frac{1}{2\pi} \int_{-\infty}^{\infty} \sum_{j=1}^4 (s_j) M_j N_j \exp(-s_j h_1 + i\lambda X) d\lambda \right\} + \right. \\ & \left. + \left\{ \frac{i\lambda}{2\pi} \int_{-\infty}^{\infty} \sum_{j=1}^4 M_j \exp(-s_j h_1 + i\lambda X) d\lambda \right\} \right], \end{aligned} \quad (2.126)$$

$$\begin{aligned} \sigma_{2XY}(X, -h_1) = \mu_2 & \left[\frac{\partial}{\partial Y} \left(\frac{1}{2\pi} \left(\frac{i\Lambda_1 |\lambda|}{2\lambda} R_3 + \frac{i\Lambda_2}{2\lambda} R_4 - h_1 \frac{i\Lambda_1 |\lambda|}{2\lambda} R_4 \right) \right) \times \right. \\ & \times \exp(-|\lambda| h_1 + i\lambda X) d\lambda \\ & \left. + \frac{\partial}{\partial X} \left\{ \frac{1}{2\pi} \int_{-\infty}^{\infty} \sum_{j=1}^4 (R_3 - h_1 R_4) \exp(-|\lambda| h_1 + i\lambda X) d\lambda \right\} \right]. \end{aligned} \quad (2.127)$$

When shear stress continuity condition is imposed, the coefficients of M_1^* , M_2^* , M_3^* and M_4^* are found as follows:

The coefficient of M_1^* ,

$$\begin{aligned} & \left(\frac{i\{-(\kappa_2 + 1)^2 + (1 - c_2^2)K_2 + 2\Lambda_2 \left(1 - \chi_1 \frac{\kappa_2 - 1}{\kappa_1 - 1}\right)\} |\lambda|^2}{2\lambda\Lambda_2} \right) + \\ & + \left(\frac{2(\kappa_2 + 1)|\lambda|N_1 - \chi_1 s_1 N_1 \Lambda_2}{\Lambda_2} \right), \end{aligned} \quad (2.128)$$

The coefficient of M_2^* ,

$$\left(\frac{-i\{-(\kappa_2 + 1)^2 + (1 - c_2^2)\mathbf{K}_2 + 2\Lambda_2 \left(1 - \chi_1 \frac{\kappa_2 - 1}{\kappa_1 - 1}\right)\}|\lambda|^2}{2\lambda\Lambda_2} \right) + \left(\frac{-2(\kappa_2 + 1)|\lambda|N_2 + \chi_1 s_2 N_2 \Lambda_2}{\Lambda_2} \right), \quad (2.129)$$

The coefficient of M_3^* ,

$$\left(\frac{i\{-(\kappa_2 + 1)^2 + (1 - c_2^2)\mathbf{K}_2 + 2\Lambda_2 \left(1 - \chi_1 \frac{\kappa_2 - 1}{\kappa_1 - 1}\right)\}|\lambda|^2}{2\lambda\Lambda_2} \right) + \left(\frac{2(\kappa_2 + 1)|\lambda|N_3 - \chi_1 s_3 N_3 \Lambda_2}{\Lambda_2} \right), \quad (2.130)$$

The coefficient of M_4^* ,

$$\left(\frac{-i\{-(\kappa_2 + 1)^2 + (1 - c_2^2)\mathbf{K}_2 + 2\Lambda_2 \left(1 - \chi_1 \frac{\kappa_2 - 1}{\kappa_1 - 1}\right)\}|\lambda|^2}{2\lambda\Lambda_2} \right) + \left(\frac{-2(\kappa_2 + 1)|\lambda|N_4 + \chi_1 s_4 N_4 \Lambda_2}{\Lambda_2} \right), \quad (2.131)$$

where

$$\mathbf{K}_2 = 2(\kappa_2^2 - 1) - (\kappa_2 - 1)^2(1 - c_2^2). \quad (2.132)$$

Normal and shear stress continuity conditions at the interface can be written in a more compact form as follows:

$$q_1 M_2^* + q_2 M_4^* = w_1 M_1^* + w_2 M_3^*, \quad (2.133)$$

$$q_3 M_2^* + q_4 M_4^* = w_3 M_1^* + w_4 M_3^*, \quad (2.134)$$

$$\begin{bmatrix} q_1 & q_2 \\ q_3 & q_4 \end{bmatrix} \begin{Bmatrix} M_2^* \\ M_4^* \end{Bmatrix} = \begin{bmatrix} w_1 & w_2 \\ w_3 & w_4 \end{bmatrix} \begin{Bmatrix} M_1^* \\ M_3^* \end{Bmatrix}, \quad (2.135)$$

where

$$q_1 = \left[\frac{\Lambda_2 [\chi_1 \frac{\kappa_2 - 1}{\kappa_1 - 1} (3 - \kappa_1) + (\kappa_2 - 3)] + 2(\kappa_2 + 1)}{\Lambda_2} \right] i\lambda N_2 + \chi_1 \frac{\kappa_2 - 1}{\kappa_1 - 1} (\kappa_1 + 1) s_2 - \left(\frac{2(\kappa_2^2 - 1)(1 - c_2^2)}{\Lambda_2} \right) |\lambda|, \quad (2.136)$$

$$q_2 = \left[\frac{\Lambda_2 [\chi_1 \frac{\kappa_2 - 1}{\kappa_1 - 1} (3 - \kappa_1) + (\kappa_2 - 3)] + 2(\kappa_2 + 1)}{\Lambda_2} \right] i\lambda N_4 + \chi_1 \frac{\kappa_2 - 1}{\kappa_1 - 1} (\kappa_1 + 1) s_4 - \left(\frac{2(\kappa_2^2 - 1)(1 - c_2^2)}{\Lambda_2} \right) |\lambda|, \quad (2.137)$$

$$q_3 = \frac{-i \left\{ -(\kappa_2 + 1)^2 + (1 - c_2^2) \mathbf{K}_2 + 2(\Lambda_2 \left(1 - \chi_1 \frac{\kappa_2 - 1}{\kappa_1 - 1} \right)) \right\} |\lambda|^2}{2\lambda \Lambda_2} - \frac{2(\kappa_2 + 1) |\lambda| N_2}{\Lambda_2} + \chi_1 \frac{\kappa_2 - 1}{\kappa_1 - 1} s_2 N_2, \quad (2.138)$$

$$q_4 = \frac{-i \left\{ -(\kappa_2 + 1)^2 + (1 - c_2^2) \mathbf{K}_2 + 2(\Lambda_2 \left(1 - \chi_1 \frac{\kappa_2 - 1}{\kappa_1 - 1} \right)) \right\} |\lambda|^2}{2\lambda \Lambda_2} - \frac{2(\kappa_2 + 1) |\lambda| N_4}{\Lambda_2} + \chi_1 \frac{\kappa_2 - 1}{\kappa_1 - 1} s_4 N_4, \quad (2.139)$$

$$w_1 = \left[\frac{\Lambda_2 \left(-\chi_1 \frac{\kappa_2 - 1}{\kappa_1 - 1} (3 - \kappa_1) + (3 - \kappa_2) \right) - 2(\kappa_2 + 1)}{\Lambda_2} \right] i\lambda N_1 - \chi_1 \frac{\kappa_2 - 1}{\kappa_1 - 1} (\kappa_1 + 1) s_1 \quad (2.140)$$

$$+ \left(\frac{2(\kappa_2^2 - 1)(1 - c_2^2)}{\Lambda_2} \right) |\lambda|,$$

$$w_2 = \left[\frac{\Lambda_2 \left[-\chi_1 \frac{\kappa_2 - 1}{\kappa_1 - 1} (3 - \kappa_1) + (3 - \kappa_2) \right] - 2(\kappa_2 + 1)}{\Lambda_2} \right] i\lambda N_3 - \chi_1 \frac{\kappa_2 - 1}{\kappa_1 - 1} (\kappa_1 + 1) s_4 \quad (2.141)$$

$$+ \left(\frac{2(\kappa_2^2 - 1)(1 - c_2^2)}{\Lambda_2} \right) |\lambda|,$$

$$w_3 = \frac{i \left\{ -(\kappa_2 + 1)^2 + (1 - c_2^2) K_2 + 2\Lambda_2 \left(1 - \chi_1 \frac{\kappa_2 - 1}{\kappa_1 - 1} \right) \right\} |\lambda|^2}{2\lambda \Lambda_2} + \frac{2(\kappa_2 + 1) |\lambda| N_1}{\Lambda_2} \quad (2.142)$$

$$- \chi_1 \frac{\kappa_2 - 1}{\kappa_1 - 1} s_1 N_1,$$

$$w_4 = \frac{i \left\{ -(\kappa_2 + 1)^2 + (1 - c_2^2) K_2 + 2\Lambda_2 \left(1 - \chi_1 \frac{\kappa_2 - 1}{\kappa_1 - 1} \right) \right\} |\lambda|^2}{2\lambda \Lambda_2} + \frac{2(\kappa_2 + 1) |\lambda| N_3}{\Lambda_2} \quad (2.143)$$

$$- \chi_1 \frac{\kappa_2 - 1}{\kappa_1 - 1} s_3 N_3.$$

In order to solve this linear algebraic equation system for M_2^* and M_4^* , we need to find the inverse of matrix $[q]$.

$$[q] \begin{Bmatrix} M_2^* \\ M_4^* \end{Bmatrix} = [w] \begin{Bmatrix} M_1^* \\ M_3^* \end{Bmatrix}, \quad (2.144)$$

$$\begin{Bmatrix} M_2^* \\ M_4^* \end{Bmatrix} = [q]^{-1} [w] \begin{Bmatrix} M_1^* \\ M_3^* \end{Bmatrix}, \quad (2.145)$$

where

$$[q]^{-1} = \frac{1}{q_1 q_4 - q_2 q_3} \begin{bmatrix} q_4 & -q_2 \\ -q_3 & q_1 \end{bmatrix}. \quad (2.146)$$

Let's define Δ_1 as:

$$\Delta_1 = q_1 q_4 - q_2 q_3. \quad (2.147)$$

$$\begin{Bmatrix} M_2^* \\ M_4^* \end{Bmatrix} = \frac{1}{\Delta_1} \begin{bmatrix} q_4 & -q_2 \\ -q_3 & q_1 \end{bmatrix} \begin{bmatrix} w_1 & w_2 \\ w_3 & w_4 \end{bmatrix} \begin{Bmatrix} M_1^* \\ M_3^* \end{Bmatrix}, \quad (2.148)$$

$$\begin{Bmatrix} M_2^* \\ M_4^* \end{Bmatrix} = \frac{1}{\Delta_1} \begin{bmatrix} q_4 w_1 - q_2 w_3 & q_4 w_2 - q_2 w_4 \\ -q_3 w_1 + q_1 w_3 & -q_3 w_2 + q_1 w_4 \end{bmatrix} \begin{Bmatrix} M_1^* \\ M_3^* \end{Bmatrix}, \quad (2.149)$$

In the final form, M_2^* and M_4^* can be rewritten below,

$$\begin{Bmatrix} M_2^* \\ M_4^* \end{Bmatrix} = \frac{1}{\Delta_1} \begin{bmatrix} r_1 & r_2 \\ r_3 & r_4 \end{bmatrix} \begin{Bmatrix} M_1^* \\ M_3^* \end{Bmatrix}, \quad (2.150)$$

where

$$r_1 = q_4 w_1 - q_2 w_3, \quad (2.151)$$

$$r_2 = q_4 w_2 - q_2 w_4, \quad (2.152)$$

$$r_3 = -q_3 w_1 + q_1 w_3, \quad (2.153)$$

$$r_4 = -q_3 w_2 + q_1 w_4, \quad (2.154)$$

$$\Delta_1 = q_1 q_4 - q_2 q_3. \quad (2.155)$$

Consequently, using the interface continuity conditions (displacement continuity conditions and the stress continuity conditions), M_2^* , M_4^* , R_3^* and R_4^* are determined. In conclusion, M_2^* , M_4^* , R_3^* and R_4^* are given as follows:

$$R_3^* = (1+h_1b_1)M_1^* + (1+h_1b_2)M_2^* + (1+h_1b_3)M_3^* + (1+h_1b_4)M_4^*, \quad (2.156)$$

$$R_4^* = b_1M_1^* + b_2M_2^* + b_3M_3^* + b_4M_4^*, \quad (2.157)$$

$$\begin{Bmatrix} M_2^* \\ M_4^* \end{Bmatrix} = \frac{1}{\Delta_1} \begin{bmatrix} r_1 & r_2 \\ r_3 & r_4 \end{bmatrix} \begin{Bmatrix} M_1^* \\ M_3^* \end{Bmatrix}. \quad (2.158)$$

M_1^* and M_3^* are already unknown functions and they are determined from the boundary conditions.

2.1.2 Boundary Conditions

Normal and shear stress outside the contact region must be zero since outside the contact surface is stress free. In the contact region, stress components can be described as:

$$\sigma_{iYY}(X,0) = \sigma_{iXY}(X,0) = 0, \quad -\infty < X < -a \quad \text{and} \quad b < X < \infty, \quad (2.159)$$

$$\sigma_{iYY}(X,0) = \sigma(X), \quad -a < X < b, \quad (2.160)$$

$$\sigma_{iXY}(X,0) = \eta \sigma(X), \quad -a < X < b, \quad (2.161)$$

The two remaining unknown functions (i.e. M_1^* and M_3^*) for the dynamic contact problem are determined using the boundary conditions on the contact surface. M_1^* and M_3^* come from the tractions along the contact surface. Remember normal and shear stress expressions for the graded coating as provided below.

$$\begin{aligned} \sigma_{1YY}(X, Y) = & \frac{\mu_{10} e^{\gamma_1 Y}}{\kappa_1 - 1} \left[(3 - \kappa_1) \left\{ \frac{i\lambda}{2\pi} \int_{-\infty}^{\infty} \sum_{j=1}^4 M_j N_j \exp(s_j Y + i\lambda X) d\lambda \right\} + \right. \\ & \left. + (\kappa_1 + 1) \left\{ \frac{1}{2\pi} \int_{-\infty}^{\infty} \sum_{j=1}^4 (s_j) M_j \exp(s_j Y + i\lambda X) d\lambda \right\} \right], \end{aligned} \quad (2.162)$$

$$\begin{aligned} \sigma_{1XY}(X, Y) = & \mu_{10} e^{\gamma_1 Y} \left[\left\{ \frac{1}{2\pi} \int_{-\infty}^{\infty} \sum_{j=1}^4 (s_j) M_j N_j \exp(s_j Y + i\lambda X) d\lambda \right\} + \right. \\ & \left. + \left\{ \frac{i\lambda}{2\pi} \int_{-\infty}^{\infty} \sum_{j=1}^4 M_j \exp(s_j Y + i\lambda X) d\lambda \right\} \right], \end{aligned} \quad (2.163)$$

When we take inverse Fourier transform of equations (2.162) and (2.163), we found following expressions:

$$\begin{aligned} (3 - \kappa_1) i\lambda \sum_{j=1}^4 M_j(\lambda) N_j(\lambda) \exp(s_j Y) + (\kappa_1 + 1) \sum_{j=1}^4 s_j M_j(\lambda) \exp(s_j Y) = \\ = \frac{(\kappa_1 - 1)}{\mu_{10} \exp(\gamma_1 Y)} \int_{-\infty}^{\infty} \sigma_{1YY}(t, Y) \exp(-i\lambda t) dt, \end{aligned} \quad (2.164)$$

$$\begin{aligned} \sum_{j=1}^4 s_j M_j(\lambda) N_j(\lambda) \exp(s_j Y) + i\lambda \sum_{j=1}^4 M_j(\lambda) \exp(s_j Y) = \\ = \frac{1}{\mu_{10} \exp(\gamma_1 Y)} \int_{-\infty}^{\infty} \sigma_{1XY}(t, Y) \exp(-i\lambda t) dt. \end{aligned} \quad (2.165)$$

Since contact surface is at $Y = 0$ plane, the normal and shear stress components on the contact surface can be written as follows:

$$\sigma_{1YY}(X, 0) = \sigma(X) \rightarrow \sigma_{YY}(t, 0) = \sigma(t), \quad (2.166)$$

$$\sigma_{1XY}(X, 0) = \eta \sigma(X) \rightarrow \sigma_{1XY}(t, 0) = \eta \sigma(t). \quad (2.167)$$

Introducing new parameters such as:

$$P(\lambda) = \int_{-\infty}^{\infty} \sigma(t) \exp(-i\lambda t) dt, \quad (2.168)$$

$$Q(\lambda) = \int_{-\infty}^{\infty} \eta \sigma(t) \exp(-i\lambda t) dt. \quad (2.169)$$

Out of the contact region, normal and shear stresses should be zero. Since normal and shear stresses are defined in the interval $-a < X < b$, we can write $P(\lambda)$ and $Q(\lambda)$ as follows:

$$P(\lambda) = \int_{-a}^b \sigma(t) \exp(-i\lambda t) dt, \quad (2.170)$$

Since coefficient of friction is constant on the contact surface, η may go out the integral.

$$Q(\lambda) = \eta \int_{-a}^b \sigma(t) \exp(-i\lambda t) dt. \quad (2.171)$$

Taking the limit of equations (2.164) and (2.165) while $Y \rightarrow 0$,

$$\begin{aligned} & (3 - \kappa_1) i \lambda \times \\ & \times [N_1 M_1 + N_2 M_2 + N_3 M_3 + N_4 M_4] + (\kappa_1 + 1) [s_1 M_1 + s_2 M_2 + s_3 M_3 + s_4 M_4] = \quad (2.172) \\ & = \frac{\kappa_1 - 1}{\mu_{10}} P(\lambda), \end{aligned}$$

$$\begin{aligned} & s_1 N_1 M_1 + s_2 N_2 M_2 + s_3 N_3 M_3 + s_4 N_4 M_4 + i \lambda [M_1 + M_2 + M_3 + M_4] \\ & = \frac{1}{\mu_{10}} Q(\lambda). \quad (2.173) \end{aligned}$$

These equations can be rewritten in a more compact form as follows:

$$\begin{bmatrix} z_{11} & z_{12} & z_{13} & z_{14} \\ z_{21} & z_{22} & z_{23} & z_{24} \end{bmatrix} \begin{Bmatrix} M_1 \\ M_2 \\ M_3 \\ M_4 \end{Bmatrix} = \frac{1}{\mu_{10}} \begin{Bmatrix} (\kappa_1 - 1)P(\lambda) \\ Q(\lambda) \end{Bmatrix}, \quad (2.174)$$

where

$$z_{11} = (3 - \kappa_1)i\lambda N_1 + (\kappa_1 + 1)s_1, \quad (2.175)$$

$$z_{12} = (3 - \kappa_1)i\lambda N_2 + (\kappa_1 + 1)s_2, \quad (2.176)$$

$$z_{13} = (3 - \kappa_1)i\lambda N_3 + (\kappa_1 + 1)s_3, \quad (2.177)$$

$$z_{14} = (3 - \kappa_1)i\lambda N_4 + (\kappa_1 + 1)s_4, \quad (2.178)$$

$$z_{21} = s_1 N_1 + i\lambda, \quad (2.179)$$

$$z_{22} = s_2 N_2 + i\lambda, \quad (2.180)$$

$$z_{23} = s_3 N_3 + i\lambda, \quad (2.181)$$

$$z_{24} = s_4 N_4 + i\lambda. \quad (2.182)$$

Remember M_2^* and M_4^* :

$$\begin{Bmatrix} M_2^* \\ M_4^* \end{Bmatrix} = \frac{1}{\Delta_1} \begin{bmatrix} r_1 & r_2 \\ r_3 & r_4 \end{bmatrix} \begin{Bmatrix} M_1^* \\ M_3^* \end{Bmatrix}. \quad (2.183)$$

Rewrite equation (2.183) as follows:

$$\begin{Bmatrix} M_2^* \\ M_4^* \end{Bmatrix} = \begin{bmatrix} r_{11} & r_{21} \\ r_{31} & r_{41} \end{bmatrix} \begin{Bmatrix} M_1^* \\ M_3^* \end{Bmatrix}, \quad (2.184)$$

where

$$r_{11} = \frac{r_1}{\Delta_1}, \quad (2.185)$$

$$r_{21} = \frac{r_2}{\Delta_1}, \quad (2.186)$$

$$r_{31} = \frac{r_3}{\Delta_1}, \quad (2.187)$$

$$r_{41} = \frac{r_4}{\Delta_1}. \quad (2.188)$$

When equations (2.184) are written explicitly for M_2^* and M_4^* , we can find the following relations:

$$M_2^* = r_{11} M_1^* + r_{21} M_3^*, \quad (2.189)$$

$$M_4^* = r_{31} M_1^* + r_{41} M_3^*, \quad (2.190)$$

After determination of M_2^* and M_4^* , we can write M_2 and M_4 as follows:

$$M_2 = r_{11} M_1 \exp((s_2 - s_1)h_1) + r_{21} M_3 \exp((s_2 - s_3)h_1), \quad (2.191)$$

$$M_4 = r_{31} M_1 \exp((s_4 - s_1)h_1) + r_{41} M_3 \exp((s_4 - s_3)h_1), \quad (2.192)$$

When equations (2.191) and (2.192) are substituted into equations (2.172) and (2.173), the following set of equations are found:

$$\begin{aligned} & \{(3 - \kappa_1)i\lambda N_1 + (3 - \kappa_1)i\lambda N_2 r_{11} \exp(s_2 - s_1)h_1 + (3 - \kappa_1)i\lambda N_4 r_{31} \exp(s_4 - s_1)h_1 + \\ & + (\kappa_1 + 1)s_1 + (\kappa_1 + 1)s_2 \exp(s_2 - s_1)h_1 + (\kappa_1 + 1)s_4 r_{31} \exp(s_2 - s_1)\} M_1 + \\ & + \{(3 - \kappa_1)i\lambda N_2 r_{21} \exp(s_2 - s_3)h_1 + (3 - \kappa_1)i\lambda N_3 + \\ & + (3 - \kappa_1)i\lambda N_4 r_{41} \exp(s_4 - s_3)h_1 + (\kappa_1 + 1)s_2 r_{21} \exp(s_2 - s_3)h_1 + \\ & + (\kappa_1 + 1)s_3 + (\kappa_1 + 1)s_4 r_{41} \exp(s_4 - s_3)h_1\} M_3 = \frac{\kappa_1 - 1}{\mu_{10}} P(\lambda), \end{aligned} \quad (2.193)$$

$$\begin{aligned}
& \{s_1 N_1 + s_2 N_2 r_{11} \exp(s_2 - s_1) h_1 + s_4 N_4 r_{31} \exp(s_4 - s_1) h_1 \\
& + i\lambda + i\lambda r_{11} \exp(s_2 - s_1) h_1 + i\lambda r_{31} \exp(s_4 - s_1) h_1\} M_1 \\
& + \{s_2 N_2 r_{21} \exp(s_2 - s_3) h_1 + s_3 N_3 + s_4 N_4 r_{41} \exp(s_4 - s_3) h_1 \\
& + i\lambda r_{21} \exp(s_2 - s_3) + i\lambda + i\lambda r_{41} \exp(s_4 - s_3) h_1\} M_3 \\
& = \frac{1}{\mu_{10}} Q(\lambda).
\end{aligned} \tag{2.194}$$

Equations (2.193) and (2.194) can be represented in matrix form as follows:

$$\begin{bmatrix} r_{51} & r_{61} \\ r_{71} & r_{81} \end{bmatrix} \begin{Bmatrix} M_1 \\ M_3 \end{Bmatrix} = \frac{1}{\mu_{10}} \begin{Bmatrix} (\kappa_1 - 1) P(\lambda) \\ Q(\lambda) \end{Bmatrix}, \tag{2.195}$$

where

$$\begin{aligned}
r_{51} = & (3 - \kappa_1) i\lambda [N_1 + N_2 r_{11} \exp(s_2 - s_1) h_1 + N_4 r_{31} \exp(s_4 - s_1) h_1] \\
& + (\kappa_1 + 1) s_1 + (\kappa_1 + 1) s_2 r_{11} \exp(s_2 - s_1) h_1 + (\kappa_1 + 1) s_4 r_{31} \exp(s_4 - s_1) h_1,
\end{aligned} \tag{2.196}$$

$$\begin{aligned}
r_{61} = & (3 - \kappa_1) i\lambda [N_2 r_{21} \exp(s_2 - s_3) h_1 + N_3 + N_4 r_{41} \exp(s_4 - s_3) h_1] \\
& + (\kappa_1 + 1) s_3 + (\kappa_1 + 1) s_2 r_{21} \exp(s_2 - s_3) h_1 + (\kappa_1 + 1) s_4 r_{41} \exp(s_4 - s_3) h_1,
\end{aligned} \tag{2.197}$$

$$\begin{aligned}
r_{71} = & s_1 N_1 + s_2 N_2 r_{11} \exp(s_2 - s_1) h_1 + s_4 N_4 r_{31} \exp(s_4 - s_1) h_1 \\
& + i\lambda (1 + r_{11} \exp(s_2 - s_1) h_1 + r_{31} \exp(s_4 - s_1) h_1),
\end{aligned} \tag{2.198}$$

$$\begin{aligned}
r_{81} = & s_2 N_2 r_{21} \exp(s_2 - s_3) h_1 + s_3 N_3 + s_4 N_4 r_{41} \exp(s_4 - s_3) h_1 \\
& + i\lambda (1 + r_{21} \exp(s_2 - s_3) h_1 + r_{41} \exp(s_4 - s_3) h_1),
\end{aligned} \tag{2.199}$$

We can write expressions r_{51} , r_{61} , r_{71} and r_{81} as follows:

$$r_{51} = z_{11} + z_{12} r_{11} \exp(s_2 - s_1) h_1 + z_{14} r_{31} \exp(s_4 - s_1) h_1, \tag{2.200}$$

$$r_{61} = z_{13} + z_{12} r_{21} \exp(s_2 - s_3) h_1 + z_{14} r_{41} \exp(s_4 - s_3) h_1, \tag{2.201}$$

$$r_{71} = z_{21} + z_{22} r_{11} \exp(s_2 - s_1) h_1 + z_{24} r_{31} \exp(s_4 - s_1) h_1, \tag{2.202}$$

$$r_{81} = z_{23} + z_{22} r_{21} \exp(s_2 - s_3) h_1 + z_{24} r_{41} \exp(s_4 - s_3) h_1. \tag{2.203}$$

The unknown functions M_1 and M_3 are determined from the following linear algebraic equation system:

$$\begin{bmatrix} r_{51} & r_{61} \\ r_{71} & r_{81} \end{bmatrix} \begin{Bmatrix} M_1 \\ M_3 \end{Bmatrix} = \frac{1}{\mu_{10}} \begin{Bmatrix} (\kappa_1 - 1)P(\lambda) \\ Q(\lambda) \end{Bmatrix}, \quad (2.204)$$

$$[r]^{-1} = \frac{1}{r_{51}r_{81} - r_{61}r_{71}} \begin{bmatrix} r_{81} & -r_{61} \\ -r_{71} & r_{51} \end{bmatrix}, \quad (2.205)$$

$$\begin{Bmatrix} M_1 \\ M_3 \end{Bmatrix} = \frac{1}{\mu_{10} \Delta_{21}} \begin{bmatrix} r_{81} & -r_{61} \\ -r_{71} & r_{51} \end{bmatrix} \begin{Bmatrix} (\kappa_1 - 1)P(\lambda) \\ Q(\lambda) \end{Bmatrix}, \quad (2.206)$$

$$\Delta_{21} = r_{51}r_{81} - r_{61}r_{71}. \quad (2.207)$$

Hence, six unknown functions appear in the displacement components for the coating and the substrate $\{M_1, M_2, M_3, M_4, R_3, R_4\}$ are determined at the end. They are given explicitly below.

$$M_1 = \frac{1}{\Delta_{21}\mu_{10}} [r_{81}(\kappa_1 - 1)P(\lambda) - r_{61}Q(\lambda)], \quad (2.208)$$

$$M_2 = [r_{11}M_1 \exp(s_2 - s_1)h_1 + r_{21}M_3 \exp(s_2 - s_3)h_1], \quad (2.209)$$

$$M_3 = \frac{1}{\Delta_{21}\mu_{10}} [-r_{71}(\kappa_1 - 1)P(\lambda) - r_{51}Q(\lambda)], \quad (2.210)$$

$$M_4 = [r_{31}M_1 \exp(s_4 - s_1)h_1 + r_{41}M_3 \exp(s_4 - s_3)h_1], \quad (2.211)$$

$$R_3 = (1 + h_1b_1)M_1 + (1 + h_1b_2)M_2 + (1 + h_1b_3)M_3 + (1 + h_1b_4)M_4, \quad (2.212)$$

$$R_4 = b_1M_1 + b_2M_2 + b_3M_3 + b_4M_4. \quad (2.213)$$

2.2 Singular integral equation of the problem

We have found all the unknown functions to determine displacement components in the FGM coating $u_1(X,Y)$, $v_1(X,Y)$ and homogenous substrate $u_2(X,Y)$, $v_2(X,Y)$ in Fourier domain. Since displacement vector of the contact problem is specified on some part of the contact surface and the traction vector is specified on the remainder part, the problem is a mixed Boundary Value Problem (B.V.P).

Input to the contact problem is the gradient of the vertical displacement component on the contact surface which is shown by $\partial/\partial X (v_1(X,0))$. Normal and shear stress components on the contact surface are expressed by $\sigma_{1YY}(X,0) = \sigma(X)$ and $\sigma_{1XY}(X,0) = \eta \sigma(X)$.

It is required to write displacement gradients on the contact surface by taking the derivatives of displacement expressions as described below.

$$\lim_{Y \rightarrow 0} \frac{\partial}{\partial X} u_1(X,Y) = \lim_{Y \rightarrow 0} \frac{1}{2\pi} \int_{-\infty}^{\infty} i\lambda \sum_{j=1}^4 M_j N_j \exp(s_j Y + i\lambda X) d\lambda, \quad (2.214)$$

$$\lim_{Y \rightarrow 0} \frac{\partial}{\partial X} v_1(X,Y) = \lim_{Y \rightarrow 0} \frac{1}{2\pi} \int_{-\infty}^{\infty} i\lambda \sum_{j=1}^4 M_j \exp(s_j Y + i\lambda X) d\lambda. \quad (2.215)$$

The right hand side of equations (2.214) and (2.215) can be written explicitly as follows:

$$\begin{aligned}
& \lim_{Y \rightarrow 0} \frac{1}{2\pi} \int_{-\infty}^{\infty} i\lambda \left\{ \frac{1}{\Delta_{21}\mu_{10}} [r_{81}(\kappa_1 - 1)P(\lambda) - r_{61}Q(\lambda)] N_1 \exp(s_1 Y + i\lambda X) + \right. \\
& + \left. \begin{aligned} & \left[r_{11} \left[\frac{1}{\Delta_{21}\mu_{10}} [r_{81}(\kappa_1 - 1)P(\lambda) - r_{61}Q(\lambda)] \exp(s_2 - s_1)h_1 \right. \right. \\ & \left. \left. + r_{21} \left[\frac{1}{\Delta_{21}\mu_{10}} [-r_{71}(\kappa_1 - 1)P(\lambda) + r_{51}Q(\lambda)] \exp(s_2 - s_3)h_1 \right] \right] N_2 \exp(s_2 Y + i\lambda X) \right. \\ & + \frac{1}{\Delta_{21}\mu_{10}} [-r_{71}(\kappa_1 - 1)P(\lambda) + r_{51}Q(\lambda)] N_3 \exp(s_3 Y + i\lambda X) \\ & + \left. \left. \begin{aligned} & \left[r_{31} \left[\frac{1}{\Delta_{21}\mu_{10}} [r_{81}(\kappa_1 - 1)P(\lambda) - r_{61}Q(\lambda)] \exp(s_4 - s_1)h_1 \right. \right. \\ & \left. \left. + r_{41} \left[\frac{1}{\Delta_{21}\mu_{10}} [-r_{71}(\kappa_1 - 1)P(\lambda) + r_{51}Q(\lambda)] \exp(s_4 - s_3)h_1 \right] \right] N_4 \exp(s_4 Y + i\lambda X) \right\} d\lambda, \end{aligned} \right. \\
\end{aligned} \tag{2.216}$$

$$\begin{aligned}
& \lim_{Y \rightarrow 0} \frac{1}{2\pi} \int_{-\infty}^{\infty} i\lambda \left\{ \frac{1}{\Delta_{21}\mu_{10}} [r_{81}(\kappa_1 - 1)P(\lambda) - r_{61}Q(\lambda)] \exp(s_1 Y + i\lambda X) \right. \\
& + r_{11} \left[\left[\frac{1}{\Delta_{21}\mu_{10}} [r_{81}(\kappa_1 - 1)P(\lambda) - r_{61}Q(\lambda)] \exp(s_2 - s_1)h_1 \right] \exp(s_2 Y + i\lambda X) \right. \\
& + r_{21} \left[\frac{1}{\Delta_{21}\mu_{10}} [-r_{71}(\kappa_1 - 1)P(\lambda) + r_{51}Q(\lambda)] \exp(s_2 - s_3)h_1 \exp(s_2 Y + i\lambda X) \right. \\
& + \left. \left[\frac{1}{\Delta_{21}\mu_{10}} [-r_{71}(\kappa_1 - 1)P(\lambda) + r_{51}Q(\lambda)] \exp(s_3 Y + i\lambda X) \right. \right. \\
& + r_{31} \left[\frac{1}{\Delta_{21}\mu_{10}} [r_{81}(\kappa_1 - 1)P(\lambda) - r_{61}Q(\lambda)] \exp(s_4 - s_1)h_1 \exp(s_4 Y + i\lambda X) \right. \\
& \left. \left. + r_{41} \left[\frac{1}{\Delta_{21}\mu_{10}} [-r_{71}(\kappa_1 - 1)P(\lambda) + r_{51}Q(\lambda)] \exp(s_4 - s_3)h_1 \exp(s_4 Y + i\lambda X) \right] \right\} d\lambda, \\
\end{aligned} \tag{2.217}$$

These displacement gradient equations given by equations (2.216) and (2.217) can be expressed in a more compact form using following integral equations:

$$\lim_{Y \rightarrow 0} 2\pi \mu_{10} \frac{\partial}{\partial X} v_1(X, Y) = \int_{-\infty}^{\infty} K_{11}(X, Y, t) \sigma(t) dt + \int_{-\infty}^{\infty} \eta K_{12}(X, Y, t) \sigma(t) dt, \quad (2.218)$$

$$\lim_{Y \rightarrow 0} 2\pi \mu_{10} \frac{\partial}{\partial X} u_1(X, Y) = \int_{-\infty}^{\infty} \eta K_{21}(X, Y, t) \sigma(t) dt + \int_{-\infty}^{\infty} K_{22}(X, Y, t) \sigma(t) dt. \quad (2.219)$$

The kernels of the integral equations are written below.

$$K_{11}(X, Y, t) = \lim_{Y \rightarrow 0} \int_{-\infty}^{\infty} h_{11}(\lambda, Y) \exp(-i\lambda(t - X)) d\lambda, \quad (2.220)$$

$$K_{12}(X, Y, t) = \lim_{Y \rightarrow 0} \int_{-\infty}^{\infty} h_{12}(\lambda, Y) \exp(-i\lambda(t - X)) d\lambda, \quad (2.221)$$

$$K_{21}(X, Y, t) = \lim_{Y \rightarrow 0} \int_{-\infty}^{\infty} h_{21}(\lambda, Y) \exp(-i\lambda(t - X)) d\lambda, \quad (2.222)$$

$$K_{22}(X, Y, t) = \lim_{Y \rightarrow 0} \int_{-\infty}^{\infty} h_{22}(\lambda, Y) \exp(-i\lambda(t - X)) d\lambda, \quad (2.223)$$

$$h_{11}(\lambda, Y) = \frac{i\lambda(\kappa_1 - 1)}{\Delta_{21}} \{r_{81}d_5 + r_{71}d_6\}, \quad (2.224)$$

$$h_{12}(\lambda, Y) = \frac{i\lambda}{\Delta_{21}} \{r_{51}d_7 + r_{61}d_8\}, \quad (2.225)$$

$$h_{21}(\lambda, Y) = \frac{i\lambda}{\Delta_{21}} \{r_{61}d_3 + r_{51}d_4\}, \quad (2.226)$$

$$h_{22}(\lambda, Y) = \frac{i\lambda(\kappa_1 - 1)}{\Delta_{21}} \{r_{81}d_1 + r_{71}d_2\}, \quad (2.227)$$

where

$$d_1 = \exp(s_1 Y) N_1 + r_{11} \exp((s_2 - s_1) h_1 + s_2 Y) N_2 + r_{31} \exp((s_4 - s_1) h_1 + s_4 Y) N_4, \quad (2.228)$$

$$d_2 = -\exp(s_3 Y) N_3 - r_{21} \exp((s_2 - s_3) h_1 + s_2 Y) N_2 - r_{41} \exp((s_4 - s_3) h_1 + s_4 Y) N_4, \quad (2.229)$$

$$d_3 = -\exp(s_1 Y) N_1 - r_{11} \exp((s_2 - s_1) h_1 + s_2 Y) N_2 - r_{31} \exp((s_4 - s_1) h_1 + s_4 Y) N_4, \quad (2.230)$$

$$d_4 = \exp(s_3 Y) N_3 + r_{21} \exp((s_2 - s_3) h_1 + s_2 Y) N_2 + r_{41} \exp((s_4 - s_3) h_1 + s_4 Y) N_4, \quad (2.231)$$

$$d_5 = \exp(s_1 Y) + r_{11} \exp((s_2 - s_1) h_1 + s_2 Y) + r_{31} \exp((s_4 - s_1) h_1 + s_4 Y), \quad (2.232)$$

$$d_6 = -\exp(s_3 Y) - r_{21} \exp((s_2 - s_3) h_1 + s_2 Y) - r_{41} \exp((s_4 - s_3) h_1 + s_4 Y), \quad (2.233)$$

$$d_7 = \exp(s_3 Y) + r_{21} \exp((s_2 - s_3) h_1 + s_2 Y) + r_{41} \exp((s_4 - s_3) h_1 + s_4 Y), \quad (2.234)$$

$$d_8 = -\exp(s_1 Y) - r_{11} \exp((s_2 - s_1) h_1 + s_2 Y) - r_{31} \exp((s_4 - s_1) h_1 + s_4 Y). \quad (2.235)$$

The next step is to find the asymptotic values of the kernels of the integral equations. First terms of asymptotic expansions are given in Appendix-A. Analyzing the asymptotic behavior of the kernels of the integral equations are important because of two reasons. First reason is that the singular behavior of the integral equation and that of its solution comes from the leading term in the large λ expansion. The second reason is to allow computational efficiency when singular integral equation is solved numerically. To do so, MATLAB's MuPad software is used to extract the asymptotic terms. After analyzing the asymptotic behavior of the integrands as $\lambda \rightarrow \infty$, following equations are found:

$$h_{11}(\lambda, Y) = i \frac{\lambda}{|\lambda|} \exp(|\lambda| \alpha_1 Y) \left\{ e_{10} + e_{11} \left| \frac{\gamma_1}{\lambda} \right| + e_{12} \left| \frac{\gamma_1}{\lambda} \right|^2 + e_{13} \left| \frac{\gamma_1}{\lambda} \right|^3 + \dots + e_{110} \left| \frac{\gamma_1}{\lambda} \right|^{10} \right\} + \quad (2.236)$$

$$+ i \frac{\lambda}{|\lambda|} \exp(|\lambda| \alpha_2 Y) \left\{ e_{20} + e_{21} \left| \frac{\gamma_1}{\lambda} \right| + e_{22} \left| \frac{\gamma_1}{\lambda} \right|^2 + e_{23} \left| \frac{\gamma_1}{\lambda} \right|^3 + \dots + e_{210} \left| \frac{\gamma_1}{\lambda} \right|^{10} \right\},$$

$$\begin{aligned}
h_{12}(\lambda, Y) = & \exp(|\lambda| \alpha_1 Y) \left\{ f_{10} + f_{11} \left| \frac{\gamma_1}{\lambda} \right| + f_{12} \left| \frac{\gamma_1}{\lambda} \right|^2 + f_{13} \left| \frac{\gamma_1}{\lambda} \right|^3 + \dots + f_{110} \left| \frac{\gamma_1}{\lambda} \right|^{10} \right\} + \\
& + \exp(|\lambda| \alpha_2 Y) \left\{ f_{20} + f_{21} \left| \frac{\gamma_1}{\lambda} \right| + f_{22} \left| \frac{\gamma_1}{\lambda} \right|^2 + f_{23} \left| \frac{\gamma_1}{\lambda} \right|^3 + \dots + f_{210} \left| \frac{\gamma_1}{\lambda} \right|^{10} \right\}, \tag{2.237}
\end{aligned}$$

$$\begin{aligned}
h_{21}(\lambda, Y) = & i \frac{\lambda}{|\lambda|} \exp(|\lambda| \alpha_1 Y) \left\{ g_{10} + g_{11} \left| \frac{\gamma_1}{\lambda} \right| + g_{12} \left| \frac{\gamma_1}{\lambda} \right|^2 + g_{13} \left| \frac{\gamma_1}{\lambda} \right|^3 + \dots + g_{110} \left| \frac{\gamma_1}{\lambda} \right|^{10} \right\} + \\
& + i \frac{\lambda}{|\lambda|} \exp(|\lambda| \alpha_2 Y) \left\{ g_{20} + g_{21} \left| \frac{\gamma_1}{\lambda} \right| + g_{22} \left| \frac{\gamma_1}{\lambda} \right|^2 + g_{23} \left| \frac{\gamma_1}{\lambda} \right|^3 + \dots + g_{210} \left| \frac{\gamma_1}{\lambda} \right|^{10} \right\}, \tag{2.238}
\end{aligned}$$

$$\begin{aligned}
h_{22}(\lambda, Y) = & \exp(|\lambda| \alpha_1 Y) \left\{ h_{10} + h_{11} \left| \frac{\gamma_1}{\lambda} \right| + h_{12} \left| \frac{\gamma_1}{\lambda} \right|^2 + h_{13} \left| \frac{\gamma_1}{\lambda} \right|^3 + \dots + h_{110} \left| \frac{\gamma_1}{\lambda} \right|^{10} \right\} + \\
& + \exp(|\lambda| \alpha_2 Y) \left\{ h_{20} + h_{21} \left| \frac{\gamma_1}{\lambda} \right| + h_{22} \left| \frac{\gamma_1}{\lambda} \right|^2 + h_{23} \left| \frac{\gamma_1}{\lambda} \right|^3 + \dots + h_{210} \left| \frac{\gamma_1}{\lambda} \right|^{10} \right\}. \tag{2.239}
\end{aligned}$$

In a more compact form, asymptotic terms of the integrands are expressed below.

$$\begin{aligned}
h_{11}(\lambda, Y) = & i \frac{\lambda}{|\lambda|} \exp(|\lambda| \alpha_1 Y) \left\{ e_{10} + e_{11} \left| \frac{\gamma_1}{\lambda} \right| + \mathcal{O}\left(\frac{1}{\lambda^2}\right) \right\} + \\
& + i \frac{\lambda}{|\lambda|} \exp(|\lambda| \alpha_2 Y) \left\{ e_{20} + e_{21} \left| \frac{\gamma_1}{\lambda} \right| + \mathcal{O}\left(\frac{1}{\lambda^2}\right) \right\}, \tag{2.240}
\end{aligned}$$

$$\begin{aligned}
h_{12}(\lambda, Y) = & \exp(|\lambda| \alpha_1 Y) \left\{ f_{10} + f_{11} \left| \frac{\gamma_1}{\lambda} \right| + \mathcal{O}\left(\frac{1}{\lambda^2}\right) \right\} + \\
& + \exp(|\lambda| \alpha_2 Y) \left\{ f_{20} + f_{21} \left| \frac{\gamma_1}{\lambda} \right| + \mathcal{O}\left(\frac{1}{\lambda^2}\right) \right\}, \tag{2.241}
\end{aligned}$$

$$\begin{aligned}
h_{21}(\lambda, Y) &= i \frac{\lambda}{|\lambda|} \exp(|\lambda| \alpha_1 Y) \left\{ g_{10} + g_{11} \left| \frac{\gamma_1}{\lambda} \right| + O\left(\frac{1}{\lambda^2}\right) \right\} + \\
&+ i \frac{\lambda}{|\lambda|} \exp(|\lambda| \alpha_2 Y) \left\{ g_{20} + g_{21} \left| \frac{\gamma_1}{\lambda} \right| + O\left(\frac{1}{\lambda^2}\right) \right\},
\end{aligned} \tag{2.242}$$

$$\begin{aligned}
h_{22}(\lambda, Y) &= \exp(|\lambda| \alpha_1 Y) \left\{ h_{10} + h_{11} \left| \frac{\gamma_1}{\lambda} \right| + O\left(\frac{1}{\lambda^2}\right) \right\} + \\
&+ \exp(|\lambda| \alpha_2 Y) \left\{ h_{20} + h_{21} \left| \frac{\gamma_1}{\lambda} \right| + O\left(\frac{1}{\lambda^2}\right) \right\}.
\end{aligned} \tag{2.243}$$

The singular behavior in the kernels of the integral equation is determined by performing asymptotic analysis. Hence, singular terms are extracted while $\lambda \rightarrow \infty$. The behavior of the integrands are given below.

$$h_{11}(\lambda, Y) = i \frac{\lambda}{|\lambda|} e_{10} \exp(|\lambda| \alpha_1 Y) + i \frac{\lambda}{|\lambda|} e_{20} \exp(|\lambda| \alpha_2 Y), \tag{2.244}$$

$$h_{12}(\lambda, Y) = f_{10} \exp(|\lambda| \alpha_1 Y) + f_{20} \exp(|\lambda| \alpha_2 Y), \tag{2.245}$$

$$h_{21}(\lambda, Y) = i \frac{\lambda}{|\lambda|} g_{10} \exp(|\lambda| \alpha_1 Y) + i \frac{\lambda}{|\lambda|} g_{20} \exp(|\lambda| \alpha_2 Y), \tag{2.246}$$

$$h_{22}(\lambda, Y) = h_{10} \exp(|\lambda| \alpha_1 Y) + h_{20} \exp(|\lambda| \alpha_2 Y). \tag{2.247}$$

where

$$\alpha_1 = \sqrt{1 - c_1^2}, \tag{2.248}$$

$$\alpha_2 = \sqrt{\frac{\kappa_1(1 - c_1^2) + (1 + c_1^2)}{\kappa_1 + 1}}. \tag{2.249}$$

$$\begin{aligned}
\lim_{Y \rightarrow 0} 2\pi \mu_{10} \frac{\partial}{\partial X} v_1(X, Y) &= \int_{-\infty}^{\infty} [K_{11}(X, Y, t) - K_{11\infty}(X, Y, t)] \sigma(t) dt + \\
&+ \int_{-\infty}^{\infty} [K_{12}(X, Y, t) - K_{12\infty}(X, Y, t)] \eta \sigma(t) dt + \\
&+ \lim_{Y \rightarrow 0} \int_{-\infty}^{\infty} K_{11\infty}(X, Y, t) \sigma(t) dt + \\
&+ \lim_{Y \rightarrow 0} \int_{-\infty}^{\infty} \eta K_{12\infty}(X, Y, t) \sigma(t) dt,
\end{aligned} \tag{2.250}$$

$$\begin{aligned}
\lim_{Y \rightarrow 0} 2\pi \mu_{10} \frac{\partial}{\partial X} u_1(X, Y) &= \int_{-\infty}^{\infty} [K_{21}(X, Y, t) - K_{21\infty}(X, Y, t)] \sigma(t) dt + \\
&+ \int_{-\infty}^{\infty} [K_{22}(X, Y, t) - K_{22\infty}(X, Y, t)] \eta \sigma(t) dt + \\
&+ \lim_{Y \rightarrow 0} \int_{-\infty}^{\infty} K_{21\infty}(X, Y, t) \sigma(t) dt + \\
&+ \lim_{Y \rightarrow 0} \int_{-\infty}^{\infty} \eta K_{22\infty}(X, Y, t) \sigma(t) dt,
\end{aligned} \tag{2.251}$$

Asymptotic values of the kernels of the integral equations while $\lambda \rightarrow \infty$ are given below.

$$\begin{aligned}
K_{11\infty}(X, Y, t) &= e_{10} \int_{-\infty}^{\infty} i \operatorname{sgn}(\lambda) \exp(|\lambda| \alpha_1 Y) \exp(-i\lambda(t - X)) d\lambda + \\
&+ e_{20} \int_{-\infty}^{\infty} i \operatorname{sgn}(\lambda) \exp(|\lambda| \alpha_2 Y) \exp(-i\lambda(t - X)) d\lambda,
\end{aligned} \tag{2.252}$$

$$\begin{aligned}
K_{12\infty}(X, Y, t) &= f_{10} \int_{-\infty}^{\infty} \exp(|\lambda| \alpha_1 Y) \exp(-i\lambda(t - X)) d\lambda + \\
&+ f_{20} \int_{-\infty}^{\infty} \exp(|\lambda| \alpha_2 Y) \exp(-i\lambda(t - X)) d\lambda,
\end{aligned} \tag{2.253}$$

$$\begin{aligned}
K_{21\infty}(X, Y, t) &= g_{10} \int_{-\infty}^{\infty} i \operatorname{sgn}(\lambda) \exp(|\lambda| \alpha_1 Y) \exp(-i\lambda(t - X)) d\lambda + \\
&+ g_{20} \int_{-\infty}^{\infty} i \operatorname{sgn}(\lambda) \exp(|\lambda| \alpha_2 Y) \exp(-i\lambda(t - X)) d\lambda,
\end{aligned} \tag{2.254}$$

$$\begin{aligned}
K_{22\infty}(X, Y, t) &= h_{10} \int_{-\infty}^{\infty} \exp(|\lambda| \alpha_1 Y) \exp(-i\lambda(t - X)) d\lambda + \\
&+ h_{20} \int_{-\infty}^{\infty} \exp(|\lambda| \alpha_2 Y) \exp(-i\lambda(t - X)) d\lambda.
\end{aligned} \tag{2.255}$$

The relationship between exponential and trigonometric functions can be written by using Euler's formula such that,

$$\exp(-i\lambda(t - X)) = \cos(\lambda(t - X)) - i \sin(\lambda(t - X)), \tag{2.256}$$

$$\int_{-\infty}^{\infty} i \operatorname{sgn}(\lambda) \exp(|\lambda| Y) \exp(-i\lambda(t - X)) d\lambda = 2 \int_0^{\infty} \exp(\lambda Y) \sin(\lambda(t - X)) d\lambda, \tag{2.257}$$

$$\int_{-\infty}^{\infty} \exp(|\lambda| Y) \exp(-i\lambda(t - X)) d\lambda = 2 \int_0^{\infty} \exp(\lambda Y) \cos(\lambda(t - X)) d\lambda. \tag{2.258}$$

The results of the following integrals are calculated analytically using the integration rules given in Abramowitz and Stegun [71].

$$\int_0^{\infty} e^{-ax} \sin(bx) dx = \frac{b}{a^2 + b^2}, \tag{2.259}$$

$$\int_0^{\infty} e^{-ax} \cos(bx) dx = \frac{a}{a^2 + b^2}, \tag{2.260}$$

Using equations given by (2.259) and (2.260), following expressions are obtained:

$$2 \int_0^{\infty} \exp(\lambda Y) \sin(\lambda(t - X)) d\lambda = \frac{2(t - X)}{Y^2 + (t - X)^2}, \tag{2.261}$$

$$2 \int_0^{\infty} \exp(\lambda Y) \cos(\lambda(t-X)) d\lambda = \frac{-2Y}{(t-X)^2 + Y^2}, \quad (2.262)$$

Therefore, equations involving $(-\infty, \infty)$ integrals are reduced to $(0, \infty)$ integrals and using integration rules provided by [71], the following expressions are obtained:

$$\int_{-\infty}^{\infty} \exp(|\lambda| \alpha_1 Y) \exp(-i\lambda(t-X)) d\lambda = \frac{-2Y}{(t-X)^2 + (\alpha_1 Y)^2}, \quad Y < 0, \quad (2.263)$$

$$\int_{-\infty}^{\infty} \exp(|\lambda| \alpha_2 Y) \exp(-i\lambda(t-X)) d\lambda = \frac{-2Y}{(t-X)^2 + (\alpha_2 Y)^2}, \quad Y < 0. \quad (2.264)$$

Asymptotic values of the kernels can be written in the following form,

$$K_{11\infty}(X, Y, t) = \frac{2e_{10}(t-X)}{(t-X)^2 + (\alpha_1 Y)^2} + \frac{2e_{20}(t-X)}{(t-X)^2 + (\alpha_2 Y)^2}, \quad (2.265)$$

$$K_{12\infty}(X, Y, t) = -\frac{2f_{10}\alpha_1 Y}{(t-X)^2 + (\alpha_1 Y)^2} - \frac{2f_{20}\alpha_2 Y}{(t-X)^2 + (\alpha_2 Y)^2}, \quad (2.266)$$

$$K_{21\infty}(X, Y, t) = \frac{2g_{10}(t-X)}{(t-X)^2 + (\alpha_1 Y)^2} + \frac{2g_{20}(t-X)}{(t-X)^2 + (\alpha_2 Y)^2}, \quad (2.267)$$

$$K_{22\infty}(X, Y, t) = -\frac{2h_{10}\alpha_1 Y}{(t-X)^2 + (\alpha_1 Y)^2} - \frac{2h_{20}\alpha_2 Y}{(t-X)^2 + (\alpha_2 Y)^2}. \quad (2.268)$$

Note that the following limit calculations are used while taking the limit as $Y \rightarrow 0^-$:

$$\lim_{Y \rightarrow 0^-} \frac{(t-X)}{(t-X)^2 + (\alpha_1 Y)^2} = \frac{1}{(t-X)}, \quad (2.269)$$

$$\lim_{Y \rightarrow 0^-} \frac{(t-X)}{(t-X)^2 + (\alpha_2 Y)^2} = \frac{1}{(t-X)}, \quad (2.270)$$

$$\lim_{Y \rightarrow 0^-} \frac{\alpha_1 Y}{(t-X)^2 + (\alpha_1 Y)^2} = -\pi \delta(t-X), \quad (2.271)$$

$$\lim_{Y \rightarrow 0^-} \frac{\alpha_2 Y}{(t-X)^2 + (\alpha_2 Y)^2} = -\pi \delta(t-X). \quad (2.272)$$

Therefore, while taking the limit of equations (2.265) – (2.268) as $Y \rightarrow 0^-$, asymptotic values $K_{11\infty}$, $K_{12\infty}$, $K_{21\infty}$ and $K_{22\infty}$ can be written as follows:

$$\lim_{Y \rightarrow 0^-} K_{11\infty} = \frac{2e_{10}}{(t-X)} + \frac{2e_{20}}{(t-X)} = \frac{2}{(t-X)}(e_{10} + e_{20}), \quad (2.273)$$

$$\begin{aligned} \lim_{Y \rightarrow 0^-} K_{12\infty} &= 2f_{10}[\pi\delta(t-X)] + 2f_{20}[\pi\delta(t-X)] \\ &= 2\pi\delta(t-X)(f_{10} + f_{20}), \end{aligned} \quad (2.274)$$

$$\lim_{Y \rightarrow 0^-} K_{21\infty} = \frac{2g_{10}}{(t-X)} + \frac{2g_{20}}{(t-X)} = \frac{2}{(t-X)}(g_{10} + g_{20}), \quad (2.275)$$

$$\begin{aligned} \lim_{Y \rightarrow 0^-} K_{22\infty} &= 2h_{10}[\pi\delta(t-X)] + 2h_{20}[\pi\delta(t-X)] \\ &= 2\pi\delta(t-X)(h_{10} + h_{20}). \end{aligned} \quad (2.276)$$

We have found all the asymptotic values $K_{11\infty}$, $K_{12\infty}$, $K_{21\infty}$ and $K_{22\infty}$ as $Y \rightarrow 0^-$. When we substitute these terms into the integral equations, we obtain following couple of equations:

$$\begin{aligned} &\lim_{Y \rightarrow 0^-} 2\pi\mu_{10} \frac{\partial}{\partial X} v_1(X, Y) = \\ &= \lim_{Y \rightarrow 0^-} \int_{-\infty}^{\infty} \left[K_{11}(X, Y, t) - \left[\frac{2e_{10}(t-X)}{(t-X)^2 + (\alpha_1 Y)^2} + \frac{2e_{20}(t-X)}{(t-X)^2 + (\alpha_2 Y)^2} \right] \right] \sigma(t) dt + \\ &+ \lim_{Y \rightarrow 0^-} \int_{-\infty}^{\infty} \left[K_{12}(X, Y, t) - \left[\frac{-2f_{10}(Y)}{(t-X)^2 + (\alpha_1 Y)^2} + \frac{-2f_{20}(Y)}{(t-X)^2 + (\alpha_2 Y)^2} \right] \right] \eta \sigma(t) dt + (2.277) \\ &+ \int_{-\infty}^{\infty} \frac{2}{(t-X)} [e_{10} + e_{20}] \sigma(t) dt + \\ &+ 2\pi [f_{10} + f_{20}] \int_{-\infty}^{\infty} \delta(t-X) \eta \sigma(t) dt, \end{aligned}$$

$$\begin{aligned}
& \lim_{Y \rightarrow 0^-} 2\pi\mu_{10} \frac{\partial}{\partial X} u_1(X, Y) = \\
& = \lim_{Y \rightarrow 0^-} \int_{-\infty}^{\infty} \left[K_{21}(X, Y, t) - \left[\frac{2g_{10}(t-X)}{(t-X)^2 + (\alpha_1 Y)^2} + \frac{2g_{20}(t-X)}{(t-X)^2 + (\alpha_2 Y)^2} \right] \right] \eta \sigma(t) dt + \\
& + \lim_{Y \rightarrow 0^-} \int_{-\infty}^{\infty} \left[K_{22}(X, Y, t) - \left[\frac{-2h_{10}(Y)}{(t-X)^2 + (\alpha_1 Y)^2} + \frac{-2h_{20}(Y)}{(t-X)^2 + (\alpha_2 Y)^2} \right] \right] \sigma(t) dt + \quad (2.278) \\
& + \int_{-\infty}^{\infty} \frac{2}{(t-X)} [g_{10} + g_{20}] \eta \sigma(t) dt + \\
& + 2\pi [h_{10} + h_{20}] \int_{-\infty}^{\infty} \delta(t-X) \sigma(t) dt.
\end{aligned}$$

After performing lengthy mathematical manipulations on the right hand side of integral equations (2.277) and (2.278), we can write the following equations:

$$\begin{aligned}
& \frac{4}{(\kappa_1 + 1)} \mu_{10} \frac{\partial}{\partial X} v_1(X, 0) = \\
& = \frac{2}{\pi(\kappa_1 + 1)} \int_{-\infty}^{\infty} \sigma(t) J_{11}(t, X) dt + \frac{2\eta}{\pi(\kappa_1 + 1)} \int_{-\infty}^{\infty} \sigma(t) J_{12}(t, X) dt + \quad (2.279) \\
& + \frac{4(e_{10} + e_{20})}{\pi(\kappa_1 + 1)} \int_{-\infty}^{\infty} \frac{\sigma(t)}{(t-X)} dt + \frac{4\eta(f_{10} + f_{20})}{(\kappa_1 + 1)} \sigma(X),
\end{aligned}$$

$$\begin{aligned}
& \frac{4}{(\kappa_1 + 1)} \mu_{10} \frac{\partial}{\partial X} u_1(X, 0) = \\
& = \frac{2\eta}{\pi(\kappa_1 + 1)} \int_{-\infty}^{\infty} \sigma(t) J_{21}(t, X) dt + \frac{2}{\pi(\kappa_1 + 1)} \int_{-\infty}^{\infty} \sigma(t) J_{22}(t, X) dt + \quad (2.280) \\
& + \frac{4\eta(g_{10} + g_{20})}{\pi(\kappa_1 + 1)} \int_{-\infty}^{\infty} \frac{\sigma(t)}{(t-X)} dt + \frac{4(h_{10} + h_{20})}{(\kappa_1 + 1)} \sigma(X).
\end{aligned}$$

where

$$J_{11}(t, X) = \int_{-\infty}^{\infty} \left\{ h_{11}(\lambda, 0) - (e_{10} + e_{20}) \frac{i\lambda}{|\lambda|} \right\} \exp(-i\lambda(t - X)) d\lambda, \quad (2.281)$$

$$J_{12}(t, X) = \int_{-\infty}^{\infty} \left\{ h_{12}(\lambda, 0) - (f_{10} + f_{20}) \right\} \exp(-i\lambda(t - X)) d\lambda, \quad (2.282)$$

$$J_{21}(t, X) = \int_{-\infty}^{\infty} \left\{ h_{21}(\lambda, 0) - (g_{10} + g_{20}) \frac{i\lambda}{|\lambda|} \right\} \exp(-i\lambda(t - X)) d\lambda, \quad (2.283)$$

$$J_{22}(t, X) = \int_{-\infty}^{\infty} \left\{ h_{22}(\lambda, 0) - (h_{10} + h_{20}) \right\} \exp(-i\lambda(t - X)) d\lambda. \quad (2.284)$$

Define new parameters ω_1 , ω_2 , ω_3 and ω_4 such as:

$$\omega_1 = \frac{4(e_{10} + e_{20})}{\pi(\kappa_1 + 1)}, \quad (2.285)$$

$$\omega_2 = \frac{4(f_{10} + f_{20})}{(\kappa_1 + 1)}, \quad (2.286)$$

$$\omega_3 = \frac{4(g_{10} + g_{20})}{\pi(\kappa_1 + 1)}, \quad (2.287)$$

$$\omega_4 = \frac{4(h_{10} + h_{20})}{(\kappa_1 + 1)}. \quad (2.288)$$

$$\begin{aligned} \frac{4\mu_{10}}{(\kappa_1 + 1)} \frac{\partial}{\partial X} v_1(X, 0) &= \frac{2}{\pi(\kappa_1 + 1)} \int_{-\infty}^{\infty} \sigma(t) J_{11}(t, X) dt + \\ &+ \frac{2\eta}{\pi(\kappa_1 + 1)} \int_{-\infty}^{\infty} \sigma(t) J_{12}(t, X) dt + \\ &+ \omega_1 \int_{-\infty}^{\infty} \frac{\sigma(t)}{t - X} dt + \omega_2 \eta \sigma(X), \end{aligned} \quad (2.289)$$

$$\begin{aligned}
\frac{4\mu_{10}}{(\kappa_1+1)} \frac{\partial}{\partial X} u_1(X,0) &= \frac{2\eta}{\pi(\kappa_1+1)} \int_{-\infty}^{\infty} \sigma(t) J_{21}(t,X) dt + \\
&+ \frac{2}{\pi(\kappa_1+1)} \int_{-\infty}^{\infty} \sigma(t) J_{22}(t,X) dt + \\
&+ \omega_3 \eta \int_{-\infty}^{\infty} \frac{\sigma(t)}{t-X} dt + \omega_4 \sigma(X).
\end{aligned} \tag{2.290}$$

Mathematical manipulations are made and kernels of the integral equations J_{11} , J_{12} , J_{21} and J_{22} can be expressed using the relations described in Ref. [45].

$$J_{11}(t, X) = 2 \int_0^{\infty} \Re \left[i \phi_{11}(\lambda) e^{-i\lambda(t-X)} \right] d\lambda = 2 \int_0^{\infty} \phi_{11}(\lambda) \sin(\lambda(t-X)) d\lambda, \tag{2.291}$$

$$J_{12}(t, X) = 2 \int_0^{\infty} \Re \left[\phi_{11}(\lambda) e^{-i\lambda(t-X)} \right] d\lambda = 2 \int_0^{\infty} \phi_{12}(\lambda) \cos(\lambda(t-X)) d\lambda, \tag{2.292}$$

$$J_{21}(t, X) = 2 \int_0^{\infty} \Re \left[i \phi_{21}(\lambda) e^{-i\lambda(t-X)} \right] d\lambda = 2 \int_0^{\infty} \phi_{21}(\lambda) \sin(\lambda(t-X)) d\lambda, \tag{2.293}$$

$$J_{22}(t, X) = 2 \int_0^{\infty} \Re \left[\phi_{22}(\lambda) e^{-i\lambda(t-X)} \right] d\lambda = 2 \int_0^{\infty} \phi_{22}(\lambda) \cos(\lambda(t-X)) d\lambda. \tag{2.294}$$

where

$$\phi_{11}(\lambda) = \frac{-\lambda(\kappa_1-1)}{\Delta_{21}} \{r_{81} d_5 + r_{71} d_6\} - (e_{10} + e_{20}), \tag{2.295}$$

$$\phi_{12}(\lambda) = \frac{i\lambda}{\Delta_{21}} \{r_{51} d_7 + r_{61} d_8\} - (f_{10} + f_{20}), \tag{2.296}$$

$$\phi_{21}(\lambda) = \frac{-\lambda}{\Delta_{21}} \{r_{61} d_3 + r_{51} d_4\} - (g_{10} + g_{20}), \tag{2.297}$$

$$\phi_{22}(\lambda) = \frac{i\lambda(\kappa_1 - 1)}{\Delta_{21}} \{r_{81}d_1 + r_{71}d_2\} - (h_{10} + h_{20}). \quad (2.298)$$

When ϕ_{11} , ϕ_{12} , ϕ_{21} and ϕ_{22} are substituted into equations (2.291) - (2.294) the following relations are obtained:

$$J_{11}(t, X) = 2 \int_0^\infty \left\{ \frac{-\lambda(\kappa_1 - 1)}{\Delta_{21}} [r_{81}d_5 + r_{71}d_6] - (e_{10} + e_{20}) \right\} \sin(\lambda(t - X)) d\lambda, \quad (2.299)$$

$$J_{12}(t, X) = 2 \int_0^\infty \left\{ \frac{i\lambda}{\Delta_{21}} [r_{51}d_7 + r_{61}d_8] - (f_{10} + f_{20}) \right\} \cos(\lambda(t - X)) d\lambda, \quad (2.300)$$

$$J_{21}(t, X) = 2 \int_0^\infty \left\{ \frac{-\lambda}{\Delta_{21}} [r_{61}d_3 + r_{51}d_4] - (g_{10} + g_{20}) \right\} \sin(\lambda(t - X)) d\lambda, \quad (2.301)$$

$$J_{22}(t, X) = 2 \int_0^\infty \left\{ \frac{i\lambda(\kappa_1 - 1)}{\Delta_{21}} [r_{81}d_1 + r_{71}d_2] - (h_{10} + h_{20}) \right\} \cos(\lambda(t - X)) d\lambda. \quad (2.302)$$

Finally, integral equations given by (2.289) and (2.290) are expressed in a more compact form as follows:

$$\begin{aligned} -\omega_2 \eta \sigma(X) + \frac{1}{\pi} \int_{-\infty}^\infty \left\{ \frac{\pi\omega_1}{t - X} - k_{11}(t, X) \right\} \sigma(t) dt - \frac{1}{\pi} \int_{-\infty}^\infty \eta k_{12}(t, X) \sigma(t) dt = \\ = \frac{4\mu_{10}}{(\kappa_1 + 1)} \frac{\partial v_1(X, 0)}{\partial X}, \end{aligned} \quad (2.303)$$

$$\begin{aligned} \omega_4 \sigma(X) + \frac{1}{\pi} \int_{-\infty}^\infty \left\{ \frac{\pi\omega_3}{t - X} - k_{21}(t, X) \right\} \eta \sigma(t) dt - \frac{1}{\pi} \int_{-\infty}^\infty k_{22}(t, X) \sigma(t) dt = \\ = \frac{4\mu_{10}}{(\kappa_1 + 1)} \frac{\partial u_1(X, 0)}{\partial X}. \end{aligned} \quad (2.304)$$

$$k_{11}(t, X) = \frac{-4}{\kappa_1 + 1} \int_0^\infty \phi_{11}(\lambda) \sin(\lambda(t - X)) d\lambda, \quad (2.305)$$

$$k_{12}(t, X) = \frac{-4}{\kappa_1 + 1} \int_0^{\infty} \phi_{12}(\lambda) \cos(\lambda(t - X)) d\lambda, \quad (2.306)$$

$$k_{21}(t, X) = \frac{-4}{\kappa_1 + 1} \int_0^{\infty} \phi_{21}(\lambda) \sin(\lambda(t - X)) d\lambda, \quad (2.307)$$

$$k_{22}(t, X) = \frac{-4}{\kappa_1 + 1} \int_0^{\infty} \phi_{22}(\lambda) \cos(\lambda(t - X)) d\lambda. \quad (2.308)$$

The singular integral equation given by equation (2.303) is solved for the unknown normal contact stress. Other integral equation provided by equation (2.304) is useful to calculate the lateral contact stress. In this study, lateral contact stress is presented since lateral contact stress plays an important role on surface related damages like surface cracking or propagation of the previously occurred cracks.

Recall the boundary conditions along the contact surface:

$$\sigma_{1YY}(X, 0) = \sigma(X) \neq 0, \quad -a < X < b \quad (2.309)$$

$$\sigma_{1YY}(X, 0) = \sigma(X) = 0, \quad X < -a, \quad X > b \quad (2.310)$$

Shear stress on the contact surface is related to the normal contact stress by a coefficient of friction according to the Coulomb's law and the shear stress on the contact surface is expressed by the following equation:

$$\sigma_{1XY}(X, 0) = \tau(X) = \eta\sigma(X), \quad (2.311)$$

In singular integral equations (2.303) and (2.304), $\sigma(X)$ is the normal contact stress and it is unknown priori. Utilizing definitions given by equations (2.309) – (2.311), the limits of the singular integral equation are modified as follows:

$$\begin{aligned}
-\omega_2 \eta \sigma(X) - \frac{1}{\pi} \int_{-a}^b \left\{ \frac{-\pi \omega_1}{t-X} + k_{11}(t, X) \right\} \sigma(t) dt - \frac{1}{\pi} \int_{-a}^b \eta k_{12}(t, X) \sigma(t) dt = \\
= \frac{4 \mu_{10}}{(\kappa_1 + 1)} \frac{\partial v_1(X, 0)}{\partial X},
\end{aligned} \tag{2.312}$$

$$\begin{aligned}
\omega_4 \sigma(X) - \frac{1}{\pi} \int_{-a}^b \left\{ \frac{-\pi \omega_3}{t-X} + k_{21}(t, X) \right\} \eta \sigma(t) dt - \frac{1}{\pi} \int_{-a}^b k_{22}(t, X) \sigma(t) dt = \\
= \frac{4 \mu_{10}}{(\kappa_1 + 1)} \frac{\partial u_1(X, 0)}{\partial X}.
\end{aligned} \tag{2.313}$$

The integration limits $-a$ and b in (2.312) and (2.313) show the contact length and these limits depend on the punch profile. Equilibrium equation simply means that the summation of the contact pressure must be equal to the force applied by the rigid punch and this condition is given by,

$$\int_{-a}^b \sigma(t) dt = -P. \tag{2.314}$$

where P is the prescribed compressive load per unit depth applied by the rigid punch.

2.3 The derivation of the lateral contact stress on the contact surface

If normal stress $\sigma_{1YY}(X, 0)$ and shear stress $\sigma_{1XY}(X, 0)$ on the contact surface are found, we are able to determine the lateral contact stress $\sigma_{1XX}(X, 0)$ on the surface of the coating. Firstly, we need to remember the elastic strain-stress field relations in three dimensional space. In the plane strain state, we can write strains in X , Y and Z axes as follows:

$$\varepsilon_{1XX} = \frac{1}{E_1} [\sigma_{1XX} - \nu_1(\sigma_{1YY} + \sigma_{1ZZ})], \tag{2.315}$$

$$\varepsilon_{1YY} = \frac{1}{E_1} [\sigma_{1YY} - \nu_1(\sigma_{1XX} + \sigma_{1ZZ})], \tag{2.316}$$

$$\varepsilon_{1ZZ} = \frac{1}{E_1} [\sigma_{1ZZ} - \nu_1(\sigma_{1XX} + \sigma_{1YY})]. \quad (2.317)$$

Since plane strain state is considered, the strain in Z direction must be zero, hence $\varepsilon_{1ZZ} = 0$. Therefore, the normal stress in Z direction can be expressed by the following relation:

$$\sigma_{1ZZ} = \nu_1(\sigma_{1XX} + \sigma_{1YY}), \quad (2.318)$$

Strain component in Y axis can be written as follows:

$$\varepsilon_{1YY} = \frac{1}{E_1} [\sigma_{1YY} - \nu_1(\sigma_{1XX} + \nu_1(\sigma_{1XX} + \sigma_{1YY}))], \quad (2.319)$$

$$\varepsilon_{1YY} = \frac{1-\nu_1^2}{E_1} \sigma_{1YY}(X, Y) - \frac{\nu_1(1+\nu_1)}{E_1} \sigma_{1XX}(X, Y), \quad (2.320)$$

Since plane strain state is considered, the Kolosov's constant for the coating can be written as:

$$\kappa_1 = 3 - 4\nu_1, \quad (2.321)$$

$$\nu_1 = \frac{3 - \kappa_1}{4} \quad (2.322)$$

Elastic modulus on the contact surface can be written as functions of shear modulus and Kolosov's constant.

$$E_{10} = 2\mu_{10}(1 + \nu_1) = 2\mu_{10} \left(1 + \frac{3 - \kappa_1}{4} \right), \quad (2.323)$$

$$E_{10} = \frac{7 - \kappa_1}{2} \mu_{10}. \quad (2.324)$$

Some required terms for the derivation of lateral contact stress are obtained using the following mathematical manipulations:

$$(1 - \nu_1^2) = -\frac{(\kappa_1 - 7)(\kappa_1 + 1)}{16}, \quad (2.325)$$

$$\frac{1 - \nu_1^2}{E_{10}} = \frac{\kappa_1 + 1}{8\mu_{10}}. \quad (2.326)$$

$$\nu_1(1 + \nu_1) = \frac{(3 - \kappa_1)(7 - \kappa_1)}{16}, \quad (2.327)$$

$$\frac{\nu_1(1 + \nu_1)}{E_{10}} = \frac{3 - \kappa_1}{8\mu_{10}}. \quad (2.328)$$

When we substitute equations (2.325) - (2.328) into the equation (2.320), we found the following equations:

$$\varepsilon_{1YY}(X, 0) = \frac{\partial v_1(X, 0)}{\partial Y} = \frac{\kappa_1 + 1}{8\mu_{10}} \sigma_{1YY}(X, 0) - \frac{3 - \kappa_1}{8\mu_{10}} \sigma_{1XX}(X, 0), \quad (2.329)$$

$$\begin{aligned} \varepsilon_{1YY}(X, 0) &= \frac{\partial v_1}{\partial Y}(X, 0) = \\ &= \frac{\kappa_1 + 1}{8\mu_{10}} \sigma_{1YY}(X, 0) - \frac{3 - \kappa_1}{8\mu_{10}} \sigma_{1XX}(X, 0). \end{aligned} \quad (2.330)$$

Remember the lateral contact stress in terms of displacement components such that,

$$\sigma_{1XX}(X, Y) = \frac{\mu_{10} e^{\gamma Y}}{\kappa_1 - 1} \left[(\kappa_1 + 1) \frac{\partial u_1(X, Y)}{\partial X} + (3 - \kappa_1) \frac{\partial v_1(X, Y)}{\partial Y} \right], \quad (2.331)$$

In order to derive the formula for the lateral contact stress, we need to use the right hand side of the singular integral equation given by (2.313).

$$\begin{aligned} \omega_4 \sigma(X) - \frac{1}{\pi} \int_{-a}^b \left\{ \frac{-\pi\omega_3}{t - X} + k_{21}(t, X) \right\} \eta \sigma(t) dt - \frac{1}{\pi} \int_{-a}^b k_{22}(t, X) \sigma(t) dt = \\ = \frac{4\mu_{10}}{(\kappa_1 + 1)} \frac{\partial u_1(X, 0)}{\partial X}, \end{aligned} \quad (2.332)$$

$$\begin{aligned}
\frac{\partial u_1(X, Y)}{\partial X} &= \\
&= \frac{\kappa_1 + 1}{4\mu_{10}} \left\{ \omega_4 \sigma(X) - \frac{1}{\pi} \int_{-a}^b \left\{ \frac{-\pi\omega_3}{t-X} + k_{21}(t, X) \right\} \eta \sigma(t) dt - \frac{1}{\pi} \int_{-a}^b k_{22}(t, X) \sigma(t) dt \right\},
\end{aligned} \tag{2.333}$$

$$\begin{aligned}
\sigma_{1XX}(X, Y) &= \frac{\mu_{10}(\kappa_1 + 1)}{\kappa_1 - 1} \left[\frac{\kappa_1 + 1}{4\mu_{10}} \omega_4 \sigma_{1YY}(X, Y) - \frac{\kappa_1 + 1}{4\mu_{10}} \frac{1}{\pi} \int_{-a}^b \frac{-\pi\omega_3}{t-X} \eta \sigma(t) dt \right] \\
&\quad - \frac{\mu_{10}(\kappa_1 + 1)}{\kappa_1 - 1} \left[\frac{\kappa_1 + 1}{4\mu_{10}} \frac{1}{\pi} \int_{-a}^b [\eta k_{21}(t, X) + k_{22}(t, X)] \sigma(t) dt \right] \\
&\quad + \frac{\mu_{10}(3 - \kappa_1)}{\kappa_1 - 1} \left[\frac{\kappa_1 + 1}{8\mu_{10}} \sigma_{1YY}(X, Y) - \frac{3 - \kappa_1}{8\mu_{10}} \sigma_{1xx}(x, y) \right],
\end{aligned} \tag{2.334}$$

By taking the limit of equation (2.334) as $Y \rightarrow 0^-$, and performing some mathematical manipulations, we obtain the lateral contact stress as follows:

$$\begin{aligned}
\sigma_{1XX}(X, 0) &= \left[2\omega_4 + \frac{3 - \kappa_1}{\kappa_1 + 1} \right] \sigma(X) + \frac{2\eta}{\pi} \int_{-a}^b \frac{\pi\omega_3}{t-X} \sigma(t) dt - \\
&\quad - \frac{2}{\pi} \int_{-a}^b [\eta k_{21}(t, X) + k_{22}(t, X)] \sigma(t) dt.
\end{aligned} \tag{2.335}$$

$(g_{10} + g_{20})$ and $(h_{10} + h_{20})$ are the leading terms of the asymptotic expansion and they are lengthy functions of κ_1 and c_1 . The explicit forms of these terms are provided in Appendix-A. Integration limits may take different forms depending on the punch profile.

CHAPTER 3

NUMERICAL SOLUTION OF THE SINGULAR INTEGRAL EQUATION

In this chapter, we focus on developing solutions for the governing singular integral equation of the problem. Singular integral equation can be solved using function theoretical methods or numerical methods. In what follows below, we describe the numerical solution methodologies for each punch profile.

3.1 Flat punch problem

The geometry of the flat punch contact problem is shown in Figure 3.1. The same numerical solution methodologies are applied for homogenous elastic coating and functionally graded coating contact problems. A coating of thickness h_1 is perfectly bonded to the substrate. The right hand side of the singular integral equation involves the displacement gradient on the contact surface. Note that, for the rigid flat punch contact problem, normal displacement beneath the punch is constant, and correspondingly the displacement gradient on the contact surface becomes zero.

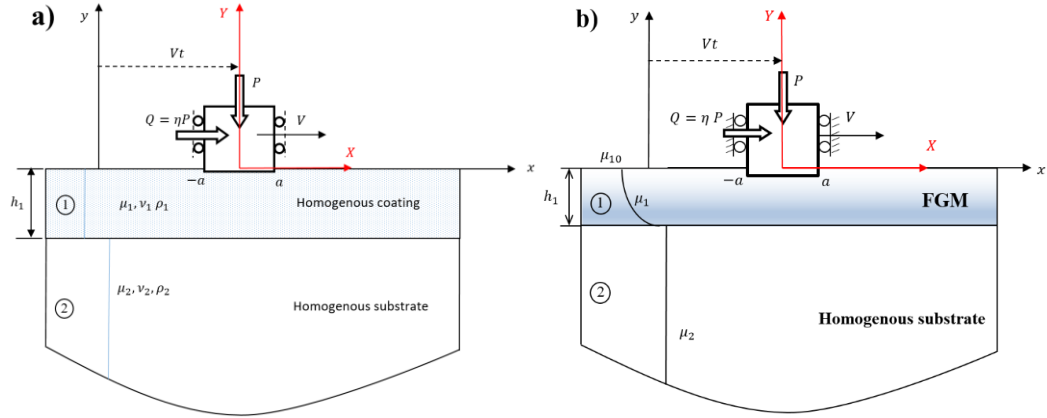


Figure 3.1: The moving rigid flat punch on (a) homogenous elastic coating (b) functionally graded coating

$$v_1(X,0) = -v_0, \quad (3.1)$$

$$\frac{\partial v_1(X,0)}{\partial X} = 0, \quad (3.2)$$

$$-\omega_2 \eta \sigma(X) - \frac{1}{\pi} \int_{-a}^a \left[\frac{-\pi \omega_1}{t-X} + k_{11}(t, X) + \eta k_{12}(t, X) \right] \sigma(t) dt = \frac{4\mu_{10}}{\kappa_1 + 1} \frac{\partial v_1(X,0)}{\partial X}, \quad (3.3)$$

$$\int_{-a}^a \sigma(t) dt = -P. \quad (3.4)$$

Equilibrium equation for the flat punch contact problem is given by equation (3.4). The summation of the normal contact stress under the flat punch equals to the applied load per depth by the flat punch. In order to solve the singular integral equation (3.3), it is required to normalize the interval from $(-a, a)$ to $(-1, 1)$. This normalization procedure is done by the following change of variables:

$$l = a, \quad (3.5)$$

$$X = ar, \quad -a < X < a, \quad -1 < r < 1, \quad (3.6)$$

$$t = as, \quad -a < t < a, \quad -1 < s < 1, \quad (3.7)$$

$$k_{11}(t, X) = \frac{1}{l} k_{11}(as, ar) = \frac{1}{a} k_{11}^*(s, r), \quad (3.8)$$

$$k_{12}(t, X) = \frac{1}{l} k_{12}(as, ar) = \frac{1}{a} k_{12}^*(s, r), \quad (3.9)$$

$$k_{21}(t, X) = \frac{1}{l} k_{21}(as, ar) = \frac{1}{a} k_{21}^*(s, r), \quad (3.10)$$

$$k_{22}(t, X) = \frac{1}{l} k_{22}(as, ar) = \frac{1}{a} k_{22}^*(s, r), \quad (3.11)$$

$$\lambda = \frac{1}{a} \xi, \quad (3.12)$$

$$\phi_{11}(\lambda) = \phi_{11}\left(\frac{\xi}{a}\right) = \phi_{11}^*(\xi), \quad (3.13)$$

$$\phi_{12}(\lambda) = \phi_{12}\left(\frac{\xi}{a}\right) = \phi_{12}^*(\xi), \quad (3.14)$$

$$\phi_{21}(\lambda) = \phi_{21}\left(\frac{\xi}{a}\right) = \phi_{21}^*(\xi), \quad (3.15)$$

$$\phi_{22}(\lambda) = \phi_{22}\left(\frac{\xi}{a}\right) = \phi_{22}^*(\xi), \quad (3.16)$$

$$\gamma_1 = \frac{1}{a} \gamma_1^*, \quad (3.17)$$

$$\sigma(X) = \sigma(ar) = -\frac{P}{a} \Theta(r), \quad \sigma(t) = \sigma(as) = -\frac{P}{a} \Theta(s). \quad (3.18)$$

When we substitute normalized quantities into the singular integral equation (3.3), the following integral equation is obtained:

$$\begin{aligned} \omega_2 \eta \Theta(r) + \frac{1}{\pi} \int_{-1}^1 \left\{ \frac{-\pi \omega_1}{(as) - (ar)} + \frac{1}{a} k_{11}^*(s, r) \right\} \Theta(s) a ds + \\ + \frac{1}{\pi} \int_{-1}^1 \frac{1}{a} \eta k_{12}^*(s, r) \Theta(s) a ds = \frac{1}{a} \frac{\partial}{\partial r} v_1(ar, 0). \end{aligned} \quad (3.19)$$

After rearranging and simplifying, we obtain the normalized singular integral equation and normalized equilibrium equation of the form,

$$\omega_2 \eta \Theta(r) + \frac{1}{\pi} \int_{-1}^1 \left\{ \frac{-\pi \omega_1}{s-r} + k_{11}^*(s, r) + \eta k_{12}^*(s, r) \right\} \Theta(s) ds = 0, \quad (3.20)$$

$$\int_{-1}^1 \Theta(s) ds = 1. \quad (3.21)$$

Terms shown with the sign *, the inhomogeneity constant γ_1 is replaced by γ_1^* . Note that for the homogenous elastic coating problem $\gamma_1 = 0$, hence $\gamma_1^* = 0$.

Kernels of the singular integral equation using normalized variables can be written as follows:

$$k_{11}^*(s, r) = a k_{11}(t, X) \rightarrow k_{11}^*(s, r) = \frac{-4}{\kappa_1 + 1} \int_0^\infty \phi_{11}^*(\xi) \sin(\xi(s-r)) d\xi, \quad (3.22)$$

$$k_{12}^*(s, r) = a k_{12}(t, X) \rightarrow k_{12}^*(s, r) = \frac{-4}{\kappa_1 + 1} \int_0^\infty \phi_{12}^*(\xi) \cos(\xi(s-r)) d\xi, \quad (3.23)$$

$$k_{21}^*(s, r) = a k_{21}(t, X) \rightarrow k_{21}^*(s, r) = \frac{-4}{\kappa_1 + 1} \int_0^\infty \phi_{21}^*(\xi) \sin(\xi(s-r)) d\xi, \quad (3.24)$$

$$k_{22}^*(s, r) = a k_{22}(t, X) \rightarrow k_{22}^*(s, r) = \frac{-4}{\kappa_1 + 1} \int_0^\infty \phi_{22}^*(\xi) \sin(\xi(s-r)) d\xi. \quad (3.25)$$

where

$$\phi_{11}^*(\xi) = \frac{-\xi(\kappa_1 - 1)}{\Delta_{21}(\xi)} \{r_{81} d_5 + r_{71} d_6\} - (e_{10} + e_{20}), \quad (3.26)$$

$$\phi_{12}^*(\xi) = \frac{i\xi}{\Delta_{21}(\xi)} \{r_{51} d_7 + r_{61} d_8\} - (f_{10} + f_{20}), \quad (3.27)$$

$$\phi_{21}^*(\xi) = \frac{-\xi}{\Delta_{21}(\xi)} \{r_{61} d_3 + r_{51} d_4\} - (g_{10} + g_{20}), \quad (3.28)$$

$$\phi_{22}^*(\xi) = \frac{i\xi(\kappa_1 - 1)}{\Delta_{21}(\xi)} \{r_{81} d_1 + r_{71} d_2\} - (h_{10} + h_{20}). \quad (3.29)$$

Since normal contact stress $\sigma(X)$ has integrative singularities at the ends of the flat punch, both powers of stress singularities must be negative. The index of the singular integral equation is $\kappa_0 = 1.0$. Determination of the index of the singular integral equation depends on the physics of the problem (Erdogan et al. [73]). The powers of the stress singularities α and β are calculated by,

If $\eta > 0$:

$$\alpha = -1 + \frac{1}{\pi} \tan^{-1} \left| \frac{1}{\omega_2 \eta} \right|, \quad \beta = -\frac{1}{\pi} \tan^{-1} \left| \frac{1}{\omega_2 \eta} \right|. \quad (3.30)$$

If $\eta < 0$:

$$\alpha = -\frac{1}{\pi} \tan^{-1} \left| \frac{1}{\omega_2 \eta} \right|, \quad \beta = -1 + \frac{1}{\pi} \tan^{-1} \left| \frac{1}{\omega_2 \eta} \right|. \quad (3.31)$$

Powers of the stress singularities α and β are functions of ω_2 and η . ω_2 involves $f_{10} + f_{20}$ term where $f_{10} + f_{20}$ is a lengthy function of κ_1 and c_1 . Hence, powers of the stress singularities depend on coefficient of friction η , dimensionless punch speed c_1 and Poisson's ratio ν_1 . Explicit form of $f_{10} + f_{20}$ is given in Appendix-A.

Some numerical values for the powers of the stress singularities with respect to various coefficient of friction and punch speed are given in Table 3.1. The Poisson's ratio along the graded coating is assumed constant since the variation of Poisson's ratio along the graded coating has a small effect on contact stresses [46].

Generally, the solution of the singular integral equations can be done by either function theoretical method or numerical methods. Function theoretical method for the solutions of singular integral equations is given in the study conducted by Muskhelishvili [72]. In the present study, we use numerical methods for the solutions of singular integral equations. By numerical methods, we try to obtain an approximate solution rather than a closed form solution. In this technique, using Jacobi orthogonal polynomials, the singular integral equation is reduced to an infinite number of linear algebraic equation set. The numerical solution for the singular integral equation consisting of infinite series and Jacobi polynomials can be expressed by,

$$\Theta(s) = \sum_{n=0}^{\infty} c_n W(s) P_n^{(\alpha,\beta)}(s), \quad (3.32)$$

$$W(s) = (1-s)^\alpha (1+s)^\beta. \quad (3.33)$$

Recall that the terms consisting of Fredholm kernels are,

$$Z_{1n}(r) = \frac{1}{\pi} \int_{-1}^1 k_{11}^*(s, r) W(s) P_n^{(\alpha,\beta)}(s) ds, \quad (3.34)$$

$$Z_{2n}(r) = \frac{1}{\pi} \int_{-1}^1 \eta k_{12}^*(s, r) W(s) P_n^{(\alpha,\beta)}(s) ds, \quad (3.35)$$

$$K_n(r) = Z_{1n}(r) + Z_{2n}(r) = \frac{1}{\pi} \int_{-1}^1 \left(k_{11}^*(s, r) + \eta k_{12}^*(s, r) \right) W(s) P_n^{(\alpha,\beta)}(s) ds. \quad (3.36)$$

When numerical solution given by (3.32) is substituted into the normalized singular integral equation (3.20), the following expression is obtained:

$$\begin{aligned} & \sum_{n=0}^{\infty} c_n \left\{ \omega_2 \eta P_n^{(\alpha, \beta)}(r) W(r) - \frac{\omega_1}{\pi} \int_{-1}^1 \frac{P_n^{(\alpha, \beta)}(s) W(s)}{s-r} ds \right\} \\ & + \sum_{n=0}^{\infty} c_n \left\{ \frac{1}{\pi} \int_{-1}^1 k_{11}^*(s, r) + \eta k_{12}^*(s, r) \right\} W(s) P_n^{(\alpha, \beta)}(s) ds = 0. \end{aligned} \quad (3.37)$$

For the rigid flat punch contact problem, the index of the singular integral equation is $\kappa_0 = 1.0$. Using the orthogonality property of Jacobi polynomials described in Appendix-C, governing singular integral equation of the problem is reduced to the following linear algebraic equation set:

$$\sum_{n=0}^{\infty} c_n \left\{ \frac{\pi \omega_1}{2 \sin \pi \alpha} P_{n-1}^{(-\alpha, -\beta)}(r) + K_n(r) \right\} = 0, \quad -1 < r < 1. \quad (3.38)$$

Governing equation of the contact problem is reduced to a system of linear algebraic equation set with undetermined coefficients c_n . These undetermined coefficients can be found using the suitable expansion-collocation technique. The accuracy of the numerical solution is highly dependent on the selection of the collocation points r_k . The collocation points r_k are selected as the roots of the Jacobi polynomial. If the density of the collocation points is increased near the ends of integration, we will obtain more accurate results. Collocation points r_k are determined by,

$$P_{N-1}^{(\alpha+1, \beta+1)}(r_k) = 0, \quad k = 1, \dots, N. \quad (3.39)$$

Truncating the infinite series at $n = N$, equation (3.38) is reduced to N number of algebraic equations in c_n by expanding both sides into series of Jacobi polynomials $P_{n-1}^{(-\alpha, -\beta)}(r)$, $n = 1, 2, \dots, N$. Hence, N equations are generated using equation (3.38)

and these equations involves $N+1$ unknown constants c_0, c_1, \dots, c_N . The additional equation for a unique solution is provided by the equilibrium condition.

$$\sum_{n=0}^N c_n \int_{-1}^1 W(s) P_n^{(\alpha, \beta)}(s) ds = 1. \quad (3.40)$$

Using the orthogonality condition discussed in Appendix-C, equation (3.40) is reduced to the following equation:

$$c_0 \int_{-1}^1 P_0^{(\alpha, \beta)}(s) P_0^{(\alpha, \beta)}(s) W(s) ds = 1, \quad (3.41)$$

$$c_0 = \frac{1}{\theta_0^{(\alpha, \beta)}}. \quad (3.42)$$

Therefore, using equilibrium equation, we found the first unknown constant. Once we have found the unknown constants $\{c_0, c_1, \dots, c_N\}$ by solving linear algebraic equation system, we can determine the normal contact stress distribution in normalized coordinates.

$$\sigma(ar) = -\frac{P}{a} \Theta(r) = -\frac{P}{a} W(r) \sum_{n=0}^N c_n P_n^{(\alpha, \beta)}(r). \quad (3.43)$$

The normal and shear stresses on the contact surface in spatial coordinates are expressed by,

$$\frac{\sigma_{IYY}(X, 0)}{(P/2a)} = -2 \left(1 - \frac{X}{a}\right)^\alpha \left(1 + \frac{X}{a}\right)^\beta \sum_{n=0}^N c_n P_n^{(\alpha, \beta)}\left(\frac{X}{a}\right), \quad (3.44)$$

$$\frac{\sigma_{IXY}(X, 0)}{(P/2a)} = -2\eta \left(1 - \frac{X}{a}\right)^\alpha \left(1 + \frac{X}{a}\right)^\beta \sum_{n=0}^N c_n P_n^{(\alpha, \beta)}\left(\frac{X}{a}\right), \quad (3.45)$$

Recall that the lateral contact stress expressed by equation (2.335):

$$\begin{aligned} \sigma_{1XX}(X, 0) = & \left[2\omega_4 + \frac{3-\kappa_1}{\kappa_1+1} \right] \sigma(X) + \frac{2\eta}{\pi} \int_{-a}^a \frac{\pi \omega_3}{t-X} \sigma(t) dt \\ & - \frac{2}{\pi} \int_{-a}^a [\eta k_{21}(t, X) + k_{22}(t, X)] \sigma(t) dt. \end{aligned} \quad (3.46)$$

Recall that $\sigma(t) = -\frac{P}{a} \Theta(s)$. In spatial coordinates, the lateral contact stress can be written as follows:

$$\begin{aligned} \frac{\sigma_{1XX}(X, 0)}{(P/2a)} = & -2 \left(2\omega_4 + \frac{3-\kappa_1}{\kappa_1+1} \right) \Theta(r) - \frac{4\eta}{\pi} \int_{-1}^1 \frac{\pi \omega_3 \Theta(s)}{s-r} ds \\ & + \frac{4}{\pi} \int_{-1}^1 [\eta k_{21}^*(s, r) + k_{22}^*(s, r)] \Theta(s) ds. \end{aligned} \quad (3.47)$$

The following equations are useful for the calculation of the punch stress intensity factors. At the ends of the rigid flat punch, mode-I stress intensity factors can be calculated by [45],

$$k_I(-a) = \lim_{X \rightarrow -a} -\frac{\sigma_{1YY}(X, 0)}{2^\alpha (a+X)^\beta} = \frac{(P/a)}{a^\alpha} \sum_{n=0}^N c_n P_n^{(\alpha, \beta)}(-1), \quad (3.48)$$

$$k_I(a) = \lim_{X \rightarrow a} -\frac{\sigma_{1YY}(X, 0)}{2^\beta (a-X)^\alpha} = \frac{(P/a)}{a^\beta} \sum_{n=0}^N c_n P_n^{(\alpha, \beta)}(1). \quad (3.49)$$

In a non-dimensional form, the normalized stress intensity factors are calculated by,

$$K_I(-a) = \frac{a^\beta}{(P/a)} k_I(-a) = \sum_{n=0}^N c_n P_n^{(\alpha, \beta)}(-1), \quad (3.50)$$

$$K_I(a) = \frac{a^\alpha}{(P/a)} k_I(a) = \sum_{n=0}^N c_n P_n^{(\alpha, \beta)}(1). \quad (3.51)$$

Powers of the stress singularities at the ends of the rigid flat punch are computed for various values of coefficient of friction η and dimensionless punch speed c_1 .

Numerical values are presented in Table 3.1. In frictionless case, the powers of the stress singularities remain the same value as -0.5 although punch speed is increased. On the other hand, in frictional cases, dimensionless punch speed begins to become effective and it significantly changes the powers of the stress singularities. The maximum variation of the powers of the stress singularities with respect to punch speed occurs at cases involving higher coefficient of friction values as it can be seen in Table 3.1.

Table 3.1: The powers of stress singularity for a flat punch $\nu_1 = 0.25$.

η	c_1	α	β
0.0	0.0	-0.500000	-0.500000
	0.4	-0.500000	-0.500000
	0.6	-0.500000	-0.500000
	0.8	-0.500000	-0.500000
0.3	0.0	-0.531725	-0.468274
	0.4	-0.539476	-0.460523
	0.6	-0.556115	-0.443884
	0.8	-0.627597	-0.372402
0.5	0.0	-0.552568	-0.447431
	0.4	-0.565206	-0.434793
	0.6	-0.591867	-0.408132
	0.8	-0.695751	-0.304248
0.7	0.0	-0.572966	-0.427033
	0.4	-0.590101	-0.409898
	0.6	-0.625392	-0.374607
	0.8	-0.748221	-0.251778

3.2 Triangular punch problem

The geometry of the triangular punch contact problem is shown in Figure 3.2. A coating of thickness h_1 is perfectly bonded to the substrate. The right hand side of the singular integral equation involves the displacement gradient on the contact surface. Note that, for the rigid triangular punch contact problem, normal displacement beneath the punch is a linear function due to the punch profile, and correspondingly the displacement gradient on the contact surface becomes constant. In Figure 3.2, θ denotes the inclination angle of the triangular punch.

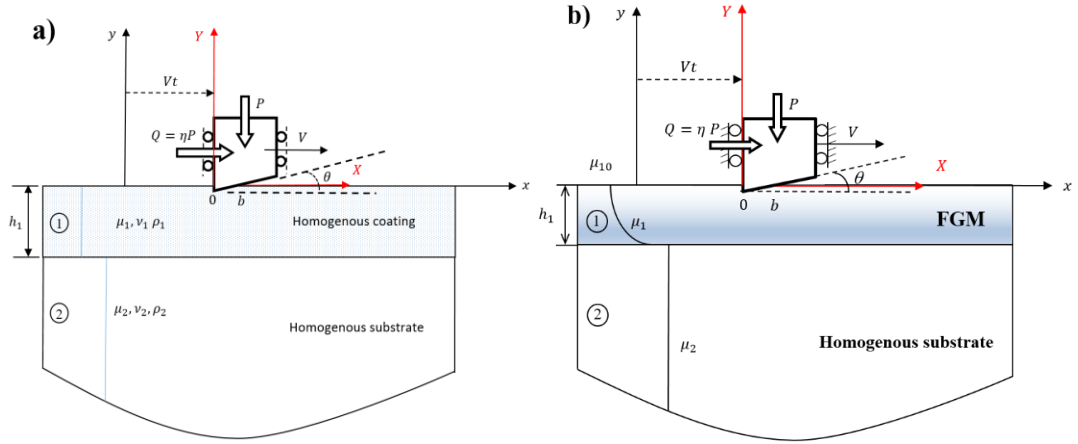


Figure 3.2: The moving rigid triangular punch on (a) homogenous elastic coating
(b) functionally graded coating

$$v_1(X,0) = -v_0 + \tan \theta X, \quad (3.52)$$

$$\frac{\partial v_1(X,0)}{\partial X} = \tan \theta, \quad (3.53)$$

$$-\omega_2 \eta \sigma(X) - \frac{1}{\pi} \int_0^b \left[\frac{-\pi \omega_1}{t-X} + k_{11}(t, X) + \eta k_{12}(t, X) \right] \sigma(t) dt = \frac{4 \mu_{10}}{\kappa_1 + 1} \frac{\partial v_1(X,0)}{\partial X}, \quad (3.54)$$

$$\int_0^b \sigma(t) dt = -P. \quad (3.55)$$

The integration limits of singular integral equation and equilibrium equation are modified as $(0, b)$ for triangular punch contact problem. In order to solve the singular integral equation, it is required to normalize the interval from $(0, b)$ to $(-1, 1)$. This normalization procedure is done by the following change of variables:

$$l = \frac{b}{2}, \quad (3.56)$$

$$X = \frac{b}{2}r + \frac{b}{2}, \quad 0 < X < b, \quad -1 < r < 1, \quad (3.57)$$

$$t = \frac{b}{2}s + \frac{b}{2}, \quad 0 < t < b, \quad -1 < s < 1, \quad (3.58)$$

$$k_{11}(t, X) = \frac{2}{b}k_{11}\left(\frac{b}{2}s + \frac{b}{2}, \frac{b}{2}r + \frac{b}{2}\right) = \frac{2}{b}k_{11}^*(s, r), \quad (3.59)$$

$$k_{12}(t, X) = \frac{2}{b}k_{12}\left(\frac{b}{2}s + \frac{b}{2}, \frac{b}{2}r + \frac{b}{2}\right) = \frac{2}{b}k_{12}^*(s, r), \quad (3.60)$$

$$k_{21}(t, X) = \frac{2}{b}k_{21}\left(\frac{b}{2}s + \frac{b}{2}, \frac{b}{2}r + \frac{b}{2}\right) = \frac{2}{b}k_{21}^*(s, r), \quad (3.61)$$

$$k_{22}(t, X) = \frac{2}{b}k_{22}\left(\frac{b}{2}s + \frac{b}{2}, \frac{b}{2}r + \frac{b}{2}\right) = \frac{2}{b}k_{22}^*(s, r), \quad (3.62)$$

$$\lambda = \frac{2}{b}\xi, \quad (3.63)$$

$$\phi_{11}(\lambda) = \phi_{11}\left(\frac{2\xi}{b}\right) = \phi_{11}^*(\xi), \quad (3.64)$$

$$\phi_{12}(\lambda) = \phi_{12}\left(\frac{2\xi}{b}\right) = \phi_{12}^*(\xi), \quad (3.65)$$

$$\phi_{21}(\lambda) = \phi_{21}\left(\frac{2\xi}{b}\right) = \phi_{21}^*(\xi), \quad (3.66)$$

$$\phi_{22}(\lambda) = \phi_{22}\left(\frac{2\xi}{b}\right) = \phi_{22}^*(\xi), \quad (3.67)$$

$$\gamma_1 = \frac{2}{b}\gamma_1^*, \quad (3.68)$$

$$\sigma(X) = \sigma\left(\frac{b}{2}r + \frac{b}{2}\right) = -\frac{4\mu_{10}}{\kappa_1 + 1} \tan \theta \Theta(r),$$

$$\sigma(t) = \sigma\left(\frac{b}{2}s + \frac{b}{2}\right) = -\frac{4\mu_{10}}{\kappa_1 + 1} \tan \theta \Theta(s). \quad (3.69)$$

When we substitute normalized quantities into the singular integral equation (3.54), the following equation is obtained:

$$\begin{aligned} \omega_2 \eta \Theta(r) + \frac{1}{\pi} \int_{-1}^1 \left\{ \frac{-\pi \omega_1}{\left(\frac{b}{2}s + \frac{b}{2}\right) - \left(\frac{b}{2}r + \frac{b}{2}\right)} + \frac{2}{b} k_{11}^*(s, r) \right\} \Theta(s) \frac{b}{2} ds \\ + \frac{1}{\pi} \int_{-1}^1 \frac{2}{b} \eta k_{12}^*(s, r) \Theta(s) \frac{b}{2} ds = 1. \end{aligned} \quad (3.70)$$

When equation (3.70) is simplified and rearranged, the following singular integral equation is derived:

$$\omega_2 \eta \Theta(r) + \frac{1}{\pi} \int_{-1}^1 \left\{ \frac{-\pi \omega_1}{s - r} + k_{11}^*(s, r) + \eta k_{12}^*(s, r) \right\} \Theta(s) ds = 1, \quad (3.71)$$

The equilibrium equation for the triangular punch contact problem is written using normalized variables as follows:

$$\int_{-1}^1 \Theta(s) ds = \frac{\kappa_1 + 1}{2\mu_{10}} \frac{P}{\tan \theta b}. \quad (3.72)$$

Terms shown with the sign *, the inhomogeneity constant γ_1 is replaced by γ_1^* . Note that for the homogenous elastic coating problem $\gamma_1 = 0$, hence $\gamma_1^* = 0$.

Kernels of the singular integral equation using normalized variables can be written as follows:

$$k_{11}^*(s, r) = \frac{b}{2} k_{11}(t, X) \rightarrow k_{11}^*(s, r) = \frac{-4}{\kappa_1 + 1} \int_0^\infty \phi_{11}^*(\xi) \sin(\xi(s-r)) d\xi, \quad (3.73)$$

$$k_{12}^*(s, r) = \frac{b}{2} k_{12}(t, X) \rightarrow k_{12}^*(s, r) = \frac{-4}{\kappa_1 + 1} \int_0^\infty \phi_{12}^*(\xi) \cos(\xi(s-r)) d\xi, \quad (3.74)$$

$$k_{21}^*(s, r) = \frac{b}{2} k_{21}(t, X) \rightarrow k_{21}^*(s, r) = \frac{-4}{\kappa_1 + 1} \int_0^\infty \phi_{21}^*(\xi) \sin(\xi(s-r)) d\xi, \quad (3.75)$$

$$k_{22}^*(s, r) = \frac{b}{2} k_{22}(t, X) \rightarrow k_{22}^*(s, r) = \frac{-4}{\kappa_1 + 1} \int_0^\infty \phi_{22}^*(\xi) \sin(\xi(s-r)) d\xi, \quad (3.76)$$

where

$$\phi_{11}^*(\xi) = \frac{-\xi(\kappa_1 - 1)}{\Delta_{21}(\xi)} \{r_{81} d_5 + r_{71} d_6\} - (e_{10} + e_{20}), \quad (3.77)$$

$$\phi_{12}^*(\xi) = \frac{i\xi}{\Delta_{21}(\xi)} \{r_{51} d_7 + r_{61} d_8\} - (f_{10} + f_{20}), \quad (3.78)$$

$$\phi_{21}^*(\xi) = \frac{-\xi}{\Delta_{21}(\xi)} \{r_{61} d_3 + r_{51} d_4\} - (g_{10} + g_{20}), \quad (3.79)$$

$$\phi_{22}^*(\xi) = \frac{i\xi(\kappa_1 - 1)}{\Delta_{21}(\xi)} \{r_{81} d_1 + r_{71} d_2\} - (h_{10} + h_{20}). \quad (3.80)$$

The triangular punch has a sharp corner at trailing end $X = 0$, and there is a smooth contact point between the punch and the coating at $X = b$. The index of the singular integral equation is $\kappa_0 = 0$, which requires that α must be positive and β must be negative. Determination of the index of the singular integral equation depends on the physics of the problem as described in the work conducted by Erdogan et al. [73]. The powers of the stress singularities α and β are calculated by,

If $\eta > 0$:

$$\alpha = \frac{1}{\pi} \tan^{-1} \left| \frac{1}{\omega_2 \eta} \right|, \quad \beta = -\frac{1}{\pi} \tan^{-1} \left| \frac{1}{\omega_2 \eta} \right|. \quad (3.81)$$

If $\eta < 0$:

$$\alpha = 1 - \frac{1}{\pi} \tan^{-1} \left| \frac{1}{\omega_2 \eta} \right|, \quad \beta = -1 + \frac{1}{\pi} \tan^{-1} \left| \frac{1}{\omega_2 \eta} \right|. \quad (3.82)$$

Powers of the stress singularities α and β are functions of ω_2 and η . ω_2 involves $f_{10} + f_{20}$ term where $f_{10} + f_{20}$ is a lengthy function of κ_1 and c_1 . Explicit form of $f_{10} + f_{20}$ is given in Appendix-A. The Poisson's ratio along the graded coating is assumed to be constant since the variation of the Poisson's ratio along the graded coating has a very small effect on contact stresses [46].

In frictional dynamic contact problems, consequently, the powers of stress singularity α and β depend on the coefficient of friction η , the Poisson's ratio ν_1 and the dimensionless punch speed c_1 .

The governing singular integral equation for the dynamic contact problem has been derived. This integral equation is a second type which involves a Cauchy kernel and Fredholm kernels. Generally, the solution of the singular integral equations can be done by either function theoretical method or numerical methods. In the present

study, we use numerical methods to solve the singular integral equation. Using Jacobi orthogonal polynomials, the singular integral equation is reduced to an infinite number of linear algebraic equation set. The numerical solution of the singular integral equation consisting of infinite series and Jacobi polynomials can be expressed by,

$$\Theta(s) = \sum_{n=0}^{\infty} c_n W(s) P_n^{(\alpha,\beta)}(s), \quad (3.83)$$

$$W(s) = (1-s)^\alpha (1+s)^\beta. \quad (3.84)$$

where c_n are the undetermined coefficients ($n = 0, 1, 2, \dots, N$). Substituting (3.83) into singular integral equation (3.71) yields the following equation:

$$\begin{aligned} & \sum_{n=0}^{\infty} c_n \left\{ \omega_2 \eta P_n^{(\alpha,\beta)}(r) W(r) - \frac{\pi \omega_1}{\pi} \int_{-1}^1 \frac{P_n^{(\alpha,\beta)}(s) W(s)}{s-r} ds \right\} \\ & + \sum_{n=0}^{\infty} c_n \left\{ \frac{1}{\pi} \int_{-1}^1 k_{11}^*(s, r) + \eta k_{12}^*(s, r) \right\} W(s) P_n^{(\alpha,\beta)}(s) ds = 1. \end{aligned} \quad (3.85)$$

For neatness, terms consisting of equation (3.85) can be grouped as follows:

$$Z_{1n}(r) = \frac{1}{\pi} \int_{-1}^1 k_{11}^*(s, r) W(s) P_n^{(\alpha,\beta)}(s) ds, \quad (3.86)$$

$$Z_{2n}(r) = \frac{1}{\pi} \int_{-1}^1 \eta k_{12}^*(s, r) W(s) P_n^{(\alpha,\beta)}(s) ds, \quad (3.87)$$

$$K_n(r) = Z_{1n}(r) + Z_{2n}(r). \quad (3.88)$$

Using orthogonality property of Jacobi polynomials described in Appendix-C, governing singular integral equation of the problem is reduced to the following set of linear algebraic equations:

$$\sum_{n=0}^{\infty} c_n \left\{ \frac{\pi \omega_1}{\sin \pi \alpha} P_n^{(-\alpha, -\beta)}(r) + K_n(r) \right\} = 1, \quad -1 < r < 1. \quad (3.89)$$

Governing equation of the contact problem is reduced to a system of linear algebraic equation set with undetermined coefficients c_n . These undetermined coefficients can be found using the suitable expansion-collocation technique. The accuracy of the numerical solution is highly dependent on the selection of the collocation points r_k . The collocation points r_k are selected as the roots of the Jacobi polynomial. If the density of the collocation points is increased near the ends of integration, we will obtain more accurate results. Collocation points are determined by,

$$P_{N+1}^{(\alpha-1, \beta+1)}(r_k) = 0, \quad k = 1, \dots, N+1. \quad (3.90)$$

The relationship between the applied load by the punch and the contact length can be determined by using equilibrium equation.

$$c_0 \theta_0 = \frac{\kappa_1 + 1}{2 \mu_{10}} \frac{P}{\tan \theta b}. \quad (3.91)$$

where θ_0 can be calculated by,

$$\theta_0 = \frac{2\pi\alpha}{\sin \pi\alpha}. \quad (3.92)$$

Triangular punch contact problem is an incomplete contact problem since there is a relation between the contact length and the load applied by the rigid triangular punch. The normalized load for a triangular punch can be calculated by the following formulation:

$$\frac{P}{\mu_{10} \tan \theta} = \frac{2c_0 \theta_0}{\kappa_1 + 1} b. \quad (3.93)$$

In normalized coordinates, the solution can be written as follows:

$$\Theta(r) = \left(\frac{1-r}{1+r} \right)^\alpha \sum_{n=0}^N c_n P_n^{(\alpha, \beta)}(r). \quad (3.94)$$

In spatial coordinates, the normal and shear stresses on the contact surface can be expressed as follows:

$$\frac{\sigma_{1YY}(X, 0)}{\mu_{10} \tan \theta} = -\frac{4}{\kappa_1 + 1} \left(\frac{b-X}{X} \right)^\alpha \sum_{n=0}^N c_n P_n^{(\alpha, \beta)} \left(\frac{2X-b}{b} \right), \quad (3.95)$$

$$\frac{\sigma_{1XY}(X, 0)}{\mu_{10} \tan \theta} = -\frac{4\eta}{\kappa_1 + 1} \left(\frac{b-X}{X} \right)^\alpha \sum_{n=0}^N c_n P_n^{(\alpha, \beta)} \left(\frac{2X-b}{b} \right). \quad (3.96)$$

The lateral contact stress on the contact surface is expressed by the following equation:

$$\begin{aligned} \sigma_{1XX}(X, 0) = & \left[2\omega_4 + \frac{3-\kappa_1}{\kappa_1 + 1} \right] \sigma(X) + \frac{2\eta}{\pi} \int_0^b \frac{\pi \omega_3}{t-X} \sigma(t) dt \\ & - \frac{2}{\pi} \int_0^b [\eta k_{21}(t, X) + k_{22}(t, X)] \sigma(t) dt, \end{aligned} \quad (3.97)$$

$$\frac{\sigma_{1XX}(X, 0)}{\mu_{10} \tan \theta} = \frac{4}{\kappa_1 + 1} \left\{ \begin{aligned} & - \left(2\omega_4 + \frac{3-\kappa_1}{\kappa_1 + 1} \right) \Theta(r) \\ & - \frac{2\eta}{\pi} \int_{-1}^1 \frac{\pi \omega_3 \Theta(s)}{s-r} ds + \frac{2}{\pi} \int_{-1}^1 (\eta k_{21}^*(s, r) + k_{22}^*(s, r)) \Theta(s) ds \end{aligned} \right\}. \quad (3.98)$$

The mode-I stress intensity factor at the sharp end of the triangular punch can be calculated by the following formula [45]:

$$k_I(0) = -\lim_{X \rightarrow 0} x^\alpha \sigma(X) = \frac{4\mu_{10} \tan \theta b^\alpha}{\kappa_1 + 1} \sum_{n=0}^N c_n P_n^{(\alpha, \beta)}(-1). \quad (3.99)$$

In a non-dimensional form, the normalized stress intensity factor can be calculated by,

$$K_I(0) = \frac{k_I(0)}{\mu_{10} \tan \theta b^\alpha} = -\frac{4}{\kappa_1 + 1} \sum_{n=0}^N c_n P_n^{(\alpha, \beta)}(-1). \quad (3.100)$$

The powers of the stress singularities are calculated for the triangular punch and some numerical values are presented with respect to various coefficient of friction η and dimensionless punch speed c_1 in Table 3.2. In frictionless contacts, although punch speed is increased, the powers of stress singularities remain the same value. However, in frictional contacts, both powers of the stress singularities begin to change. The higher coefficient of friction value we take, the greater variation in the powers of stress singularities we observe.

Table 3.2: The powers of stress singularity for a triangular punch $\nu_1 = 0.25$.

η	c_1	α	β
0.0	0.0	0.500000	-0.500000
	0.4	0.500000	-0.500000
	0.7	0.500000	-0.500000
	0.8	0.500000	-0.500000
0.3	0.0	0.468274	-0.468274
	0.4	0.460523	-0.460523
	0.6	0.443885	-0.443885
	0.8	0.372402	-0.372402
0.5	0.0	0.447432	-0.447432
	0.4	0.434794	-0.434794
	0.6	0.408132	-0.408132
	0.8	0.304248	-0.304248
0.7	0.0	0.427033	-0.427033
	0.4	0.409898	-0.409898
	0.6	0.374607	-0.374607
	0.8	0.251779	-0.251779

3.3 Semi-circular punch problem

The geometry of the semi-circular punch contact problem is shown in Figure 3.3. A coating of thickness h_1 is perfectly bonded to the substrate. The right hand side of the singular integral equation involves the displacement gradient on the contact surface. Note that, for the rigid semi-circular punch contact problem, normal displacement beneath the punch is a quadratic function due to the semi-circular profile, and correspondingly the displacement gradient on the contact surface becomes a linear function. R_1 denotes the radius of the semi-circular punch.

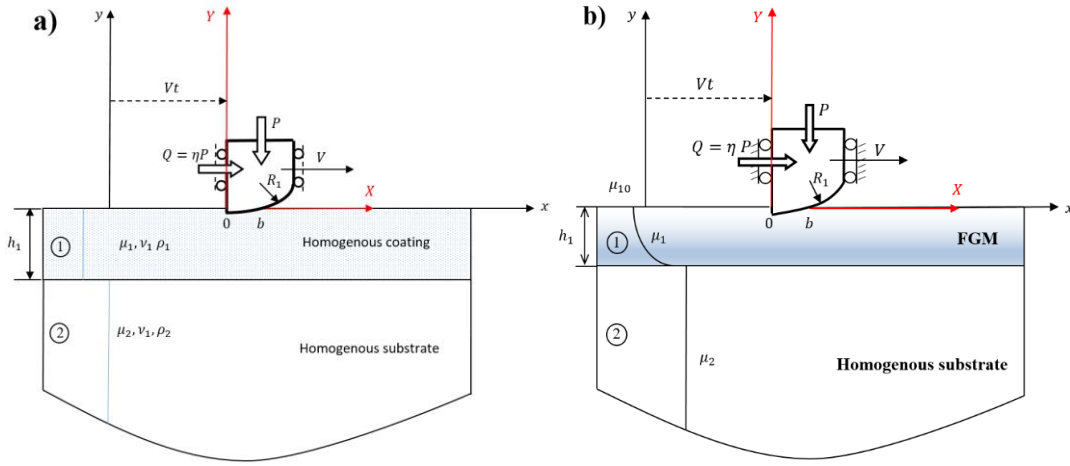


Figure 3.3: The moving rigid semi-circular punch on (a) homogenous elastic coating (b) functionally graded coating

$$v_1(X,0) = -v_0 + \frac{X^2}{2R_1}, \quad (3.101)$$

$$\frac{\partial v_1(X,0)}{\partial X} = \frac{X}{R_1}, \quad (3.102)$$

$$-\omega_2 \eta \sigma(X) - \frac{1}{\pi} \int_0^b \left[\frac{-\pi \omega_1}{t-X} + k_{11}(t,X) + \eta k_{12}(t,X) \right] \sigma(t) dt = \frac{4\mu_{10}}{\kappa_1 + 1} \frac{\partial v_1(X,0)}{\partial X}, \quad (3.103)$$

$$\int_0^b \sigma(t) dt = -P. \quad (3.104)$$

The equilibrium equation for the semi-circular punch contact problem is shown by equation (3.104). In order to solve the singular integral equation, normalization procedure is needed. The normalization procedure for semi-circular punch contact problem is performed in two parts. First part is carried out as follows:

$$t = t^* R_1, \quad (3.105)$$

$$X = X^* R_1, \quad (3.106)$$

$$b = b^* R_1, \quad (3.107)$$

$$\sigma(t) = \sigma^*(t^*), \quad (3.108)$$

$$k_{11}(t, X) = \frac{1}{R_1} k_{11}^*(t^*, X^*), \quad (3.109)$$

$$k_{12}(t, X) = \frac{1}{R_1} k_{12}^*(t^*, X^*), \quad (3.110)$$

$$k_{21}(t, X) = \frac{1}{R_1} k_{21}^*(t^*, X^*), \quad (3.111)$$

$$k_{22}(t, X) = \frac{1}{R_1} k_{22}^*(t^*, X^*), \quad (3.112)$$

$$\begin{aligned} -\omega_2 \eta \sigma^*(t^*) - \frac{1}{\pi} \int_0^{b^*} \left[-\frac{\pi \omega_1}{t^* - X^*} + k_{11}^*(t^*, X^*) + \eta k_{12}^*(t^*, X^*) \right] \sigma^*(t^*) dt^* = \\ = \frac{4\mu_{10}}{\kappa_1 + 1} X^*, \end{aligned} \quad (3.113)$$

The second normalization step is conducted to normalize the interval from $(0, b)$ to $(-1, 1)$. This normalization procedure is performed by the following change of variables:

$$l = \frac{b^*}{2}, \quad (3.114)$$

$$X^* = \frac{b^*}{2}r + \frac{b^*}{2}, \quad 0 < X^* < b^*, \quad -1 < r < 1, \quad (3.115)$$

$$t^* = \frac{b^*}{2}s + \frac{b^*}{2}, \quad 0 < t^* < b^*, \quad -1 < s < 1, \quad (3.116)$$

$$\sigma^*(X^*) = \sigma^*\left(\frac{b^*}{2}r + \frac{b^*}{2}\right) = \Theta(r), \quad \sigma^*(t^*) = \sigma^*\left(\frac{b^*}{2}s + \frac{b^*}{2}\right) = \Theta(s), \quad (3.117)$$

$$k_{11}^*(t^*, X^*) = \frac{1}{l} k_{11}^*\left(\frac{b^*}{2}s + \frac{b^*}{2}, \frac{b^*}{2}r + \frac{b^*}{2}\right) = \frac{2}{b^*} \overline{k_{11}}(s, r), \quad (3.118)$$

$$k_{12}^*(t, X) = \frac{1}{l} k_{12}^*\left(\frac{b^*}{2}s + \frac{b^*}{2}, \frac{b^*}{2}r + \frac{b^*}{2}\right) = \frac{2}{b^*} \overline{k_{12}}(s, r), \quad (3.119)$$

$$k_{21}^*(t^*, X^*) = \frac{1}{l} k_{21}^*\left(\frac{b^*}{2}s + \frac{b^*}{2}, \frac{b^*}{2}r + \frac{b^*}{2}\right) = \frac{2}{b^*} \overline{k_{21}}(s, r), \quad (3.120)$$

$$k_{22}^*(t^*, X^*) = \frac{1}{l} k_{22}^*\left(\frac{b^*}{2}s + \frac{b^*}{2}, \frac{b^*}{2}r + \frac{b^*}{2}\right) = \frac{2}{b^*} \overline{k_{22}}(s, r), \quad (3.121)$$

$$\lambda = \frac{2}{b^*} \xi, \quad (3.122)$$

$$\gamma_1 = \frac{2}{b^*} \gamma_1^*, \quad (3.123)$$

$$\omega_2 \eta \Theta(r) + \frac{1}{\pi} \int_{-1}^1 \left\{ \frac{-\pi \omega_1}{\left(\frac{b^*}{2} s + \frac{b^*}{2}\right) - \left(\frac{b^*}{2} r + \frac{b^*}{2}\right)} + \frac{2}{b^*} \overline{k_{11}}(s, r) \right\} \Theta(s) \frac{b^*}{2} ds \quad (3.124)$$

$$+ \frac{1}{\pi} \int_{-1}^1 \frac{2}{b^*} \eta \overline{k_{12}}(s, r) \Theta(s) \frac{b^*}{2} ds = (r+1),$$

After rearranging and simplification of equation (3.124), we found the normalized singular integral equation for the semi-circular punch contact problem.

$$\omega_2 \eta \Theta(r) + \frac{1}{\pi} \int_{-1}^1 \left\{ -\frac{\pi \omega_1}{s-r} + \overline{k_{11}}(s, r) + \eta \overline{k_{12}}(s, r) \right\} \Theta(s) ds = r+1, \quad (3.125)$$

The equilibrium equation for the semi-circular punch contact problem in normalized form can be written as follows:

$$\int_{-1}^1 \Theta(s) ds = -\frac{\kappa_1 + 1}{\mu_{10}} \frac{P}{R_1 b^{*2}}. \quad (3.126)$$

$$\phi_{11}(\lambda) = \phi_{11} \left(\frac{2\xi}{b^*} \right) = \phi_{11}^*(\xi), \quad (3.127)$$

$$\phi_{12}(\lambda) = \phi_{12} \left(\frac{2\xi}{b^*} \right) = \phi_{12}^*(\xi), \quad (3.128)$$

$$\phi_{21}(\lambda) = \phi_{21} \left(\frac{2\xi}{b^*} \right) = \phi_{21}^*(\xi), \quad (3.129)$$

$$\phi_{22}(\lambda) = \phi_{22} \left(\frac{2\xi}{b^*} \right) = \phi_{22}^*(\xi), \quad (3.130)$$

Terms denoted with the sign *, the inhomogeneity constant γ_1 is replaced by γ_1^* .

Note that for the homogenous elastic coating problem $\gamma_1 = 0$, hence $\gamma_1^* = 0$.

Kernels of the singular integral equation using normalized variables can be written as follows:

$$\bar{k}_{11}(s, r) = \frac{b^*}{2} k_{11}^*(t^*, X^*) \rightarrow \bar{k}_{11}(s, r) = \frac{-4}{\kappa_1 + 1} \int_0^\infty \phi_{11}^*(\xi) \sin(\xi(s-r)) d\xi, \quad (3.131)$$

$$\bar{k}_{12}(s, r) = \frac{b^*}{2} k_{12}^*(t^*, X^*) \rightarrow \bar{k}_{12}(s, r) = \frac{-4}{\kappa_1 + 1} \int_0^\infty \phi_{12}^*(\xi) \cos(\xi(s-r)) d\xi, \quad (3.132)$$

$$\bar{k}_{21}(s, r) = \frac{b^*}{2} k_{21}^*(t^*, X^*) \rightarrow \bar{k}_{21}(s, r) = \frac{-4}{\kappa_1 + 1} \int_0^\infty \phi_{21}^*(\xi) \sin(\xi(s-r)) d\xi, \quad (3.133)$$

$$\bar{k}_{22}(s, r) = \frac{b^*}{2} k_{22}^*(t^*, X^*) \rightarrow \bar{k}_{22}(s, r) = \frac{-4}{\kappa_1 + 1} \int_0^\infty \phi_{22}^*(\xi) \sin(\xi(s-r)) d\xi. \quad (3.134)$$

where

$$\phi_{11}^*(\xi) = \frac{-\xi(\kappa_1 - 1)}{\Delta_{21}(\xi)} \{r_{81} d_5 + r_{71} d_6\} - (e_{10} + e_{20}), \quad (3.135)$$

$$\phi_{12}^*(\xi) = \frac{i\xi}{\Delta_{21}(\xi)} \{r_{51} d_7 + r_{61} d_8\} - (f_{10} + f_{20}), \quad (3.136)$$

$$\phi_{21}^*(\xi) = \frac{-\xi}{\Delta_{21}(\xi)} \{r_{61} d_3 + r_{51} d_4\} - (g_{10} + g_{20}), \quad (3.137)$$

$$\phi_{22}^*(\xi) = \frac{i\xi(\kappa_1 - 1)}{\Delta_{21}(\xi)} \{r_{81} d_1 + r_{71} d_2\} - (h_{10} + h_{20}), \quad (3.138)$$

Singular behavior of the unknown normal contact stress can be determined through the function-theoretic analysis as described by Erdogan [73]. Since normal contact stress is unbounded at the sharp end and bounded at the smooth contact point, the powers of the stress singularities should be $\alpha > 0$, $\beta < 0$. The index of the integral

equation should be $\kappa_0 = 0$. Powers of stress singularities α and β are calculated by the following formulations:

If $\eta > 0$:

$$\alpha = \frac{1}{\pi} \tan^{-1} \left| \frac{1}{\omega_2 \eta} \right|, \quad \beta = -\frac{1}{\pi} \tan^{-1} \left| \frac{1}{\omega_2 \eta} \right|. \quad (3.139)$$

If $\eta < 0$:

$$\alpha = 1 - \frac{1}{\pi} \tan^{-1} \left| \frac{1}{\omega_2 \eta} \right|, \quad \beta = -1 + \frac{1}{\pi} \tan^{-1} \left| \frac{1}{\omega_2 \eta} \right|. \quad (3.140)$$

Powers of the stress singularities α and β are functions of ω_2 and η . ω_2 involves $f_{10} + f_{20}$ where $f_{10} + f_{20}$ is a lengthy function of κ_1 and c_1 . Explicit form of $f_{10} + f_{20}$ is given in Appendix-A. The Poisson's ratio along the graded coating is assumed to be constant since the variation of Poisson's ratio along the graded coating has a small effect on contact stresses [46].

In frictional dynamic contact problems, the powers of stress singularity α and β depend on the coefficient of friction η , the Poisson's ratio ν_1 and dimensionless punch speed c_1 .

The governing singular integral equation of the dynamic contact problem is obtained. This integral equation is a second type equation involving a Cauchy kernel and Fredholm kernels. Generally, the solution of the singular integral equations can be done by either function theoretical method or numerical methods. In present study, we use numerical methods to solve the singular integral equation. Using Jacobi orthogonal polynomials, the singular integral equation is reduced to an infinite number of linear algebraic equation set. The numerical solution of the singular

integral equation consisting of infinite series and Jacobi polynomials can be expressed by,

$$\Theta(s) = \sum_{n=0}^{\infty} c_n W(s) P_n^{(\alpha,\beta)}(s), \quad (3.141)$$

$$W(s) = (1-s)^\alpha (1+s)^\beta. \quad (3.142)$$

where c_n are the undetermined coefficients ($n = 0, 1, 2, \dots, N$). Substituting (3.141) into (3.125) yields the following equation:

$$\begin{aligned} & \sum_{n=0}^{\infty} c_n \left\{ \omega_2 \eta P_n^{(\alpha,\beta)}(r) W(r) - \frac{1}{\pi} \int_{-1}^1 \frac{\pi \omega_1 P_n^{(\alpha,\beta)}(s) W(s)}{s-r} ds \right\} \\ & + \sum_{n=0}^{\infty} c_n \left\{ \frac{1}{\pi} \int_{-1}^1 \overline{k_{11}}(s, r) + \eta \overline{k_{12}}(s, r) \right\} W(s) P_n^{(\alpha,\beta)}(s) ds = r + 1, \end{aligned} \quad (3.143)$$

For neatness, equation (3.143) can be divided into minor parts as follows:

$$Z_{1n}(r) = \frac{1}{\pi} \int_{-1}^1 \overline{k_{11}}(s, r) W(s) P_n^{(\alpha,\beta)}(s) ds, \quad (3.144)$$

$$Z_{2n}(r) = \frac{1}{\pi} \int_{-1}^1 \eta \overline{k_{12}}(s, r) W(s) P_n^{(\alpha,\beta)}(s) ds, \quad (3.145)$$

$$K_n(r) = Z_{1n}(r) + Z_{2n}(r). \quad (3.146)$$

Using the orthogonality property of Jacobi polynomials described in Appendix-C, governing singular integral equation is reduced to the following set of linear algebraic equations with undetermined coefficients c_n .

$$\sum_{n=0}^{\infty} c_n \left\{ \frac{\pi \omega_1}{\sin \pi \alpha} P_n^{(-\alpha, -\beta)}(r) + K_n(r) \right\} = r + 1, \quad -1 < r < 1. \quad (3.147)$$

These undetermined coefficients can be found using the suitable expansion-collocation technique. The accuracy of the numerical solution is highly dependent on the selection of the collocation points r_k . The collocation points are selected as the roots of the Jacobi polynomial. If the density of the collocation points r_k is increased near the ends of integration, we will obtain more accurate results. Collocation points are determined by,

$$P_{N+1}^{(\alpha-1, \beta+1)}(r_k) = 0, \quad k = 1, \dots, N+1. \quad (3.148)$$

The relationship between the punch load and the contact length is found using equilibrium equation and this equation is given by the following formula:

$$c_0 \theta_0 = \frac{(\kappa_1 + 1)}{\mu_{10}} \frac{P}{R_1 b^{*2}}, \quad (3.149)$$

where θ_0 can be calculated from the following equation:

$$\theta_0 = \frac{2\pi\alpha}{\sin \pi\alpha}. \quad (3.150)$$

Semi-circular punch contact problem is an incomplete contact problem since there is a relation between the contact length and the load applied by the rigid semi-circular punch. The normalized load applied by the semi-circular punch can be calculated using the following equation:

$$\frac{P}{\mu_{10} R_1} = \frac{c_0 \theta_0}{\kappa_1 + 1} b^{*2}. \quad (3.151)$$

The normal contact stress beneath the semi-circular punch in normalized coordinates is calculated by the following equation:

$$\sigma^*(X^*) = -\frac{2\mu_{10}}{(\kappa_1 + 1)} b^* \left(\frac{1-r}{1+r} \right)^\alpha \sum_{n=0}^N c_n P_n^{(\alpha, \beta)}(r), \quad (3.152)$$

In spatial coordinates, the normal and shear contact stresses can be expressed as follows:

$$\frac{\sigma_{1YY}(X^*, 0)}{\mu_{10}} = -\frac{2\mu_{10}}{(\kappa_1 + 1)} b^* \left(\frac{b^* - X^*}{X^*} \right)^\alpha \sum_{n=0}^N c_n P_n^{(\alpha, \beta)} \left(\frac{2X^* - b^*}{b^*} \right), \quad (3.153)$$

$$\frac{\sigma_{1XY}(X^*, 0)}{\mu_{10}} = -\frac{2\eta\mu_{10}}{(\kappa_1 + 1)} b^* \left(\frac{b^* - X^*}{X^*} \right)^\alpha \sum_{n=0}^N c_n P_n^{(\alpha, \beta)} \left(\frac{2X^* - b^*}{b^*} \right), \quad (3.154)$$

The lateral contact stress distribution is expressed by the following equation:

$$\begin{aligned} \sigma_{1XX}(X, 0) = & \left[2\omega_4 + \frac{3 - \kappa_1}{\kappa_1 + 1} \right] \sigma(X) + \frac{2\eta}{\pi} \int_0^b \frac{\pi \omega_3}{t - X} \sigma(t) dt \\ & - \frac{2}{\pi} \int_0^b [\eta k_{21}(t, X) + k_{22}(t, X)] \sigma(t) dt, \end{aligned} \quad (3.155)$$

In normalized coordinates, the lateral contact stress distribution is written as follows:

$$\frac{\sigma_{1XX}(X, 0)}{\mu_{10}} = \frac{2}{\kappa_1 + 1} b^* \left\{ \begin{aligned} & - \left[2\omega_4 + \frac{3 - \kappa_1}{\kappa_1 + 1} \right] \Theta(r) \\ & - \frac{2\eta}{\pi} \int_{-1}^1 \frac{\pi \omega_3 \Theta(s)}{s - r} ds + \frac{2}{\pi} \int_{-1}^1 [\eta \bar{k}_{21}(s, r) + \bar{k}_{22}(s, r)] \Theta(s) ds \end{aligned} \right\}. \quad (3.156)$$

The following equation is useful to calculate the mode-I stress intensity factor at the sharp end of the semi-circular punch [45]:

$$k_I(0) = -\lim_{X \rightarrow 0} X^\alpha \sigma(X) = -\frac{2\mu_{10}}{\kappa_1 + 1} \frac{b^{1+\alpha}}{R_1} \sum_{n=0}^N c_n P_n^{(\alpha, \beta)}(-1). \quad (3.157)$$

In a non-dimensional form, the normalized mode-I stress intensity factor at the sharp end is defined by,

$$K_I(0) = \frac{k_I(0)}{\mu_{10} b^{1+\alpha} / R_1} = \frac{2}{\kappa_1 + 1} \sum_{n=0}^N c_n P_n^{(\alpha, \beta)}(-1). \quad (3.158)$$

The powers of the stress singularities α and β are calculated for various values of coefficient of friction η and dimensionless punch speed c_1 . Table 3.3 tabulates the powers of the stress singularities. Since physics of the problem is similar to that of triangular punch contact problem, results are the same. In frictionless contacts, α and β remain the same value although punch speed is increased from 0.0 to 0.8. Nevertheless, variations begin with respect to punch speed for frictional cases and the highest variation of the powers of the stress singularity occur when friction coefficient is taken as $\eta = 0.7$.

Table 3.3: The powers of stress singularity for a semi-circular punch $\nu_1 = 0.25$.

η	c_1	α	β
0.0	0.0	0.500000	-0.500000
	0.4	0.500000	-0.500000
	0.7	0.500000	-0.500000
	0.8	0.500000	-0.500000
0.3	0.0	0.468274	-0.468274
	0.4	0.460523	-0.460523
	0.6	0.443885	-0.443885
	0.8	0.372402	-0.372402
0.5	0.0	0.447432	-0.447432
	0.4	0.434794	-0.434794
	0.6	0.408132	-0.408132
	0.8	0.304248	-0.304248
0.7	0.0	0.427033	-0.427033
	0.4	0.409898	-0.409898
	0.6	0.374607	-0.374607
	0.8	0.251779	-0.251779

3.4 Cylindrical punch problem

The geometry of the cylindrical punch contact problem is shown in Figure 3.4. A coating of thickness h_1 is perfectly bonded to the substrate. The contact area $(b-a)$ is assumed much smaller than the radius of the punch R_1 . The right hand side of the singular integral equation involves the displacement gradient on the contact surface. Note that, for the rigid cylindrical punch contact problem, normal displacement beneath the punch is a quadratic function due to the cylindrical profile, and correspondingly the displacement gradient on the contact surface becomes a linear function.

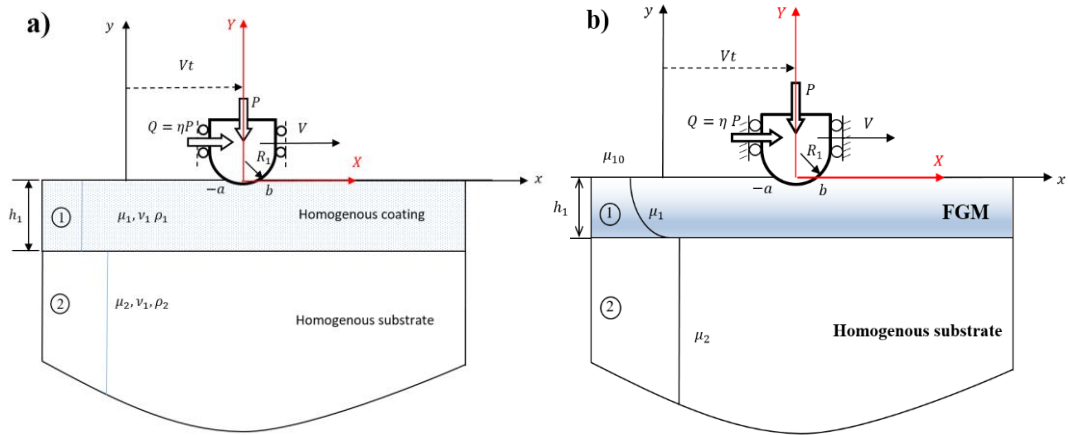


Figure 3.4: The moving rigid cylindrical punch on (a) homogenous elastic coating
(b) functionally graded coating

$$v_1(X,0) = -v_0 + \frac{X^2}{2R_1}, \quad (3.159)$$

$$\frac{\partial v_1(X,0)}{\partial X} = \frac{X}{R_1}, \quad (3.160)$$

$$-\omega_2 \eta \sigma(X) - \frac{1}{\pi} \int_{-a}^b \left[\frac{-\pi \omega_1}{t-X} + k_{11}(t, X) + \eta k_{12}(t, X) \right] \sigma(t) dt = \frac{4\mu_{10}}{\kappa_1 + 1} \frac{\partial v_1(X,0)}{\partial X}, \quad (3.161)$$

$$\int_{-a}^b \sigma(t) dt = -P. \quad (3.162)$$

The equilibrium equation is given by equation (3.162) and it simply indicates that the summation of the normal contact stress on the contact zone equals to the applied load by the rigid cylindrical punch. The integration limits for the cylindrical punch contact problem are $-a$ and b . For the cylindrical punch contact problem, the normalization procedure should be carried out in two steps. In the first step, the following definitions are required:

$$t = t^* R_1, \quad (3.163)$$

$$X = X^* R_1, \quad (3.164)$$

$$a = a^* R_1, \quad (3.165)$$

$$b = b^* R_1, \quad (3.166)$$

$$k_{11}(t, X) = \frac{1}{R_1} k_{11}^*(t^*, X^*), \quad (3.167)$$

$$k_{12}(t, X) = \frac{1}{R_1} k_{12}^*(t^*, X^*), \quad (3.168)$$

$$k_{21}(t, X) = \frac{1}{R_1} k_{21}^*(t^*, X^*), \quad (3.169)$$

$$k_{22}(t, X) = \frac{1}{R_1} k_{22}^*(t^*, X^*), \quad (3.170)$$

$$\sigma(t) = \sigma^*(t^*). \quad (3.171)$$

Using variables shown by * at the end of the first normalization step, the singular integral equation and the equilibrium equation are written as follows:

$$\begin{aligned}
-\omega_2 \eta \sigma(X) - \frac{1}{\pi} \int_{-a^*}^{b^*} \left[\frac{\pi \omega_1}{t^* - X^*} + k_{11}^*(t^*, X^*) + \eta k_{12}^*(t^*, X^*) \right] \sigma^*(t^*) dt^* = \\
= \frac{4\mu_{10}}{\kappa_1 + 1} X^*,
\end{aligned} \tag{3.172}$$

$$\int_{-a^*}^{b^*} \sigma^*(t^*) dt^* = -\frac{P}{R_1}. \tag{3.173}$$

In the second normalization step, in order to solve the singular integral equation numerically, it is required to normalize the interval from $(-a^*, b^*)$ to $(-1, 1)$. This normalization procedure is performed by the following change of variables:

$$l = \frac{b^* + a^*}{2}, \tag{3.174}$$

$$X^* = \frac{b^* + a^*}{2} r + \frac{b^* - a^*}{2}, \quad -a^* < X^* < b^*, \quad -1 < r < 1, \tag{3.175}$$

$$t^* = \frac{b^* + a^*}{2} s + \frac{b^* - a^*}{2}, \quad -a^* < t^* < b^*, \quad -1 < s < 1, \tag{3.176}$$

$$\begin{aligned}
k_{11}^*(t^*, X^*) &= \frac{1}{l} k_{11}^* \left(\frac{b^* + a^*}{2} s + \frac{b^* - a^*}{2}, \frac{b^* + a^*}{2} r + \frac{b^* - a^*}{2} \right) = \\
&= \frac{2}{b^* + a^*} \overline{k_{11}}(s, r),
\end{aligned} \tag{3.177}$$

$$\begin{aligned}
k_{12}^*(t^*, X^*) &= \frac{1}{l} k_{12}^* \left(\frac{b^* + a^*}{2} s + \frac{b^* - a^*}{2}, \frac{b^* + a^*}{2} r + \frac{b^* - a^*}{2} \right) = \\
&= \frac{2}{b^* + a^*} \overline{k_{12}}(s, r),
\end{aligned} \tag{3.178}$$

$$\begin{aligned}
k_{21}^*(t^*, X^*) &= \frac{1}{l} k_{21}^* \left(\frac{b^* + a^*}{2} s + \frac{b^* - a^*}{2}, \frac{b^* + a^*}{2} r + \frac{b^* - a^*}{2} \right) = \\
&= \frac{2}{b^* + a^*} \overline{k_{21}}(s, r),
\end{aligned} \tag{3.179}$$

$$\begin{aligned}
k_{22}^*(t^*, X^*) &= \frac{1}{l} k_{22}^* \left(\frac{b^* + a^*}{2} s + \frac{b^* - a^*}{2}, \frac{b^* + a^*}{2} r + \frac{b^* - a^*}{2} \right) = \\
&= \frac{2}{b^* + a^*} \overline{k_{22}}(s, r),
\end{aligned} \tag{3.180}$$

$$\sigma^*(t^*) = -\frac{2\mu_{10}}{\kappa_1 + 1} \Theta(s), \tag{3.181}$$

Using normalized quantities, the integral equation and the equilibrium equation can be written as follows:

$$\begin{aligned}
\omega_2 \eta \Theta(r) + \frac{1}{\pi} \int_{-1}^1 \left[-\frac{\pi \omega_1}{s-r} + \overline{k_{11}}(s, r) + \eta \overline{k_{12}}(s, r) \right] \Theta(s) ds = \\
= (b^* + a^*)r + (b^* - a^*),
\end{aligned} \tag{3.182}$$

$$\int_{-1}^1 \Theta(s) ds = \frac{\kappa_1 + 1}{b^* + a^*} \frac{P}{\mu_{10} R_1}. \tag{3.183}$$

$$\phi_{11}(\lambda) = \phi_{11} \left(\frac{2\xi}{b^* + a^*} \right) = \phi_{11}^*(\xi), \tag{3.184}$$

$$\phi_{12}(\lambda) = \phi_{12} \left(\frac{2\xi}{b^* + a^*} \right) = \phi_{12}^*(\xi), \tag{3.185}$$

$$\phi_{21}(\lambda) = \phi_{21} \left(\frac{2\xi}{b^* + a^*} \right) = \phi_{21}^*(\xi), \tag{3.186}$$

$$\phi_{22}(\lambda) = \phi_{22} \left(\frac{2\xi}{b^* + a^*} \right) = \phi_{22}^*(\xi), \tag{3.187}$$

$$\gamma_1 = \frac{2\gamma_1^*}{b^* + a^*}. \quad (3.188)$$

Terms denoted with the sign *, the inhomogeneity constant γ_1 is replaced by γ_1^* .

Note that for the homogenous elastic coating problem $\gamma_1 = 0$, hence $\gamma_1^* = 0$.

Kernels of the singular integral equation using normalized variables can be written as follows:

$$\overline{k}_{11}(s, r) = \frac{b^* + a^*}{2} k_{11}^*(t^*, X^*) \rightarrow \overline{k}_{11}(s, r) = \frac{-4}{\kappa_1 + 1} \int_0^\infty \phi_{11}^*(\xi) \sin(\xi(s-r)) d\xi, \quad (3.189)$$

$$\overline{k}_{12}(s, r) = \frac{b^* + a^*}{2} k_{12}^*(t^*, X^*) \rightarrow \overline{k}_{12}(s, r) = \frac{-4}{\kappa_1 + 1} \int_0^\infty \phi_{12}^*(\xi) \cos(\xi(s-r)) d\xi, \quad (3.190)$$

$$\overline{k}_{21}(s, r) = \frac{b^* + a^*}{2} k_{21}^*(t^*, X^*) \rightarrow \overline{k}_{21}(s, r) = \frac{-4}{\kappa_1 + 1} \int_0^\infty \phi_{21}^*(\xi) \sin(\xi(s-r)) d\xi, \quad (3.191)$$

$$\overline{k}_{22}(s, r) = \frac{b^* + a^*}{2} k_{22}^*(t^*, X^*) \rightarrow \overline{k}_{22}(s, r) = \frac{-4}{\kappa_1 + 1} \int_0^\infty \phi_{22}^*(\xi) \sin(\xi(s-r)) d\xi, \quad (3.192)$$

where

$$\phi_{11}^*(\xi) = \frac{-\xi(\kappa_1 - 1)}{\Delta_{21}(\xi)} \{r_{81} d_5 + r_{71} d_6\} - (e_{10} + e_{20}), \quad (3.193)$$

$$\phi_{12}^*(\xi) = \frac{i\xi}{\Delta_{21}(\xi)} \{r_{51} d_7 + r_{61} d_8\} - (f_{10} + f_{20}), \quad (3.194)$$

$$\phi_{21}^*(\xi) = \frac{-\xi}{\Delta_{21}(\xi)} \{r_{61} d_3 + r_{51} d_4\} - (g_{10} + g_{20}), \quad (3.195)$$

$$\phi_{22}^*(\xi) = \frac{i\xi(\kappa_1 - 1)}{\Delta_{21}(\xi)} \{r_{81} d_1 + r_{71} d_2\} - (h_{10} + h_{20}), \quad (3.196)$$

Singular behavior of the unknown normal contact stress can be determined through the function-theoretic analysis as described by Erdogan [73]. Since normal contact stress is bounded at trailing and leading ends of the cylindrical punch, the powers of the stress singularities should be $\alpha > 0$, $\beta > 0$. The index of the integral equation should be $\kappa_0 = -1$. Powers of stress singularities α and β are calculated by the following formulations:

If $\eta > 0$:

$$\alpha = \frac{1}{\pi} \tan^{-1} \left| \frac{1}{\omega_2 \eta} \right|, \quad \beta = 1 - \frac{1}{\pi} \tan^{-1} \left| \frac{1}{\omega_2 \eta} \right|. \quad (3.197)$$

If $\eta < 0$:

$$\alpha = 1 - \frac{1}{\pi} \tan^{-1} \left| \frac{1}{\omega_2 \eta} \right|, \quad \beta = \frac{1}{\pi} \tan^{-1} \left| \frac{1}{\omega_2 \eta} \right|. \quad (3.198)$$

Powers of stress singularities α and β are functions of ω_2 and η . ω_2 involves $f_{10} + f_{20}$ where $f_{10} + f_{20}$ is a lengthy function of κ_1 and c_1 . Explicit form of $f_{10} + f_{20}$ is provided in Appendix-A. The Poisson's ratio along the graded coating is assumed to be constant since the variation of Poisson's ratio along the graded coating has a small effect on contact stresses [46].

In frictional dynamic contact problems, consequently, the powers of stress singularities α and β depend on the coefficient of friction η , the Poisson's ratio ν_1 and the normalized punch speed c_1 .

The governing singular integral equation for the dynamic contact problem has been obtained in normalized form. This equation is a second type singular integral equation involving a Cauchy kernel and the Fredholm kernels. Generally, the solution of the singular integral equations can be done by either function theoretical

method or numerical methods. In present study, we use numerical methods to solve the singular integral equation. Using Jacobi orthogonal polynomials, the singular integral equation is reduced to an infinite number of linear algebraic equations. The numerical solution of the singular integral equation consisting of infinite series and Jacobi polynomials can be expressed by,

$$\Theta(s) = \sum_{n=0}^{\infty} c_n W(s) P_n^{(\alpha, \beta)}(s), \quad (3.199)$$

$$W(s) = (1-s)^\alpha (1+s)^\beta, \quad (3.200)$$

$W(s)$ is the corresponding weight function for numerical solution given by equation (3.199). We need one more normalization step. Quantities involving $\bar{\quad}$ symbol are written as described in Ref. [45].

$$P^* = \frac{P}{\mu_{10} R_1}, \quad (3.201)$$

$$\bar{c}_n = \frac{c_n}{\sqrt{P^*}}, \quad (3.202)$$

$$\bar{a} = \frac{a^*}{\sqrt{P^*}}, \quad (3.203)$$

$$\bar{b} = \frac{b^*}{\sqrt{P^*}}, \quad (3.204)$$

$$\bar{X} = \frac{X^*}{\sqrt{P^*}}, \quad (3.205)$$

Using the orthogonality property of the Jacobi polynomials described in Appendix-C, and truncating the series expansion to $N-1$, the singular integral equation can be expressed by the following linear algebraic equation.

$$\sum_{n=0}^{N-1} c_n \left[\frac{2\pi\omega_1}{\sin \pi\alpha} P_{n+1}^{(\alpha,\beta)}(r) + K_n(r) \right] = (r+1)\bar{b} + (r-1)\bar{a}, \quad (3.206)$$

$$K_n(r) = Z_{1n}(r) + Z_{2n}(r), \quad (3.207)$$

$$Z_{1n}(r) = \frac{1}{\pi} \int_{-1}^1 \overline{k_{11}}(s,r) W(s) P_n^{(\alpha,\beta)}(s) ds, \quad (3.208)$$

$$Z_{2n} = \frac{1}{\pi} \int_{-1}^1 \eta \overline{k_{12}}(s,r) W(s) P_n^{(\alpha,\beta)}(s) ds. \quad (3.209)$$

Using the orthogonality property of the Jacobi polynomials, equilibrium equation for the cylindrical punch contact problem can be written as follows:

$$\overline{c_0} \theta_0 = \frac{2\pi\alpha(1-\alpha)}{\sin \pi\alpha}. \quad (3.210)$$

The index of the singular integral equation is $\kappa_0 = -1$, and the consistency condition for the cylindrical punch contact problem is given by,

$$\int_{-1}^1 \left[(b^* + a^*)r + (b^* - a^*) - \frac{1}{\pi} \int_{-1}^1 [\overline{k_{11}}(s,r) + \eta \overline{k_{12}}(s,r)] \Theta(s) ds \right] \frac{dr}{W(r)} = 0. \quad (3.211)$$

Using the normalized singular integral equation, we can write the following equation:

$$\begin{aligned} & (b^* + a^*)r + (b^* - a^*) - \frac{1}{\pi} \int_{-1}^1 [\overline{k_{11}}(s,r) + \eta \overline{k_{12}}(s,r)] \Theta(s) ds \\ & = \omega_2 \eta \Theta(r) - \frac{1}{\pi} \int_{-1}^1 \frac{\pi \omega_1 \Theta(s)}{s-r} ds. \end{aligned} \quad (3.212)$$

When numerical solution is put into the singular integral equation, the following linear algebraic equation set is obtained.

$$\begin{aligned}
& \sum_{n=0}^{\infty} c_n \left[\omega_2 \eta W(r) P_n^{(\alpha, \beta)}(r) - \frac{1}{\pi} \int_{-1}^1 \frac{\pi \omega_1 W(s) P_n^{(\alpha, \beta)}(s)}{s-r} ds \right] = \\
& = \frac{2\pi\omega_1}{\sin \pi\alpha} \sum_{n=0}^{\infty} c_n P_{n+1}^{(-\alpha, -\beta)}(r).
\end{aligned} \tag{3.213}$$

We obtain the following expression by integrating equation (3.213).

$$\frac{2\pi \omega_1}{\sin \pi\alpha} \sum_{n=0}^{\infty} c_n \int_{-1}^1 \frac{P_{n+1}^{(-\alpha, -\beta)}(s)}{W(s)} ds = 0. \tag{3.214}$$

The consistency condition is satisfied. If equation (3.206) is examined, this equation system involves $N+2$ unknowns $(\bar{c}_0, \bar{c}_1, \bar{c}_2, \dots, \bar{a}, \bar{b})$. However, this equation produces $N+1$ equations for r_k ($k=1, \dots, N+1$). The functional equation for the cylindrical contact problem can be written in the following form,

$$\sum_{n=0}^{N-1} c_n \left[\frac{2\pi\omega_1}{\sin \pi\alpha} P_{n+1}^{(-\alpha, -\beta)}(r_k) + K_n(r_k) \right] - (r_k + 1)\bar{b} = (r_k - 1)\bar{a}, \quad k=1, \dots, N+1. \tag{3.215}$$

The collocation points r_k are the roots of the Jacobi polynomial and they are determined by,

$$P_{N+1}^{(\alpha-1, \beta-1)}(r_k) = 0, \quad k=1, \dots, N+1. \tag{3.216}$$

In matrix form, the linear algebraic equation system is written as follows:

$$\begin{bmatrix} S_o(r_1) & \cdot & S_{N-1}(r_1) & -(r_1+1) \\ S_o(r_2) & \cdot & S_{N-1}(r_2) & -(r_2+1) \\ \cdot & \cdot & \cdot & \cdot \\ \cdot & \cdot & \cdot & \cdot \\ S_o(r_N) & \cdot & S_{N-1}(r_N) & -(r_N+1) \\ S_o(r_{N+1}) & \cdot & S_{N-1}(r_{N+1}) & -(r_{N+1}+1) \end{bmatrix} \begin{bmatrix} \bar{c}_0 \\ \bar{c}_1 \\ \cdot \\ \cdot \\ \bar{c}_{N-1} \\ \bar{b} \end{bmatrix} = \begin{bmatrix} (r_1-1) \\ (r_2-1) \\ \cdot \\ \cdot \\ (r_N-1) \\ (r_{N+1}-1) \end{bmatrix} \bar{a}. \tag{3.217}$$

The above system is solved iteratively for $N + 1$ unknowns $(\bar{c}_0, \bar{c}_1, \bar{c}_2, \dots, \bar{b})$. In order to solve this system iteratively, the following algorithm is used [45].

Algorithm:

- 1- Initialize the parameter \bar{a} .
- 2- Solve this matrix system for $N + 1$ unknowns $(\bar{c}_0, \bar{c}_1, \bar{c}_2, \dots, \bar{b})$.
- 3- Using obtained \bar{c}_0 and \bar{b} , calculate the new \bar{a} parameter by the following equation:

$$\bar{a} = \frac{\kappa_1 + 1}{c_0 \theta_0} \bar{b}. \quad (3.218)$$

- 4- Do iterations until absolute percent relative error between new \bar{a} and previously obtained \bar{a} value is below a certain limit. (In present study, this certain limit is specified as $\varepsilon_s = 0.1\%$)

$$|\varepsilon_a| = \left| \frac{\bar{a}_j - \bar{a}_{j-1}}{\bar{a}_j} \right| \times 100 \quad (3.219)$$

After solution process is completed, the normal and shear stress components on the contact surface are calculated from the following equations.

$$\frac{\sigma_{1YY}(X^*, 0)}{\mu_{10}} = -\frac{2}{\kappa_1 + 1} W(r) \sum_{n=0}^{N+1} c_n P_n^{(\alpha, \beta)}(r), \quad (3.220)$$

$$\frac{\sigma_{1XY}(X^*, 0)}{\mu_{10}} = -\frac{2\eta}{\kappa_1 + 1} W(r) \sum_{n=0}^{N+1} c_n P_n^{(\alpha, \beta)}(r). \quad (3.221)$$

where

$$r = \frac{2X^* - (b^* - a^*)}{b^* + a^*}. \quad (3.222)$$

Cylindrical punch contact problem is an incomplete contact problem since there is a relation between the contact length and the load applied by the rigid cylindrical punch. The normalized load applied by the cylindrical punch can be calculated by the following equation.

$$P^* = \frac{P}{\mu_{10} R_1} = \left(\frac{a^* + b^*}{a + b} \right)^2. \quad (3.223)$$

where a^* , b^* and c_n are obtained from the back transformation as follows:

$$a^* = \bar{a} \sqrt{P^*}, \quad (3.224)$$

$$b^* = \bar{b} \sqrt{P^*}, \quad (3.225)$$

$$c_n = \bar{c}_n \sqrt{P^*}. \quad (3.226)$$

The lateral contact stress on the contact surface is calculated using the following equation:

$$\begin{aligned} \sigma_{1XX}(X^*, 0) = & \left(2\omega_4 + \frac{3 - \kappa_1}{\kappa_1 + 1} \right) \sigma(X^*) + \frac{2\eta}{\pi} \int_{-a^*}^{b^*} \frac{\pi \omega_3}{t^* - X^*} \sigma^*(t^*) dt^* \\ & - \frac{2}{\pi} \int_{-a^*}^{b^*} \left[\eta k_{21}^*(t^*, X^*) + k_{22}^*(t^*, X^*) \right] \sigma^*(t^*) dt^*. \end{aligned} \quad (3.227)$$

In normalized form, the lateral contact stress is written by,

$$\frac{\sigma_{1XX}(X^*, 0)}{\mu_{10}} = \frac{2}{\kappa_1 + 1} \left\{ \begin{aligned} & - \left(2\omega_4 + \frac{3 - \kappa_1}{\kappa_1 + 1} \right) \Theta(r) \\ & - \frac{2}{\pi} \int_{-1}^1 \frac{\pi \omega_3}{s - r} \Theta(s) ds + \frac{2}{\pi} \int_{-1}^1 \left[\eta \bar{k}_{21}(s, r) + \bar{k}_{22}(s, r) \right] \Theta(s) ds \end{aligned} \right\}. \quad (3.228)$$

Table 3.4 tabulates the powers of stress singularities α and β with respect to various values of coefficient of friction η and dimensionless punch speed c_1 . In frictionless elastodynamic contacts, the powers of the stress singularities remain the same value as 0.5 although punch speed is increased. However, in frictional elastodynamic contacts, powers of the stress singularities significantly change with respect to punch speed and the highest change occurs when coefficient of friction is taken as $\eta = 0.7$.

Table 3.4: The powers of stress singularity for a cylindrical punch $\nu_1 = 0.25$.

η	c_1	α	β
0.0	0.0	0.500000	0.500000
	0.4	0.500000	0.500000
	0.7	0.500000	0.500000
	0.8	0.500000	0.500000
0.3	0.0	0.468274	0.531726
	0.4	0.460523	0.539477
	0.6	0.443885	0.556115
	0.8	0.372402	0.627598
0.5	0.0	0.447432	0.552568
	0.4	0.434794	0.565206
	0.6	0.408132	0.591868
	0.8	0.304248	0.695752
0.7	0.0	0.427033	0.572967
	0.4	0.409898	0.590102
	0.6	0.374607	0.625393
	0.8	0.251779	0.748221

CHAPTER 4

NUMERICAL RESULTS FOR THE HOMOGENOUS ELASTIC COATING AND THE SUBSTRATE SYSTEM

In this chapter, dynamic contact mechanics of homogenous elastic coatings is investigated. The main results in this chapter are normal contact stress $\sigma_{1YY}(X,0)$, lateral contact stress $\sigma_{1XX}(X,0)$ and normalized stress intensity factors K_I at sharp ends of the rigid punch. Required contact load applied by the punch is also computed for incomplete contact problems consisting of triangular, semi-circular and cylindrical punch profiles. Computer codes are developed for the implementation of the numerical procedures described in Appendix-B, C and D. Numerical results of the present analytical procedure is compared with those obtained by computational methods. ANSYS Mechanical APDL [74] is used to generate the computational results. Verification of our results corresponding to elastostatic contact is satisfied by ANSYS Mechanical APDL [74]. For the verification study of the elastodynamic solution procedure, results of the present study are compared to those provided by Eringen and Suhubi [75] for a homogenous half-plane. In this section, numerical results are presented to show the influences of mass density ratio, dimensionless punch speed, coefficient of friction, relative contact length, and Poisson's ratio on elastodynamic contact stresses and stress intensity factors. In Chapter 2, general analytical formulations were derived for elastodynamic contact problem of FGM

coatings. However, we investigate elastodynamic contact problem of homogenous elastic coatings by applying the following assumptions in the general formulation.

$$\Gamma_1 = \frac{\mu_{20}}{\mu_{10}} = 1.0, \quad (4.1)$$

$$\chi_1 = \frac{\mu_{20}}{\mu_2} \neq 1.0. \quad (4.2)$$

μ_i, ν_i, ρ_i ($i=1,2$) show the shear modulus, the Poisson's ratio and the mass density of homogenous coating and the substrate, respectively. Homogenous coating is perfectly bonded to the substrate. Governing partial differential equations (PDEs) for the homogenous elastic coating are given below.

$$\left(\frac{\kappa_1 + 1}{\kappa_1 - 1} - c_1^2 \right) \frac{\partial^2 u_1}{\partial X^2} + \frac{2}{(\kappa_1 - 1)} \frac{\partial^2 v_1}{\partial X \partial Y} + \frac{\partial^2 u_1}{\partial Y^2} = 0, \quad (4.3)$$

$$(1 - c_1^2) \frac{\partial^2 v_1}{\partial X^2} + \frac{2}{(\kappa_1 - 1)} \frac{\partial^2 u_1}{\partial X \partial Y} + \frac{(\kappa_1 + 1)}{(\kappa_1 - 1)} \frac{\partial^2 v_1}{\partial Y^2} = 0, \quad (4.4)$$

Governing partial differential equations (PDEs) for the homogenous substrate are,

$$\left(\frac{\kappa_2 + 1}{\kappa_2 - 1} - c_2^2 \right) \frac{\partial^2 u_2}{\partial X^2} + \frac{2}{(\kappa_2 - 1)} \frac{\partial^2 v_2}{\partial X \partial Y} + \frac{\partial^2 u_2}{\partial Y^2} = 0, \quad (4.5)$$

$$(1 - c_2^2) \frac{\partial^2 v_2}{\partial X^2} + \frac{2}{(\kappa_2 - 1)} \frac{\partial^2 u_2}{\partial X \partial Y} + \frac{(\kappa_2 + 1)}{(\kappa_2 - 1)} \frac{\partial^2 v_2}{\partial Y^2} = 0. \quad (4.6)$$

Roots of the characteristic equation for the dynamic contact problem of homogenous elastic coatings are obtained as follows:

$$s_1 = \frac{1}{2} \left\{ + \sqrt{4 \left(1 - \frac{\kappa_1 c_1^2}{\kappa_1 + 1} \right) + 4i\lambda \frac{\sqrt{-\lambda^2 c_1^4}}{\kappa_1 + 1}} \right\}; \quad \Re(s_1) > 0, \quad (4.7)$$

$$s_2 = \frac{1}{2} \left\{ -\sqrt{4 \left(1 - \frac{\kappa_1 c_1^2}{\kappa_1 + 1} \right) + 4i\lambda \frac{\sqrt{-\lambda^2 c_1^4}}{\kappa_1 + 1}} \right\}; \quad \Re(s_2) < 0, \quad (4.8)$$

$$s_3 = \frac{1}{2} \left\{ +\sqrt{4 \left(1 - \frac{\kappa_1 c_1^2}{\kappa_1 + 1} \right) - 4i\lambda \frac{\sqrt{-\lambda^2 c_1^4}}{\kappa_1 + 1}} \right\}; \quad \Re(s_3) > 0, \quad (4.9)$$

$$s_4 = \frac{1}{2} \left\{ -\sqrt{4 \left(1 - \frac{\kappa_1 c_1^2}{\kappa_1 + 1} \right) - 4i\lambda \frac{\sqrt{-\lambda^2 c_1^4}}{\kappa_1 + 1}} \right\}; \quad \Re(s_4) < 0. \quad (4.10)$$

Dimensionless punch speeds for homogenous elastic coating and homogenous substrate can be calculated by,

$$c_1 = \frac{V}{c_{s1}}, \quad (4.11)$$

$$c_2 = \frac{V}{c_{s2}}, \quad (4.12)$$

where

$$c_{s1} = \sqrt{\frac{\mu_1}{\rho_1}}, \quad (4.13)$$

$$c_{s2} = \sqrt{\frac{\mu_2}{\rho_2}}, \quad (4.14)$$

For homogenous elastic coating contact problem, function appears in the horizontal displacement component $u_1(X, Y)$ becomes:

$$N_j(\lambda) = \frac{1}{\lambda} \frac{(2 - c_1^2) i \lambda^2}{2s_j}, \quad j = 1, \dots, 4. \quad (4.15)$$

Detailed investigations for the influence of mass density ratio on dynamic contact mechanics of less stiff and stiffer coatings are made and obtained results and discussions are provided in Appendix-E.

4.1 Finite Element Analysis Study

Verification of the developed analytical method is provided by utilizing the computational results for elastostatic contacts generated through the general purpose finite element analysis software ANSYS Mechanical APDL [74]. Fig. 4.1 illustrates the computational model constructed to calculate contact stresses for the elastostatic problem. The finite element mesh involves a total of 97536 quadrilateral finite elements. Fig. 4.1(a) displays the quadrilateral finite elements used in analyses.

In Fig. 4.1(b), the dimensions l_p , l_m , h_1 , and h_2 respectively denote punch width, substrate width, coating thickness, and substrate thickness. Homogenous substrate dimensions are kept large since it is modeled as an half-plane in the analytical solution. Therefore, in the constructed model, dimensional ratios are determined as $l_p/l_m = 3/40$, and $l_p/h_2 = 3/24$. Fig. 4.1(c) illustrates a close-up view of the contact region. In discretization of the contact zone, line contact elements are employed as it can be seen in Fig. 4.1(c). A total of 300 line contact elements and 597 contact nodes exist in the finite element model. The contact between the rigid punch and the coating is defined by CONTA169 and TARGE172 elements available in ANSYS Mechanical APDL [74]. Deformable coating surface is modelled by 298 CONTA169 elements, whereas 2 TARGE172 elements are used for the rigid punch. Each CONTA169 element has three nodes. Hence, a total of 597 contact nodes are created. The density of the finite element mesh around the contact zone is refined in order to capture the sharp variations in the contact stresses. Implicit integration scheme is employed in the finite element simulations.

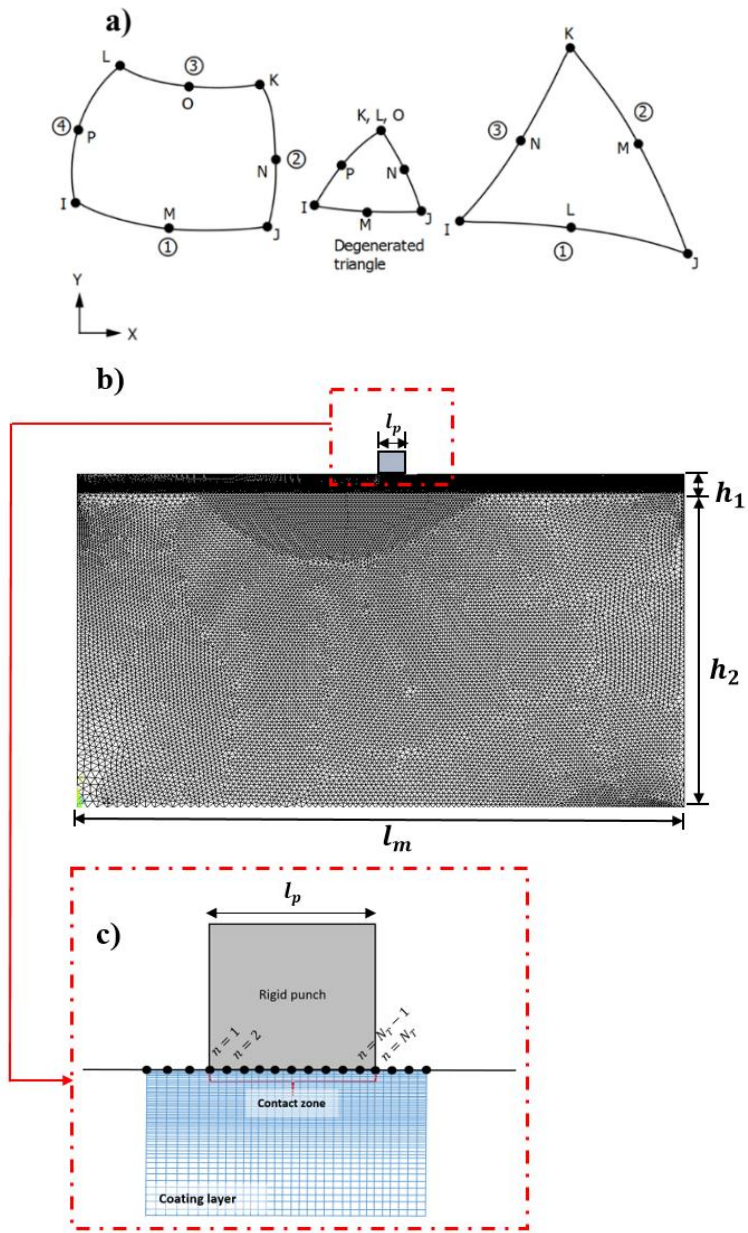


Figure 4.1: Constructed finite element model: (a) Quadrilateral finite element and its 8-noded triangular option; (b) Dimensions in the finite element mesh; (c) close-up view of the contact zone

4.2 Numerical Results for the Rigid Flat Punch

General schematic for the contact problem between a rigid flat punch and a homogenous elastic coating is depicted in Figure 4.2. Homogenous elastic coating of thickness h_1 is perfectly bonded to a homogenous substrate, and the rigid flat punch slides over the coating at a speed of V .

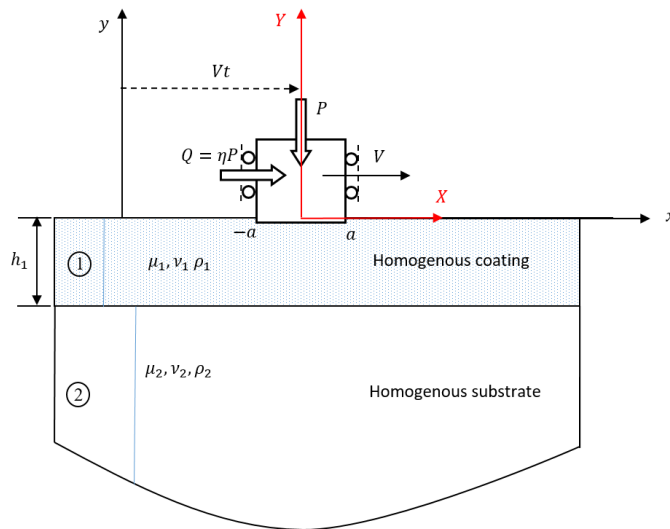


Figure 4.2: General schematic for the contact between a homogenous elastic coating and a rigid flat punch

Our results corresponding to elastostatic contact are verified by ANSYS Mechanical APDL [74]. In the verification study of the elastodynamic solution procedure, we compare our findings to those provided by Eringen and Suhubi [75] for a homogenous half-plane. Good agreement is observed in elastostatic and elastodynamic verification studies. However, sufficiently accurate results for elastodynamic contact could not be generated by ANSYS Mechanical APDL [74] and the finite element method. The main reason for this problem lies in the modeling difficulty of the half-plane geometry. In analytical modeling, the coating-substrate structure is assumed to constitute a half-plane thus there is no reflection of stress

waves back from surrounding boundaries. Unboundedness of the domain cannot be incorporated into finite element model. This causes reflections in finite element simulations from the boundaries. As a result, mismatches occur between analytically and computationally found contact stresses. The difference becomes significant especially for higher punch speeds.

Figures 4.3 - 4.5 show a comparison of contact stresses computed by the analytical method to those generated via finite element analysis for the case of elastostatic contact. The results are calculated by assuming $V = 0$ and using four different values of the stiffness ratio μ_1/μ_2 . Coefficient of friction is assumed to be equal to 0.3. It can be seen that contact stresses evaluated by the analytical technique developed are in excellent agreement with those found by finite element analysis.

A verification study for elastodynamic contact analysis is conducted by utilizing the analytical results of Eringen and Suhubi [75]. The results given in Ref. [75] are applicable for a homogenous half-plane. Figure 4.6 displays a comparison of our results to those available in Ref. [75]. Half-plane geometry and material homogeneity are accounted for by taking $a/h_1 = 0.001$ and $\mu_1/\mu_2 = 1$. The contact is assumed to be frictionless. Figures 4.6(a)-(b) indicate that the results are in perfect agreement. It is seen that normal contact stress is not affected by dimensionless punch speed c_1 in this type of contact. Magnitude of dimensionless lateral contact stress in the contact zone however increases as c_1 is increased from 0 to 0.8.

In parametric analyses presented below for coating-substrate systems, we provide contact stresses computed for different values of shear modulus ratio μ_1/μ_2 and density ratio ρ_1/ρ_2 . As one of these ratios is varied while the other is fixed, dimensionless speed ratio c_1/c_2 also changes. Table 4.1 tabulates c_1/c_2 ratios

computed for different values of density ratio ρ_1/ρ_2 . Note that these results follow from the relation:

$$c_2 = c_1 \sqrt{\frac{\mu_1 \rho_2}{\mu_2 \rho_1}}. \quad (4.16)$$

Table 4.1: Dimensionless punch speed ratios

	$\frac{\rho_1}{\rho_2} = 10$	$\frac{\rho_1}{\rho_2} = 5$	$\frac{\rho_1}{\rho_2} = 1$	$\frac{\rho_1}{\rho_2} = \frac{1}{10}$
	c_1/c_2	c_1/c_2	c_1/c_2	c_1/c_2
$\mu_1/\mu_2 = 1/10$	10	7.071	3.163	1
$\mu_1/\mu_2 = 10$	1	0.707	0.316	0.1

Figures 4.7 – 4.8 show elastodynamic contact stress distributions for less stiff and stiffer coatings for which modulus ratio μ_1/μ_2 is respectively defined as 1/10 and 10. The contact is assumed to be frictional and coefficient of friction η is taken as 0.3. It is interesting to note that density ratio ρ_1/ρ_2 has almost no effect on contact stresses for a less stiff coating. However, density ratio affect is found to be highly significant for the stiffer coating. Figure 4.8 illustrates the effect of density ratio ρ_1/ρ_2 on normal and lateral contact stress distributions for the stiffer coating. Figures 4.9 - 4.12 show the effect of dimensionless punch speed c_1 on contact stresses for less stiff and stiffer coatings, respectively. Analyses are carried out in

frictional conditions and coefficient of friction η is taken as 0.3. Two different relative contact length parameter are utilized ($a/h_1 = 0.1$, $a/h_1 = 0.4$).

Contact stresses are in general sensitive to the change in punch speed. Normal contact stress tends to be more compressive near the trailing end, and less compressive near the leading end of the contact zone, hence normal contact stresses become skewed curve formations. Tensile lateral contact stresses are formed behind the trailing end of the contact zone. Increase in the punch speed intensify the tensile behavior of the lateral contact stress. It should also be noted that the lateral contact stress reaches slightly positive values ahead of the contact zone and this behavior can be seen in Figures 4.9(b) and 4.11(b).

The influence of coefficient of friction η on elastodynamic contact stresses is examined in Figures 4.13 - 4.14. It should be noted that generated lateral contact stresses in a stiffer coating are more compressive than those generated in a less stiff coating, and general trend in the variation of the contact stresses with respect to coefficient of friction is similar for less stiff and stiffer coatings. Increase in the coefficient of friction leads to more compressive lateral contact stresses ahead of the contact. In all cases, larger coefficient of friction leads to a larger tensile peak at the trailing end of contact zone. Thus, in elastodynamic contacts with friction, trailing end of the contact zone is a possible site for cracking type failure. This finding is in line with experimental results observed in scratch tests. Adjustment of the coefficient of friction and modulus ratio could be possible ways of avoiding such fracture related failures. For both less stiff and stiffer coatings, and all values of coefficient of friction, normal contact stress tends to slant towards the leading end of the contact zone.

Figures 4.15 - 4.16 show the elastodynamic contact stresses as functions of the relative contact length which is denoted by ratio a/h_1 . The variation of both normal

and lateral contact stresses with respect to increasing a/h_1 is quite different for the less stiff and stiffer coatings. Normal contact stress tends to be more compressive as a/h_1 is increased from 0.01 to 0.8. However, normal contact stress becomes less compressive around the trailing end and more compressive around the leading end of the contact zone. When lateral contact stresses are examined, increase in the ratio a/h_1 leads to less compressive stresses for the less stiff coating and more compressive stresses for the stiffer coating throughout the contact.

In Figures 4.17 - 4.18, we present elastodynamic contact stresses as functions of ν_1/ν_2 . ν_1 and ν_2 being Poisson's ratios of the coating and substrate, respectively. It can be inferred from Figure 4.17(a) and Figure 4.18(a) that the impact of ν_1/ν_2 on normal contact stress is minimal. Increase in the ratio ν_1/ν_2 leads to different influences on lateral contact stress distributions. As the ratio ν_1/ν_2 is increased from 0.6 to 1.2, lateral contact stress in the contact zone decreases for the less stiff coating and increases for the stiffer coating.

Normalized stress intensity factors evaluated at the ends of the moving flat punch are provided in Tables 4.2 - 4.6. Table 4.2 shows the normalized stress intensity factors for different values of a/h_1 in elastostatic case. Coefficient of friction is taken as 0.0, results are generated and provided in this table. Hence, the effect of a/h_1 and μ_1/μ_2 on normalized stress intensity factors is merely observed. For the less stiff coating, as a/h_1 ratio is increased, the normalized stress intensity factors at both ends decrease. However, reverse trend is observed for the stiffer coating. Tables 4.3 and 4.4 tabulate the normalized stress intensity factors at the trailing and leading ends of the moving flat punch for various values of the modulus ratio μ_1/μ_2 and dimensionless punch speed c_1 . Coefficient of friction is assumed to be 0.3 in these tables. The form of dependence of K_I on the dimensionless punch speed c_1 is a

function of many parameters including relative contact length a/h_1 , modulus ratio μ_1/μ_2 , density ratio ρ_1/ρ_2 , coefficient of friction η , and punch profile. For example, from Table 4.3 it is seen that the mode I SIF at the flat punch end $X = a$ first increases and then decreases as c_1 gets larger when $\mu_1/\mu_2 = 1/10$ and $\mu_1/\mu_2 = 10$. However, mode I SIF results are equal at both ends of the flat punch for the half-plane and gradual decrease is seen when $\mu_1/\mu_2 = 1$. For example, from Table 4.4 it is seen that the mode I SIF at both ends of the flat punch is a decreasing function of the dimensionless punch speed c_1 . It clearly shows us that the variation of the mode I SIF depends on various dynamic, geometric and elastic parameters. Tables 4.5 - 4.6 display the normalized stress intensity factors with respect to various coefficient of friction for a less stiff ($\mu_1/\mu_2 = 1/5$) and a stiffer coating ($\mu_1/\mu_2 = 5$). Stress intensity factors for the stiffer coating is greater than those for the less stiff coating. In frictionless case, the mode I SIF at trailing and leading ends of the rigid flat punch are equal, however, in frictional case, they are not equal. As dimensionless punch speed c_1 is increased, a decreasing trend is observed for mode I SIF at both ends of the flat punch for the less stiff coating. When Table 4.6 is investigated, the values of mode I SIF decrease suddenly at a punch speed of $c_1 = 0.4$, and then increase at $c_1 = 0.6$, then decrease again.

Tables 4.7- 4.10 tabulate the results of normal and lateral contact stresses calculated based on elastostatic and elastodynamic theories. In these tables, percent differences are given between contact stresses computed considering elastostatic and elastodynamic conditions. Contact stresses are calculated for four different values of dimensionless punch speed c_1 . The case $c_1 = 0.0$ corresponds to elastostatic contact. The contacts for which $c_1 > 0$ are elastodynamic. The percent difference $\varepsilon\%$ in each case is computed with respect to contact stress evaluated at $c_1 = 0.0$. Tables 4.7 and

4.8 show respectively normal and lateral contact stresses for the less stiff coating ($\mu_1/\mu_2 = 1/10$). The differences found for the normal contact stress $\sigma_{1yy}(X,0)$ are in general significant. Larger deviations from the stresses obtained for the elastostatic case occur near the sharp ends. Table 4.8 indicates that percent differences between lateral contact stresses generated in elastostatic and elastodynamic contacts are even larger. Difference is larger especially behind the trailing end of the contact and it reaches up to 426% for $c_1 = 0.8$. Tables 4.9 and 4.10 display contact stress results computed for stiffer coatings ($\mu_1/\mu_2 = 10$) based on elastostatic and elastodynamic theories. Again the difference between elastostatic and elastodynamic contact stresses are highly considerable. The most difference between elastodynamic and elastostatic normal contact stresses occur around the sharp ends of the flat punch (see Table 4.9). The value of percent difference gradually increases as punch speed is increased. For stiffer coatings ($\mu_1/\mu_2 = 10$), again the value of percent difference is much greater around trailing end of the flat punch. It should also be noted that the orders of the percent difference generally greater for less stiff coatings. It can be concluded that less stiff coatings are more sensitive to dynamic influences when compared to stiffer coatings.

Hence, determination of elastodynamic contact stresses is highly critical for contact problems involving moving punches.

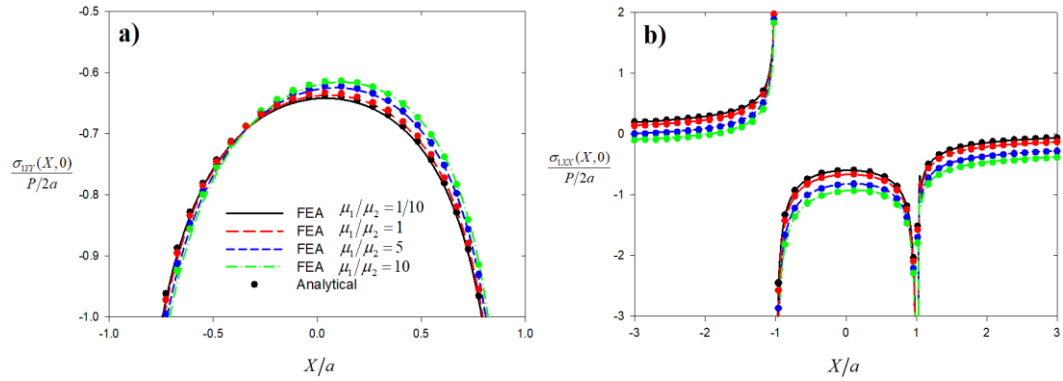


Figure 4.3: Normal and lateral contact stress distribution on the homogenous coating indented by a flat punch for different stiffness ratio of the coating and the substrate (a) Normal contact stress distribution; (b) Lateral contact stress distribution, $a/h_1 = 0.1$, $\eta = 0.3$, $c_1 = 0.0$.

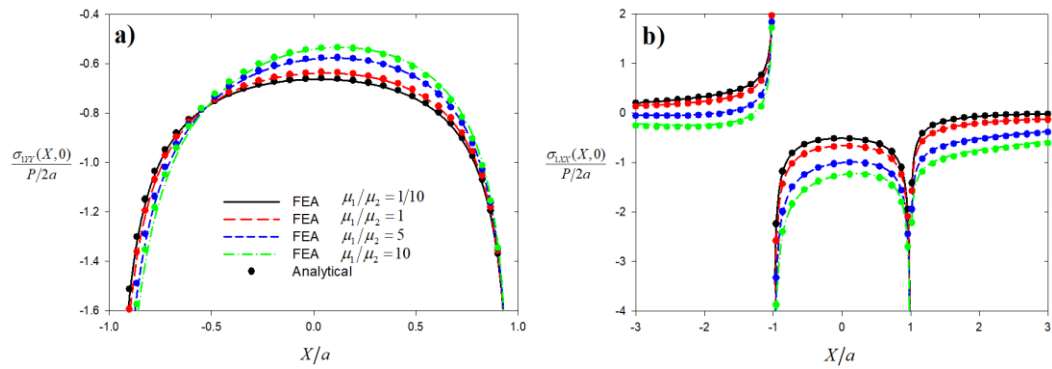


Figure 4.4: Normal and lateral contact stress distribution on the homogenous coating indented by a flat punch for different stiffness ratio of the coating and the substrate (a) Normal contact stress distribution; (b) Lateral contact stress distribution, $a/h_1 = 0.25$, $\eta = 0.3$, $c_1 = 0.0$.

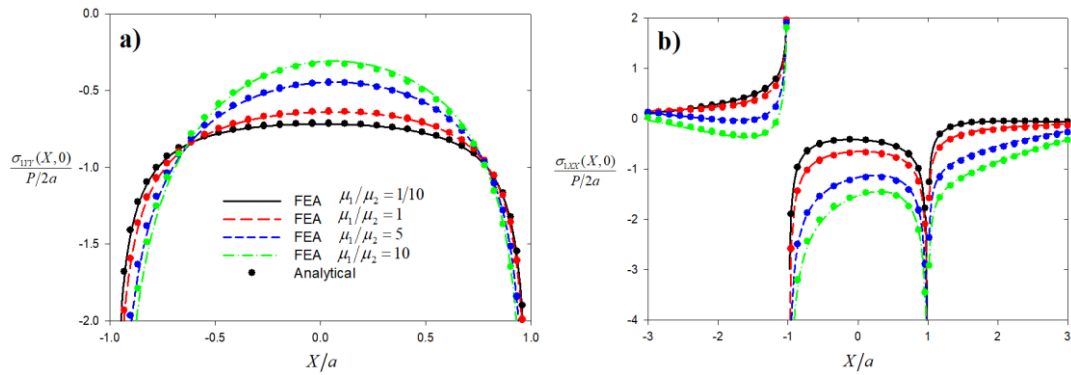


Figure 4.5: Normal and lateral contact stress distribution on the homogenous coating indented by a flat punch for different stiffness ratio of the coating and the substrate (a) Normal contact stress distribution; (b) Lateral contact stress distribution, $a/h_1 = 0.5$, $\eta = 0.3$, $c_1 = 0.0$.

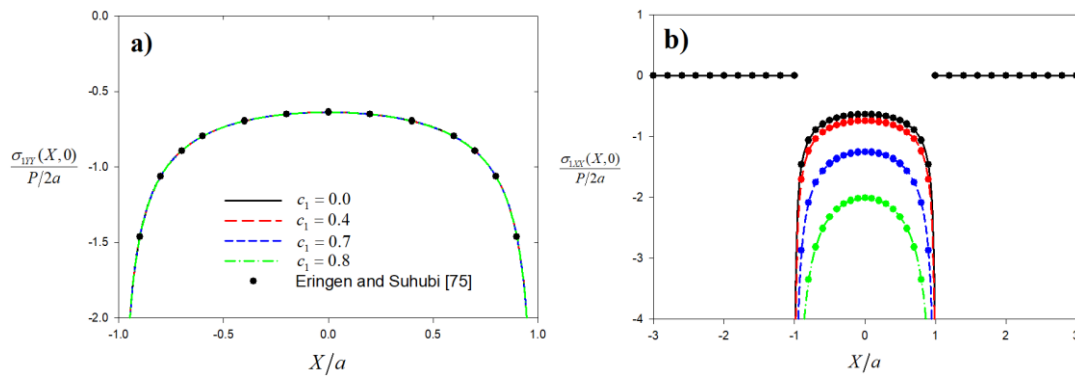


Figure 4.6: Normal and lateral contact stress distribution on the half-plane indented by frictionless moving punch for various punch speed $\eta = 0.0$. (a) Normal contact stress distribution; (b) Lateral contact stress distribution.

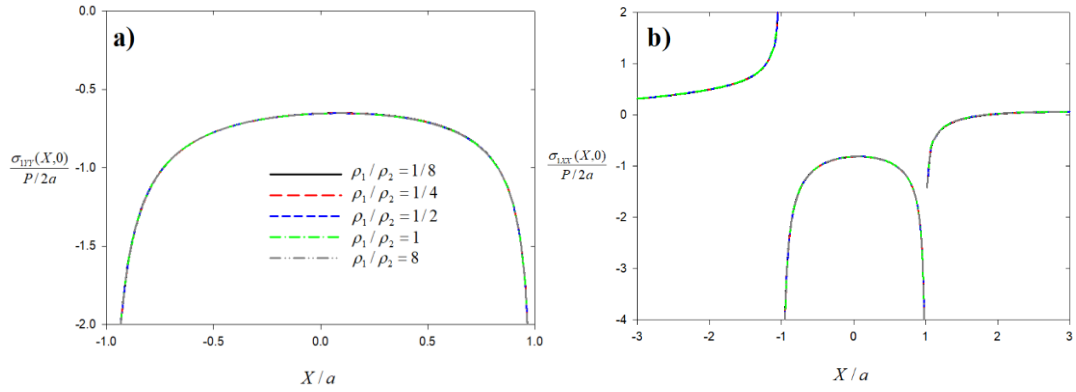


Figure 4.7: Normal and lateral elastodynamic contact stresses on homogeneous coating indented by a moving flat punch for various mass density ratio (a) Normal contact stress distribution; (b) Lateral contact stress distribution, $\mu_1/\mu_2 = 1/10$, $a/h_1 = 0.2$, $c_1 = 0.6$, $\eta = 0.3$, $v_1/v_2 = 0.8$.

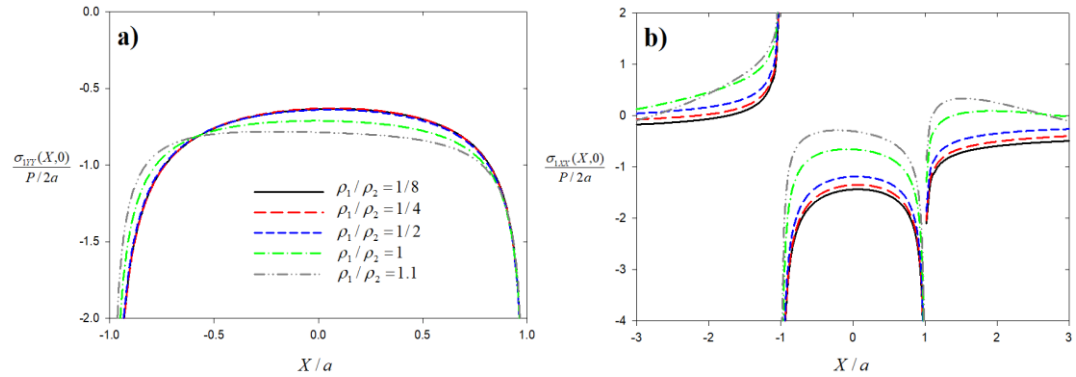


Figure 4.8: Normal and lateral elastodynamic contact stresses on homogeneous coating indented by a moving flat punch for various mass density ratio (a) Normal contact stress distribution; (b) Lateral contact stress distribution, $\mu_1/\mu_2 = 10$, $a/h_1 = 0.2$, $c_1 = 0.6$, $\eta = 0.3$, $v_1/v_2 = 0.8$.

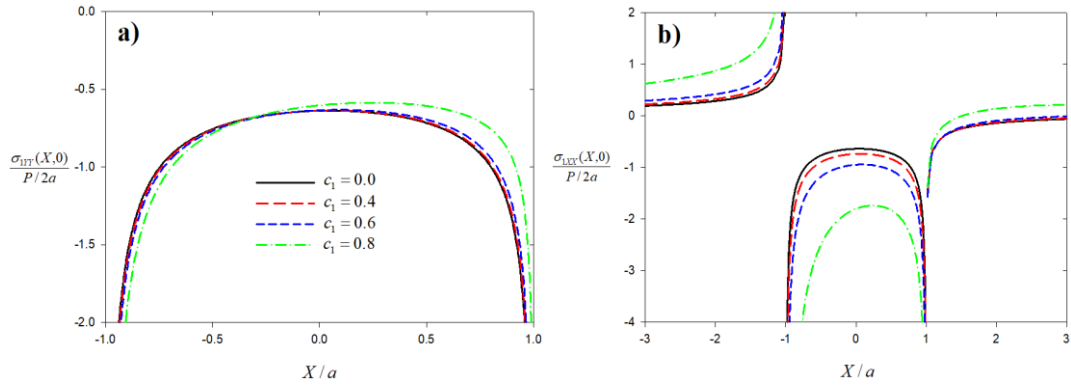


Figure 4.9: Normal and lateral elastodynamic contact stresses on homogenous coating indented by a moving flat punch for various values of punch speed (a) Normal contact stress distribution; (b) Lateral contact stress distribution, $\mu_1 / \mu_2 = 1/10$, $a / h_1 = 0.1$, $\eta = 0.3$, $\rho_1 / \rho_2 = 1/8$, $v_1 / v_2 = 0.8$.

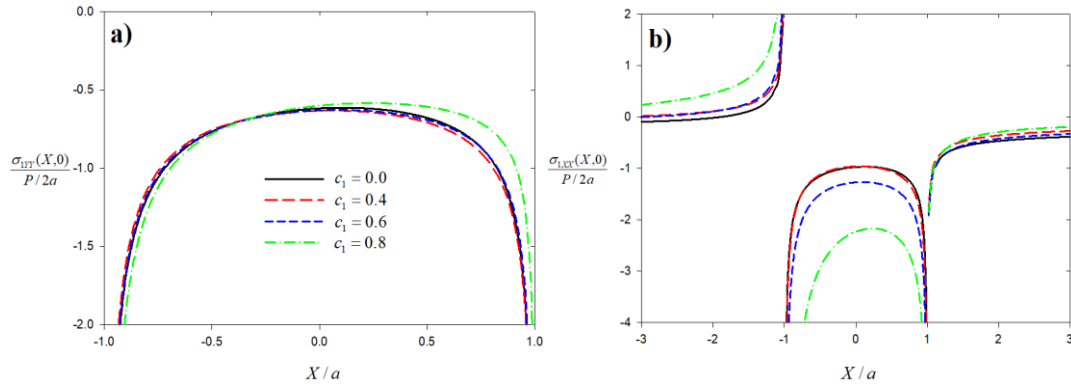


Figure 4.10: Normal and lateral elastodynamic contact stresses on homogenous coating indented by a moving flat punch for various values of punch speed (a) Normal contact stress distribution; (b) Lateral contact stress distribution, $\mu_1 / \mu_2 = 10$, $a / h_1 = 0.1$, $\eta = 0.3$, $\rho_1 / \rho_2 = 1/8$, $v_1 / v_2 = 0.8$.

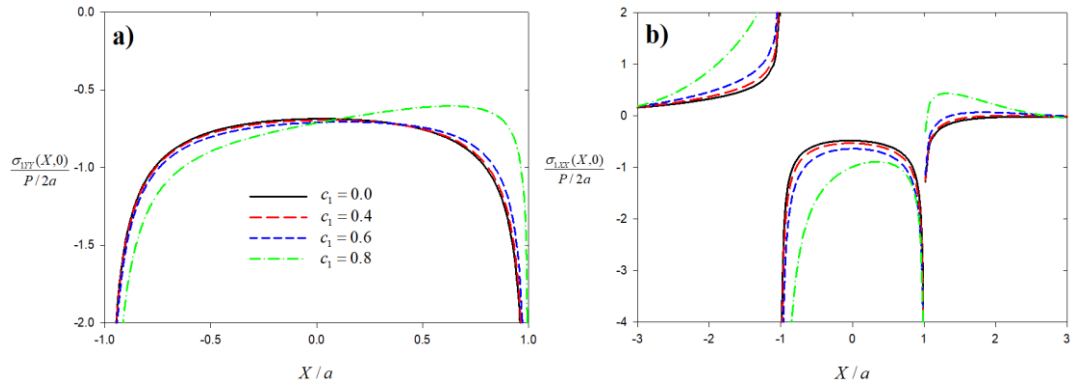


Figure 4.11: Normal and lateral elastodynamic contact stresses on homogeneous coating indented by a moving flat punch for various values of punch speed (a) Normal contact stress distribution; (b) Lateral contact stress distribution, $\mu_1/\mu_2 = 1/10$, $a/h_1 = 0.4$, $\eta = 0.3$, $\rho_1/\rho_2 = 1/8$, $\nu_1/\nu_2 = 0.8$.

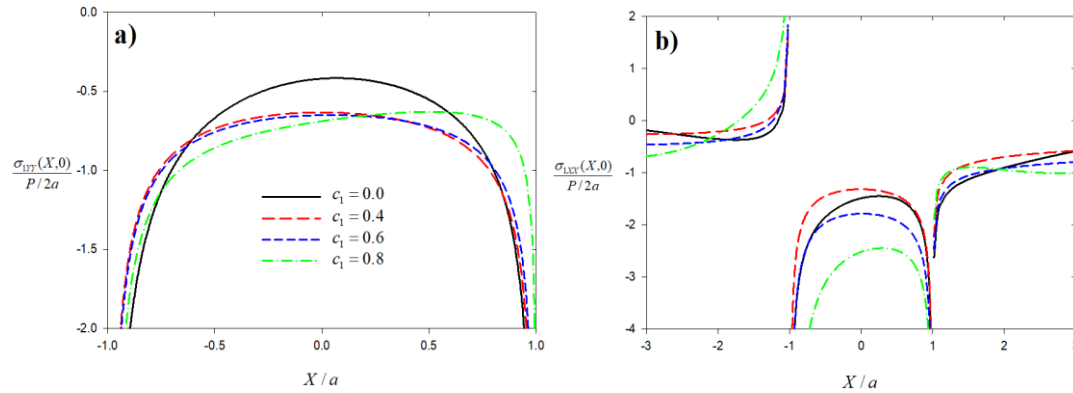


Figure 4.12: Normal and lateral elastodynamic contact stresses on homogeneous coating indented by a moving flat punch for various values of punch speed (a) Normal contact stress distribution; (b) Lateral contact stress distribution, $\mu_1/\mu_2 = 10$, $a/h_1 = 0.4$, $\eta = 0.3$, $\rho_1/\rho_2 = 1/8$, $\nu_1/\nu_2 = 0.8$.

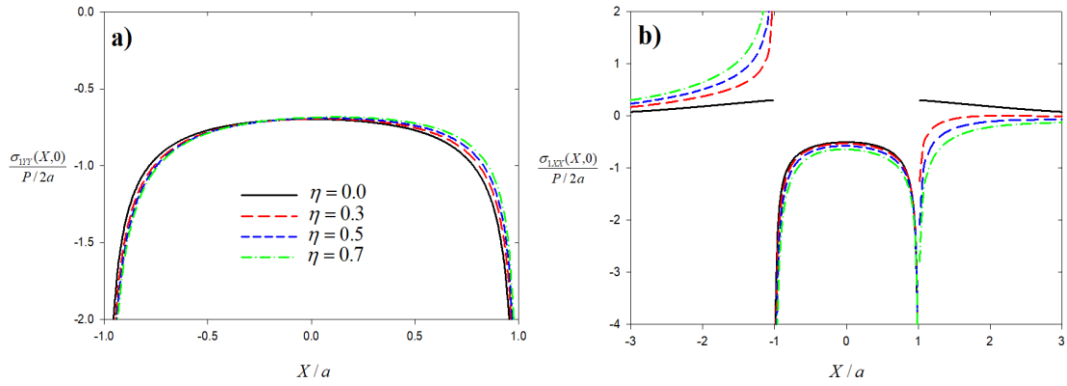


Figure 4.13: Normal and lateral elastodynamic contact stresses on homogenous coating indented by a moving flat punch for various values of coefficient of friction (a) Normal contact stress distribution; (b) Lateral contact stress distribution, $\mu_1 / \mu_2 = 1/10$, $a / h_1 = 0.4$, $c_1 = 0.4$, $\rho_1 / \rho_2 = 1/8$, $v_1 / v_2 = 0.8$.

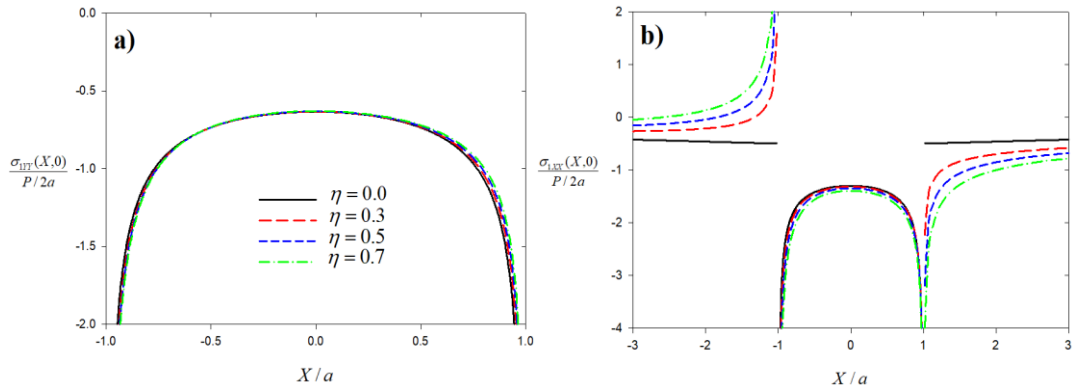


Figure 4.14: Normal and lateral elastodynamic contact stresses on homogenous coating indented by a moving flat punch for various values of coefficient of friction (a) Normal contact stress distribution; (b) Lateral contact stress distribution, $\mu_1 / \mu_2 = 10$, $a / h_1 = 0.4$, $c_1 = 0.4$, $\rho_1 / \rho_2 = 1/8$, $v_1 / v_2 = 0.8$.

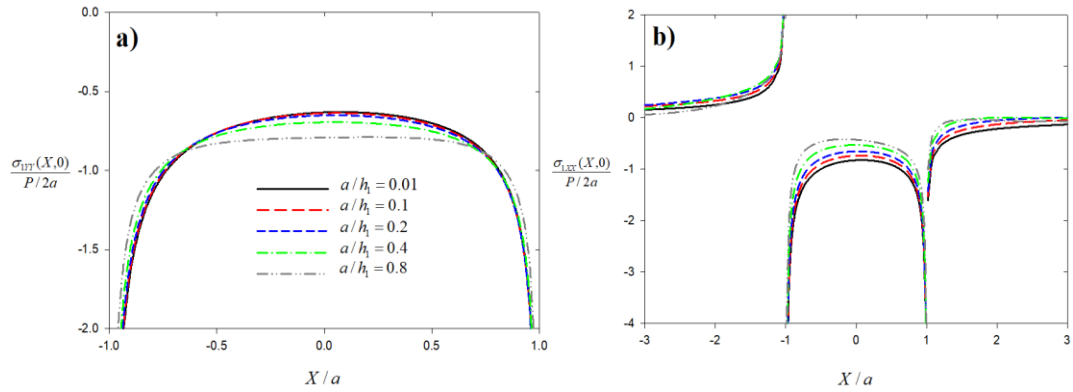


Figure 4.15: Normal and lateral elastodynamic contact stresses on homogenous coating indented by a moving flat punch for various values of relative coating thickness (a) Normal contact stress distribution; (b) Lateral contact stress distribution, $\mu_1 / \mu_2 = 1/10$, $c_1 = 0.4$, $\eta = 0.3$, $\rho_1 / \rho_2 = 1/8$, $\nu_1 / \nu_2 = 0.8$.

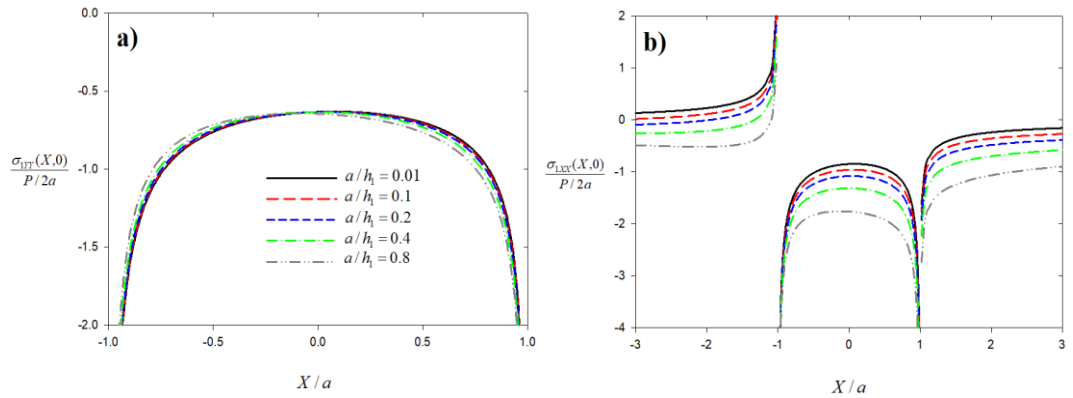


Figure 4.16: Normal and lateral elastodynamic contact stresses on homogenous coating indented by a moving flat punch for various values of relative coating thickness (a) Normal contact stress distribution; (b) Lateral contact stress distribution, $\mu_1 / \mu_2 = 10$, $c_1 = 0.4$, $\eta = 0.3$, $\rho_1 / \rho_2 = 1/8$, $\nu_1 / \nu_2 = 0.8$.

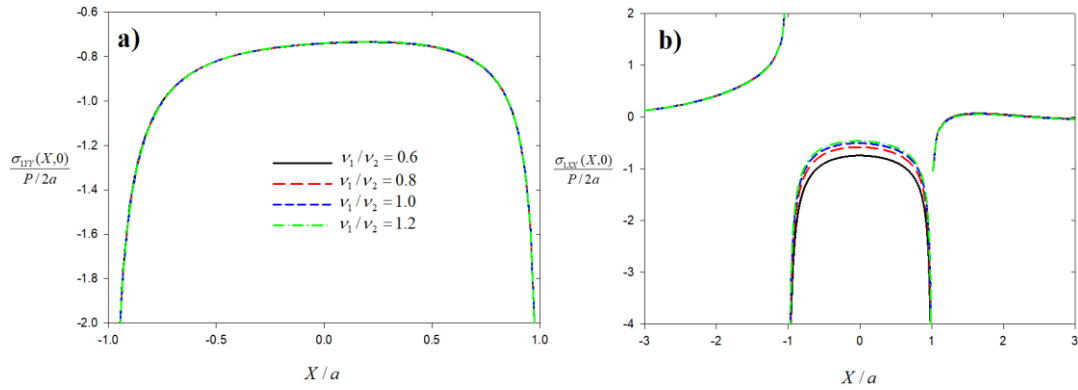


Figure 4.17: Normal and lateral elastodynamic contact stresses on homogeneous coating indented by a moving flat punch for various values of Poisson's ratio (a) Normal contact stress distribution; (b) Lateral contact stress distribution, $\mu_1 / \mu_2 = 1/10$, $a / h_1 = 0.5$, $c_1 = 0.6$, $\eta = 0.3$, $\rho_1 / \rho_2 = 1/8$, $v_1 / v_2 = 0.8$.

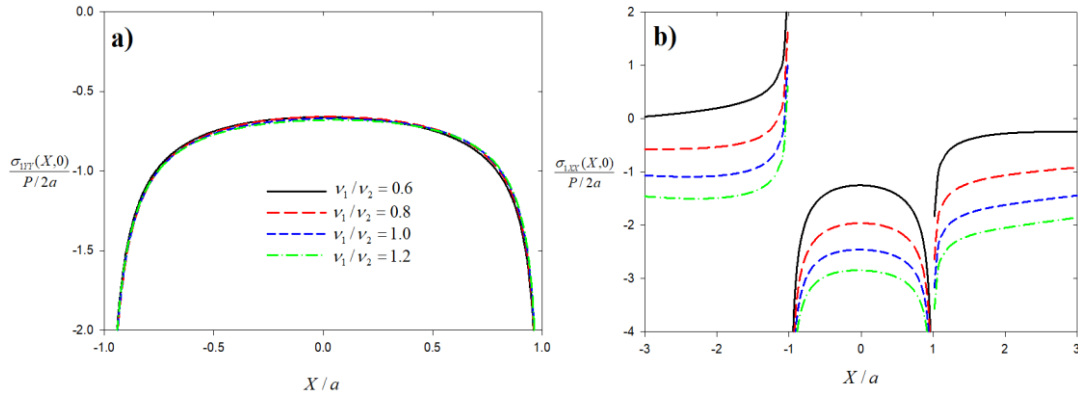


Figure 4.18: Normal and lateral elastodynamic contact stresses on homogeneous coating indented by a moving flat punch for various values of Poisson's ratio (a) Normal contact stress distribution; (b) Lateral contact stress distribution, $\mu_1 / \mu_2 = 10$, $a / h_1 = 0.5$, $c_1 = 0.6$, $\eta = 0.3$, $\rho_1 / \rho_2 = 1/8$, $v_1 / v_2 = 0.8$.

Table 4.2: Normalized stress intensity factors for the moving flat punch $c_1 = 0.0$, $\eta = 0.0$, $\nu_1 / \nu_2 = 0.8$.

μ_1 / μ_2	$a/h_1 = 0.1$		$a/h_1 = 0.2$		$a/h_1 = 0.3$		$a/h_1 = 0.4$	
	$K_I(-a)$	$K_I(a)$	$K_I(-a)$	$K_I(a)$	$K_I(-a)$	$K_I(a)$	$K_I(-a)$	$K_I(a)$
1/10	0.3165	0.3165	0.3113	0.3113	0.2941	0.2941	0.2555	0.2555
1/5	0.3167	0.3167	0.3122	0.3122	0.2972	0.2972	0.2636	0.2636
1	0.3183	0.3183	0.3183	0.3183	0.3183	0.3183	0.3183	0.3183
10	0.3256	0.3256	0.3468	0.3468	0.4204	0.4204	0.5919	0.5919

Table 4.3: Normalized stress intensity factors for the moving flat punch $a/h_1 = 0.1$, $\eta = 0.3$, $\rho_1 / \rho_2 = 1/8$, $\nu_1 / \nu_2 = 0.8$.

μ_1 / μ_2	$c_1 = 0.0$		$c_1 = 0.4$		$c_1 = 0.6$		$c_1 = 0.7$	
	$K_I(-a)$	$K_I(a)$	$K_I(-a)$	$K_I(a)$	$K_I(-a)$	$K_I(a)$	$K_I(-a)$	$K_I(a)$
1/10	0.3103	0.3102	0.3085	0.3198	0.3044	0.3179	0.2991	0.3140
1/5	0.3111	0.3197	0.3097	0.3190	0.3067	0.3165	0.3028	0.3116
1	0.3167	0.3167	0.3159	0.3159	0.3134	0.3134	0.3092	0.3092
10	0.3399	0.3060	0.3103	0.3228	0.3069	0.3202	0.3008	0.3165

Table 4.4: Normalized stress intensity factors for the moving flat punch $a/h_1 = 0.4$, $\eta = 0.3$, $\rho_1 / \rho_2 = 1/8$, $\nu_1 / \nu_2 = 0.8$.

μ_1 / μ_2	$c_1 = 0.0$		$c_1 = 0.4$		$c_1 = 0.6$		$c_1 = 0.7$	
	$K_I(-a)$	$K_I(a)$	$K_I(-a)$	$K_I(a)$	$K_I(-a)$	$K_I(a)$	$K_I(-a)$	$K_I(a)$
1/10	0.2795	0.3074	0.2743	0.3029	0.2658	0.2910	0.2591	0.2725
1/5	0.2844	0.3085	0.2814	0.3042	0.2777	0.2937	0.2773	0.2797
1	0.3167	0.3167	0.3159	0.3159	0.3134	0.3134	0.3092	0.3092
10	0.4472	0.3862	0.2945	0.3437	0.2850	0.3305	0.2708	0.3105

Table 4.5: Normalized stress intensity factors for the moving flat punch $a/h_1 = 0.4$,

$\mu_1/\mu_2 = 1/5$, $\rho_1/\rho_2 = 1/8$, $\nu_1/\nu_2 = 0.8$.

η	$c_1 = 0.0$		$c_1 = 0.4$		$c_1 = 0.6$		$c_1 = 0.7$	
	$K_I(-a)$	$K_I(a)$	$K_I(-a)$	$K_I(a)$	$K_I(-a)$	$K_I(a)$	$K_I(-a)$	$K_I(a)$
0.0	0.2972	0.2972	0.2942	0.2942	0.2892	0.2892	0.2862	0.2862
0.3	0.2844	0.3085	0.2814	0.3042	0.2777	0.2937	0.2773	0.2797
0.5	0.2753	0.3150	0.2717	0.3091	0.2666	0.2928	0.2698	0.2928
0.7	0.2659	0.2648	0.2613	0.3126	0.2542	0.2894	0.2474	0.2552

Table 4.6: Normalized stress intensity factors for the moving flat punch $a/h_1 = 0.4$,

$\mu_1/\mu_2 = 5$, $\rho_1/\rho_2 = 1/8$, $\nu_1/\nu_2 = 0.8$.

η	$c_1 = 0.0$		$c_1 = 0.4$		$c_1 = 0.6$		$c_1 = 0.7$	
	$K_I(-a)$	$K_I(a)$	$K_I(-a)$	$K_I(a)$	$K_I(-a)$	$K_I(a)$	$K_I(-a)$	$K_I(a)$
0.0	0.3774	0.3774	0.2913	0.2913	0.2921	0.2921	0.2817	0.2817
0.3	0.3941	0.3549	0.2572	0.3264	0.2652	0.3157	0.2578	0.2959
0.5	0.4017	0.3371	0.2358	0.3495	0.2467	0.3284	0.2387	0.2994
0.7	0.4065	0.3176	0.2159	0.3718	0.2287	0.3385	0.2191	0.2991

Table 4.7: Percent difference between elastostatic and elastodynamic normal contact stresses $\mu_1 / \mu_2 = 1/10$, $a/h_1 = 0.1$, $\eta = 0.3$, $\rho_1 / \rho_2 = 1/8$, $\nu_1 / \nu_2 = 0.8$.

X/a	$c_1 = 0.0$		$c_1 = 0.4$		$c_1 = 0.6$		$c_1 = 0.8$	
	$\frac{\sigma_{yy}(X,0)}{P/(2a)}$	$\frac{\sigma_{yy}(X,0)}{P/(2a)}$	$\varepsilon\%$	$\frac{\sigma_{yy}(X,0)}{P/(2a)}$	$\varepsilon\%$	$\frac{\sigma_{yy}(X,0)}{P/(2a)}$	$\varepsilon\%$	
-0.90	-1.58576	-1.61436	1.80	-1.67613	5.70	-1.93012	21.72	
-0.82	-1.18923	-1.20545	1.36	-1.23985	4.26	-1.36946	15.15	
-0.73	-0.96813	-0.97815	1.04	-0.99895	3.18	-1.06852	10.37	
-0.61	-0.83246	-0.83888	0.77	-0.85180	2.32	-0.88723	6.58	
-0.41	-0.71430	-0.71746	0.44	-0.72321	1.25	-0.72787	1.90	
-0.19	-0.65578	-0.65673	0.14	-0.65761	0.28	-0.64115	2.23	
-0.04	-0.63943	-0.63908	0.06	-0.63709	0.37	-0.60807	4.90	
0.19	-0.64363	-0.64122	0.37	-0.63468	1.39	-0.58576	8.99	
0.41	-0.68435	-0.67930	0.74	-0.66698	2.54	-0.59309	13.33	
0.61	-0.77525	-0.76623	1.16	-0.74528	3.87	-0.63507	18.08	
0.73	-0.88106	-0.86787	1.50	-0.83794	4.89	-0.69098	21.57	
0.82	-1.05196	-1.03207	1.89	-0.98786	6.09	-0.78404	25.47	
0.90	-1.35150	-1.31933	2.38	-1.24925	7.57	-0.94585	30.02	

Table 4.8: Percent difference between elastostatic and elastodynamic lateral contact stresses $\mu_1 / \mu_2 = 1/10$, $a/h_1 = 0.1$, $\eta = 0.3$, $\rho_1 / \rho_2 = 1/8$, $\nu_1 / \nu_2 = 0.8$.

X/a	$c_1 = 0.0$		$c_1 = 0.4$		$c_1 = 0.6$		$c_1 = 0.8$	
	$\frac{\sigma_{xx}(X,0)}{P/(2a)}$	$\frac{\sigma_{xx}(X,0)}{P/(2a)}$	$\varepsilon\%$	$\frac{\sigma_{xx}(X,0)}{P/(2a)}$	$\varepsilon\%$	$\frac{\sigma_{xx}(X,0)}{P/(2a)}$	$\varepsilon\%$	
-1.22	0.62893	0.70554	12.18	0.87105	38.50	1.69584	169.64	
-0.99	-5.98980	-7.30696	21.99	-10.49468	75.21	-31.51114	426.08	
-0.82	-1.25235	-1.48411	18.51	-2.00951	60.46	-4.77932	281.63	
-0.67	-0.92008	-1.08166	17.56	-1.44118	56.64	-3.21739	249.69	
-0.41	-0.72068	-0.84023	16.59	-1.10049	52.70	-2.28728	217.38	
-0.27	-0.67161	-0.78037	16.19	-1.01472	51.09	-2.04134	203.95	
-0.04	-0.63755	-0.73764	15.70	-0.95008	49.02	-1.82513	186.27	
0.27	-0.65331	-0.75254	15.19	-0.95907	46.80	-1.74032	166.38	
0.41	-0.68913	-0.79237	14.98	-1.00518	45.86	-1.77570	157.67	
0.67	-0.84443	-0.96780	14.61	-1.21710	44.13	-2.04083	141.68	
0.82	-1.10252	-1.26016	14.30	-1.57322	42.69	-2.52963	129.44	
0.99	-4.37889	-4.92702	12.52	-5.93114	35.45	-8.03705	83.54	
1.22	-0.42393	-0.42834	1.04	-0.41972	0.99	-0.22919	45.94	

Table 4.9: Percent difference between elastostatic and elastodynamic normal contact stresses $\mu_1 / \mu_2 = 10$, $a/h_1 = 0.1$, $\eta = 0.3$, $\rho_1 / \rho_2 = 1/8$, $\nu_1 / \nu_2 = 0.8$.

X/a	$c_1 = 0.0$			$c_1 = 0.4$			$c_1 = 0.6$			$c_1 = 0.8$		
	$\frac{\sigma_{1yy}(X,0)}{P/(2a)}$	$\frac{\sigma_{1yy}(X,0)}{P/(2a)}$	$\varepsilon\%$	$\frac{\sigma_{1yy}(X,0)}{P/(2a)}$	$\frac{\sigma_{1yy}(X,0)}{P/(2a)}$	$\varepsilon\%$	$\frac{\sigma_{1yy}(X,0)}{P/(2a)}$	$\frac{\sigma_{1yy}(X,0)}{P/(2a)}$	$\varepsilon\%$	$\frac{\sigma_{1yy}(X,0)}{P/(2a)}$	$\frac{\sigma_{1yy}(X,0)}{P/(2a)}$	$\varepsilon\%$
-0.90	-1.70845	-1.61968	5.20	-1.68472	-1.68472	1.39	-1.93127	-1.93127	13.04	-1.93127	-1.93127	13.04
-0.82	-1.26532	-1.20712	4.60	-1.24358	-1.24358	1.72	-1.36869	-1.36869	8.17	-1.36869	-1.36869	8.17
-0.73	-1.01482	-0.97743	3.68	-0.99956	-0.99956	1.50	-1.06658	-1.06658	5.10	-1.06658	-1.06658	5.10
-0.61	-0.85839	-0.83647	2.55	-0.85025	-0.85025	0.95	-0.88455	-0.88455	3.05	-0.88455	-0.88455	3.05
-0.41	-0.71815	-0.71344	0.66	-0.71957	-0.71957	0.20	-0.72465	-0.72465	0.91	-0.72465	-0.72465	0.91
-0.19	-0.64417	-0.65197	1.21	-0.65289	-0.65289	1.35	-0.63794	-0.63794	0.97	-0.63794	-0.63794	0.97
0.04	-0.61432	-0.63137	2.78	-0.62769	-0.62769	2.18	-0.59457	-0.59457	3.21	-0.59457	-0.59457	3.21
0.19	-0.61517	-0.63701	3.55	-0.63005	-0.63005	2.42	-0.58367	-0.58367	5.12	-0.58367	-0.58367	5.12
0.41	-0.64898	-0.67649	4.24	-0.66344	-0.66344	2.23	-0.59231	-0.59231	8.73	-0.59231	-0.59231	8.73
0.61	-0.73367	-0.76568	4.36	-0.74360	-0.74360	1.35	-0.63607	-0.63607	13.30	-0.63607	-0.63607	13.30
0.73	-0.83464	-0.86944	4.17	-0.83800	-0.83800	0.40	-0.69348	-0.69348	16.91	-0.69348	-0.69348	16.91
0.82	-0.99861	-1.03647	3.79	-0.99020	-0.99020	0.84	-0.78843	-0.78843	21.05	-0.78843	-0.78843	21.05
0.90	-1.28613	-1.32781	3.24	-1.25474	-1.25474	2.44	-0.95277	-0.95277	25.92	-0.95277	-0.95277	25.92

Table 4.10: Percent difference between elastostatic and elastodynamic lateral contact stresses $\mu_1 / \mu_2 = 10$, $a/h_1 = 0.1$, $\eta = 0.3$, $\rho_1 / \rho_2 = 1/8$, $\nu_1 / \nu_2 = 0.8$.

X/a	$c_1 = 0.0$			$c_1 = 0.4$			$c_1 = 0.6$			$c_1 = 0.8$		
	$\frac{\sigma_{1xx}(X,0)}{P/(2a)}$	$\frac{\sigma_{1xx}(X,0)}{P/(2a)}$	$\varepsilon\%$	$\frac{\sigma_{1xx}(X,0)}{P/(2a)}$	$\frac{\sigma_{1xx}(X,0)}{P/(2a)}$	$\varepsilon\%$	$\frac{\sigma_{1xx}(X,0)}{P/(2a)}$	$\frac{\sigma_{1xx}(X,0)}{P/(2a)}$	$\varepsilon\%$	$\frac{\sigma_{1xx}(X,0)}{P/(2a)}$	$\frac{\sigma_{1xx}(X,0)}{P/(2a)}$	$\varepsilon\%$
-1.22	0.33412	0.48381	44.80	0.55140	0.55140	65.03	1.26996	1.26996	280.09	1.26996	1.26996	280.09
-0.99	-6.92933	-7.57922	9.38	-10.90958	-10.90958	57.44	-32.01416	-32.01416	362.01	-32.01416	-32.01416	362.01
-0.82	-1.70689	-1.71629	0.55	-2.34813	-2.34813	37.57	-5.21374	-5.21374	205.45	-5.21374	-5.21374	205.45
-0.67	-1.32742	-1.30940	1.36	-1.77242	-1.77242	33.52	-3.64640	-3.64640	174.70	-3.64640	-3.64640	174.70
-0.41	-1.08927	-1.06450	2.27	-1.42628	-1.42628	30.94	-2.71361	-2.71361	149.12	-2.71361	-2.71361	149.12
-0.27	-1.02600	-1.00360	2.18	-1.33890	-1.33890	30.50	-2.46757	-2.46757	140.50	-2.46757	-2.46757	140.50
-0.04	-0.97458	-0.96002	1.49	-1.27289	-1.27289	30.61	-2.25241	-2.25241	131.12	-2.25241	-2.25241	131.12
0.27	-0.97232	-0.97513	0.29	-1.28180	-1.28180	31.83	-2.17103	-2.17103	123.28	-2.17103	-2.17103	123.28
0.41	-1.00054	-1.01569	1.51	-1.32862	-1.32862	32.79	-2.20901	-2.20901	120.78	-2.20901	-2.20901	120.78
0.67	-1.14138	-1.19415	4.62	-1.54371	-1.54371	35.25	-2.48162	-2.48162	117.42	-2.48162	-2.48162	117.42
0.82	-1.38569	-1.49089	7.59	-1.90439	-1.90439	37.43	-2.97921	-2.97921	115.00	-2.97921	-2.97921	115.00
0.99	-4.51852	-5.19684	15.01	-6.29930	-6.29930	39.41	-8.54844	-8.54844	89.19	-8.54844	-8.54844	89.19
1.22	-0.74239	-0.65993	11.11	-0.75212	-0.75212	1.31	-0.66820	-0.66820	9.99	-0.66820	-0.66820	9.99

4.3 Numerical Results for the Rigid Triangular Punch

General schematic for the contact problem between a rigid triangular punch and a homogenous elastic coating is illustrated in Figure 4.19. Homogenous elastic coating of thickness h_1 is perfectly bonded to a homogenous substrate, and the rigid triangular punch slides over the coating at a speed of V .

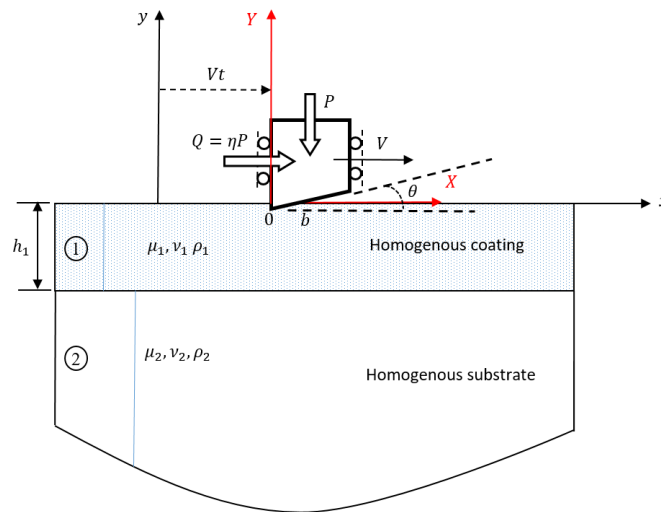


Figure 4.19: General schematic for the contact between a homogenous elastic coating and a rigid triangular punch

Figures 4.20 - 4.21 show the influence of mass density ratio on elastodynamic contact stresses for the triangular punch contact problem. For the less stiff coating, although the mass density ratio is changed, both normal and lateral contact stresses almost remain the same value. Hence, the effect of mass density ratio on contact stresses for the less stiff coating is minimal. However, the variation of the mass density ratio significantly changes the contact stresses as can be seen in Fig. 4.21. As mass density ratio ρ_1/ρ_2 is increased, the magnitude of normal contact stress increases and the magnitude of lateral contact stress decreases in the contact zone. Increase in the mass

density ratio enhances the tensile behavior of the lateral contact stress behind the trailing end of the contact zone.

Figures 4.22 - 4.25 show the effect of dimensionless punch speed c_1 on elastodynamic contact stresses due to a triangular punch. Normal contact stress is unbounded at the sharp end. Influence of the dimensionless punch speed on normal contact stress is found to be significant. Normal contact stress becomes less compressive as the dimensionless punch speed is increased from 0.0 to 0.8. Although the curves generated for the normalized lateral contact stress are generally close to each other, there is a notable increase in the tensile stress around the trailing end at larger punch speeds. For both less stiff and stiffer coatings, lateral contact stress tends to become less compressive near the leading end of the contact zone.

Figures 4.26 - 4.27 present the effect of coefficient of friction η on elastodynamic contact stresses generated by a moving triangular punch. Normal contact stresses in the contact zone slightly change due to the friction. However, change in the lateral contact stress is rather significant. The impact of the coefficient of friction especially on the tensile stress is important. A rise in the coefficient of friction again causes an increase in the tensile stresses behind the trailing end of the triangular punch. Lateral contact stresses in the contact zone and ahead of the leading end are compressive.

Figures 4.28 - 4.29 depict the effect of relative contact length b/h_1 on elastodynamic contact stresses. Increase in the ratio b/h_1 influences contact stresses generated on the less stiff and stiffer coatings in different ways. Figure 4.28 shows contact stress distributions for the less stiff coating. As the ratio b/h_1 is increased from 0.1 to 1.2, normal contact stress tends to be compressive whereas lateral contact stress becomes less compressive throughout the contact. Tensile behavior of the lateral contact stresses behind the trailing end of the triangular punch is enhanced for larger b/h_1 ratios. Hence, behind locations of the triangular punch is more critical for surface

related failures in the less stiff coating especially at higher b/h_1 ratios. The reverse trend is observed for the stiffer coating. As the ratio b/h_1 is increased, less compressive normal contact stresses are formed. Lateral contact stress tends to become compressive along the contact surface for higher values of b/h_1 .

Figure 4.30 - 4.31 illustrate normal and lateral contact stress variations with respect to different values of the ratio ν_1/ν_2 . Normal contact stress curves calculated for different values of the ratio ν_1/ν_2 are rather close to each other hence the effect is minimal. A considerable change in the lateral contact stress however can be seen with the corresponding change in the ratio ν_1/ν_2 . Lateral contact stress in the contact zone decreases as ν_1/ν_2 is increased from 0.6 to 1.2 for a less stiff coating. In the case of the stiffer coating however, lateral contact stress throughout the contact tends to be compressive.

Triangular punch contact problem is a type of the incomplete contact problems. There is a relationship between the required load applied by the punch and the contact length. In this study, for the solutions of the triangular punch contact problem, we have assigned a contact length b/h_1 initially. The normalized applied load by the triangular punch is computed by using the equilibrium equation after solution is completed. Tables 4.11 - 4.15 show the normalized applied load by the triangular punch for various parameters. Table 4.11 depicts the normalized load for various relative contact length b/h_1 in elastostatic case. The normalized load for the less stiff coating ($\mu_1/\mu_2 = 1/10$) is always greater than that for the stiffer coating ($\mu_1/\mu_2 = 10$), and the normalized load is an increasing function of b/h_1 for all type of coatings. Tables 4.12 - 4.15 show the normalized load for different values of modulus ratio μ_1/μ_2 and punch speed c_1 . When Tables 4.12 and 4.13 are examined,

the values of the normalized load for $b/h_1 = 0.2$ is less than those calculated for $b/h_1 = 0.4$. In both situations, the normalized load is a decreasing function of dimensionless punch speed c_1 . Tables 4.14 and 4.15 show the normalized load for different values of coefficient of friction and dimensionless punch speed for the less stiff and stiffer coatings. In all cases, the normalized load is a decreasing function of the dimensionless punch speed. When Tables 4.14 and 4.15 are investigated, the amount of decrease in the normalized load for the less stiff coating is greater than that for the stiffer coating in frictionless case. Nevertheless, the amount of decrease in the normalized load for the stiffer coating is greater than that for the less stiff coating at highly frictional situation.

Tables 4.16 – 4.20 tabulate the normalized stress intensity factor at the sharp corner of the triangular punch. Table 4.16 shows the normalized stress intensity factors for different values of modulus ratio μ_1/μ_2 and relative contact length b/h_1 in elastostatic case. The mode I SIF denoted by $K_I(0)$ is an increasing function of the ratio b/h_1 for the less stiff coating whereas it is a decreasing function of the ratio b/h_1 for the stiffer coating. Tables 4.17 – 4.18 show the normalized stress intensity factor for various values of modulus ratio μ_1/μ_2 and dimensionless punch speed c_1 . In all cases, as punch speed is increased, the mode I SIF decreases. Tables 4.19 – 4.20 provide the normalized stress intensity factors for various values of coefficient of friction η and dimensionless punch speed c_1 . The amount of fall in the mode I SIF with respect to punch speed is greater for the less stiff coating in the frictionless case. However, in highly frictional cases, the amount of fall in the mode I SIF is greater for stiffer coatings.

Tables 4.21 - 4.24 provide results on percent differences between contact stresses computed considering elastostatic and elastodynamic conditions. Such a comparison

is critical in assessment of influence of punch dynamics on the contact stress distributions. Contact stresses are calculated for four different values of dimensionless punch speed c_1 . The case $c_1 = 0$ corresponds to elastostatic contact. The contacts for which $c_1 > 0$ are elastodynamic. The percent difference $\varepsilon\%$ in each case is computed with respect to contact stress evaluated for $c_1 = 0$. Tables 4.21 and 4.22 show respectively normal and lateral contact stresses induced by the moving frictional flat punch for the less stiff coating ($\mu_1/\mu_2 = 1/10$). The difference found for the normal contact stresses $\sigma_{1YY}(X, 0)$ are significant. When we investigate Table 4.21, the difference values in all the contact points gradually increase as punch speed is increased from 0.0 to 0.8. The orders of the percent difference are greater at positions near the leading end of the contact zone, and percent difference reaches up to 89% at that locations. Percent differences for the lateral contact stress are also remarkable. The value of percent differences gradually increase as punch speed is increased. The highest difference is observed at the trailing end (sharp corner) of the triangular punch. Moreover, the percent difference values gradually increase ahead of the contact zone.

Tables 4.23 – 4.24 tabulate elastostatic and elastodynamic contact stresses and percent difference values evaluated at several contact points for the stiffer coating ($\mu_1/\mu_2 = 10$). The percent difference values for the normal contact stress are significant. For all contact points, the percent differences gradually increase as punch speed is increased and it reaches up to 88.6%. The values of the percent difference between elastostatic and elastodynamic results for the lateral contact stresses are provided in Table 4.24. Values of the percent difference for the lateral contact stress are also remarkable. The highest difference is seen around trailing end (sharp corner) of the triangular punch.

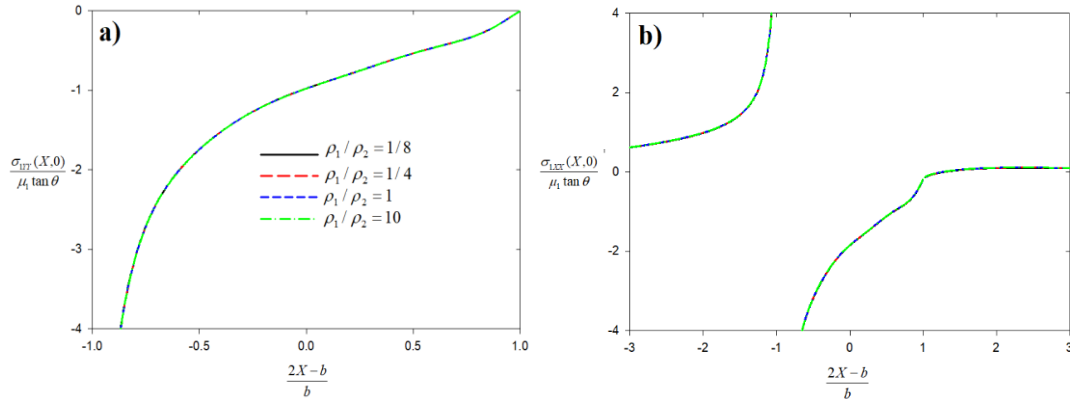


Figure 4.20: Normal and lateral elastodynamic contact stresses on homogeneous coating indented by a moving triangular punch for various mass density ratios (a) Normal contact stress distribution; (b) Lateral contact stress distribution, $\mu_1 / \mu_2 = 1/10$, $b/h_1 = 0.4$, $c_1 = 0.6$, $\eta = 0.3$, $\nu_1/\nu_2 = 0.8$.

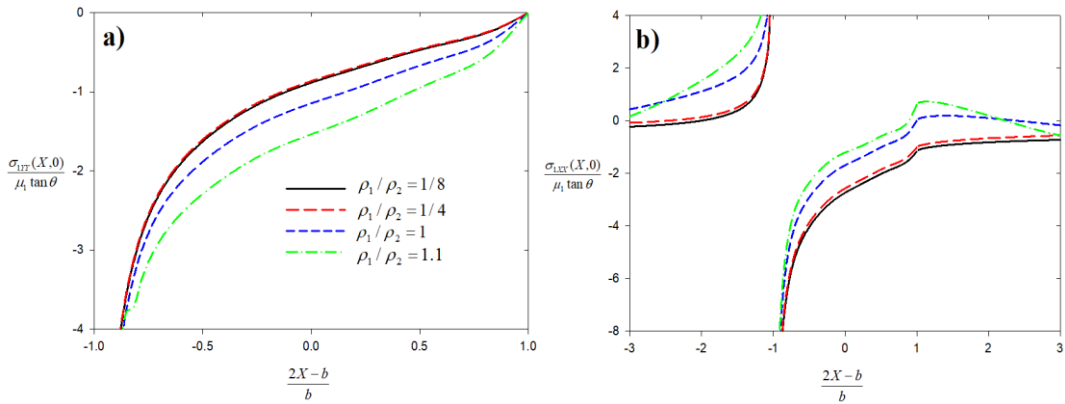


Figure 4.21: Normal and lateral elastodynamic contact stresses on homogeneous coating indented by a moving triangular punch for various mass density ratios (a) Normal contact stress distribution; (b) Lateral contact stress distribution, $\mu_1 / \mu_2 = 10$, $b/h_1 = 0.4$, $c_1 = 0.6$, $\eta = 0.3$, $\nu_1/\nu_2 = 0.8$.

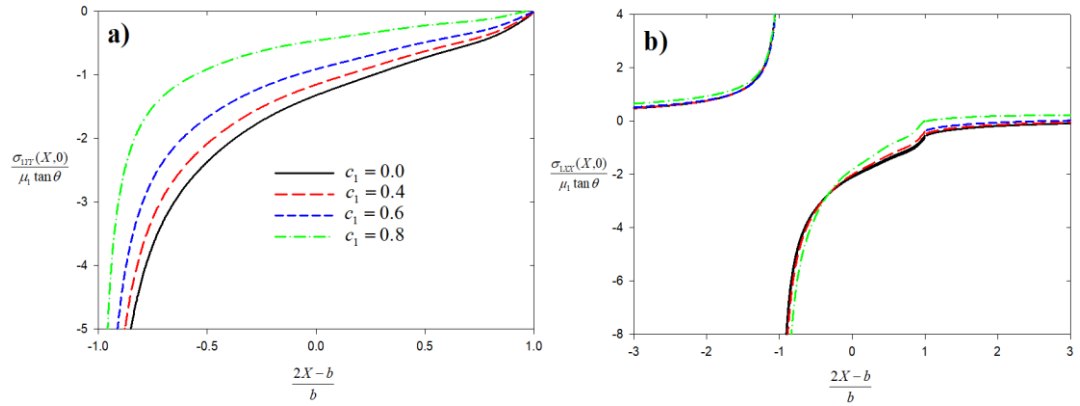


Figure 4.22: Normal and lateral elastodynamic contact stresses on homogenous coating indented by a moving triangular punch for various values of punch speed (a) Normal contact stress distribution; (b) Lateral contact stress distribution, $\mu_1 / \mu_2 = 1/10$, $b/h_1 = 0.2$, $\eta = 0.3$, $\rho_1 / \rho_2 = 1/8$, $v_1 / v_2 = 0.8$.

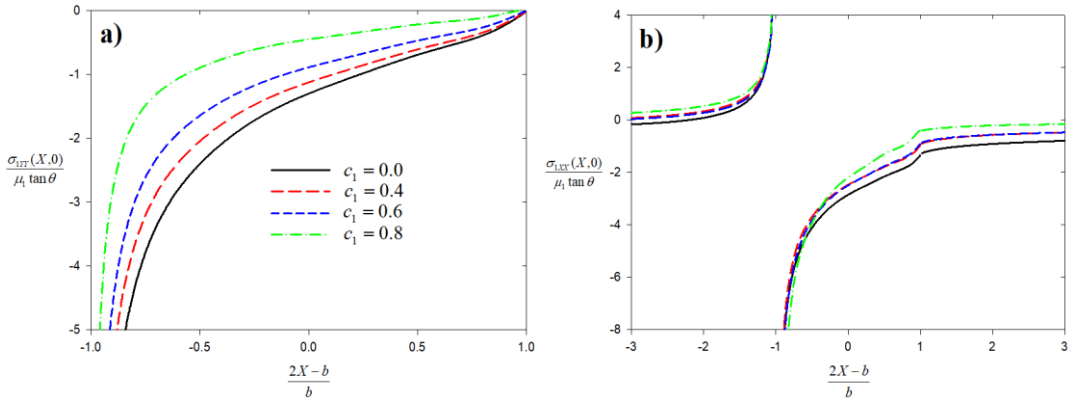


Figure 4.23: Normal and lateral elastodynamic contact stresses on homogenous coating indented by a moving triangular punch for various values of punch speed (a) Normal contact stress distribution; (b) Lateral contact stress distribution, $\mu_1 / \mu_2 = 10$, $b/h_1 = 0.2$, $\eta = 0.3$, $\rho_1 / \rho_2 = 1/8$, $v_1 / v_2 = 0.8$.

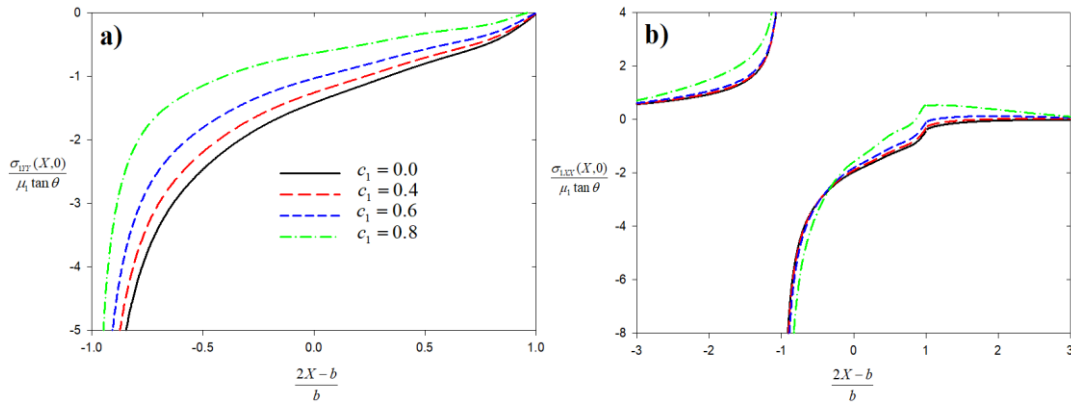


Figure 4.24: Normal and lateral elastodynamic contact stresses on homogenous coating indented by a moving triangular punch for various values of punch speed (a) Normal contact stress distribution; (b) Lateral contact stress distribution, $\mu_1 / \mu_2 = 1/10$, $b/h_1 = 0.5$, $\eta = 0.3$, $\rho_1 / \rho_2 = 1/8$, $v_1/v_2 = 0.8$.

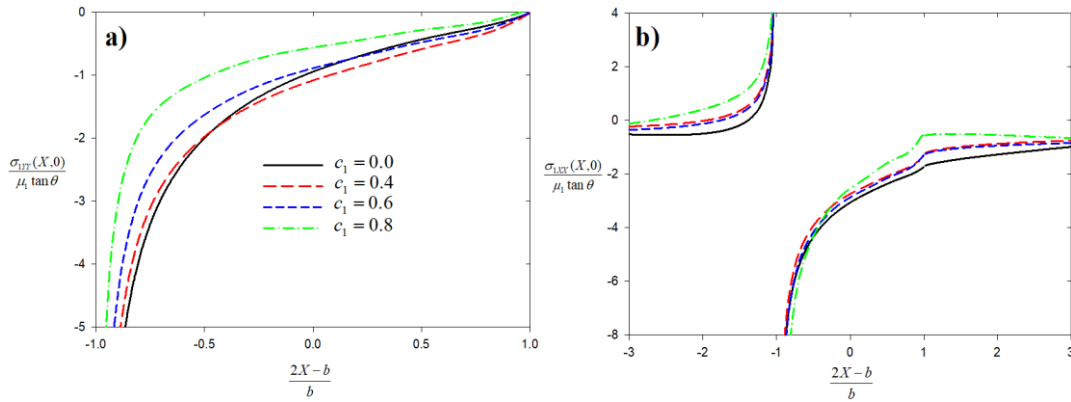


Figure 4.25: Normal and lateral elastodynamic contact stresses on homogenous coating indented by a moving triangular punch for various values of punch speed (a) Normal contact stress distribution; (b) Lateral contact stress distribution, $\mu_1 / \mu_2 = 10$, $b/h_1 = 0.5$, $\eta = 0.3$, $\rho_1 / \rho_2 = 1/8$, $v_1/v_2 = 0.8$.

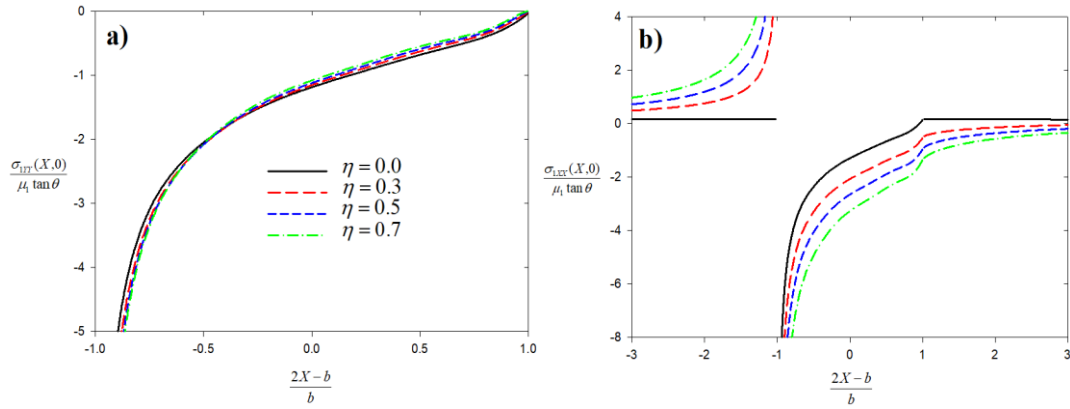


Figure 4.26: Normal and lateral elastodynamic contact stresses on homogeneous coating indented by a moving triangular punch for various values of coefficient of friction (a) Normal contact stress distribution; (b) Lateral contact stress distribution, $\mu_1 / \mu_2 = 1/10$, $b/h_1 = 0.2$, $c_1 = 0.4$, $\rho_1 / \rho_2 = 1/8$, $\nu_1 / \nu_2 = 0.8$.

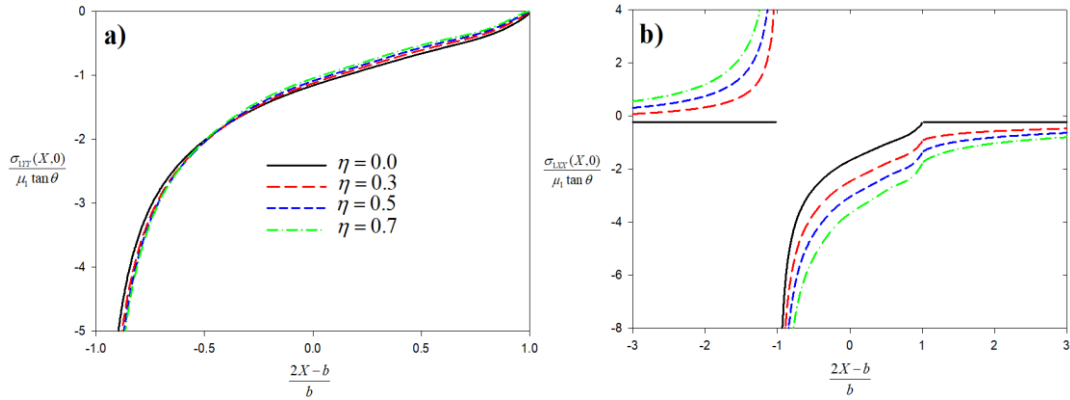


Figure 4.27: Normal and lateral elastodynamic contact stresses on homogeneous coating indented by a moving triangular punch for various values of coefficient of friction (a) Normal contact stress distribution; (b) Lateral contact stress distribution, $\mu_1 / \mu_2 = 10$, $b/h_1 = 0.2$, $c_1 = 0.4$, $\rho_1 / \rho_2 = 1/8$, $\nu_1 / \nu_2 = 0.8$.

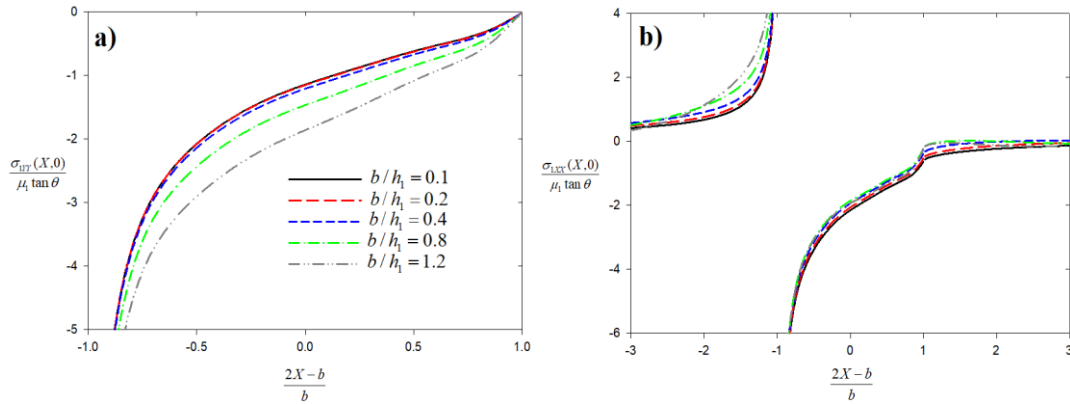


Figure 4.28: Normal and lateral elastodynamic contact stresses on homogenous coating indented by a moving triangular punch for various values of relative coating thickness (a) Normal contact stress distribution; (b) Lateral contact stress distribution, $\mu_1 / \mu_2 = 1/10$, $c_1 = 0.4$, $\eta = 0.3$, $\rho_1 / \rho_2 = 1/8$, $\nu_1 / \nu_2 = 0.8$.

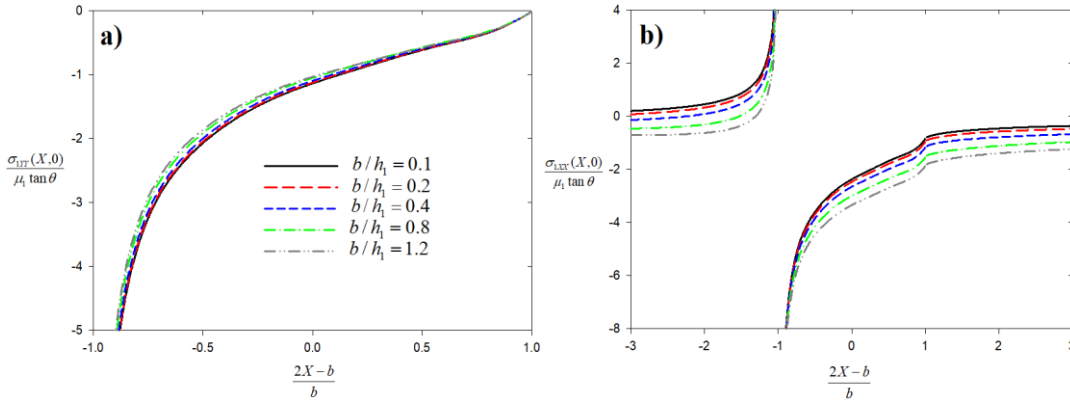


Figure 4.29: Normal and lateral elastodynamic contact stresses on homogenous coating indented by a moving triangular punch for various values of relative coating thickness (a) Normal contact stress distribution; (b) Lateral contact stress distribution, $\mu_1 / \mu_2 = 10$, $c_1 = 0.4$, $\eta = 0.3$, $\rho_1 / \rho_2 = 1/8$, $\nu_1 / \nu_2 = 0.8$.

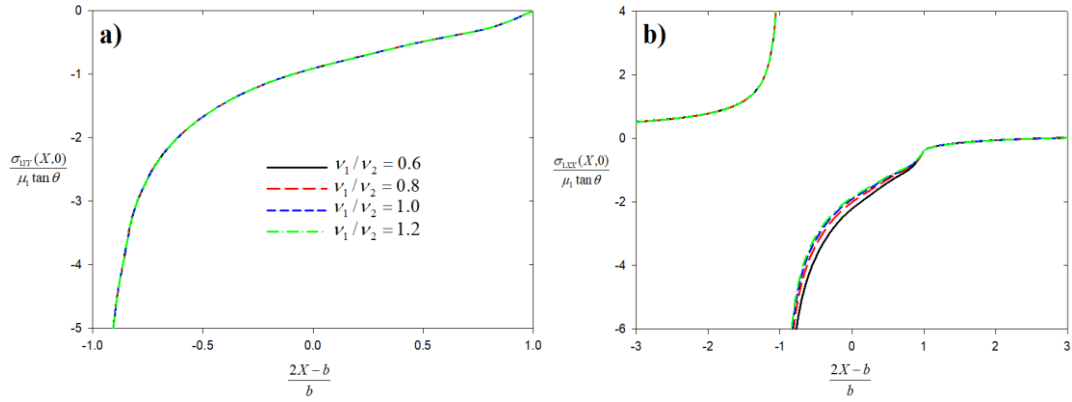


Figure 4.30: Normal and lateral elastodynamic contact stresses on homogeneous coating indented by a moving triangular punch for various values of Poisson's ratio (a) Normal contact stress distribution; (b) Lateral contact stress distribution, $\mu_1 / \mu_2 = 1/10$, $b/h_1 = 0.2$, $c_1 = 0.6$, $\eta = 0.3$, $\rho_1 / \rho_2 = 1/8$.

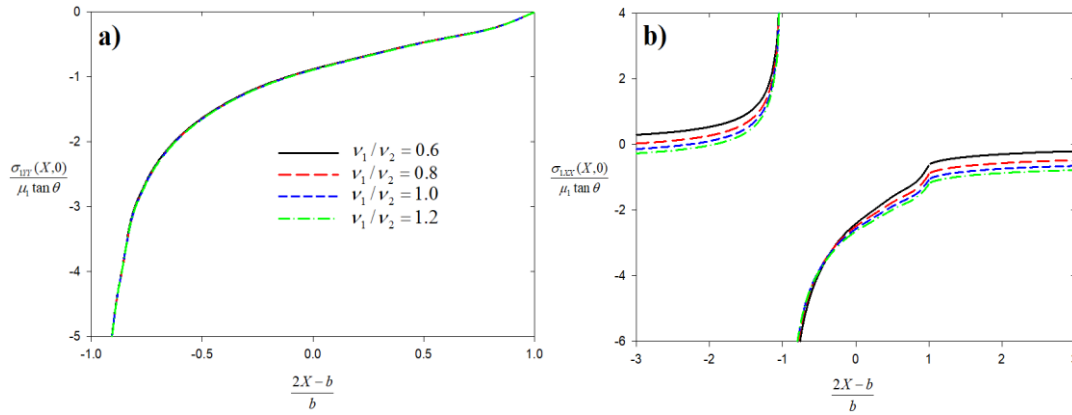


Figure 4.31: Normal and lateral elastodynamic contact stresses on homogeneous coating indented by a moving triangular punch for various values of Poisson's ratio (a) Normal contact stress distribution; (b) Lateral contact stress distribution, $\mu_1 / \mu_2 = 10$, $b/h_1 = 0.2$, $c_1 = 0.6$, $\eta = 0.3$, $\rho_1 / \rho_2 = 1/8$.

Table 4.11: The normalized load for homogenous coating indented by a moving triangular punch $c_1 = 0$, $\eta = 0.0$, $\nu_1 / \nu_2 = 0.8$.

	$b/h_1 = 0.2$	$b/h_1 = 0.4$	$b/h_1 = 0.8$	$b/h_1 = 1.2$
μ_1/μ_2	P	P	P	P
	$\mu_1 \tan(\theta)$	$\mu_1 \tan(\theta)$	$\mu_1 \tan(\theta)$	$\mu_1 \tan(\theta)$
1/10	0.421671	0.870991	1.945252	3.357045
1/5	0.421049	0.866031	1.906162	3.217368
1	0.416952	0.833905	1.667809	2.501214
10	0.398958	0.705983	0.969333	0.999572

Table 4.12: The normalized load for homogenous coating indented by a moving triangular punch $b/h_1 = 0.2$, $\eta = 0.3$, $\rho_1 / \rho_2 = 1/8$, $\nu_1 / \nu_2 = 0.8$.

	$c_1 = 0.0$	$c_1 = 0.4$	$c_1 = 0.6$	$c_1 = 0.7$	$c_1 = 0.8$
μ_1/μ_2	P	P	P	P	P
	$\mu_1 \tan(\theta)$	$\mu_1 \tan(\theta)$	$\mu_1 \tan(\theta)$	$\mu_1 \tan(\theta)$	$\mu_1 \tan(\theta)$
1/10	0.440287	0.389985	0.318719	0.265112	0.191240
1/5	0.440530	0.390444	0.319456	0.266068	0.193229
1	0.442468	0.391993	0.320205	0.265859	0.189928
10	0.447603	0.383546	0.314108	0.261359	0.188564

Table 4.13: The normalized load for homogenous coating indented by a moving triangular punch $b/h_1 = 0.4$, $\eta = 0.3$, $\rho_1 / \rho_2 = 1/8$, $\nu_1 / \nu_2 = 0.8$.

	$c_1 = 0.0$	$c_1 = 0.4$	$c_1 = 0.6$	$c_1 = 0.7$	$c_1 = 0.8$
μ_1/μ_2	P	P	P	P	P
	$\mu_1 \tan(\theta)$	$\mu_1 \tan(\theta)$	$\mu_1 \tan(\theta)$	$\mu_1 \tan(\theta)$	$\mu_1 \tan(\theta)$
1/10	0.897830	0.799932	0.662422	0.560996	0.427338
1/5	0.896008	0.798068	0.659417	0.555144	0.403873
1	0.884936	0.783985	0.640410	0.531718	0.379855
10	0.816886	0.749701	0.622156	0.528455	0.403790

Table 4.14: The normalized load for homogenous coating indented by a moving triangular punch $b/h_1 = 0.4$, $\mu_1/\mu_2 = 1/5$, $\rho_1/\rho_2 = 1/8$, $\nu_1/\nu_2 = 0.8$.

η	$c_1 = 0.0$	$c_1 = 0.4$	$c_1 = 0.6$	$c_1 = 0.7$	$c_1 = 0.8$
	$\frac{P}{\mu_1 \tan(\theta)}$	$\frac{P}{\mu_1 \tan(\theta)}$	$\frac{P}{\mu_1 \tan(\theta)}$	$\frac{P}{\mu_1 \tan(\theta)}$	$\frac{P}{\mu_1 \tan(\theta)}$
0.0	0.866031	0.761991	0.611807	0.495656	0.319328
0.3	0.896008	0.798068	0.659417	0.555144	0.403873
0.5	0.912833	0.817897	0.684410	0.584566	0.442670
0.7	0.926917	0.833968	0.703111	0.604097	0.463034

Table 4.15: The normalized load for homogenous coating indented by a moving triangular punch $b/h_1 = 0.4$, $\mu_1/\mu_2 = 5$, $\rho_1/\rho_2 = 1/8$, $\nu_1/\nu_2 = 0.8$.

η	$c_1 = 0.0$	$c_1 = 0.4$	$c_1 = 0.6$	$c_1 = 0.7$	$c_1 = 0.8$
	$\frac{P}{\mu_1 \tan(\theta)}$	$\frac{P}{\mu_1 \tan(\theta)}$	$\frac{P}{\mu_1 \tan(\theta)}$	$\frac{P}{\mu_1 \tan(\theta)}$	$\frac{P}{\mu_1 \tan(\theta)}$
0.0	0.754082	0.765176	0.607343	0.499091	0.349693
0.3	0.843994	0.771813	0.636854	0.540387	0.413025
0.5	0.911643	0.771194	0.648633	0.555646	0.427282
0.7	0.986265	0.766940	0.654174	0.561238	0.422749

Table 4.16: Normalized stress intensity factors for a moving triangular punch $c_1 = 0$, $\eta = 0.0$, $\nu_1/\nu_2 = 0.8$.

μ_1/μ_2	$b/h_1 = 0.2$	$b/h_1 = 0.4$	$b/h_1 = 0.8$	$b/h_1 = 1.2$
	$K_I(0)$	$K_I(0)$	$K_I(0)$	$K_I(0)$
1/10	1.3345	1.3558	1.4311	1.5328
1/5	1.3336	1.3520	1.4169	1.5013
1	1.3272	1.3272	1.3272	1.3272
10	1.2988	1.2231	1.0165	0.8447

Table 4.17: Normalized stress intensity factors for a moving triangular punch
 $b/h_1 = 0.2$, $\eta = 0.3$, $\rho_1/\rho_2 = 1/8$, $\nu_1/\nu_2 = 0.8$.

	$c_1 = 0.0$	$c_1 = 0.4$	$c_1 = 0.6$	$c_1 = 0.7$	$c_1 = 0.8$
μ_1/μ_2	$K_I(0)$	$K_I(0)$	$K_I(0)$	$K_I(0)$	$K_I(0)$
1/10	1.3043	1.1342	0.8902	0.7032	0.4397
1/5	1.3060	1.1368	0.8941	0.7084	0.4504
1	1.3183	1.1482	0.9030	0.7141	0.4449
10	1.3640	1.1240	0.8841	0.6979	0.4358

Table 4.18: Normalized stress intensity factors for a moving triangular punch
 $b/h_1 = 0.4$, $\eta = 0.3$, $\rho_1/\rho_2 = 1/8$, $\nu_1/\nu_2 = 0.8$.

	$c_1 = 0.0$	$c_1 = 0.4$	$c_1 = 0.6$	$c_1 = 0.7$	$c_1 = 0.8$
μ_1/μ_2	$K_I(0)$	$K_I(0)$	$K_I(0)$	$K_I(0)$	$K_I(0)$
1/10	1.3076	1.1395	0.8998	0.7181	0.4670
1/5	1.3088	1.1419	0.9031	0.7212	0.4648
1	1.3183	1.1482	0.9030	0.7141	0.4449
10	1.3259	1.1000	0.8706	0.6940	0.4495

Table 4.19: Normalized stress intensity factors for a moving triangular punch
 $b/h_1 = 0.4$, $\mu_1/\mu_2 = 1/5$, $\rho_1/\rho_2 = 1/8$, $\nu_1/\nu_2 = 0.8$.

	$c_1 = 0.0$	$c_1 = 0.4$	$c_1 = 0.6$	$c_1 = 0.7$	$c_1 = 0.8$
η	$K_I(0)$	$K_I(0)$	$K_I(0)$	$K_I(0)$	$K_I(0)$
0.0	1.3520	1.1854	0.9461	0.7631	0.4985
0.3	1.3088	1.1419	0.9031	0.7212	0.4648
0.5	1.2721	1.1024	0.8584	0.6712	0.4105
0.7	1.2302	1.0565	0.8052	0.6117	0.3504

Table 4.20: Normalized stress intensity factors for a moving triangular punch
 $b/h_1 = 0.4$, $\mu_1/\mu_2 = 5$, $\rho_1/\rho_2 = 1/8$, $\nu_1/\nu_2 = 0.8$.

	$c_1 = 0.0$	$c_1 = 0.4$	$c_1 = 0.6$	$c_1 = 0.7$	$c_1 = 0.8$
η	$K_I(0)$	$K_I(0)$	$K_I(0)$	$K_I(0)$	$K_I(0)$
0.0	1.2633	1.1878	0.9428	0.7656	0.5212
0.3	1.3244	1.1016	0.8753	0.6993	0.4549
0.5	1.3656	1.0367	0.8162	0.6353	0.3806
0.7	1.4077	0.9687	0.7514	0.5658	0.3085

Table 4.21: Percent difference between elastostatic and elastodynamic normal contact stresses $\mu_1/\mu_2 = 1/10$, $b/h_1 = 0.2$, $\eta = 0.3$, $\rho_1/\rho_2 = 1/8$, $\nu_1/\nu_2 = 0.8$.

	$c_1 = 0.0$		$c_1 = 0.4$		$c_1 = 0.6$		$c_1 = 0.8$	
$\frac{2X-b}{b}$	$\frac{\sigma_{1YY}(X,0)}{\mu_1 \tan \theta}$	$\frac{\sigma_{1YY}(X,0)}{\mu_1 \tan \theta}$	$\varepsilon\%$	$\frac{\sigma_{1YY}(X,0)}{\mu_1 \tan \theta}$	$\varepsilon\%$	$\frac{\sigma_{1YY}(X,0)}{\mu_1 \tan \theta}$	$\varepsilon\%$	
-0.94	-8.09109	-7.22887	10.66	-6.01239	25.69	-3.81489	52.85	
-0.82	-4.49617	-3.98267	11.42	-3.25150	27.68	-1.90101	57.72	
-0.70	-3.30291	-2.91371	11.78	-2.35793	28.61	-1.32838	59.78	
-0.61	-2.78459	-2.45156	11.96	-1.97551	29.06	-1.09428	60.70	
-0.50	-2.38210	-2.09320	12.13	-1.67982	29.48	-0.91430	61.62	
-0.22	-1.65577	-1.44745	12.58	-1.14839	30.64	-0.59229	64.23	
-0.03	-1.36163	-1.18782	12.77	-0.93819	31.10	-0.47553	65.08	
0.22	-1.05313	-0.91611	13.01	-0.71918	31.71	-0.35502	66.29	
0.50	-0.72074	-0.62287	13.58	-0.48176	33.16	-0.21988	69.49	
0.61	-0.61739	-0.53266	13.72	-0.41058	33.50	-0.18513	70.01	
0.70	-0.52645	-0.45368	13.82	-0.34892	33.72	-0.15663	70.25	
0.82	-0.38378	-0.32881	14.32	-0.24953	34.98	-0.10347	73.04	
0.94	-0.17124	-0.14193	17.12	-0.09914	42.11	-0.01829	89.32	

Table 4.22: Percent difference between elastostatic and elastodynamic lateral contact stresses $\mu_1 / \mu_2 = 1/10$, $b/h_1 = 0.2$, $\eta = 0.3$, $\rho_1 / \rho_2 = 1/8$, $\nu_1 / \nu_2 = 0.8$.

$\frac{2X-b}{b}$	$c_1 = 0.0$		$c_1 = 0.4$		$c_1 = 0.6$		$c_1 = 0.8$	
	$\frac{\sigma_{1xx}(X,0)}{\mu_1 \tan \theta}$	$\frac{\sigma_{1xx}(X,0)}{\mu_1 \tan \theta}$	$\varepsilon\%$	$\frac{\sigma_{1xx}(X,0)}{\mu_1 \tan \theta}$	$\varepsilon\%$	$\frac{\sigma_{1xx}(X,0)}{\mu_1 \tan \theta}$	$\varepsilon\%$	
-1.50	1.19013	1.17838	0.99	1.17981	0.87	1.32734	11.53	
-1.22	1.99647	1.95841	1.91	1.92717	3.47	2.07416	3.89	
-0.99	-32.75225	-34.99146	6.84	-40.11392	22.48	-65.63974	100.41	
-0.82	-5.66980	-5.81109	2.49	-6.13882	8.27	-7.42274	30.92	
-0.50	-3.29464	-3.30953	0.45	-3.36489	2.13	-3.57637	8.55	
-0.22	-2.48513	-2.46158	0.95	-2.43514	2.01	-2.33812	5.92	
-0.03	-2.14979	-2.11303	1.71	-2.05925	4.21	-1.87567	12.75	
0.22	-1.81241	-1.76294	2.73	-1.68343	7.12	-1.42394	21.43	
0.50	-1.44067	-1.37706	4.42	-1.26813	11.98	-0.90854	36.94	
0.82	-1.07204	-0.99833	6.88	-0.87036	18.81	-0.47589	55.61	
0.99	-0.63663	-0.55560	12.73	-0.41377	35.01	-0.00076	99.88	
1.22	-0.38802	-0.32756	15.58	-0.22180	42.84	0.08116	120.92	
1.50	-0.28556	-0.23169	18.86	-0.13658	52.17	0.13916	148.73	

Table 4.23: Percent difference between elastostatic and elastodynamic normal contact stresses $\mu_1 / \mu_2 = 10$, $b/h_1 = 0.2$, $\eta = 0.3$, $\rho_1 / \rho_2 = 1/8$, $\nu_1 / \nu_2 = 0.8$.

$\frac{2X-b}{b}$	$c_1 = 0.0$		$c_1 = 0.4$		$c_1 = 0.6$		$c_1 = 0.8$	
	$\frac{\sigma_{1yy}(X,0)}{\mu_1 \tan \theta}$	$\frac{\sigma_{1yy}(X,0)}{\mu_1 \tan \theta}$	$\varepsilon\%$	$\frac{\sigma_{1yy}(X,0)}{\mu_1 \tan \theta}$	$\varepsilon\%$	$\frac{\sigma_{1yy}(X,0)}{\mu_1 \tan \theta}$	$\varepsilon\%$	
-0.94	-8.42655	-7.15457	15.09	-5.96314	29.23	-3.77606	55.19	
-0.82	-4.65217	-3.93530	15.41	-3.21933	30.80	-1.87935	59.60	
-0.70	-3.39285	-2.87332	15.31	-2.32970	31.34	-1.31104	61.36	
-0.61	-2.84365	-2.41343	15.13	-1.94835	31.48	-1.07841	62.08	
-0.50	-2.41716	-2.05695	14.90	-1.65362	31.59	-0.89973	62.78	
-0.22	-1.65113	-1.41613	14.23	-1.12528	31.85	-0.58092	64.82	
-0.03	-1.34217	-1.15846	13.69	-0.91628	31.73	-0.46522	65.34	
0.22	-1.02208	-0.88968	12.95	-0.69931	31.58	-0.34621	66.13	
0.50	-0.68655	-0.60244	12.25	-0.46645	32.06	-0.21382	68.86	
0.61	-0.58422	-0.51428	11.97	-0.39680	32.08	-0.17979	69.23	
0.70	-0.49539	-0.43722	11.74	-0.33660	32.05	-0.15191	69.33	
0.82	-0.35825	-0.31632	11.70	-0.24028	32.93	-0.10024	72.02	
0.94	-0.15671	-0.13686	12.67	-0.09562	38.98	-0.01781	88.64	

Table 4.24: Percent difference between elastostatic and elastodynamic lateral contact stresses $\mu_1 / \mu_2 = 10$, $b / h_1 = 0.2$, $\eta = 0.3$, $\rho_1 / \rho_2 = 1/8$, $\nu_1 / \nu_2 = 0.8$.

$\frac{2X-b}{b}$	$c_1 = 0.0$		$c_1 = 0.4$		$c_1 = 0.6$		$c_1 = 0.8$	
	$\frac{\sigma_{1xx}(X,0)}{\mu_1 \tan \theta}$	$\frac{\sigma_{1xx}(X,0)}{\mu_1 \tan \theta}$	$\frac{\sigma_{1xx}(X,0)}{\mu_1 \tan \theta}$	$\varepsilon\%$	$\frac{\sigma_{1xx}(X,0)}{\mu_1 \tan \theta}$	$\varepsilon\%$	$\frac{\sigma_{1xx}(X,0)}{\mu_1 \tan \theta}$	$\varepsilon\%$
-1.50	0.51088	0.73231	43.34	0.65836	28.87	0.90972	78.07	
-1.22	1.33995	1.50015	11.96	1.39484	4.10	1.64469	22.74	
-0.99	-35.01885	-35.12308	0.30	-40.36371	15.26	-65.45765	86.92	
-0.82	-6.64605	-6.19195	6.83	-6.60705	0.59	-7.75646	16.71	
-0.50	-4.12521	-3.70401	10.21	-3.84306	6.84	-3.93820	4.53	
-0.22	-3.26050	-2.86046	12.27	-2.91691	10.54	-2.71112	16.85	
-0.03	-2.90134	-2.51333	13.37	-2.54207	12.38	-2.25220	22.37	
0.22	-2.54022	-2.16433	14.80	-2.16711	14.69	-1.80398	28.98	
0.50	-2.15167	-1.78314	17.13	-1.75648	18.37	-1.29623	39.76	
0.82	-1.77674	-1.41033	20.62	-1.36456	23.20	-0.87010	51.03	
0.99	-1.35774	-0.98299	27.60	-0.92295	32.02	-0.40785	69.96	
1.22	-1.12111	-0.76047	32.17	-0.73468	34.47	-0.32488	71.02	
1.50	-1.01764	-0.66542	34.61	-0.64910	36.21	-0.26465	73.99	

4.4 Numerical Results for the Rigid Semi-circular Punch

General schematic for the contact problem between a rigid semi-circular punch and a homogenous elastic coating is shown in Figure 4.32. Homogenous elastic coating of thickness h_1 is perfectly bonded to a homogenous substrate, and the rigid semi-circular punch slides over the coating at a speed of V .

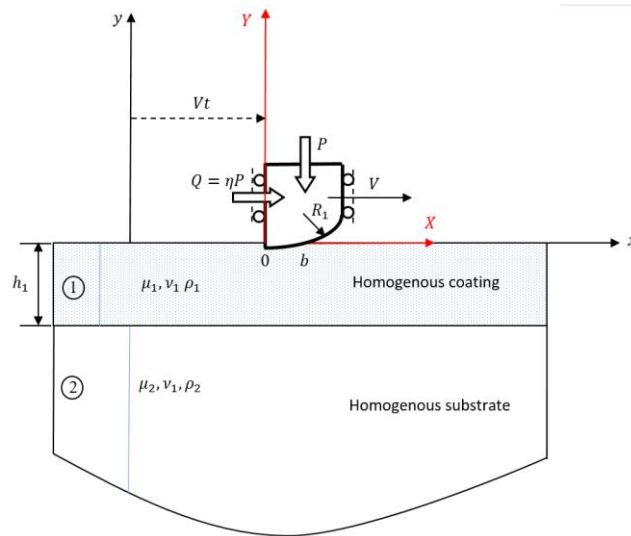


Figure 4.32: General schematic for the contact between a homogenous elastic coating and a rigid triangular punch

Figures 4.33 - 4.34 show elastodynamic contact stress distributions for less stiff and stiffer coatings for which modulus ratio μ_1/μ_2 is respectively defined as 1/10 and 10. The contact is assumed to be frictional and coefficient of friction η is taken as 0.3. It is interesting to note that the mass density ratio ρ_1/ρ_2 does not considerably affect the contact stress distribution for a less stiff coating. However, density ratio ρ_1/ρ_2 significantly affect the contact stress distribution for the stiffer coating.

Figures 4.35 – 4.38 display the effect of dimensionless punch speed c_1 on contact stress induced frictional contacts of less stiff and stiffer coatings for two different

relative contact lengths defined by the ratio b/R_1 . The ratio R_1/h_1 is kept constant as 20 in these figures. Figure 4.35 - 4.36 respectively show elastodynamic contact stresses on the less stiff and stiffer coatings for different values of the dimensionless punch speed c_1 at the ratio $b/R_1 = 0.01$. Contact stresses are in general sensitive to the change in punch speed and normal contact stresses become less compressive as punch speed is increased (see Figures 4.35(a) and 4.36(a)). For both less stiff and stiffer coatings, lateral contact stress increases near the trailing end and decreases near the leading end of the contact zone and skewed lateral contact stress curves are formed. Figures 4.37 – 4.38 show the elastodynamic contact stresses for different values of dimensionless punch speed at the ratio $b/R_1 = 0.05$. Figure 4.37 shows elastodynamic contact stresses for the less stiff coating ($\mu_1/\mu_2 = 1/10$). The general trend in the variation of the normal and lateral contact stresses is similar to that observed in Figure 4.35. Figure 4.38 illustrates elastodynamic contact stresses for the stiffer coating ($\mu_1/\mu_2 = 10$). However, the behavior of normal and lateral contact stresses are different from that observed in Figure 4.36. Both normal and lateral contact stresses decrease as punch speed c_1 is increased. The change in the ratio b/R_1 leads to different elastodynamic contact stresses.

The influence of coefficient of friction η on elastodynamic contact stresses is examined in Figures 4.39 - 4.40. Figures 4.39(a) and 4.40(a) illustrate the effect of the coefficient of friction on normal contact stresses for the less stiff and stiffer coatings, respectively. It can be seen that increase in the coefficient of friction influences the normal contact stresses in a similar way for both coating types. Normal contact stresses slightly increase near the trailing end (sharp corner) and decrease near the leading end (smooth contact) of the semi-circular punch, hence skewed stress curves are formed. When Figures 4.39(b) and 4.40(b) are examined, in all cases, larger coefficient of friction leads to a larger tensile peak at the trailing end of

the contact zone. Thus, in elastodynamic contacts with friction, trailing end of the contact zone is a possible site for cracking type failure. Ahead of the leading end of the contact zone however, lateral contact stress is compressive.

Figures 4.41 – 4.42 show respectively the elastodynamic contact stresses for the less stiff and stiffer coatings as functions of the ratio R_1/h_1 . The magnitude of normal contact stress for the less stiff coating ($\mu_1/\mu_2 = 1/10$) increases as the ratio R_1/h_1 is increased from 5 to 60. The magnitude of lateral contact stress slightly decreases in the contact zone and ahead of the leading end. However, tensile behavior of the lateral contact stress is intensified behind the trailing end. The reverse trend is observed on the variations of elastodynamic contact stresses for the stiffer coating. Increase in the ratio R_1/h_1 leads to slightly less compressive normal contact stresses on the contact zone and more compressive lateral contact stresses throughout the contact.

In Figures 4.43 - 4.44, we present elastodynamic contact stresses as functions of ν_1/ν_2 . ν_1 and ν_2 being Poisson's ratios of the coating and the substrate, respectively. It can be inferred from Figures 4.43(a) and 4.44(a) that the impact of ν_1/ν_2 on normal contact stress in the contact zone is minimal. The magnitude of lateral contact stress in the contact zone decreases for the less stiff coating and increases for the stiffer coating as ν_1/ν_2 is increased from 0.6 to 1.2.

The contact problem of a semi-circular punch is a type of incomplete contact problems since there is a relationship between the contact length and required load applied by the punch. Normalized applied load by the semi-circular punch for different values of the relative contact length is calculated and results are provided in Tables 4.25 – 4.29. Table 4.25 shows the values of normalized punch load for different modulus ratio μ_1/μ_2 and relative contact length b/R_1 in elastostatic case.

The normalized punch load for the less stiff coatings is greater than that for the stiffer coatings. Moreover, the normalized punch load is an increasing function of b/R_1 . Tables 4.26 - 4.27 show the normalized punch load in elastodynamic case for different modulus ratio μ_1/μ_2 and dimensionless punch speed c_1 . The values of the normalized punch load given in Table 4.26 and 4.27 are computed at length ratios $b/R_1 = 0.01$ and $b/R_1 = 0.04$, respectively. When Table 4.26 is examined, the normalized punch loads in all cases decrease as dimensionless punch speed is increased from 0.0 to 0.8. When Table 4.27 is examined, the normalized punch load is a decreasing function of punch speed c_1 for $\mu_1/\mu_2 = 1/10$ - $\mu_1/\mu_2 = 1$. However, the normalized punch load first increases and then decreases as punch speed is increased from 0.0 to 0.8 for the stiffer coating ($\mu_1/\mu_2 = 10$). Tables 4.28 and 4.29 demonstrate the normalized punch load for different values of coefficient of friction and dimensionless punch speed for a less stiff ($\mu_1/\mu_2 = 1/5$) and stiffer coatings ($\mu_1/\mu_2 = 5$), respectively. Again, the normalized punch load is a decreasing function of punch speed c_1 and values are always greater at highly frictional cases.

Tables 4.30 - 4.34 show the normalized stress intensity factors at the sharp corner of the semi-circular punch. Table 4.30 provides mode I SIFs in elastostatic case for different values of modulus ratio μ_1/μ_2 and relative contact length b/R_1 . Mode I SIFs are always greater for the less stiff coating than those found for the stiffening coating. Moreover, as the ratio b/R_1 is increased, the values of mode I SIF increases for the less stiff coating and decreases for the stiffer coating and remain the same value for homogenous half-plane. The influences of punch speed and modulus ratio on mode I SIF are shown in Tables 4.31 and 4.32. In all cases, the mode I SIF is a decreasing function of the punch speed c_1 . Tables 4.33 and 4.34 illustrate the normalized stress intensity factors for different values of coefficient of friction and

dimensionless punch speed for the less stiff ($\mu_1/\mu_2 = 1/5$) and stiffer coatings ($\mu_1/\mu_2 = 5$), respectively. Again, the values of normalized stress intensity factors decrease as punch speed is increased. The amount of fall in the mode I SIF is greater at highly frictional conditions.

Tables 4.35 - 4.38 tabulate numerical results based on percent differences between contact stresses computed considering elastostatic and elastodynamic conditions. Such a comparison is important in evaluation of the effect of punch dynamics on contact stresses. Contact stresses are calculated for four different values of dimensionless punch speed c_1 . The case $c_1 = 0.0$ corresponds to elastostatic contact and contacts for which $c_1 > 0$ are elastodynamic. The percent difference is computed based on elastostatic results. Table 4.35 - 4.36 show elastostatic and elastodynamic contact stress results involving percent differences for the less stiff coatings. The percent differences between elastodynamic and elastostatic normal contact stresses gradually increase as punch speed c_1 is increased from 0.0 to 0.8. It reaches considerable values such as 86.72% near the leading end of the contact zone. Results for the lateral contact stress are given in Table 4.36. Percent differences between elastodynamic and elastostatic lateral contact stresses are also significant. Percent difference is relatively high at the trailing end of the contact zone. Moreover, ahead of the leading end is also critical since percent difference at that location reaches up to 142.11%.

Tables 4.37 - 4.38 show percent differences between elastostatic and elastodynamic contact stresses for the stiffer coating ($\mu_1/\mu_2 = 10$). Percent differences gradually increase as punch speed is increased from 0.0 to 0.8. The values of percent difference reach up to 86.08% near the leading end of the contact zone. The values of percent difference for the lateral contact stress are also remarkable. Critical locations for the

lateral contact stress are the out of the contact zone since the values of percent difference are relatively high at those locations.

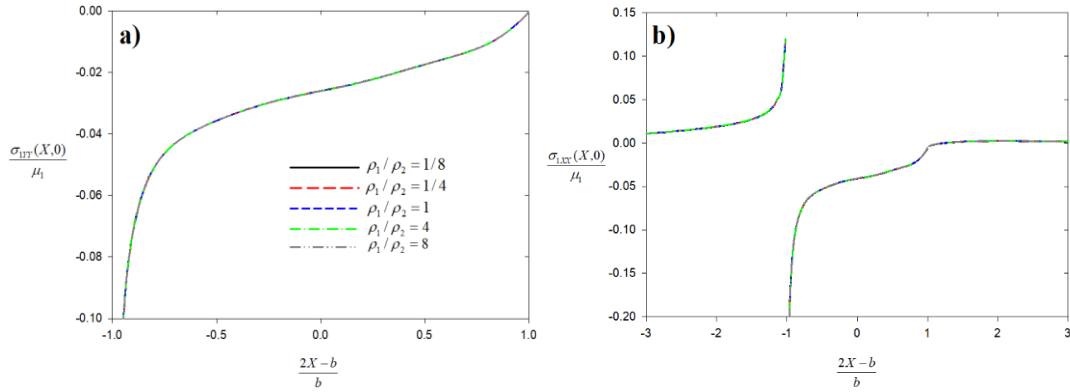


Figure 4.33: Normal and lateral elastodynamic contact stresses on homogenous coating indented by a moving semi-circular punch for various mass density ratios (a) Normal contact stress distribution; (b) Lateral contact stress distribution, $\mu_1/\mu_2 = 1/10$, $b/R_1 = 0.025$, $R_1/h_1 = 20$, $c_1 = 0.6$, $\eta = 0.3$, $\nu_1/\nu_2 = 0.8$.

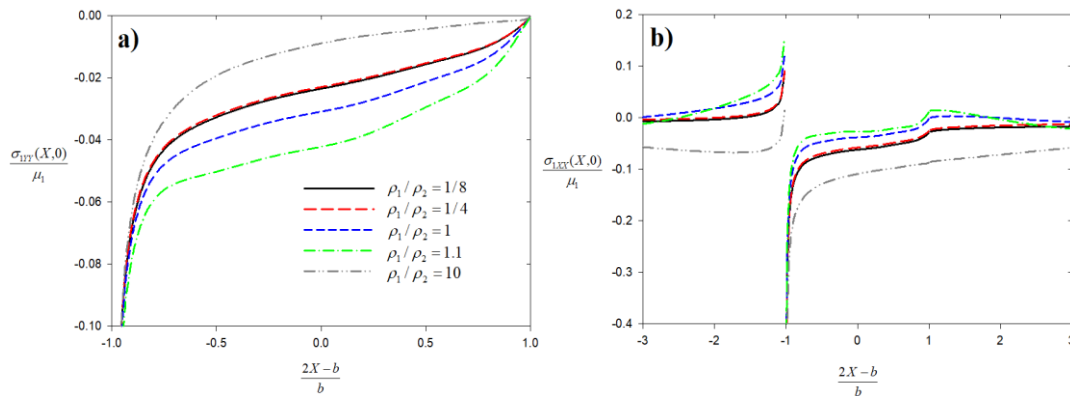


Figure 4.34: Normal and lateral elastodynamic contact stresses on homogenous coating indented by a moving semi-circular punch for various mass density ratios (a) Normal contact stress distribution; (b) Lateral contact stress distribution, $\mu_1/\mu_2 = 10$, $b/R_1 = 0.025$, $R_1/h_1 = 20$, $c_1 = 0.6$, $\eta = 0.3$, $\nu_1/\nu_2 = 0.8$.

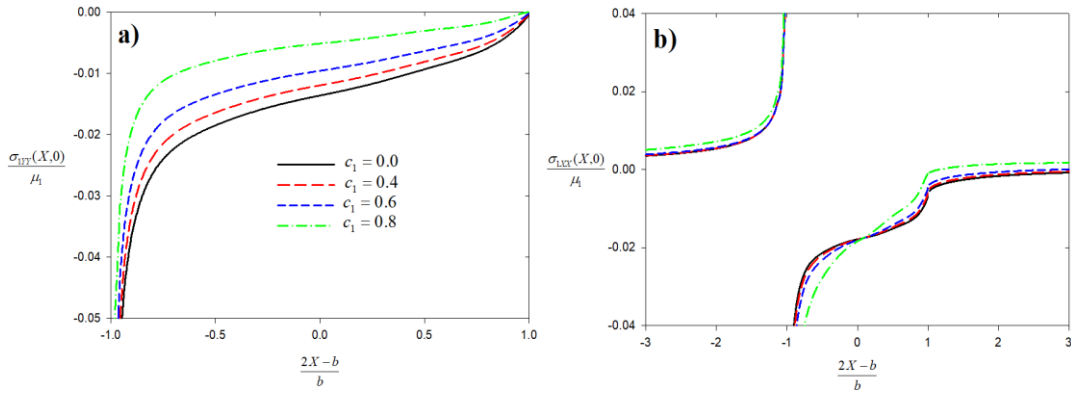


Figure 4.35: Normal and lateral elastodynamic contact stresses on homogeneous coating indented by a moving semi-circular punch for various values of punch speed (a) Normal contact stress distribution; (b) Lateral contact stress distribution, $\mu_1 / \mu_2 = 1/10$, $b / R_1 = 0.01$, $R_1 / h_1 = 20$, $\eta = 0.3$, $\rho_1 / \rho_2 = 1/8$, $v_1 / v_2 = 0.8$.

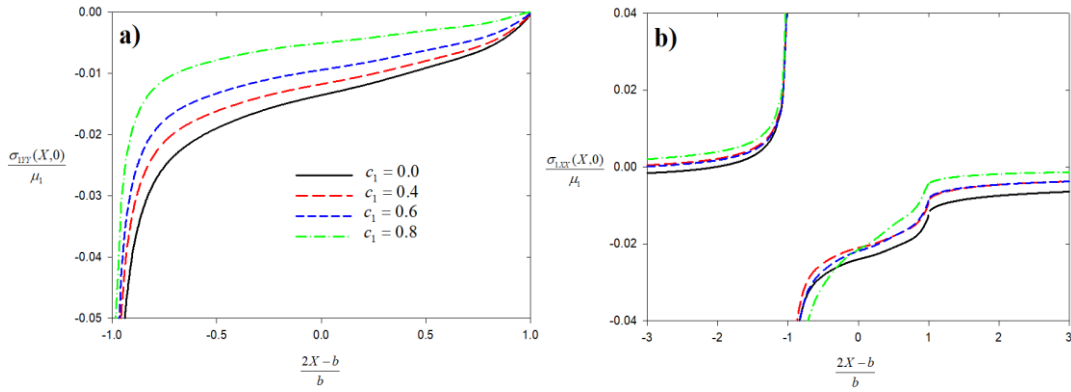


Figure 4.36: Normal and lateral elastodynamic contact stresses on homogeneous coating indented by a moving semi-circular punch for various values of punch speed (a) Normal contact stress distribution; (b) Lateral contact stress distribution, $\mu_1 / \mu_2 = 10$, $b / R_1 = 0.01$, $R_1 / h_1 = 20$, $\eta = 0.3$, $\rho_1 / \rho_2 = 1/8$, $v_1 / v_2 = 0.8$.

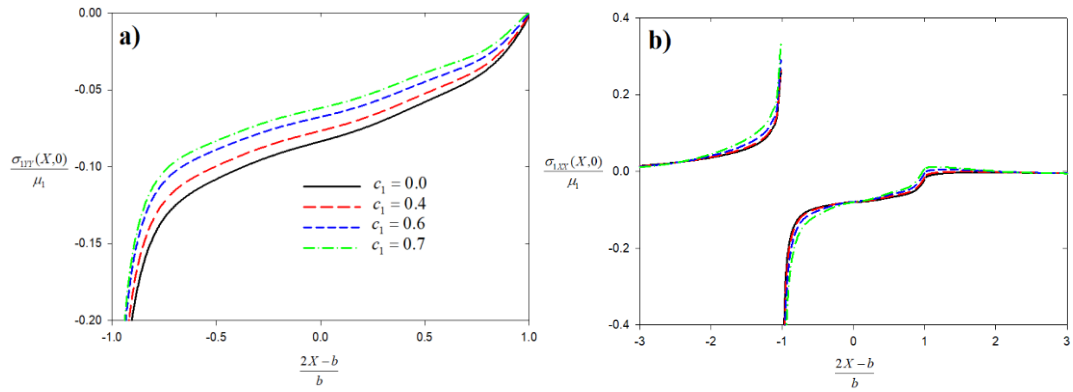


Figure 4.37: Normal and lateral elastodynamic contact stresses on homogeneous coating indented by a moving semi-circular punch for various values of punch speed (a) Normal contact stress distribution; (b) Lateral contact stress distribution, $\mu_1 / \mu_2 = 1/10$, $b / R_1 = 0.05$, $R_1 / h_1 = 20$, $\eta = 0.3$, $\rho_1 / \rho_2 = 1/8$, $v_1 / v_2 = 0.8$.

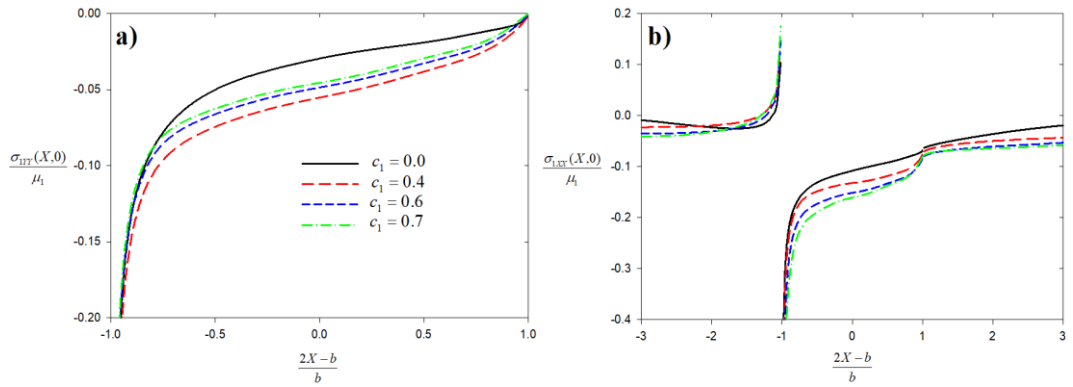


Figure 4.38: Normal and lateral elastodynamic contact stresses on homogeneous coating indented by a moving semi-circular punch for various values of punch speed (a) Normal contact stress distribution; (b) Lateral contact stress distribution, $\mu_1 / \mu_2 = 10$, $b / R_1 = 0.05$, $R_1 / h_1 = 20$, $\eta = 0.3$, $\rho_1 / \rho_2 = 1/8$, $v_1 / v_2 = 0.8$.

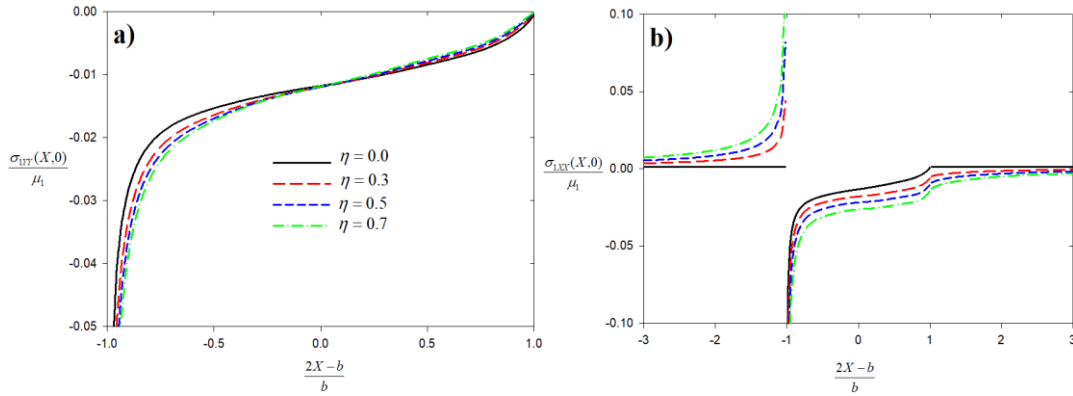


Figure 4.39: Normal and lateral elastodynamic contact stresses on homogeneous coating indented by a moving semi-circular punch for various values of coefficient of friction (a) Normal contact stress distribution; (b) Lateral contact stress distribution, $\mu_1 / \mu_2 = 1/10$, $b / R_1 = 0.01$, $R_1 / h_1 = 20$, $c_1 = 0.4$, $\rho_1 / \rho_2 = 1/8$, $v_1 / v_2 = 0.8$.

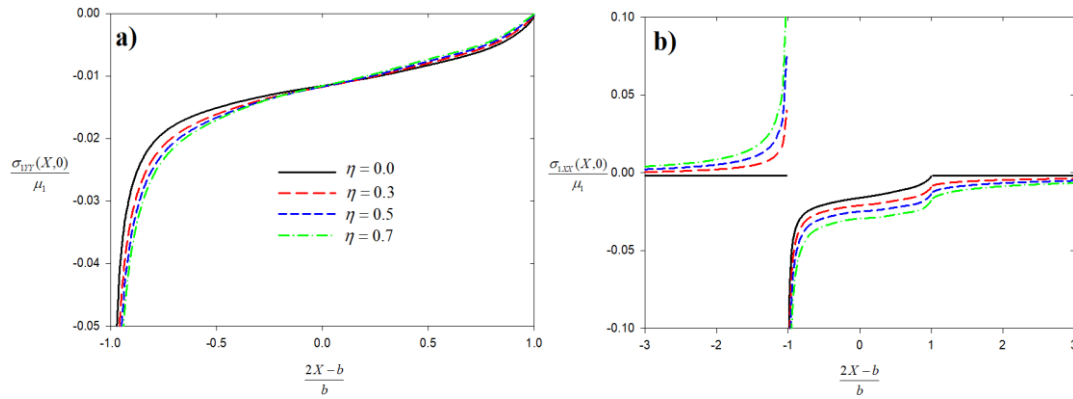


Figure 4.40: Normal and lateral elastodynamic contact stresses on homogeneous coating indented by a moving semi-circular punch for various values of coefficient of friction (a) Normal contact stress distribution; (b) Lateral contact stress distribution, $\mu_1 / \mu_2 = 10$, $b / R_1 = 0.01$, $R_1 / h_1 = 20$, $c_1 = 0.4$, $\rho_1 / \rho_2 = 1/8$, $v_1 / v_2 = 0.8$.

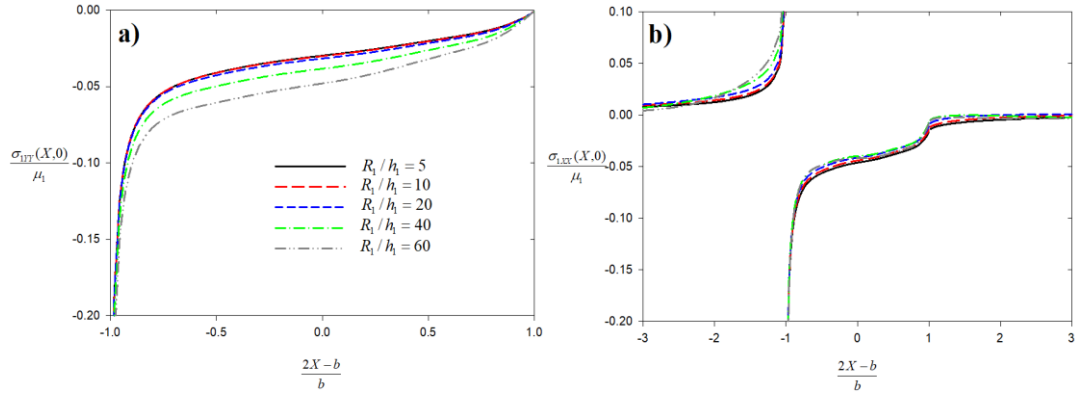


Figure 4.41: Normal and lateral elastodynamic contact stresses on homogenous coating indented by a moving semi-circular punch for various values of relative coating thickness (a) Normal contact stress distribution; (b) Lateral contact stress distribution, $\mu_1 / \mu_2 = 1/10$, $b / R_1 = 0.025$, $c_1 = 0.4$, $\eta = 0.3$, $\rho_1 / \rho_2 = 1/8$, $\nu_1 / \nu_2 = 0.8$.

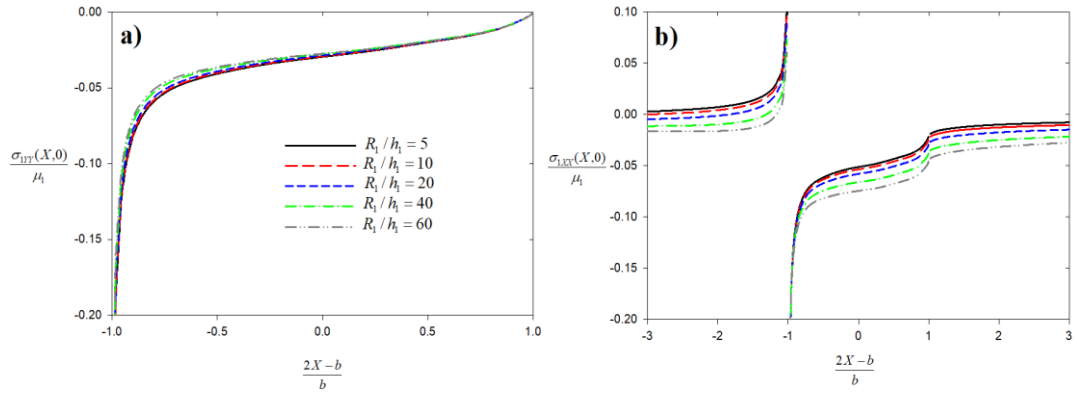


Figure 4.42: Normal and lateral elastodynamic contact stresses on homogenous coating indented by a moving semi-circular punch for various values of relative coating thickness (a) Normal contact stress distribution; (b) Lateral contact stress distribution, $\mu_1 / \mu_2 = 10$, $b / R_1 = 0.025$, $c_1 = 0.4$, $\eta = 0.3$, $\rho_1 / \rho_2 = 1/8$, $\nu_1 / \nu_2 = 0.8$.

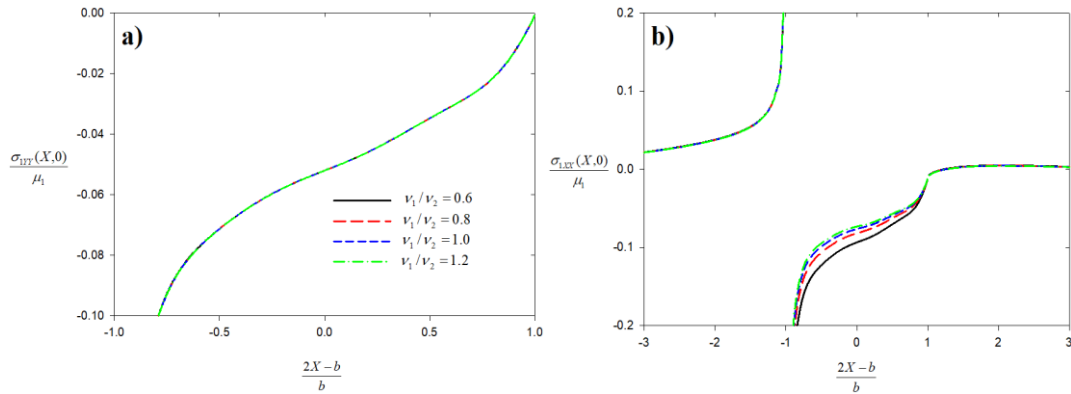


Figure 4.43: Normal and lateral elastodynamic contact stresses on homogeneous coating indented by a moving semi-circular punch for various values of Poisson's ratio (a) Normal contact stress distribution; (b) Lateral contact stress distribution, $\mu_1 / \mu_2 = 1/10$, $b / R_1 = 0.05$, $c_1 = 0.6$, $\eta = 0.3$, $\rho_1 / \rho_2 = 1/8$.

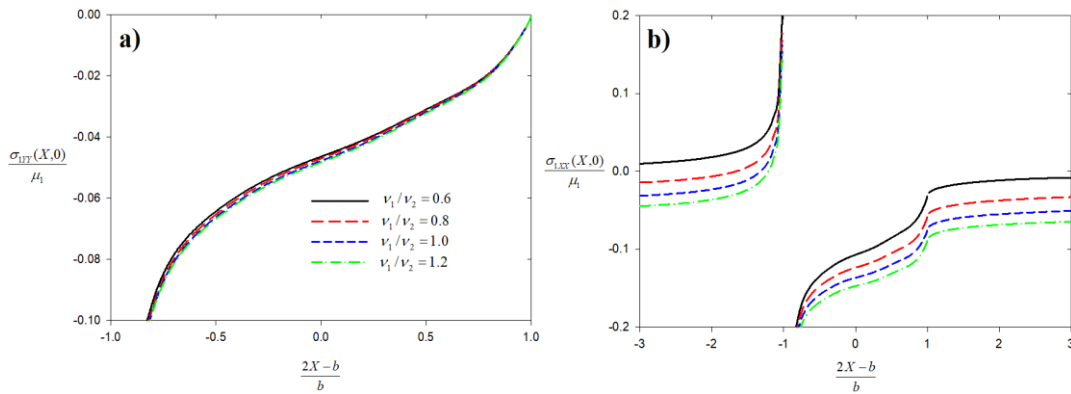


Figure 4.44: Normal and lateral elastodynamic contact stresses on homogeneous coating indented by a moving semi-circular punch for various values of Poisson's ratio (a) Normal contact stress distribution; (b) Lateral contact stress distribution, $\mu_1 / \mu_2 = 10$, $b / R_1 = 0.05$, $c_1 = 0.6$, $\eta = 0.3$, $\rho_1 / \rho_2 = 1/8$.

Table 4.25: The normalized load for homogenous coating indented by a moving semi-circular punch $c_1 = 0$, $R_1/h_1 = 20$, $\eta = 0.0$, $\nu_1/\nu_2 = 0.8$.

	$b/R_1 = 0.01$	$b/R_1 = 0.025$	$b/R_1 = 0.04$	$b/R_1 = 0.05$
μ_1/μ_2	$\frac{P}{\mu_1 R_1}$	$\frac{P}{\mu_1 R_1}$	$\frac{P}{\mu_1 R_1}$	$\frac{P}{\mu_1 R_1}$
1/10	1.576e-4	1.032e-3	2.846e-3	4.726e-3
1/5	1.574e-4	1.024e-3	2.798e-3	4.600e-3
1	1.561e-4	9.757e-4	2.498e-3	3.902e-3
10	1.503e-4	7.908e-4	1.577e-3	2.091e-3

Table 4.26: The normalized load for homogenous coating indented by a moving semi-circular punch $b/R_1 = 0.01$, $R_1/h_1 = 20$, $\eta = 0.3$, $\rho_1/\rho_2 = 1/8$, $\nu_1/\nu_2 = 0.8$.

	$c_1 = 0.0$	$c_1 = 0.4$	$c_1 = 0.6$	$c_1 = 0.7$	$c_1 = 0.8$
μ_1/μ_2	$\frac{P}{\mu_1 R_1}$	$\frac{P}{\mu_1 R_1}$	$\frac{P}{\mu_1 R_1}$	$\frac{P}{\mu_1 R_1}$	$\frac{P}{\mu_1 R_1}$
1/10	1.679e-4	1.494e-4	1.233e-4	1.037e-4	7.696e-5
1/5	1.681e-4	1.496e-4	1.237e-4	1.042e-4	7.811e-5
1	1.691e-4	1.505e-4	1.243e-4	1.044e-4	7.691e-5
10	1.726e-4	1.473e-4	1.218e-4	1.025e-4	7.601e-5

Table 4.27: The normalized load for homogenous coating indented by a moving semi-circular punch $b/R_1 = 0.04$, $R_1/h_1 = 20$, $\eta = 0.3$, $\rho_1/\rho_2 = 1/8$, $\nu_1/\nu_2 = 0.8$.

	$c_1 = 0.0$	$c_1 = 0.4$	$c_1 = 0.6$	$c_1 = 0.7$	$c_1 = 0.8$
μ_1/μ_2	$\frac{P}{\mu_1 R_1}$	$\frac{P}{\mu_1 R_1}$	$\frac{P}{\mu_1 R_1}$	$\frac{P}{\mu_1 R_1}$	$\frac{P}{\mu_1 R_1}$
1/10	2.941e-3	2.678e-3	2.328e-3	2.102e-3	1.942e-3
1/5	2.910e-3	2.639e-3	2.262e-3	1.979e-3	1.425e-3
1	2.705e-3	2.409e-3	1.988e-3	1.671e-3	1.231e-3
10	1.851e-3	2.211e-3	1.922e-3	1.750e-3	1.615e-3

Table 4.28: The normalized load for homogenous coating indented by a moving semi-circular punch $b/R_1 = 0.01$, $R_1/h_1 = 20$, $\mu_1/\mu_2 = 1/5$, $\rho_1/\rho_2 = 1/8$, $\nu_1/\nu_2 = 0.8$.

	$c_1 = 0.0$	$c_1 = 0.4$	$c_1 = 0.6$	$c_1 = 0.7$	$c_1 = 0.8$
η	$\frac{P}{\mu_1 R_1}$	$\frac{P}{\mu_1 R_1}$	$\frac{P}{\mu_1 R_1}$	$\frac{P}{\mu_1 R_1}$	$\frac{P}{\mu_1 R_1}$
0.0	1.574e-4	1.377e-4	1.096e-4	8.820e-5	5.808e-5
0.3	1.681e-4	1.497e-4	1.237e-4	1.042e-4	7.811e-5
0.5	1.748e-4	1.571e-4	1.322e-4	1.135e-4	8.810e-5
0.7	1.812e-4	1.640e-4	1.396e-3	1.210e-4	9.410e-5

Table 4.29: The normalized load for homogenous coating indented by a moving semi-circular punch $b/R_1 = 0.01$, $R_1/h_1 = 20$, $\mu_1/\mu_2 = 5$, $\rho_1/\rho_2 = 1/8$, $\nu_1/\nu_2 = 0.8$.

	$c_1 = 0.0$	$c_1 = 0.4$	$c_1 = 0.6$	$c_1 = 0.7$	$c_1 = 0.8$
η	$\frac{P}{\mu_1 R_1}$	$\frac{P}{\mu_1 R_1}$	$\frac{P}{\mu_1 R_1}$	$\frac{P}{\mu_1 R_1}$	$\frac{P}{\mu_1 R_1}$
0.0	1.526e-4	1.379e-4	1.094e-4	8.830e-5	5.924e-5
0.3	1.712e-4	1.470e-4	1.218e-4	1.026e-4	7.620e-5
0.5	1.847e-4	1.523e-4	1.290e-4	1.103e-4	8.311e-5
0.7	1.991e-4	1.568e-4	1.350e-4	1.161e-4	8.614e-5

Table 4.30: Normalized stress intensity factors for a moving semi-circular punch $c_1 = 0$, $R_1/h_1 = 20$, $\eta = 0.0$, $\nu_1/\nu_2 = 0.8$.

	$b/R_1 = 0.01$	$b/R_1 = 0.025$	$b/R_1 = 0.04$	$b/R_1 = 0.05$
μ_1/μ_2	$K_I(0)$	$K_I(0)$	$K_I(0)$	$K_I(0)$
1/10	0.6641	0.6822	0.7112	0.7355
1/5	0.6637	0.6791	0.7044	0.7244
1	0.6605	0.6605	0.6605	0.6605
10	0.6463	0.5848	0.5054	0.4594

Table 4.31: Normalized stress intensity factors for a moving semi-circular punch $b/R_1 = 0.01$, $R_1/h_1 = 20$, $\eta = 0.3$, $\rho_1/\rho_2 = 1/8$, $\nu_1/\nu_2 = 0.8$.

	$c_1 = 0.0$	$c_1 = 0.4$	$c_1 = 0.6$	$c_1 = 0.7$	$c_1 = 0.8$
μ_1/μ_2	$K_I(0)$	$K_I(0)$	$K_I(0)$	$K_I(0)$	$K_I(0)$
1/10	0.6844	0.6030	0.4867	0.3977	0.2699
1/5	0.6859	0.6053	0.4902	0.4025	0.2801
1	0.6971	0.6158	0.4989	0.4085	0.2763
10	0.7423	0.5974	0.4838	0.3948	0.2673

Table 4.32: Normalized stress intensity factors for a moving semi-circular punch $b/R_1 = 0.04$, $R_1/h_1 = 20$, $\eta = 0.3$, $\rho_1/\rho_2 = 1/8$, $\nu_1/\nu_2 = 0.8$.

	$c_1 = 0.0$	$c_1 = 0.4$	$c_1 = 0.6$	$c_1 = 0.7$	$c_1 = 0.8$
μ_1/μ_2	$K_I(0)$	$K_I(0)$	$K_I(0)$	$K_I(0)$	$K_I(0)$
1/10	0.6974	0.6218	0.5188	0.4447	0.3744
1/5	0.6979	0.6230	0.5194	0.4431	0.3157
1	0.6971	0.6158	0.4989	0.4085	0.2763
10	0.6143	0.5466	0.4567	0.3917	0.3191

Table 4.33: Normalized stress intensity factors for a moving semi-circular punch $b/R_1 = 0.01$, $R_1/h_1 = 20$, $\mu_1/\mu_2 = 1/5$, $\rho_1/\rho_2 = 1/8$, $\nu_1/\nu_2 = 0.8$.

	$c_1 = 0.0$	$c_1 = 0.4$	$c_1 = 0.6$	$c_1 = 0.7$	$c_1 = 0.8$
η	$K_I(0)$	$K_I(0)$	$K_I(0)$	$K_I(0)$	$K_I(0)$
0.0	0.6637	0.5804	0.4613	0.3709	0.2448
0.3	0.6859	0.6053	0.4902	0.4025	0.2801
0.5	0.6952	0.6143	0.4970	0.4047	0.2697
0.7	0.6998	0.6171	0.4941	0.3937	0.2441

Table 4.34: Normalized stress intensity factors for a moving semi-circular punch
 $b/R_1 = 0.01$, $R_1/h_1 = 20$, $\mu_1/\mu_2 = 5$, $\rho_1/\rho_2 = 1/8$, $\nu_1/\nu_2 = 0.8$.

	$c_1 = 0.0$	$c_1 = 0.4$	$c_1 = 0.6$	$c_1 = 0.7$	$c_1 = 0.8$
η	$K_I(0)$	$K_I(0)$	$K_I(0)$	$K_I(0)$	$K_I(0)$
0.0	0.6519	0.5806	0.4609	0.3712	0.2476
0.3	0.7242	0.5892	0.4806	0.3933	0.2672
0.5	0.7713	0.5872	0.4813	0.3893	0.2478
0.7	0.8169	0.5795	0.4728	0.3734	0.2173

Table 4.35: Percent difference between elastostatic and elastodynamic normal contact stresses $\mu_1/\mu_2 = 1/10$, $b/R_1 = 0.01$, $R_1/h_1 = 20$, $\eta = 0.3$, $\rho_1/\rho_2 = 1/8$, $\nu_1/\nu_2 = 0.8$.

	$c_1 = 0.0$		$c_1 = 0.4$		$c_1 = 0.6$		$c_1 = 0.8$	
$\frac{2X-b}{b}$	$\frac{\sigma_{1YY}(X,0)}{\mu_1}$	$\frac{\sigma_{1YY}(X,0)}{\mu_1}$	$\varepsilon\%$	$\frac{\sigma_{1YY}(X,0)}{\mu_1}$	$\varepsilon\%$	$\frac{\sigma_{1YY}(X,0)}{\mu_1}$	$\varepsilon\%$	
-0.96	-0.05548	-0.05040	9.15	-0.04344	21.69	-0.03200	42.32	
-0.82	-0.02790	-0.02502	10.33	-0.02097	24.86	-0.01363	51.15	
-0.73	-0.02316	-0.02067	10.72	-0.01716	25.89	-0.01071	53.73	
-0.61	-0.02029	-0.01806	11.02	-0.01488	26.67	-0.00902	55.57	
-0.48	-0.01823	-0.01616	11.34	-0.01322	27.50	-0.00776	57.45	
-0.20	-0.01506	-0.01326	11.93	-0.01069	29.03	-0.00587	61.03	
-0.04	-0.01387	-0.01218	12.15	-0.00977	29.57	-0.00525	62.12	
0.20	-0.01217	-0.01065	12.46	-0.00847	30.37	-0.00441	63.76	
0.48	-0.00948	-0.00824	13.08	-0.00645	31.94	-0.00311	67.22	
0.61	-0.00821	-0.00711	13.32	-0.00554	32.51	-0.00261	68.23	
0.73	-0.00694	-0.00601	13.53	-0.00465	33.02	-0.00215	69.06	
0.82	-0.00547	-0.00471	13.99	-0.00360	34.17	-0.00156	71.52	
0.96	-0.00210	-0.00175	16.79	-0.00123	41.21	-0.00028	86.72	

Table 4.36: Percent difference between elastostatic and elastodynamic lateral contact stresses $\mu_1 / \mu_2 = 1/10$, $b/R_1 = 0.01$, $R_1/h_1 = 20$, $\eta = 0.3$, $\rho_1 / \rho_2 = 1/8$, $\nu_1 / \nu_2 = 0.8$.

$2X - b$ b	$c_1 = 0.0$		$c_1 = 0.4$		$c_1 = 0.6$		$c_1 = 0.8$	
	$\sigma_{1xx}(X,0)$	$\sigma_{1xx}(X,0)$	$\varepsilon\%$	$\sigma_{1xx}(X,0)$	$\varepsilon\%$	$\sigma_{1xx}(X,0)$	$\varepsilon\%$	
	μ_1	μ_1		μ_1		μ_1		
-1.58	0.00751	0.00752	0.13	0.00770	2.55	0.00935	24.52	
-1.22	0.01289	0.01277	0.91	0.01283	0.42	0.01492	15.78	
-0.99	-0.13325	-0.14412	8.16	-0.16938	27.12	-0.30419	128.29	
-0.82	-0.03069	-0.03215	4.75	-0.03538	15.30	-0.04907	59.90	
-0.48	-0.02117	-0.02170	2.53	-0.02291	8.25	-0.02738	29.36	
-0.20	-0.01878	-0.01898	1.03	-0.01947	3.64	-0.02088	11.18	
-0.04	-0.01802	-0.01809	0.37	-0.01833	1.69	-0.01883	4.51	
0.20	-0.01710	-0.01700	0.60	-0.01690	1.15	-0.01629	4.72	
0.48	-0.01528	-0.01494	2.21	-0.01438	5.88	-0.01213	20.58	
0.82	-0.01223	-0.01164	4.80	-0.01062	13.16	-0.00720	41.13	
0.99	-0.00729	-0.00654	10.28	-0.00522	28.38	-0.00123	83.11	
1.22	-0.00365	-0.00315	13.52	-0.00229	37.31	0.00027	107.29	
1.58	-0.00240	-0.00198	17.37	-0.00124	48.44	0.00101	142.11	

Table 4.37: Percent difference between elastostatic and elastodynamic normal contact stresses $\mu_1 / \mu_2 = 10$, $b/R_1 = 0.01$, $R_1/h_1 = 20$, $\eta = 0.3$, $\rho_1 / \rho_2 = 1/8$, $\nu_1 / \nu_2 = 0.8$.

$2X - b$ b	$c_1 = 0.0$		$c_1 = 0.4$		$c_1 = 0.6$		$c_1 = 0.8$	
	$\sigma_{1yy}(X,0)$	$\sigma_{1yy}(X,0)$	$\varepsilon\%$	$\sigma_{1yy}(X,0)$	$\varepsilon\%$	$\sigma_{1yy}(X,0)$	$\varepsilon\%$	
	μ_1	μ_1		μ_1		μ_1		
-0.96	-0.05986	-0.04984	16.74	-0.04304	28.11	-0.03139	47.56	
-0.82	-0.02959	-0.02472	16.46	-0.02074	29.89	-0.01340	54.72	
-0.73	-0.02428	-0.02040	15.97	-0.01696	30.15	-0.01054	56.59	
-0.61	-0.02104	-0.01780	15.39	-0.01469	30.18	-0.00888	57.81	
-0.48	-0.01867	-0.01593	14.67	-0.01305	30.09	-0.00766	58.99	
-0.20	-0.01513	-0.01305	13.76	-0.01053	30.41	-0.00579	61.77	
-0.04	-0.01383	-0.01198	13.36	-0.00962	30.46	-0.00518	62.57	
0.20	-0.01201	-0.01046	12.92	-0.00833	30.66	-0.00434	63.87	
0.48	-0.00927	-0.00809	12.67	-0.00634	31.57	-0.00306	66.97	
0.61	-0.00799	-0.00698	12.62	-0.00544	31.93	-0.00257	67.88	
0.73	-0.00675	-0.00589	12.66	-0.00457	32.31	-0.00211	68.65	
0.82	-0.00530	-0.00462	12.88	-0.00354	33.29	-0.00154	71.05	
0.96	-0.00201	-0.00172	14.28	-0.00122	39.40	-0.00028	86.08	

Table 4.38: Percent difference between elastostatic and elastodynamic lateral contact stresses $\mu_1 / \mu_2 = 10, b / R_1 = 0.01, R_1 / h_1 = 20, \eta = 0.3, \rho_1 / \rho_2 = 1/8, \nu_1 / \nu_2 = 0.8.$

$\frac{2X-b}{b}$	$c_1 = 0.0$		$c_1 = 0.4$		$c_1 = 0.6$		$c_1 = 0.8$	
	$\sigma_{1xx}(X,0)$		$\sigma_{1xx}(X,0)$		$\sigma_{1xx}(X,0)$		$\sigma_{1xx}(X,0)$	
	μ_1	μ_1	$\varepsilon\%$	μ_1	$\varepsilon\%$	μ_1	$\varepsilon\%$	
-1.58	0.00221	0.00414	87.85	0.00371	68.13	0.00603	173.34	
-1.22	0.00783	0.00929	18.66	0.00875	11.70	0.01149	46.68	
-0.99	-0.15086	-0.14617	3.11	-0.17239	14.27	-0.30455	101.87	
-0.82	-0.03892	-0.03518	9.62	-0.03914	0.54	-0.05186	33.24	
-0.48	-0.02799	-0.02480	11.40	-0.02669	4.64	-0.03036	8.47	
-0.20	-0.02512	-0.02209	12.06	-0.02326	7.42	-0.02394	4.71	
-0.04	-0.02418	-0.02121	12.30	-0.02212	8.54	-0.02190	9.42	
0.20	-0.02306	-0.02012	12.76	-0.02070	10.26	-0.01939	15.94	
0.48	-0.02107	-0.01809	14.13	-0.01820	13.61	-0.01528	27.46	
0.82	-0.01794	-0.01483	17.30	-0.01448	19.26	-0.01040	42.00	
0.99	-0.01308	-0.00985	24.74	-0.00919	29.72	-0.00454	65.32	
1.22	-0.00953	-0.00650	31.82	-0.00628	34.05	-0.00303	68.22	
1.58	-0.00827	-0.00533	35.48	-0.00523	36.71	-0.00226	72.64	

4.5 Numerical Results for the Rigid Cylindrical Punch

General schematic for the contact problem between a rigid cylindrical punch and a homogenous elastic coating is depicted in Figure 4.45. Homogenous elastic coating of thickness h_1 is perfectly bonded to a homogenous substrate, and the rigid cylindrical punch slides over the coating at a speed of V .

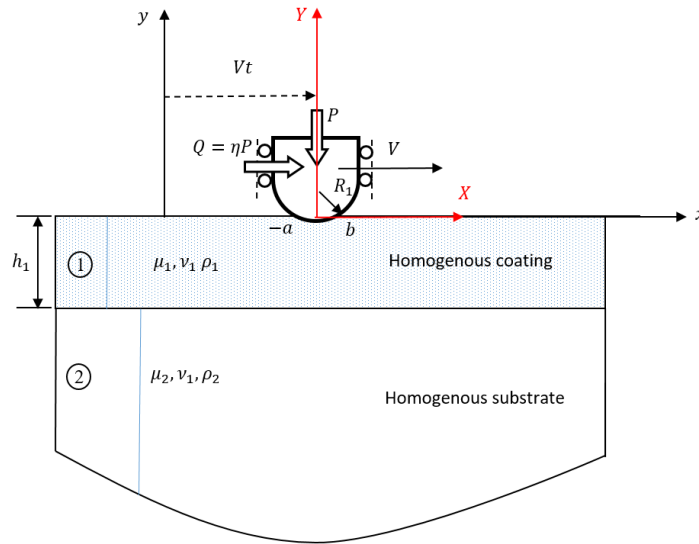


Figure 4.45: General schematic for the contact between a homogenous elastic coating and a rigid cylindrical punch

Figures 4.46 and 4.47 depict the influence of mass density ratio on contact stress distributions for the less stiff and stiffer coatings, respectively. It is interesting to note that the mass density ratio ρ_1/ρ_2 has almost no effect on contact stresses for the less stiff coating (see Figure 4.46). However, the mass density ratio significantly affect the contact stress distributions for the stiffer coating as can be seen from Figure 4.47.

Figure 4.48 shows the influence of dimensionless punch speed c_1 on elastodynamic contact stress distributions in frictionless contacts for the less stiff coating ($\mu_1/\mu_2 = 1/10$). As punch speed is increased from 0.0 to 0.7, the normal contact

stress becomes less compressive in the contact zone and the magnitude of tensile lateral contact stress increases at the ends of the cylindrical punch. Normal and lateral elastodynamic contact stresses are generated for the frictionless contacts of the half-plane ($\mu_1/\mu_2 = 1$). Again, normal contact stress becomes less compressive in the contact zone as shown in Figure 4.49(a). When lateral contact stress is examined, surface outside the contact zone is stress free although dimensionless punch speed is increased. However, lateral contact stress becomes more compressive in the contact zone. The influence of punch speed on elastodynamic contact stresses for the stiffer coating ($\mu_1/\mu_2 = 10$) is shown in Figure 4.50. Normal contact stress increases suddenly and then decrease gradually in the contact zone. The magnitude of the lateral contact stress also increases in the contact zone. The slope of the lateral contact stress outside the contact zone decreases and lateral contact stress tends to become compressive there. Figure 4.51 shows the elastodynamic contact stresses in frictional case for the less stiff coating ($\mu_1/\mu_2 = 1/10$). Normal and lateral contact stresses become less compressive in the contact zone. Due to the friction, tensile lateral contact stresses are generated around the trailing end of the contact zone. The magnitude of tensile stresses slightly increases at higher punch speeds. Moreover, the lateral contact stresses become slightly tensile around the leading end. Figure 4.52 shows elastodynamic contact stress distributions on a half-plane in a frictional case. As punch speed is increased, normal contact stresses become less compressive in the contact zone, and normal contact stress distribution is not symmetric due to the friction. The variation of the lateral contact stress with respect to punch speed is observed in Figure 4.52(b). Elastodynamic contact stresses for the stiffer coating ($\mu_1/\mu_2 = 10$) in frictional case is depicted in Figure 4.53. As dimensionless punch speed is increased, firstly the normal contact stress increases suddenly and then decreases in the contact zone. The lateral contact stress in the contact zone increases

at higher punch speeds. The magnitude of tensile lateral contact stresses at the trailing end increases at higher punch speeds.

The influence of coefficient of friction η on elastodynamic contact stresses is examined in Figure 4.54 – 4.55. Variations of normal contact stresses with respect to η are more pronounced for a stiffer coating ($\mu_1/\mu_2 = 5$). This conclusion can be drawn by examining Figures 4.54(a) and 4.55(a). In all cases, larger coefficient of friction leads to a larger tensile peak at the trailing end of the contact zone. Thus, in elastodynamic contacts with friction, trailing end of the contact zone is a possible site for cracking type failure. Adjustment of the coefficient of friction η and modulus ratio μ_1/μ_2 could be possible ways of avoiding such fracture related failures.

Figures 4.56 – 4.57 show the elastodynamic contact stresses as functions of the ratio R_1/h_1 . As the ratio R_1/h_1 is increased from 20 to 150, the magnitude of normal contact stress increases in the contact zone for both less stiff and stiffer coatings. However, the variations on the lateral contact stresses with respect to various R_1/h_1 ratio are quite different for less stiff and stiffer coatings. Lateral contact stresses become slightly less compressive around the trailing end and ahead of the contact zone for a less stiff coating however, lateral stresses become more compressive throughout the contact for a stiffer coating.

In Figures 4.58 – 4.59, we present elastodynamic contact stresses as functions of ν_1/ν_2 . ν_1 and ν_2 being Poisson's ratios of the coating and the substrate, respectively. It can be inferred from Figure 4.58(a) that the impact of ν_1/ν_2 on normal contact stress is minimal for a less stiff coating ($\mu_1/\mu_2 = 1/10$). For a stiffer coating ($\mu_1/\mu_2 = 10$) however, the effect of the ratio ν_1/ν_2 on normal contact stress can be seen from Figure 4.59(a). When lateral contact stress distributions are examined, the

influence of the ratio ν_1/ν_2 on contact stresses generated for the less stiff and stiffer coatings is quite different. For a less stiff coating, as ν_1/ν_2 is increased from 0.6 to 1.2, lateral contact stress tends to become less compressive in the contact zone and there is no considerable change outside the contact zone. Nevertheless, lateral contact stresses are compressive throughout the contact for a stiffer coating (see Figure 4.59(b)).

Table 4.39 shows the normalized load applied by the cylindrical punch for various values of the modulus ratio μ_1/μ_2 and relative contact length $(b+a)/R_1$ in elastostatic case. The normalized punch load is always greater for the less stiff coatings. In all cases, as relative contact length $(b+a)/R_1$ is increased, the values of the normalized punch load increase. Tables 4.40 - 4.41 tabulate normalized punch loads for two different relative contact length specified by $(b+a)/R_1 = 0.01$ and $(b+a)/R_1 = 0.05$. For less stiff coatings $\mu_1/\mu_2 < 1$ and half-planes $\mu_1/\mu_2 = 1$, the normalized punch load decreases as punch speed c_1 is increased. For stiffer coatings $\mu_1/\mu_2 = 10$ however, the trend of change is different. The normalized punch load increases first ($c_1 = 0.4$), and then gradually decreases for higher punch speeds.

Table 4.42 shows the normalized punch load generated on a less stiff coating for different values of coefficient of friction η and dimensionless punch speed c_1 . In all cases, normalized punch load gradually decreases as dimensionless punch speed is increased. Table 4.43 tabulates the normalized punch load generated on a stiffer coating for different values of coefficient of friction and dimensionless punch speed. The trend of the change in the normalized punch load is different from that observed in a less stiff coating. The normalized punch load increases first ($c_1 = 0.4$) and then gradually decreases with respect to the increasing punch speed.

Tables 4.44 and 4.45 show elastostatic and elastodynamic normal and lateral contact stresses for a less stiff coating ($\mu_1/\mu_2 = 1/10$). The percent difference between elastodynamic and elastostatic results are calculated at several contact points and it is denoted by $\varepsilon\%$. As dimensionless punch speed is increased, the difference between elastodynamic and elastostatic normal contact stresses increases and larger values of percent difference are observed towards the leading end of the contact zone. The values of percent difference reaches up to 50.42% (see Table 4.44). Percent differences between elastodynamic and elastostatic lateral contact stresses are provided in Table 4.45. Percent differences gradually increase as punch speed is increased. Higher values of the percent difference are observed ahead of the leading end of the contact zone.

Table 4.46 and 4.47 depict elastostatic and elastodynamic normal and lateral contact stresses for a stiffer coating ($\mu_1/\mu_2 = 10$). The general trend of change with respect to punch speed is different from that observed for a less stiff coating. For the stiffer coating, as punch speed is increased from 0.0 to 0.4, a sudden increase in normal contact stress occurs in the contact zone and normal stress gradually decreases as punch speed is increased from 0.4 to 0.8. Normal contact stress again starts to come close to the elastostatic normal stress curve at higher punch speeds. This behavior can be inferred from Figure 4.46 and 4.49. Therefore, percent difference between elastodynamic and elastostatic normal contact stress has larger values at punch speed $c_1 = 0.4$. As punch speed is increased from 0.4 to 0.7, percent difference value becomes smaller. Table 4.47 depicts elastostatic and elastodynamic lateral contact stresses for a stiffer coating ($\mu_1/\mu_2 = 10$), at some of the contacting points the percent difference increases whereas at some of them it decreases. Thus, in this case, general conclusion regarding dependence of percent difference $\varepsilon\%$ on c_1 can not be made.

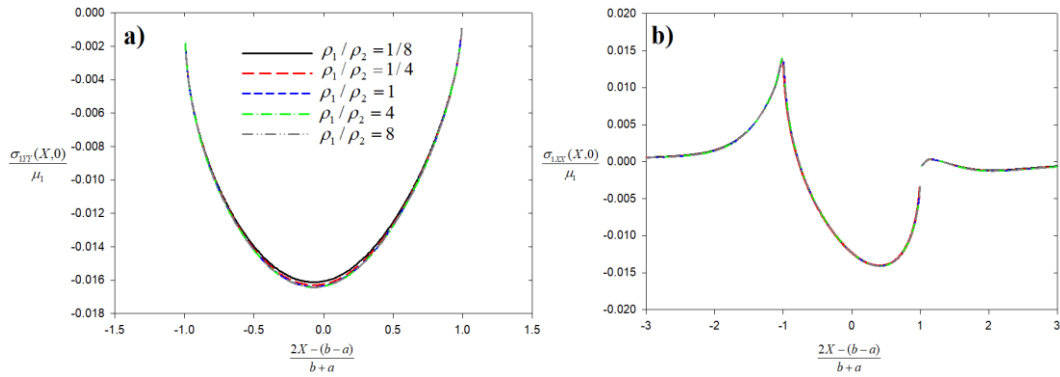


Figure 4.46: Normal and lateral elastodynamic contact stresses on homogeneous coating indented by a moving cylindrical punch for various mass density ratios (a) Normal contact stress distribution; (b) Lateral contact stress distribution, $\mu_1/\mu_2 = 1/10$, $(b+a)/R_1 = 0.02$, $R_1/h_1 = 100$, $c_1 = 0.6$, $\eta = 0.3$, $\nu_1/\nu_2 = 0.8$.

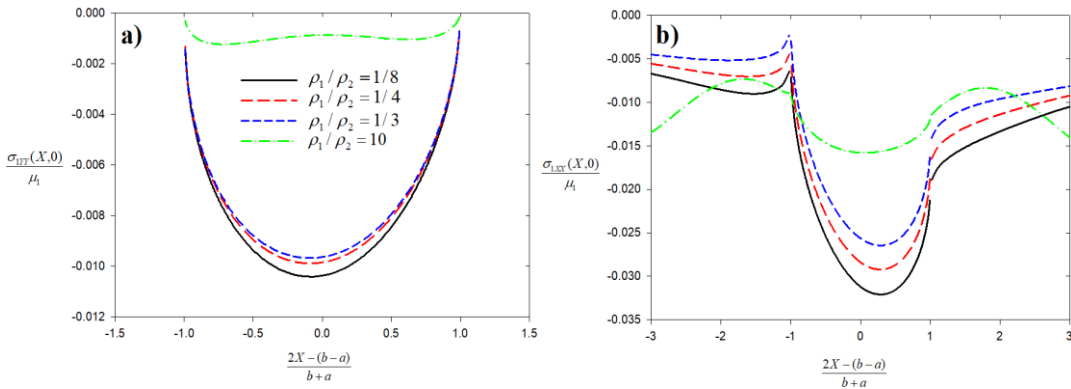


Figure 4.47: Normal and lateral elastodynamic contact stresses on homogeneous coating indented by a moving cylindrical punch for various mass density ratios (a) Normal contact stress distribution; (b) Lateral contact stress distribution, $\mu_1/\mu_2 = 1/10$, $(b+a)/R_1 = 0.02$, $R_1/h_1 = 100$, $c_1 = 0.6$, $\eta = 0.3$, $\nu_1/\nu_2 = 0.8$.

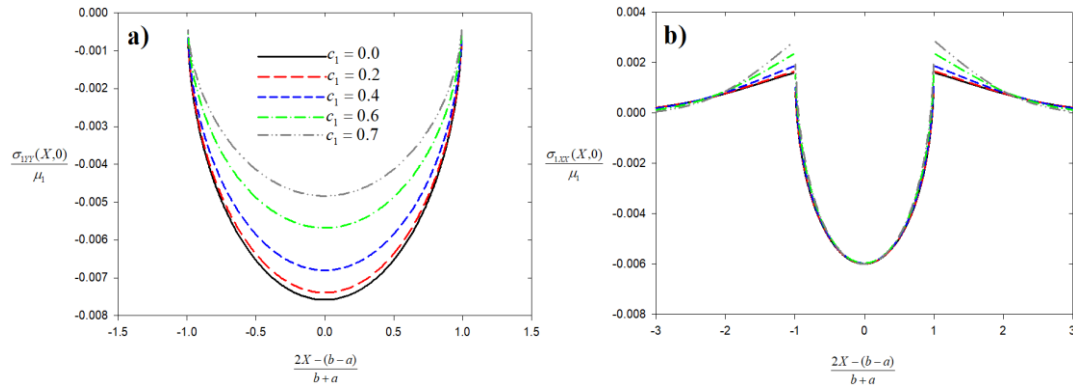


Figure 4.48: Normal and lateral elastodynamic contact stresses on homogeneous coating indented by a moving cylindrical punch for various values of punch speed (a) Normal contact stress distribution; (b) Lateral contact stress distribution, $\mu_1 / \mu_2 = 1/10$, $(b+a)/R_1 = 0.01$, $R_1/h_1 = 100$, $\eta = 0.0$, $\rho_1/\rho_2 = 1/8$, $v_1/v_2 = 0.8$.

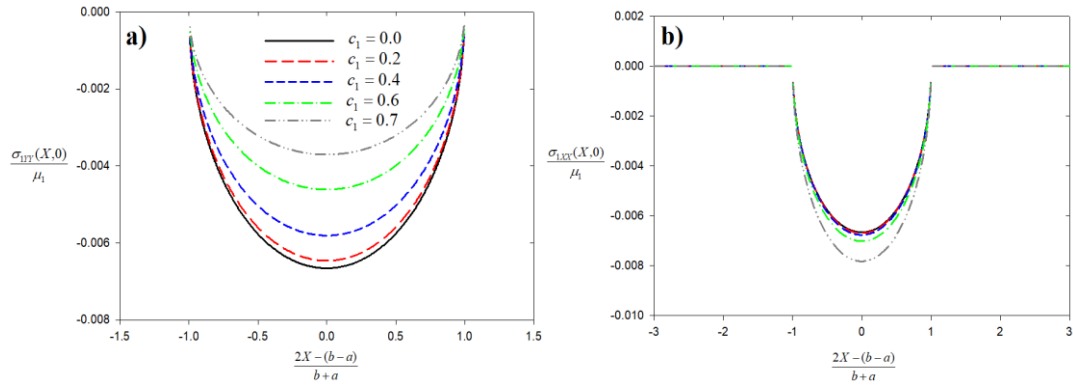


Figure 4.49: Normal and lateral elastodynamic contact stresses on homogeneous coating indented by a moving cylindrical punch for various values of punch speed (a) Normal contact stress distribution; (b) Lateral contact stress distribution, $\mu_1 / \mu_2 = 1$, $(b+a)/R_1 = 0.01$, $R_1/h_1 = 100$, $\eta = 0.0$, $\rho_1/\rho_2 = 1/8$, $v_1/v_2 = 1.0$.

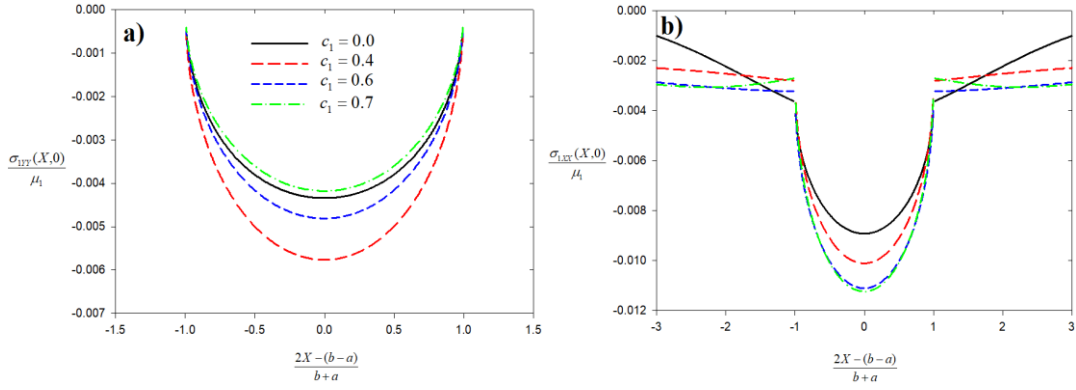


Figure 4.50: Normal and lateral elastodynamic contact stresses on homogeneous coating indented by a moving cylindrical punch for various values of punch speed (a) Normal contact stress distribution; (b) Lateral contact stress distribution, $\mu_1 / \mu_2 = 10$, $(b+a) / R_1 = 0.01$, $R_1 / h_1 = 100$, $\eta = 0.0$, $\rho_1 / \rho_2 = 1/8$, $v_1 / v_2 = 0.8$.

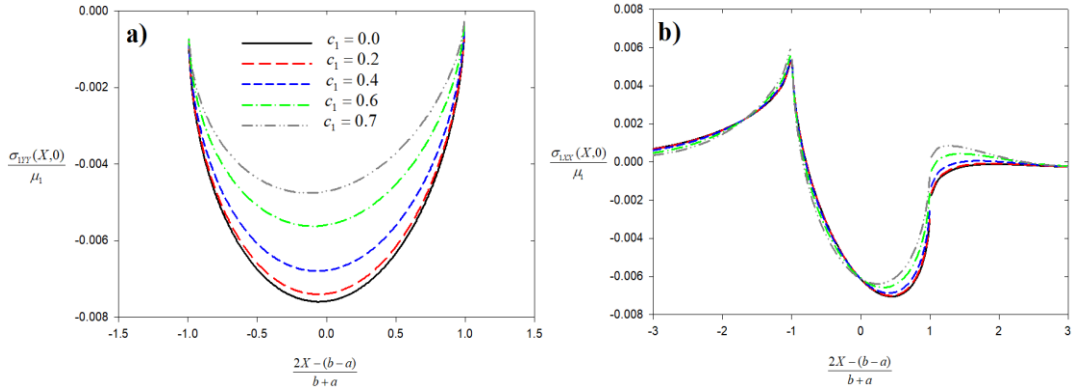


Figure 4.51: Normal and lateral elastodynamic contact stresses on homogeneous coating indented by a moving cylindrical punch for various values of punch speed (a) Normal contact stress distribution; (b) Lateral contact stress distribution, $\mu_1 / \mu_2 = 1/10$, $(b+a) / R_1 = 0.01$, $R_1 / h_1 = 100$, $\eta = 0.3$, $\rho_1 / \rho_2 = 1/8$, $v_1 / v_2 = 0.8$.

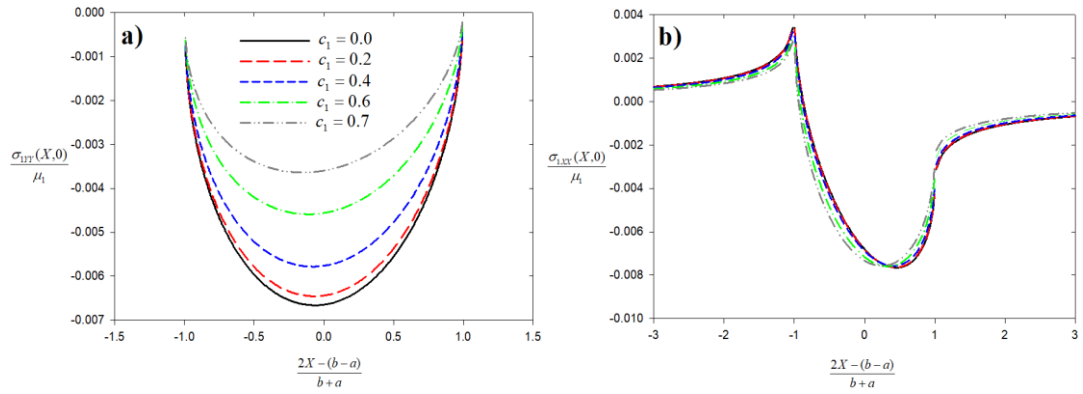


Figure 4.52: Normal and lateral elastodynamic contact stresses on homogenous coating indented by a moving cylindrical punch for various values of punch speed (a) Normal contact stress distribution; (b) Lateral contact stress distribution, $\mu_1/\mu_2=1$, $(b+a)/R_1=0.01$, $R_1/h_1=100$, $\eta=0.3$, $\rho_1/\rho_2=1/8$, $v_1/v_2=1.0$.

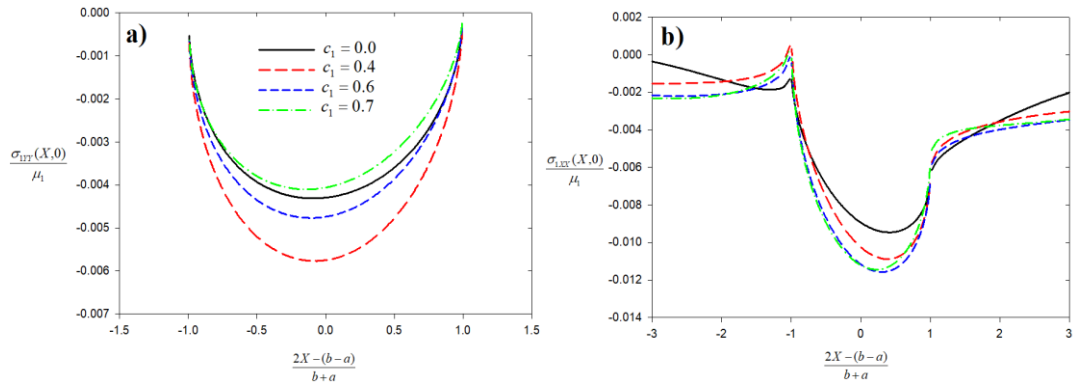


Figure 4.53: Normal and lateral elastodynamic contact stresses on homogenous coating indented by a moving cylindrical punch for various values of punch speed (a) Normal contact stress distribution; (b) Lateral contact stress distribution, $\mu_1/\mu_2=10$, $(b+a)/R_1=0.01$, $R_1/h_1=100$, $\eta=0.3$, $\rho_1/\rho_2=1/8$, $v_1/v_2=0.8$.

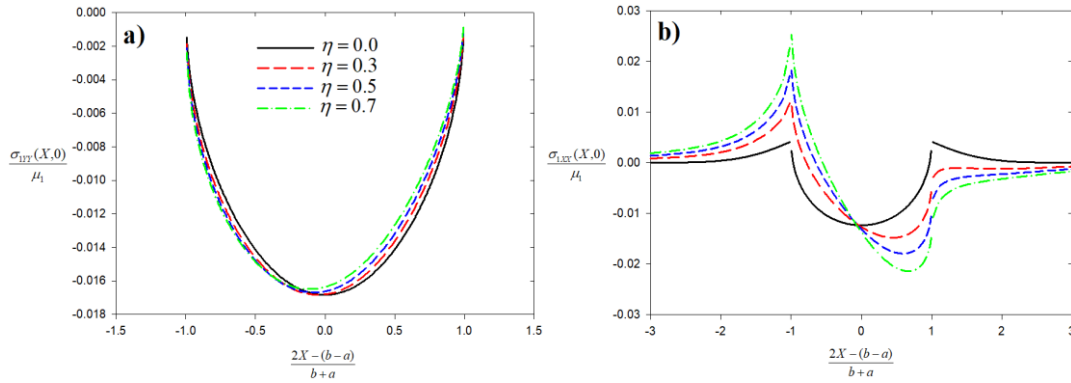


Figure 4.54: Normal and lateral elastodynamic contact stresses on homogenous coating indented by a moving cylindrical punch for various values of coefficient of friction (a) Normal contact stress distribution; (b) Lateral contact stress distribution, $\mu_1 / \mu_2 = 1/5$, $(b + a) / R_1 = 0.02$, $R_1 / h_1 = 100$, $c_1 = 0.4$, $\rho_1 / \rho_2 = 1/8$, $\nu_1 / \nu_2 = 0.8$.

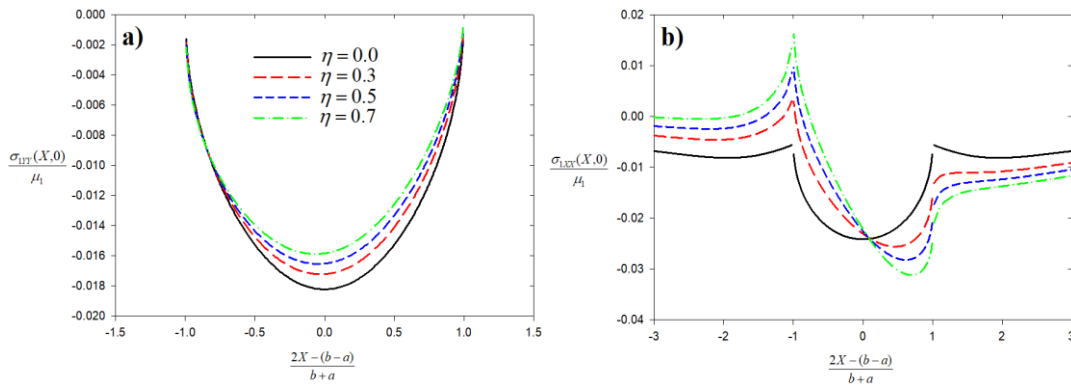


Figure 4.55: Normal and lateral elastodynamic contact stresses on homogenous coating indented by a moving cylindrical punch for various values of coefficient of friction (a) Normal contact stress distribution; (b) Lateral contact stress distribution, $\mu_1 / \mu_2 = 5$, $(b + a) / R_1 = 0.02$, $R_1 / h_1 = 100$, $c_1 = 0.4$, $\rho_1 / \rho_2 = 1/8$, $\nu_1 / \nu_2 = 0.8$.

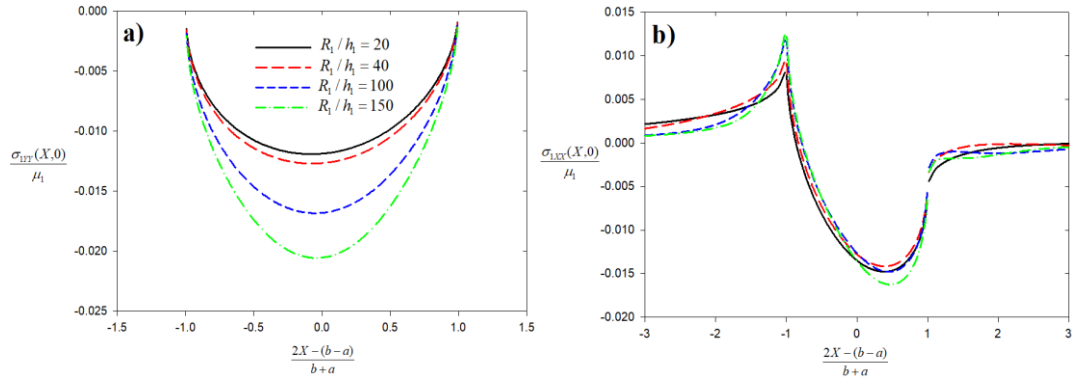


Figure 4.56: Normal and lateral elastodynamic contact stresses on homogeneous coating indented by a moving cylindrical punch for various values of relative coating thickness (a) Normal contact stress distribution; (b) Lateral contact stress distribution, $\mu_1 / \mu_2 = 1/5$, $(b + a) / R_1 = 0.02$, $c_1 = 0.4$, $\eta = 0.3$, $\rho_1 / \rho_2 = 1/8$, $\nu_1 / \nu_2 = 0.8$.

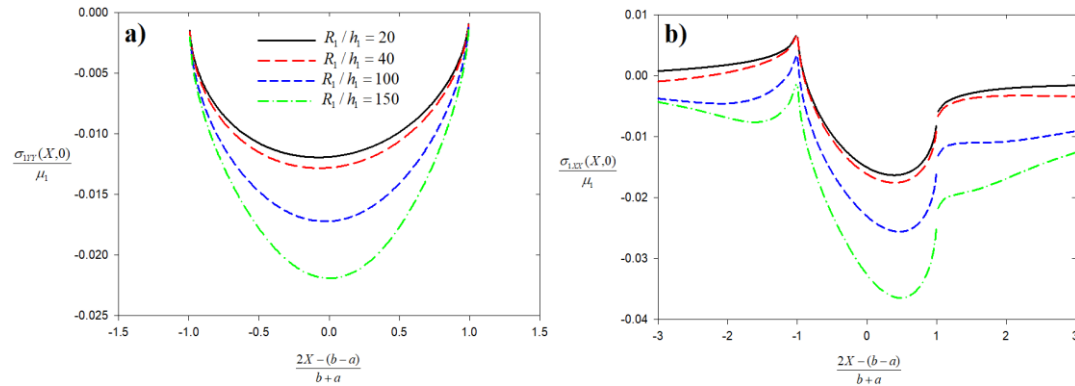


Figure 4.57: Normal and lateral elastodynamic contact stresses on homogeneous coating indented by a moving cylindrical punch for various values of relative coating thickness (a) Normal contact stress distribution; (b) Lateral contact stress distribution, $\mu_1 / \mu_2 = 5$, $(b + a) / R_1 = 0.02$, $c_1 = 0.4$, $\eta = 0.3$, $\rho_1 / \rho_2 = 1/8$, $\nu_1 / \nu_2 = 0.8$.

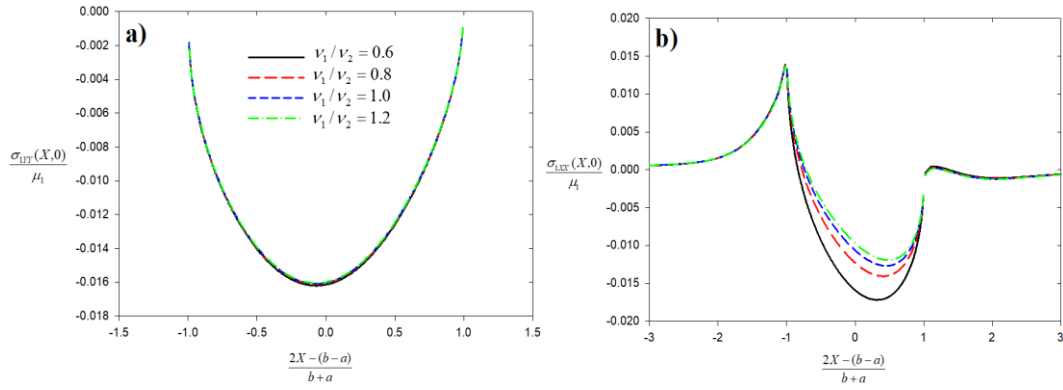


Figure 4.58: Normal and lateral elastodynamic contact stresses on homogeneous coating indented by a moving cylindrical punch for various values of Poisson's ratio (a) Normal contact stress distribution; (b) Lateral contact stress distribution, $\mu_1 / \mu_2 = 1/10$, $(b + a) / R_1 = 0.02$, $R_1 / h_1 = 100$, $c_1 = 0.6$, $\eta = 0.3$, $\rho_1 / \rho_2 = 1/8$.

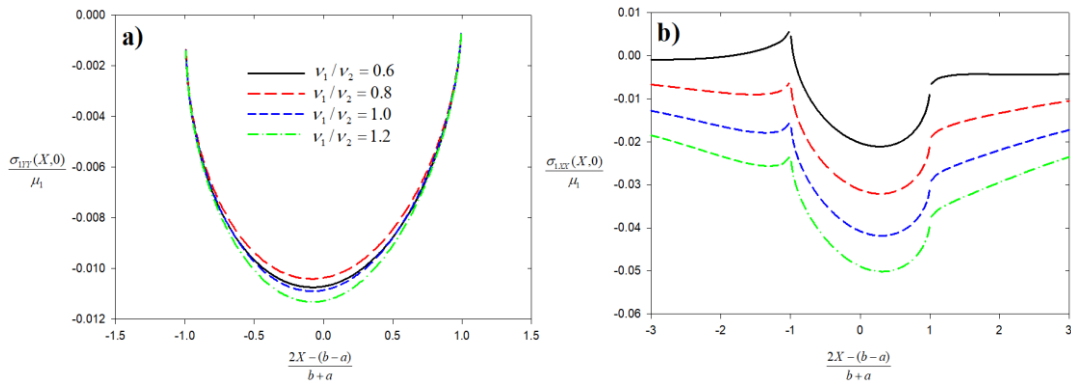


Figure 4.59: Normal and lateral elastodynamic contact stresses on homogeneous coating indented by a moving cylindrical punch for various values of Poisson's ratio (a) Normal contact stress distribution; (b) Lateral contact stress distribution, $\mu_1 / \mu_2 = 10$, $(b + a) / R_1 = 0.02$, $R_1 / h_1 = 100$, $c_1 = 0.6$, $\eta = 0.3$, $\rho_1 / \rho_2 = 1/8$.

Table 4.39: The normalized load for homogenous coating indented by a moving cylindrical punch $c_1 = 0$, $R_1/h_1 = 100$, $\eta = 0.0$, $\nu_1/\nu_2 = 1.0$.

	$\frac{(b+a)}{R_1} = 0.01$	$\frac{(b+a)}{R_1} = 0.02$	$\frac{(b+a)}{R_1} = 0.03$	$\frac{(b+a)}{R_1} = 0.05$
μ_1/μ_2	$\frac{P}{\mu_1 R_1}$	$\frac{P}{\mu_1 R_1}$	$\frac{P}{\mu_1 R_1}$	$\frac{P}{\mu_1 R_1}$
1/10	5.9e-5	2.9e-4	8.3e-4	3.1e-3
1/5	5.8e-5	2.8e-4	7.6e-4	2.7e-3
1	5.2e-5	2.1e-4	4.7e-4	1.3e-3
10	3.3e-5	8.1e-5	1.3e-4	2.7e-4

Table 4.40: The normalized load for homogenous coating indented by a moving cylindrical punch $(b+a)/R_1 = 0.01$, $R_1/h_1 = 100$, $\eta = 0.3$, $\rho_1/\rho_2 = 1/8$, $\nu_1/\nu_2 = 0.8$.

	$c_1 = 0.0$	$c_1 = 0.4$	$c_1 = 0.6$	$c_1 = 0.7$	$c_1 = 0.8$
μ_1/μ_2	$\frac{P}{\mu_1 R_1}$	$\frac{P}{\mu_1 R_1}$	$\frac{P}{\mu_1 R_1}$	$\frac{P}{\mu_1 R_1}$	$\frac{P}{\mu_1 R_1}$
1/10	5.9e-5	5.3e-5	4.4e-5	3.7e-5	2.6e-5
1/5	5.8e-5	5.2e-5	4.2e-5	3.4e-5	1.9e-5
1	5.2e-5	4.5e-5	3.6e-5	2.8e-5	1.8e-5
10	3.5e-5	4.5e-5	3.7e-5	3.2e-5	2.3e-5

Table 4.41: The normalized load for homogenous coating indented by a moving cylindrical punch $(b+a)/R_1 = 0.05$, $R_1/h_1 = 100$, $\eta = 0.3$, $\rho_1/\rho_2 = 1/8$, $\nu_1/\nu_2 = 0.8$.

	$c_1 = 0.0$	$c_1 = 0.4$	$c_1 = 0.6$	$c_1 = 0.7$	$c_1 = 0.8$
μ_1/μ_2	$\frac{P}{\mu_1 R_1}$	$\frac{P}{\mu_1 R_1}$	$\frac{P}{\mu_1 R_1}$	$\frac{P}{\mu_1 R_1}$	$\frac{P}{\mu_1 R_1}$
1/10	3.122e-3	2.950e-3	2.680e-3	2.4e-3	1.494e-3
1/5	2.683e-3	2.398e-3	1.898e-3	1.4e-3	4.660e-4
1	1.307e-3	1.134e-3	8.980e-4	7.1e-4	4.520e-4
10	2.750e-4	1.218e-3	1.216e-3	1.3e-3	1.151e-3

Table 4.42: The normalized load for homogenous coating indented by a moving cylindrical punch $(b + a)/R_1 = 0.01$, $R_1/h_1 = 100$, $\mu_1/\mu_2 = 1/5$, $\rho_1/\rho_2 = 1/8$, $\nu_1/\nu_2 = 0.8$.

	$c_1 = 0.0$	$c_1 = 0.4$	$c_1 = 0.6$	$c_1 = 0.7$	$c_1 = 0.8$
η	$\frac{P}{\mu_1 R_1}$	$\frac{P}{\mu_1 R_1}$	$\frac{P}{\mu_1 R_1}$	$\frac{P}{\mu_1 R_1}$	$\frac{P}{\mu_1 R_1}$
0.0	5.828e-5	5.188e-5	4.224e-5	3.452e-5	2.078e-5
0.3	5.834e-5	5.172e-5	4.171e-5	3.382e-5	1.939e-5
0.5	5.796e-5	5.116e-5	4.095e-5	3.238e-5	1.747e-5
0.7	5.736e-5	5.013e-5	3.956e-5	2.225e-4	1.537e-5

Table 4.43: The normalized load for homogenous coating indented by a moving cylindrical punch $(b + a)/R_1 = 0.01$, $R_1/h_1 = 100$, $\mu_1/\mu_2 = 5$, $\rho_1/\rho_2 = 1/8$, $\nu_1/\nu_2 = 0.8$.

	$c_1 = 0.0$	$c_1 = 0.4$	$c_1 = 0.6$	$c_1 = 0.7$	$c_1 = 0.8$
η	$\frac{P}{\mu_1 R_1}$	$\frac{P}{\mu_1 R_1}$	$\frac{P}{\mu_1 R_1}$	$\frac{P}{\mu_1 R_1}$	$\frac{P}{\mu_1 R_1}$
0.0	4.029e-5	5.269e-5	4.157e-5	3.452e-5	2.707e-5
0.3	4.014e-5	5.258e-5	4.106e-5	3.469e-5	2.484e-5
0.5	4.001e-5	5.205e-5	4.020e-5	3.316e-5	2.197e-5
0.7	3.957e-5	5.128e-5	3.915e-5	3.146e-5	1.903e-5

Table 4.44: Percent difference between elastostatic and elastodynamic normal contact stresses $\mu_1 / \mu_2 = 1/10$, $(b + a) / R_1 = 0.01$, $R_1 / h_1 = 100$, $\eta = 0.3$, $\rho_1 / \rho_2 = 1/8$, $\nu_1 / \nu_2 = 0.8$.

$\frac{2X - (b - a)}{(b + a)}$	$c_1 = 0.0$		$c_1 = 0.4$		$c_1 = 0.6$		$c_1 = 0.7$	
	$\frac{\sigma_{1YY}(X, 0)}{\mu_1}$	$\frac{\sigma_{1YY}(X, 0)}{\mu_1}$	$\varepsilon\%$	$\frac{\sigma_{1YY}(X, 0)}{\mu_1}$	$\varepsilon\%$	$\frac{\sigma_{1YY}(X, 0)}{\mu_1}$	$\varepsilon\%$	
-0.97	-0.00190	-0.00175	8.11	-0.00153	19.51	-0.00139	26.94	
-0.89	-0.00377	-0.00342	9.12	-0.00293	22.27	-0.00258	31.47	
-0.65	-0.00600	-0.00541	9.81	-0.00455	24.12	-0.00393	34.45	
-0.43	-0.00699	-0.00629	10.10	-0.00525	24.89	-0.00450	35.69	
-0.32	-0.00732	-0.00657	10.23	-0.00547	25.24	-0.00466	36.27	
-0.19	-0.00752	-0.00674	10.37	-0.00559	25.61	-0.00475	36.87	
-0.06	-0.00759	-0.00680	10.52	-0.00562	26.00	-0.00475	37.51	
0.19	-0.00736	-0.00656	10.86	-0.00538	26.93	-0.00449	38.99	
0.32	-0.00705	-0.00627	11.07	-0.00512	27.47	-0.00424	39.85	
0.43	-0.00663	-0.00588	11.29	-0.00477	28.06	-0.00393	40.78	
0.65	-0.00548	-0.00484	11.81	-0.00387	29.41	-0.00314	42.84	
0.89	-0.00319	-0.00278	12.82	-0.00217	31.96	-0.00170	46.61	
0.97	-0.00146	-0.00126	13.92	-0.00096	34.65	-0.00072	50.42	

Table 4.45: Percent difference between elastostatic and elastodynamic lateral contact stresses $\mu_1 / \mu_2 = 1/10$, $(b + a) / R_1 = 0.01$, $R_1 / h_1 = 100$, $\eta = 0.3$, $\rho_1 / \rho_2 = 1/8$, $\nu_1 / \nu_2 = 0.8$.

$\frac{2X - (b - a)}{(b + a)}$	$c_1 = 0.0$		$c_1 = 0.4$		$c_1 = 0.6$		$c_1 = 0.7$	
	$\frac{\sigma_{1XX}(X, 0)}{\mu_1}$	$\frac{\sigma_{1XX}(X, 0)}{\mu_1}$	$\varepsilon\%$	$\frac{\sigma_{1XX}(X, 0)}{\mu_1}$	$\varepsilon\%$	$\frac{\sigma_{1XX}(X, 0)}{\mu_1}$	$\varepsilon\%$	
-2.05	0.00161	0.00157	2.35	0.00147	8.45	0.00136	15.53	
-1.62	0.00237	0.00239	0.94	0.00240	1.57	0.00242	2.07	
-0.94	0.00277	0.00267	3.49	0.00247	10.68	0.00226	18.44	
-0.74	-0.00070	-0.00085	21.82	-0.00116	66.61	-0.00154	120.64	
-0.55	-0.00277	-0.00290	4.78	-0.00317	14.63	-0.00352	27.13	
-0.19	-0.00525	-0.00530	0.83	-0.00539	2.69	-0.00556	5.78	
-0.06	-0.00587	-0.00587	0.06	-0.00589	0.37	-0.00597	1.68	
0.19	-0.00673	-0.00665	1.30	-0.00649	3.64	-0.00637	5.33	
0.55	-0.00700	-0.00676	3.40	-0.00632	9.67	-0.00591	15.55	
0.74	-0.00648	-0.00614	5.22	-0.00552	14.78	-0.00493	23.94	
0.94	-0.00473	-0.00426	9.91	-0.00342	27.66	-0.00262	44.54	
1.62	-0.00016	0.00006	137.90	0.00040	346.78	0.00065	503.21	
2.05	-0.00011	0.00001	108.17	0.00017	245.60	0.00025	314.48	

Table 4.46: Percent difference between elastostatic and elastodynamic normal contact stresses $\mu_1 / \mu_2 = 10$, $(b + a) / R_1 = 0.01$, $R_1 / h_1 = 100$, $\eta = 0.3$, $\rho_1 / \rho_2 = 1/8$, $\nu_1 / \nu_2 = 0.8$.

$\frac{2X - (b - a)}{(b + a)}$	$c_1 = 0.0$		$c_1 = 0.4$		$c_1 = 0.6$		$c_1 = 0.7$	
	$\sigma_{1YY}(X, 0)$	$\sigma_{1YY}(X, 0)$	$\varepsilon\%$	$\sigma_{1YY}(X, 0)$	$\varepsilon\%$	$\sigma_{1YY}(X, 0)$	$\varepsilon\%$	
	μ_1	μ_1		μ_1		μ_1		
-0.97	-0.00116	-0.00153	31.31	-0.00134	15.21	-0.00123	6.05	
-0.89	-0.00228	-0.00298	30.65	-0.00255	11.87	-0.00228	0.04	
-0.65	-0.00354	-0.00466	31.59	-0.00392	10.72	-0.00344	2.92	
-0.43	-0.00405	-0.00537	32.65	-0.00449	10.75	-0.00390	3.69	
-0.32	-0.00421	-0.00560	33.13	-0.00466	10.77	-0.00404	4.04	
-0.19	-0.00429	-0.00573	33.52	-0.00475	10.70	-0.00410	4.48	
-0.06	-0.00431	-0.00577	33.77	-0.00476	10.51	-0.00409	5.07	
0.19	-0.00416	-0.00556	33.76	-0.00456	9.61	-0.00387	6.82	
0.32	-0.00399	-0.00533	33.49	-0.00434	8.88	-0.00367	8.01	
0.43	-0.00376	-0.00500	33.05	-0.00406	7.97	-0.00341	9.41	
0.65	-0.00314	-0.00413	31.78	-0.00332	5.70	-0.00274	12.71	
0.89	-0.00185	-0.00240	29.30	-0.00188	1.31	-0.00150	18.87	
0.97	-0.00086	-0.00109	27.21	-0.00083	2.97	-0.00064	24.87	

Table 4.47: Percent difference between elastostatic and elastodynamic lateral contact stresses $\mu_1 / \mu_2 = 10$, $(b + a) / R_1 = 0.01$, $R_1 / h_1 = 100$, $\eta = 0.3$, $\rho_1 / \rho_2 = 1/8$, $\nu_1 / \nu_2 = 0.8$.

$\frac{2X - (b - a)}{(b + a)}$	$c_1 = 0.0$		$c_1 = 0.4$		$c_1 = 0.6$		$c_1 = 0.7$	
	$\sigma_{1XX}(X, 0)$	$\sigma_{1XX}(X, 0)$	$\varepsilon\%$	$\sigma_{1XX}(X, 0)$	$\varepsilon\%$	$\sigma_{1XX}(X, 0)$	$\varepsilon\%$	
	μ_1	μ_1		μ_1		μ_1		
-2.05	-0.00127	-0.00145	13.67	-0.00212	66.38	-0.00216	70.06	
-1.62	-0.00170	-0.00126	26.10	-0.00189	11.44	-0.00179	5.13	
-0.94	-0.00285	-0.00198	30.53	-0.00297	4.11	-0.00305	7.15	
-0.74	-0.00520	-0.00528	1.44	-0.00640	23.16	-0.00668	28.46	
-0.55	-0.00664	-0.00722	8.71	-0.00835	25.66	-0.00862	29.80	
-0.19	-0.00836	-0.00949	13.58	-0.01050	25.68	-0.01065	27.44	
-0.06	-0.00877	-0.01003	14.39	-0.01098	25.21	-0.01106	26.12	
0.19	-0.00930	-0.01072	15.17	-0.01151	23.74	-0.01143	22.88	
0.55	-0.00940	-0.01075	14.40	-0.01128	20.00	-0.01092	16.23	
0.74	-0.00902	-0.01013	12.36	-0.01047	16.14	-0.00993	10.16	
0.94	-0.00791	-0.00839	6.10	-0.00849	7.40	-0.00772	2.35	
1.62	-0.00423	-0.00394	6.87	-0.00429	1.30	-0.00391	7.75	
2.05	-0.00342	-0.00353	3.17	-0.00395	15.47	-0.00375	9.55	

CHAPTER 5

NUMERICAL RESULTS FOR THE FUNCTIONALLY GRADED COATING AND THE SUBSTRATE SYSTEM

In this chapter, dynamic contact mechanics of functionally graded coatings is investigated. The main results in this chapter are normal contact stress $\sigma_{1YY}(X,0)$, lateral contact stress $\sigma_{1XX}(X,0)$ and normalized stress intensity factors K_I at sharp ends of the punch. Required contact load applied by the punch is also computed for incomplete contact problems which are triangular punch, semi-circular punch and cylindrical punch contact problems. Computer programs are developed for the implementation of the numerical procedures described in Appendix-B, C and D. Numerical results of the present analytical method are compared with those available in the literature. In this section, numerical results are presented to show the influences of dimensionless punch speed, coefficient of friction, material inhomogeneity and relative contact length on elastodynamic contact stresses and stress intensity factors. In Chapter 2, general analytical formulations were derived for the dynamic contact problem of FGM coatings. Therefore, these formulations and procedures are utilized. The shear modulus of FGM coating is expressed by $\mu_1 = \mu_{10} e^{\gamma_1 Y}$, where γ_1 is the inhomogeneity constant, and it controls the gradient of shear modulus of the coating. The relation between stiffness ratio and inhomogeneity constant can be denoted as

$\ln(\Gamma_1) = -\gamma_1 h_1$. It is useful to define following parameters for FGM coating contact problem.

$$\Gamma_1 = \frac{\mu_{20}}{\mu_{10}} < 1.0, \quad \gamma_1 h_1 > 0, \quad \text{softening FGM coating}, \quad (5.1)$$

$$\Gamma_1 = \frac{\mu_{20}}{\mu_{10}} = 1.0, \quad \gamma_1 h_1 = 0, \quad \text{homogenous half-plane}, \quad (5.2)$$

$$\Gamma_1 = \frac{\mu_{20}}{\mu_{10}} > 1.0, \quad \gamma_1 h_1 < 0, \quad \text{stiffening FGM coating}. \quad (5.3)$$

Equations (5.1) - (5.3) depict the stiffness ratio of the materials. When softer material is used at the interface, the stiffness ratio becomes $\Gamma_1 < 1$, and it means FGM coating is softening through the thickness. When stiffness of the ingredient materials are equal, it means the material is homogenous half-plane, and finally when stiffer material is used at the interface, the stiffness ratio becomes $\Gamma_1 > 1$, and it means FGM coating is stiffening through the thickness.

For FGM coating problem, the shear modulus ratio between the interface material and the homogenous substrate is defined by,

$$\chi_1 = \frac{\mu_{20}}{\mu_2} = 1.0. \quad (5.4)$$

It means that the continuity on the material property at the interface is satisfied for FGM coating problem.

5.1 Numerical Results for the Rigid Flat Punch

The general schematic of the rigid flat punch contact problem is depicted in Figure 5.1. An FGM coating of thickness h_1 is perfectly bonded to a homogenous substrate. The rigid flat punch slides over the FGM coating at a speed of V .

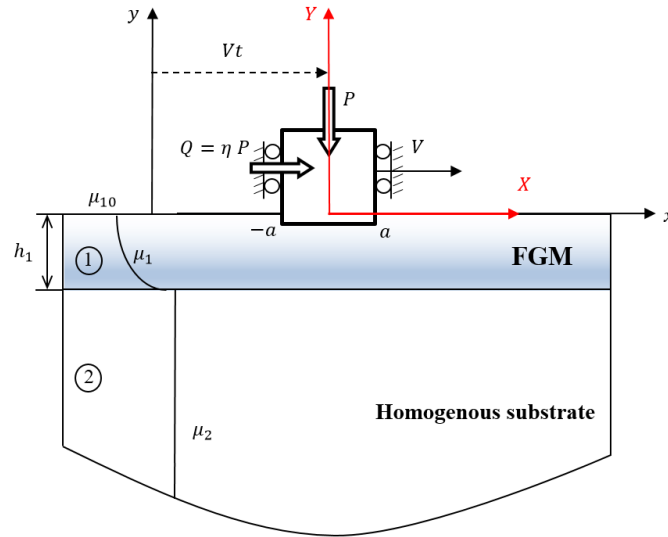


Figure 5.1: The schematic of the flat punch on the surface of the FGM coating bonded to a homogenous substrate

In order to be able verify the developed formulations, elastostatic contact stress results obtained for the rigid flat punch contact problem are compared to those provided by Guler [45]. Figures 5.2 - 5.5 show normal and lateral contact stress distributions for various values of the stiffness ratio of the FGM coating. In Figures 5.4 - 5.5, the frictional force is reversed since the frictional force is taken towards left in Guler [45]. It can be inferred from Figures 5.2 - 5.5 that results of the present study are in excellent agreement between those provided by Guler [45].

Figures 5.6 - 5.7 show elastodynamic contact stress distributions for homogenous half-planes for which stiffness ratio $\Gamma_1 = \mu_2 / \mu_{10}$ is defined as 1. In frictionless case, the normal contact stress distribution remain the same although dimensionless punch

speed c_1 is increased. When Figure 5.6(b) is examined, the magnitude of lateral contact stress increases in the contact zone. The surface outside the contact zone is stress free. Figure 5.7 indicates the normal and lateral elastodynamic contact stresses in frictional case. When dimensionless punch speed c_1 is increased from 0.0 to 0.8, normal contact stress slants towards the leading end of the contact zone. Lateral elastodynamic contact stress gradually increases when punch speed c_1 is increased. The tensile behavior of the lateral elastodynamic contact stress at trailing end is enhanced at higher punch speeds.

Figures 5.8 – 5.13 show elastodynamic contact stress distributions for softening ($\Gamma_1 = 1/6$) and stiffening coatings ($\Gamma_1 = 6$) for different relative contact lengths adjusted as $a/h_1 = 0.05$, $a/h_1 = 0.1$ and $a/h_1 = 0.2$, respectively. The influence of dimensionless punch speed c_1 on elastodynamic contact stress distributions is different for softening and stiffening coatings as it can be inferred from Figures 5.8 and 5.9. Normal contact stresses become less compressive in the contact zone for the softening coating ($\Gamma_1 = 1/6$). However, normal contact stresses become more compressive towards the trailing end, and become less compressive around the leading end of the contact zone for the stiffening coating ($\Gamma_1 = 6$). Hence, skewed normal stress curves are formed for the stiffening coating. The influence of dimensionless punch speed on lateral contact stress can be seen from Figures 5.8(b) and 5.9(b). As dimensionless punch speed is increased, compressive elastodynamic lateral contact stresses are formed in the contact zone. However, behind the trailing end of the contact, lateral elastodynamic contact stresses become more compressive for the softening coating whereas, lateral elastodynamic contact stresses increase in tensile way for the stiffening coating. For a softening coating ($\Gamma_1 = 1/6$), tensile lateral contact stresses behind the trailing end of the contact tend to be compressive

especially at higher punch speeds. Nevertheless, for a stiffening coatings ($\Gamma_1 = 6$), the tensile behavior of the lateral contact stress is enhanced behind the trailing end. Trailing end of the contact for the stiffening coatings is more critical for cracking type failures due to the formations of high tensile lateral contact stresses. The effect of dimensionless punch speed on contact stress distributions for $a/h_1 = 0.1$ and $a/h_1 = 0.2$ are similar to those obtained in Figures 5.8 - 5.9. However, the difference between curves generated for elastodynamic contact stresses are greater at higher values of a/h_1 . This behavior can easily be inferred from Figure 5.8 and 5.12. It should also be noted that contact stresses for softening coatings ($\Gamma_1 = 1/6$) are relatively more sensitive to the change in punch speed when compared to stiffening coatings ($\Gamma_1 = 6$).

The influence of coefficient of friction η on elastodynamic contact stresses is examined in Figures 5.14 – 5.15. The general trend of variations of normal and lateral elastodynamic contact stresses observed for softening and a stiffening coatings is similar. For both softening and stiffening coatings, and all values of coefficient of friction, normal contact stress slant towards the leading end of the contact zone. Moreover, in all cases, larger coefficient of friction leads to a larger tensile peak at the trailing end of the contact. Thus, the trailing end of the contact is a possible site for cracking type failure. This finding is in line with experimental results observed in scratch tests. The magnitude of elastodynamic contact stresses are different for softening and stiffening coatings. Hence, adjustment of the coefficient of friction and stiffness ratio could be possible methods for avoiding surface related failures. Ahead of the leading end of the contact, lateral contact stress is compressive for both softening and stiffening coatings.

Figures 5.16 – 5.17 illustrate the effect of stiffness ratio Γ_1 on elastodynamic normal and lateral contact stresses. The contact is assumed to be frictional, hence $\eta = 0.3$.

The results are provided for different relative contact length parameters such as $a/h_1 = 0.1$ and $a/h_1 = 0.4$. Normalized contact stresses are seen to be quite sensitive to the change in stiffness ratio. Normal contact stress in softening coatings is less compressive than that found for the stiffening coating. As stiffness ratio Γ_1 is increased from 1/6 to 6, elastodynamic lateral contact stress comes close to the zero stress line as observed in Figures 5.16 and 5.17.

Figures 5.18 – 5.19 show the elastodynamic contact stresses as functions of the relative contact length denoted by the ratio a/h_1 . Variations of the contact stresses with respect to a/h_1 are more pronounced for the softening coating ($\Gamma_1 = 1/6$). Increase in the ratio a/h_1 leads to less compressive normal stresses in the case of a softening coating however, it leads to more compressive normal stresses in the case of a stiffening coating. Lateral contact stress within the contact zone becomes more compressive as a/h_1 is increased from 0.01 to 0.4 in the case of a softening coating. However, the reverse trend is seen to be valid for a stiffening coating ($\Gamma_1 = 6$).

Normalized stress intensity factors evaluated at the sharp end points of the flat punch are provided in Tables 5.1 – 5.7. Table 5.1 shows the normalized stress intensity factors at the trailing and leading ends of the flat punch for various values of stiffness ratio and coefficient of friction in elastostatic case. Results obtained in this study are compared to those found by Guler [45] for the verification purpose. It can be inferred from Table 5.1 that a very good agreement is achieved. Table 5.2 shows the elastostatic normalized stress intensity factors for various values of stiffness ratio Γ_1 and relative contact length a/h_1 . The mode I SIF is an increasing function of a/h_1 for softening coatings however, the mode I SIF is a decreasing function of a/h_1 for stiffening coatings, in elastostatic case. Elastodynamic mode I SIFs generated for different values of stiffness ratio and dimensionless punch speed is presented in

Tables 5.3 – 5.5. The mode I SIFs are presented in these tables for $a/h_1 = 0.1$, $a/h_1 = 0.25$ and $a/h_1 = 0.4$, respectively. Coefficient of friction is assumed to be $\eta = 0.3$. In all cases, the mode I SIF at the trailing end of the punch $K_I(-a)$ for the softening coating is greater than the mode I SIF at the trailing end $K_I(-a)$ for the stiffening coating. As punch speed c_1 is increased from 0.0 to 0.7, the mode SIF at the leading end $K_I(a)$ gradually increases in the case of a softening coating. However, the reverse trend is observed in the case of a stiffening coating. The normalized stress intensity factor at the leading end $K_I(a)$ is a decreasing function of punch speed c_1 . In Table 5.3, the same behavior is observed for the variation of the mode I SIF at the trailing end $K_I(-a)$. However, this behavior is slightly changed when the ratio a/h_1 is adjusted as 0.25 and 0.4. The mode I SIF at the trailing end $K_I(-a)$ decreases when punch speed is increased from 0.0 to 0.6, and then slightly increases when punch speed is $c_1 = 0.7$. For the half-plane contact problem $\Gamma_1 = 1$, the mode I SIF at both ends are equal and they are decreasing functions of punch speed c_1 . Tables 5.6 and 5.7 show the mode I SIF for various values of coefficient of friction and dimensionless punch speed. In the case of a softening coating $\Gamma_1 = 1/6$, the mode I SIF at both ends are increasing functions of punch speed between $\eta = 0.0$ and $\eta = 0.5$. However, when coefficient of friction is adjusted as $\eta = 0.7$, $K_I(a)$ slightly decreases with respect to increasing punch speed. Moreover, the mode I SIF at the trailing end $K_I(-a)$ is greater than the mode I SIF at the leading end $K_I(a)$.

Table 5.7 shows the normalized stress intensity factors in the case of a stiffening coating $\Gamma_1 = 6$. In all cases, the mode I SIF at both ends are decreasing functions of punch speed c_1 . Although the difference between the normalized stress intensity

factors $K_I(-a)$ and $K_I(a)$ are considerable in frictional elastostatic case, this difference starts to diminish at higher punch speeds. In general, the mode-I SIF at the leading end $K_I(a)$ is greater than the mode-I SIF at the trailing end $K_I(-a)$ however, at a punch speed of $c_1 = 0.7$, $K_I(-a)$ becomes greater than $K_I(a)$.

Tables 5.8 - 5.11 provide tabulated results on percent differences between contact stresses computed considering elastostatic and elastodynamic conditions. Such a comparison is critical in assessment of the influence of punch dynamics on contact stresses. Contact stresses are calculated for four different values of dimensionless punch speed c_1 . When punch speed is adjusted as $c_1 = 0.0$, it corresponds to elastostatic contact, and contacts for which $c_1 > 0$ are elastodynamic. Percent differences $\varepsilon\%$ are computed based on elastostatic results. Tables 5.8 – 5.9 show results for the softening coating ($\Gamma_1 = 1/6$). Percent differences between elastodynamic and elastostatic normal contact stress increase as punch speed is increased from 0.0 to 0.7. The values of percent difference are relatively high towards the leading end of the contact zone. The values of percent difference between elastodynamic and elastostatic lateral contact stresses are also considerable. Again, percent differences gradually increase as punch speed is increased from 0.0 to 0.7. Relatively high percent difference values are observed behind the trailing end of the contact and percent difference reaches up to 858.7% at those locations.

Tables 5.10 - 5.11 show percent differences between elastodynamic and elastostatic contact stresses for the stiffening coating ($\Gamma_1 = 6$). The percent differences for the normal contact stress increase as punch speed c_1 is increased, and larger differences are observed near the ends of the contact. When Table 4.11 is examined, the percent differences for the lateral contact stress increase as the punch speed is increased. Higher values of percent difference are observed especially near the trailing end of

the contact. When Tables 5.9 and 5.11 are compared, it can also be noted that values of the percent difference are quite high for softening coatings.

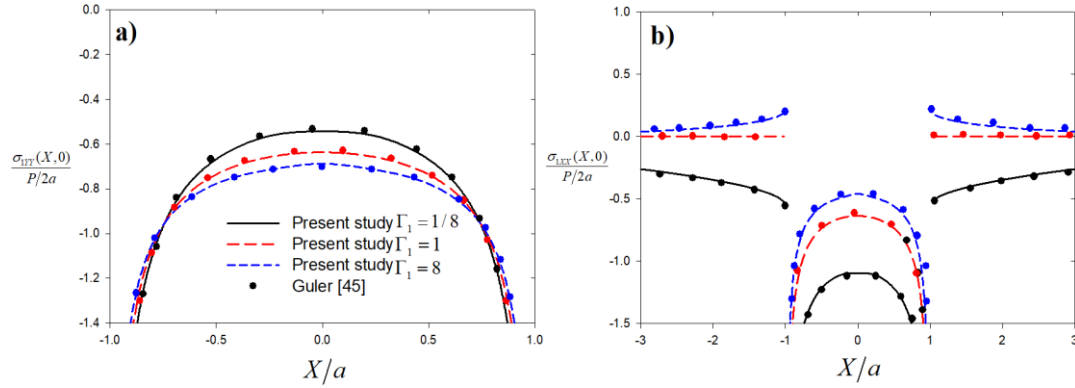


Figure 5.2: Normal and lateral contact stress distribution on FGM coating indented by a flat punch for different stiffness ratio of the coating (a) Normal contact stress distribution; (b) Lateral contact stress distribution, $a/h_1 = 0.1$, $\Gamma_1 = \mu_2 / \mu_{10}$, $\eta = 0.0$, $c_1 = 0.0$.

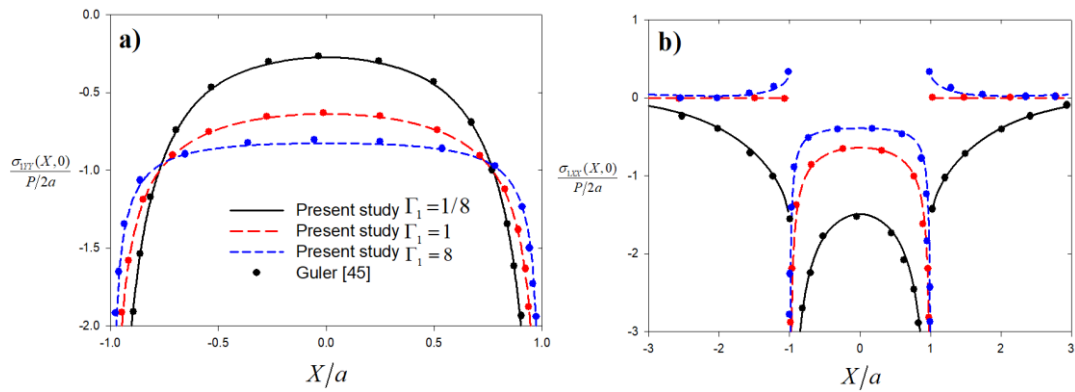


Figure 5.3: Normal and lateral contact stress distribution on FGM coating indented by a flat punch for different stiffness ratio of the coating (a) Normal contact stress distribution; (b) Lateral contact stress distribution, $a/h_1 = 0.5$, $\Gamma_1 = \mu_2 / \mu_{10}$, $\eta = 0.0$, $c_1 = 0.0$.

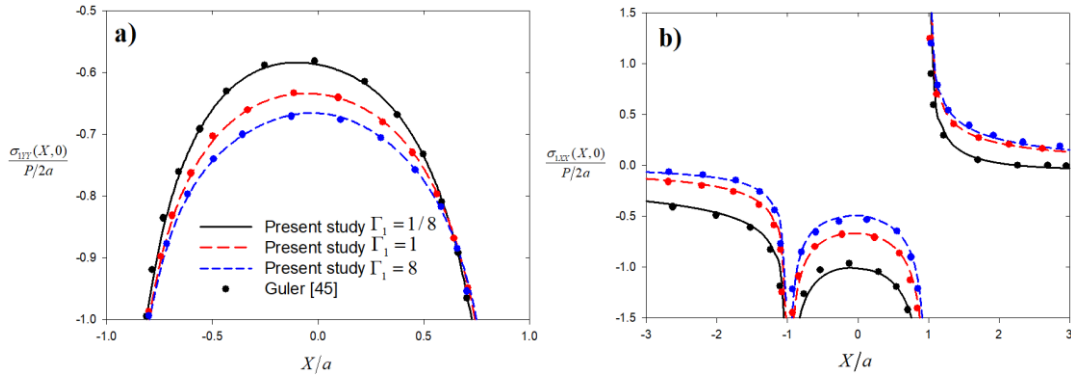


Figure 5.4: Normal and lateral contact stress distribution on FGM coating indented by a flat punch for different stiffness ratio of the coating (a) Normal contact stress distribution; (b) Lateral contact stress distribution, $a/h_1 = 0.05$, $\Gamma_1 = \mu_2 / \mu_{10}$, $\eta = 0.3$, $c_1 = 0.0$.

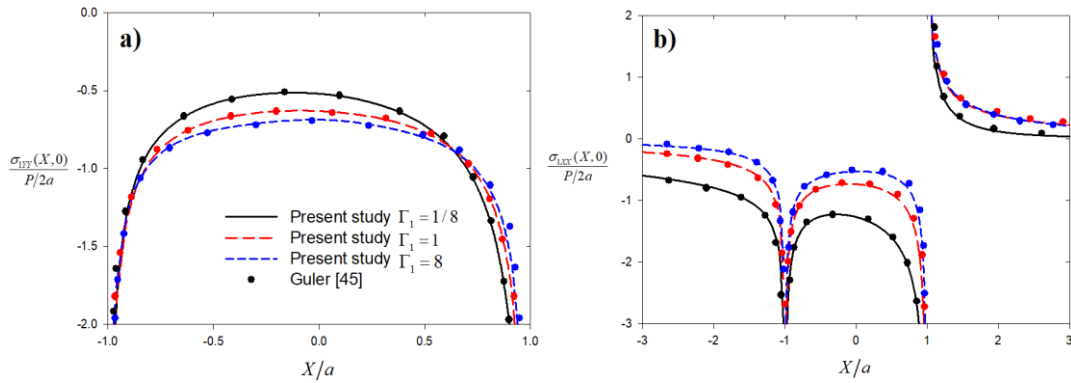


Figure 5.5: Normal and lateral contact stress distribution on FGM coating indented by a flat punch for different stiffness ratio of the coating (a) Normal contact stress distribution; (b) Lateral contact stress distribution, $a/h_1 = 0.1$, $\Gamma_1 = \mu_2 / \mu_{10}$, $\eta = 0.5$, $c_1 = 0.0$.

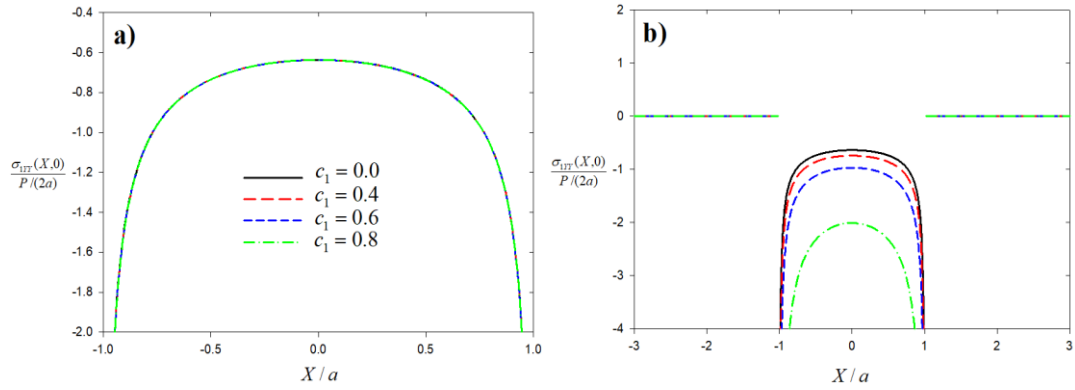


Figure 5.6: Normal and lateral elastodynamic contact stresses on FGM coating indented by a moving flat punch for various values of punch speed (a) Normal contact stress distribution; (b) Lateral contact stress distribution, $a/h_1 = 0.1$, $\Gamma_1 = 1$, $\eta = 0.0$, $\nu_1/\nu_2 = 1$.

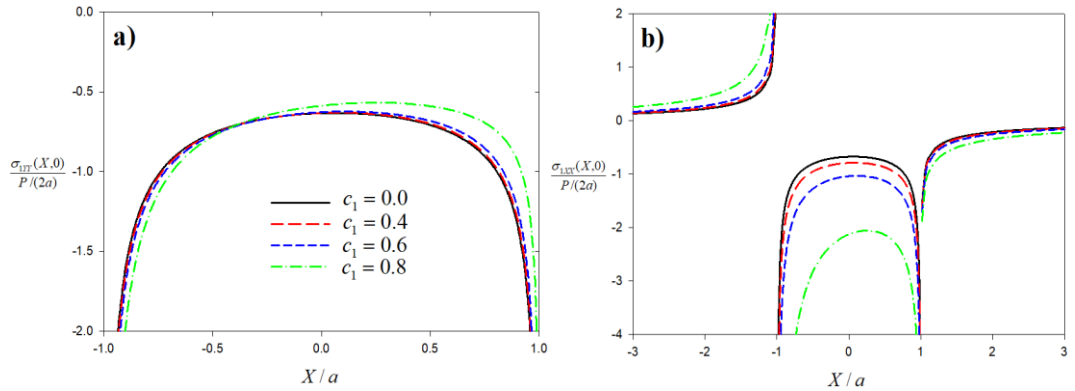


Figure 5.7: Normal and lateral elastodynamic contact stresses on FGM coating indented by a moving flat punch for various values of punch speed (a) Normal contact stress distribution; (b) Lateral contact stress distribution, $a/h_1 = 0.1$, $\Gamma_1 = 1$, $\eta = 0.3$, $\nu_1/\nu_2 = 1$.

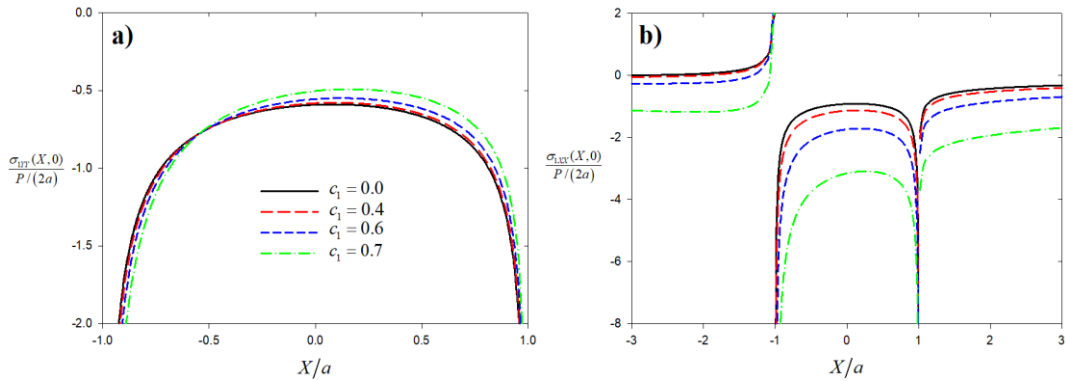


Figure 5.8: Normal and lateral elastodynamic contact stresses on FGM coating indented by a moving flat punch for various values of punch speed (a) Normal contact stress distribution; (b) Lateral contact stress distribution, $a/h_1 = 0.05$, $\Gamma_1 = 1/6$, $\eta = 0.3$, $\nu_1/\nu_2 = 1$.

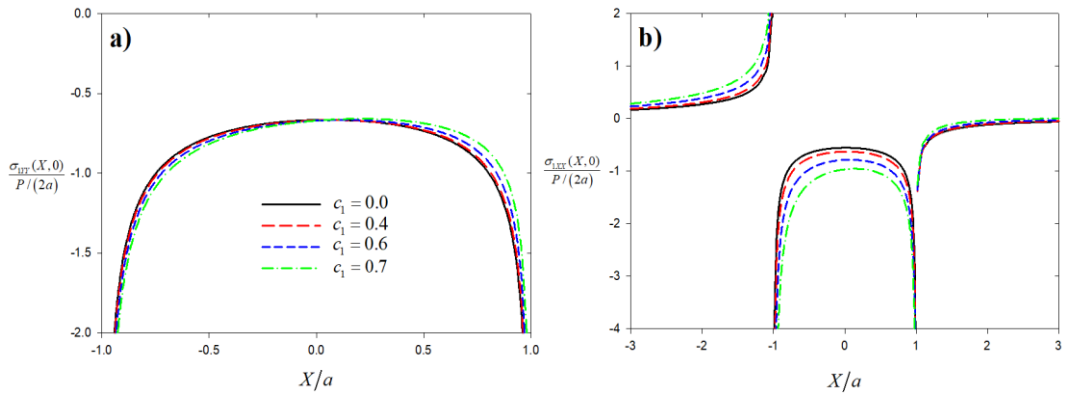


Figure 5.9: Normal and lateral elastodynamic contact stresses on FGM coating indented by a moving flat punch for various values of punch speed (a) Normal contact stress distribution; (b) Lateral contact stress distribution, $a/h_1 = 0.05$, $\Gamma_1 = 6$, $\eta = 0.3$, $\nu_1/\nu_2 = 1$.

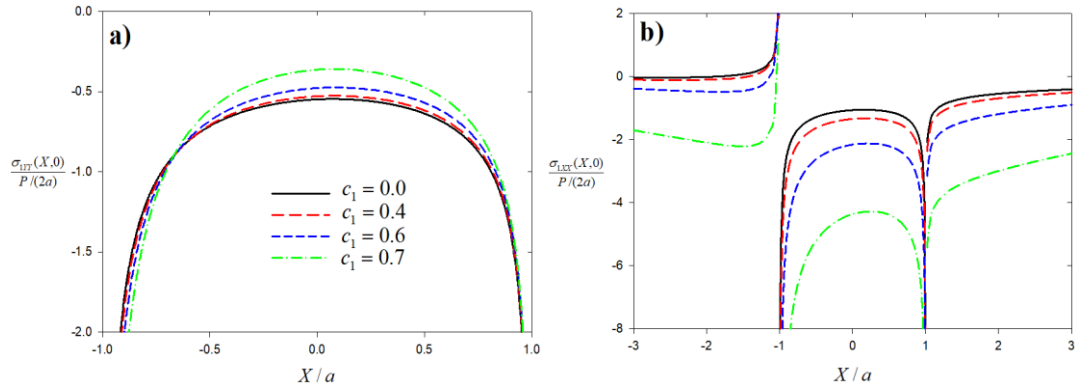


Figure 5.10: Normal and lateral elastodynamic contact stresses on FGM coating indented by a moving flat punch for various values of punch speed (a) Normal contact stress distribution; (b) Lateral contact stress distribution, $a/h_1 = 0.1$, $\Gamma_1 = 1/6$, $\eta = 0.3$, $\nu_1/\nu_2 = 1$.

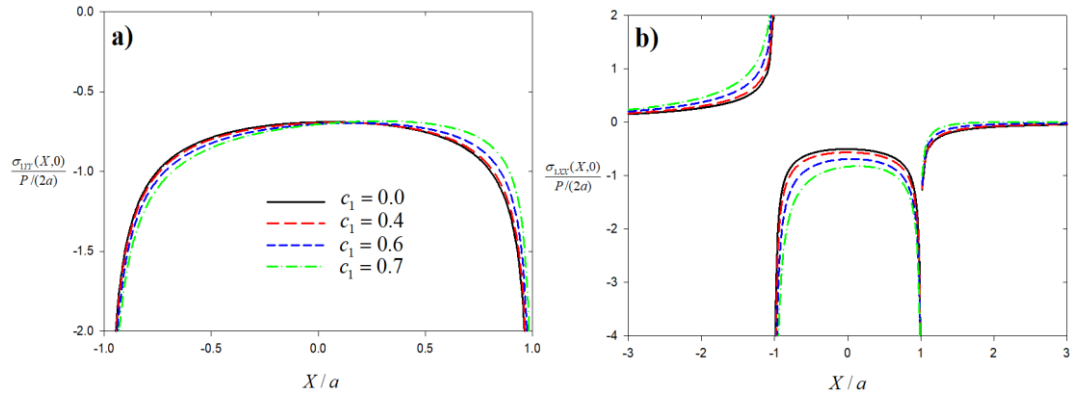


Figure 5.11: Normal and lateral elastodynamic contact stresses on FGM coating indented by a moving flat punch for various values of punch speed (a) Normal contact stress distribution; (b) Lateral contact stress distribution, $a/h_1 = 0.1$, $\Gamma_1 = 6$, $\eta = 0.3$, $\nu_1/\nu_2 = 1$.

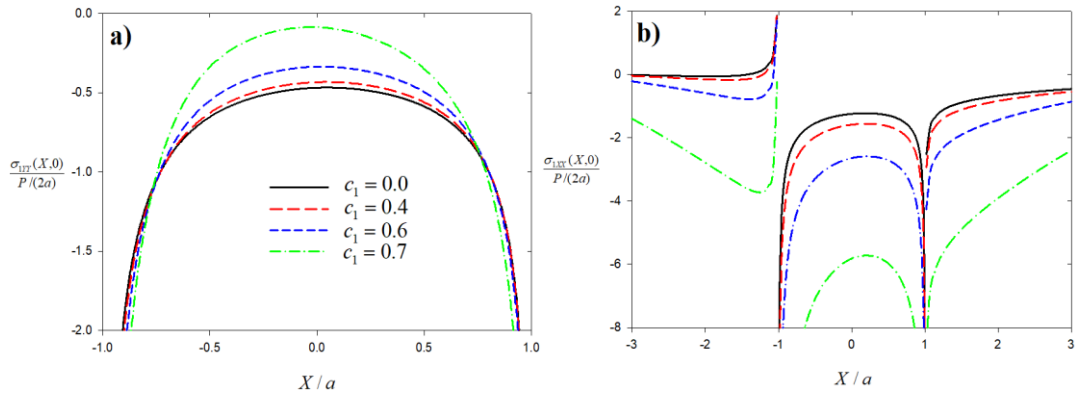


Figure 5.12: Normal and lateral elastodynamic contact stresses on FGM coating indented by a moving flat punch for various values of punch speed (a) Normal contact stress distribution; (b) Lateral contact stress distribution, $a/h_1 = 0.2$, $\Gamma_1 = 1/6$, $\eta = 0.3$, $\nu_1/\nu_2 = 1$.

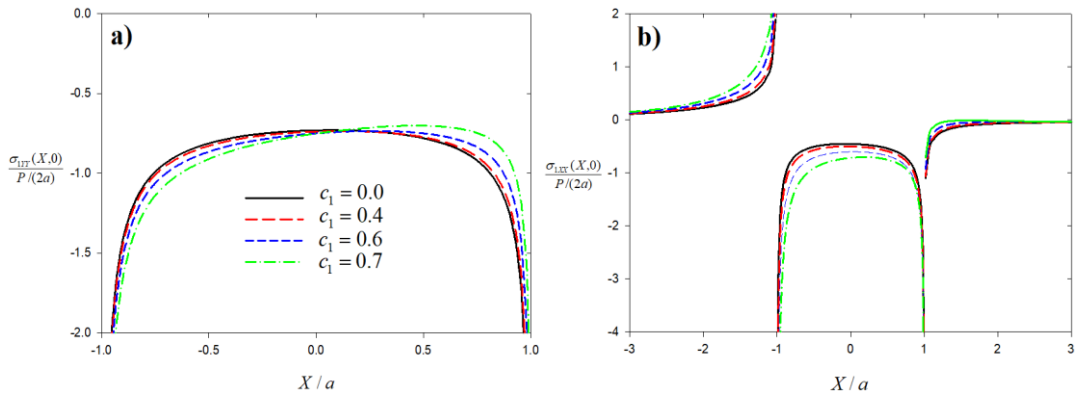


Figure 5.13: Normal and lateral elastodynamic contact stresses on FGM coating indented by a moving flat punch for various values of punch speed (a) Normal contact stress distribution; (b) Lateral contact stress distribution, $a/h_1 = 0.2$, $\Gamma_1 = 6$, $\eta = 0.3$, $\nu_1/\nu_2 = 1$.

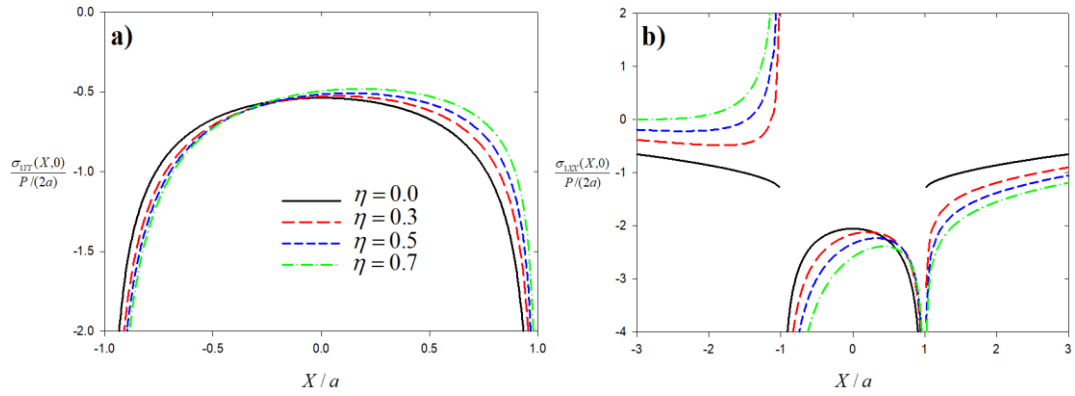


Figure 5.14: Normal and lateral elastodynamic contact stresses on FGM coating indented by a moving flat punch for various values of coefficient of friction (a) Normal contact stress distribution; (b) Lateral contact stress distribution, $a/h_1 = 0.1$, $\Gamma_1 = 1/6$, $c_1 = 0.4$, $v_1/v_2 = 1$.

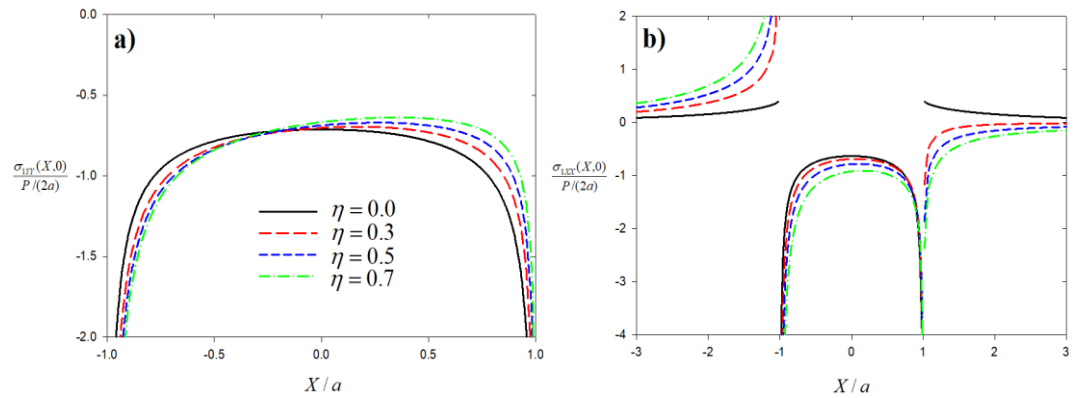


Figure 5.15: Normal and lateral elastodynamic contact stresses on FGM coating indented by a moving flat punch for various values of coefficient of friction (a) Normal contact stress distribution; (b) Lateral contact stress distribution, $a/h_1 = 0.1$, $\Gamma_1 = 6$, $c_1 = 0.4$, $v_1/v_2 = 1$.

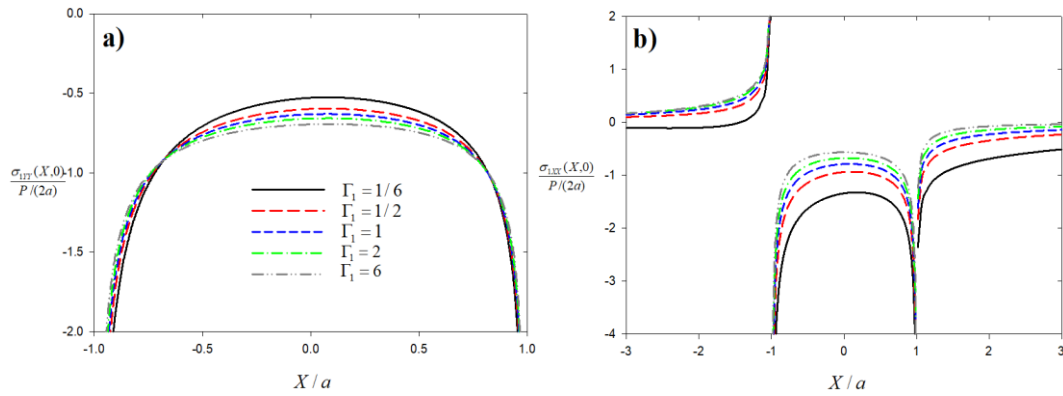


Figure 5.16: Normal and lateral elastodynamic contact stresses on FGM coating indented by a moving flat punch for various values of stiffness ratio (a) Normal contact stress distribution; (b) Lateral contact stress distribution, $a/h_1 = 0.1$, $c_1 = 0.4$, $\eta = 0.3$, $\nu_1/\nu_2 = 1$.

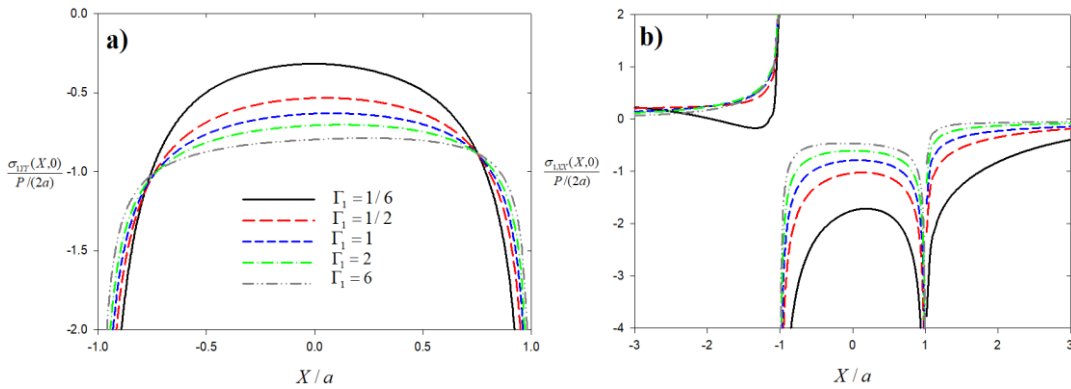


Figure 5.17: Normal and lateral elastodynamic contact stresses on FGM coating indented by a moving flat punch for various values of stiffness ratio (a) Normal contact stress distribution; (b) Lateral contact stress distribution, $a/h_1 = 0.4$, $c_1 = 0.4$, $\eta = 0.3$, $\nu_1/\nu_2 = 1$.

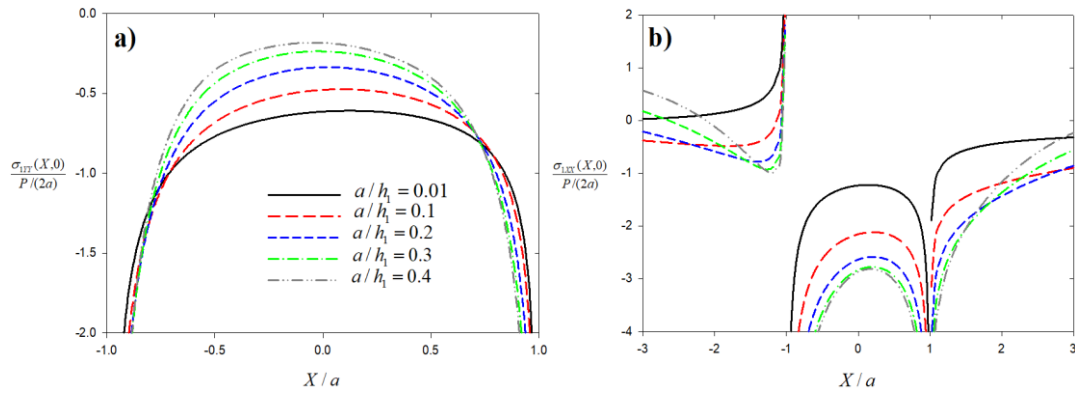


Figure 5.18: Normal and lateral elastodynamic contact stresses on FGM coating indented by a moving flat punch for various values of relative coating thickness (a) Normal contact stress distribution; (b) Lateral contact stress distribution, $\Gamma_1 = 1/6$, $c_1 = 0.6$, $\eta = 0.3$, $\nu_1/\nu_2 = 1$.

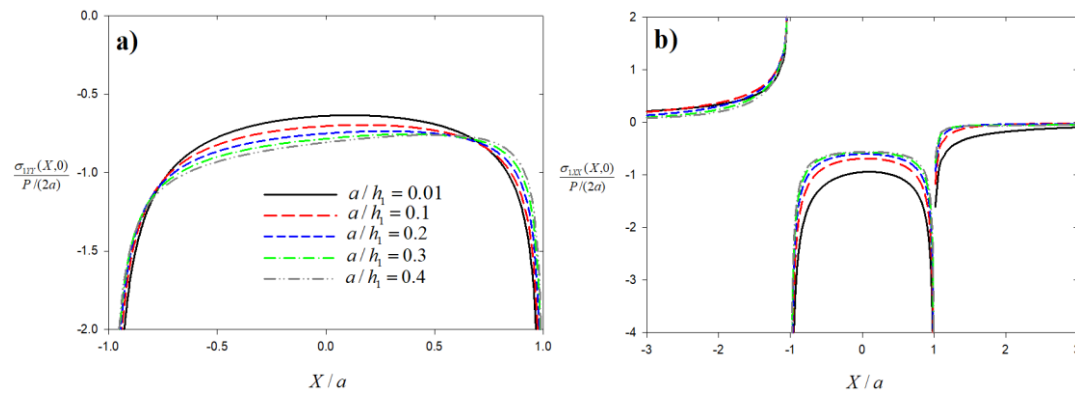


Figure 5.19: Normal and lateral elastodynamic contact stresses on FGM coating indented by a moving flat punch for various values of relative coating thickness (a) Normal contact stress distribution; (b) Lateral contact stress distribution, $\Gamma_1 = 6$, $c_1 = 0.6$, $\eta = 0.3$, $\nu_1/\nu_2 = 1$.

Table 5.1: Normalized stress intensity factors for the contact between a rigid flat punch and an FGM coating $a/h_1 = 0.1$, $c_1 = 0.0$.

	$\eta = 0.0$			$\eta = 0.3$			$\eta = 0.5$			
Γ_1	$K_I(a)$	$K_I^*(a)$	$K_I(-a)$	$K_I(a)$	$K_I^*(-a)$	$K_I^*(a)$	$K_I(-a)$	$K_I(a)$	$K_I^*(-a)$	$K_I^*(a)$
1/8	0.3822	0.3813	0.4028	0.3567	0.3933	0.3673	0.4137	0.3376	0.3999	0.3572
1/2	0.3358	0.3355	0.3402	0.3285	0.3382	0.3305	0.3414	0.3220	0.3386	0.3261
1	0.3183	0.3183	0.3171	0.3171	0.3171	0.3171	0.3151	0.3151	0.3151	0.3151
2	0.3034	0.3038	0.2981	0.3061	0.2991	0.3060	0.2937	0.3081	0.2949	0.3062
8	0.2790	0.2802	0.2686	0.2883	0.2696	0.2885	0.2612	0.2938	0.2615	0.2926

Note that K_I^* value shows the normalized stress intensity factor presented by Guler [45].

Table 5.2: Normalized stress intensity factors for the moving rigid flat punch $c_1 = 0.0$, $\eta = 0.0$, $\nu_1/\nu_2 = 1$.

	$a/h_1 = 0.1$		$a/h_1 = 0.2$		$a/h_1 = 0.3$		$a/h_1 = 0.4$	
Γ_1	$K_I(-a)$	$K_I(a)$	$K_I(-a)$	$K_I(a)$	$K_I(-a)$	$K_I(a)$	$K_I(-a)$	$K_I(a)$
1/6	0.3688	0.3688	0.4208	0.4208	0.4678	0.4678	0.5075	0.5075
1/2	0.3351	0.3351	0.3506	0.3506	0.3639	0.3639	0.3751	0.3751
1	0.3183	0.3183	0.3183	0.3183	0.3183	0.3183	0.3183	0.3183
2	0.3039	0.3039	0.2925	0.2925	0.2832	0.2832	0.2756	0.2756
6	0.2847	0.2847	0.2608	0.2608	0.2423	0.2423	0.2275	0.2275

Table 5.3: Normalized stress intensity factors for the moving rigid flat punch $a/h_1 = 0.1$, $\eta = 0.3$, $\nu_1/\nu_2 = 1$.

	$c_1 = 0.0$		$c_1 = 0.4$		$c_1 = 0.6$		$c_1 = 0.7$	
Γ_1	$K_I(-a)$	$K_I(a)$	$K_I(-a)$	$K_I(a)$	$K_I(-a)$	$K_I(a)$	$K_I(-a)$	$K_I(a)$
1/6	0.3840	0.3479	0.3951	0.3538	0.4211	0.3707	0.4813	0.4058
1/2	0.3388	0.3275	0.3410	0.3286	0.3442	0.3313	0.3455	0.3355
1	0.3167	0.3167	0.3159	0.3159	0.3134	0.3134	0.3092	0.3092
2	0.2984	0.3069	0.2961	0.3039	0.2917	0.2965	0.2870	0.2854
6	0.2752	0.2925	0.2712	0.2872	0.2652	0.2741	0.2610	0.2549

Table 5.4: Normalized stress intensity factors for the moving rigid flat punch $a/h_1 = 0.25$, $\eta = 0.3$, $\nu_1/\nu_2 = 1$.

Γ_1	$c_1 = 0.0$		$c_1 = 0.4$		$c_1 = 0.6$		$c_1 = 0.7$	
	$K_I(-a)$	$K_I(a)$	$K_I(-a)$	$K_I(a)$	$K_I(-a)$	$K_I(a)$	$K_I(-a)$	$K_I(a)$
1/6	0.4607	0.4235	0.4844	0.4504	0.5433	0.5342	0.6932	0.7719
1/2	0.3620	0.3488	0.3671	0.3543	0.3752	0.3686	0.3812	0.3917
1	0.3167	0.3167	0.3159	0.3159	0.3134	0.3134	0.3092	0.3092
2	0.2812	0.2917	0.2785	0.2863	0.2746	0.2734	0.2718	0.2557
6	0.2395	0.2613	0.2350	0.2514	0.2306	0.2282	0.2318	0.1968

Table 5.5: Normalized stress intensity factors for the moving rigid flat punch $a/h_1 = 0.4$, $\eta = 0.3$, $\nu_1/\nu_2 = 1$.

Γ_1	$c_1 = 0.0$		$c_1 = 0.4$		$c_1 = 0.6$		$c_1 = 0.7$	
	$K_I(-a)$	$K_I(a)$	$K_I(-a)$	$K_I(a)$	$K_I(-a)$	$K_I(a)$	$K_I(-a)$	$K_I(a)$
1/6	0.5182	0.4908	0.5495	0.5338	0.6287	0.6676	0.8384	1.0539
1/2	0.3788	0.3673	0.3855	0.3762	0.3962	0.3995	0.4045	0.4371
1	0.3167	0.3167	0.3159	0.3159	0.3134	0.3134	0.3092	0.3092
2	0.2693	0.2796	0.2671	0.2727	0.2647	0.2571	0.2644	0.2369
6	0.2161	0.2378	0.2123	0.2251	0.2108	0.1962	0.2174	0.1592

Table 5.6: Normalized stress intensity factors for the rigid flat punch $a/h_1 = 0.1$, $\Gamma_1 = 1/6$, $\nu_1/\nu_2 = 1$.

η	$c_1 = 0.0$		$c_1 = 0.4$		$c_1 = 0.6$		$c_1 = 0.7$	
	$K_I(-a)$	$K_I(a)$	$K_I(-a)$	$K_I(a)$	$K_I(-a)$	$K_I(a)$	$K_I(-a)$	$K_I(a)$
0.0	0.3688	0.3688	0.3790	0.3790	0.4057	0.4057	0.4664	0.4664
0.3	0.3840	0.3479	0.3951	0.3538	0.4211	0.3707	0.4813	0.4058
0.5	0.3907	0.3313	0.4005	0.3329	0.4208	0.3382	0.4700	0.3446
0.7	0.3947	0.3130	0.4019	0.3094	0.4135	0.3011	0.4475	0.2748

Table 5.7: Normalized stress intensity factors for the moving rigid flat punch $a/h_1 = 0.1$, $\Gamma_1 = 6$, $\nu_1/\nu_2 = 1$.

η	$c_1 = 0.0$		$c_1 = 0.4$		$c_1 = 0.6$		$c_1 = 0.7$	
	$K_I(-a)$	$K_I(a)$	$K_I(-a)$	$K_I(a)$	$K_I(-a)$	$K_I(a)$	$K_I(-a)$	$K_I(a)$
0.0	0.2847	0.2847	0.2808	0.2808	0.2731	0.2731	0.2647	0.2647
0.3	0.2752	0.2925	0.2712	0.2872	0.2652	0.2741	0.2610	0.2549
0.5	0.2680	0.2966	0.2635	0.2897	0.2565	0.2713	0.2509	0.2438
0.7	0.2602	0.2997	0.2548	0.2908	0.2458	0.2665	0.2368	0.2314

Table 5.8: Percent difference between elastostatic and elastodynamic normal contact stresses $\Gamma_1 = 1/6$, $a/h_1 = 0.1$, $\eta = 0.3$, $\nu_1/\nu_2 = 1$.

X/a	$c_1 = 0.0$			$c_1 = 0.4$			$c_1 = 0.6$			$c_1 = 0.7$		
	$\frac{\sigma_{iyy}(X,0)}{P/(2a)}$	$\frac{\sigma_{iyy}(X,0)}{P/(2a)}$	$\varepsilon\%$	$\frac{\sigma_{iyy}(X,0)}{P/(2a)}$	$\frac{\sigma_{iyy}(X,0)}{P/(2a)}$	$\varepsilon\%$	$\frac{\sigma_{iyy}(X,0)}{P/(2a)}$	$\frac{\sigma_{iyy}(X,0)}{P/(2a)}$	$\varepsilon\%$	$\frac{\sigma_{iyy}(X,0)}{P/(2a)}$	$\frac{\sigma_{iyy}(X,0)}{P/(2a)}$	$\varepsilon\%$
-0.90	-1.81344	-1.88383	3.88	-2.04431	-1.88383	12.73	-2.34655	-1.88383	29.40	-2.34655	-1.88383	29.40
-0.82	-1.29816	-1.33123	2.55	-1.40144	-1.33123	7.96	-1.52575	-1.33123	17.53	-1.52575	-1.33123	17.53
-0.73	-1.00533	-1.01788	1.25	-1.03893	-1.01788	3.34	-1.06515	-1.01788	5.95	-1.06515	-1.01788	5.95
-0.61	-0.82172	-0.82159	0.02	-0.81263	-0.82159	1.11	-0.77863	-0.82159	5.24	-0.77863	-0.82159	5.24
-0.41	-0.65900	-0.64790	1.68	-0.61367	-0.64790	6.88	-0.52909	-0.64790	19.71	-0.52909	-0.64790	19.71
-0.19	-0.57597	-0.55915	2.92	-0.51264	-0.55915	10.99	-0.40467	-0.55915	29.74	-0.40467	-0.55915	29.74
-0.04	-0.55067	-0.53169	3.45	-0.48112	-0.53169	12.63	-0.36671	-0.53169	33.41	-0.36671	-0.53169	33.41
0.19	-0.55144	-0.53105	3.70	-0.47913	-0.53105	13.11	-0.36602	-0.53105	33.63	-0.36602	-0.53105	33.63
0.41	-0.59894	-0.57851	3.41	-0.52906	-0.57851	11.67	-0.42725	-0.57851	28.67	-0.42725	-0.57851	28.67
0.61	-0.70781	-0.68804	2.79	-0.64352	-0.68804	9.08	-0.56119	-0.68804	20.71	-0.56119	-0.68804	20.71
0.73	-0.83404	-0.81472	2.32	-0.77421	-0.81472	7.17	-0.70918	-0.81472	14.97	-0.70918	-0.81472	14.97
0.82	-1.03406	-1.01421	1.92	-0.97652	-1.01421	5.56	-0.93069	-1.01421	10.00	-0.93069	-1.01421	10.00
0.90	-1.37765	-1.35424	1.70	-1.31438	-1.35424	4.59	-1.28681	-1.35424	6.59	-1.28681	-1.35424	6.59

Table 5.9: Percent difference between elastostatic and elastodynamic lateral contact stresses $\Gamma_1 = 1/6$, $a/h_1 = 0.1$, $\eta = 0.3$, $\nu_1/\nu_2 = 1$.

X/a	$c_1 = 0.0$		$c_1 = 0.4$		$c_1 = 0.6$		$c_1 = 0.7$	
	$\frac{\sigma_{1xx}(X,0)}{P/(2a)}$	$\frac{\sigma_{1xx}(X,0)}{P/(2a)}$	$\varepsilon\%$	$\frac{\sigma_{1xx}(X,0)}{P/(2a)}$	$\varepsilon\%$	$\frac{\sigma_{1xx}(X,0)}{P/(2a)}$	$\varepsilon\%$	
-1.22	0.26832	0.17771	33.77	-0.24508	191.34	-2.03592	858.77	
-0.99	-7.65534	-9.73231	27.13	-15.40241	101.20	-27.17313	254.96	
-0.82	-1.94587	-2.46846	26.86	-3.93597	102.27	-7.47159	283.97	
-0.67	-1.50501	-1.91009	26.91	-3.06378	103.57	-5.97327	296.89	
-0.41	-1.21643	-1.54271	26.82	-2.48498	104.29	-4.96107	307.84	
-0.27	-1.13690	-1.44048	26.70	-2.32137	104.18	-4.66824	310.61	
-0.04	-1.06804	-1.35013	26.41	-2.17229	103.39	-4.39281	311.30	
0.27	-1.05583	-1.32838	25.81	-2.12267	101.04	-4.27742	305.13	
0.41	-1.08411	-1.35932	25.39	-2.15866	99.12	-4.31804	298.30	
0.67	-1.23846	-1.53786	24.18	-2.39361	93.27	-4.64700	275.22	
0.82	-1.51072	-1.85468	22.77	-2.81342	86.23	-5.23502	246.53	
0.99	-4.93542	-5.76238	16.76	-7.74267	56.88	-11.57837	134.60	
1.22	-0.91562	-1.11367	21.63	-1.75204	91.35	-3.80532	315.60	

Table 5.10: Percent difference between elastostatic and elastodynamic normal contact stresses $\Gamma_1 = 6$, $a/h_1 = 0.1$, $\eta = 0.3$, $\nu_1/\nu_2 = 1$.

X/a	$c_1 = 0.0$		$c_1 = 0.4$		$c_1 = 0.6$		$c_1 = 0.7$	
	$\frac{\sigma_{1yy}(X,0)}{P/(2a)}$	$\frac{\sigma_{1yy}(X,0)}{P/(2a)}$	$\varepsilon\%$	$\frac{\sigma_{1yy}(X,0)}{P/(2a)}$	$\varepsilon\%$	$\frac{\sigma_{1yy}(X,0)}{P/(2a)}$	$\varepsilon\%$	
-0.90	-1.49033	-1.51546	1.69	-1.58115	6.09	-1.67963	12.70	
-0.82	-1.15084	-1.16883	1.56	-1.21456	5.54	-1.28096	11.31	
-0.73	-0.96408	-0.97860	1.51	-1.01394	5.17	-1.06281	10.24	
-0.61	-0.85130	-0.86375	1.46	-0.89248	4.84	-0.92976	9.22	
-0.41	-0.75370	-0.76366	1.32	-0.78457	4.10	-0.80823	7.24	
-0.19	-0.70543	-0.71286	1.05	-0.72637	2.97	-0.73784	4.59	
0.04	-0.68979	-0.69424	0.65	-0.69980	1.45	-0.69915	1.36	
0.19	-0.69443	-0.69638	0.28	-0.69573	0.19	-0.68628	1.17	
0.41	-0.72697	-0.72413	0.39	-0.71219	2.03	-0.68773	5.40	
0.61	-0.80175	-0.79198	1.22	-0.76464	4.63	-0.72101	10.07	
0.73	-0.89031	-0.87370	1.87	-0.83165	6.59	-0.77044	13.46	
0.82	-1.03666	-1.00987	2.58	-0.94630	8.72	-0.85998	17.04	
0.90	-1.29819	-1.25414	3.39	-1.15463	11.06	-1.02724	20.87	

Table 5.11: Percent difference between elastostatic and elastodynamic lateral contact stresses $\Gamma_1 = 6$, $a/h_1 = 0.1$, $\eta = 0.3$, $\nu_1/\nu_2 = 1$.

X/a	$c_1 = 0.0$			$c_1 = 0.4$			$c_1 = 0.6$			$c_1 = 0.7$		
	$\frac{\sigma_{1xx}(X,0)}{P/(2a)}$	$\frac{\sigma_{1xx}(X,0)}{P/(2a)}$	$\varepsilon\%$	$\frac{\sigma_{1xx}(X,0)}{P/(2a)}$	$\frac{\sigma_{1xx}(X,0)}{P/(2a)}$	$\varepsilon\%$	$\frac{\sigma_{1xx}(X,0)}{P/(2a)}$	$\frac{\sigma_{1xx}(X,0)}{P/(2a)}$	$\varepsilon\%$	$\frac{\sigma_{1xx}(X,0)}{P/(2a)}$	$\frac{\sigma_{1xx}(X,0)}{P/(2a)}$	$\varepsilon\%$
-1.22	0.64722	0.73496	13.56	0.92832	43.43	1.18326	82.82					
-0.99	-4.83975	-5.81532	20.16	-8.20338	69.50	-11.78561	143.52					
-0.82	-0.95157	-1.10148	15.75	-1.44733	52.10	-1.92422	102.21					
-0.67	-0.69634	-0.79743	14.52	-1.02590	47.33	-1.33082	91.12					
-0.41	-0.55248	-0.62593	13.29	-0.78657	42.37	-0.98939	79.08					
-0.27	-0.51988	-0.58643	12.80	-0.72915	40.25	-0.90318	73.73					
-0.04	-0.50194	-0.56319	12.20	-0.69017	37.50	-0.83586	66.53					
0.27	-0.52434	-0.58491	11.55	-0.70406	34.28	-0.82770	57.86					
0.41	-0.55747	-0.62047	11.30	-0.74109	32.94	-0.85952	54.18					
0.67	-0.69090	-0.76625	10.91	-0.90275	30.66	-1.02171	47.88					
0.82	-0.90804	-1.00513	10.69	-1.17449	29.34	-1.30966	44.23					
0.99	-3.70072	-4.05950	9.69	-4.62106	24.87	-4.95856	33.99					
1.22	0.64722	0.73496	13.56	0.92832	43.43	1.18326	82.82					

5.2 Numerical Results for the Rigid Triangular Punch

The general schematic of the rigid triangular punch contact problem is illustrated in Figure 5.20. An FGM coating of thickness h_1 is perfectly bonded to a homogenous substrate. The rigid triangular punch slides over the FGM coating at a speed of V and θ denotes the inclination angle of the triangular punch.

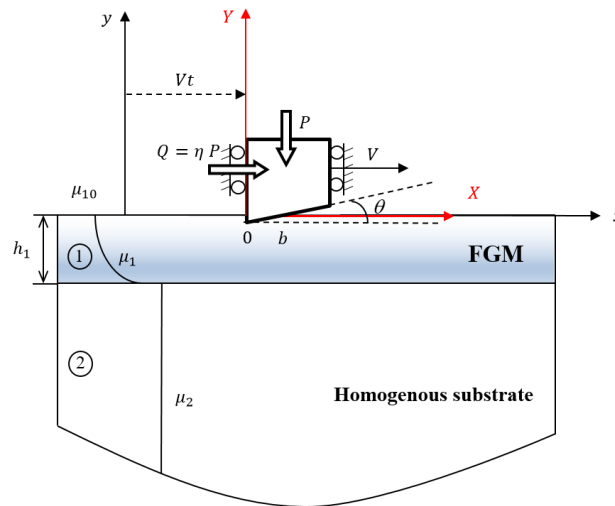


Figure 5.20: The schematic of the triangular punch on the surface of the FGM coating bonded to a homogenous substrate

Our results depicted in Figures 5.21 – 5.24 corresponding to elastostatic contact are verified by those presented by Guler [45]. It can be inferred from Figures 5.21 - 5.24 that an excellent agreement is achieved.

Figure 5.25 shows the effect of dimensionless punch speed c_1 on elastodynamic contact stresses due to a triangular punch for the half-plane problem. Normal contact stress is unbounded at the sharp trailing end, and zero at the leading end where there is a smooth contact. Figure 5.26 illustrates the effect of dimensionless punch speed c_1 on elastodynamic contact stresses for the half-plane in a frictional case. It can be inferred from Figures 5.25 - 5.26 that the influence of dimensionless punch speed on

normal contact stress is found to be significant. Normal contact stress tends to be less compressive as punch speed is increased. Increase in the punch speed slightly changes the lateral contact stress distribution as observed in Figure 5.25(b) and 5.26(b).

Figure 5.27 shows the effect of dimensionless punch speed c_1 on elastodynamic contact stresses for a softening coating ($\Gamma_1 = 1/6$). As punch speed is increased, the normal contact stress in the contact zone becomes less compressive and lateral contact stress becomes more compressive throughout the contact. Figure 5.28 depicts the effect of dimensionless punch speed on elastodynamic contact stresses for a stiffening coating ($\Gamma_1 = 6$). Higher punch speeds leads to less compressive normal contact stresses in the contact zone. The variation of the lateral contact stress with respect to punch speed is minimal. Slightly less compressive lateral stresses are formed around the leading end and lateral tensile stresses are slightly increased at the trailing end. Figures 5.29 – 5.32 illustrate the effect of dimensionless punch speed c_1 on elastodynamic contact stresses for different values of relative contact length shown by $b/h_1 = 0.2$, $b/h_1 = 0.4$. Although, the variation of the relative contact length influences elastodynamic contact stresses, the general trend of change with respect to punch speed is similar.

Figures 5.33 – 5.34 present the effect of coefficient of friction η on elastodynamic contact stresses in the case of softening and stiffening coatings, respectively. In both situations, normal elastodynamic contact stress in the contact zone tends to slant towards the trailing end due to the friction. The major influence of the coefficient of friction on lateral elastodynamic contact stress is the formation of high tensile stresses at the trailing end of the contact zone. Lateral contact stresses ahead of the contact zone is compressive. Thus, trailing end of the contact zone is critical for possible occurrence of cracking failure due to high lateral tensile stresses.

Representative results on the influence of the stiffness ratio Γ_1 on normal and lateral elastodynamic contact stresses are shown in Figures 5.35 – 5.36. As stiffness ratio Γ_1 is increased from 1/6 to 6, more compressive normal contact stresses are formed in the contact zone. Increase in the stiffness ratio leads to greater tensile lateral stresses behind the trailing end of the contact zone.

Figures 5.37 – 5.38 show the elastodynamic contact stresses as functions of b/h_1 for softening and stiffening coatings. In the case of a softening coating ($\Gamma_1 = 1/6$), as the ratio b/h_1 is increased from 0.1 to 0.5, normal contact stress becomes less compressive. Lateral contact stress also tends to become less compressive in the contact zone and more compressive around the trailing end of the contact. In the case of a stiffening coating ($\Gamma_1 = 6$) however, as the ratio b/h_1 is increased from 0.1 to 0.5, normal contact stress tends to be more compressive. The lateral contact stress becomes more compressive in the contact zone. Slightly greater lateral stresses are observed behind the trailing end.

Table 5.12 shows the normalized punch load for different values of the stiffness ratio Γ_1 and relative contact length b/h_1 in elastostatic case. In all cases, the normalized punch load increases gradually as b/h_1 is increased. Tables 5.13 – 5.15 show the normalized punch load for different values of stiffness ratio Γ_1 and dimensionless punch speed c_1 . It can be seen in tables that normalized punch load gradually decreases as punch speed c_1 is increased from 0.0 to 0.7. Tables 5.16 – 5.17 tabulate the normalized punch load for various values of coefficient of friction η and dimensionless punch speed c_1 . It can be seen in these tables that normalized punch load is greater for a stiffening coating than that generated for a softening coating. Moreover, the normalized load computed at higher coefficient of friction is greater

than that computed at frictionless case. In all cases, the normalized load gradually decreases as punch speed is increased from 0.0 to 0.7.

Table 5.18 tabulates the elastostatic normalized stress intensity factors computed for various values of stiffness ratio Γ_1 and coefficient of friction η . Results obtained in this study are in a very good agreement with those provided by Guler [45].

Table 5.19 show the normalized stress intensity factor $K_I(0)$ evaluated at the sharp corner of the triangular punch for various values of stiffness ratio Γ_1 and relative contact length b/h_1 in elastostatic case. Normalized stress intensity factors for the softening coating decreases as b/h_1 is increased, however normalized stress intensity factor for the stiffening coating increases as b/h_1 is increased. Tables 5.20 and 5.21 show normalized elastodynamic stress intensity factors for different values of stiffness ratio Γ_1 and dimensionless punch speed c_1 . In all cases, the mode I SIF is a decreasing function of the punch speed c_1 . Tables 5.22 and 5.23 show the mode I SIFs for various values of coefficient of friction η and dimensionless punch speed c_1 . Again, in all cases, the mode I SIF is a decreasing function of dimensionless punch speed c_1 .

Tables 5.24 – 5.27 provide tabulated results on percent differences between contact stresses computed considering elastostatic and elastodynamic conditions. Contact stresses are calculated for four different values of dimensionless punch speed c_1 . The $c_1 = 0$ condition indicates elastostatic contact whereas $c_1 > 0$ condition indicates elastodynamic contact. Percent difference $\varepsilon\%$ is calculated based on elastostatic contact stress results. Tables 5.24 – 5.25 show percent differences between elastodynamic and elastostatic normal and lateral contact stresses in the case of a softening coating ($\Gamma_1 = 1/6$). As punch speed c_1 is increased, percent differences

gradually increase. The largest difference in the normal contact stress distribution is observed near the leading end of the contact. However, the largest difference in the lateral contact stress is observed behind the trailing end of the contact. Tables 5.26 - 5.27 show percent differences in the case of a stiffening coating ($\Gamma_1 = 6$). Percent differences for the normal and lateral contact stresses gradually increase as punch speed is increased from 0.0 to 0.7. The largest difference in the normal contact stress is observed around the leading end of the contact. However, the largest difference in the lateral contact stress is observed ahead of the contact.

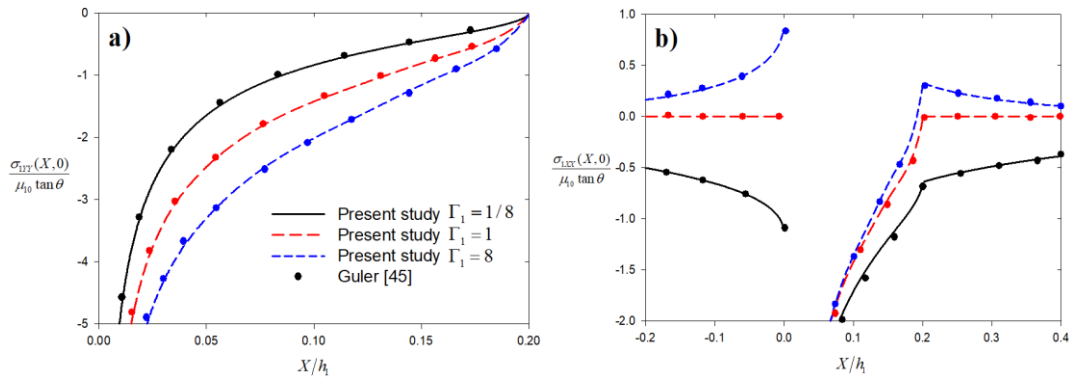


Figure 5.21: Normal and lateral contact stress distribution on FGM coating indented by a triangular punch for different stiffness ratio of the coating (a) Normal contact stress distribution; (b) Lateral contact stress distribution, $b/h_1 = 0.2$, $\eta = 0.0$, $c_1 = 0.0$.

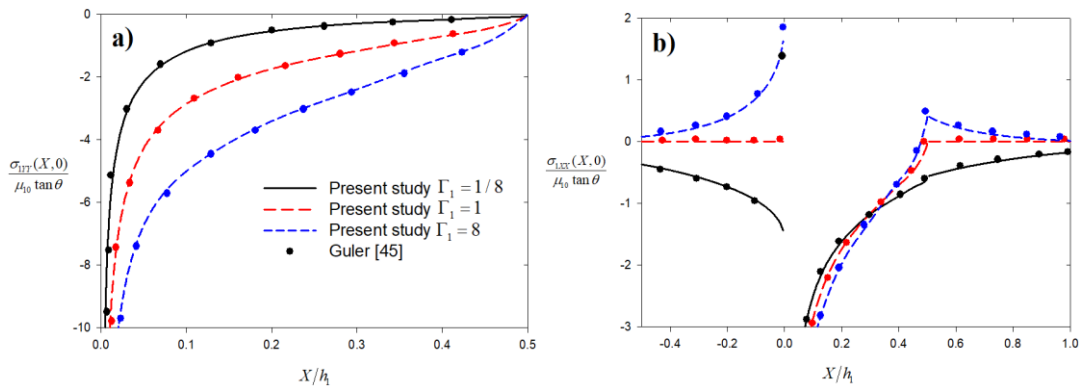


Figure 5.22: Normal and lateral contact stress distribution on FGM coating indented by a triangular punch for different stiffness ratio of the coating (a) Normal contact stress distribution; (b) Lateral contact stress distribution, $b/h_1 = 0.5$, $\eta = 0.0$, $c_1 = 0.0$.

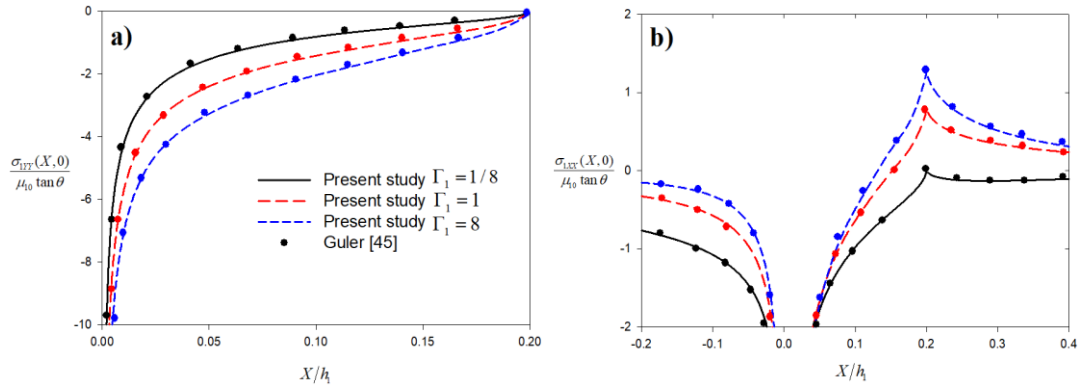


Figure 5.23: Normal and lateral contact stress distribution on FGM coating indented by a frictional triangular punch for different stiffness ratio of the coating (a) Normal contact stress distribution; (b) Lateral contact stress distribution, $b/h_1 = 0.2$, $\eta = 0.3$, $c_1 = 0.0$.

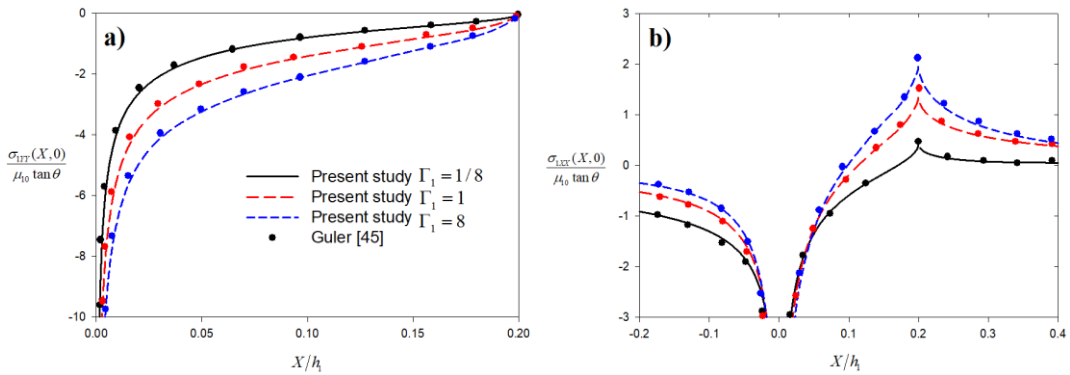


Figure 5.24: Normal and lateral contact stress distribution on FGM coating indented by a frictional triangular punch for different stiffness ratio of the coating (a) Normal contact stress distribution; (b) Lateral contact stress distribution, $b/h_1 = 0.2$, $\eta = 0.5$, $c_1 = 0.0$.

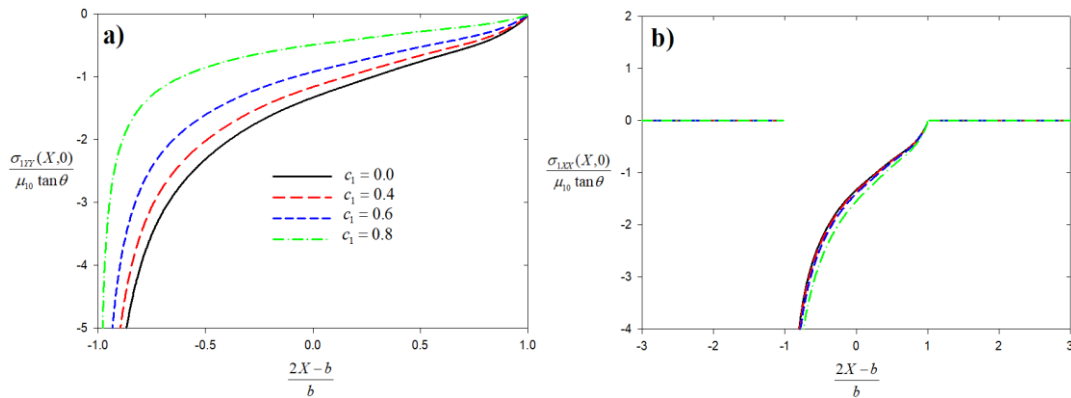


Figure 5.25: Normal and lateral elastodynamic contact stresses on FGM coating indented by a moving triangular punch for various values of punch speed (a) Normal contact stress distribution; (b) Lateral contact stress distribution, $b/h_1 = 0.1$, $\Gamma_1 = 1$, $\eta = 0.0$, $v_1/v_2 = 1$.

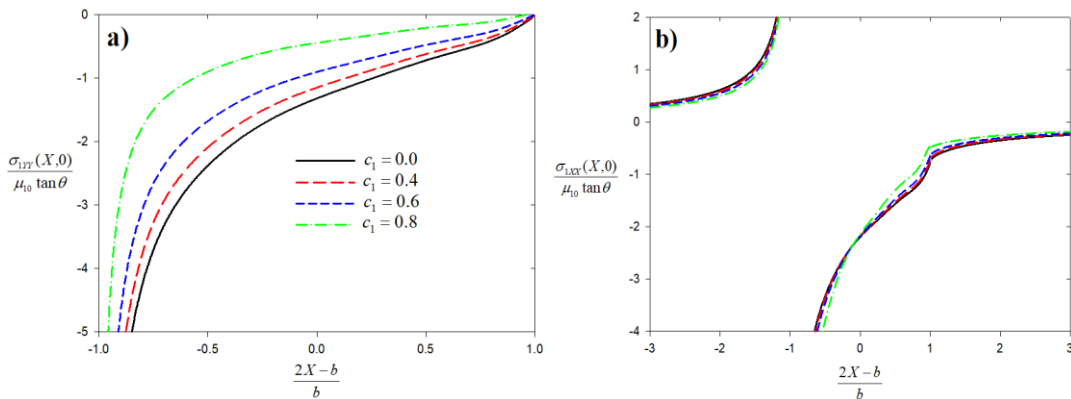


Figure 5.26: Normal and lateral elastodynamic contact stresses on FGM coating indented by a moving triangular punch for various values of punch speed (a) Normal contact stress distribution; (b) Lateral contact stress distribution, $b/h_1 = 0.1$, $\Gamma_1 = 1$, $\eta = 0.3$, $v_1/v_2 = 1$.

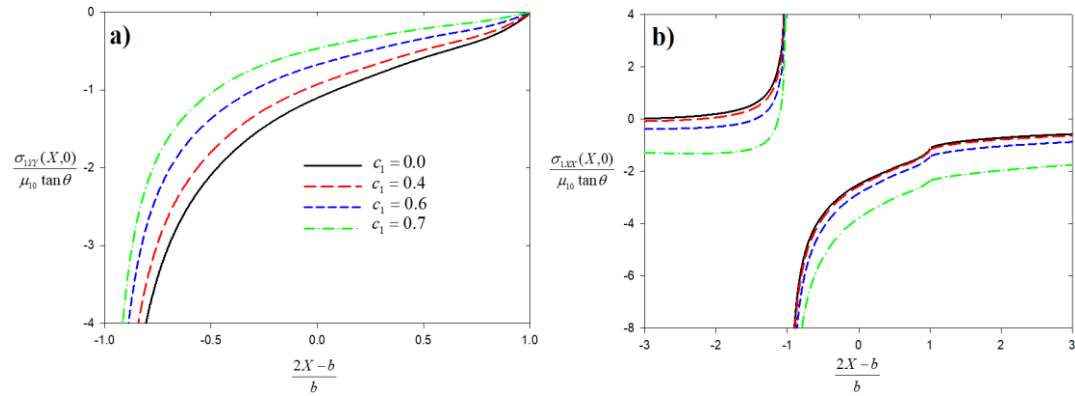


Figure 5.27: Normal and lateral elastodynamic contact stresses on FGM coating indented by a moving triangular punch for various values of punch speed (a) Normal contact stress distribution; (b) Lateral contact stress distribution, $b/h_1 = 0.1$, $\Gamma_1 = 1/6$, $\eta = 0.3$, $\nu_1/\nu_2 = 1$.

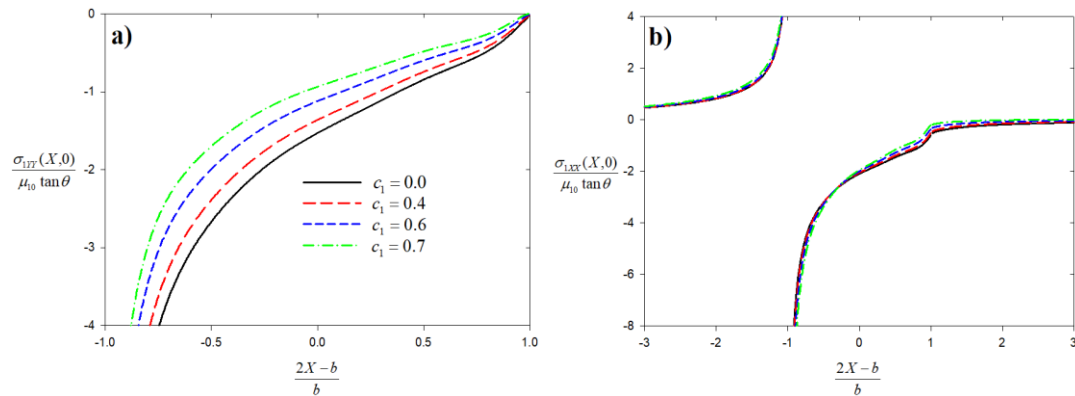


Figure 5.28: Normal and lateral elastodynamic contact stresses on FGM coating indented by a moving triangular punch for various values of punch speed (a) Normal contact stress distribution; (b) Lateral contact stress distribution, $b/h_1 = 0.1$, $\Gamma_1 = 6$, $\eta = 0.3$, $\nu_1/\nu_2 = 1$.

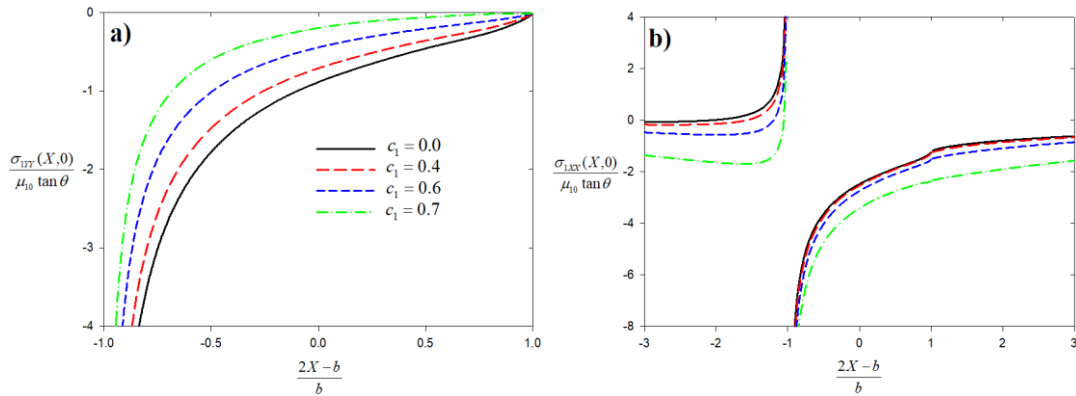


Figure 5.29: Normal and lateral elastodynamic contact stresses on FGM coating indented by a moving triangular punch for various values of punch speed (a) Normal contact stress distribution; (b) Lateral contact stress distribution, $b/h_1 = 0.2$, $\Gamma_1 = 1/6$, $\eta = 0.3$, $\nu_1/\nu_2 = 1$.

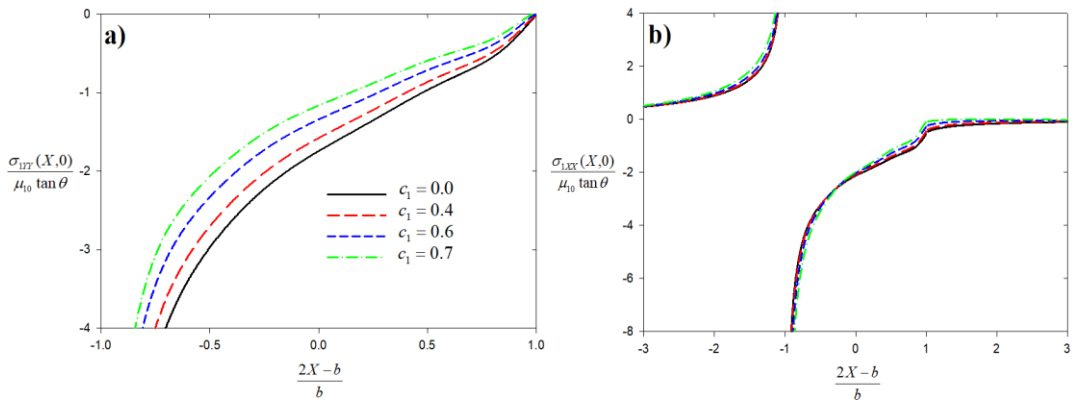


Figure 5.30: Normal and lateral elastodynamic contact stresses on FGM coating indented by a moving triangular punch for various values of punch speed (a) Normal contact stress distribution; (b) Lateral contact stress distribution, $b/h_1 = 0.2$, $\Gamma_1 = 6$, $\eta = 0.3$, $\nu_1/\nu_2 = 1$.

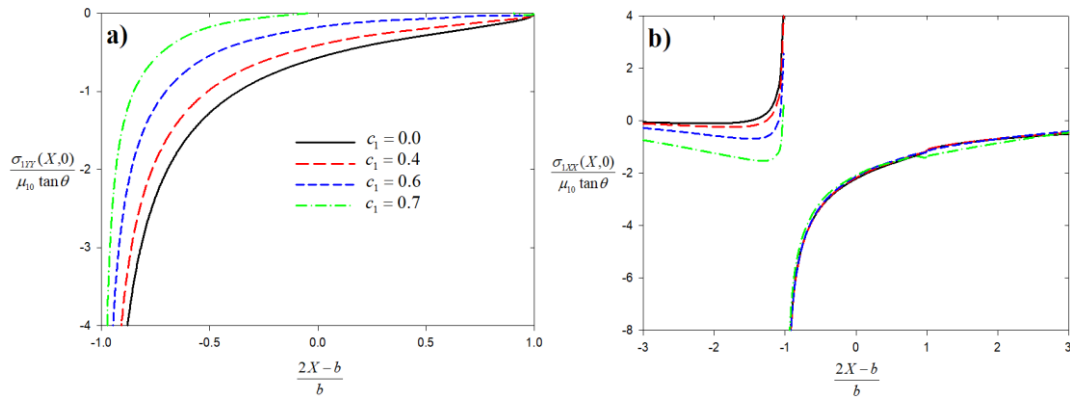


Figure 5.31: Normal and lateral elastodynamic contact stresses on FGM coating indented by a moving triangular punch for various values of punch speed (a) Normal contact stress distribution; (b) Lateral contact stress distribution, $b/h_1 = 0.4$, $\Gamma_1 = 1/6$, $\eta = 0.3$, $\nu_1/\nu_2 = 1$.

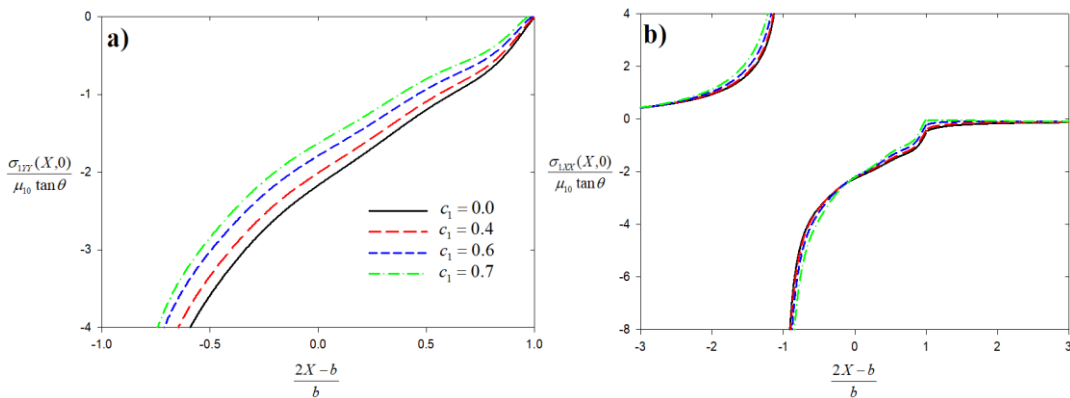


Figure 5.32: Normal and lateral elastodynamic contact stresses on FGM coating indented by a moving triangular punch for various values of punch speed (a) Normal contact stress distribution; (b) Lateral contact stress distribution, $b/h_1 = 0.4$, $\Gamma_1 = 6$, $\eta = 0.3$, $\nu_1/\nu_2 = 1$.

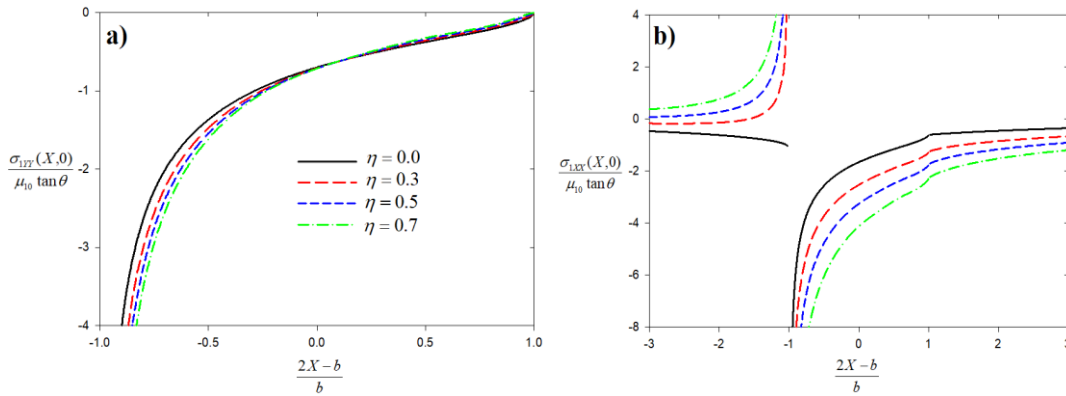


Figure 5.33: Normal and lateral elastodynamic contact stresses on FGM coating indented by a moving triangular punch for various values of coefficient of friction (a) Normal contact stress distribution; (b) Lateral contact stress distribution, $b/h_1 = 0.2$, $\Gamma_1 = 1/6$, $c_1 = 0.4$, $\nu_1/\nu_2 = 1$.

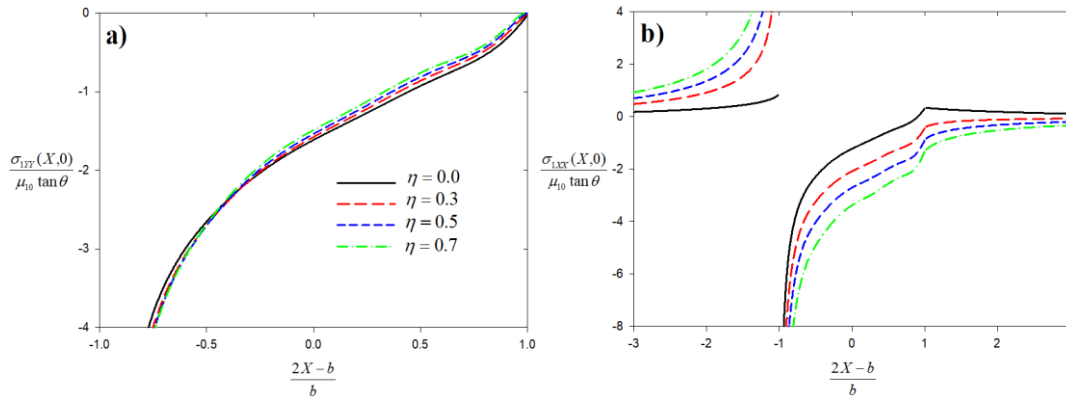


Figure 5.34: Normal and lateral elastodynamic contact stresses on FGM coating indented by a moving triangular punch for various values of coefficient of friction (a) Normal contact stress distribution; (b) Lateral contact stress distribution, $b/h_1 = 0.2$, $\Gamma_1 = 6$, $c_1 = 0.4$, $\nu_1/\nu_2 = 1$.

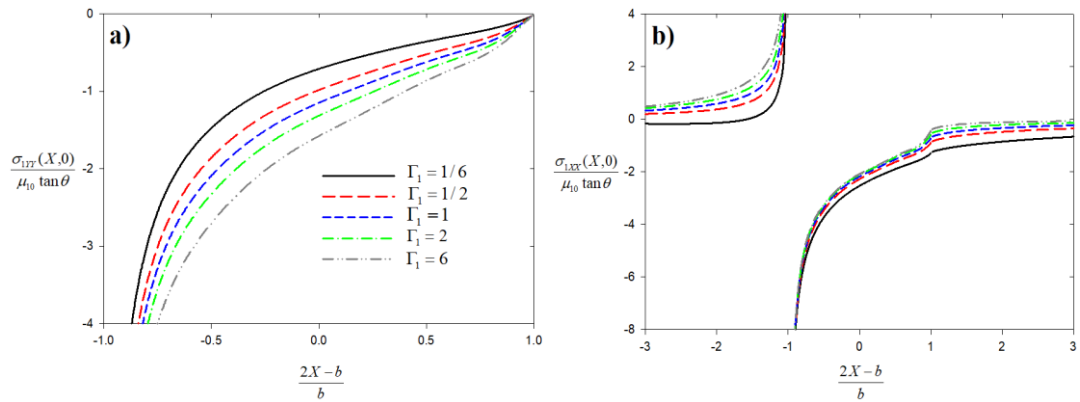


Figure 5.35: Normal and lateral elastodynamic contact stresses on FGM coating indented by a moving triangular punch for various values of stiffness ratio (a) Normal contact stress distribution; (b) Lateral contact stress distribution, $b/h_1 = 0.2$, $\eta = 0.3$, $c_1 = 0.4$, $\nu_1/\nu_2 = 1$.

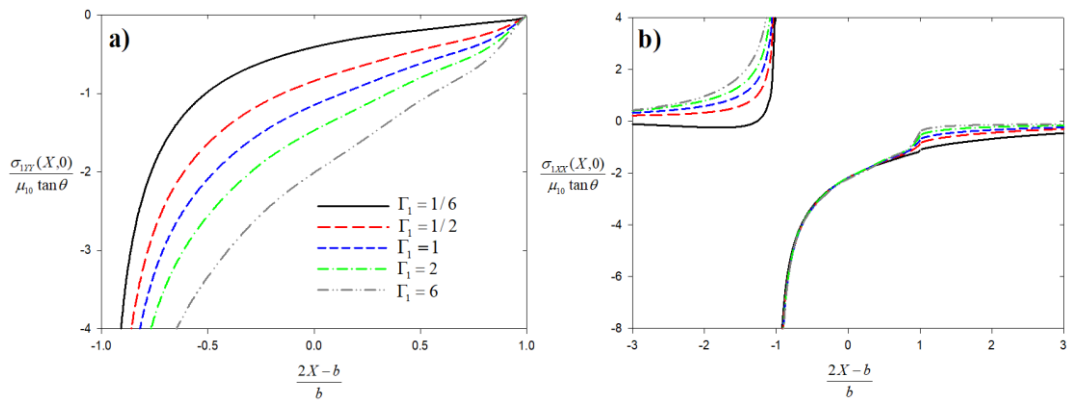


Figure 5.36: Normal and lateral elastodynamic contact stresses on FGM coating indented by a moving triangular punch for various values of stiffness ratio (a) Normal contact stress distribution; (b) Lateral contact stress distribution, $b/h_1 = 0.4$, $\eta = 0.3$, $c_1 = 0.4$, $\nu_1/\nu_2 = 1$.

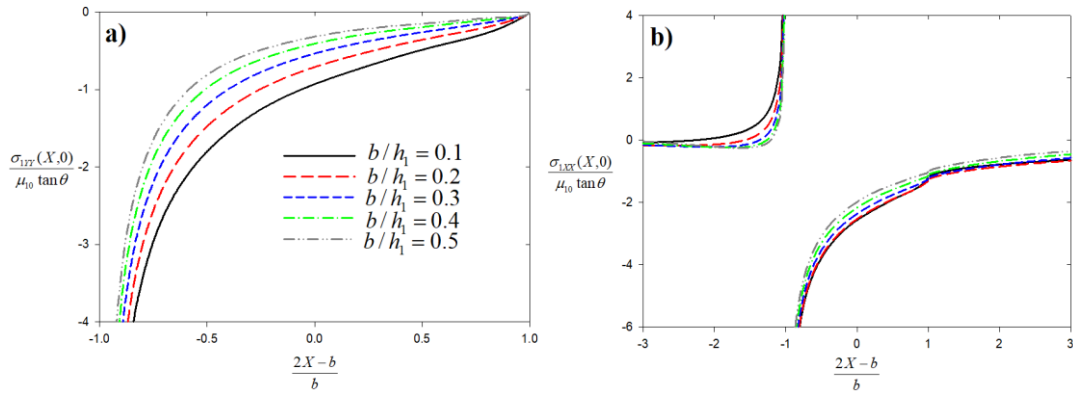


Figure 5.37: Normal and lateral elastodynamic contact stresses on FGM coating indented by a moving triangular punch for various values of relative coating thickness (a) Normal contact stress distribution; (b) Lateral contact stress distribution, $\Gamma_1 = 1/6$, $\eta = 0.3$, $c_1 = 0.4$, $\nu_1/\nu_2 = 1$.

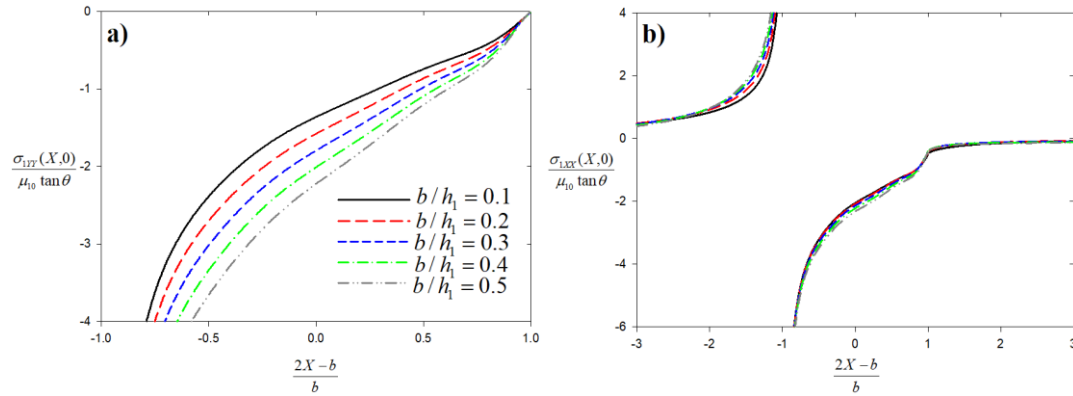


Figure 5.38: Normal and lateral elastodynamic contact stresses on FGM coating indented by a moving triangular punch for various values of relative coating thickness (a) Normal contact stress distribution; (b) Lateral contact stress distribution, $\Gamma_1 = 6$, $\eta = 0.3$, $c_1 = 0.4$, $\nu_1/\nu_2 = 1$.

Table 5.12: The normalized load for FGM coating indented by a moving triangular punch $c_1 = 0$, $\eta = 0.0$, $\nu_1 / \nu_2 = 1.0$.

Γ_1	$b/h_1 = 0.1$	$b/h_1 = 0.2$	$b/h_1 = 0.3$	$b/h_1 = 0.4$
	$\frac{P}{\mu_1 \tan(\theta)}$	$\frac{P}{\mu_1 \tan(\theta)}$	$\frac{P}{\mu_1 \tan(\theta)}$	$\frac{P}{\mu_1 \tan(\theta)}$
1/6	0.181066	0.313938	0.411790	0.485992
1/2	0.198217	0.377717	0.541621	0.692910
1	0.208467	0.416952	0.625428	0.883905
2	0.218419	0.455422	0.709475	0.979108
6	0.233716	0.515125	0.842102	1.213105

Table 5.13: The normalized load for FGM coating indented by a moving triangular punch $b/h_1 = 0.2$, $\eta = 0.3$, $\nu_1 / \nu_2 = 1$.

Γ_1	$c_1 = 0.0$	$c_1 = 0.2$	$c_1 = 0.4$	$c_1 = 0.6$	$c_1 = 0.7$
	$\frac{P}{\mu_1 \tan(\theta)}$	$\frac{P}{\mu_1 \tan(\theta)}$	$\frac{P}{\mu_1 \tan(\theta)}$	$\frac{P}{\mu_1 \tan(\theta)}$	$\frac{P}{\mu_1 \tan(\theta)}$
1/6	0.349818	0.337109	0.296464	0.216059	0.143286
1/2	0.407394	0.395100	0.356197	0.282155	0.224397
1	0.442468	0.430300	0.391993	0.320205	0.265858
2	0.477110	0.465168	0.427734	0.358484	0.307449
6	0.531803	0.520139	0.483884	0.418673	0.373801

Table 5.14: The normalized load for FGM coating indented by a moving triangular punch $b/h_1 = 0.4$, $\eta = 0.3$, $\nu_1 / \nu_2 = 1$.

Γ_1	$c_1 = 0.0$	$c_1 = 0.2$	$c_1 = 0.4$	$c_1 = 0.6$	$c_1 = 0.7$
	$\frac{P}{\mu_1 \tan(\theta)}$	$\frac{P}{\mu_1 \tan(\theta)}$	$\frac{P}{\mu_1 \tan(\theta)}$	$\frac{P}{\mu_1 \tan(\theta)}$	$\frac{P}{\mu_1 \tan(\theta)}$
1/6	0.538183	0.512978	0.432209	0.272091	0.128836
1/2	0.747916	0.723165	0.644545	0.493407	0.373639
1	0.884936	0.860600	0.783986	0.640411	0.531718
2	1.023374	0.999804	0.926129	0.791055	0.693514
6	1.244415	1.222238	1.154484	1.040316	0.976631

Table 5.15: The normalized load for FGM coating indented by a moving triangular punch $b/h_1 = 0.4$, $\eta = 0.3$, $\nu_1/\nu_2 = 1.0$.

	$c_1 = 0.0$	$c_1 = 0.2$	$c_1 = 0.4$	$c_1 = 0.6$	$c_1 = 0.7$
Γ_1	$\frac{P}{\mu_1 \tan(\theta)}$	$\frac{P}{\mu_1 \tan(\theta)}$	$\frac{P}{\mu_1 \tan(\theta)}$	$\frac{P}{\mu_1 \tan(\theta)}$	$\frac{P}{\mu_1 \tan(\theta)}$
1/6	0.599161	0.568709	0.471517	0.281768	0.119851
1/2	0.899356	0.868485	0.770338	0.581381	0.431607
1	1.106170	1.075750	0.979982	0.800513	0.664647
2	1.320054	1.290668	1.198876	1.030899	0.910100
6	1.666611	1.639630	1.558066	1.426529	1.365757

Table 5.16: The normalized load for FGM coating indented by a moving triangular punch $b/h_1 = 0.2$, $\Gamma_1 = 1/6$, $\nu_1/\nu_2 = 1.0$.

	$c_1 = 0.0$	$c_1 = 0.2$	$c_1 = 0.4$	$c_1 = 0.6$	$c_1 = 0.7$
η	$\frac{P}{\mu_1 \tan(\theta)}$	$\frac{P}{\mu_1 \tan(\theta)}$	$\frac{P}{\mu_1 \tan(\theta)}$	$\frac{P}{\mu_1 \tan(\theta)}$	$\frac{P}{\mu_1 \tan(\theta)}$
0.0	0.313938	0.301066	0.260152	0.180692	0.110262
0.3	0.349818	0.337109	0.296464	0.216590	0.143286
0.5	0.376502	0.364048	0.324115	0.244719	0.174903
0.7	0.405628	0.393574	0.354898	0.278460	0.219114

Table 5.17: The normalized load for FGM coating indented by a moving triangular punch $b/h_1 = 0.2$, $\Gamma_1 = 6$, $\nu_1/\nu_2 = 1.0$.

	$c_1 = 0.0$	$c_1 = 0.2$	$c_1 = 0.4$	$c_1 = 0.6$	$c_1 = 0.7$
η	$\frac{P}{\mu_1 \tan(\theta)}$	$\frac{P}{\mu_1 \tan(\theta)}$	$\frac{P}{\mu_1 \tan(\theta)}$	$\frac{P}{\mu_1 \tan(\theta)}$	$\frac{P}{\mu_1 \tan(\theta)}$
0.0	0.515125	0.502385	0.462175	0.386338	0.328552
0.3	0.531803	0.520140	0.483884	0.418674	0.373801
0.5	0.541026	0.529920	0.495650	0.435226	0.394724
0.7	0.548607	0.537903	0.504979	0.446951	0.406343

Table 5.18: Normalized stress intensity factors for the moving rigid triangular punch
 $b/h_1 = 0.2$, $c_1 = 0.0$.

	$\eta = 0.0$		$\eta = 0.1$		$\eta = 0.3$		$\eta = 0.5$	
Γ_1	$K_I(0)$	$K_I^*(0)$	$K_I(0)$	$K_I^*(0)$	$K_I(0)$	$K_I^*(0)$	$K_I(0)$	$K_I^*(0)$
1/8	1.1976	1.1912	1.1740	1.1677	1.1283	1.1224	1.0844	1.0789
1/2	1.3530	1.3550	1.3452	1.3467	1.3270	1.3279	1.3058	1.3063
1	1.4220	1.4286	1.4218	1.4280	1.4183	1.4234	1.4100	1.4142
2	1.4862	1.4976	1.4933	1.5041	1.5033	1.5128	1.5076	1.5160
8	1.6029	1.6247	1.6219	1.6430	1.6554	1.6751	1.6823	1.7005

Note that K_I^* value shows the normalized stress intensity factor presented by Guler [45].

Table 5.19: Normalized stress intensity factors for the moving triangular punch
 $c_1 = 0$, $\eta = 0.0$, $\nu_1/\nu_2 = 1.0$.

	$b/h_1 = 0.1$	$b/h_1 = 0.2$	$b/h_1 = 0.3$	$b/h_1 = 0.4$
Γ_1	$K_I(0)$	$K_I(0)$	$K_I(0)$	$K_I(0)$
1/6	1.2396	1.1563	1.0831	1.0204
1/2	1.2952	1.2652	1.2379	1.2134
1	1.3272	1.3272	1.3272	1.3272
2	1.3574	1.3848	1.4101	1.4336
6	1.4023	1.4689	1.5301	1.5867

Table 5.20: Normalized stress intensity factors for the moving triangular punch
 $b/h_1 = 0.2$, $\eta = 0.3$, $\nu_1/\nu_2 = 1.0$.

	$c_1 = 0.0$	$c_1 = 0.2$	$c_1 = 0.4$	$c_1 = 0.6$	$c_1 = 0.7$
Γ_1	$K_I(0)$	$K_I(0)$	$K_I(0)$	$K_I(0)$	$K_I(0)$
1/6	1.2114	1.1696	1.0360	0.7742	0.5549
1/2	1.2796	1.2386	1.1084	0.8579	0.6629
1	1.3183	1.2775	1.1482	0.9030	0.7141
2	1.3557	1.3153	1.1880	0.9488	0.7676
6	1.4132	1.3733	1.2480	1.0166	0.8481

Table 5.21: Normalized stress intensity factors for the moving triangular punch
 $b/h_1 = 0.4$, $\eta = 0.3$, $\nu_1/\nu_2 = 1.0$.

	$c_1 = 0.0$	$c_1 = 0.2$	$c_1 = 0.4$	$c_1 = 0.6$	$c_1 = 0.7$
Γ_1	$K_I(0)$	$K_I(0)$	$K_I(0)$	$K_I(0)$	$K_I(0)$
1/6	1.0665	1.0233	0.8839	0.6042	0.3511
1/2	1.2300	1.1887	1.0570	0.8022	0.5995
1	1.3183	1.2775	1.1482	0.9030	0.7141
2	1.3978	1.3578	1.2322	0.9977	0.8226
6	1.5106	1.4716	1.3501	1.1334	0.9897

Table 5.22: Normalized stress intensity factors for the moving triangular punch
 $b/h_1 = 0.2$, $\Gamma_1 = 1/6$, $\nu_1/\nu_2 = 1.0$.

	$c_1 = 0.0$	$c_1 = 0.2$	$c_1 = 0.4$	$c_1 = 0.6$	$c_1 = 0.7$
η	$K_I(0)$	$K_I(0)$	$K_I(0)$	$K_I(0)$	$K_I(0)$
0.0	1.1563	1.1152	0.9846	0.7320	0.5135
0.3	1.2114	1.1696	1.0360	0.7742	0.5549
0.5	1.2476	1.2052	1.0690	0.8006	0.5890
0.7	1.2835	1.2405	1.1016	0.8281	0.6387

Table 5.23: Normalized stress intensity factors for the moving triangular punch
 $b/h_1 = 0.2$, $\Gamma_1 = 6$, $\nu_1/\nu_2 = 1.0$.

	$c_1 = 0.0$	$c_1 = 0.2$	$c_1 = 0.4$	$c_1 = 0.6$	$c_1 = 0.7$
η	$K_I(0)$	$K_I(0)$	$K_I(0)$	$K_I(0)$	$K_I(0)$
0.0	1.4689	1.4282	1.2997	1.0572	0.8722
0.3	1.4132	1.3733	1.2480	1.0166	0.8481
0.5	1.3681	1.3280	1.2022	0.9699	0.7993
0.7	1.3180	1.2773	1.1495	0.9117	0.7326

Table 5.24: Percent difference between elastostatic and elastodynamic normal contact stresses $\Gamma_1 = 1/6$, $b/h_1 = 0.2$, $\eta = 0.3$, $\nu_1/\nu_2 = 1.0$.

$\frac{2X-b}{b}$	$c_1 = 0.0$			$c_1 = 0.4$			$c_1 = 0.6$			$c_1 = 0.7$		
	$\frac{\sigma_{iyy}(X,0)}{\mu_0 \tan \theta}$	$\frac{\sigma_{iyy}(X,0)}{\mu_0 \tan \theta}$	$\varepsilon\%$	$\frac{\sigma_{iyy}(X,0)}{\mu_0 \tan \theta}$	$\frac{\sigma_{iyy}(X,0)}{\mu_0 \tan \theta}$	$\varepsilon\%$	$\frac{\sigma_{iyy}(X,0)}{\mu_0 \tan \theta}$	$\frac{\sigma_{iyy}(X,0)}{\mu_0 \tan \theta}$	$\varepsilon\%$	$\frac{\sigma_{iyy}(X,0)}{\mu_0 \tan \theta}$	$\frac{\sigma_{iyy}(X,0)}{\mu_0 \tan \theta}$	$\varepsilon\%$
-0.94	-7.18099	-6.25644	12.88	-4.85800	32.35	-3.61439	49.67					
-0.82	-3.78496	-3.23764	14.46	-2.41106	36.30	-1.68226	55.55					
-0.70	-2.65689	-2.24294	15.58	-1.61797	39.10	-1.06442	59.94					
-0.61	-2.16614	-1.81207	16.35	-1.27724	41.04	-0.79995	63.07					
-0.50	-1.79277	-1.48615	17.10	-1.02293	42.94	-0.60670	66.16					
-0.22	-1.16276	-0.94407	18.81	-0.61444	47.16	-0.31468	72.94					
-0.03	-0.91985	-0.73799	19.77	-0.46359	49.60	-0.21003	77.17					
0.22	-0.67989	-0.53719	20.99	-0.32151	52.71	-0.11795	82.65					
0.50	-0.45428	-0.35399	22.08	-0.20295	55.32	-0.05922	86.96					
0.61	-0.38547	-0.29879	22.49	-0.16812	56.39	-0.04255	88.96					
0.70	-0.32473	-0.25023	22.94	-0.13769	57.60	-0.02834	91.27					
0.82	-0.23608	-0.18053	23.53	-0.09707	58.88	-0.01655	92.99					
0.94	-0.11627	-0.08899	23.46	-0.04991	57.08	-0.01671	85.62					

Table 5.25: Percent difference between elastostatic and elastodynamic lateral contact stresses $\Gamma_1 = 1/6$, $b/h_1 = 0.2$, $\eta = 0.3$, $\nu_1/\nu_2 = 1.0$.

$\frac{2X-b}{b}$	$c_1 = 0.0$			$c_1 = 0.4$			$c_1 = 0.6$			$c_1 = 0.7$		
	$\frac{\sigma_{lxx}(X,0)}{\mu_0 \tan \theta}$	$\frac{\sigma_{lxx}(X,0)}{\mu_0 \tan \theta}$	$\varepsilon\%$	$\frac{\sigma_{lxx}(X,0)}{\mu_0 \tan \theta}$	$\frac{\sigma_{lxx}(X,0)}{\mu_0 \tan \theta}$	$\varepsilon\%$	$\frac{\sigma_{lxx}(X,0)}{\mu_0 \tan \theta}$	$\frac{\sigma_{lxx}(X,0)}{\mu_0 \tan \theta}$	$\varepsilon\%$	$\frac{\sigma_{lxx}(X,0)}{\mu_0 \tan \theta}$	$\frac{\sigma_{lxx}(X,0)}{\mu_0 \tan \theta}$	$\varepsilon\%$
-1.50	0.26384	0.05659	78.55	-0.47514	280.09	-1.67926	736.47					
-1.22	0.85837	0.58393	31.97	-0.07559	108.81	-1.42666	266.20					
-0.99	-19.36992	-20.30565	4.83	-22.19170	14.57	-24.09914	24.42					
-0.82	-5.93585	-6.14285	3.49	-6.62583	11.62	-7.49011	26.18					
-0.50	-3.64327	-3.74640	2.83	-4.03917	10.87	-4.75911	30.63					
-0.22	-2.84994	-2.92070	2.48	-3.15821	10.82	-3.84480	34.91					
-0.03	-2.51961	-2.57789	2.31	-2.79393	10.89	-3.46550	37.54					
0.22	-2.18247	-2.22757	2.07	-2.42109	10.93	-3.07740	41.01					
0.50	-1.85202	-1.89042	2.07	-2.07840	12.22	-2.75531	48.77					
0.82	-1.53457	-1.56993	2.30	-1.76014	14.70	-2.47017	60.97					
0.99	-1.27760	-1.32842	3.98	-1.56337	22.37	-2.37897	86.21					
1.22	-1.03518	-1.10335	6.58	-1.36657	32.01	-2.21758	114.22					
1.50	-0.92149	-0.98893	7.32	-1.24699	35.32	-2.09137	126.95					

Table 5.26: Percent difference between elastostatic and elastodynamic normal contact stresses $\Gamma_1 = 6$, $b/h_1 = 0.2$, $\eta = 0.3$, $\nu_1/\nu_2 = 1.0$.

$\frac{2X-b}{b}$	$c_1 = 0.0$		$c_1 = 0.4$		$c_1 = 0.6$		$c_1 = 0.7$	
	$\frac{\sigma_{1YY}(X,0)}{\mu_0 \tan \theta}$	$\frac{\sigma_{1YY}(X,0)}{\mu_0 \tan \theta}$	$\frac{\sigma_{1YY}(X,0)}{\mu_0 \tan \theta}$	$\varepsilon\%$	$\frac{\sigma_{1YY}(X,0)}{\mu_0 \tan \theta}$	$\varepsilon\%$	$\frac{\sigma_{1YY}(X,0)}{\mu_0 \tan \theta}$	$\varepsilon\%$
-0.94	-9.10464	-8.30622	8.77	-7.25190	20.35	-6.57716	27.76	
-0.82	-5.26412	-4.78574	9.09	-4.14130	21.33	-3.70735	29.57	
-0.70	-3.98568	-3.62135	9.14	-3.12596	21.57	-2.78468	30.13	
-0.61	-3.42934	-3.11652	9.12	-2.68907	21.59	-2.39101	30.28	
-0.50	-2.98896	-2.71613	9.13	-2.34100	21.68	-2.07549	30.56	
-0.22	-2.14841	-1.94694	9.38	-1.66383	22.56	-1.45367	32.34	
-0.03	-1.79313	-1.62261	9.51	-1.38064	23.00	-1.19754	33.22	
0.22	-1.40523	-1.26795	9.77	-1.07057	23.81	-0.91761	34.70	
0.50	-0.95852	-0.85687	10.61	-0.70752	26.19	-0.58754	38.70	
0.61	-0.81920	-0.73034	10.85	-0.59937	26.83	-0.49380	39.72	
0.70	-0.69789	-0.62104	11.01	-0.50764	27.26	-0.41628	40.35	
0.82	-0.50435	-0.44517	11.73	-0.35699	29.22	-0.28494	43.50	
0.94	-0.20946	-0.17570	16.12	-0.12333	41.12	-0.07790	62.81	

Table 5.27: Percent difference between elastostatic and elastodynamic lateral contact stresses $\Gamma_1 = 6$, $b/h_1 = 0.2$, $\eta = 0.3$, $\nu_1/\nu_2 = 1.0$.

$\frac{2X-b}{b}$	$c_1 = 0.0$		$c_1 = 0.4$		$c_1 = 0.6$		$c_1 = 0.7$	
	$\frac{\sigma_{1XX}(X,0)}{\mu_0 \tan \theta}$	$\frac{\sigma_{1XX}(X,0)}{\mu_0 \tan \theta}$	$\frac{\sigma_{1XX}(X,0)}{\mu_0 \tan \theta}$	$\varepsilon\%$	$\frac{\sigma_{1XX}(X,0)}{\mu_0 \tan \theta}$	$\varepsilon\%$	$\frac{\sigma_{1XX}(X,0)}{\mu_0 \tan \theta}$	$\varepsilon\%$
-1.50	1.49612	1.53738	2.76	1.65124	10.37	1.82493	21.98	
-1.22	2.52700	2.58613	2.34	2.77076	9.65	3.07694	21.76	
-0.99	-20.37155	-21.74252	6.73	-25.13117	23.36	-30.05751	47.55	
-0.82	-5.49769	-5.64149	2.62	-6.04219	9.90	-6.64494	20.87	
-0.50	-3.24140	-3.25329	0.37	-3.33471	2.88	-3.48834	7.62	
-0.22	-2.47861	-2.45020	1.15	-2.43186	1.89	-2.44348	1.42	
-0.03	-2.16136	-2.11985	1.92	-2.06929	4.26	-2.03684	5.76	
0.22	-1.84749	-1.79474	2.86	-1.71678	7.07	-1.64818	10.79	
0.50	-1.46660	-1.39626	4.80	-1.27633	12.97	-1.15229	21.43	
0.82	-1.08769	-1.00694	7.42	-0.86564	20.42	-0.72148	33.67	
0.99	-0.60606	-0.50543	16.60	-0.32198	46.87	-0.13030	78.50	
1.22	-0.31137	-0.24334	21.85	-0.12619	59.47	-0.01527	95.10	
1.50	-0.22307	-0.16836	24.53	-0.07612	65.88	0.00833	103.74	

5.3 Numerical Results for the Rigid Semi-circular Punch

The general schematic of the rigid semi-circular punch contact problem is illustrated in Figure 5.39. An FGM coating of thickness h_1 is perfectly bonded to a homogenous substrate. The rigid semi-circular punch slides over the FGM coating at a speed of V . R_1 shows the radius of the semi-circular punch.

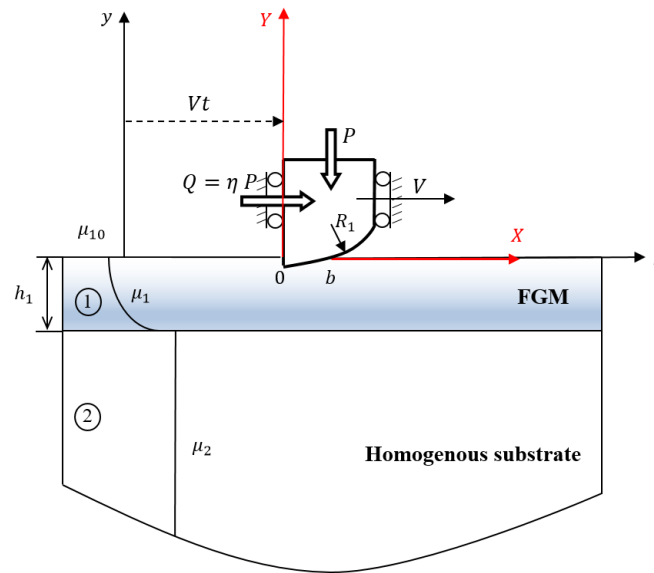


Figure 5.39: The schematic of the semi-circular punch on the surface of the FGM coating bonded to a homogenous substrate

Figures 5.40 – 5.41 illustrate the comparison of contact stresses computed by the present analytical method to those provided by Guler [45] for the case of elastostatic contact. The results are calculated by assuming $V = 0$ and using three different values of the stiffness ratio Γ_1 . It can be seen that contact stresses evaluated by the present analytical method are in excellent agreement with those provided by Guler [45].

Figures 5.42 and 5.43 show frictionless and frictional elastodynamic contact stresses for different values of dimensionless punch speed c_1 in half-plane contacts respectively. For both cases, as punch speed c_1 is increased, less compressive normal

contact stress is obtained in the contact zone. When elastodynamic lateral contact stresses are examined, the magnitude of lateral contact stress increases in the contact zone and surface outside the contact zone is stress free. However, tensile spike in lateral contact stress forms at the trailing end in the case of frictional contact. Figures 5.44 – 5.45 show the influence of punch speed c_1 on contact stresses for softening ($\Gamma_1 = 1/6$) and stiffening coatings ($\Gamma_1 = 6$), respectively. The influence of punch speed on elastodynamic contact stresses is very similar to those obtained for triangular punch contact problem. Normal contact stress becomes less compressive for both softening ($\Gamma_1 = 1/6$) and stiffening coatings ($\Gamma_1 = 6$). However, the variation of lateral contact stress with respect to punch speed is different for softening and stiffening coatings. As punch speed is increased, the magnitude of lateral contact stress increases throughout the contact for a softening coating. In the case of a stiffening coating, the change in the lateral contact stress is minimal. The tensile behavior of the lateral stress at the trailing end is slightly enhanced and slightly less compressive lateral stresses are formed around the leading end of the contact. Figures 5.46 – 5.49 depict elastodynamic contact stresses with respect to dimensionless punch speed for different values of relative contact length denoted by the ratio b/R_1 . Although some minor differences are observed due to the length parameters, obtained results are similar to those presented in Figures 5.44 - 5.45. In the case of a softening coating ($\Gamma_1 = 1/6$), the magnitude of the compressive lateral contact stress at trailing end increases as the ratio b/R_1 is increased, and lateral contact stresses become slightly less compressive in the contact zone.

The influence of coefficient of friction η on elastodynamic contact stresses is examined in Figures 5.50 – 5.51. Normal contact stress in the contact zone slants towards the trailing end as coefficient of friction is increased from 0.0 to 0.7. Normal contact stresses evaluated for the softening coating ($\Gamma_1 = 1/6$) are less compressive

when compared to stiffening coating ($\Gamma_1 = 6$). In all cases, larger coefficient of friction leads to a larger tensile peak at the trailing end of the contact. Thus, in elastodynamic contacts with friction, trailing end of the contact is a possible site for cracking type failure.

Figures 5.52 – 5.53 depict the elastodynamic contact stresses with respect to different values of stiffness ratio Γ_1 . As Γ_1 is increased from 1/6 to 6, the magnitude of the normal contact stress increases in the contact zone. However, slightly less compressive lateral contact stresses are generated in the contact zone and tensile behavior of the lateral stress behind the trailing end is enhanced at greater values of Γ_1 .

Figures 5.54 – 5.55 show respectively the elastodynamic contact stresses for softening and stiffening coatings as functions of the ratio R_1/h_1 . As the ratio R_1/h_1 is increased from 5 to 40, normal contact stress tends to be less compressive in the case of a softening coating whereas more compressive in the case of a stiffening coating. The effect of the ratio R_1/h_1 on elastodynamic lateral contact stress distributions generated for softening and stiffening coatings are quite different. Lateral contact stress in the contact zone becomes less compressive for a softening coating while it becomes more compressive for a stiffening coating.

Figures 5.56 - 5.57 show the elastodynamic contact stresses for softening and stiffening coatings as functions of relative contact length b/R_1 . Increase in the ratio b/R_1 leads to more compressive normal stresses in the contact zone. The variation of the normal contact stress with respect to the ratio b/R_1 is significant for the stiffening coating when compared to the softening coating. The magnitude of lateral elastodynamic contact stress in the contact zone increases at higher values of b/R_1 .

Table 5.28 shows the normalized punch load applied by the rigid semi-circular punch for different values of stiffness ratio Γ_1 and relative contact length b/R_1 in elastostatic case. The values computed for the stiffening coating is greater than those computed for the softening coating. In all cases, the normalized punch load is an increasing function of b/R_1 . Table 5.29 - 5.31 show the normalized punch load for different values of stiffness ratio Γ_1 and dimensionless punch speed c_1 . In all cases, the normalized punch load is a decreasing function of punch speed c_1 . Tables 5.32 – 5.33 show normalized punch loads for various values of coefficient of friction η and dimensionless punch speed c_1 . We obtain higher values of the normalized punch load at cases in which higher values of coefficient of friction is used. The normalized punch load is again a decreasing function of dimensionless punch speed c_1 as observed in these tables.

Table 5.34 tabulates the normalized stress intensity factors evaluated at the sharp end of the semi-circular punch. Results of present analytical study and those generated by Guler [45] are presented together in the same table. It can be inferred from Table 5.34 that a very good agreement is achieved. Table 5.35 shows the normalized stress intensity factor for different values of stiffness ratio Γ_1 and relative contact length b/R_1 in elastostatic case. As the ratio b/R_1 is increased from 0.01 to 0.04, the values of mode I SIF at the sharp end $K_I(0)$ decrease for softening coatings while they increase for stiffening coatings.

Tables 5.36 - 5.38 show elastodynamic mode I SIFs calculated at different stiffness ratio Γ_1 and dimensionless punch speed c_1 at several relative contact lengths such as $b/R_1 = 0.01$, $b/R_1 = 0.02$ and $b/R_1 = 0.04$. The mode I SIFs calculated for the

stiffening coatings are greater than those calculated for the softening coatings. In all cases, the mode I SIF is a decreasing function of punch speed c_1 .

Tables 5.39 - 5.40 show the normalized stress intensity factors for different values of coefficient of friction η and dimensionless punch speed c_1 . In all cases, the mode I SIF is a decreasing function of punch speed c_1 .

Tables 5.41 - 5.44 provide tabulated results on percent differences between contact stresses computed considering elastostatic and elastodynamic conditions. Such a comparison is important since it provides assessment of the effect of punch dynamics on contact stresses. Contact stresses are calculated for four different values of dimensionless punch speed c_1 . The case $c_1 = 0$ corresponds to elastostatic contact while contacts for which $c_1 > 0$ are elastodynamic. The percent difference $\varepsilon\%$ in each case is computed with respect to elastostatic results. Tables 5.41 - 5.42 show a comparison for a softening coating ($\Gamma_1 = 1/6$) while Tables 5.43 - 5.44 indicate a comparison for a stiffening coating ($\Gamma_1 = 6$). When Table 5.41 is investigated, percent differences for the normal contact stress increase as punch speed is increased from 0.0 to 0.7. The values of percent difference is greater around the leading end (smooth contact point). Percent differences for the lateral contact stress again increase as punch speed is increased and they reach great values behind the trailing end of the contact. In the case of a stiffening coating, percent differences between elastodynamic and elastostatic normal contact stress are also considerable. The values of percent difference gradually increase as punch speed c_1 is increased from 0.0 to 0.7. The percent differences for the lateral contact stress are provided in Table 5.44. Percent difference values reach up to 100% ahead of the leading end of the contact zone.

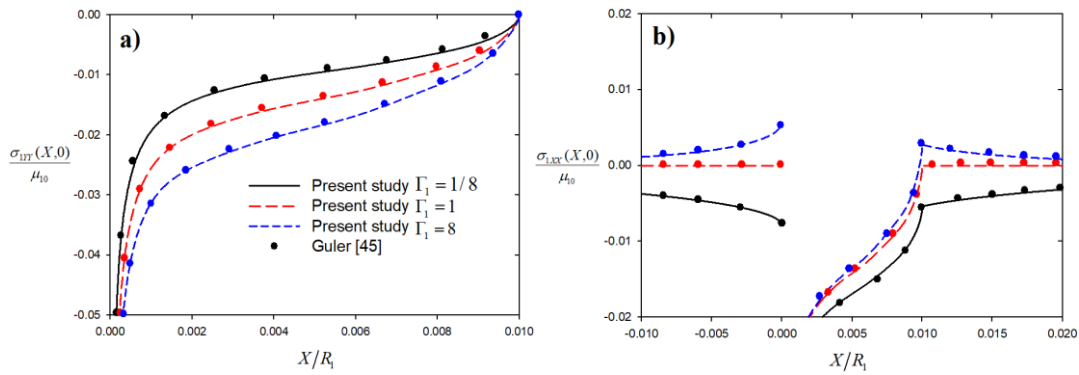


Figure 5.40: Normal and lateral contact stress distribution on FGM coating indented by a frictional semi-circular punch for different stiffness ratio of the coating (a) Normal contact stress distribution; (b) Lateral contact stress distribution, $\Gamma_1 = \mu_2 / \mu_{10}$, $\eta = 0.0$, $b / R_1 = 0.01$, $R_1 / h_1 = 20$.

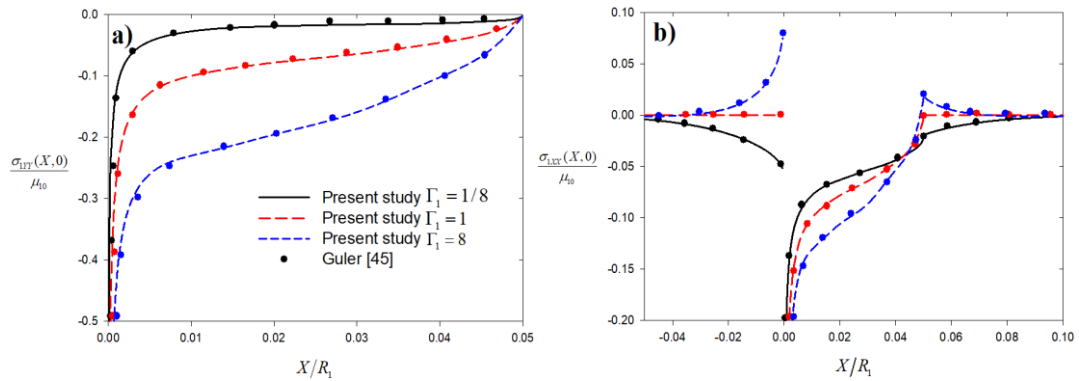


Figure 5.41: Normal and lateral contact stress distribution on FGM coating indented by a frictional semi-circular punch for different stiffness ratio of the coating (a) Normal contact stress distribution; (b) Lateral contact stress distribution, $\Gamma_1 = \mu_2 / \mu_{10}$, $\eta = 0.0$, $b / R_1 = 0.05$, $R_1 / h_1 = 20$.

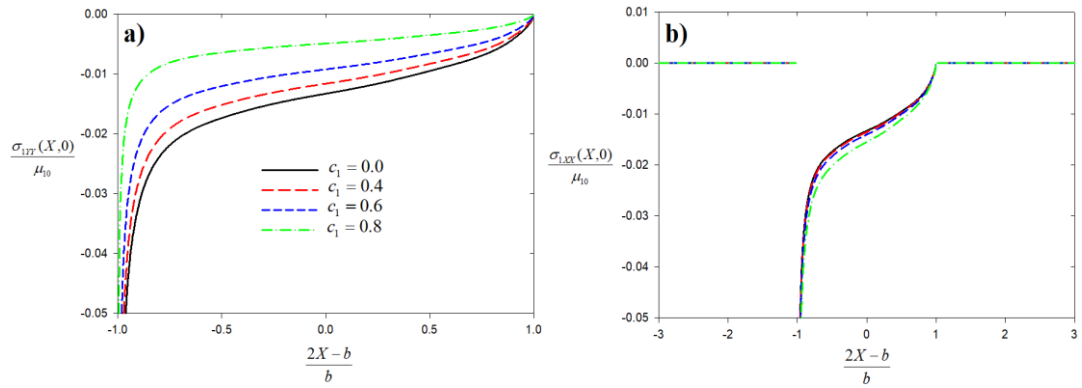


Figure 5.42: Normal and lateral elastodynamic contact stresses on FGM coating indented by a moving semi-circular punch for various values of punch speed (a) Normal contact stress distribution; (b) Lateral contact stress distribution, $b/R_1 = 0.01$, $R_1/h_1 = 20$, $\Gamma_1 = 1$, $\eta = 0.0$, $\nu_1/\nu_2 = 1$.

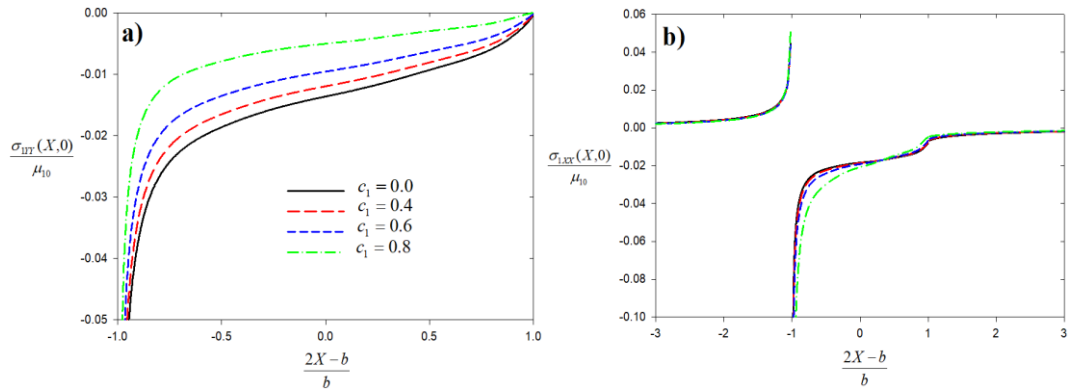


Figure 5.43: Normal and lateral elastodynamic contact stresses on FGM coating indented by a moving semi-circular punch for various values of punch speed (a) Normal contact stress distribution; (b) Lateral contact stress distribution, $b/R_1 = 0.01$, $R_1/h_1 = 20$, $\Gamma_1 = 1$, $\eta = 0.3$, $\nu_1/\nu_2 = 1$.

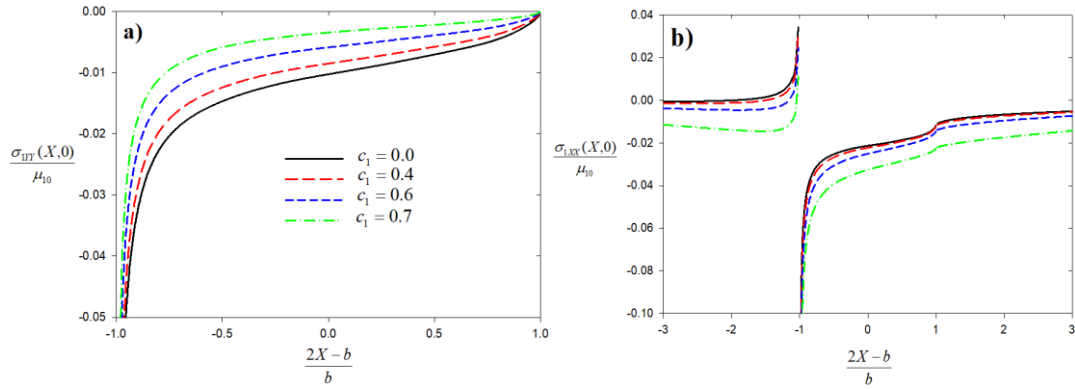


Figure 5.44: Normal and lateral elastodynamic contact stresses on FGM coating indented by a moving semi-circular punch for various values of punch speed (a) Normal contact stress distribution; (b) Lateral contact stress distribution, $b/R_1 = 0.01$, $R_1/h_1 = 20$, $\Gamma_1 = 1/6$, $\eta = 0.3$, $\nu_1/\nu_2 = 1$.

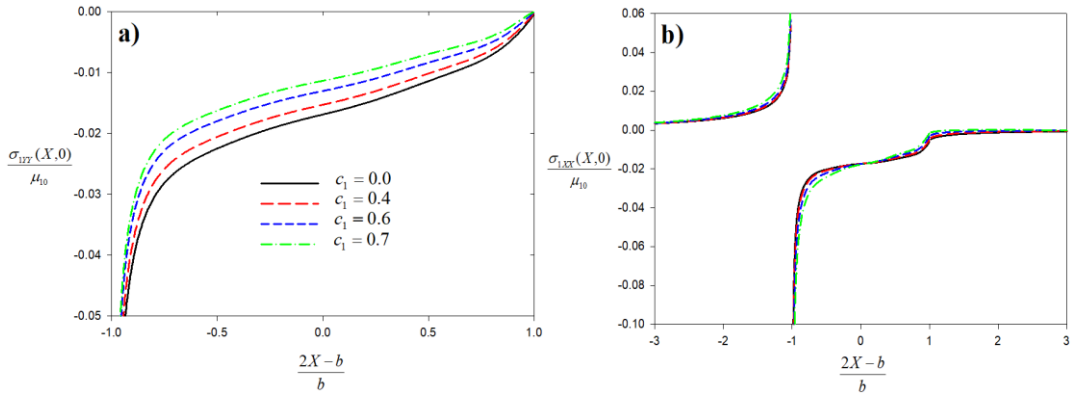


Figure 5.45: Normal and lateral elastodynamic contact stresses on FGM coating indented by a moving semi-circular punch for various values of relative coating thickness (a) Normal contact stress distribution; (b) Lateral contact stress distribution, $b/R_1 = 0.01$, $R_1/h_1 = 20$, $\Gamma_1 = 6$, $\eta = 0.3$, $\nu_1/\nu_2 = 1$.

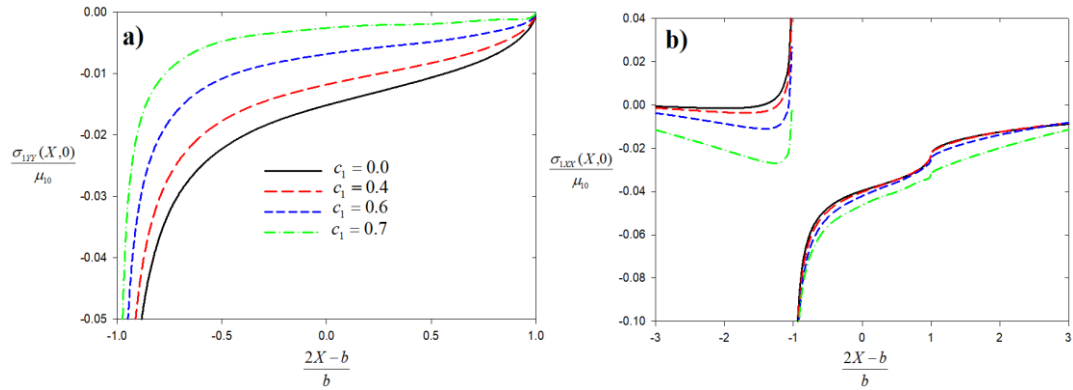


Figure 5.46: Normal and lateral elastodynamic contact stresses on FGM coating indented by a moving semi-circular punch for various values of punch speed (a) Normal contact stress distribution; (b) Lateral contact stress distribution, $b/R_1 = 0.02$, $R_1/h_1 = 20$, $\Gamma_1 = 1/6$, $\eta = 0.3$, $\nu_1/\nu_2 = 1$.

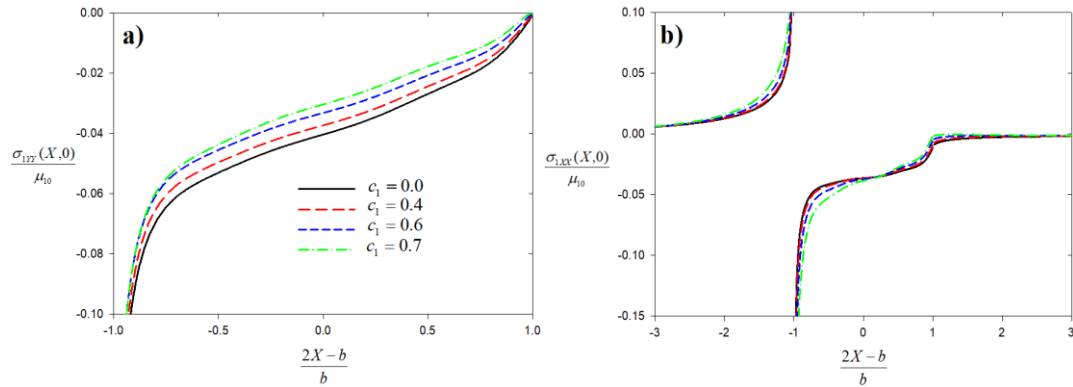


Figure 5.47: Normal and lateral elastodynamic contact stresses on FGM coating indented by a moving semi-circular punch for various values of punch speed (a) Normal contact stress distribution; (b) Lateral contact stress distribution, $b/R_1 = 0.02$, $R_1/h_1 = 20$, $\Gamma_1 = 6$, $\eta = 0.3$, $\nu_1/\nu_2 = 1$.

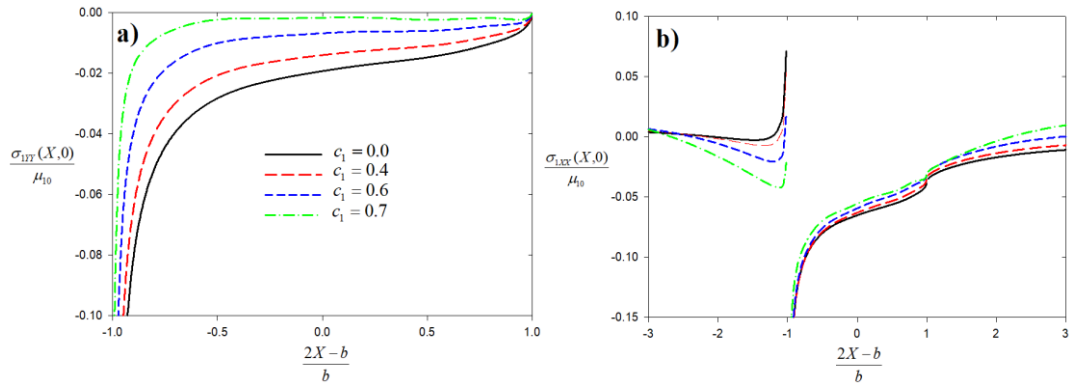


Figure 5.48: Normal and lateral elastodynamic contact stresses on FGM coating indented by a moving semi-circular punch for various values of punch speed (a) Normal contact stress distribution; (b) Lateral contact stress distribution, $b/R_1 = 0.04$, $R_1/h_1 = 20$, $\Gamma_1 = 1/6$, $\eta = 0.3$, $\nu_1/\nu_2 = 1$.

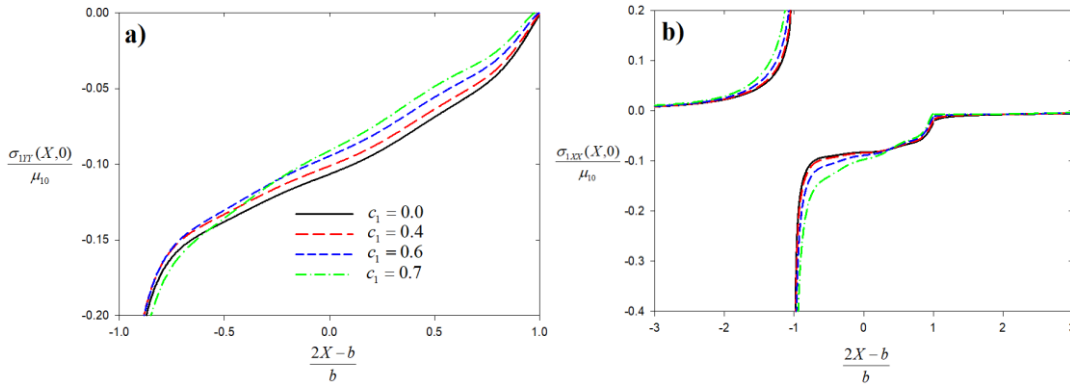


Figure 5.49: Normal and lateral elastodynamic contact stresses on FGM coating indented by a moving semi-circular punch for various values of punch speed (a) Normal contact stress distribution; (b) Lateral contact stress distribution, $b/R_1 = 0.04$, $R_1/h_1 = 20$, $\Gamma_1 = 6$, $\eta = 0.3$, $\nu_1/\nu_2 = 1$.

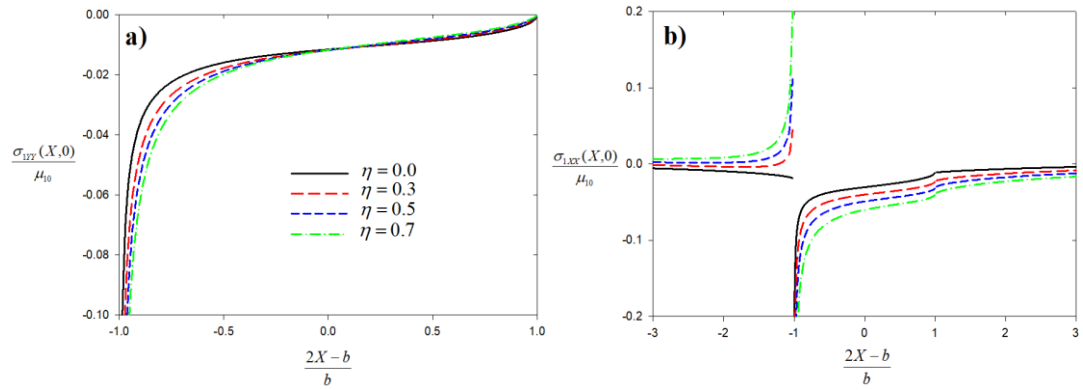


Figure 5.50: Normal and lateral elastodynamic contact stresses on FGM coating indented by a moving semi-circular punch for various values of coefficient of friction (a) Normal contact stress distribution; (b) Lateral contact stress distribution, $b/R_1 = 0.02$, $R_1/h_1 = 20$, $\Gamma_1 = 1/6$, $c_1 = 0.4$, $\nu_1/\nu_2 = 1$.

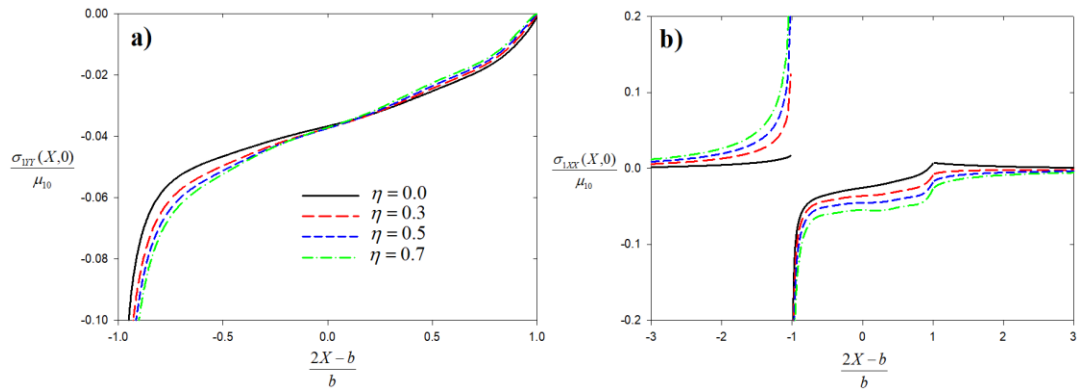


Figure 5.51: Normal and lateral elastodynamic contact stresses on FGM coating indented by a moving semi-circular punch for various values of coefficient of friction (a) Normal contact stress distribution; (b) Lateral contact stress distribution, $b/R_1 = 0.02$, $R_1/h_1 = 20$, $\Gamma_1 = 6$, $c_1 = 0.4$, $\nu_1/\nu_2 = 1$.

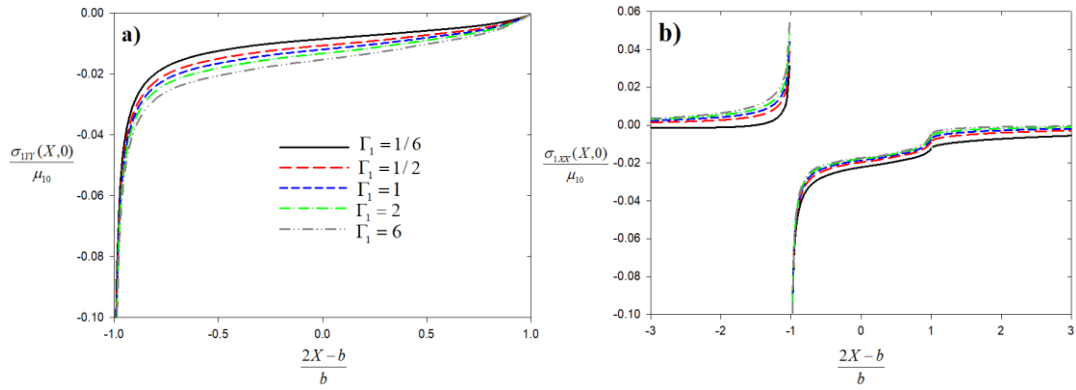


Figure 5.52: Normal and lateral elastodynamic contact stresses on FGM coating indented by a moving semi-circular punch for various values of stiffness ratio (a) Normal contact stress distribution; (b) Lateral contact stress distribution, $b/R_1 = 0.01$, $R_1/h_1 = 20$, $c_1 = 0.4$, $\eta = 0.3$, $\nu_1/\nu_2 = 1$.

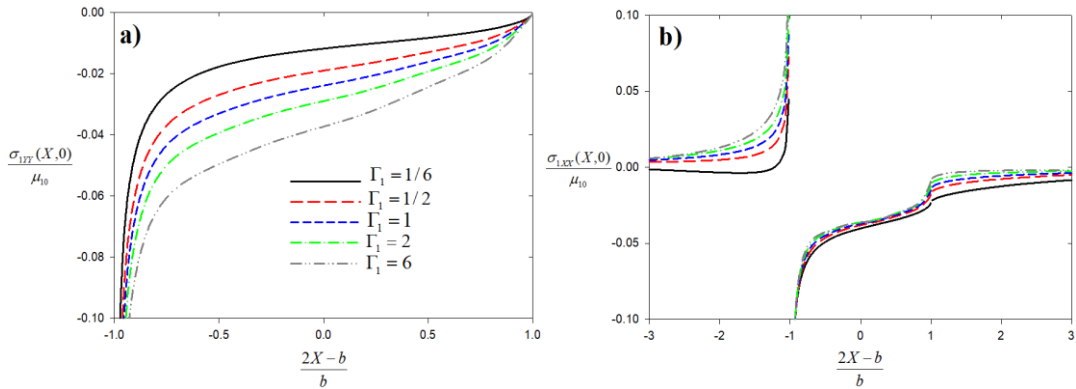


Figure 5.53: Normal and lateral elastodynamic contact stresses on FGM coating indented by a moving semi-circular punch for various values of stiffness ratio (a) Normal contact stress distribution; (b) Lateral contact stress distribution, $b/R_1 = 0.02$, $R_1/h_1 = 20$, $c_1 = 0.4$, $\eta = 0.3$, $\nu_1/\nu_2 = 1$.

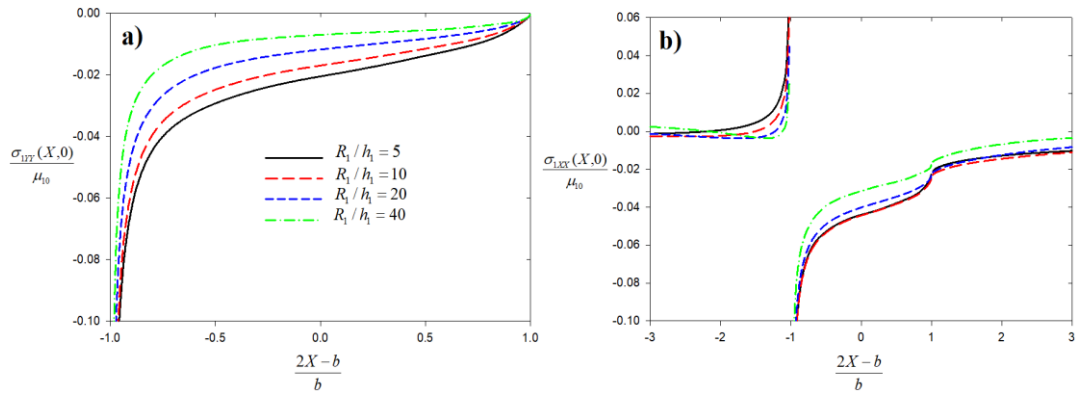


Figure 5.54: Normal and lateral elastodynamic contact stresses on FGM coating indented by a moving semi-circular punch for various values of relative coating thickness (a) Normal contact stress distribution; (b) Lateral contact stress distribution, $b/R_1 = 0.02$, $\Gamma_1 = 1/6$, $c_1 = 0.4$, $\eta = 0.3$, $\nu_1/\nu_2 = 1$.

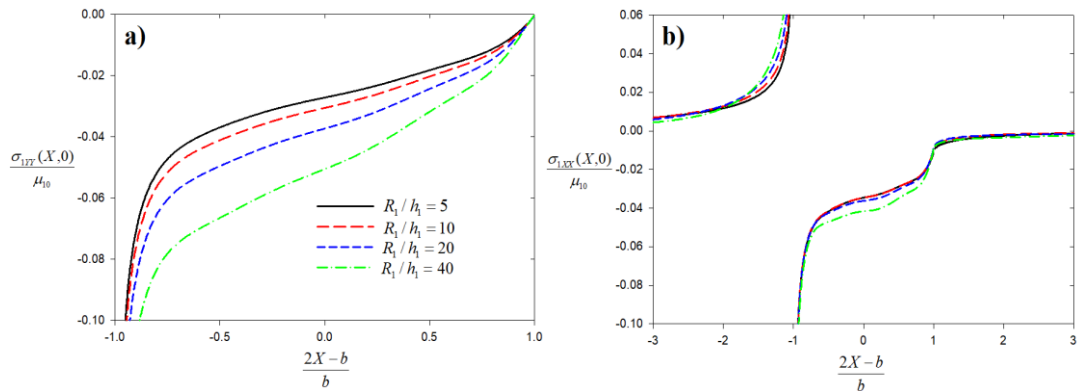


Figure 5.55: Normal and lateral elastodynamic contact stresses on FGM coating indented by a moving semi-circular punch for various values of relative coating thickness (a) Normal contact stress distribution; (b) Lateral contact stress distribution, $b/R_1 = 0.02$, $\Gamma_1 = 6$, $c_1 = 0.4$, $\eta = 0.3$, $\nu_1/\nu_2 = 1$.

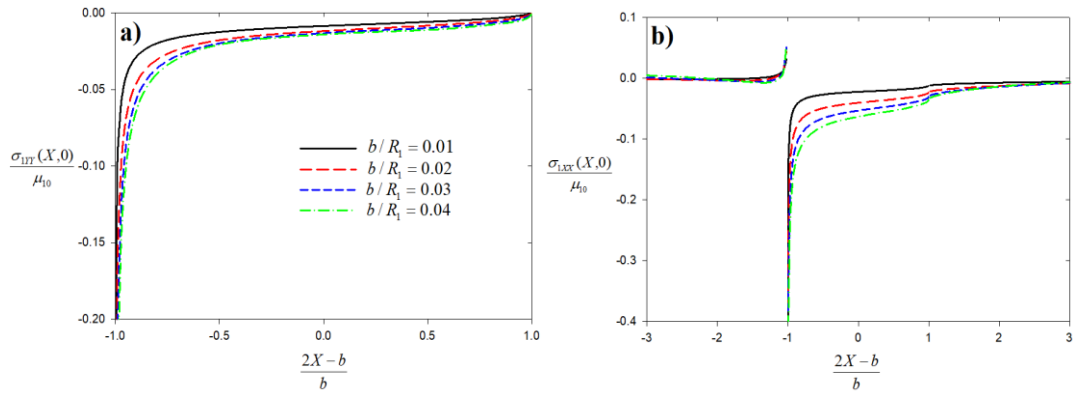


Figure 5.56: Normal and lateral elastodynamic contact stresses on FGM coating indented by a moving semi-circular punch for various values of punch radius (a) Normal contact stress distribution; (b) Lateral contact stress distribution, $\Gamma_1 = 1/6$, $R_1 / h_1 = 20$, $c_1 = 0.4$, $\eta = 0.3$, $\nu_1 / \nu_2 = 1$.

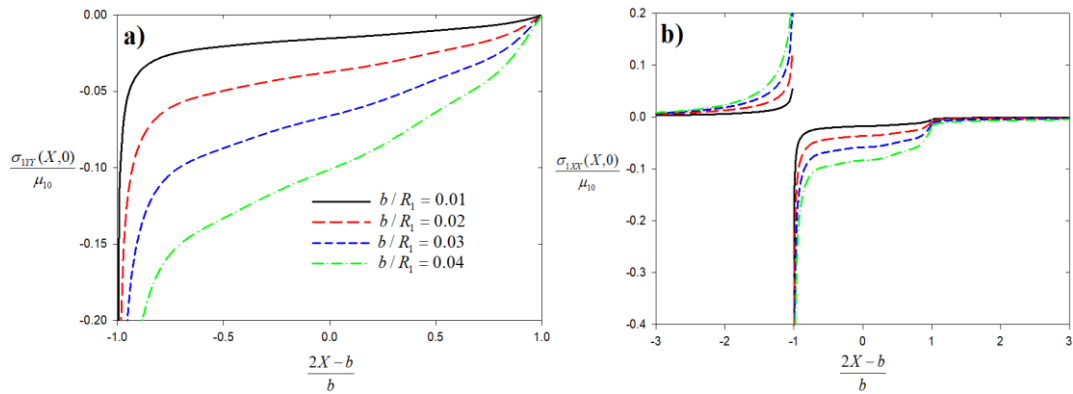


Figure 5.57: Normal and lateral elastodynamic contact stresses on FGM coating indented by a moving semi-circular punch for various values of punch radius (a) Normal contact stress distribution; (b) Lateral contact stress distribution, $\Gamma_1 = 6$, $R_1 / h_1 = 20$, $c_1 = 0.4$, $\eta = 0.3$, $\nu_1 / \nu_2 = 1$.

Table 5.28: The normalized load for FGM coating indented by a moving semi-circular punch $c_1 = 0$, $\eta = 0.0$, $R_1 / h_1 = 20$, $\nu_1 / \nu_2 = 1.0$.

	$b/R_1 = 0.01$	$b/R_1 = 0.02$	$b/R_1 = 0.03$	$b/R_1 = 0.04$
Γ_1	$\frac{P}{\mu_{10}R_1}$	$\frac{P}{\mu_{10}R_1}$	$\frac{P}{\mu_{10}R_1}$	$\frac{P}{\mu_{10}R_1}$
1/6	0.00012143	0.00038692	0.00072335	0.00111056
1/2	0.00014293	0.00052895	0.00111482	0.00187796
1	0.00015612	0.00062446	0.00140505	0.00249786
2	0.00016903	0.00072233	0.00171867	0.00320342
6	0.00018906	0.00087941	0.00224378	0.00443774

Table 5.29: The normalized load for FGM coating indented by a moving semi-circular punch $b/R_1 = 0.01$, $R_1 / h_1 = 20$, $\eta = 0.3$, $\nu_1 / \nu_2 = 1.0$.

	$c_1 = 0.0$	$c_1 = 0.2$	$c_1 = 0.4$	$c_1 = 0.6$	$c_1 = 0.7$
Γ_1	$\frac{P}{\mu_{10}R_1}$	$\frac{P}{\mu_{10}R_1}$	$\frac{P}{\mu_{10}R_1}$	$\frac{P}{\mu_{10}R_1}$	$\frac{P}{\mu_{10}R_1}$
1/6	0.00013835	0.00013365	0.00011860	0.00008884	0.00006211
1/2	0.00015745	0.00015291	0.00013857	0.00011129	0.00008998
1	0.00016908	0.00016461	0.00015053	0.00012425	0.00010445
2	0.00018061	0.00017624	0.00016256	0.00013745	0.00011923
6	0.00019889	0.00019464	0.00018151	0.00015826	0.00014289

Table 5.30: The normalized load for FGM coating indented by a moving semi-circular punch $b/R_1 = 0.02$, $R_1 / h_1 = 20$, $\eta = 0.3$, $\nu_1 / \nu_2 = 1.0$.

	$c_1 = 0.0$	$c_1 = 0.2$	$c_1 = 0.4$	$c_1 = 0.6$	$c_1 = 0.7$
Γ_1	$\frac{P}{\mu_{10}R_1}$	$\frac{P}{\mu_{10}R_1}$	$\frac{P}{\mu_{10}R_1}$	$\frac{P}{\mu_{10}R_1}$	$\frac{P}{\mu_{10}R_1}$
1/6	0.00043874	0.00041967	0.00035838	0.00023557	0.00012302
1/2	0.00058344	0.00056508	0.00050674	0.00039433	0.00030460
1	0.00067634	0.00065843	0.00060213	0.00049699	0.00041781
2	0.00076958	0.00075243	0.00069902	0.00060238	0.00053456
6	0.00091807	0.00090216	0.00085404	0.00077598	0.00073855

Table 5.31: The normalized load for FGM coating indented by a moving semi-circular punch $b/R_1 = 0.04$, $R_1/h_1 = 20$, $\eta = 0.3$, $\nu_1/\nu_2 = 1.0$.

	$c_1 = 0.0$	$c_1 = 0.2$	$c_1 = 0.4$	$c_1 = 0.6$	$c_1 = 0.7$
Γ_1	$\frac{P}{\mu_{10}R_1}$	$\frac{P}{\mu_{10}R_1}$	$\frac{P}{\mu_{10}R_1}$	$\frac{P}{\mu_{10}R_1}$	$\frac{P}{\mu_{10}R_1}$
1/6	0.00122894	0.00116237	0.00095131	0.00054837	0.00022405
1/2	0.00206032	0.00198775	0.00175651	0.00130980	0.00095456
1	0.00270536	0.00263371	0.00240851	0.00198798	0.00167123
2	0.00341564	0.00334766	0.00313657	0.00275680	0.00249289
6	0.00462066	0.00456601	0.00441130	0.00423572	0.00432052

Table 5.32: The normalized load for FGM coating indented by a moving semi-circular punch $b/R_1 = 0.02$, $R_1/h_1 = 20$, $\Gamma_1 = 1/6$, $\nu_1/\nu_2 = 1.0$.

	$c_1 = 0.0$	$c_1 = 0.2$	$c_1 = 0.4$	$c_1 = 0.6$	$c_1 = 0.7$
η	$\frac{P}{\mu_{10}R_1}$	$\frac{P}{\mu_{10}R_1}$	$\frac{P}{\mu_{10}R_1}$	$\frac{P}{\mu_{10}R_1}$	$\frac{P}{\mu_{10}R_1}$
0.0	0.00038692	0.00036847	0.00031000	0.00019747	0.00010065
0.3	0.00043874	0.00041967	0.00035838	0.00023557	0.00012302
0.5	0.00047717	0.00045775	0.00039470	0.00026484	0.00014127
0.7	0.00051893	0.00049922	0.00043453	0.00029766	0.00016317

Table 5.33: The normalized load for FGM coating indented by a moving semi-circular punch $b/R_1 = 0.02$, $R_1/h_1 = 20$, $\Gamma_1 = 6$, $\nu_1/\nu_2 = 1.0$.

	$c_1 = 0.0$	$c_1 = 0.2$	$c_1 = 0.4$	$c_1 = 0.6$	$c_1 = 0.7$
η	$\frac{P}{\mu_{10}R_1}$	$\frac{P}{\mu_{10}R_1}$	$\frac{P}{\mu_{10}R_1}$	$\frac{P}{\mu_{10}R_1}$	$\frac{P}{\mu_{10}R_1}$
0.0	0.00087941	0.00086013	0.00079923	0.00068399	0.00059573
0.3	0.00091807	0.00090216	0.00085404	0.00077598	0.00073855
0.5	0.00094055	0.00092662	0.00088590	0.00082867	0.00081638
0.7	0.00096003	0.00094776	0.00091309	0.00087077	0.00086878

Table 5.34: Normalized stress intensity factors for the moving rigid semi-circular punch $b/R_1 = 0.025$, $R_1/h_1 = 20$, $c_1 = 0.0$.

	$\eta = 0.0$		$\eta = 0.1$		$\eta = 0.3$		$\eta = 0.5$	
Γ_1	$K_I(0)$	$K_I^*(0)$	$K_I(0)$	$K_I^*(0)$	$K_I(0)$	$K_I^*(0)$	$K_I(0)$	$K_I^*(0)$
1/8	0.4800	0.4725	0.4570	0.4501	0.4124	0.4066	0.3702	0.3653
1/2	0.6335	0.6342	0.6152	0.6157	0.5782	0.5783	0.5409	0.5408
1	0.7077	0.7143	0.6950	0.7010	0.6679	0.6729	0.6390	0.6342
2	0.7778	0.7914	0.7719	0.7847	0.7574	0.7688	0.7399	0.7500
8	0.9027	0.9336	0.9108	0.9411	0.9239	0.9528	0.9327	0.9603

Note that K_I^* value shows the normalized stress intensity factor presented by Guler [45].

Table 5.35: Normalized stress intensity factor for the moving semi-circular punch $c_1 = 0.0$, $\eta = 0.0$, $R_1/h_1 = 20$, $\nu_1/\nu_2 = 1.0$.

	$b/R_1 = 0.01$	$b/R_1 = 0.02$	$b/R_1 = 0.03$	$b/R_1 = 0.04$
Γ_1	$K_I(0)$	$K_I(0)$	$K_I(0)$	$K_I(0)$
1/6	0.5763	0.5093	0.4612	0.4271
1/2	0.6300	0.6045	0.5841	0.5682
1	0.6605	0.6605	0.6605	0.6605
2	0.6889	0.7129	0.7333	0.7506
6	0.7303	0.7882	0.8381	0.8812

Table 5.36: Normalized stress intensity factor for the moving semi-circular punch $b/R_1 = 0.01$, $R_1/h_1 = 20$, $\eta = 0.3$, $\nu_1/\nu_2 = 1.0$.

	$c_1 = 0.0$	$c_1 = 0.2$	$c_1 = 0.4$	$c_1 = 0.6$	$c_1 = 0.7$
Γ_1	$K_I(0)$	$K_I(0)$	$K_I(0)$	$K_I(0)$	$K_I(0)$
1/6	0.6604	0.6403	0.5758	0.4483	0.3429
1/2	0.6834	0.6637	0.6012	0.4807	0.3844
1	0.6971	0.6775	0.6158	0.4989	0.4085
2	0.7111	0.6920	0.6321	0.5207	0.4377
6	0.7344	0.7157	0.6579	0.5539	0.4827

Table 5.37: Normalized stress intensity factor for the moving semi-circular punch
 $b/R_1 = 0.02$, $R_1/h_1 = 20$, $\eta = 0.3$, $\nu_1/\nu_2 = 1.0$.

	$c_1 = 0.0$	$c_1 = 0.2$	$c_1 = 0.4$	$c_1 = 0.6$	$c_1 = 0.7$
Γ_1	$K_I(0)$	$K_I(0)$	$K_I(0)$	$K_I(0)$	$K_I(0)$
1/6	0.5847	0.5632	0.4932	0.3490	0.2127
1/2	0.6588	0.6388	0.5749	0.4495	0.3468
1	0.6971	0.6775	0.6158	0.4989	0.4085
2	0.7312	0.7125	0.6544	0.5479	0.4712
6	0.7800	0.7623	0.7084	0.6184	0.5699

Table 5.38: Normalized stress intensity factor for the moving semi-circular punch
 $b/R_1 = 0.04$, $R_1/h_1 = 20$, $\eta = 0.3$, $\nu_1/\nu_2 = 1.0$.

	$c_1 = 0.0$	$c_1 = 0.2$	$c_1 = 0.4$	$c_1 = 0.6$	$c_1 = 0.7$
Γ_1	$K_I(0)$	$K_I(0)$	$K_I(0)$	$K_I(0)$	$K_I(0)$
1/6	0.4769	0.4557	0.3869	0.2481	0.1262
1/2	0.6166	0.5964	0.5313	0.4022	0.2957
1	0.6971	0.6675	0.6158	0.4989	0.4085
2	0.7681	0.7501	0.6942	0.5938	0.5241
6	0.8619	0.8461	0.8001	0.7399	0.7447

Table 5.39: Normalized stress intensity factor for the moving semi-circular punch
 $b/R_1 = 0.02$, $R_1/h_1 = 20$, $\Gamma_1 = 1/6$, $\nu_1/\nu_2 = 1.0$.

	$c_1 = 0.0$	$c_1 = 0.2$	$c_1 = 0.4$	$c_1 = 0.6$	$c_1 = 0.7$
η	$K_I(0)$	$K_I(0)$	$K_I(0)$	$K_I(0)$	$K_I(0)$
0.0	0.5093	0.4889	0.4241	0.2972	0.1826
0.3	0.5847	0.5632	0.4932	0.3490	0.2127
0.5	0.6359	0.6133	0.5388	0.3799	0.2281
0.7	0.6874	0.6635	0.5834	0.4078	0.2413

Table 5.40: Normalized stress intensity factor for the moving semi-circular punch $b/R_1 = 0.02$, $R_1/h_1 = 20$, $\Gamma_1 = 6$, $\nu_1/\nu_2 = 1.0$.

	$c_1 = 0.0$	$c_1 = 0.2$	$c_1 = 0.4$	$c_1 = 0.6$	$c_1 = 0.7$
η	$K_I(0)$	$K_I(0)$	$K_I(0)$	$K_I(0)$	$K_I(0)$
0.0	0.7882	0.7675	0.7022	0.5781	0.4825
0.3	0.7800	0.7623	0.7084	0.6184	0.5699
0.5	0.7685	0.7522	0.7034	0.6275	0.5944
0.7	0.7527	0.7372	0.6915	0.6218	0.5876

Table 5.41: Percent difference between elastostatic and elastodynamic normal contact stresses $\Gamma_1 = 1/6$, $b/R_1 = 0.01$, $R_1/h_1 = 20$, $\eta = 0.3$, $\nu_1/\nu_2 = 1.0$.

	$c_1 = 0.0$		$c_1 = 0.4$		$c_1 = 0.6$		$c_1 = 0.7$	
$\frac{2X-b}{b}$	$\frac{\sigma_{11Y}(X,0)}{\mu_0}$	$\frac{\sigma_{11Y}(X,0)}{\mu_0}$	$\varepsilon\%$	$\frac{\sigma_{11Y}(X,0)}{\mu_0}$	$\varepsilon\%$	$\frac{\sigma_{11Y}(X,0)}{\mu_0}$	$\varepsilon\%$	
-0.96	-0.05075	-0.04527	10.80	-0.03698	27.13	-0.02975	41.37	
-0.82	-0.02408	-0.02095	12.98	-0.01620	32.72	-0.01199	50.20	
-0.70	-0.01866	-0.01604	14.08	-0.01204	35.51	-0.00845	54.73	
-0.61	-0.01642	-0.01399	14.76	-0.01031	37.23	-0.00697	57.57	
-0.50	-0.01471	-0.01245	15.37	-0.00901	38.76	-0.00588	60.05	
-0.22	-0.01168	-0.00975	16.53	-0.00683	41.53	-0.00417	64.33	
-0.03	-0.01042	-0.00864	17.04	-0.00596	42.75	-0.00351	66.32	
0.22	-0.00893	-0.00736	17.56	-0.00500	44.00	-0.00283	68.32	
0.50	-0.00698	-0.00573	17.96	-0.00385	44.81	-0.00215	69.27	
0.61	-0.00624	-0.00511	18.10	-0.00342	45.12	-0.00189	69.76	
0.70	-0.00549	-0.00449	18.26	-0.00299	45.51	-0.00162	70.42	
0.82	-0.00423	-0.00345	18.54	-0.00228	46.07	-0.00123	70.94	
0.96	-0.00180	-0.00145	19.04	-0.00097	46.25	-0.00057	68.03	

Table 5.42: Percent difference between elastostatic and elastodynamic lateral contact stresses $\Gamma_1 = 1/6$, $b/R_1 = 0.01$, $R_1/h_1 = 20$, $\eta = 0.3$, $\nu_1/\nu_2 = 1.0$.

$\frac{2X-b}{b}$	$c_1 = 0.0$		$c_1 = 0.4$		$c_1 = 0.6$		$c_1 = 0.7$	
	$\frac{\sigma_{1xx}(X,0)}{\mu_0}$	$\frac{\sigma_{1xx}(X,0)}{\mu_0}$	$\varepsilon\%$	$\frac{\sigma_{1xx}(X,0)}{\mu_0}$	$\varepsilon\%$	$\frac{\sigma_{1xx}(X,0)}{\mu_0}$	$\varepsilon\%$	
-1.51	0.00152	0.00001	99.51	-0.00410	370.39	-0.01444	1052.52	
-1.22	0.00510	0.00320	37.17	-0.00167	132.78	-0.01296	354.22	
-0.99	-0.10492	-0.11283	7.55	-0.13004	23.95	-0.15371	46.51	
-0.82	-0.03486	-0.03727	6.93	-0.04298	23.30	-0.05390	54.63	
-0.50	-0.02529	-0.02680	5.94	-0.03066	21.21	-0.03937	55.68	
-0.22	-0.02252	-0.02366	5.05	-0.02682	19.12	-0.03478	54.47	
-0.03	-0.02142	-0.02239	4.51	-0.02524	17.81	-0.03285	53.33	
0.22	-0.02025	-0.02101	3.77	-0.02348	15.99	-0.03070	51.65	
0.50	-0.01857	-0.01915	3.12	-0.02133	14.89	-0.02843	53.10	
0.82	-0.01611	-0.01652	2.53	-0.01846	14.56	-0.02556	58.60	
0.99	-0.01268	-0.01312	3.50	-0.01527	20.46	-0.02312	82.32	
1.22	-0.00911	-0.00977	7.29	-0.01229	34.92	-0.02056	125.80	
1.51	-0.00791	-0.00857	8.34	-0.01104	39.51	-0.01923	143.04	

Table 5.43: Percent difference between elastostatic and elastodynamic normal contact stresses $\Gamma_1 = 6$, $b/R_1 = 0.01$, $R_1/h_1 = 20$, $\eta = 0.3$, $\nu_1/\nu_2 = 1.0$.

$\frac{2X-b}{b}$	$c_1 = 0.0$		$c_1 = 0.4$		$c_1 = 0.6$		$c_1 = 0.7$	
	$\frac{\sigma_{1yy}(X,0)}{\mu_0}$	$\frac{\sigma_{1yy}(X,0)}{\mu_0}$	$\varepsilon\%$	$\frac{\sigma_{1yy}(X,0)}{\mu_0}$	$\varepsilon\%$	$\frac{\sigma_{1yy}(X,0)}{\mu_0}$	$\varepsilon\%$	
-0.96	-0.06036	-0.05592	7.35	-0.05058	16.20	-0.04804	20.42	
-0.82	-0.03199	-0.02941	8.06	-0.02611	18.38	-0.02416	24.47	
-0.70	-0.02646	-0.02426	8.30	-0.02139	19.15	-0.01958	25.98	
-0.61	-0.02426	-0.02222	8.41	-0.01952	19.55	-0.01777	26.78	
-0.50	-0.02253	-0.02060	8.57	-0.01801	20.05	-0.01628	27.75	
-0.22	-0.01884	-0.01712	9.15	-0.01473	21.84	-0.01300	31.01	
-0.03	-0.01713	-0.01551	9.46	-0.01324	22.74	-0.01155	32.60	
0.22	-0.01485	-0.01338	9.92	-0.01128	24.06	-0.00967	34.86	
0.50	-0.01134	-0.01011	10.86	-0.00832	26.65	-0.00691	39.10	
0.61	-0.01004	-0.00892	11.16	-0.00729	27.42	-0.00599	40.28	
0.70	-0.00878	-0.00778	11.40	-0.00632	28.04	-0.00516	41.20	
0.82	-0.00661	-0.00581	12.11	-0.00464	29.91	-0.00369	44.13	
0.96	-0.00237	-0.00198	16.44	-0.00139	41.40	-0.00090	62.31	

Table 5.44: Percent difference between elastostatic and elastodynamic lateral contact stresses $\Gamma_1 = 6$, $b/R_1 = 0.01$, $R_1/h_1 = 20$, $\eta = 0.3$, $\nu_1/\nu_2 = 1.0$.

$\frac{2X-b}{b}$	$c_1 = 0.0$		$c_1 = 0.4$		$c_1 = 0.6$		$c_1 = 0.7$	
	$\frac{\sigma_{1XX}(X,0)}{\mu_0}$	$\frac{\sigma_{1XX}(X,0)}{\mu_0}$	$\frac{\sigma_{1XX}(X,0)}{\mu_0}$	$\frac{\sigma_{1XX}(X,0)}{\mu_0}$	$\frac{\sigma_{1XX}(X,0)}{\mu_0}$	$\frac{\sigma_{1XX}(X,0)}{\mu_0}$	$\frac{\sigma_{1XX}(X,0)}{\mu_0}$	$\frac{\sigma_{1XX}(X,0)}{\mu_0}$
-1.51	0.00999	0.01033	3.41	0.01126	12.65	0.01268	26.87	
-1.22	0.01617	0.01669	3.22	0.01821	12.66	0.02071	28.10	
-0.99	-0.10202	-0.11091	8.71	-0.13348	30.83	-0.16787	64.54	
-0.82	-0.02846	-0.02982	4.77	-0.03337	17.24	-0.03865	35.82	
-0.50	-0.02028	-0.02076	2.34	-0.02213	9.09	-0.02419	19.24	
-0.22	-0.01821	-0.01832	0.63	-0.01883	3.43	-0.01966	7.96	
-0.03	-0.01746	-0.01743	0.19	-0.01760	0.79	-0.01796	2.89	
0.22	-0.01673	-0.01652	1.20	-0.01633	2.37	-0.01623	2.96	
0.50	-0.01489	-0.01443	3.07	-0.01368	8.14	-0.01288	13.52	
0.82	-0.01209	-0.01140	5.66	-0.01020	15.57	-0.00895	25.92	
0.99	-0.00687	-0.00594	13.63	-0.00422	38.54	-0.00242	64.78	
1.22	-0.00288	-0.00229	20.36	-0.00127	55.73	-0.00029	89.81	
1.51	-0.00196	-0.00150	23.46	-0.00072	63.45	0.00002	100.81	

5.4 Numerical Results for the Rigid Cylindrical Punch

The general schematic of the rigid cylindrical punch contact problem is illustrated in Figure 5.58. An FGM coating of thickness h_1 is perfectly bonded to a homogenous substrate. The rigid cylindrical punch slides over the FGM coating at a speed of V . It is assumed that contact area $(b-a)$ is much smaller than the radius of the cylindrical punch R_1 .

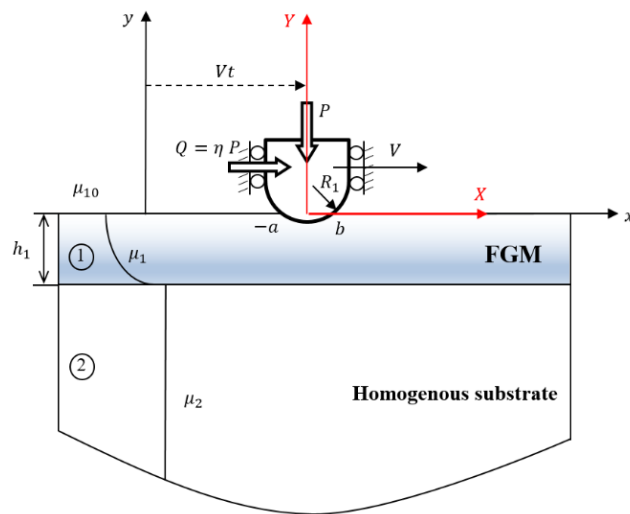


Figure 5.58: The schematic of the cylindrical punch on the surface of the FGM coating bonded to a homogenous substrate

Figures 5.59 – 5.62 show the elastostatic contact stress results obtained by present analytical study with those obtained by Guler [45] for different values of stiffness ratio Γ_1 . Comparisons are made for both frictionless and frictional contacts. It can be seen in Figures 5.59 – 5.62 that a very good agreement is achieved.

The influence of dimensionless punch speed c_1 on contact stresses generated on the half-plane is depicted in Figure 5.63 and 5.64. Figure 5.63 illustrates normal and lateral elastodynamic contact stress distributions in frictionless case. As punch speed

is increased, less compressive elastodynamic normal contact stresses are observed in the contact zone. However, the compressive behavior of the lateral elastodynamic contact stress is strengthened in the contact zone. The surface outside of the contact zone is stress free as seen in Figure 5.63(b). In frictional case, normal elastodynamic contact stress becomes less compressive as observed in Figure 5.64(a). The results presented in Figure 5.64(b) indicate that a tensile spike in lateral stress forms at the trailing end of the contact. It can also be noted that the variation of the normal contact stress with respect to punch speed is greater than that of the lateral contact stress.

Figures 5.65 – 5.70 show the effect of dimensionless punch speed on elastodynamic contact stresses for softening ($\Gamma_1 = 1/6$) and stiffening coatings ($\Gamma_1 = 6$). Results are provided for three different relative contact lengths such as $(b+a)/R_1 = 0.01$, $(b+a)/R_1 = 0.02$ and $(b+a)/R_1 = 0.04$. When Figures 5.65(a) – 5.70(a) are examined, the magnitude of normal contact stress is different because of utilizing different geometric and elastic parameters, however, the general trend in the variation of the normal contact stress with respect to punch speed is very similar. As punch speed c_1 is increased, less compressive normal contact stresses are formed in the contact zone. Lateral elastodynamic contact stress distributions are presented in Figures 5.65(b) – 5.70(b). In all cases, at the same value of $(b+a)/R_1$, the magnitude of tensile lateral contact stress at the trailing end is greater for stiffening coating when compared to softening coating. Moreover, tensile lateral contact stresses are formed outside the contact zone in the case of softening coating especially at higher punch speeds.

Figures 5.71 – 5.72 illustrate the influence of coefficient of friction η on elastodynamic contact stresses generated by a moving cylindrical punch. The magnitude of normal elastodynamic contact stress for the stiffening coating is greater than that for the softening coating. As punch speed c_1 is increased, normal

elastodynamic stress slants towards the trailing end of the contact. The impact of the coefficient of friction on tensile lateral stress is highly significant. A rise in the coefficient of friction causes an increase in the tensile stresses behind the trailing end. In the case of a stiffening coating, tensile lateral contact stresses are greater at those locations.

Figures 5.73 – 5.74 illustrate the effect of stiffness ratio Γ_1 on elastodynamic normal and lateral contact stresses. As stiffness ratio Γ_1 is increased from 1/6 to 6, the magnitude of normal and lateral contact stresses increase in the contact zone. It should also be noted that the tensile behavior of the lateral stress at the trailing end is enhanced as Γ_1 is increased from 1/6 to 6.

Representative results on the influence of the ratio R_1/h_1 on normal and lateral elastodynamic contact stresses on the surface of softening and stiffening coatings are provided in Figures 5.75 – 5.76. As the ratio R_1/h_1 is increased from 50 to 200, less compressive normal stresses are formed in the contact zone for the softening coating ($\Gamma_1 = 1/6$). However, normal contact stresses become more compressive in the contact zone for the stiffening coating ($\Gamma_1 = 6$). The variation of the lateral contact stresses in the contact zone is quite different for softening and stiffening coatings. Lateral contact stress becomes less compressive for the softening coating whereas it tends to be more compressive for the stiffening coating.

The effect of the relative contact length $(b+a)/R_1$ on normal and lateral elastodynamic contact stresses is illustrated in Figures 5.77 and 5.78. The variation of normal and lateral contact stresses with respect to the ratio $(b+a)/R_1$ are very similar for softening ($\Gamma_1 = 1/6$) and stiffening coatings ($\Gamma_1 = 6$). As the ratio $(b+a)/R_1$ is increased from 0.01 to 0.04, the magnitude of normal and lateral contact

stress increase in the contact zone. Tensile lateral elastodynamic contact stress tends to increase especially at higher values of $(b+a)/R_1$.

Table 5.45 tabulates the normalized load applied by the cylindrical punch for various values of stiffness ratio Γ_1 and relative contact length $(b+a)/R_1$ in elastostatic case. The values of the normalized load is greater for stiffening coatings when compared to softening coatings. Increase in the relative contact length $(b+a)/R_1$ leads to greater values of normalized punch loads.

Tables 5.46 – 5.48 show the normalized punch load for various values of stiffness ratio Γ_1 and dimensionless punch speed c_1 . In all cases, the values of normalized load gradually decreases as punch speed is increased.

Tables 5.49 and 5.50 indicate the normalized punch load for various values of coefficient of friction η and dimensionless punch speed c_1 . In all cases, again the normalized punch load is a decreasing function of punch speed c_1 .

Dynamic effect on normal and lateral contact stress distributions is provided quantitatively in Tables 5.51 – 5.54. Contact stresses are computed considering both elastostatic and elastodynamic theories. Contacts for which $c_1 = 0$ corresponds to elastostatic contact whereas contacts for which $c_1 > 0$ corresponds to elastodynamic. Elastodynamic contact stresses are computed for four different values of dimensionless punch speed. In each case, the percent difference $\varepsilon\%$ is computed based on elastostatic contact stresses. Tables 5.51 and 5.52 illustrate dynamic effect for a softening coating ($\Gamma_1 = 1/6$). As punch speed is increased, percent differences for the normal contact stress gradually increase, and they reach up to 82.6%. Percent differences for the lateral contact stress are also considerable. The largest change

occurs around the trailing end of the contact. Percent differences reach up to 172% at those locations.

Tables 5.53 – 5.54 show percent difference between elastodynamic and elastostatic contact stress results for a stiffening coating ($\Gamma_1 = 6$). When Table 5.53 is examined, percent differences gradually increase as punch speed is increased. The largest difference in the normal contact stress is observed around the leading end of the contact. This difference reaches up to 52% at that location. When percent difference for the lateral contact stress is examined, larger values of difference are seen especially at higher punch speeds. The values of percent difference reach up to 335% around the trailing end of the contact zone.

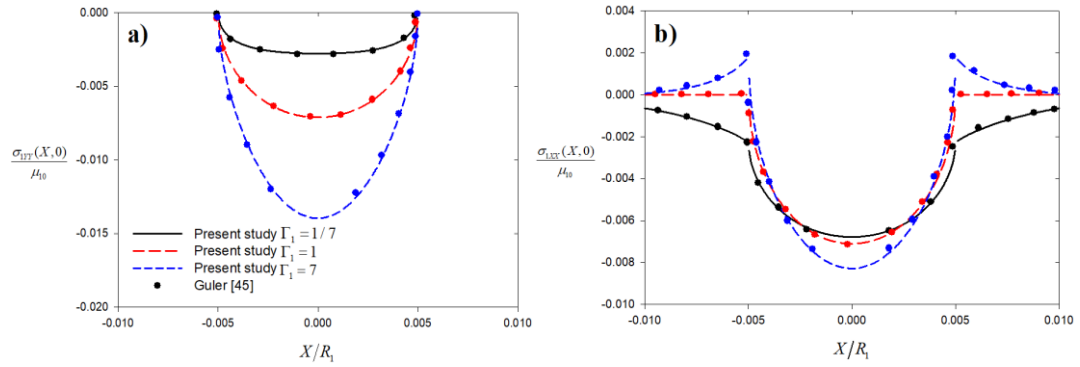


Figure 5.59: Normal and lateral contact stress distribution on FGM coating indented by a cylindrical punch for different stiffness ratio of the coating (a) Normal contact stress distribution; (b) Lateral contact stress distribution, $\Gamma_1 = \mu_2 / \mu_{10}$, $(b+a)/R_1 = 0.01$, $R_1/h_1 = 100$, $\eta = 0.0$, $c_1 = 0.0$.

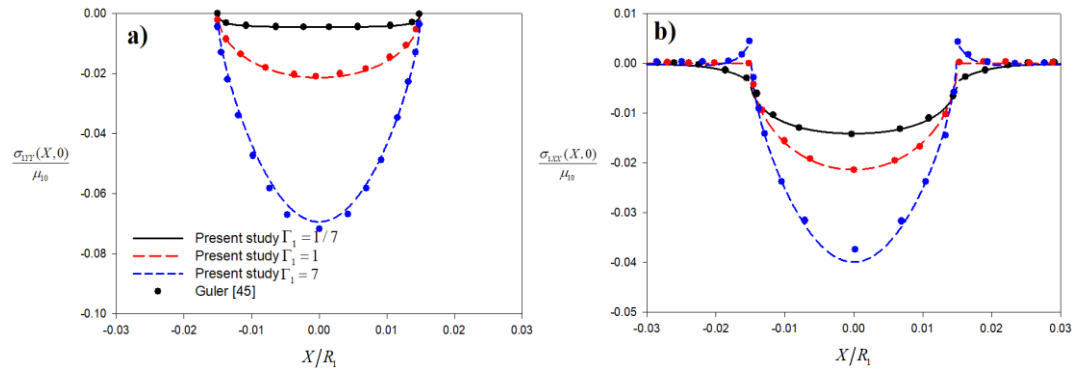


Figure 5.60: Normal and lateral contact stress distribution on FGM coating indented by a cylindrical punch for different stiffness ratio of the coating (a) Normal contact stress distribution; (b) Lateral contact stress distribution, $\Gamma_1 = \mu_2 / \mu_{10}$, $(b+a)/R_1 = 0.03$, $R_1/h_1 = 100$, $\eta = 0.0$, $c_1 = 0.0$.

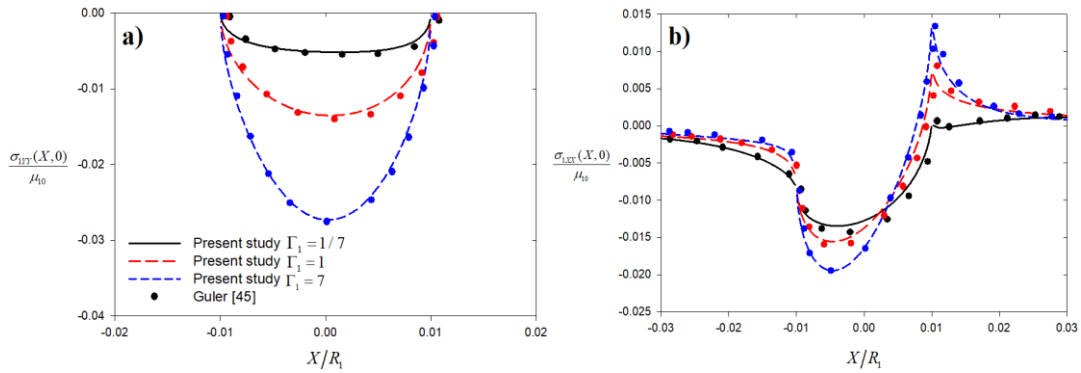


Figure 5.61: Normal and lateral contact stress distribution on FGM coating indented by a cylindrical punch for different stiffness ratio of the coating (a) Normal contact stress distribution; (b) Lateral contact stress distribution, $\Gamma_1 = \mu_2 / \mu_{10}$, $(b + a) / R_1 = 0.02$, $R_1 / h_1 = 50$, $\eta = 0.3$, $c_1 = 0.0$.

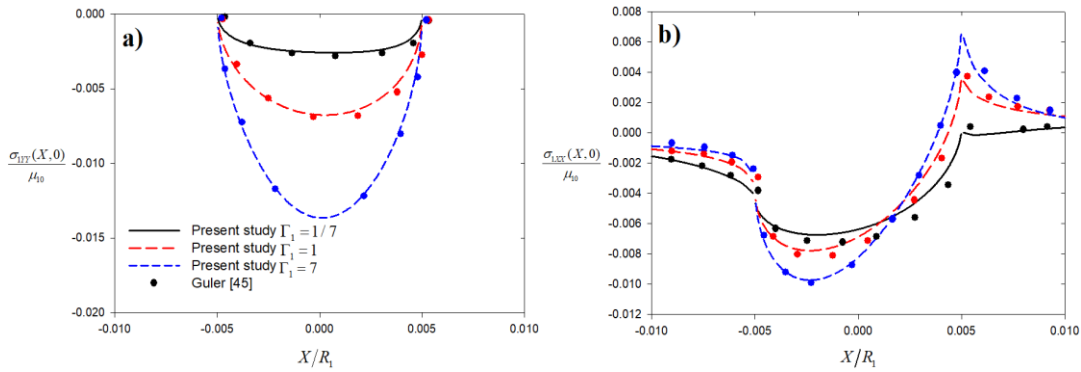


Figure 5.62: Normal and lateral contact stress distribution on FGM coating indented by a cylindrical punch for different stiffness ratio of the coating (a) Normal contact stress distribution; (b) Lateral contact stress distribution, $\Gamma_1 = \mu_2 / \mu_{10}$, $(b + a) / R_1 = 0.01$, $R_1 / h_1 = 100$, $\eta = 0.3$, $c_1 = 0.0$.

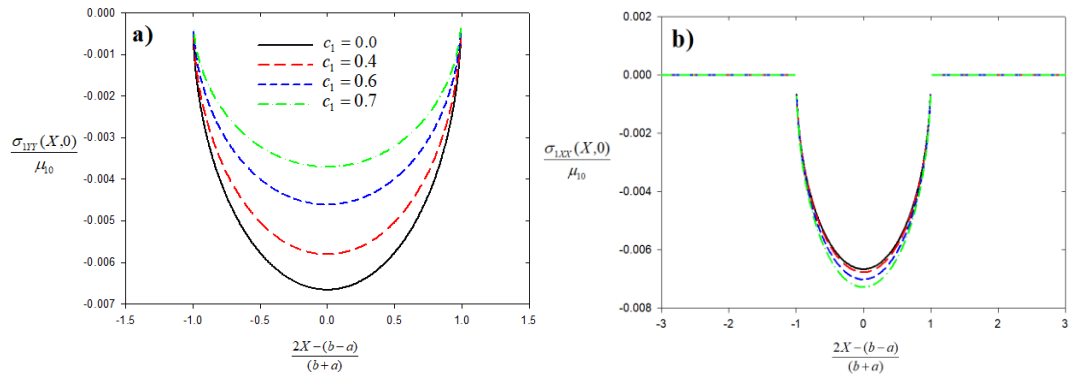


Figure 5.63: Normal and lateral elastodynamic contact stresses on FGM coating indented by a moving cylindrical punch for various values of punch speed (a) Normal contact stress distribution; (b) Lateral contact stress distribution, $(b+a)/R_1 = 0.01$, $R_1/h_1 = 100$, $\Gamma_1 = 1$, $\eta = 0.0$, $\nu_1/\nu_2 = 1$.

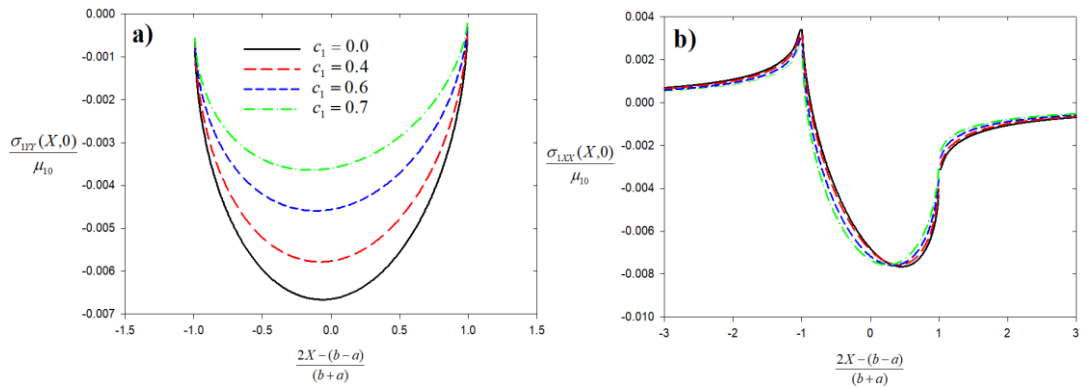


Figure 5.64: Normal and lateral elastodynamic contact stresses on FGM coating indented by a moving cylindrical punch for various values of punch speed (a) Normal contact stress distribution; (b) Lateral contact stress distribution, $(b+a)/R_1 = 0.01$, $R_1/h_1 = 100$, $\Gamma_1 = 1$, $\eta = 0.3$, $\nu_1/\nu_2 = 1$.

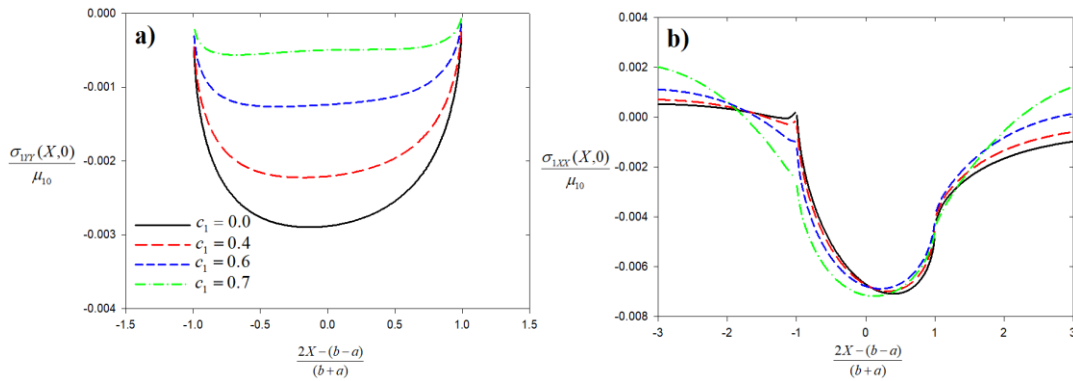


Figure 5.65: Normal and lateral elastodynamic contact stresses on FGM coating indented by a moving cylindrical punch for various values of punch speed (a) Normal contact stress distribution; (b) Lateral contact stress distribution, $(b+a)/R_1 = 0.01$, $R_1/h_1 = 100$, $\Gamma_1 = 1/6$, $\eta = 0.3$, $v_1/v_2 = 1$.

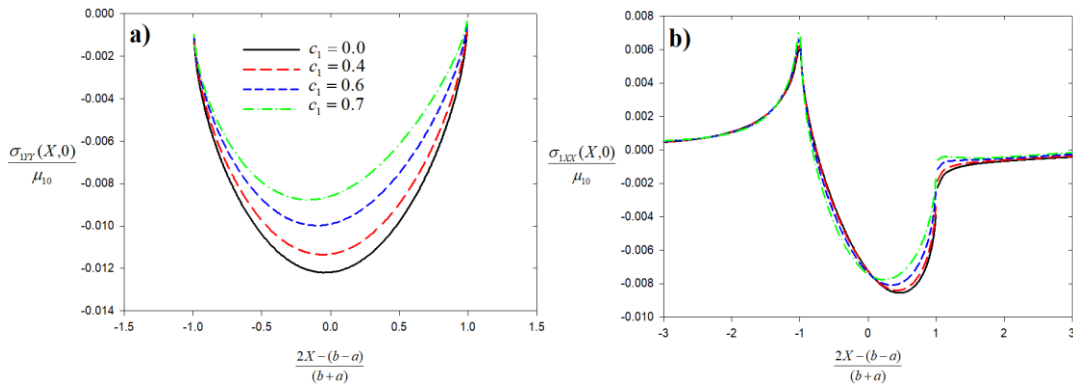


Figure 5.66: Normal and lateral elastodynamic contact stresses on FGM coating indented by a moving cylindrical punch for various values of punch speed (a) Normal contact stress distribution; (b) Lateral contact stress distribution, $(b+a)/R_1 = 0.01$, $R_1/h_1 = 100$, $\Gamma_1 = 6$, $\eta = 0.3$, $v_1/v_2 = 1$.

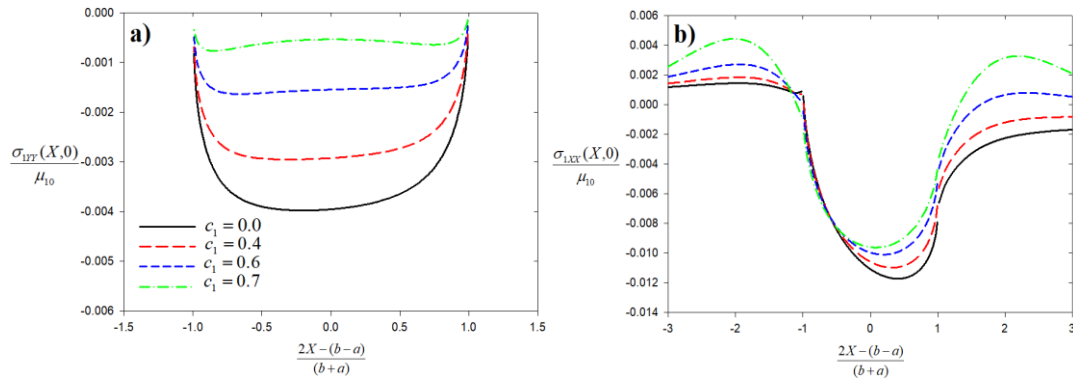


Figure 5.67: Normal and lateral elastodynamic contact stresses on FGM coating indented by a moving cylindrical punch for various values of punch speed (a) Normal contact stress distribution; (b) Lateral contact stress distribution, $(b+a)/R_1 = 0.02$, $R_1/h_1 = 100$, $\Gamma_1 = 1/6$, $\eta = 0.3$, $\nu_1/\nu_2 = 1$.

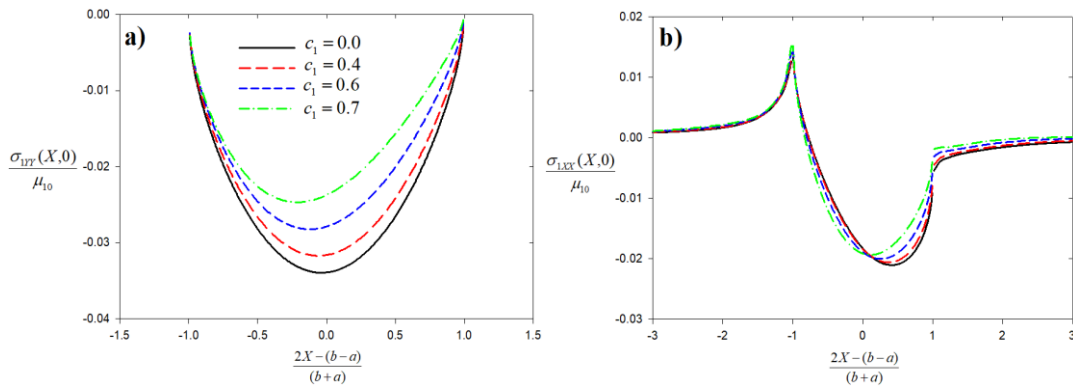


Figure 5.68: Normal and lateral elastodynamic contact stresses on FGM coating indented by a moving cylindrical punch for various values of punch speed (a) Normal contact stress distribution; (b) Lateral contact stress distribution, $(b+a)/R_1 = 0.02$, $R_1/h_1 = 100$, $\Gamma_1 = 6$, $\eta = 0.3$, $\nu_1/\nu_2 = 1$.

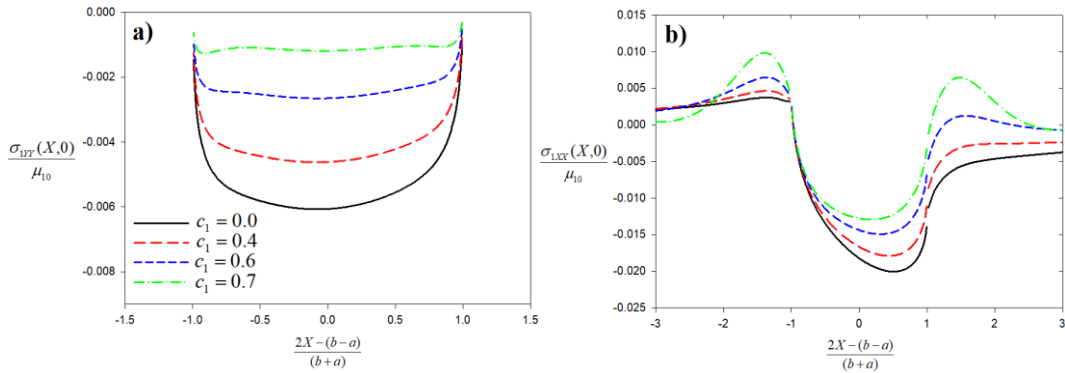


Figure 5.69: Normal and lateral elastodynamic contact stresses on FGM coating indented by a moving cylindrical punch for various values of punch speed (a) Normal contact stress distribution; (b) Lateral contact stress distribution, $(b+a)/R_1 = 0.04$, $R_1/h_1 = 100$, $\Gamma_1 = 1/6$, $\eta = 0.3$, $\nu_1/\nu_2 = 1$.

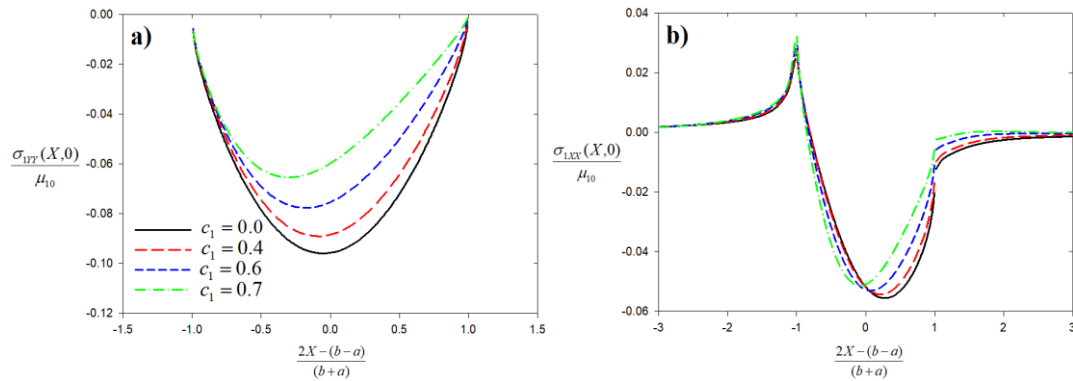


Figure 5.70: Normal and lateral elastodynamic contact stresses on FGM coating indented by a moving cylindrical punch for various values of punch speed (a) Normal contact stress distribution; (b) Lateral contact stress distribution, $(b+a)/R_1 = 0.04$, $R_1/h_1 = 100$, $\Gamma_1 = 6$, $\eta = 0.3$, $\nu_1/\nu_2 = 1$.

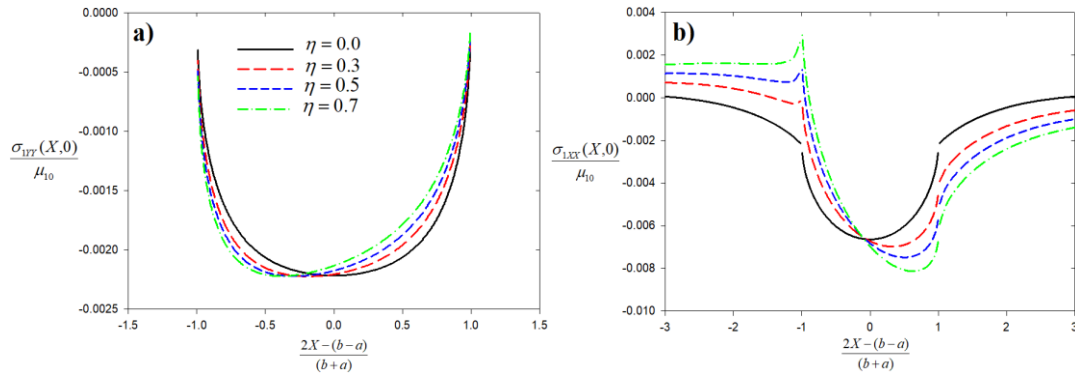


Figure 5.71: Normal and lateral elastodynamic contact stresses on FGM coating indented by a moving cylindrical punch for various values of coefficient of friction (a) Normal contact stress distribution; (b) Lateral contact stress distribution, $(b+a)/R_1 = 0.01$, $R_1/h_1 = 100$, $\Gamma_1 = 1/6$, $c_1 = 0.4$, $\nu_1/\nu_2 = 1$.

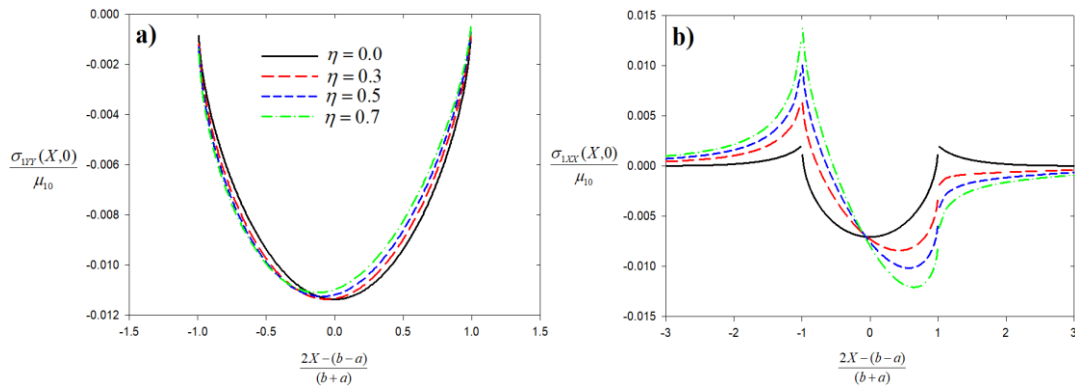


Figure 5.72: Normal and lateral elastodynamic contact stresses on FGM coating indented by a moving cylindrical punch for various values of coefficient of friction (a) Normal contact stress distribution; (b) Lateral contact stress distribution, $(b+a)/R_1 = 0.01$, $R_1/h_1 = 100$, $\Gamma_1 = 6$, $c_1 = 0.4$, $\nu_1/\nu_2 = 1$.

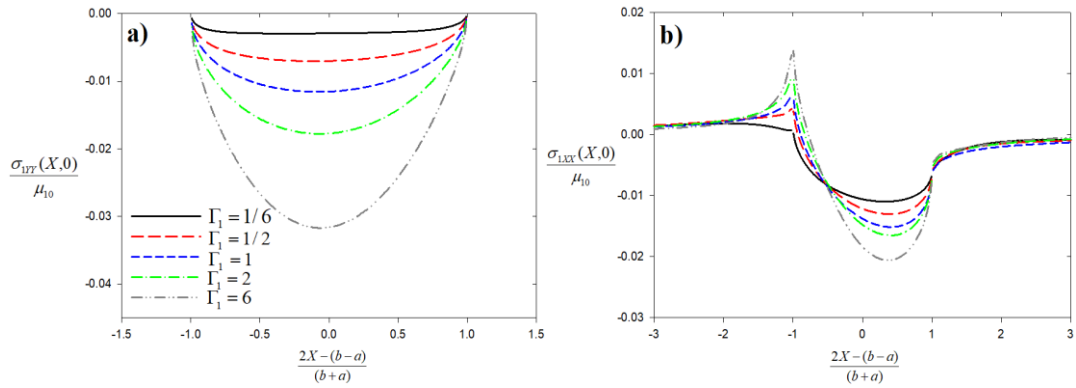


Figure 5.73: Normal and lateral elastodynamic contact stresses on FGM coating indented by a moving cylindrical punch for various values of stiffness ratio (a) Normal contact stress distribution; (b) Lateral contact stress distribution, $(b+a)/R_1 = 0.02$, $R_1/h_1 = 100$, $c_1 = 0.4$, $\eta = 0.3$, $\nu_1/\nu_2 = 1$.

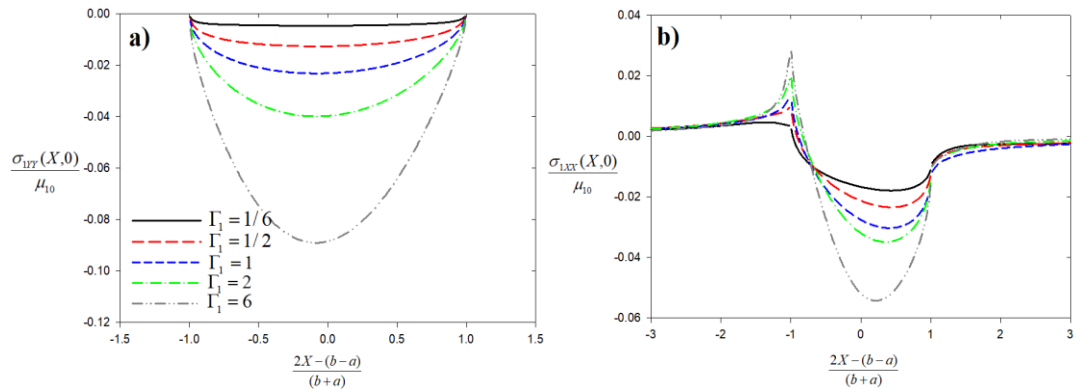


Figure 5.74: Normal and lateral elastodynamic contact stresses on FGM coating indented by a moving cylindrical punch for various values of stiffness ratio (a) Normal contact stress distribution; (b) Lateral contact stress distribution, $(b+a)/R_1 = 0.04$, $R_1/h_1 = 100$, $c_1 = 0.4$, $\eta = 0.3$, $\nu_1/\nu_2 = 1$.

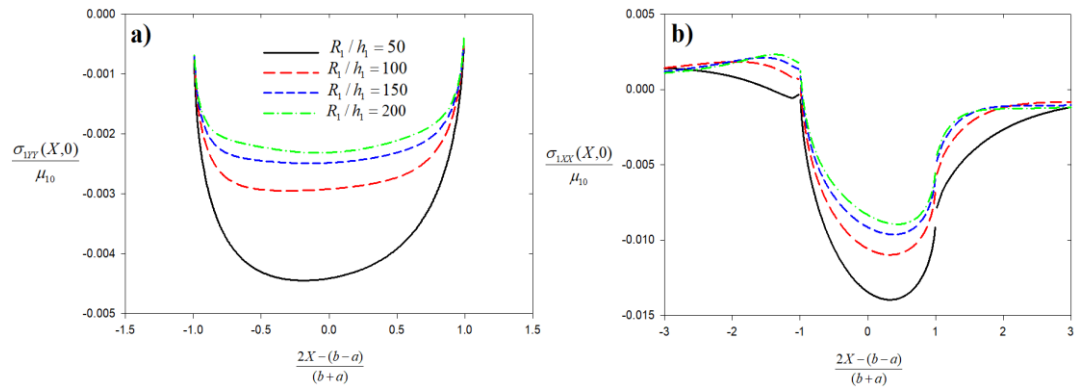


Figure 5.75: Normal and lateral elastodynamic contact stresses on FGM coating indented by a moving cylindrical punch for various values of relative coating thickness (a) Normal contact stress distribution; (b) Lateral contact stress distribution, $(b+a)/R_1 = 0.02$, $\Gamma_1 = 1/6$, $c_1 = 0.4$, $\eta = 0.3$, $\nu_1/\nu_2 = 1$.

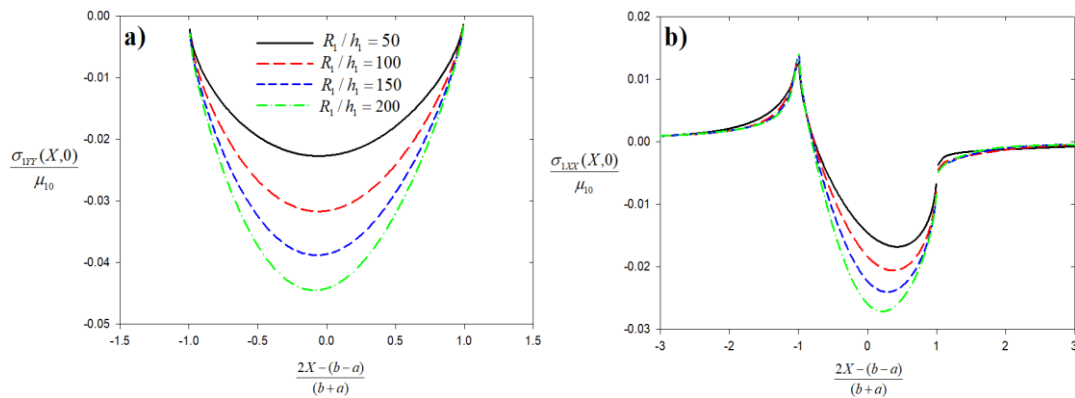


Figure 5.76: Normal and lateral elastodynamic contact stresses on FGM coating indented by a moving cylindrical punch for various values of relative coating thickness (a) Normal contact stress distribution; (b) Lateral contact stress distribution, $(b+a)/R_1 = 0.02$, $\Gamma_1 = 6$, $c_1 = 0.4$, $\eta = 0.3$, $\nu_1/\nu_2 = 1$.

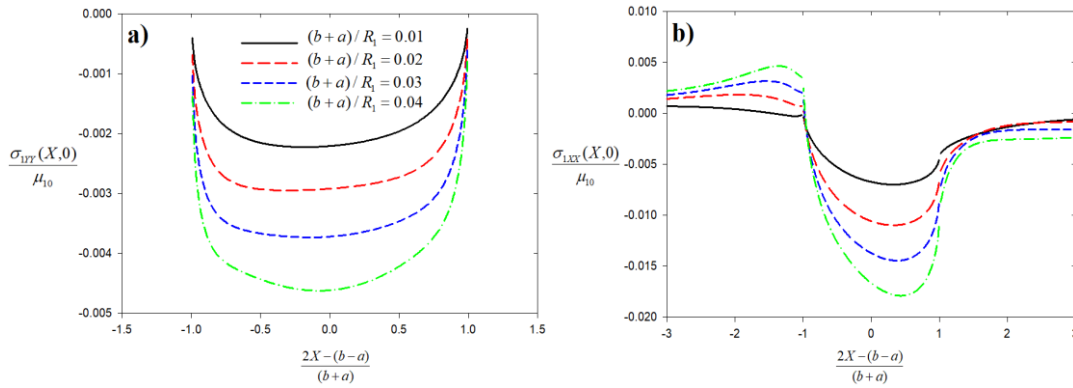


Figure 5.77: Normal and lateral elastodynamic contact stresses on FGM coating indented by a moving cylindrical punch for various values of $(b+a)/R_1$ (a) Normal contact stress distribution; (b) Lateral contact stress distribution, $R_1/h_1=100$, $\Gamma_1=1/6$, $c_1=0.4$, $\eta=0.3$, $\nu_1/\nu_2=1$.

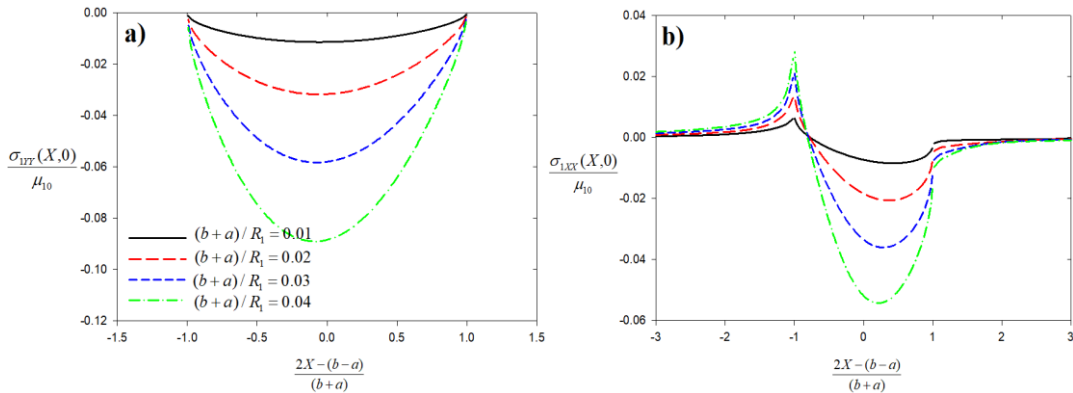


Figure 5.78: Normal and lateral elastodynamic contact stresses on FGM coating indented by a moving cylindrical punch for various values of $(b+a)/R_1$ (a) Normal contact stress distribution; (b) Lateral contact stress distribution, $R_1/h_1=100$, $\Gamma_1=6$, $c_1=0.4$, $\eta=0.3$, $\nu_1/\nu_2=1$.

Table 5.45: The normalized load for FGM coating indented by a moving cylindrical punch $c_1 = 0$, $\eta = 0.0$, $R_1/h_1 = 100$, $\nu_1/\nu_2 = 1.0$.

	$(b+a)/R_1 = 0.01$	$(b+a)/R_1 = 0.02$	$(b+a)/R_1 = 0.03$	$(b+a)/R_1 = 0.04$
Γ_1	$\frac{P}{\mu_{10}R_1}$	$\frac{P}{\mu_{10}R_1}$	$\frac{P}{\mu_{10}R_1}$	$\frac{P}{\mu_{10}R_1}$
1/6	2.433e-5	6.953e-5	1.328e-4	2.146e-4
1/2	3.978e-5	1.395e-4	2.933e-4	5.008e-4
1	5.230e-5	2.092e-4	4.707e-4	8.369e-4
2	6.648e-5	3.017e-4	7.295e-4	1.358e-3
6	9.174e-5	4.962e-4	1.347e-3	2.729e-3

Table 5.46: The normalized load for FGM coating indented by a moving cylindrical punch $(b+a)/R_1 = 0.01$, $R_1/h_1 = 100$, $\eta = 0.3$, $\nu_1/\nu_2 = 1.0$.

	$c_1 = 0.0$	$c_1 = 0.2$	$c_1 = 0.4$	$c_1 = 0.6$	$c_1 = 0.7$
Γ_1	$\frac{P}{\mu_{10}R_1}$	$\frac{P}{\mu_{10}R_1}$	$\frac{P}{\mu_{10}R_1}$	$\frac{P}{\mu_{10}R_1}$	$\frac{P}{\mu_{10}R_1}$
1/6	2.423e-5	2.301e-5	1.881e-5	1.093e-5	4.790e-6
1/2	3.963e-5	3.808e-5	3.388e-5	2.419e-5	1.722e-5
1	5.227e-5	5.065e-5	4.534e-5	3.594e-5	2.840e-5
2	6.656e-5	6.483e-5	5.938e-5	4.860e-5	4.034e-5
6	9.142e-5	8.970e-5	8.461e-5	7.355e-5	6.370e-5

Table 5.47: The normalized load for FGM coating indented by a moving cylindrical punch $(b+a)/R_1 = 0.02$, $R_1/h_1 = 100$, $\eta = 0.3$, $\nu_1/\nu_2 = 1.0$.

	$c_1 = 0.0$	$c_1 = 0.2$	$c_1 = 0.4$	$c_1 = 0.6$	$c_1 = 0.7$
Γ_1	$\frac{P}{\mu_{10}R_1}$	$\frac{P}{\mu_{10}R_1}$	$\frac{P}{\mu_{10}R_1}$	$\frac{P}{\mu_{10}R_1}$	$\frac{P}{\mu_{10}R_1}$
1/6	6.962e-5	6.552e-5	5.247e-5	2.927e-5	1.185e-5
1/2	1.390e-4	1.339e-4	1.152e-4	8.216e-5	5.696e-5
1	2.091e-4	2.026e-4	1.814e-4	1.438e-4	1.136e-4
2	3.020e-4	2.942e-4	2.692e-4	2.194e-4	1.787e-4
6	4.945e-4	4.860e-4	4.588e-4	4.026e-4	3.449e-4

Table 5.48: The normalized load for FGM coating indented by a moving cylindrical punch $(b+a)/R_1 = 0.04$, $R_1/h_1 = 100$, $\eta = 0.3$, $\nu_1/\nu_2 = 1.0$.

	$c_1 = 0.0$	$c_1 = 0.2$	$c_1 = 0.4$	$c_1 = 0.6$	$c_1 = 0.7$
Γ_1	$\frac{P}{\mu_{10}R_1}$	$\frac{P}{\mu_{10}R_1}$	$\frac{P}{\mu_{10}R_1}$	$\frac{P}{\mu_{10}R_1}$	$\frac{P}{\mu_{10}R_1}$
1/6	2.141e-4	2.019e-4	1.641e-4	9.563e-5	4.426e-5
1/2	5.016e-4	4.787e-4	4.142e-4	2.971e-4	2.099e-4
1	8.363e-4	8.104e-4	7.255e-4	5.750e-4	4.544e-4
2	1.358e-3	1.320e-3	1.198e-3	9.600e-4	7.710e-4
6	2.716e-3	2.664e-3	2.500e-3	2.140e-3	1.743e-3

Table 5.49: The normalized load for FGM coating indented by a moving cylindrical punch $(b+a)/R_1 = 0.04$, $R_1/h_1 = 100$, $\Gamma_1 = 1/6$, $\nu_1/\nu_2 = 1.0$.

	$c_1 = 0.0$	$c_1 = 0.2$	$c_1 = 0.4$	$c_1 = 0.6$	$c_1 = 0.7$
η	$\frac{P}{\mu_{10}R_1}$	$\frac{P}{\mu_{10}R_1}$	$\frac{P}{\mu_{10}R_1}$	$\frac{P}{\mu_{10}R_1}$	$\frac{P}{\mu_{10}R_1}$
0.0	2.146e-4	2.026e-4	1.647e-4	9.610e-5	4.442e-5
0.3	2.141e-4	2.019e-4	1.641e-4	9.563e-5	4.426e-5
0.5	2.130e-4	2.001e-4	1.628e-4	9.469e-5	4.364e-5
0.7	2.114e-4	1.988e-4	1.614e-4	9.324e-5	4.277e-5

Table 5.50: The normalized load for FGM coating indented by a moving cylindrical punch $(b+a)/R_1 = 0.04$, $R_1/h_1 = 100$, $\Gamma_1 = 6$, $\nu_1/\nu_2 = 1.0$.

	$c_1 = 0.0$	$c_1 = 0.2$	$c_1 = 0.4$	$c_1 = 0.6$	$c_1 = 0.7$
η	$\frac{P}{\mu_{10}R_1}$	$\frac{P}{\mu_{10}R_1}$	$\frac{P}{\mu_{10}R_1}$	$\frac{P}{\mu_{10}R_1}$	$\frac{P}{\mu_{10}R_1}$
0.0	2.723e-3	2.678e-3	2.531e-3	2.241e-3	2.004e-3
0.3	2.716e-3	2.664e-3	2.500e-3	2.140e-3	1.743e-3
0.5	2.694e-3	2.641e-3	2.466e-3	1.981e-3	1.460e-3
0.7	2.670e-3	2.622e-3	2.389e-3	1.803e-3	1.220e-3

Table 5.51: Percent difference between elastostatic and elastodynamic normal contact stresses $\Gamma_1 = 1/6$, $(b+a)/R_1 = 0.01$, $R_1/h_1 = 100$, $\eta = 0.3$, $\nu_1/\nu_2 = 1.0$.

$\frac{2X-(b-a)}{(b+a)}$	$c_1 = 0.0$		$c_1 = 0.4$		$c_1 = 0.6$		$c_1 = 0.7$	
	$\frac{\sigma_{1Y}(X,0)}{\mu_0}$	$\frac{\sigma_{1Y}(X,0)}{\mu_0}$	$\epsilon\%$	$\frac{\sigma_{1Y}(X,0)}{\mu_0}$	$\epsilon\%$	$\frac{\sigma_{1Y}(X,0)}{\mu_0}$	$\epsilon\%$	
-0.97	-0.00100	-0.00083	16.76	-0.00056	43.72	-0.00031	68.55	
-0.89	-0.00183	-0.00149	18.74	-0.00096	47.85	-0.00050	72.97	
-0.65	-0.00258	-0.00203	21.17	-0.00122	52.75	-0.00056	78.26	
-0.43	-0.00281	-0.00218	22.38	-0.00126	55.17	-0.00054	80.84	
-0.32	-0.00287	-0.00221	22.84	-0.00126	56.05	-0.00052	81.76	
-0.19	-0.00289	-0.00222	23.17	-0.00125	56.68	-0.00051	82.40	
-0.06	-0.00289	-0.00222	23.39	-0.00124	57.07	-0.00050	82.75	
0.19	-0.00281	-0.00215	23.48	-0.00121	57.10	-0.00049	82.61	
0.32	-0.00273	-0.00209	23.36	-0.00118	56.77	-0.00049	82.15	
0.43	-0.00262	-0.00202	23.15	-0.00115	56.26	-0.00049	81.48	
0.65	-0.00230	-0.00178	22.54	-0.00104	54.87	-0.00047	79.71	
0.89	-0.00150	-0.00117	21.65	-0.00071	52.83	-0.00034	77.09	
0.97	-0.00073	-0.00058	21.69	-0.00035	52.78	-0.00017	76.74	

Table 5.52: Percent difference between elastostatic and elastodynamic lateral contact stresses $\Gamma_1 = 1/6$, $(b+a)/R_1 = 0.01$, $R_1/h_1 = 100$, $\eta = 0.3$, $\nu_1/\nu_2 = 1.0$.

$\frac{2X-(b-a)}{(b+a)}$	$c_1 = 0.0$		$c_1 = 0.4$		$c_1 = 0.6$		$c_1 = 0.7$	
	$\frac{\sigma_{1X}(X,0)}{\mu_0}$	$\frac{\sigma_{1X}(X,0)}{\mu_0}$	$\epsilon\%$	$\frac{\sigma_{1X}(X,0)}{\mu_0}$	$\epsilon\%$	$\frac{\sigma_{1X}(X,0)}{\mu_0}$	$\epsilon\%$	
-2.05	0.00036	0.00046	26.22	0.00063	73.57	0.00074	104.67	
-1.62	0.00018	0.00017	2.62	0.00009	49.78	-0.00037	310.45	
-0.94	-0.00138	-0.00176	27.67	-0.00252	83.11	-0.00376	172.73	
-0.74	-0.00356	-0.00386	8.45	-0.00441	23.94	-0.00530	48.73	
-0.55	-0.00482	-0.00505	4.73	-0.00545	13.06	-0.00615	27.41	
-0.19	-0.00624	-0.00633	1.58	-0.00651	4.32	-0.00697	11.72	
-0.06	-0.00656	-0.00661	0.79	-0.00671	2.23	-0.00710	8.28	
0.19	-0.00697	-0.00693	0.61	-0.00688	1.37	-0.00717	2.74	
0.55	-0.00702	-0.00685	2.49	-0.00661	5.96	-0.00678	3.50	
0.74	-0.00669	-0.00645	3.65	-0.00612	8.65	-0.00626	6.45	
0.94	-0.00572	-0.00543	5.18	-0.00505	11.70	-0.00528	7.80	
1.62	-0.00217	-0.00190	12.43	-0.00155	28.82	-0.00169	22.35	
2.05	-0.00160	-0.00127	20.72	-0.00073	54.24	-0.00041	74.27	

Table 5.53: Percent difference between elastostatic and elastodynamic normal contact stresses $\Gamma_1 = 6$, $(b+a)/R_1 = 0.01$, $R_1/h_1 = 100$, $\eta = 0.3$, $\nu_1/\nu_2 = 1.0$.

$\frac{2X-(b-a)}{(b+a)}$	$c_1 = 0.0$		$c_1 = 0.4$		$c_1 = 0.6$		$c_1 = 0.7$	
	$\frac{\sigma_{1YY}(X,0)}{\mu_0}$	$\frac{\sigma_{1YY}(X,0)}{\mu_0}$	$\epsilon\%$	$\frac{\sigma_{1YY}(X,0)}{\mu_0}$	$\epsilon\%$	$\frac{\sigma_{1YY}(X,0)}{\mu_0}$	$\epsilon\%$	
-0.97	-0.00246	-0.00232	5.86	-0.00213	13.29	-0.00203	17.43	
-0.89	-0.00516	-0.00484	6.25	-0.00440	14.80	-0.00410	20.47	
-0.65	-0.00895	-0.00839	6.24	-0.00757	15.47	-0.00693	22.53	
-0.43	-0.01089	-0.01020	6.35	-0.00913	16.20	-0.00823	24.42	
-0.32	-0.01157	-0.01082	6.48	-0.00963	16.74	-0.00860	25.63	
-0.19	-0.01201	-0.01121	6.66	-0.00992	17.41	-0.00876	27.02	
-0.06	-0.01219	-0.01135	6.89	-0.00997	18.21	-0.00871	28.57	
0.19	-0.01177	-0.01089	7.52	-0.00940	20.17	-0.00799	32.08	
0.32	-0.01118	-0.01030	7.91	-0.00880	21.32	-0.00738	34.00	
0.43	-0.01038	-0.00951	8.35	-0.00804	22.56	-0.00664	36.00	
0.65	-0.00825	-0.00748	9.39	-0.00616	25.34	-0.00493	40.23	
0.89	-0.00443	-0.00393	11.33	-0.00309	30.22	-0.00234	47.11	
0.97	-0.00193	-0.00167	13.05	-0.00127	34.31	-0.00091	52.55	

Table 5.54: Percent difference between elastostatic and elastodynamic lateral contact stresses $\Gamma_1 = 6$, $(b+a)/R_1 = 0.01$, $R_1/h_1 = 100$, $\eta = 0.3$, $\nu_1/\nu_2 = 1.0$.

$\frac{2X-(b-a)}{(b+a)}$	$c_1 = 0.0$		$c_1 = 0.4$		$c_1 = 0.6$		$c_1 = 0.7$	
	$\frac{\sigma_{1XX}(X,0)}{\mu_0}$	$\frac{\sigma_{1XX}(X,0)}{\mu_0}$	$\epsilon\%$	$\frac{\sigma_{1XX}(X,0)}{\mu_0}$	$\epsilon\%$	$\frac{\sigma_{1XX}(X,0)}{\mu_0}$	$\epsilon\%$	
-2.05	0.00101	0.00100	1.07	0.00099	2.85	0.00097	4.48	
-1.62	0.00173	0.00172	0.54	0.00169	2.42	0.00164	5.24	
-0.94	0.00355	0.00352	0.73	0.00337	5.08	0.00309	13.01	
-0.74	-0.00032	-0.00045	39.06	-0.00082	155.82	-0.00140	335.43	
-0.55	-0.00281	-0.00295	4.96	-0.00334	18.92	-0.00392	39.54	
-0.19	-0.00603	-0.00612	1.50	-0.00635	5.46	-0.00666	10.60	
-0.06	-0.00687	-0.00692	0.81	-0.00706	2.89	-0.00722	5.22	
0.19	-0.00807	-0.00803	0.45	-0.00794	1.64	-0.00775	3.89	
0.55	-0.00851	-0.00830	2.42	-0.00782	8.08	-0.00717	15.76	
0.74	-0.00789	-0.00758	3.99	-0.00689	12.72	-0.00604	23.44	
0.94	-0.00581	-0.00537	7.56	-0.00451	22.35	-0.00361	37.86	
1.62	-0.00082	-0.00072	11.58	-0.00059	28.35	-0.00049	40.43	
2.05	-0.00066	-0.00060	9.02	-0.00050	23.59	-0.00041	36.79	

CHAPTER 6

CONCLUSIONS AND FUTURE WORK

6.1 Concluding Remarks

Graded materials, also known as *functionally graded materials* (FGMs) are a kind of advanced composites involving two or more constituent phases with gradual and functionally variable composition of microstructure and material properties. They are used as protective coatings and interfacial zones in engineering applications. FGM coatings have significant advantages over conventional homogenous elastic coatings. They reduce stresses resulting from the material property mismatch, increase the bonding strength and improve material durability for the surface wear and abrasion. This study presents a general theory of dynamic frictional contact mechanics of homogenous elastic coatings and FGM coatings pressed by a rigid punch which moves at constant subsonic speed. Chapter 1 is the introduction part which consists of subsections regarding general knowledge about FGMs, tribological applications, literature survey and the scope of the research.

In Chapter 2, the problem definition is proposed and formulations regarding dynamic frictional contact mechanics of functionally graded materials (FGMs) are made. Stress displacement relations are expressed in plane strain state. Stresses obtained by means of theory of elasticity is substituted into the equations of elastodynamics. The relation between stationary and moving coordinates are determined by the use of Galilean transformation and time dependent problem becomes tractable. Governing

partial differential equations (PDEs) for the elastodynamic contact problem are solved analytically by utilizing Fourier transformation technique. Displacement expressions for the functionally graded coating and the homogenous substrate have six unknown functions in total. Then, these six unknown functions appearing in displacement fields are determined through imposing interface continuity and boundary conditions. The surface displacement gradients are derived in order to get the singular integral equation of the contact problem. In the derivation part, we have derived two singular integral equations, one of which is solved for the unknown normal contact stress. The other singular integral equation is utilized in the derivation of lateral contact stress distribution. Asymptotic analysis is performed in order to extract the Cauchy singularity of the integral equations. Asymptotic analysis is performed because of two reasons. First reason is to see the singular behavior of the integral equation and that of its solution comes from the leading term in the large λ expansion of the kernels of the integral equations. The second reason is to allow the computational efficiency when singular integral equation is solved numerically. Terms of asymptotic expansion are calculated by using a symbolic processor and singular integral equations of the second kind are obtained.

In Chapter 3, the numerical solution techniques of the singular integral equations are described. Firstly, different normalization procedures are conducted for four different punch profiles, and boundaries of the integration are changed to $(-1,1)$ in order to solve the integral equations numerically. Computing the Fredholm kernels in integral equations is important. Calculation procedure on how to evaluate 0 to ∞ integrals are described in Appendix-B. Numerical evaluation of the Fredholm kernels are important to get accurate results. Details on the numerical computation of Fredholm kernels are given in Appendix-D. As described in Appendix-B, right hand sides of the singular integral equations are treated separately which compromise from evaluation of bounded integrals and evaluation of unbounded integrals. For each

punch profile, formulations for normal contact stress, lateral contact stress and normalized punch stress intensity factors are provided. For incomplete contact problems such as, triangular, semi-circular and cylindrical punch profiles, the formulation for the normalized required load applied by the punch is also provided. Formulation and solution procedures of dynamic frictional contact problem are completed. Computer programs are developed for the implementation of the numerical procedures. In Chapter 4, numerical results obtained for homogenous elastic coatings are presented. The effects of mass density ratio ρ_1/ρ_2 , dimensionless punch speed c_1 , coefficient of friction η , shear modulus ratio μ_1/μ_2 and length parameters are examined. Results obtained for homogenous elastic coatings are compared to those found by finite element analysis using ANSYS Mechanical APDL [74] in elastostatic case. It can be seen that results of the present analytical study are in excellent agreement with those of finite element analysis. Results obtained for elastodynamic contact problem of homogenous half-planes are compared those presented by Eringen and Suhubi [75]. Again, an excellent agreement is achieved. Thus, verification of the present analytical method is provided. Results obtained for the flat, triangular, semi-circular and cylindrical profiles are presented in subsections of Chapter 4.

The basic conclusions obtained for elastodynamic contact mechanics of homogenous elastic coatings can be summarized as follows:

- (i) Powers of stress singularities depend on material properties κ , friction coefficient η , and the dimensionless punch speed c_1 .
- (ii) Although change in the mass density ratio ρ_1/ρ_2 does not influence elastodynamic contact stresses for a less stiff coating ($\mu_1/\mu_2 = 1/10$), it significantly affects the contact stress distribution for a stiffer coating ($\mu_1/\mu_2 = 10$). Appendix-E describes the effect of mass density ratio on

contact stresses and punch stress intensity factors in detail. (see Figures 4.7, 4.8, 4.20, 4.21, 4.33, 4.34, 4.46, 4.47).

- (iii) The influence of the dimensionless punch speed c_1 on contact stress distributions for the less stiff coating, stiffer coating and the half-plane is examined. In frictional case, normal contact stress tends to slant towards the leading end and skewed stress curves are formed in the contact zone. Lateral contact stress increases in the contact zone, and the magnitude of tensile peak generated at the trailing end increases. Thus, increase in the punch speed may be critical for cracking type failure at trailing end of the contact. (see Figures 4.9, 4.10, 4.11, 4.12, 4.22, 4.23, 4.24, 4.25, 4.35, 4.36, 4.37, 4.38, 4.48, 4.49, 4.50, 4.51, 4.52, 4.53).
- (iv) The effect of the coefficient of friction η on elastodynamic contact stresses generated on the less stiff ($\mu_1/\mu_2 = 1/10$) and stiffer ($\mu_1/\mu_2 = 10$) coatings are presented. In all cases, larger coefficient of friction leads to a larger tensile peak at the trailing end of the contact. Thus, in elastodynamic contacts with friction, trailing end of the contact is a possible site for surface cracking type failures. This finding is in line with experimental results observed in scratch tests. (see Figures 4.13, 4.14, 4.26, 4.27, 4.39, 4.40, 4.54, 4.55).
- (v) Representative results on the effect of geometric parameters on contact stress distributions are examined. Geometric parameters utilized in analyses are a/h_1 for the flat punch, b/h_1 for the triangular punch, R_1/h_1 for the semi-circular and cylindrical punches. Results of geometric parameters on elastodynamic contact stresses are quite different for the less stiff and stiffer coatings. For example, increase in the ratio a/h_1 for the less stiff coating leads to the increase in the normal contact stress and

decrease in the lateral stress in the contact zone. However, increase in the ratio a/h_1 for the stiffer coating leads to the formation of skewed normal contact stresses, and it leads to formation of more compressive lateral contact stresses in the contact zone. The effects of geometric parameters on contact problems for flat, triangular, semi-circular and cylindrical punches can be seen in Figures 4.15, 4.16, 4.28, 4.29, 4.41, 4.42, 4.56, 4.57.

- (vi) The influence of the Poisson's ratio of the coating and the substrate material ν_1/ν_2 on elastodynamic contact stresses is investigated. For the flat punch contact problem, although the effect on normal contact stress is seen to be minimal, a notable change is observed in the lateral stress variation. As the ratio ν_1/ν_2 is increased from 0.6 to 1.2, less compressive lateral stresses are observed in the contact zone for the less stiff coating. The magnitude of the lateral contact stress increases throughout the contact for the stiffer coating. Effect of the ratio ν_1/ν_2 on contact stresses for the flat, triangular, semi-circular and cylindrical punches can be seen in Figures 4.17, 4.18, 4.30, 4.31, 4.43, 4.44, 4.58, 4.59.
- (vii) Normalized stress intensity factors at sharp end of the flat, triangular and semi-circular punches are computed and they are presented as a series of tables. Tables are provided for different elastodynamic parameters however, the main parameter is the dimensionless punch speed c_1 . In the case of half-plane contact with a flat punch, the normalized mode I SIF gradually decreases as punch speed is increased. The mode I SIF at the trailing end of the flat punch $K_I(-a)$ gradually decreases for all the shear modulus ratios μ_1/μ_2 however, $K_I(a)$ first increases and then decreases in some cases. Hence, the conclusion regarding dependence of $K_I(a)$ on

c_1 can not be made because many parameters such as a/h_1 , ρ_1/ρ_2 are also influential. The normalized stress intensity factor at the trailing end (sharp corner) of the triangular and semi-circular punch is shown by $K_I(0)$. In all cases, values of the mode I SIF gradually decrease as punch speed is increased. (see Tables 4.2, 4.3, 4.4, 4.5, 4.6, 4.16, 4.17, 4.18, 4.19, 4.20, 4.30, 4.31, 4.32, 4.33, 4.34)

- (viii) For incomplete contact problems (triangular, semi-circular and cylindrical) there is a relationship between required load applied by the punch and the contact length. Applied punch load is normalized and presented in tables. In elastostatic case, as the relative contact length is increased, the normalized punch load increases for all the shear modulus ratio of the coating. Numerical values obtained for stiffer coatings are greater than those obtained for less stiff coatings. Normalized punch load in less stiff coatings is a decreasing function of dimensionless punch speed. However, general conclusion regarding dependency of the normalized load for the stiffer coatings can not be made. Normalized punch load increases first and then decrease however in some cases normalized punch load gradually decreases since relative contact length is also influential.
- (ix) The influence of punch dynamics on contact mechanics of homogenous elastic coatings is investigated. Tabulated results based on percent differences between contact stresses computed considering elastostatic and elastodynamic conditions are provided. Therefore, assessment of the effect of punch dynamics on the contact stresses is made by quantitatively. Contact stresses are calculated for four different dimensionless punch speed c_1 . The case $c_1 = 0$ corresponds to elastostatic contact whereas contacts for which $c_1 > 0$ are elastodynamic. Percent

difference $\varepsilon\%$ in each case is computed with respect to the elastostatic contact stress results. Results are presented for four different punch profiles. See Tables 4.7, 4.8, 4.9, 4.10, 4.21, 4.22, 4.23, 4.24, 4.35, 4.36, 4.37, 4.38, 4.44, 4.45, 4.46, 4.47 for further investigation. It can be observed in these tables that influence of the punch dynamics on contact stress distributions for all type of coatings is significant. Percent difference reaches great values especially at higher punch speeds.

In Chapter 5, elastodynamic frictional contact problem of functionally graded coatings is investigated. The graded coating has a thickness of h_1 and it is assumed to have an exponential variation in shear modulus. Poisson's ratio is assumed to be constant in the coating. Numerical results are provided for different parameters such as dimensionless punch speed c_1 , coefficient of friction η , stiffness ratio Γ_1 and related geometric parameters. Geometric parameters can be simply expressed by a/h_1 for the flat punch, b/h_1 for the triangular punch, b/R_1 and R_1/h_1 for semi-circular punch, $(b+a)/R_1$ and R_1/h_1 for the cylindrical punch. The main trends concerning these elastodynamic and geometric parameters can be summarized as follows:

- (i) Powers of stress singularities depend on material properties κ , friction coefficient η and the dimensionless punch speed c_1 .
- (ii) The influence of dimensionless punch speed c_1 on elastodynamic contact stresses for softening coatings, stiffening coatings and half-planes are investigated. It is interesting that in half-plane contacts without friction, the normal contact stress does not change although dimensionless punch speed is increased. The magnitude of the lateral contact stress tends to increase in the contact zone. In a frictional case, normal contact stress slants towards the leading end of the contact zone. The tensile behavior

of the lateral contact stress at the trailing end is enhanced, and lateral stress tends to be compressive ahead of the contact. For a softening coating ($\Gamma_1 = 1/6$), normal contact stress tends to be less compressive at higher speeds, however normal contact stress become slanted stress curve formations for a stiffening coating ($\Gamma_1 = 6$). Thus, punch speed has different influences on contact stresses generated for the softening and stiffening coatings. The effect of dimensionless punch speed on contact stresses obtained by flat, triangular, semi-circular and cylindrical punches can be seen in Figures 5.6, 5.7, 5.8, 5.9, 5.10, 5.11, 5.12, 5.13, 5.25, 5.26, 5.27, 5.28, 5.29, 5.30, 5.31, 5.32, 5.42, 5.43, 5.44, 5.45, 5.46, 5.47, 5.48, 5.49, 5.63, 5.64, 5.65, 5.66, 5.67, 5.68, 5.69, 5.70.

- (iii) The influence of coefficient of friction η on normal and lateral elastodynamic contact stresses generated by a moving punch for the softening and stiffening coatings are investigated. The impact of the coefficient of friction especially on the tensile lateral stress is highly important. A rise in the coefficient of friction causes an increase in the tensile stresses behind the trailing end of the contact. The trailing end of the contact is a likely location of crack initiation due to the formations of high tensile lateral stresses and stress concentrations. Lateral elastodynamic contact stresses ahead of the leading end is compressive for both softening and stiffening coatings. The effect of coefficient of friction on contact stresses generated by flat, triangular, semi-circular and cylindrical punches can be seen in Figures 5.14, 5.15, 5.33, 5.34, 5.50, 5.51, 5.71, 5.72.
- (iv) The stiffness ratio Γ_1 of the graded coating has a significant effect on elastodynamic contact stresses. As stiffness ratio Γ_1 is increased from 1/6 to 6, normal contact stress increases in the contact zone. However, less

compressive lateral contact stresses are generated in the contact zone. Lateral stress ahead of the contact zone tends to be less compressive. Increase in the stiffness ratio Γ_1 leads to the enhancement of tensile lateral stress at the trailing end. Elastodynamic contact stresses obtained on graded coating by different punch profiles such as flat, triangular, semi-circular and cylindrical are illustrated in Figures 5.16, 5.17, 5.35, 5.36, 5.52, 5.53, 5.73, 5.74.

- (v) The effects of geometric parameters on elastodynamic contact stresses are examined. Relative contact length for the flat punch contact problem is defined by the ratio a/h_1 where h_1 shows the coating thickness. The ratio a/h_1 has different influences on contact stresses generated for softening and stiffening coatings. In the case of a softening coating ($\Gamma_1 = 1/6$), as the ratio a/h_1 is increased, less compressive normal contact stresses are generated. However, lateral stress throughout the contact tends to be compressive. The reverse trend is seen for a stiffening coating ($\Gamma_1 = 6$). As the ratio a/h_1 is increased, normal contact stress tends to increase, and lateral contact stress throughout the contact decreases. For a triangular punch contact problem, the similar variation trend is observed for the contact stresses with respect to different b/h_1 ratio. Geometric parameters for the semi-cylindrical punch contact problem are R_1/h_1 and b/R_1 . In the case of a softening coating ($\Gamma_1 = 1/6$), as the ratio R_1/h_1 is increased, less compressive normal stresses are formed in the contact zone. The reverse trend is observed for a stiffening coating ($\Gamma_1 = 6$). The variations of the lateral contact stresses generated for softening and stiffening coatings with respect to R_1/h_1 are rather different. Increase in the relative contact

length b/R_1 leads to the increase in the normal contact stress. Lateral contact stress obtained for softening and stiffening coatings increases as the ratio b/R_1 is increased. The amount of change with respect to the increase in the ratio b/R_1 is greater for stiffening coating ($\Gamma_1 = 6$) when compared to the softening coating ($\Gamma_1 = 1/6$). The influences of geometric parameters R_1/h_1 and $(b+a)/R_1$ on elastodynamic contact stresses generated for softening and stiffening coatings pressed by a moving cylindrical punch are also examined. The variation of the normal and lateral contact stresses is similar to those described for the semi-circular punch contact problem. Details on how geometric factors affect elastodynamic contact stresses can be seen in Figures 5.18, 5.19, 5.37, 5.38, 5.54, 5.55, 5.56, 5.57, 5.75, 5.76, 5.77, 5.78.

- (vi) Normalized stress intensity factors at sharp ends of the punch are calculated and results are presented as a series of tables. Normalized stress intensity factors obtained by the present analytical method are compared to those available in the literature and a very good agreement is achieved. In elastostatic case, as the relative contact length a/h_1 is increased, the mode I SIF for softening coatings gradually increases however, the mode I SIF for stiffening coating gradually decreases. In elastodynamic case, as punch speed c_1 is increased, the mode I SIF at trailing and leading ends shown by $K_I(-a)$ and $K_I(a)$ are equal and they gradually decrease in the case of a half-plane contact. In elastodynamic case, the mode I SIF at trailing end $K_I(-a)$ is generally greater than the mode I SIF at the leading end $K_I(a)$ for softening coatings. However, the reverse trend is observed in stiffening coatings. As punch speed c_1 is

- increased, $K_I(-a)$ and $K_I(a)$ for softening coatings increase however, $K_I(-a)$ and $K_I(a)$ for stiffening coatings decrease. Normalized stress intensity factors calculated for flat, triangular and semi-circular punch contact problems are provided in Tables 5.1, 5.2, 5.3, 5.4, 5.5, 5.6, 5.7, 5.18, 5.19, 5.20, 5.21, 5.22, 5.23, 5.34, 5.35, 5.36, 5.37, 5.38, 5.39, 5.40.
- (vii) Triangular, semi-circular and cylindrical punch contact problems are a kind of incomplete contact problems since there is a relationship between the contact length and required punch load. The required punch load is normalized using contact related parameters and results are presented in tables. For a triangular punch contact problem, the normalized punch load is an increasing function of relative contact length b/h_1 . Normalized punch loads calculated for stiffening coatings are greater than those calculated for softening coatings. In all cases, the normalized punch load is a decreasing function of dimensionless punch speed c_1 . Normalized punch loads calculated for triangular, semi-circular and cylindrical punch contact problems are provided in Tables 5.12, 5.13, 5.14, 5.15, 5.16, 5.17, 5.28, 5.29, 5.30, 5.31, 5.32, 5.33, 5.45, 5.46, 5.47, 5.48, 5.49, 5.50.
- (viii) The influence of punch dynamics on contact mechanics of functionally graded coatings is investigated. Tabulated results based on percent differences between contact stresses computed considering elastostatic and elastodynamic conditions are provided. Contact stress results at punch speed $c_1 = 0$ are elastostatic and contact stress results for which $c_1 > 0$ are elastodynamic. Percent difference $\varepsilon\%$ in each case is computed based on elastostatic stress results. For all punch profiles (flat, triangular, semi-circular and cylindrical), percent difference between elastodynamic and elastostatic contact stresses are presented. See Tables

5.8, 5.9, 5.10, 5.11, 5.24, 5.25, 5.26, 5.27, 5.41, 5.42, 5.43, 5.44, 5.51, 5.52, 5.53, 5.54. It can be inferred from these tables that punch speed significantly affect the contact stresses generated for functionally graded coatings. Therefore, punch dynamics must be taken into account in frictional sliding contact problems involving sliding punches with relatively high speeds.

6.2 Future work

In this study, elastodynamic contact mechanics of the homogenous elastic coatings and functionally graded coatings are examined and contact stresses and stress intensity factors are presented. The following topics may be considered as a further research of the present study:

- In the present study, the stiffness of the punch is much greater than that of the contacting material, hence punch is assumed to be rigid. A future study can be conducted to examine the contact mechanics of deformable elastic punch and the coating in elastodynamic case. Results of that study will be interesting since it clearly shows the influences of elastic properties of the punch on elastodynamic contact problem.
- The speed of the rigid punch is less than the shear wave propagation speed of the elastic solid ($c_1 < 1.0$). As a further research, the behavior of the contact (stresses, and stress intensity factors) may be examined at higher punch speeds, i.e. for shear wave propagation speed and for the super shear wave speeds of the punch. Rayleigh wave speed is very critical for elastodynamic boundary value problems. Moreover, investigation of contact stresses at Rayleigh and super Rayleigh speeds will be interesting.
- Subsurface stresses in FGM coatings under frictional elastodynamic contact conditions will be studied as a further research.

- Dynamic contact mechanics of layered structures and substrates coated with functionally graded materials can be examined considering the damping ratio of the coating and the substrate material.
- Due to the friction, frictional heat may be influential and this effect may be added to the dynamic contact mechanics of solids. Generated frictional heat will be important for contact problems involving sliding punches especially at higher speeds.
- Porous FGMs have a great importance in sensor electronics and biomedical applications. Contact mechanics problems involving porous FGMs may take an attention.
- Surface crack problem subjected to the elastodynamic contact conditions will be analyzed and contribution of the dynamic influences on the stress intensity factors at the tip of a surface crack will be proposed.

REFERENCES

- [1] Agarwal, B.D., Broutman, L.J., 1990, *Analysis and Performance of Fiber Composites*, John Wiley&Sons, USA.
- [2] Holmberg, K., Matthews, A., 2009, *Coatings Tribology Properties, Mechanisms, Techniques and Applications in Surface Engineering, Second Edition*, Tribology and Interface Engineering Series, 56, Elsevier.
- [3] Parks, W.P., Hoffman, E.E., Lee, W.Y., Wright, I.G., 1995, “Thermal Barrier Coatings Issues in Advanced Land-Based Gas Turbines”, *NASA Conference Publication 3312*, pp. 35-47.
- [4] Hogmark, S., Jacobson, S., Larsson, M., 2000, “Design and evaluation of tribological coatings”, *Wear*, Vol.246, pp. 20-33.
- [5] Rickerby, D.S, Matthews, A., 1991, *Advanced Surface Coatings: A Handbook of Surface Engineering*, Glasgow, UK, Blackie, pp. 364.
- [6] Wang, M., Miyake, S., Saito, S., 2005, “Nanoindentation and nanowear of extremely thin protective layers of C-N and B-C-N.”, *Tribology International*, Vol. 38, pp. 657-664.
- [7] Koizumi, M., 1997, “FGM Activities in Japan”, *Composites Part-B*, Vol. 28B, pp. 1-4.
- [8] Niino, M., Maeda, S., 1990, “Recent Development Status of Functionally Gradient Materials”, *ISIJ International*, Vol.30, pp. 699-703.

- [9] Birman, V., Byrd, L.W., 2007, "Modeling and Analysis of Functionally Graded Materials and Structures", *Applied Mechanics Reviews*, ASME, Vol. 60(5), pp. 195-216.
- [10] Bhushan, B., 2013, *Introduction to tribology*, 2nd ed. John Wiley & Sons.
- [11] Suh, N., 1986, *Tribophysics*, Prentice-Hall, NJ, USA.
- [12] Bhadeshia HKDH, 2012, "Steels for bearings", *Prog Mater Sci*. Vol. 57, pp. 268-435.
- [13] Erdemir A., 1992, "Rolling-contact fatigue and wear resistance of hard coatings on bearing- steel substartes", *Surface and Coatings Technology*, Vol. 54-55, pp. 482-9.
- [14] Kuhn M., Gold P.W., Loos J., 2004, "Wear and friction characteristics of PVD-coated roller bearings", *Surface and Coating Technology*, Vol. 174-175, pp. 469-76.
- [15] Igartua A., Laucirica J., Aranzabe A., Leyendecker T., Lemmer O., Erkens G., et al., 1996, "Application of low temperature PVD coatings in roller bearings: Tribological tests and experiences with spindle bearing systems", *Surface and Coatings Technology*, Vol. 86-87, pp. 460-6.
- [16] Meetham, G.W., ed., 1981, *The Development of Gas Turbine Materials*, Applied Science Publishers, London, UK.
- [17] Alanou M.P., Snidle R.W., Evans, H.P., Krantz, T.L., 2002, "On the performance of thin hard coatings for gearing applications", *Tribology Transactions*, Vol. 45, pp. 334-44.
- [18] Page T.F., Knight J.C., 1989, "Factors Affecting the Tribological Behavior of Thin Hard TiN and TiC Coatings", *Surface and Coatings Technology*, Vol 39-40, 339-354.

- [19] Bull S.J., 1991, "Failure Modes in Scratch Adhesion Testing", *Surface and Coatings Technology*, Vol. 50, pp. 25-32.
- [20] Fischer-Cripps, A.C., 2000, *Introduction to Contact Mechanics*, Springer-Verlag, NY, USA.
- [21] Lawn, B., 1995, *Fracture of Brittle Solids*, Cambridge University Press, Cambridge, UK.
- [22] Suresh, S., Olsson, M., Giannakopoulos, A.E., Padture, N.P., Jitcharoen, J., 1999, "Engineering the Resistance to Sliding-Contact Damage through Controlled Gradients in Elastic Properties at Contact Surfaces", *Acta Materialia*, Vol. 47, pp. 3915-3926.
- [23] Cho J.R., Park H.J., 2002, "High strength FGM cutting tools: finite element analysis on thermoelastic characteristics", *Journal of Materials Processing Technology*, Vol. 130-131, pp. 351-356.
- [24] DeMassi-Marchin, J.T., Gupta D.K., 1994, "Protective Coatings in the Gas Turbine Engine", *Surface and Coatings Technology*, Vol. 68-69, pp. 1-9.
- [25] Hertz, H., 1882, "On the contact of elastic Solids". *J. Reine Angewandte Mathematics*, Vol. 92, pp. 156-171.
- [26] Galin, L. A. 1961, *Contact problems in the Theory of Elasticity* (translated by H. Moss). North Carolina State College, Raleigh.
- [27] Muskhelishvili, N. I., 1963, *Some Basic Problems of the Mathematical Theory of Elasticity*. Noordhoff, Groningen, The Netherlands.
- [28] Johnson K.L., 1985, *Contact Mechanics*, Cambridge University Press.

- [29] Adams, G.G., Nosonovski, M., 2000, "Contact modeling – forces", *Tribology International*, Vol. 33, pp. 431-442.
- [30] Kikuchi, N., Oden, J.T., 1985, *Contact Problems in Elasticity*, SIAM, Philadelphia.
- [31] Khludnev, A.M., Sokolowski J., 1997, *Modelling and Control in Solid Mechanics*, Birkhauser Verlag, Basel.
- [32] Ratwani, M. and Erdoğan F., 1973, "On the Plane Contact Problem for a Frictionless Elastic Layer", *Journal of Solids and Structures*, Vol. 9, pp. 921-936.
- [33] Bakırtaş I., 1980, "The Problem of a Rigid Punch on a Non-Homogenous Elastic Half Space", *International Journal of Engineering Science*, Vol. 18, pp. 597-610.
- [34] Gupta, P.K., Walowit, J.A., 1974, "Contact Stress Between an Elastic Cylinder and a Layered Elastic Solid", *Transactions of the ASME, Journal of Lubrication Technology*, Vol. 96(2), pp. 250-257.
- [35] Gupta, P.K., Walowit, J.A., Finkin, E.F., 1973, "Stress Distribution in Plane Strain Layered Elastic Solids Subjected to Arbitrary Boundary Loading", *Transactions of the ASME, Journal of Lubrication Technology*, Vol. 95(4), pp. 427-433.
- [36] Chiu Y.P., Hartnett, M.J., 1983, "A Numerical solution for Layered Solid Contact Problems with Application to Bearings", *Transactions of the ASME, Journal of Lubrication Technology*, Vol. 105, pp. 585-590.

- [37] Komvopoulos, K., 1988, "Finite Element Analysis of a Layered Elastic Solid in Normal Contact with a Rigid Surface", *Transactions of the ASME, Journal of Tribology*, Vol. 110, pp. 477-485.
- [38] Kulchytsky-Zhyhailo R., Rogowski, G., 2007, "Stresses of Hard Coating Under Sliding Contact", *Journal of Theoretical and Applied Mechanics*, Vol. 45, pp. 753-771.
- [39] Giannakopoulos A.E. and Pallot P., 2000, "Two dimensional contact analysis of elastic graded materials", *Journal of the Mechanics and Physics of Solids*, Vol. 48, pp. 1596-1631.
- [40] Giannakopoulos, A.E., Suresh, S., 1997, "Indentation of solids with gradients in elastic properties: Part-I. Point force solution", *International Journal of Solids and Structures*, Vol. 34, pp. 2357-2392.
- [41] Giannakopoulos, A.E., Suresh S., 1997, "Indentation of Solids with Gradients in Elastic Properties: Part-II. Axisymmetric indentors", *International Journal of Solids and Structures*, Vol. 34, pp. 2393-2428.
- [42] Suresh, S., Giannakopoulos, A.E., Alcala, J., 1997, "Spherical Indentation of Compositionally Graded Materials: Theory and Experiments", *Acta Materialia*, Vol. 45, pp. 1307-1321.
- [43] Barber, J.R., 1990, "Contact Problems for the Thin Elastic Layer", *International Journal of Mechanical Science*, Vol. 32, pp. 129-132.
- [44] Guler, M. A., 1996, "The Problem of a Rigid Punch with Friction on a Graded Elastic Medium", M.S. Thesis, Lehigh University.

- [45] Guler, M. A., 2001, "Contact Mechanics of FGM coatings", Ph.D. dissertation, Lehigh University.
- [46] Guler, M. A, and Erdogan F., 2004, "Contact mechanics of graded coatings", *International Journal of Mechanical Sciences*, Vol. 41, pp. 3865-3889.
- [47] Guler, M. A, and Erdogan F., 2007, "The frictional sliding contact problems of rigid parabolic and cylindrical stamps on graded coatings", *International Journal of Mechanical Sciences*, Vol. 49, pp. 161-182.
- [48] Dag, S. and Erdogan F., 2002, "A surface crack in a graded medium loaded by a sliding rigid stamp", *Engineering Fracture Mechanics*, Vol. 69, pp. 1729-1751.
- [49] Ke, L.L., and Wang Y.S, 2006, "Two dimensional contact mechanics of functionally graded materials with arbitrary spatial variations of material properties", *International Journal of Solids and Structures*, Vol. 43, pp. 5579-5798.
- [50] Ke, L.L., and Wang Y.S, 2006, "Two dimensional sliding contact of functionally graded materials", *European Journal of Mechanics A- Solids*, Vol. 26, pp. 171-188.
- [51] Liu, T.J., Wang, Y.S., 2008, "Axisymmetric frictionless contact problem of a functionally graded coating with exponentially varying modulus", *Acta Mechanica*, Vol. 199, pp. 151-165.
- [52] Choi, H.J., Paulino, G. H., 2010, "Interfacial cracking in a graded coating /substrate system loaded by a frictional sliding flat punch", *Proceedings of the Royal Society A*, Vol. 466, pp. 853-880.

- [53] Choi, H.J., Paulinoi, G.H., 2008, “Thermoelastic contact mechanics for a flat punch sliding over a graded coating/substrate system with frictional heat generation”, *Journal of the Mechanics and Physics of Solids*, Vol.56, pp. 1673-1692.
- [54] Balci, M.N., Dag, S., Yildirim, B., 2017, “Subsurface stresses in graded coatings subjected to frictional contact with heat generation”, *Journal of Thermal Stresses*, Vol. 40, pp. 517-534.
- [55] Dag, S., Guler, M.A., Yildirim B., Ozatag A.C., 2009, “Sliding frictional contact between a rigid punch and a laterally graded elastic medium”, *International Journal of Solids and Structures*, Vol. 46, pp. 4038-4053.
- [56] Dag, S., 2015, “Consideration of spatial variation of the friction coefficient in the contact mechanics analysis of laterally graded materials”, *Zeitschrift Angewandte. Mathematik und Mechanik*, Vol. 96, pp. 121-136.
- [57] Dag, S., Apatay, T., Guler, M.A., Gulgeç, M., 2012, “A surface crack in a graded coating subjected to sliding frictional contact”, *Engineering Fracture Mechanics*, Vol. 80, pp. 72-91.
- [58] Chen P., Chen S., 2012, “Contact behaviors of a rigid punch and a homogenous half-space coated with a graded layer”, *Acta Mechanica*, Vol. 223, pp. 563-577.
- [59] Guler, M. A., Adibnazari, S., Alinia, Y., 2012, “Tractive rolling contact mechanics of graded coatings”, *International Journal of Solids and Structures*, Vol. 49, pp. 929-945.

- [60] Alinia, Y., Guler, M. A., Adibnazari, S., 2014, "The effect of material property grading on the rolling contact stress field", *Mechanics Research Communications*, Vol. 55, pp. 45-52.
- [61] Sneddon, I. N., 1952, "Stress produced by a Pulse of Pressure Moving along the Surface of Semi-infinite Solid", *Rend. Circ. Mat. Palermo*, Vol.2, pp. 57-62.
- [62] Cole, J., Huth, J., 1958, "Stresses Produced in a Half Plane by Moving Loads", *ASME Journal of Applied Mechanics*, Vol. 25, pp. 433-436.
- [63] Craggs J., W, and Roberts, A.M., 1970, "On the motion of a heavy cylinder over the surface of an elastic solid", *ASME Journal of Applied Mechanics*, Vol. 19, pp. 116-124.
- [64] Georgidas, H.G. and Barber J.R., 1993, "On the super-Rayleigh/subseismic elastodynamic indentation problem", *Journal of Elasticity*, Vol. 31, pp. 141-161.
- [65] Barber, J.R., and Comninou, M., 1982, "Rolling of elastic cylinders with friction at supersonic speed", *International Journal of Solids and Structures*, Vol. 18, pp. 783-789.
- [66] Zhou Y., T., Lee K.Y., Jang Y.H., 2013, "Influences of the moving velocity and material property on frictionless contact problem of orthotropic materials indented by a moving punch", *Archives of Mechanics*, Vol. 65, pp. 195-217.
- [67] Zhou Y., T., Lee K.Y., Jang Y.H., 2014, "Indentation theory on orthotropic materials subjected to a frictional moving punch", *Archives of Mechanics*, Vol. 66, pp. 71-94.

- [68] Zhou, Y.T., Lee, K.Y., 2014, “Dynamic behavior of a moving frictional punch over the surface of anisotropic materials”, *Applied Mathematical Modelling*, Vol. 38, pp. 2311-2327.
- [69] Zhou, Y.T., Kim, T-W., 2013, “Frictional moving contact over the surface between a rigid punch and piezomagnetic materials – Terfanol-D as example”, *International Journal of Solids and Structures*, Vol. 50, pp. 4030-4042.
- [70] Comez, I., 2015, “Contact problem for a functionally graded layer indented by a moving punch”, *International Journal of Mechanical Sciences*, Vol. 100, pp. 339-344.
- [71] Abramowitz, M. and Stegun, I.A., 1964, *Handbook of Mathematical Functions*, National Bureau of Standards, Applied Mathematics Series.
- [72] N.I., Muskhelishvili, 1953, *Singular Integral Equations*, P. Noordhoff, Groningen.
- [73] Erdogan, F., Gupta G.D., and Cook T.S., 1973, “*Numerical Solution of Singular Integral Equations*”, *Method of Analysis and Solution of Crack Problems*, G.C. Sih (ed), Noordhoff Int. publ., Leyden, pp. 368-425.
- [74] ANSYS, Ansys Basic Analysis Procedures Guide, Release 5.4. Canonsburg P.A., USA, ANSYS Inc., 1997.
- [75] Eringen, C., Suhubi, E.S., 1975, *Elastodynamics: Linear Theory*, v2, Academic Press Inc, Fifth Avenue, NewYork, 10003.
- [76] Tricomi, F.G., 1957, *Integral Equations*, Interscience, New York, 1957.

[77] Szegő, G., 1939, *Orthogonal Polynomials*, Colloquium Publications, 23, Am.,
Math. Soc.

APPENDICES

APPENDIX-A FIRST TERMS OF ASYMPTOTIC EXPRESSIONS

First terms of the asymptotic expansion are given as follows:

$$(e_{10} + e_{20}) = -\frac{c_1^2 \delta_1 \delta_3}{4 \delta_1 \delta_2 - 4 \delta_3 + 4 c_1^2 \delta_3 - 4 c_1^2 \delta_1 \delta_2 + c_1^4 \delta_1 \delta_2}, \quad (\text{A.1})$$

$$(f_{10} + f_{20}) = -\frac{\delta_2 (c_1^2 - 2)}{4i \delta_1 \delta_4} + \frac{\delta_1^2 \delta_4}{2\delta_1^2 \delta_4 - i \delta_1 \delta_2 (c_1^2 - 2)^2}, \quad (\text{A.2})$$

$$(g_{10} + g_{20}) = \frac{2i \delta_1^2 \delta_2}{4 \delta_1^2 \delta_4 - i \delta_1 \delta_2 (c_1^2 - 2)^2} + \frac{i (c_1^2 - 2) \delta_1^2 \delta_2}{4 \delta_1^2 \delta_4 - i \delta_1 \delta_2 (c_1^2 - 2)^2}, \quad (\text{A.3})$$

$$(h_{10} + h_{20}) = -\frac{\delta_1 \delta_2 (c_1^2 - 2)}{\left(4 \delta_1^2 \delta_4 - i \delta_1 \delta_2 (c_1^2 - 2)^2\right) (\kappa_1 - 1)} - \frac{2i \delta_1^2 \delta_4}{\left(4 \delta_1^2 \delta_4 + i \delta_1 \delta_2 (c_1^2 - 2)^2\right) (\kappa_1 - 1)}, \quad (\text{A.4})$$

$$\delta_1 = \sqrt{1 - c_1^2}, \quad (\text{A.5})$$

$$\delta_2 = \sqrt{1 + \kappa_1}, \quad (\text{A.6})$$

$$\delta_3 = \sqrt{\kappa_1 (1 - c_1^2) + (1 + c_1^2)}, \quad (\text{A.7})$$

$$\delta_4 = \sqrt{\kappa_1 (1 - c_1^2) + (i + c_1^2)}, \quad (\text{A.8})$$

APPENDIX-B METHOD TO CALCULATE INDEFINITE INTEGRALS

We need to calculate following integrals that appear in the problem.

$$I_{211}(r, s) = \int_{A_{11}^*}^{\infty} \left\{ \sum_{k=1}^{k=N} [e_{1k} + e_{2k}] \left| \frac{\gamma_1^*}{\xi} \right|^k \right\} \sin(\xi(s-r)) d\xi, \quad (\text{B.1})$$

$$I_{212}(r, s) = \int_{A_{12}^*}^{\infty} \left\{ \sum_{k=1}^{k=N} [f_{1k} + f_{2k}] \left| \frac{\gamma_1^*}{\xi} \right|^k \right\} \cos(\xi(s-r)) d\xi, \quad (\text{B.2})$$

$$I_{221}(r, s) = \int_{A_{21}^*}^{\infty} \left\{ \sum_{k=1}^{k=N} [g_{1k} + g_{2k}] \left| \frac{\gamma_1^*}{\xi} \right|^k \right\} \sin(\xi(s-r)) d\xi, \quad (\text{B.3})$$

$$I_{222}(r, s) = \int_{A_{22}^*}^{\infty} \left\{ \sum_{k=1}^{k=N} [h_{1k} + h_{2k}] \left| \frac{\gamma_1^*}{\xi} \right|^k \right\} \cos(\xi(s-r)) d\xi. \quad (\text{B.4})$$

Recall that sine and cosine integrals can be written as the following form,

$$Si(x) = \int_0^x \frac{\sin(t)}{t} dt = \int_0^{\infty} \frac{\sin(t)}{t} dt - \int_x^{\infty} \frac{\sin(t)}{t} dt = \frac{\pi}{2} \frac{|x|}{x} - \int_x^{\infty} \frac{\sin(t)}{t} dt, \quad (\text{B.5})$$

$$Ci(x) = \int_0^x \frac{\cos(t)}{t} dt = \gamma_0 + \log|x| - \int_0^{|x|} \frac{1-\cos(t)}{t} dt. \quad (\text{B.6})$$

where γ_0 is the Euler number and $\gamma_0 = 0.57721566490$. We can express the integrals such that:

$$\int_x^{\infty} \frac{\sin(t)}{t} dt = \frac{\pi}{2} \frac{|x|}{x} - Si(x), \quad (\text{B.7})$$

$$\int_x^\infty \frac{\cos(t)}{t} dt = -\gamma_0 - \log|x| + \int_0^{|x|} \frac{1 - \cos(t)}{t} dt. \quad (\text{B.8})$$

We may call the indefinite integrals such that,

$$S_k = \int_{A_{i1}^*}^\infty \frac{\sin(\xi(s-r))}{\xi^k} d\xi, \quad k = 1, 2, 3, \dots, N \quad (\text{B.9})$$

$$C_k = \int_{A_{i2}^*}^\infty \frac{\cos(\xi(s-r))}{\xi^k} d\xi. \quad k = 1, 2, 3, \dots, N \quad (\text{B.10})$$

Therefore,

$$S_1 = \frac{|s-r|}{s-r} \int_{A_{i1}^*}^\infty \frac{\sin(\xi(s-r))}{\xi} d\xi = \frac{|s-r|}{s-r} \left[\frac{\pi}{2} - Si(A_{i1}^* |s-r|) \right], \quad i = 1, 2. \quad (\text{B.11})$$

$$C_1 = \int_{A_{i2}^*}^\infty \frac{\cos(\xi(s-r))}{\xi} d\xi = -Ci(A_{i2}^* |s-r|), \quad i = 1, 2. \quad (\text{B.12})$$

Then the required formulation for higher order terms can be obtained by integration by parts and they are expressed as the following recursive formulation:

$$S_k = \frac{1}{k-1} \left(\frac{\sin(A_{i1}^* |s-r|)}{A_{i1}^{*k-1}} + |s-r| C_{k-1} \right) \frac{s-r}{|s-r|} \text{ for } k > 1, \quad (\text{B.13})$$

$$C_k = \frac{1}{k-1} \left(\frac{\cos(A_{i2}^* |s-r|)}{A_{i2}^{*k-1}} - (s-r) S_{k-1} \right) \text{ for } k > 1. \quad (\text{B.14})$$

APPENDIX-C USEFUL PROPERTIES OF JACOBI POLYNOMIALS

For the index $\kappa_0 = (-1, 0, 1)$, the following relations can be written (see Guler [45], Tricomi [76], Szegő [77]).

$$\begin{aligned} \frac{1}{\pi} \int_{-1}^1 \frac{W(t) P_n^{(\alpha, \beta)}(t)}{t-x} dt &= \frac{\cos \pi \alpha}{\sin \pi \alpha} W(x) P_n^{(\alpha, \beta)}(x) - \\ &- \frac{2^{\alpha+\beta} \Gamma(\alpha) \Gamma(n+\beta+1)}{\pi \Gamma(n+\alpha+\beta+1)} F\left(n+1, -n-\alpha-\beta, 1-\alpha, \frac{1-x}{2}\right). \end{aligned} \quad (\text{C.1})$$

where

$$-1 < x < 1, \Re(\alpha) > -1 \text{ and } \Re(\beta) > -1 \quad \alpha + \beta = -\kappa_0 \text{ and } \Re(\alpha) \neq (0, 1, 2, \dots)$$

The relation between Jacobi polynomials and hypergeometric function can be expressed as follows:

$$P_{n-\kappa_0}^{(-\alpha, -\beta)}(x) = \frac{\Gamma(n-\kappa_0-\alpha+1)}{\Gamma(n-\kappa_0+1)\Gamma(1-\alpha)} F\left(n+1, -n+\kappa_0, 1-\alpha, \frac{1-x}{2}\right). \quad (\text{C.2})$$

By substituting $\kappa_0 = -(\alpha + \beta)$ into (C.1), we found the following equation:

$$F\left(n+1, -n+\kappa_0, 1-\alpha, \frac{1-x}{2}\right) = \frac{\Gamma(n+\alpha+\beta+1)}{\Gamma(n+\beta+1)} P_{n-\kappa_0}^{(-\alpha, -\beta)}(x). \quad (\text{C.3})$$

By substituting (C.2) into (C.1), we found the following equation:

$$\frac{1}{\pi} \int_{-1}^1 \frac{W(t) P_n^{(\alpha, \beta)}(t)}{t-x} dt = \frac{\cos(\pi \alpha)}{\sin(\pi \alpha)} W(x) P_n^{(\alpha, \beta)}(x) - 2^{-\kappa_0} \frac{\Gamma(\alpha) \Gamma(1-\alpha)}{\pi} P_{n-\kappa_0}^{(-\alpha, -\beta)}(x). \quad (\text{C.4})$$

$$\Gamma(\alpha) \Gamma(1-\alpha) = \frac{\pi}{\sin \pi \alpha}. \quad (\text{C.5})$$

Integral equation for the contact problem can be written as follows:

$$A P_n^{(\alpha, \beta)}(r) W(r) + \frac{B}{\pi} \int_{-1}^1 \frac{P_n^{(\alpha, \beta)}(s) W(s)}{s-r} ds = -2^{-\kappa_0} \frac{B}{\sin(\pi\alpha)} P_{n-\kappa_0}^{(-\alpha, -\beta)}(r). \quad (\text{C.6})$$

for $-1 < r < 1$, $\Re(\alpha) > -1$ and $\Re(\beta) > -1$, and $\Re(\alpha) \neq (0, 1, 2, \dots)$

The orthogonality condition states that:

$$\int_{-1}^1 P_n^{(\alpha, \beta)}(t) P_j^{(\alpha, \beta)}(t) W(t) dt = \begin{cases} 0 & n \neq j \\ \theta_j^{(\alpha, \beta)} & n = j \end{cases} \quad j = 0, 1, 2, \dots \quad (\text{C.7})$$

where

$$\theta_0^{(\alpha, \beta)} = \int_{-1}^1 W(t) dt = \frac{2^{\alpha+\beta+1} \Gamma(\alpha+1) \Gamma(\beta+1)}{\Gamma(\alpha+\beta+2)}, \quad (\text{C.8})$$

$$\theta_j^{(\alpha, \beta)} = \frac{2^{\alpha+\beta+1} \Gamma(j+\alpha+1) \Gamma(j+\beta+1)}{(2j+\alpha+\beta+1) j! \Gamma(j+\alpha+\beta+1)}. \quad (\text{C.9})$$

Rodrigues formula states that the following formula:

$$W^{(\alpha, \beta)}(t) P_n^{(\alpha, \beta)}(t) = -\frac{(-1)^n}{2^n n!} \frac{d^n}{dt^n} [W^{(\alpha+n, \beta+n)}(t)] \quad n = 0, 1, 2, \dots \quad (\text{C.10})$$

$$W^{(\alpha, \beta)}(t) P_n^{(\alpha, \beta)}(t) = -\frac{1}{2n} \frac{d}{dt} [W^{(\alpha+1, \beta+1)}(t) P_{n-1}^{(\alpha+1, \beta+1)}(t)]. \quad (\text{C.11})$$

The recurrence relation on Jacobi polynomials is given by,

$$P_{n+1}^{(\alpha, \beta)}(x) P_n^{(\alpha, \beta)}(y) - P_{n+1}^{(\alpha, \beta)}(y) P_n^{(\alpha, \beta)}(x) = (x-y) \frac{\theta_n^{(\alpha, \beta)}}{A_n^{(\alpha, \beta)}} \sum_{k=0}^n \frac{P_k^{(\alpha, \beta)}(x) P_k^{(\alpha, \beta)}(y)}{\theta_k^{(\alpha, \beta)}}, \quad (\text{C.12})$$

where

$$A_n^{(\alpha, \beta)} = \frac{2(n+1)(\alpha + \beta + n + 1)}{(\alpha + \beta + 2n + 1)(\alpha + \beta + 2n + 2)}. \quad (\text{C.13})$$

APPENDIX-D THE METHOD OF EVALUATION OF THE FREDHOLM KERNELS

Numerical evaluation of Fredholm Kernels in the singular integral equations is highly important and the accuracy of the results depend on the correct evaluation of the Fredholm kernels. These Fredholm kernels contain improper integrals with upper limit of ∞ . In this part, it is required to calculate these indefinite integrals as accurate as possible. First of all, we need to separate these indefinite integrals into three main parts as shown in equations (D.1) – (D.4).

$$\begin{aligned}
 k_{11}^*(s, r) &= \frac{-4}{\kappa_1 + 1} \int_0^{A_{11}^*} \phi_{11}^*(\xi) \sin(\xi(s-r)) d\xi + \\
 &+ \frac{-4}{\kappa_1 + 1} \int_{A_{11}^*}^{\infty} \left[\phi_{11}^*(\xi) - \frac{[e_{11} + e_{21}]}{\xi} - \frac{[e_{12} + e_{22}]}{\xi^2} - \dots - \frac{[e_{110} + e_{210}]}{\xi^{10}} \right] \sin(\xi(s-r)) d\xi \\
 &+ \frac{-4}{\kappa_1 + 1} \int_{A_{11}^*}^{\infty} \left[\frac{[e_{11} + e_{21}]}{\xi} + \frac{[e_{12} + e_{22}]}{\xi^2} + \dots + \frac{[e_{110} + e_{210}]}{\xi^{10}} \right] \sin(\xi(s-r)) d\xi,
 \end{aligned} \tag{D.1}$$

$$\begin{aligned}
 k_{12}^*(s, r) &= \frac{-4}{\kappa_1 + 1} \int_0^{A_{12}^*} \phi_{12}^*(\xi) \cos(\xi(s-r)) d\xi + \\
 &+ \frac{-4}{\kappa_1 + 1} \int_{A_{12}^*}^{\infty} \left[\phi_{12}^*(\xi) - \frac{[f_{11} + f_{21}]}{\xi} - \frac{[f_{12} + f_{22}]}{\xi^2} - \dots - \frac{[f_{110} + f_{210}]}{\xi^{10}} \right] \cos(\xi(s-r)) d\xi \\
 &+ \frac{-4}{\kappa_1 + 1} \int_{A_{12}^*}^{\infty} \left[\frac{[f_{11} + f_{21}]}{\xi} + \frac{[f_{12} + f_{22}]}{\xi^2} + \dots + \frac{[f_{110} + f_{210}]}{\xi^{10}} \right] \cos(\xi(s-r)) d\xi,
 \end{aligned} \tag{D.2}$$

$$\begin{aligned}
k_{21}^*(s, r) &= \frac{-4}{\kappa_1 + 1} \int_0^{A_{21}^*} \phi_{21}^*(\xi) \sin(\xi(s-r)) d\xi + \\
&+ \frac{-4}{\kappa_1 + 1} \int_{A_{21}^*}^{\infty} \left[\phi_{21}^*(\xi) - \frac{[g_{11} + g_{21}]}{\xi} - \frac{[g_{12} + g_{22}]}{\xi^2} - \dots - \frac{[g_{110} + g_{210}]}{\xi^{10}} \right] \sin(\xi(s-r)) d\xi \\
&+ \frac{-4}{\kappa_1 + 1} \int_{A_{21}^*}^{\infty} \left[\frac{[g_{11} + g_{21}]}{\xi} + \frac{[g_{12} + g_{22}]}{\xi^2} + \dots + \frac{[g_{110} + g_{210}]}{\xi^{10}} \right] \sin(\xi(s-r)) d\xi,
\end{aligned} \tag{D.3}$$

$$\begin{aligned}
k_{22}^*(s, r) &= \frac{-4}{\kappa_1 + 1} \int_0^{A_{22}^*} \phi_{22}^*(\xi) \cos(\xi(s-r)) d\xi + \\
&+ \frac{-4}{\kappa_1 + 1} \int_{A_{22}^*}^{\infty} \left[\phi_{22}^*(\xi) - \frac{[h_{11} + h_{21}]}{\xi} - \frac{[h_{12} + h_{22}]}{\xi^2} - \dots - \frac{[h_{110} + h_{210}]}{\xi^{10}} \right] \sin(\xi(s-r)) d\xi \\
&+ \frac{-4}{\kappa_1 + 1} \int_{A_{22}^*}^{\infty} \left[\frac{[h_{11} + h_{21}]}{\xi} + \frac{[h_{12} + h_{22}]}{\xi^2} + \dots + \frac{[h_{110} + h_{210}]}{\xi^{10}} \right] \sin(\xi(s-r)) d\xi.
\end{aligned} \tag{D.4}$$

A_{11}^* , A_{12}^* , A_{21}^* and A_{22}^* are the integration cut-off points. They are used to calculate the integrals numerically from zero to A_{ij} using Gauss-Quadrature rule and $A_{ij}^* = A_{ij} l$ for $i, j = 1, 2$. Large values of A_{ij}^* increases the numerical effort for the computation of the second term in the right hand side of equations (D.1) - (D.4). On the other hand, choosing lower values of integration cut off points A_{ij}^* leads to a combination of right hand side equations with higher order of asymptotic expansions and it brings complexity of the asymptotic expansions. Instead, we have chosen large values of A_{ij}^* and we may assume that these terms will go to zero and hence it provides less computational effort. Consequently, second terms in the right hand side of the equations (D.1) - (D.4) will tend to zero so only first and third terms are considered.

D.1. Evaluation of bounded Fredholm kernels

First integrals in equations (D.1) - (D.4) are bounded and they can be evaluated numerically using the Gaussian Quadrature Rule. Hence, we apply the Gauss-Quadrature integration scheme for zero to A_{ij}^* part. Selection of integration cut off points A_{ij}^* has no significant importance on total integral evaluation of the kernels but we try to select A_{ij}^* so that γ_1^*/A_{ij}^* is small. If higher values of integration cut off points are used, more computing effort is observed and correspondingly so much computation time is needed.

$$I_{111}(r, s) = \int_0^{A_{11}^*} \phi_{11}^*(\xi) \sin(\xi(s-r)) d\xi, \quad (\text{D.5})$$

$$I_{112}(r, s) = \int_0^{A_{12}^*} \phi_{12}^*(\xi) \cos(\xi(s-r)) d\xi, \quad (\text{D.6})$$

$$I_{121}(r, s) = \int_0^{A_{21}^*} \phi_{21}^*(\xi) \sin(\xi(s-r)) d\xi, \quad (\text{D.7})$$

$$I_{122}(r, s) = \int_0^{A_{22}^*} \phi_{22}^*(\xi) \cos(\xi(s-r)) d\xi. \quad (\text{D.8})$$

We need to change the variables in order to make the integration limits from $(-a, b)$ to $(-1, 1)$. Hence the following change of variable is applied:

$$\xi = \frac{A_{ij}^* - 0}{2} \varsigma + \frac{A_{ij}^* + 0}{2} = \frac{A_{ij}^*}{2} \varsigma + \frac{A_{ij}^*}{2}, \quad i, j = 1, 2. \quad (\text{D.9})$$

$$d\xi = \frac{A_{ij}^*}{2} d\varsigma, \quad i, j = 1, 2. \quad (\text{D.10})$$

$$I_{111}(r, s) = \frac{A_{11}^*}{2} \int_{-1}^1 \phi_{11}^* \left(\frac{A_{11}^*}{2} \zeta + \frac{A_{11}^*}{2} \right) \sin \left(\left(\frac{A_{11}^*}{2} \zeta + \frac{A_{11}^*}{2} \right) (s-r) \right) d\zeta \cong \sum_{k=1}^M w_k n_{11}(\zeta_k), \quad (\text{D.11})$$

$$I_{112}(r, s) = \frac{A_{12}^*}{2} \int_{-1}^1 \phi_{12}^* \left(\frac{A_{12}^*}{2} \zeta + \frac{A_{12}^*}{2} \right) \cos \left(\left(\frac{A_{12}^*}{2} \zeta + \frac{A_{12}^*}{2} \right) (s-r) \right) d\zeta \cong \sum_{k=1}^M w_k n_{12}(\zeta_k), \quad (\text{D.12})$$

$$I_{121}(r, s) = \frac{A_{21}^*}{2} \int_{-1}^1 \phi_{21}^* \left(\frac{A_{21}^*}{2} \zeta + \frac{A_{21}^*}{2} \right) \sin \left(\left(\frac{A_{21}^*}{2} \zeta + \frac{A_{21}^*}{2} \right) (s-r) \right) d\zeta \cong \sum_{k=1}^M w_k n_{21}(\zeta_k), \quad (\text{D.13})$$

$$I_{122}(r, s) = \frac{A_{22}^*}{2} \int_{-1}^1 \phi_{22}^* \left(\frac{A_{22}^*}{2} \zeta + \frac{A_{22}^*}{2} \right) \cos \left(\left(\frac{A_{22}^*}{2} \zeta + \frac{A_{22}^*}{2} \right) (s-r) \right) d\zeta \cong \sum_{k=1}^M w_k n_{22}(\zeta_k). \quad (\text{D.14})$$

where

$$n_{11}(\zeta_k) = \phi_{11}^* \left(\frac{A_{11}^*}{2} \zeta_k + \frac{A_{11}^*}{2} \right) \sin \left(\left(\frac{A_{11}^*}{2} \zeta_k + \frac{A_{11}^*}{2} \right) (s-r) \right), \quad (\text{D.15})$$

$$n_{12}(\zeta_k) = \phi_{12}^* \left(\frac{A_{12}^*}{2} \zeta_k + \frac{A_{12}^*}{2} \right) \cos \left(\left(\frac{A_{12}^*}{2} \zeta_k + \frac{A_{12}^*}{2} \right) (s-r) \right), \quad (\text{D.16})$$

$$n_{21}(\zeta_k) = \phi_{21}^* \left(\frac{A_{21}^*}{2} \zeta_k + \frac{A_{21}^*}{2} \right) \sin \left(\left(\frac{A_{21}^*}{2} \zeta_k + \frac{A_{21}^*}{2} \right) (s-r) \right), \quad (\text{D.17})$$

$$n_{22}(\zeta_k) = \phi_{22}^* \left(\frac{A_{22}^*}{2} \zeta_k + \frac{A_{22}^*}{2} \right) \cos \left(\left(\frac{A_{22}^*}{2} \zeta_k + \frac{A_{22}^*}{2} \right) (s-r) \right). \quad (\text{D.18})$$

w_k are the Gauss weights and ζ_k are the roots of the Legendre functions $P_k(\zeta)$.

Actually, the integration interval is divided into 100 parts. For each part, the Gaussian Quadrature integration scheme is applied.

Consequently, we have found $I_{11}(r, s)$, $I_{12}(r, s)$, $I_{21}(r, s)$ and $I_{22}(r, s)$ for 0 to A_{ij}^* ($i, j = 1, 2$) interval.

D.2. Evaluation of unbounded Fredholm kernels

The third terms of the equations (D.1) - (D.4) consist of unbounded integrals and they can be expressed as the following form:

$$I_{211}(r, s) = \int_{A_{11}^*}^{\infty} \phi_{11}^*(\xi) \sin(\xi(s-r)) d\xi, \quad (\text{D.19})$$

$$I_{212}(r, s) = \int_{A_{12}^*}^{\infty} \phi_{12}^*(\xi) \cos(\xi(s-r)) d\xi, \quad (\text{D.20})$$

$$I_{221}(r, s) = \int_{A_{21}^*}^{\infty} \phi_{21}^*(\xi) \sin(\xi(s-r)) d\xi, \quad (\text{D.21})$$

$$I_{222}(r, s) = \int_{A_{22}^*}^{\infty} \phi_{22}^*(\xi) \cos(\xi(s-r)) d\xi. \quad (\text{D.22})$$

For A_{ij}^* to ∞ part, the integrands ϕ_{11}^* , ϕ_{12}^* , ϕ_{21}^* and ϕ_{22}^* are asymptotically expanded.

For $\xi \rightarrow \infty$:

$$h_{11}(\xi, Y) = \frac{i\xi}{|\xi|} e^{|\xi|\alpha_1 Y} h_{111}^{\infty}(\xi, Y) + \frac{i\xi}{|\xi|} e^{|\xi|\alpha_2 Y} h_{112}^{\infty}(\xi, Y), \quad (\text{D.23})$$

$$h_{12}(\xi, Y) = e^{|\xi|\alpha_1 Y} h_{121}^{\infty}(\xi, Y) + e^{|\xi|\alpha_2 Y} h_{122}^{\infty}(\xi, Y), \quad (\text{D.24})$$

$$h_{21}(\xi, Y) = \frac{i\xi}{|\xi|} e^{|\xi|\alpha_1 Y} h_{211}^{\infty}(\xi, Y) + \frac{i\xi}{|\xi|} e^{|\xi|\alpha_2 Y} h_{212}^{\infty}(\xi, Y), \quad (\text{D.25})$$

$$h_{22}(\xi, Y) = e^{|\xi|\alpha_1 Y} h_{221}^{\infty}(\xi, Y) + e^{|\xi|\alpha_2 Y} h_{222}^{\infty}(\xi, Y), \quad (\text{D.26})$$

where

$$h_{111}^{\infty}(\xi, Y) = \left\{ e_{11} \left| \frac{\gamma_1^*}{\xi} \right| + e_{12} \left| \frac{\gamma_1^*}{\xi} \right|^2 + e_{13} \left| \frac{\gamma_1^*}{\xi} \right|^3 + \dots + e_{110} \left| \frac{\gamma_1^*}{\xi} \right|^{10} \right\}, \quad (\text{D.27})$$

$$h_{112}^{\infty}(\xi, Y) = \left\{ e_{21} \left| \frac{\gamma_1^*}{\xi} \right| + e_{22} \left| \frac{\gamma_1^*}{\xi} \right|^2 + e_{23} \left| \frac{\gamma_1^*}{\xi} \right|^3 + \dots + e_{210} \left| \frac{\gamma_1^*}{\xi} \right|^{10} \right\}, \quad (\text{D.28})$$

$$h_{121}^{\infty}(\xi, Y) = \left\{ f_{11} \left| \frac{\gamma_1^*}{\xi} \right| + f_{12} \left| \frac{\gamma_1^*}{\xi} \right|^2 + f_{13} \left| \frac{\gamma_1^*}{\xi} \right|^3 + \dots + f_{110} \left| \frac{\gamma_1^*}{\xi} \right|^{10} \right\}, \quad (\text{D.29})$$

$$h_{122}^{\infty}(\xi, Y) = \left\{ f_{21} \left| \frac{\gamma_1^*}{\xi} \right| + f_{22} \left| \frac{\gamma_1^*}{\xi} \right|^2 + f_{23} \left| \frac{\gamma_1^*}{\xi} \right|^3 + \dots + f_{210} \left| \frac{\gamma_1^*}{\xi} \right|^{10} \right\}, \quad (\text{D.30})$$

$$h_{211}^{\infty}(\xi, Y) = \left\{ g_{11} \left| \frac{\gamma_1^*}{\xi} \right| + g_{12} \left| \frac{\gamma_1^*}{\xi} \right|^2 + g_{13} \left| \frac{\gamma_1^*}{\xi} \right|^3 + \dots + g_{110} \left| \frac{\gamma_1^*}{\xi} \right|^{10} \right\}, \quad (\text{D.31})$$

$$h_{212}^{\infty}(\xi, Y) = \left\{ g_{21} \left| \frac{\gamma_1^*}{\xi} \right| + g_{22} \left| \frac{\gamma_1^*}{\xi} \right|^2 + g_{23} \left| \frac{\gamma_1^*}{\xi} \right|^3 + \dots + g_{210} \left| \frac{\gamma_1^*}{\xi} \right|^{10} \right\}, \quad (\text{D.32})$$

$$h_{221}^{\infty}(\xi, Y) = \left\{ h_{11} \left| \frac{\gamma_1^*}{\xi} \right| + h_{12} \left| \frac{\gamma_1^*}{\xi} \right|^2 + h_{13} \left| \frac{\gamma_1^*}{\xi} \right|^3 + \dots + h_{110} \left| \frac{\gamma_1^*}{\xi} \right|^{10} \right\}, \quad (\text{D.33})$$

$$h_{222}^{\infty}(\xi, Y) = \left\{ h_{21} \left| \frac{\gamma_1^*}{\xi} \right| + h_{22} \left| \frac{\gamma_1^*}{\xi} \right|^2 + h_{23} \left| \frac{\gamma_1^*}{\xi} \right|^3 + \dots + h_{210} \left| \frac{\gamma_1^*}{\xi} \right|^{10} \right\}. \quad (\text{D.34})$$

On the contact surface, asymptotic expansions can be written as the following form:

$$h_{11}(\xi, 0) = \frac{i\xi}{|\xi|} \left\{ [e_{11} + e_{21}] \left| \frac{\gamma_1^*}{\xi} \right| + [e_{12} + e_{22}] \left| \frac{\gamma_1^*}{\xi} \right|^2 + \dots + [e_{110} + e_{210}] \left| \frac{\gamma_1^*}{\xi} \right|^{10} \right\}, \quad (\text{D.35})$$

$$h_{12}(\xi, 0) = \left\{ [f_{11} + f_{21}] \left| \frac{\gamma_1^*}{\xi} \right| + [f_{12} + f_{22}] \left| \frac{\gamma_1^*}{\xi} \right|^2 + \dots + [f_{110} + f_{210}] \left| \frac{\gamma_1^*}{\xi} \right|^{10} \right\}, \quad (\text{D.36})$$

$$h_{21}(\xi, 0) = \frac{i\xi}{|\xi|} \left\{ [g_{11} + g_{21}] \left| \frac{\gamma_1^*}{\xi} \right| + [g_{12} + g_{22}] \left| \frac{\gamma_1^*}{\xi} \right|^2 + \dots + [g_{110} + g_{210}] \left| \frac{\gamma_1^*}{\xi} \right|^{10} \right\}, \quad (\text{D.37})$$

$$h_{22}(\xi, 0) = \left\{ [h_{11} + h_{21}] \left| \frac{\gamma_1^*}{\xi} \right| + [h_{12} + h_{22}] \left| \frac{\gamma_1^*}{\xi} \right|^2 + \dots + [h_{110} + h_{210}] \left| \frac{\gamma_1^*}{\xi} \right|^{10} \right\}. \quad (\text{D.38})$$

Therefore, when these expressions are substituted A_{ij}^* to ∞ part integral equations, the following relations are obtained:

$$I_{211}(r, s) = \int_{A_{11}^*}^{\infty} \left\{ \sum_{k=1}^{k=N} [e_{1k} + e_{2k}] \left| \frac{\gamma_1^*}{\xi} \right|^k \right\} \sin(\xi(s-r)) d\xi, \quad (\text{D.39})$$

$$I_{212}(r, s) = \int_{A_{12}^*}^{\infty} \left\{ \sum_{k=1}^{k=N} [f_{1k} + f_{2k}] \left| \frac{\gamma_1^*}{\xi} \right|^k \right\} \cos(\xi(s-r)) d\xi, \quad (\text{D.40})$$

$$I_{221}(r, s) = \int_{A_{21}^*}^{\infty} \left\{ \sum_{k=1}^{k=N} [g_{1k} + g_{2k}] \left| \frac{\gamma_1^*}{\xi} \right|^k \right\} \sin(\xi(s-r)) d\xi, \quad (\text{D.41})$$

$$I_{222}(r, s) = \int_{A_{22}^*}^{\infty} \left\{ \sum_{k=1}^{k=N} [h_{1k} + h_{2k}] \left| \frac{\gamma_1^*}{\xi} \right|^k \right\} \cos(\xi(s-r)) d\xi. \quad (\text{D.42})$$

$[e_{1k} + e_{2k}]$, $[f_{1k} + f_{2k}]$, $[g_{1k} + g_{2k}]$ and $[h_{1k} + h_{2k}]$, $k = 1, 2, \dots, 10$ are found and first terms of the asymptotic expansion are given in Appendix-A. We can calculate the indefinite integrals I_{211} , I_{212} , I_{221} and I_{222} in closed form using the procedure explained in Appendix-B.

APPENDIX-E THE EFFECT OF MASS DENSITY RATIO ON DYNAMIC CONTACT MECHANICS OF HOMOGENOUS ELASTIC COATINGS

Governing partial differential equations for the contact problem of homogenous elastic coating and the homogenous substrate are derived as:

$$\left(\frac{\kappa_1+1}{\kappa_1-1}-c_1^2\right)\frac{\partial^2 u_1}{\partial X^2}+\frac{2}{\kappa_1-1}\frac{\partial^2 v_1}{\partial X \partial Y}+\frac{\partial^2 u_1}{\partial Y^2}=0, \quad (\text{E.1})$$

$$(1-c_1^2)\frac{\partial^2 v_1}{\partial X^2}+\frac{2}{\kappa_1-1}\frac{\partial^2 u_1}{\partial X \partial Y}+\frac{\kappa_1+1}{\kappa_1-1}\frac{\partial^2 v_1}{\partial Y^2}=0, \quad (\text{E.2})$$

$$\left(\frac{\kappa_2+1}{\kappa_2-1}-c_2^2\right)\frac{\partial^2 u_2}{\partial X^2}+\frac{2}{\kappa_2-1}\frac{\partial^2 v_2}{\partial X \partial Y}+\frac{\partial^2 u_2}{\partial Y^2}=0, \quad (\text{E.3})$$

$$(1-c_2^2)\frac{\partial^2 v_2}{\partial X^2}+\frac{2}{\kappa_2-1}\frac{\partial^2 u_2}{\partial X \partial Y}+\frac{\kappa_2+1}{\kappa_2-1}\frac{\partial^2 v_2}{\partial Y^2}=0, \quad (\text{E.4})$$

Roots of the characteristic equation for the dynamic contact problem of homogenous elastic coatings are obtained as follows:

$$s_1 = \frac{1}{2} \left\{ + \sqrt{4 \left(1 - \frac{\kappa_1 c_1^2}{\kappa_1 + 1} \right) + 4i\lambda \frac{\sqrt{-\lambda^2 c_1^4}}{\kappa_1 + 1}} \right\}; \quad \Re(s_1) > 0, \quad (\text{E.5})$$

$$s_2 = \frac{1}{2} \left\{ - \sqrt{4 \left(1 - \frac{\kappa_1 c_1^2}{\kappa_1 + 1} \right) + 4i\lambda \frac{\sqrt{-\lambda^2 c_1^4}}{\kappa_1 + 1}} \right\}; \quad \Re(s_2) < 0, \quad (\text{E.6})$$

$$s_3 = \frac{1}{2} \left\{ + \sqrt{4 \left(1 - \frac{\kappa_1 c_1^2}{\kappa_1 + 1} \right) - 4i\lambda \frac{\sqrt{-\lambda^2 c_1^4}}{\kappa_1 + 1}} \right\}; \quad \Re(s_3) > 0, \quad (\text{E.7})$$

$$s_4 = \frac{1}{2} \left\{ -\sqrt{4 \left(1 - \frac{\kappa_1 c_1^2}{\kappa_1 + 1} \right) - 4i\lambda \frac{\sqrt{-\lambda^2 c_1^4}}{\kappa_1 + 1}} \right\}; \quad \Re(s_4) < 0, \quad (\text{E.8})$$

Dimensionless punch speeds for homogenous elastic coating and homogenous substrate can be calculated by,

$$c_1 = \frac{V}{c_{s1}}, \quad c_2 = \frac{V}{c_{s2}}, \quad (\text{E.9})$$

where

$$c_{s1} = \sqrt{\frac{\mu_1}{\rho_1}}, \quad c_{s2} = \sqrt{\frac{\mu_2}{\rho_2}}, \quad (\text{E.10})$$

μ_1, ρ_1 denote the shear modulus and mass density of the coating material while μ_2, ρ_2 denote the shear modulus and mass density of the substrate material. Using expressions described above, the relationship between dimensionless punch speeds c_1 and c_2 can be expressed as follows:

$$c_2 = c_1 \sqrt{\frac{\mu_1 \rho_2}{\mu_2 \rho_1}} \quad (\text{E.11})$$

In this part, the effect of mass density ratio on elastodynamic contact mechanics of less stiff and stiffer coatings is examined.

- Dynamic contact mechanics analysis for the less stiff coating $\mu_1 / \mu_2 = 1/10$,
 $a / h_1 = 0.5, c_1 = 0.6, \eta = 0.3$.

$$c_2 = 0.31623 c_1 \sqrt{\frac{\rho_2}{\rho_1}}$$

Table E. 1. Dimensionless punch speeds and normalized punch stress intensity factors for various values of mass density ratio

ρ_1 / ρ_2	$c_1 = 0.6$	c_2	$K_I(-a)$	$K_I(a)$
1/10		0.6	0.2543	0.2763
1/5		0.424	0.2528	0.2760
1		0.190	0.2518	0.2759
3.6		0.167	0.2517	0.2759
5		0.085	0.2517	0.2759
10		0.060	0.2517	0.2759

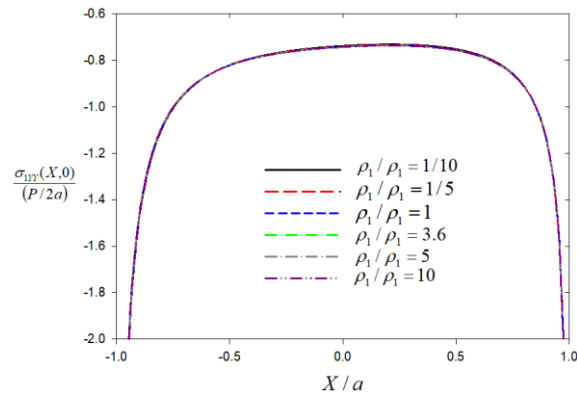


Fig. E.1 Normal elastodynamic contact stresses for various values of the mass density ratio $\mu_1 / \mu_2 = 1/10$, $a / h_1 = 0.5$, $\eta = 0.3$, $c_1 = 0.6$, $\nu_1 / \nu_2 = 1.0$.

- Dynamic contact mechanics analysis for the stiffer coating $\mu_1 / \mu_2 = 10$,
 $a / h_1 = 0.5$, $c_1 = 0.6$, $\eta = 0.3$.

$$c_2 = 3.1623 c_1 \sqrt{\frac{\rho_2}{\rho_1}}$$

Table E.2. Dimensionless punch speeds and normalized punch stress intensity factors for various values of mass density ratio

ρ_1 / ρ_2	$c_1 = 0.6$	c_2	$K_I(-a)$	$K_I(a)$
1/10		6.000	0.2677	0.3156
1/5		4.243	0.2845	0.3372
1		1.897	0.1578	0.2761
3.6		1.000	0.3404	0.3836
5		0.849	0.3808	0.4476
10		0.600	1.3005	1.3036

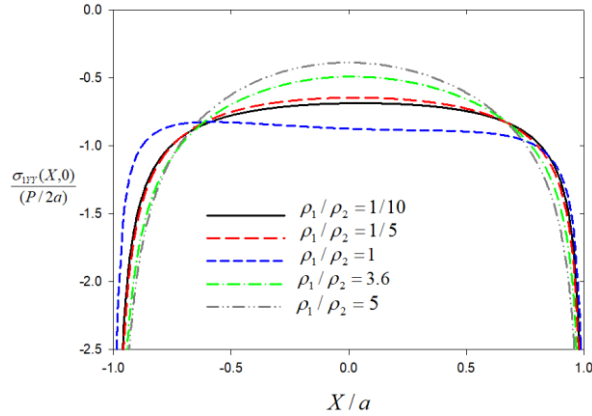


Fig. E.2 Normal elastodynamic contact stresses for various values of the density ratio $\mu_1 / \mu_2 = 10$, $a / h_1 = 0.5$, $\eta = 0.3$, $c_1 = 0.6$, $v_1 / v_2 = 1.0$.

- Investigation of the normalized punch stress intensity factors for different type coatings $\rho_1 / \rho_2 = 1/2$.

$$c_2 = 1.4142 c_1 \sqrt{\frac{\mu_1}{\mu_2}}$$

Table E.3. Numerical relations between c_1 and c_2 , $\rho_1/\rho_2=1/2$.

	$c_1 = 0.0$	$c_1 = 0.2$	$c_1 = 0.4$	$c_1 = 0.6$	$c_1 = 0.8$
μ_1/μ_2	c_2	c_2	c_2	c_2	c_2
1/10	0.0	0.089	0.179	0.268	0.358
1/5	0.0	0.127	0.253	0.380	0.506
1	0.0	0.283	0.566	0.849	1.131
5	0.0	0.633	1.265	1.897	2.530
10	0.0	0.895	1.789	2.683	3.578

Table E.4. Normalized stress intensity factors for the rigid flat punch, $a/h_1=0.1$, $\eta=0.3$, $\rho_1/\rho_2=1/2$, $\nu_1/\nu_2=1$.

	$c_1 = 0.0$		$c_1 = 0.2$		$c_1 = 0.4$		$c_1 = 0.6$		$c_1 = 0.8$	
μ_1/μ_2	$K_I(-a)$	$K_I(a)$	$K_I(-a)$	$K_I(a)$	$K_I(-a)$	$K_I(a)$	$K_I(-a)$	$K_I(a)$	$K_I(-a)$	$K_I(a)$
1/10	0.3103	0.3201	0.3099	0.3201	0.3084	0.3198	0.3042	0.3180	0.2821	0.2967
1/5	0.3113	0.3196	0.3109	0.3195	0.3094	0.3192	0.3053	0.3175	0.2829	0.2965
1	0.3167	0.3167	0.3166	0.3166	0.3159	0.3159	0.3134	0.3134	0.2931	0.2931
5	0.3310	0.3098	0.3389	0.3039	0.2155	0.3837	0.2941	0.3255	0.2811	0.3002
10	0.3409	0.3050	0.3847	0.2723	0.2772	0.3350	0.3058	0.3217	0.2867	0.3012

- Investigation of the normalized punch stress intensity factors for different type coatings $\rho_1/\rho_2=2$.

$$c_2 = 0.7071 c_1 \sqrt{\frac{\mu_1}{\mu_2}}$$

Table E. 5. Numerical relations between c_1 and c_2 , $\rho_1/\rho_2=2$.

	$c_1 = 0.0$	$c_1 = 0.2$	$c_1 = 0.4$	$c_1 = 0.6$	$c_1 = 0.8$
μ_1/μ_2	c_2	c_2	c_2	c_2	c_2
1/10	0.0	0.0447	0.0894	0.134	0.179
1/5	0.0	0.0633	0.127	0.189	0.253
1	0.0	0.1414	0.283	0.424	0.566
5	0.0	0.3162	0.632	0.949	1.265
10	0.0	0.4472	0.894	1.342	1.789

Table E.6. Normalized stress intensity factors for the rigid flat punch, $a/h_1 = 0.1$, $\eta = 0.3$, $\rho_1 / \rho_2 = 2$, $\nu_1 / \nu_2 = 1$.

μ_1 / μ_2	$c_1 = 0.0$		$c_1 = 0.2$		$c_1 = 0.4$		$c_1 = 0.6$		$c_1 = 0.8$	
	$K_I(-a)$	$K_I(a)$	$K_I(-a)$	$K_I(a)$	$K_I(-a)$	$K_I(a)$	$K_I(-a)$	$K_I(a)$	$K_I(-a)$	$K_I(a)$
1/10	0.3103	0.3201	0.3099	0.3201	0.3084	0.3198	0.3042	0.3180	0.2820	0.2967
1/5	0.3113	0.3196	0.3108	0.3196	0.3093	0.3193	0.3051	0.3176	0.2826	0.2966
1	0.3167	0.3167	0.3166	0.3166	0.3159	0.3159	0.3134	0.3134	0.2931	0.2931
5	0.3310	0.3098	0.3329	0.3084	0.3436	0.3007	0.6886	0.2327	0.3161	0.3519
10	0.3409	0.3050	0.3468	0.3010	0.5797	0.1586	0.2919	0.3384	0.2714	0.2986

- Investigation of the normalized punch stress intensity factors for different type coatings $\rho_1 / \rho_2 = 1/8$.

$$c_2 = 2.8284 c_1 \sqrt{\frac{\mu_1}{\mu_2}}$$

Table E.7. Numerical relations between c_1 and c_2 , $\rho_1 / \rho_2 = 1/8$.

μ_1 / μ_2	$c_1 = 0.0$	$c_1 = 0.2$	$c_1 = 0.4$	$c_1 = 0.6$	$c_1 = 0.8$
	c_2	c_2	c_2	c_2	c_2
1/10	0.0	0.179	0.358	0.537	0.716
1/5	0.0	0.253	0.506	0.759	1.012
1	0.0	0.566	1.131	1.697	2.263
5	0.0	1.265	2.530	3.795	5.060
10	0.0	1.789	3.578	5.367	7.155

Table E.8. Normalized stress intensity factors for the rigid flat punch, $a/h_1 = 0.1$, $\eta = 0.3$, $\rho_1 / \rho_2 = 1/8$, $\nu_1 / \nu_2 = 1$.

μ_1 / μ_2	$c_1 = 0.0$		$c_1 = 0.2$		$c_1 = 0.4$		$c_1 = 0.6$		$c_1 = 0.8$	
	$K_I(-a)$	$K_I(a)$	$K_I(-a)$	$K_I(a)$	$K_I(-a)$	$K_I(a)$	$K_I(-a)$	$K_I(a)$	$K_I(-a)$	$K_I(a)$
1/10	0.3103	0.3201	0.3100	0.3200	0.3085	0.3197	0.3045	0.3178	0.2824	0.2965
1/5	0.3113	0.3196	0.3110	0.3195	0.3099	0.3189	0.3068	0.3164	0.2900	0.2919
1	0.3167	0.3167	0.3166	0.3166	0.3159	0.3159	0.3134	0.3134	0.2931	0.2931
5	0.3310	0.3098	0.4035	0.2865	0.3053	0.3243	0.3036	0.3208	0.2813	0.2987
10	0.3409	0.3050	0.2668	0.3386	0.3112	0.3219	0.3065	0.3199	0.2820	0.2988

Results show that the mass density ratio of the coating and the substrate material does not significantly affect the normal elastodynamic contact stress and the punch stress

intensity factors in the case of a less stiff coating. However, mass density ratio significantly affects the normal elastodynamic contact stress and accordingly punch stress intensity factors for the stiffer coating. Hence, selection of the mass density ratio plays an important role on dynamic contact behavior of stiffer coatings.

Normalized punch stress intensity factors depend on various parameters including dimensionless punch speed, coefficient of friction, Poisson's ratio, mass density ratio, coating thickness and shear modulus ratio. Performed analyses show that when c_2 close to 1.0, a sudden change is observed for the values of normalized punch stress intensity factors for the stiffer coatings.

APPENDIX-F SOLUTION OF DYNAMIC CONTACT PROBLEM BETWEEN A RIGID PUNCH AND A HALF PLANE BY COMPLEX FUNCTIONS

The contact problem between a moving punch and the half-plane is analyzed by Eringen and Suhubi [75] and they developed analytical method by means of complex functions. In this study, a rigid punch moves steadily at a constant subsonic speed on the contact surface and there is no friction between the rigid punch and the contact surface. When the applied vertical force is increased thoroughly indents the half-plane, general stress singularities are occurred at the punch corners. The vertical displacement component is known priori which depends on the punch profile. Figure F.1 illustrates the general description of the moving flat punch on a half plane.

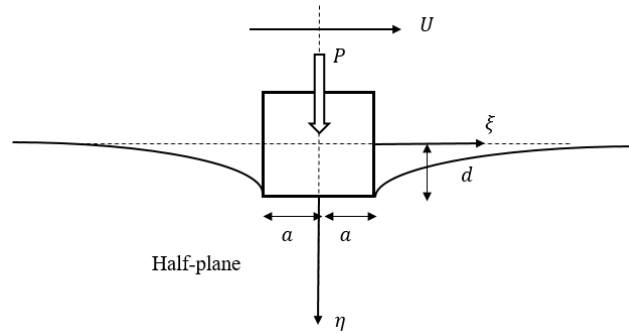


Figure F.1: Schematic of the moving flat punch sliding over the half plane

For the contact of a rigid flat punch, the indentation depth is denoted as d and it is constant.

$$\xi = x_1 - Ut, \quad \eta = x_2. \quad (\text{F.1})$$

Normal and lateral elastodynamic contact stresses over the the half plane are given by,

$$t_{22} = \begin{cases} -\frac{P}{\pi(a^2 - \zeta^2)^{1/2}} & |\zeta| \leq a \\ 0 & |\zeta| > a \end{cases} \quad (\text{F.2})$$

$$t_{11} = \begin{cases} -\frac{(1 + 2\beta_1^2 - \beta_2^2)(1 + \beta_2^2) - 4\beta_1\beta_2}{4\beta_1\beta_2 - (1 + \beta_2^2)^2} \frac{P}{\pi(a^2 - \zeta^2)^{1/2}}, & |\zeta| \leq a \\ 0 & |\zeta| > a \end{cases} \quad (\text{F.3})$$

where t_{22} and t_{11} and denote the surface normal and lateral contact stresses, respectively.

$$\beta_1 = (1 - M_1^2)^{1/2}, \quad \beta_2 = (1 - M_2^2)^{1/2}, \quad (\text{F.4})$$

$$M_1 = \frac{U}{c_1}, \quad M_2 = \frac{U}{c_2}, \quad (\text{F.5})$$

M_1 and M_2 are Mach numbers of the moving source relative to the dilatational and equivoluminal (shear) waves, respectively.

$$c_1 = \sqrt{\frac{E}{\rho}}, \quad (\text{F.6})$$

$$c_2 = \sqrt{\frac{\mu}{\rho}}, \quad (\text{F.7})$$

$$\mu = \frac{E}{2(1 + \nu)}. \quad (\text{F.8})$$

CURRICULUM VITAE

PERSONAL INFORMATION

Surname, Name: Balci, Mehmet Nurullah

Nationality: Turkish (T.C.)

Date and Place of Birth: 06 August 1988, Çankırı

Marital Status: Married

Phone: +90 312 297 62 08 / 147

Fax: +90 312 297 62 08

Email: mehmetbalci@hacettepe.edu.tr, balci.mehmet06@gmail.com

EDUCATION

Degree Graduation	Institution	Year of
MSc	Hacettepe U. Mechanical Eng. Dept.	2012
BSc	Baskent U. Mechanical Eng. Dept. (Full scholarship)	2010
High School	Mehmet Emin Resulzade Anatolian High School	2006

WORK EXPERIENCE

Year	Place	Enrollment
2011- Present	Hacettepe U. Mechanical Eng. Dept.	Teaching Assistant
2009 June	Mercedes-Benz Türk A.Ş.	Intern Engineering Student
2008 June	Turkish Aerospace Industries (TAI)	Intern Engineering Student

FOREIGN LANGUAGES

English

PUBLICATIONS

1. Balci, M.N., Dag, S., “Dynamic frictional contact problems involving elastic coatings”, Tribology International, Vol. 124, pp. 70-92 (2018).
2. Balci, M.N., Dag, S., Yildirim, B., “Subsurface stresses in graded coatings subjected to frictional contact with heat generation”, Journal of Thermal Stresses, Vol. 40, pp. 517-534 (2017).
3. Balci, M.N., Yildirim, B., Dag, S., “Analysis of frictional contacts with heat generation considering temperature dependent properties”, International Journal of Mechanical Sciences, Vol. 101-102, pp. 59-69 (2015).